PROCEEDINGS OF ASPL2019 - 8TH ASIAN-OCEANIAN SYMPOSIUM ON PLANT LIPIDS

EDITED BY: Xue-Rong Zhou, Ikuo Nishida, Mi Chung Suh and Thomas Vanhercke

PUBLISHED IN: Frontiers in Plant Science

frontiers Research Topics

ISSN 1664-8714
ISBN 978-2-88966-433-7
DOI 10.3389/978-2-88966-433-7

About Frontiers

Frontiers is more than just an open-access publisher of scholarly articles: it is a pioneering approach to the world of academia, radically improving the way scholarly research is managed. The grand vision of Frontiers is a world where all people have an equal opportunity to seek, share and generate knowledge. Frontiers provides immediate and permanent online open access to all its publications, but this alone is not enough to realize our grand goals.

Frontiers Journal Series

The Frontiers Journal Series is a multi-tier and interdisciplinary set of open-access, online journals, promising a paradigm shift from the current review, selection and dissemination processes in academic publishing. All Frontiers journals are driven by researchers for researchers; therefore, they constitute a service to the scholarly community. At the same time, the Frontiers Journal Series operates on a revolutionary invention, the tiered publishing system, initially addressing specific communities of scholars, and gradually climbing up to broader public understanding, thus serving the interests of the lay society, too.

Dedication to Quality

Each Frontiers article is a landmark of the highest quality, thanks to genuinely collaborative interactions between authors and review editors, who include some of the world's best academicians. Research must be certified by peers before entering a stream of knowledge that may eventually reach the public - and shape society; therefore, Frontiers only applies the most rigorous and unbiased reviews.
Frontiers revolutionizes research publishing by freely delivering the most outstanding research, evaluated with no bias from both the academic and social point of view. By applying the most advanced information technologies, Frontiers is catapulting scholarly publishing into a new generation.

What are Frontiers Research Topics?

Frontiers Research Topics are very popular trademarks of the Frontiers Journals Series: they are collections of at least ten articles, all centered on a particular subject. With their unique mix of varied contributions from Original Research to Review Articles, Frontiers Research Topics unify the most influential researchers, the latest key findings and historical advances in a hot research area! Find out more on how to host your own Frontiers Research Topic or contribute to one as an author by contacting the Frontiers Editorial Office: frontiersin.org/about/contact

PROCEEDINGS OF ASPL2019 - 8TH ASIAN-OCEANIAN SYMPOSIUM ON PLANT LIPIDS

Topic Editors:
Xue-Rong Zhou, Commonwealth Scientific and Industrial Research Organisation (CSIRO), Australia
Ikuo Nishida, Saitama University, Japan
Mi Chung Suh, Sogang University, South Korea
Thomas Vanhercke, Commonwealth Scientific and Industrial Research Organisation (CSIRO), Australia

Citation: Zhou, X.-R., Nishida, I., Suh, M. C., Vanhercke, T., eds. (2021). Proceedings of ASPL2019 - 8th Asian-Oceanian Symposium on Plant Lipids. Lausanne: Frontiers Media SA. doi: 10.3389/978-2-88966-433-7

Table of Contents

frontiers in Plant Science

EDITORIAL
published: 08 December 2020
doi: 10.3389/fpls.2020.617094

Editorial: Proceedings of ASPL2019 - 8th Asian-Oceanian Symposium on Plant Lipids

Xue-Rong Zhou[1]*, *Ikuo Nishida*[2], *Mi Chung Suh*[3] and *Thomas Vanhercke*[1]

[1] CSIRO Agriculture and Food, Canberra, ACT, Australia, [2] Division of Life Science, The Graduate School of Science and Engineering, Saitama University, Saitama, Japan, [3] Department of Life Science, Sogang University, Seoul, South Korea

Keywords: ASPL2019, lipid synthesis and storage, lipid functions, lipid production, lipid platform

Editorial on the Research Topic

Proceedings of ASPL2019 - 8th Asian-Oceanian Symposium on Plant Lipids

The 8th Asian-Oceanian Symposium on Plant Lipids (ASPL2019) was held in Canberra, Australia, on November 19-22, 2019, accommodated 55 oral talks and 24 posters. ASPL2019 covered a broad range of both fundamental and applied Research Topics related to plant and algal lipid metabolism including lipidomic and lipid metabolic analysis; membrane lipids and environment; wax, sphingolipids, sterols and isoprenoids; lipid droplets and storage lipids; algal and microbial lipids; lipids for food and nutrition; lipase and lipid catabolism; lipids and plant biotechnology; synthetic biology. A Research Topic from Frontiers in Plant Science was open to participants of ASPL2019 to contribute. This Research Topic presents 14 peer reviewed articles contributed by 113 authors.

OPEN ACCESS

Edited and reviewed by:
Wanchai De-Eknamkul, Chulalongkorn University, Thailand

***Correspondence:**
Xue-Rong Zhou
xue-rong.zhou@csiro.au

Specialty section:
This article was submitted to Plant Metabolism and Chemodiversity, a section of the journal Frontiers in Plant Science

Received: *14 October 2020*
Accepted: *26 October 2020*
Published: *08 December 2020*

Citation:
Zhou X-R, Nishida I, Suh MC and Vanhercke T (2020) Editorial: Proceedings of ASPL2019 - 8th Asian-Oceanian Symposium on Plant Lipids. Front. Plant Sci. 11:617094. doi: 10.3389/fpls.2020.617094

LIPID SYNTHESIS AND STORAGE

WRINKLED1 (WRI1) transcription factor plays a central role in the transcriptional regulation of plant fatty acid biosynthesis in seed. Kong et al. summarized the recent understanding of the regulatory mechanism of WRI1 in plant oil biosynthesis and other regulators controlling the expression of *WRI1*. These recent advances provide novel approaches for engineering oil production in plants.

Chlorophyll biosynthesis is important for maintaining high photosynthetic productivity in crops. Wang et al. identified a wheat mutant defective in chlorophyll biosynthesis, displaying an altered leaf color. The mutant has a single G664A substitution in the gene *TaCHLI-7A* encoding the subunit I of the Mg-chelatase, and the resultant D221N substitution in the mutant protein abolishes an interaction with the normal TaCHLI-7A protein, which is required for Mg-chelatase function. Interestingly, the mutant also displayed reduced FA content in seed and leaf. Thus, the mutant may serve as a useful resource for a better understanding chlorophyll and lipid biosynthetic pathways in common wheat.

In recent years, advances in plant lipid metabolic engineering have led to transgenic strategies that allow for the storage lipid triacylglycerol (TAG) to accumulate in non-seed tissues of tobacco, sorghum, and sugarcane. Xu, Vanhercke et al. overexpressed WRI1, diacylglycerol acyltransferase 1 (DGAT1), and Oleosin oil body protein in potato leaves. The combined "Push, Pull, Protect" strategy resulted in a 30-fold increase in TAG levels. The authors observed an inverse correlation between lipid and starch content, suggesting a redistribution of carbon toward TAG as a new sink. Interestingly, transgenic mesophyll chloroplasts contained a large number of plastoglobuli, hinting at phytol esters competing with TAG for photosynthetic carbon. The second paper

also by Xu, Akbar et al. explored the effect of downregulating TAG turnover and inhibition of starch biosynthesis in a previously established transgenic potato line that accumulates TAG levels in tubers. To this end, the SDP1 lipase and AGPase were downregulated *via* RNA interference (RNAi) to further optimize the flux of storage carbon toward lipids. Super-transformed events accumulated up to 7% TAG in transgenic tubers. In addition, the authors observed increased levels of polar membrane lipids, as well as significant changes in starch granule composition, morphology, and functionality.

Erucic acid is a valuable industrial fatty acid with many applications for biodegradable and environmentally safe oil products such as biodiesel, lubricants, surfactants, pharmaceuticals, cosmetics, soaps, rubber, and nylon. There are low- and high-erucic acid accessions of *Brassica napus*. Lu et al. examined the distribution of erucic acid-containing lipids and the gene transcripts encoding the enzymes involved in pathways for its synthesis and incorporation into triacylglycerols in seeds. This is also another excellent example of application of matrix assisted laser desorption/ionization-mass spectrometry imaging, linked to the molecular mechanism.

Oil bodies and lipid droplets are the major lipid particles of neutral lipids assembling, storing, and suppling in plants. These particles and the oil body proteins are also involved in many other cellular processes. Shao et al. reviewed recent work on the structural or metabolic roles of these proteins in oil body biogenesis, stabilization and degradation, lipid homeostasis and mobilization, hormone signal transduction, stress defenses, and various aspects of plant growth and development. The review suggested opportunities for increasing stress resistance, enhancing plant yield or increasing the total TAG content in plant for a variety of industrial applications.

In addition to seed oil storage, silique dehiscence plays another important role in seed oil production. Silique dehiscence enables mature seeds to be released from plants, thus its timing and degree affect the harvest and yield. The review article contributed by Yu Y.-K. et al. summarizes the recent understanding of the mechanism and regulation of silique dehiscence, especially the genetic elements controlling silique dehiscence and their silique dehiscence.

PHYSIOLOGICAL FUNCTIONS OF PLANT LIPIDS

Lipidomics is an emerging technology that allows us to globally characterize and quantify lipids within biological matrices including biofluids, cells, whole organs, and tissues. Yu D. et al. applied this technology in characterizing the changes in individual lipid molecular species among salinity-stress-treated barley cultivars displaying different salinity tolerance. They found a general decrease in most of the galactolipids in plastid membranes, and an increase of glycerophospholipids and acylated steryl glycosides in extraplastidial membranes in barley roots. They also revealed salinity-induced oxidative damages to plastidial and extraplastidial membrane lipids, which are associated with sensitivity to salinity stress in barley.

Terrestrial crop productivity is significantly reduced by drought. The aerial organs of land plants increase total loads of cuticular waxes to decrease non-stomatal water loss under drought. Yang et al. revealed that an AP2/DREB-type transcription factor RAP2.4, which is induced by ABA-, drought-, osmotic-, and salt-stress upregulates the expression of *KCS2* and *CER1*, which are required for the production of alkanes, and thereby, contributes to an increase in total wax loads in *Arabidopsis* leaves. This study shows that RAP2.4 might be applicable in the production of alkanes and the development of crops with enhanced drought tolerance.

LIPID PRODUCTION

The long-chain omega-3 polyunsaturated fatty acids such as EPA and DHA are essential components of animal cell membranes and important contributors to human health. However, increased demand for these fatty acids has led to overfishing of many source species. Petrie et al. developed a novel form of canola, containing fish oil-levels of DHA in its seed oil, the first such crop to obtain regulatory approval in any jurisdiction, with a significant decrease of the ω6:ω3 ratio. Multiple field trials have confirmed the crop to be a reliable land-based source of these essential fatty acids.

Nutritional value and health benefits of peanut seed oil, which contains 2.5 to 8.5% very long chain saturated fatty acids (VLCSFAs) can be enhanced by the reduction of VLCSFA levels. The first step of very long chain fatty acid (VLCFA) synthesis is processed by 3-ketoacyl-CoA synthase (KCS), which catalyzes the condensation of a C2 unit from malonyl-CoA to acyl-CoA. Among 30 putative *KCS* isoforms identified from the peanut genome, Huai et al. revealed that *AhKCS1* and *AhKCS28*, which are predominantly expressed in the developing seeds and localized in the ER, are the key genes involved in the synthesis of VLCFAs in seeds.

Fatty alcohols are widely used in industrial applications, but their production process is accompanied by a harsh work environment and environmental contamination. It is desirable to find organisms that efficiently produce fatty alcohols. Munawaroh et al. revealed that disruption of *HetN* and *PatS*, the repressors of heterocyst differentiation enhanced accumulation of fatty alcohols in the heterocysts of *Anabaena* sp. PCC 7120 *hglT*, which is a loss-of-function mutation in glycosyltransferase required for the synthesis of heterocyst-specific glycolipids. This result provides a novel strategy to produce fatty alcohols in atmospheric nitrogen-fixing Anabaena, which is a great candidate for bioproduction.

Branched fatty acids are widely used in the petrochemical industry due to their high oxidative stability and low melting temperature. Hydrogenation of cyclopropane fatty acids such as dihydrosterculic acid (DHSA) can convert them into branched fatty acids, thus providing potential feedstock. Okada et al. reported that overexpression of *E. coli* or cotton

cyclopropane fatty acid synthases and Arabidopsis DGAT1 silencing endogenous oleoyl desaturase resulted in 15% of DHSA in *Nicotiana benthamiana* leaf TAGs. This study shows a possible route to DHSA production in vegetative tissue.

NEW PLATFORM

Traditional genetic studies in plants are both time-consuming and labor-intensive. The need to generate stably transformed plants means that the engineering of multi-gene metabolic pathways quickly becomes daunting. Current transient assays are typically limited to hundreds of genes depending on the lab infrastructure. In an attempt to develop a high throughput screening platform that is amenable to large complex libraries, Pouvreau et al. explored tobacco protoplasts as a new plant synthetic biology chassis to identify regulators of lipid metabolism. The authors show that protoplasts can be successfully engineered to hyper-accumulate storage lipids, and subsequently isolated individually by fluorescence-activated cell sorting.

AUTHOR CONTRIBUTIONS

X-RZ, IN, MCS, and TV all contributed to writing this Editorial of the Research Topic on Proceedings of ASPL2019 - 8th Asian-Oceanian Symposium on Plant Lipids edited in 2019-2020. All authors contributed to the article and approved the submitted version.

FUNDING

MCS was supported by the New Breeding Technologies Development Program (Project No. PJ04781022020) of the Rural Development Administration, Republic of Korea.

ACKNOWLEDGMENTS

The authors thank to the handling editors and reviewers for their contribution of the Research Topic.

Conflict of Interest: The authors declare that the research was conducted in the absence of any commercial or financial relationships that could be construed as a potential conflict of interest.

frontiers in Plant Science

ORIGINAL RESEARCH
published: 12 November 2019
doi: 10.3389/fpls.2019.01444

Upregulated Lipid Biosynthesis at the Expense of Starch Production in Potato (*Solanum tuberosum*) Vegetative Tissues *via* Simultaneous Downregulation of *ADP-Glucose Pyrophosphorylase* and *Sugar Dependent1* Expressions

Xiaoyu Xu[1,2], Thomas Vanhercke[1], Pushkar Shrestha[1], Jixun Luo[1], Sehrish Akbar[1], Christine Konik-Rose[1], Lauren Venugoban[1], Dawar Hussain[1], Lijun Tian[1], Surinder Singh[1], Zhongyi Li[1], Peter J. Sharp[2]* and Qing Liu[1]**

[1] Research Program of Traits, CSIRO Agriculture and Food, Canberra, ACT, Australia, [2] Plant Breeding Institute and Sydney Institute of Agriculture, School of Life and Environmental Sciences, The University of Sydney, Sydney, NSW, Australia

OPEN ACCESS

Edited by:
Heiko Rischer,
VTT Technical Research Centre of Finland Ltd, Finland

Reviewed by:
Robert D. Hancock,
The James Hutton Institute, United Kingdom
Hiroyuki Ohta,
Tokyo Institute of Technology, Japan

***Correspondence:**
Zhongyi Li
zhong-yi.li@csiro.au
Peter J. Sharp
peter.sharp@sydney.edu.au
Qing Liu
qing.liu@csiro.au

Specialty section:
This article was submitted to Plant Metabolism and Chemodiversity, a section of the journal Frontiers in Plant Science

Received: 01 August 2019
Accepted: 17 October 2019
Published: 12 November 2019

Citation:
Xu X, Vanhercke T, Shrestha P, Luo J, Akbar S, Konik-Rose C, Venugoban L, Hussain D, Tian L, Singh S, Li Z, Sharp PJ and Liu Q (2019) Upregulated Lipid Biosynthesis at the Expense of Starch Production in Potato (Solanum tuberosum) Vegetative Tissues via Simultaneous Downregulation of ADP-Glucose Pyrophosphorylase and Sugar Dependent1 Expressions. Front. Plant Sci. 10:1444. doi: 10.3389/fpls.2019.01444

Triacylglycerol is a major component of vegetable oil in seeds and fruits of many plants, but its production in vegetative tissues is rather limited. It would be intriguing and important to explore any possibility to expand current oil production platforms, for example from the plant vegetative tissues. By expressing a suite of transgenes involved in the triacylglycerol biosynthesis, we have previously observed substantial accumulation of triacylglycerol in tobacco (*Nicotiana tabacum*) leaf and potato (*Solanum tuberosum*) tuber. In this study, simultaneous RNA interference (RNAi) downregulation of *ADP-glucose pyrophosphorylase* (AGPase) and *Sugar-dependent1* (SDP1), was able to increase the accumulation of triacylglycerol and other lipids in both wild type potato and the previously generated high oil potato line 69. Particularly, a 16-fold enhancement of triacylglycerol production was observed in the mature transgenic tubers derived from the wild type potato, and a two-fold increase in triacylglycerol was observed in the high oil potato line 69, accounting for about 7% of tuber dry weight, which is the highest triacylglycerol accumulation ever reported in potato. In addition to the alterations of lipid content and fatty acid composition, sugar accumulation, starch content of the RNAi potato lines in both tuber and leaf tissues were also substantially changed, as well as the tuber starch properties. Microscopic analysis further revealed variation of lipid droplet distribution and starch granule morphology in the mature transgenic tubers compared to their parent lines. This study reflects that the carbon partitioning between lipid and starch in both leaves and non-photosynthetic tuber tissues, respectively, are highly orchestrated in potato, and it is promising to convert low-energy starch to storage lipids *via* genetic manipulation of the carbon metabolism pathways.

Keywords: *Solanum tuberosum*, potato, RNA interference, *ADP-glucose pyrophosphorylase*, sugar dependent1, triacylglycerol

INTRODUCTION

Oil and fats, in the major form of triacylglycerols (TAGs), are one of the most energy-dense compounds in nature (Sanjaya et al., 2011). However, vegetable oil is mostly produced in the seeds or fruits; only a few vegetative tissues (*e.g. Cyperus esculentus*) have significant levels (Rahman et al., 2016). This is because most plant species rely on photosynthesis for carbon assimilation (O'Leary, 1988), from which the carbohydrate remains the typical carbon reservoir in vegetative tissues (Stitt, 1995), whereas TAG synthesized concomitantly is usually regarded as a byproduct of starch production (Chapman et al., 2013). Recently, a series of genetic engineering approaches have explored the potential of TAG production in plant biomass tissues mostly focused on the leaf, in attempts to exploit more sustainable and reliable vegetable oil production platforms (Xu and Shanklin, 2016; Xu et al., 2018; Vanhercke et al., 2019). It was revealed that through manipulating critical metabolic nodes involved in TAG metabolism, this product naturally at low levels could be remarkably accumulated in plant vegetative tissues without severely compromising plant development (Vanhercke et al., 2014; Vanhercke et al., 2017).

As reported in most recent studies, enhancement of TAG biosynthesis in plant vegetative tissues is usually accompanied by a reduction in starch accumulation (Vanhercke et al., 2014; Zale et al., 2016; Liu et al., 2017; Vanhercke et al., 2018). It was hypothesized that the carbon competition from starch is the dominant factor contributing to the boost of TAG accumulation in transgenic plants (Sanjaya et al., 2011). It is well known that pyruvate, the direct carbon source for the plastid *de novo* fatty acids biosynthesis, is derived from cytosolic glycolysis, which also supports starch production in the plastid (Rawsthorne, 2002; Zeeman et al., 2010; Chapman and Ohlrogge, 2012), so it still remains to be further investigated how the oil increase is compensated by the starch biosynthesis even with the same carbon source. Potato (*Solanum tuberosum*), which is the current 4th largest staple food in the world and produces considerable amount of starch in the stolon tubers for both energy deposition and propagation (Levy et al., 2013; Pinhero et al., 2016; Zaheer and Akhtar, 2016), may provide a good platform to study the interrelationship between lipids and starch biosynthesis.

Mitchell et al. (2017) first investigated the starch quality and multiple nutritional properties in the high oil transgenic potato tubers overexpressing *WRINKLED1* (*WRI1*) - *DIACYLGLYCEROL ACYLTRANSFERASE 1* (*DGAT1*)— *OLEOSIN* genes under a tuber-specific manner. It was found that the starch amylose content and peak viscosity were significantly reduced, while gelatinization temperature was increased in the starch isolated from the transgenic tubers rich in oil compared to the wild type (WT). However, the transgenic potato, which showed the highest TAG accumulation of 3.3% on a tuber dry weight (DW) basis (almost 100-fold increase relative to WT), was generated through the enhancement of the TAG biosynthetic pathway, while the starch metabolism was not manipulated (Liu et al., 2017). It would be therefore of importance to further explore the intrinsic connections between starch and lipid in potato tubers concerning such a correlation reflected in the high oil transgenic potato. For example, the oil enhancement may also be realized through engineering the diversion of carbon flux from the starch biosynthesis, or suppressing the lipase activity.

Presently, metabolic pathways regulating starch anabolism and TAG catabolism in plants are basically elucidated (Zeeman et al., 2010; Tjellström et al., 2015). In potato tuber, a series of enzymes are involved in starch biosynthesis, such as the *AGPase*, granule-bound starch synthase (*GBSS*), starch synthase II (*SSII*) and starch branching enzyme (*SBE*) (Schwall et al., 2000; Jobling et al., 2002; Grommers and van der Krogt, 2009). Among these, *AGPase* is the key rate-limiting enzyme initiating starch biosynthesis, and could therefore be manipulated to regulate the carbon flux (Geigenberger, 2003; Tetlow et al., 2004; Hwang et al., 2007; Jonik et al., 2012). The *SDP1* gene, which was reported to account for over 95% of TAG turnover by disintegrating the lipid droplets (LD) in plants (Kelly and Feussner, 2016), is thought to be the primary lipase for oil degradation (Scherer et al., 2010; Fan et al., 2014; Thazar-Poulot et al., 2015).

Studies on *AGPase* in terms of oil accumulation were mainly reported in algae, from which the downregulation of *AGPase* was able to boost TAG production (Radakovits et al., 2010; Li et al., 2010; Siaut et al., 2011), which was similar to an Arabidopsis (*Arabidopsis thaliana*) mutant deficient in starch (Yu et al., 2018). However, a similar result was not observed in potato tubers by repressing the same gene as the content of total fatty acids was barely changed despite considerable reduction in starch accumulation (Klaus et al., 2004). This suggests the possible necessity to co-regulate *AGPase* together with other genes involved in the lipid metabolism in order to enhance lipids accumulation in potato tubers. Indeed, it was later revealed that the inhibition of *AGPase* expression, together with the ectopic overexpression of *WRI1* had cooperatively boosted TAG accumulation in Arabidopsis leaves (Sanjaya et al., 2011). A similar result was also reported in transgenic sugarcane (*Saccharum officinarum*), where downregulation of *AGPase* and manipulation of several other genes involved in TAG biosynthesis and fatty acid β-oxidation dramatically increased TAG content (Zale et al., 2016). Likewise, in terms of the lipase *SDP1*, Kelly et al. (2013) reported that the suppression of *SDP1* had increased the TAG content of Arabidopsis leaves, and was further enhanced when co-expressed with *WRI1* and *DGAT1*. By disrupting the expression of *SDP1* in a trigalactosyldiacylglycerol1-1 (*tgd1-1*) mutant of Arabidopsis, 9% TAG was produced on a leaf DW basis (Fan et al., 2014). Further, through RNAi downregulation of *SDP1* expression in the high oil transgenic tobacco (*Nicotiana tabacum*) expressing *AtWRI1-AtDGAT1-* sesame (*Sesamum indicum*) *OLEOSIN1* (*SiOLEOSIN1*), TAG accumulation was doubled from 15% to 30% of leaf DW compared to the original transgenic line (Vanhercke et al., 2017). These studies demonstrate the possibility to further enhance oil accumulation in plant vegetative tissues by diverting more carbon away from starch and towards lipid biosynthesis, whilst preventing TAG turnover from lipase activity. In contrast, the singular manipulation of either *AGPase* or *SDP1* was proven to be less effective.

In this study, the endogenous *StAGPase* and *StSDP1* genes of potato were downregulated with a duplex RNAi approach in both WT and the high-oil transgenic potato line known as HO69

with more than 3% TAG in the tuber. Through simultaneously manipulating the carbon flux in potato tubers from the "starch source" (Jonik et al., 2012) and 'TAG sink' (Du and Benning, 2016; Bozhkov, 2018), it was anticipated that the carbon partitioning between carbohydrate and lipid would be reconstituted. A series of biochemical and microscopic analyses were thereafter carried out to characterize the biosynthesis of lipids and starch in the transgenic potatoes. With a particular focus on the carbohydrate and lipid metabolisms, the conversion of relatively low-energy starch to the energy-dense storage lipids was realized in potato tubers through these genetic engineering approaches, which may provide insight and further advance our understanding of the carbon reallocation and equilibration in plant biomass tissues.

RESULTS

Regeneration and Selection of Transgenic Potato Plants Expressing the RNAi Cassette Targeting the *StaGPase* and *StSDP1* Genes Simultaneously

WT potato and the HO69 were simultaneously transformed with a construct harboring a RNAi cassette simultaneously targeting the downregulations of *StAGPase* and *StSDP1* expression driven by the *CaMV-35S* promoter. A total of eleven and three independent T_0 plants were obtained from the WT- and HO69-derived transformations respectively, as verified by polymerase chain reaction (PCR) amplification of a DNA fragment of the hygromycin-B-phosphotransferase (*HPH*) gene, which confers hygromycin resistance as the selectable marker during gene transformation, from developing leaves of the regenerated potato plants (**data not shown**).

Analysis of the contents of total fatty acids (TFA), starch and total soluble sugars in transgenic tubers were carried out for an overview of the RNAi effects. The eleven WT-derived lines showed 1.9 to 9.8-fold increase in the content of TFA (**Figure 1**), 1.7 to 7.3-fold increase in total soluble sugars content (**Figure 1**), and 1.7 to 10.8-fold reductions in starch content compared to WT (**Figure 1**). Regression analysis showed that the accumulation of TFA was negatively correlated with starch (a coefficient of -0.88), but positively correlated to total soluble sugars (a coefficient of 0.89); the contents of total soluble sugars and starch were negatively correlated (a coefficient of -0.86) (**Figure 1**).

Two transgenic lines, WT-L5 and WT-L10, with enhanced lipid accumulation relative to WT in mature tubers (0.3% of tuber DW), representing the highest level of TFA at 2.95% and

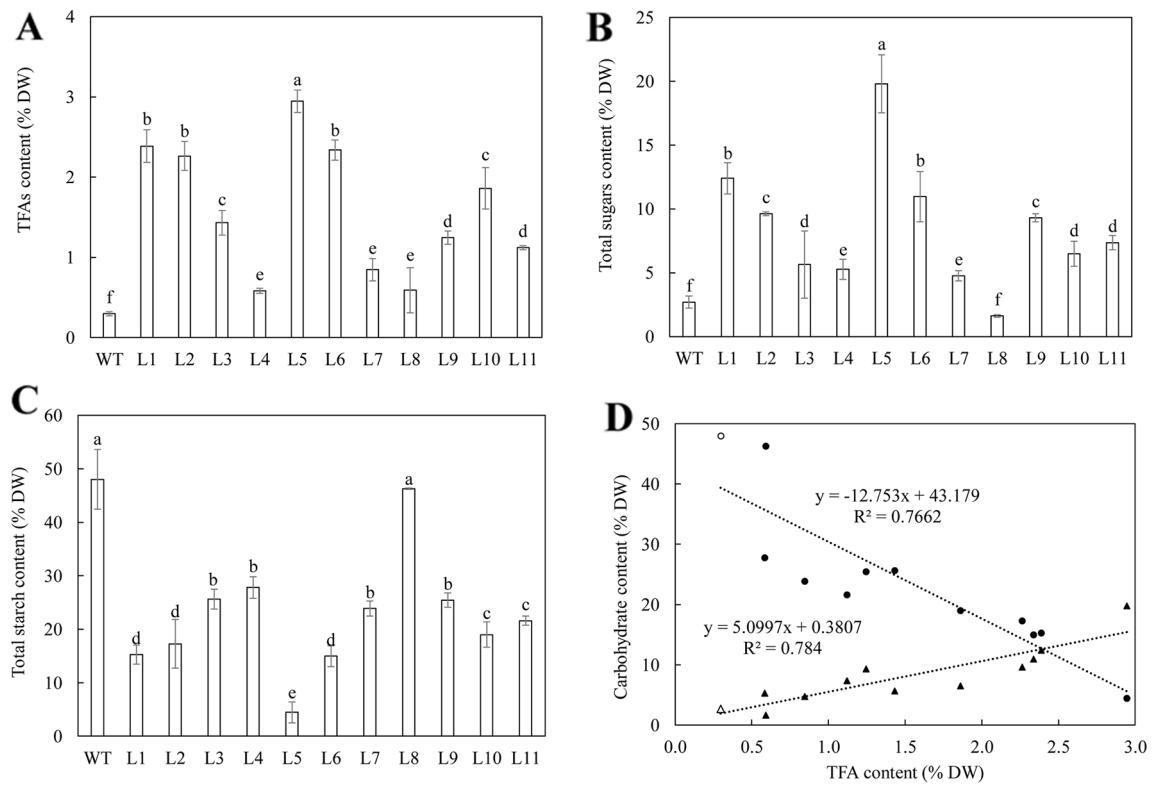

FIGURE 1 | Contents of total fatty acids (TFA) and major carbohydrate in the mature potato tubers of WT and the eleven selected T_0 generation plants. **(A)** TFA content; **(B)** Total soluble sugars content; **(C)** Total starch content; **(D)** Regression analysis among TFA, total soluble sugars (triangles) and starch (circles) in WT (open symbols) and transgenic lines (black symbols). The relationship between TFA and starch is negative (y = -12.753x + 43.179, R^2 = 0.7662), while the relationship between TFA and the total soluble sugars is positive (y = 5.0997x + 0.3807, R^2 = 0.784). The data represent the mean values ± standard deviation (SD) of three biological replicates. Letters (a, b, c, etc.) above the bars are all based on the least significant difference (LSD). Different letters between lines are statistically significantly different at $P < 0.05$.

a moderate level at 1.86% respectively, were selected for further analysis. In the HO69-derived super-transformation, due to a limited transgenic population, all the 3 super-transformed lines, named 69-L1, 69-L2, and 69-L3, were proceeded to synchronically propagate with HO69, WT, WT-L5, and WT-L10 for characterization at two developmental stages, the flowering stage and mature stage in a new generation.

Downregulation of Target Genes and Alteration in the Accumulation of Lipids and Carbohydrate in the Leaves of WT-Derived Transgenic Lines

Assessments of *StAGPase* and *StSDP1* gene expression in the fully expanded leaves of WT and the two selected transgenic lines, WT-L5 and WT-L10, were carried out in both the flowering and mature stages (**Supplementary Figures 1A**, **B**). Significant downregulation of both these two genes were detected, with WT-L5 displaying the lowest expression levels at the mature stage (**Supplementary Figure 1B**). Alterations in the accumulation of carbohydrate and TFA were also observed. WT-L10 displayed significantly enhanced TFA production (6.61% of leaf DW) relative to WT at the mature stage, representing a 1.3-fold increase (**Supplementary Figure 1D**), while WT-L5 did not show substantial variation in both stages. The starch content of WT-L5 were lower at 1.99% and 0.8% of leaf DW at both the flowering stage and mature stage respectively, compared to 7.23% and 17.41% in WT at the respective stages. The content of total soluble sugars was increased to 11.49% at the flowering stage and 7.81% at the mature stage, representing 4.4-fold and 1.7-fold increase relative to WT, respectively (**Supplementary Figures 1C, D**). WT-L10 also exhibited a significant decrease in starch contents at the two developmental stages relative to WT, displaying a 1.3 and 1.1-fold reduction respectively, but not in total soluble sugars content, which was significantly increased in the flowering stage (**Supplementary Figure 1D**).

The TAG content in WT-L5 was not increased relative to WT over the two developmental stages, instead, a declining trend in TAG accumulation was observed (**Supplementary Figure 2A**), while in WT-L10, the accumulation of TAG peaked at 0.07% (almost a 2-fold increase) in the flowering stage, but dropped thereafter. Furthermore, WT-L5 did not show significant alteration in the contents of polar lipids relative to WT, whereas WT-L10 exhibited significantly decreased monogalactosyldiacylglycerol (MGDG) and digalactosyldiacylglycerol (DGDG) at the flowering stage (0.7% and 0.31% of leaf DW, respectively) (**Supplementary Figure 2B**), but subsequently increased to the maximum level at the mature stage (**Supplementary Figure 2C**). In particular, the galactolipids demonstrated an almost 2-fold increase in WT-L10 compared to WT, and the contents of the phospholipids including phosphotidylcholine (PC) and phosphatidylethanolamine (PE) were also significantly increased, but to a lesser extent. In contrast, the content of phosphatidylglycerol (PG) did not show significant variation among WT and the two transgenic lines. Significantly enhanced free fatty acids (FFA) accumulation was observed in WT-L10, but was reduced in WT-L5 compared to the WT at the mature stage, but not at the flowering stage (**Supplementary Figure 2D**).

The significant change in the proportion of C18 polyunsaturated fatty acids (PUFA) represented the major fatty acid variation in leaf between transgenic and WT potatoes (**Supplementary Figure 3**). At the flowering stage, TAG in the two selected lines showed significantly increased linoleic acid (LA, C18:$2^{\Delta 9,12}$) and reduced α-linolenic acid (ALA, C18:$3^{\Delta 9,12,15}$) levels relative to WT (**Supplementary Figure 3A**). Oleic acid (C18:$1^{\Delta 9}$) and long chain fatty acids (LCFA, ≥ C20) were also increased in the two transgenic lines. Such a trend was persistent in WT-L5 in the mature stage, however WT-L10 showed significantly reduced LA but increased ALA levels relative to WT (**Supplementary Figure 3B**). Similarly, LA and ALA ratios of PC were altered in the two transgenic lines relative to WT (**Supplementary Figures 3C**, **D**). However, MGDG and DGDG did not show consistent variations in the fatty acid compositions in the two selected transgenic lines compared to WT, except for that WT-L5 showed significantly increased LA and decreased ALA at the mature stage (**Supplementary Figures 3F**, **H**).

Enhancement in Lipid Accumulation at the Expense of Starch in the Tubers of WT-Derived Transgenic Lines

As shown in **Figure 2A**, expression of both *StAGPase* and *StSDP1* was significantly suppressed in the tubers of the two transgenic lines compared to WT, with WT-L5 displaying more severe downregulations than WT-L10 at the flowering stage. Both WT-L5 and WT-L10 had significantly enhanced accumulation of TFA at the flowering stage relative to WT (**Figure 2C**), which were further elevated to 2.18% and 1.35% of tuber DW, respectively, at the mature stage. Relative to WT, the TFA content was an approximately 8-fold higher in WT-L5, and 3.2-fold higher in WT-L10 (**Figure 2D**). A significant reduction in starch content was observed in WT-L5, which was almost 10-fold lower relative to WT at the mature stage (5.62%), accompanied by significantly increased accumulation of total soluble sugars (18.03%), which was 9-fold higher than that in WT (**Figure 2D**). Likewise, significant reduction in starch content and increase in total soluble sugars relative to WT were observed in WT-L10 over the two developmental stages, but to a lesser extent relative to WT-L5.

The contents of TAG, diacylglycerol (DAG), and FFA were further analyzed following fractionation through thin layer chromatography (TLC) (**Figures 3A**, **B**). TAG accumulation in the tubers of WT-L5 had significantly increased throughout the tuber development, which was 0.15% of tuber DW at the flowering stage, further increased to 0.32% at the mature stage, representing a 16-fold enhancement relative to WT in the mature stage (**Figure 3B**). In WT-L10, the TAG content in tubers peaked at the flowering stage as 0.17%, but reduced thereafter. The accumulations of DAG and FFA in transgenic tubers were also significantly increased compared to WT. For example, WT-L10 displayed 6-fold and almost 3-fold increase in DAG

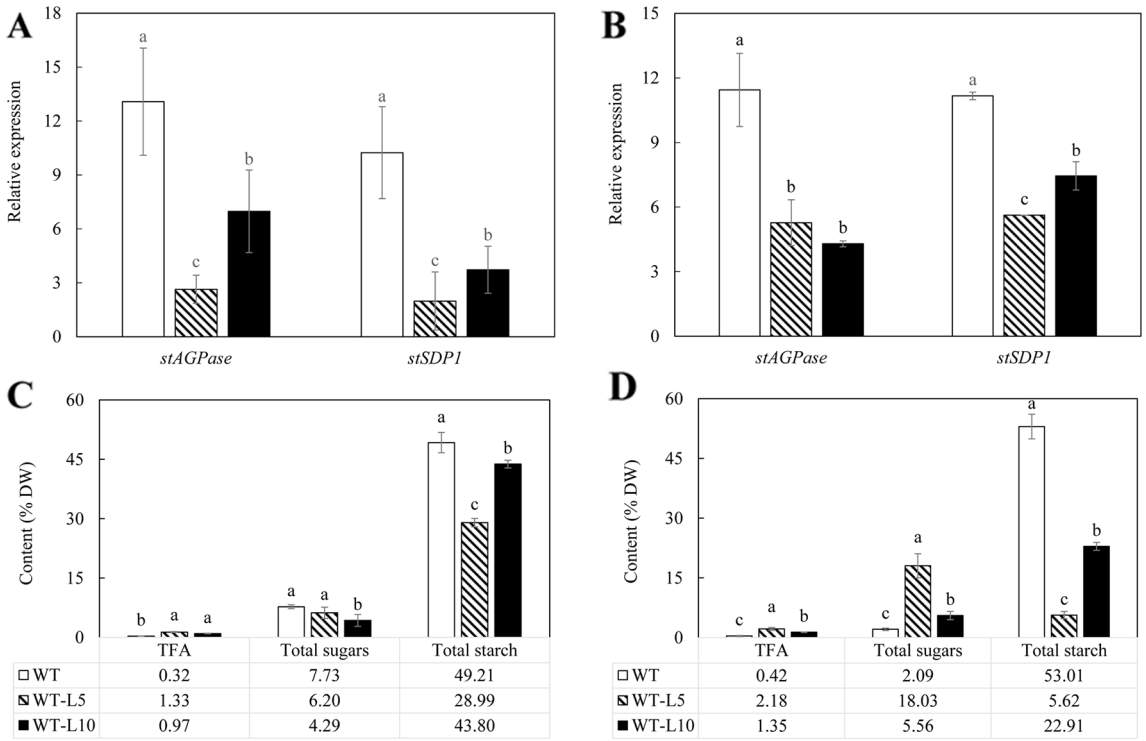

FIGURE 2 | Gene expression analysis and total carbon allocation in the potato tubers of WT (open bars) and the two selected WT-derived lines, WT-L5 (hatched bars) and WT-L10 (black bars) at two developmental stages. **(A)** Real-time quantitative reverse transcription polymerase chain reaction (qRT-PCR) result at the flowering stage; **(B)** Real-time qRT-PCR result at the mature stage; **(C)** Total carbon allocation at the flowering stage; **(D)** Total carbon allocation at the mature stage. The data represent the mean values ± SD of three biological replicates. Letters (a, b, c) above the bars are based on LSD, bars marked with different letters are statistically significantly different at $P < 0.05$.

and FFA, respectively, at the mature stage (**Figure 3B**). Likewise, the significant increase in phospholipids was detected in the two transgenic lines. At the flowering stage, the contents of PC were increased 5 and 3-fold, respectively in WT-L5 and WT-L10 compared to WT, as well as in PE, where WT-L5 and WT-L10 showed 3- and 2.6-fold increases, respectively, compared to WT (**Figure 3C**). However, at the mature stage, significant increase in the accumulation of phospholipids was only observed in WT-L5, while it was dropped to the WT level in WT-L10 (**Figure 3D**). Significant increases in the contents of galactolipids were also observed in the two transgenic lines, particularly prominent in WT-L5, which showed nearly 5-fold increase in MGDG and 6- fold increase in DGDG relative to WT at the flowering stage (**Figure 3C**). At the mature stage, further increase of MGDG in WT-L10 have also been observed (**Figure 3D**).

The fatty acid composition of TAG in the tubers of WT-L5 and WT-L10 mainly showed perturbations in the saturated and monounsaturated fatty acids relative to WT at the flowering stage, while WT-L5 also displayed significantly reduced ALA level (**Supplementary Figure 4A**). In the mature stage, the two transgenic lines both showed similar fatty acid profiles, featured by significantly reduced LA and saturated fatty acids but increased ALA compared to WT (**Supplementary Figure 4B**). In contrast, PC exhibited a relatively constant fatty acid composition in the two transgenic lines over the two stages, demonstrating significantly increased LA but reduced ALA levels relative to WT (**Supplementary Figures 4C**, **D**). In MGDG and DGDG, the variation of fatty acid compositions was reflected by the significantly decreased saturated fatty acids and alteration in the ratio of C18 PUFAs in transgenic tubers, as exemplified by the significant increase in ALA at the expense of LA in MGDG in WT-L10 relative to WT at the flowering stage (**Supplementary Figure 4E**). However, the ratio of LA/ALA dropped significantly at the mature stage in both WT-L5 and WT-L10 (**Supplementary Figure 4F**).

Starch Property Analysis of the Mature Potato Tubers in the WT-Derived Transgenic Lines

The biochemical analysis of starch properties, including the structure and functionality, was carried out using the starch isolated from mature potato tubers. Significant reduction in amylose content in the tubers of WT-L5 and WT-L10, relative to WT, was observed. In particular, the amylose contents in WT-L5 and WT-L10 tuber were approximately 4- and 2-fold lesser, respectively, than that in WT (**Figure 4A**). An altered chain length distribution (CLD), which was reflected as the

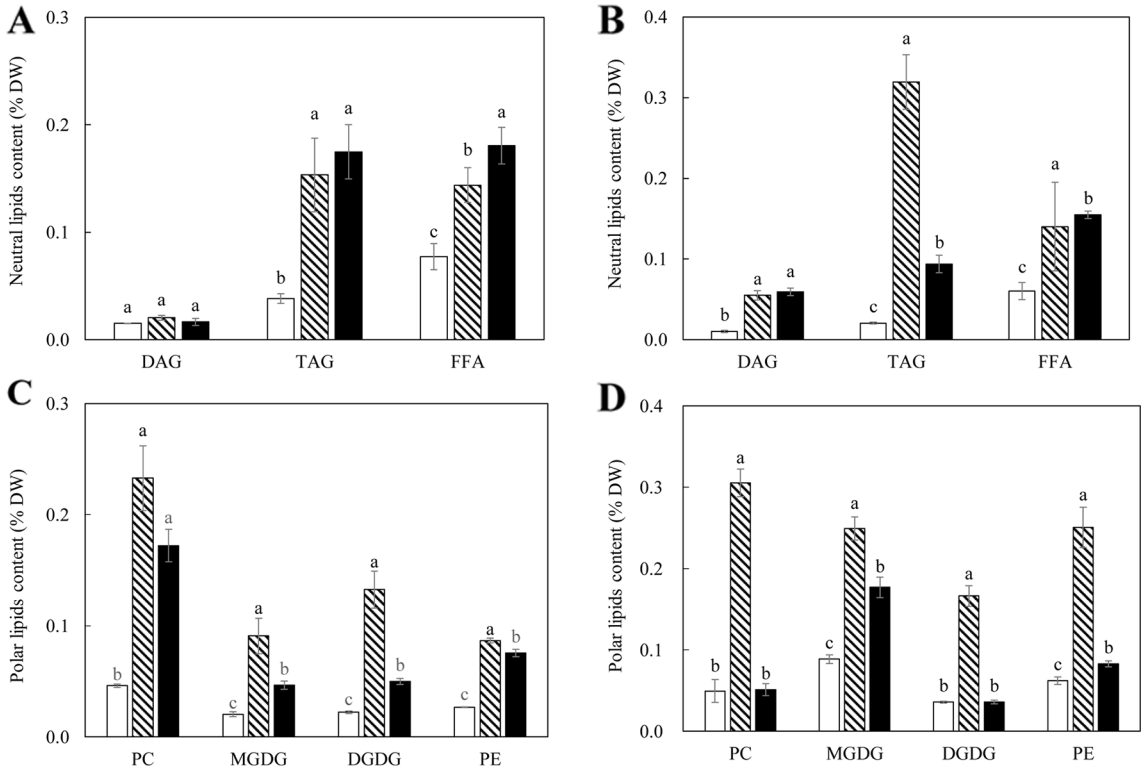

FIGURE 3 | Contents of neutral and polar lipids in the potato tubers of WT (open bars) and the two selected WT-derived lines, WT-L5 (hatched bars) and WT-L10 (black bars) at two developmental stages. **(A)** Neutral lipids contents at the flowering stage; **(B)** Neutral lipids contents at the mature stage; **(C)** Polar lipids contents at the flowering stage; **(D)** Polar lipids contents at the mature stage. The data represent the mean values ± SD of three biological replicates. Letters (a, b, c) above the bars are based on LSD, bars marked with different letters are statistically significantly different at $P < 0.05$.

degree of polymerization (DP) of the debranched starch was demonstrated. Compared to WT, both WT-L5 and WT-L10 showed a preference for the accumulation of short chains (DP < 11). In WT-L5, a decrease in the accumulation of intermediate chains between DP12 and DP16, although not statistically significant relative to WT, was observed (**Figure 4B**). In WT-L10, a tendency of significant reduction in the intermediate chains between DP12 and DP19 relative to WT, was observed (**Figure 4C**). As a result, the swelling power of the tuber flours of the two transgenic lines were altered differently. The swelling power of WT-L5 showed over 2-fold reduction compared to WT, whereas that of WT-L10 increased significantly (**Figure 4D**). Two main protein bands were identified in the SDS-PAGE gel, which were recognized as the granule bound proteins (GBPs) of the potato starch. According to the protein ladder standard, the potato GBSS band was localized near the size of 60 kDa and the SSII/SBE band was at the size of 90 kDa. Visual increase in the GBSS abundance relative to WT was observed in the two transgenic lines, while SSII/SBE reflected a visually discernible decrease in both the two transgenic lines (**Figure 4E**). The digital analysis of the protein band intensity on SDS gel revealed a consistent trend (**Supplementary Table 1**), the GBSS protein bands of WT-L5 and WT-L10 both displayed an average 1.2-fold enhancement compared to WT, while the SSII/SBE proteins showed 0.65- and 0.57-folds decrease of the band intensity, respectively.

Suppression of Target Genes Expression and Alteration in Lipids and Carbohydrate in the Leaves of the HO69-Derived Super-Transformed Potato Lines

Downregulation of the *StAGPase* and *StSDP1* expression in the leaves of the three super-transformed potato lines was reflected over the two developmental stages. Although the RNAi targeted DNA fragments derived from *StAGPase* and *StSDP1* gene sequences were physically linked in the RNAi cassette, these two genes were differentially downregulated. For example, at the flowering stage, the strongest *StAGPase* suppression was observed in 69-L1 while the strongest *StSDP1* suppression was observed in 69-L3 (**Supplementary Figure 5A**). However, the downregulation levels of the two target genes were basically consistent among the three super-transformed lines at the mature stage (**Supplementary Figure 5B**).

Significant fluctuations of the carbon allocation between lipids and carbohydrate were displayed corresponding to the alteration in the expression levels of *StAGPase* and *StSDP1*. Up to 5.31% TFA (DW) was observed in the leaves of 69-L3 at the flowering stage, which was accompanied by a 2.5-fold increase in the total soluble sugars and significantly reduced starch relative to HO69 (**Supplementary Figure 5C**). However in 69-L1 and 69-L2, the variations were relatively less significant. At the mature stage,

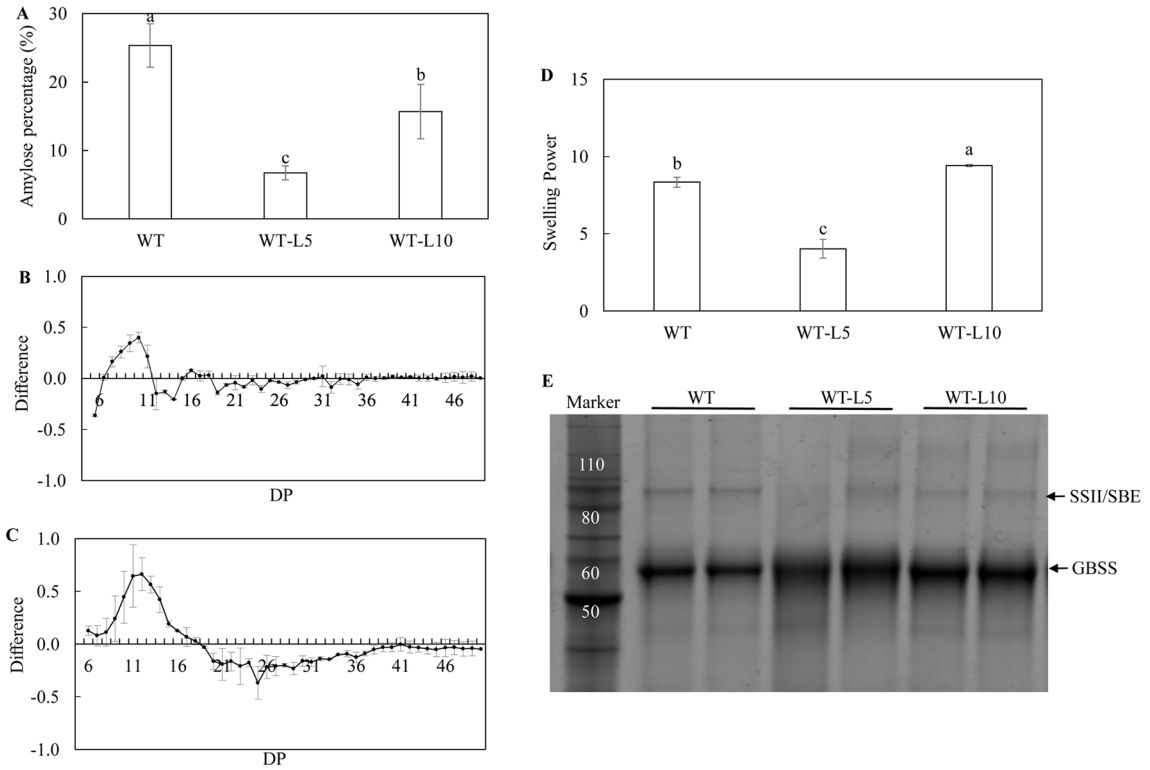

FIGURE 4 | Analysis of the starch properties in the mature potato tubers. **(A)** Amylose content; **(B)** Chain length distribution (CLD) variation in debranched starch samples of WT-L5 relative to WT; **(C)** CLD variation in debranched starch samples of WT-L10 relative to WT; The CLD was reflected as the degree of polymerization (DP), each mark above the horizontal axis corresponds to the difference of a chain length in mole percentage. The error bars represent the standard errors, and the difference value was obtained by subtracting the CLD of WT from the two selected RNAi lines, respectively. **(D)** Swelling power of potato flour; **(E)** SDS-PAGE of potato starch granule bound proteins (GBPs). The data represent the mean values ± SD of three biological replicates. Letters (a, b, c) above the bars are based on least significant difference (LSD), bars marked with different letters are statistically significantly different at $P < 0.05$.

enhanced accumulation in the total soluble sugars were observed in 69-L1 (11.04%) and 69-L3 (7.19%), followed by a nearly 2-fold reduction in the starch content relative to HO69, while the TFA levels were not significantly varied (**Supplementary Figure 5D**).

Among the three super-transformed lines, 69-L3 displayed the highest accumulation of TAG at the flowering stage (1.84%), which was nearly 5-fold higher than HO69, while both 69-L1 and 69-L2 showed moderate yet significant increases (**Supplementary Figure 6A**). At the mature stage, all the three super-transformed lines showed almost doubled TAG accumulations compared to HO69. By comparison, most polar lipids in the three super-transformed lines remained unchanged relative to HO69 at the flowering stage, except that 69-L2 and 69-L3 displayed significant reduction in PC content, and increase in the content of DGDG in 69-L2 (**Supplementary Figure 6B**). At the mature stage, 69-L3 exhibited significant increase in the contents of PC (0.6%), MGDG (0.86%) and DGDG (0.52%) (**Supplementary Figure 6C**). Similar increases in the phospholipids were also observed in 69-L1, but not in 69-L2. The accumulations of FFAs, on the contrary, were all significantly decreased in the three super-transformed lines compared to HO69 over the two developmental stages (**Supplementary Figure 6D**).

Compared to HO69, the variation in the fatty acid compositions of TAG in the three super-transformed lines was mainly reflected in the levels of palmitic (C16:0) and oleic acids (**Supplementary Figures 7A, B**). Specifically, 69-L2 and 69-L3 showed significant reduction in palmitic acid over the two developmental stages, while the relative content of oleic acid was almost doubled at flowering stage (**Supplementary Figure 7A**). The fluctuations in the relative contents of other fatty acids were also observed, such as the decline of ALA at the flowering stage and significant increase in 69-L2 at mature stage (**Supplementary Figure 7B**). A similar trend of variation in the fatty acid composition in PC was observed, while LA was significantly increased in 69-L1 and 69-L3 relative to HO69 at the flowering stage (**Supplementary Figure 7C**). Significant reduction in ALA was observed in the galactolipids of 69-L2 and 69-L3 at the flowering stage relative to HO69 (**Supplementary Figures 7E, G**), but not in the mature stage.

Suppression of Target Gene Expression and Alteration in the Accumulation of Lipids and Carbohydrate in the Tubers of HO69-Derived Super-Transformation Lines

Assessment of the expression of target genes, *StAGPase* and *StSDP1*, in the tubers of three super-transformed potato lines revealed the anticipated downregulations of both genes relative

to the parent line HO69 at both the flowering and mature stages. The most severe suppression occurred in 69-L3 relative to HO69, with *StAGPase* being drastically downregulated at the flowering stage and *StSDP1* in the mature stage, while 69-L1 and 69-L2 displayed comparatively less severe reduction in expression (**Figures 5A**, **B**).

Corresponding to the genetic downregulation of *StAGPase* and *StSDP1* in tubers, significantly higher contents of TFA and total soluble sugars were observed in 69-L2 and 69-L3 at the flowering stage, accompanied by a reduction in starch content in 69-L1 (**Figure 5C**). At the mature stage, 69-L3 showed the biggest enhancement in TFA content up to 7.70% (DW), which was more than 2-fold increase relative to HO69 (**Figure 5D**). The accumulation of twice amount of the total soluble sugars relative to HO69 was also observed in 69-L2. All the three super-transformed lines showed significant reductions in starch contents between 21% and 24% of tuber DW from 32% in WT (**Figure 5D**).

A significant increase in TAG accumulation was mainly observed in 69-L3, which peaked at 7.02% at the mature stage, displaying a 2-fold increase relative to HO69 (**Figure 6B**), however not showed in the flowering stage (**Figure 6A**). Similarly, the contents of DAG and FFA were also increased, with 69-L3 showed nearly three-fold increase in DAG and four-fold increase in FFA relative to HO69. In comparison, PC contents were significantly reduced in all the three super-transformed lines compared to HO69 at the flowering stage, but DGDG was significantly increased in 69-L1 and 69-L3 (**Figure 6C**). At the mature stage, 69-L3 showed significantly enhanced accumulation of polar lipids, with MGDG being three-fold higher relative to HO69 (**Figure 6D**). Moderate yet significant variations in the amounts of polar lipids were also observed in both 69-L1 and 69-L2.

The variation of fatty acid composition in TAG of the three super-transformed lines was mainly featured by a significant reduction in oleic acid relative to HO69 at the flowering stage (**Supplementary Figure 8A**), while at the mature stage, 69-L3 showed a significant increase in oleic acid and reduction in palmitic acid (**Supplementary Figure 8B**). Moderate yet significant reduction in LA of TAG relative to HO69 was also observed in 69-L1 and 69-L2 (**Supplementary Figure 8B**). In PC, a significant increase in palmitic acid and reduction in LA relative to HO69 were observed in 69-L2 and 69-L3 at the flowering stage (**Supplementary Figure 8C**), while all the three super-transformed lines showed enhanced oleic acids relative to HO69 at the mature stage, and 69-L1 and 69-L2 displayed reduction in the LA levels (**Supplementary Figure 8D**). Relative to HO69, MGDG in these three super-transformed lines featured significantly reduced oleic acid and increased LA levels at the flowering stage (**Supplementary Figure 8E**), and a significant reduction in stearic acid at the mature stage (**Supplementary**

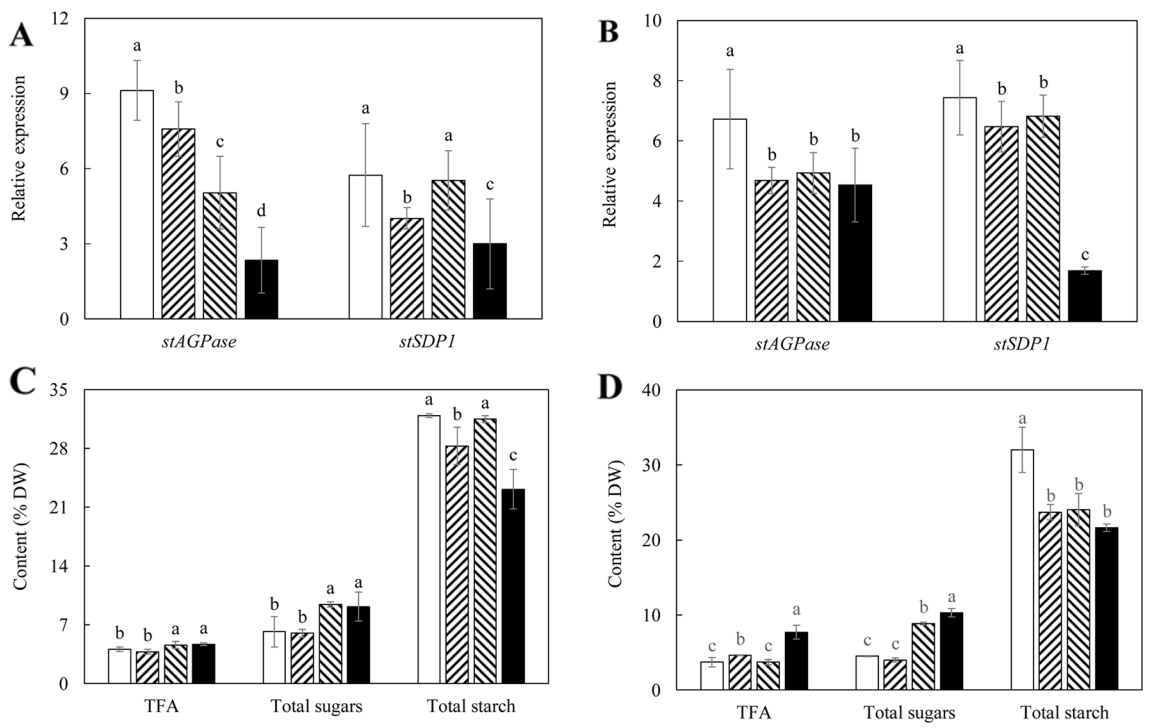

FIGURE 5 | Gene expression analysis and total carbon allocation in the potato tubers of the HO69 (open bars) and three super-transformed lines, 69-L1 (bar with upward trend), 69-L2 (hatched bars) and 69-L3 (black bars) at two developmental stages. **(A)** Real-time quantitative reverse transcription polymerase chain reaction (qRT-PCR) result at the flowering stage; **(B)** Real-time qRT-PCR result at the mature stage; **(C)** Total carbon allocation at the flowering stage; **(D)** Total carbon allocation at the mature stage. The data represent the mean values ± SD of three biological replicates. Letters (a, b, c) above the bars are based on LSD, bars marked with different letters are statistically significantly different at $P < 0.05$.

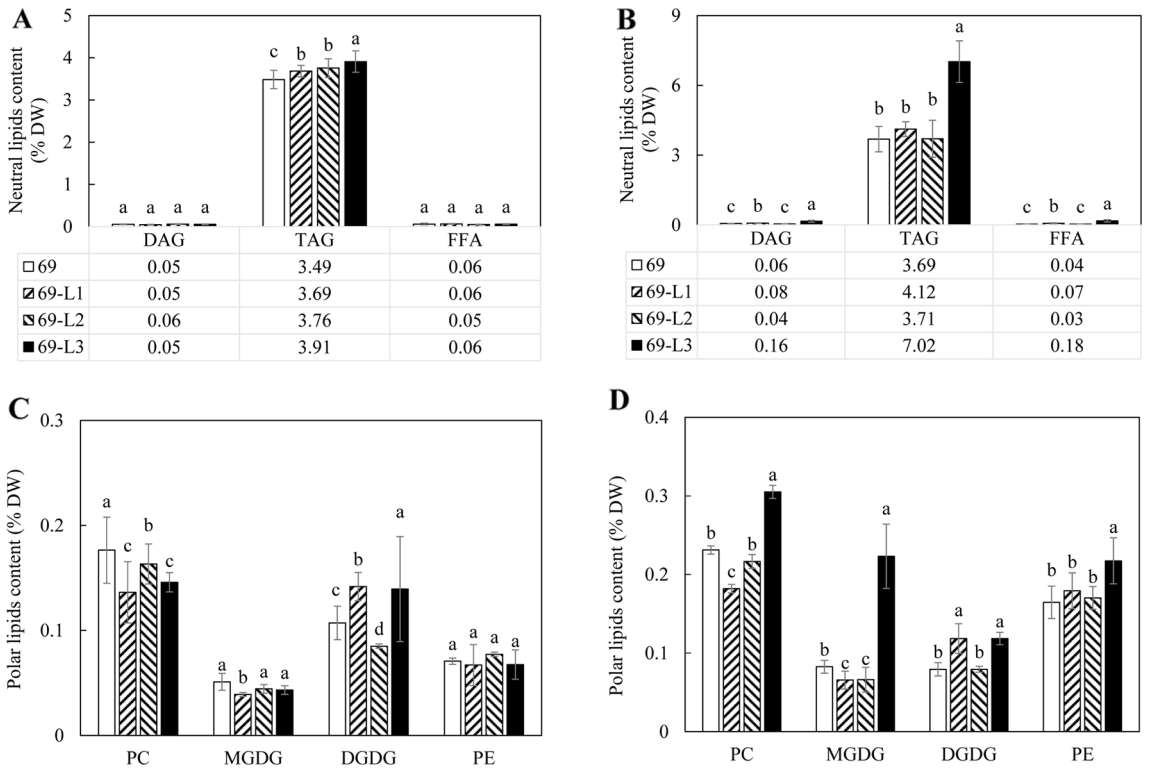

FIGURE 6 | Contents of neutral and polar lipids in the potato tubers of the HO69 (open bars) and three super-transformed lines, 69-L1 (bar with upward trend), 69-L2 (hatched bars) and 69-L3 (black bars) at two developmental stages. **(A)** Neutral lipids contents at the flowering stage; **(B)** Neutral lipids contents at the mature stage; **(C)** Polar lipids contents at the flowering stage; **(D)** Polar lipids contents at the mature stage. The data represent the mean values ± SD of three biological replicates. Letters (a, b, c) above the bars are based on LSD, bars marked with different letters are statistically significantly different at $P < 0.05$.

Figure 8F). In DGDG, 69-L1 displayed significant increase in ALA, which was nearly three-fold increase compared to HO69, at the expense of both oleic acid and LA at the flowering stage (**Supplementary Figure 8G**). Similarly, almost twice as much ALA, mainly at the expense of LA, relative to HO69 was found in the DGDG of 69-L3 at the mature stage (**Supplementary Figure 8H**).

Starch Property Analysis of the Mature Potato Tubers in the Three Super-Transformed Potato Lines

Among the three super-transformed lines, 69-L3 had a significant reduction in amylose content, which was 18.19%, nearly 1.5-fold lower than that in HO69 (**Figure 7A**). CLD analysis revealed that the parent line HO69 with enhanced TAG accumulation, compared to the WT potato, displayed a preference to short chains (DP <11) rather than intermediate chains between DP12 and DP19 (**Figure 7B**). However, in the debranched starch of the three super-transformed lines, significantly reduced formation of short chains was observed in 69-L2 and 69-L3 compared to HO69 (**Figures 7D**, **E**), and to a lesser extent in 69-L1 but not statistically significant (**Figure 7C**). Meanwhile the accumulation of intermediate chains was significantly reduced in 69-L2 which also showed significant increase in long chains (DP >19) relative to HO69 (**Supplementary Table 2**). Only 69-L3 displayed significantly enhanced swelling power of the tuber flour compared to HO69, which was not identified in the other two lines (**Figure 7F**). The SDS-PAGE analysis of GBPs showed visually enhanced accumulation of GBSS protein in 69-L1 and 69-L2 relative to HO69, but relatively decreased in 69-L3. The protein bands representing the SSII/SBE showed a decreased abundance in 69-L3 relative to HO69 (**Figure 7G**), analogous to the analysis made in the digitalization of protein bands intensity, of which 69-L3 showed almost 0.9-fold drop in both GBSS and SSII/SBE (**Supplementary Table 1**).

Microscopic Analysis of Lipid Droplets and Starch Granules in Mature Transgenic Potato Tubers

The cellular distribution of LDs in the mature potato tubers was visualized with confocal scanning microscopy. Two transgenic lines, WT-L5 and 69-L3, which displayed the most significant alterations in the contents of TAG and starch were selected for comparison with WT and HO69. Both round and oval shaped LDs were observed following the staining with BODIPY, with unstained starch granules in the background. Compared to WT, which displayed highly abundant starch granules and rather limited numbers of LDs (**Figures 8A**, **B**), enhanced accumulation

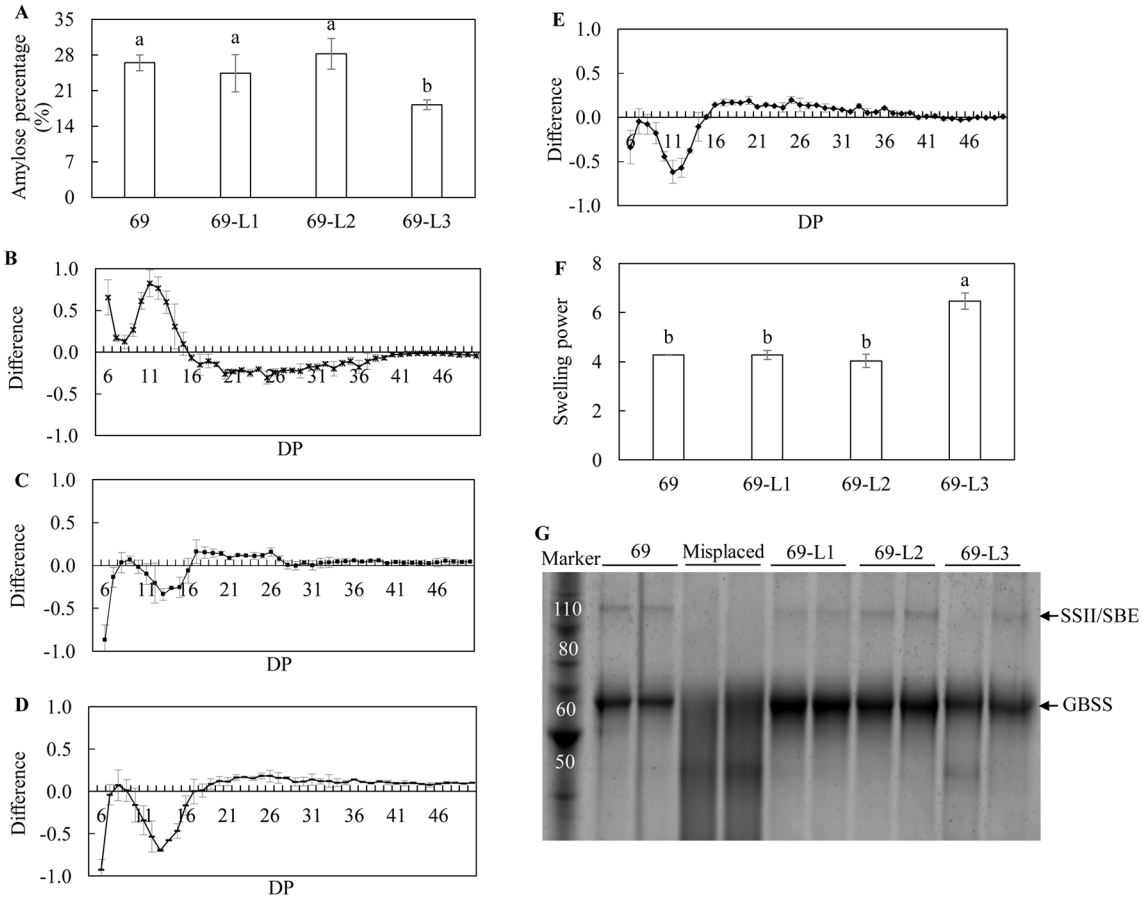

FIGURE 7 | Analysis of the starch properties in the mature potato tubers. **(A)** Amylose ratio; **(B)** Difference of chain length distribution (CLD) between debranched starch of 69 and WT; **(C)** Difference of CLD between debranched starch of 69-L1 and 69; **(D)** Difference of CLD between debranched starch of 69-L2 and 69; **(E)** Difference of CLD between debranched starch of 69-L3 and 69; The CLD was reflected as DP. Each mark above the horizontal axis corresponds to the difference of a chain length in mole percentage. The error bars are standard errors. The difference value was obtained by subtracting the CLD of 69 from the three super-transformed lines, respectively. **(F)** Swelling power of potato flour; **(G)** SDS-PAGE of potato starch GBPs. The two obscure tracks between 69-L3 and 69-L2 are misplaced samples which are irrelevant with other samples. The data represent the mean values ± SD of three biological replicates. Letters (a, b, c) above the bars are based on LSD, bars marked with different letters are statistically significantly different at $P < 0.05$.

of LDs was displayed in WT-L5 but accompanied with apparent reduction in the abundance and size of starch granules (**Figures 8C**, **D**). In the high oil parent line HO69, abundant LDs were observed and broadly distributed in the tuber section, with starch granules of variable sizes distributed within the cell compartments (**Figures 8E**, **F**). Such observations on HO69 was consistent with our previous study (Liu et al., 2017). By comparison, the super-transformed line 69-L3, appeared to have enlarged LDs and reduced number of small LDs compared to HO69 (**Figure 8G**). Relatively, fewer starch granules than in HO69 were also evident in 69-L3 (**Figure 8H**).

Morphological variation of starch granules in the mature tubers was analyzed with the scanning electron microscopy (SEM). Regular and evenly distributed starch granules in WT were found, about 20–60 μm in length and in an oval or spherical shape with a smooth surface (**Figure 9A**). However, in WT-L5, the size and number of the starch granules were drastically reduced, many of them with an irregular ellipsoid shape (**Figure 9B**). The starch granules in WT-L5 showed a nearly 10-fold reduction in the size (< 2 μm) when compared to WT, while the largest was around 10 μm. In contrast, the alteration in size and shape of starch granules in WT-L10 was relatively moderate but still apparent relative to WT (**Figure 9C**). Compared to HO69 (**Figure 9C**), 69-L3 did not show any evident morphological differences but had a declining trend in starch granule size (**Figure 9D**). The observation through light microscopy revealed that the birefringence of starch granules, featured by the Maltese cross and brightness, remained almost unaltered between the transgenic potatoes and their parent lines under the polarized light. Specifically, the crystalline order of the starch granules between WT (**Figure 9F**) and the two selected WT-derived transgenic lines (**Figure 9G–H**) did not appear to be affected, even though WT-L5 showed significant reduction in starch granule size (**Figure 9E**). There was no discernible difference between HO69 and the super-transformed line 69-L3 on the starch crystalline order either (**Figures 9I**, **J**).

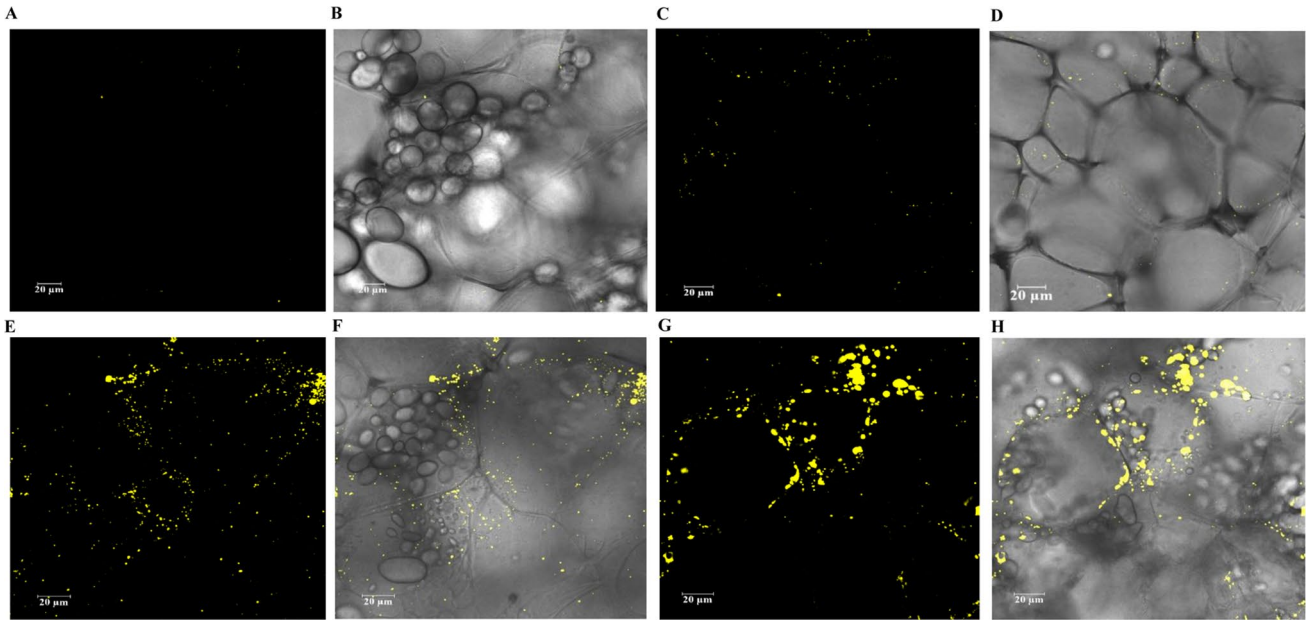

FIGURE 8 | Confocal scanning microscopy analysis of the LDs distribution in mature potato tubers. The LDs were stained with BODIPY (yellow), bright-field images of the unstained starch granules and cell wall structures formed the major background contrasted to the LDs. **(A**, **B)** Visualization of LDs in WT. **(C**, **D)** Visualization of LDs in WT-L5. **(E**, **F)** Visualization of LDs in HO69. **(G**, **H)** Visualization of LDs in 69-L3. The scale bars are located in the lower left corner for each photograph, sizes of the scale bars are all normalized to 20 μm.

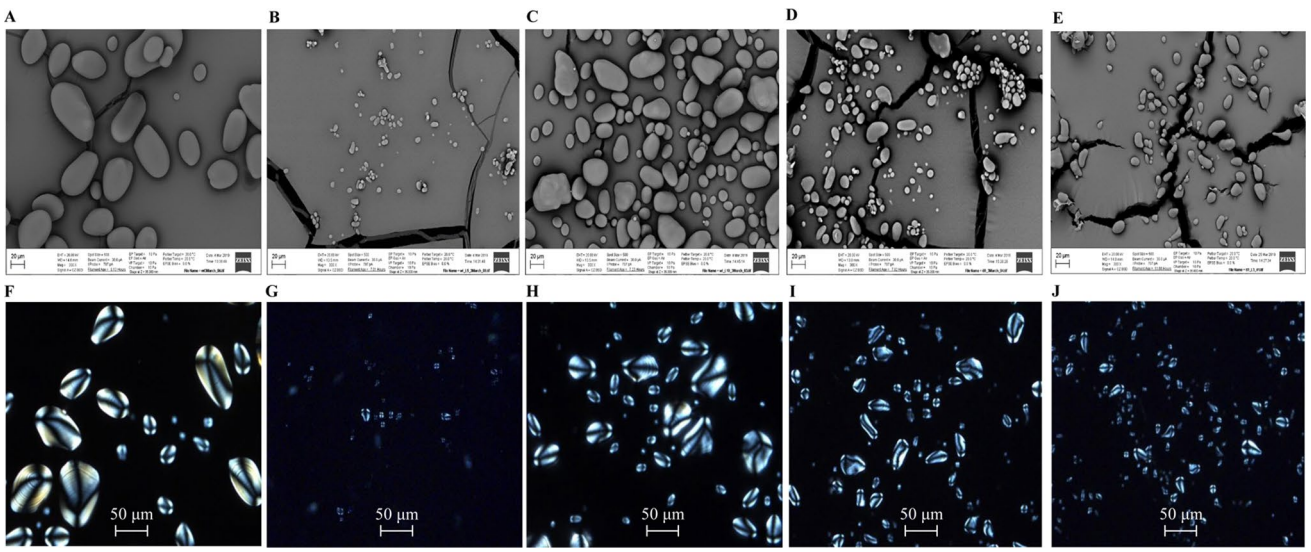

FIGURE 9 | Microscopic observation of starch granules in mature potato tubers. **(A)** scanning electron microscopy (SEM) image of WT; **(B)** SEM image of WT-L5; **(C)** SEM image of WT-L10; **(D)** SEM image of HO69; **(E)** SEM image of 69-L3; **(F**) Polarized light image of WT; **(G)** Polarized light image of WT-L5; **(H)** Polarized light image of WT-L10; **(I)** Polarized light image of HO69; **(J)** Polarized light image of 69-L3. The starch granules were observed under a view of 300× magnification in the SEM, with scale bars located in the lower left corner for each photograph. Sizes of the scale bars are all normalized to 20 μm. For the images taken by light microscopy, the scale bars are located in the lower middle position of each photograph. Size of the scale bars are normalized to 50 μm.

DISCUSSION

In this study, we have shown that the simultaneous downregulation of *StAGPase* and *StSDP1* induced significant reconstitution in the carbon partitioning in potato vegetative tissues. This was concluded from the transgenic potato plants with a duplex RNAi construct specifically targeting the expression of *AGPase* and *SDP1* genes, which displayed significant alteration in the composition of lipids, total soluble sugars and starch, representing a coordinated carbon redistribution in the transgenic potatoes.

This is consistent with the previous studies on high oil potatoes (Hofvander et al., 2016; Liu et al., 2017). Variation in the carbon metabolism of the two WT-derived transgenic lines selected for this study may represent the difference in the effectiveness of RNAi downregulation of the two selected target genes. However, in the HO69-derived super-transformation, due to the low-regeneration rate of transgenic potato plants, only three lines were obtained, with 69-L3 displaying the most distinct RNAi phenotype. Therefore, all of the three super-transformed lines were used for further analysis.

Potato mainly propagates through tuber-cutting, a form of vegetative propagation, which does not facilitate transgene stacking by sexual crossing. The selected HO69 was hence super-transformed with the duplex RNAi construct through the Agrobacterium-mediated gene transformation approach. Because the kanamycin resistance conferred by neomycin phosphotransferase II (*NPTII*) had already been used as the selectable maker in the generation of HO69 (Liu et al., 2017), hygromycin was used as an alternative selectable agent in the super-transformation. The use of *HPH* as the selectable marker is clearly less effective than *NPTII* in our experiment as the hygromycin could impose some level of stress on the explants (Barrell et al., 2002; Sundar and Sakthivel, 2008), which may explain the relatively lower frequency of transgenic plants compared with our previous study (Liu et al., 2017). However, we could not rule out the possibility that the stacking of *StAGPase-StSDP1* RNAi cassettes with the original three transgenes, *AtWRI1-AtDGAT1-siOLEOSIN* contained in the pJP3506 vector (Liu et al., 2017) may also have had some potential repercussions on the transformed cells in terms of metabolism (Halpin, 2005; Baltes and Voytas, 2015), thereby severely restricting the number of transgenic plants coming through the plant regeneration system.

In the leaves of the selected transgenic lines, WT-L10 and 69-L3 displayed enhanced lipid biosynthesis, whereas other lines showed alteration in the accumulation of carbohydrates at variable levels. In the tubers, the two selected WT-derived lines, WT-L5 and WT-L10, as well as the super-transformed line 69-L3 all showed enhanced lipid production. This may be largely due to the variable RNAi effects of the two target genes. As a direct result of the carbon reallocation following *StAGPase* suppression, it is evident that more carbon molecules released from the starch anabolism would be diverted into other carbon metabolic pathways (Sweetlove et al., 1998). AGPase is the rate-limiting enzyme exclusively catalyzing the production of ADP-glucose, which is the direct substrate for starch biosynthesis, thus it is also considered the "valve" controlling the carbon flux distribution from glycolysis (Barıs et al., 2009; Lee et al., 2009). Downregulation of *AGPase* expression in plant would inevitably lead to the re-distribution of carbon flux, which may have potentially provided more available carbon donors for the lipid biosynthesis and compartmentalization (Sanjaya et al., 2011; Yu et al., 2018), as well as the accumulation of soluble sugars (Muller-Rober et al., 1992; Geigenberger 2003; Klaus et al., 2004).

Meanwhile, the suppression of *StSDP1* may have prevented the rapid turnover of TAG and enabled their accumulation in the form of LDs (Eastmond, 2006; Walther and Farese, 2012; D'Andrea, 2016). Kelly et al. (2013) reported that the individual disruption of *SDP1* led to a substantial and continuous accumulation of TAG in the root and stem tissues of Arabidopsis during plant development, and to a lesser extent in leaf. Similarly in the transgenic potato leaves, the enhancement of TAG biosynthesis was observed, but not in WT-L5. This may be due to the difference in RNAi effects, the amount of soluble sugars was increased in WT-L5 leaf as a result of the carbon reallocation from starch decrease *via* the downregulation of *StAGPase*. However, the simultaneous suppression of *StSDP1* did not effectively contribute to TAG maintenance (**Figure 2C**). But the TAG abundance, particularly in the mature tubers of 69-L3, which was doubled to 7.02% of tuber DW relative to parent line HO69, could be the direct result of downregulating *StSDP1*, which is consistent with the study in tobacco (Vanhercke et al., 2017). The enhancement of PC and PE in the mature tubers of WT-L5 (**Figures 3C**, **D**) and 69-L3 (**Figure 6D**) could be a side effect of the *StSDP1* suppression. As recent study has revealed that *SDP1* plays a key role in TAG turnover through being timely delivered *via* the peroxisomal extension to disintegrate LDs from the surrounding phospholipid membranes (Thazar-Poulot et al., 2015). Through the inhibition in the activity of *SDP1*, the packaging of LDs *via* the phospholipid monolayer might be indirectly re-enforced (Matos and Pham-Thi, 2009). By contrast, the increase of galactolipids in transgenic potato vegetative tissues, to a certain extent, may be owing to the expanded carbon provision for the *de novo* plastidial fatty acid biosynthesis after repressing starch production (Li et al., 2010; Yu et al., 2013; Takahashi et al., 2018).

Nevertheless, in the transgenic potatoes, for both WT and the high oil genetic background, the TAG biosynthetic pathway may not have been able to utilize all the extra carbon derived from the repression of starch production and TAG turnover, which may have also resulted in the increased accumulation of soluble sugars. Although we could not rule out the possibility that the enhancement of sugars and TAG productions may be two independent metabolic events as a result of the downregulation of *StAGPase* and *StSDP1* in potatoes, the significant increase in lipid biosynthesis, which are the byproducts of carbohydrate metabolism in potato tubers suggests that the carbon allocations between lipids and carbohydrate are highly orchestrated in potato non-photosynthetic tissues. Likewise, the carbon re-allocation in the transgenic potato leaves also showed the same tendency, particularly in WT-L10 and 69-L3, which was generally consistent with the study in the Arabidopsis mutant deficient in starch biosynthesis, leading to the enhanced lipid biosynthesis and turnover (Yu et al., 2018). Consequently, it was hypothesized that the *CaMV-35S* promoter induced constitutive RNAi silencing of *StAGPase* may be the dominant factor for the overall carbon partitioning variation in transgenic potato plants, including both the increased sugar levels and fatty acid biosynthesis, while the accumulation of TAG, and phospholipids to a lesser extent, may be mainly due to the downregulation of *StSDP1*. Similar results were also observed in the mutagenesis of the *SSIIa* gene in barley, which encodes one of the major starch biosynthetic enzymes localized on the downstream of AGPase. The starch content in the barley mutant was significantly reduced relative to WT,

while lipid and sugar contents were increased to 1.7 and 8.6-fold, respectively (Clarke et al., 2008; Li et al., 2011). However, the differentiated RNAi effects on transgenic potato leaves and tubers, as well as the discrepancy for the discriminatory synthesis of sugars and lipids, still warrant further investigation (Tiessen and Padilla-Chacon, 2013; Zhai et al., 2017; Zhai et al., 2018).

The fatty acid composition in TAG of both leaf and tuber of the two selected WT-derived lines showed significantly increased ALA but decreased LA levels relative to WT at the mature stage, which was consistent with the study in Arabidopsis (Fan et al., 2014). In the super-transformed potato lines, the fatty acid composition was different. Consistent with the high oil transgenic tobacco leaf with the downregulation of *SDP1* expression (Vanhercke et al., 2017), drastic reduction in ALA was observed in the leaves of 69-L2 and 69-L3 at the flowering stage, as well as in PC and galactolipids, but not in tubers. To a certain degree, the variations in fatty acid composition among species and tissues at disparate physiological stages may be due to the differential acyl flux regulation (Ohlrogge and Jaworski, 1997; Slocombe et al., 2009; Bates et al., 2009; Bates et al., 2016; Marchive et al., 2014). The synergistic manipulation of *AtWRI1-AtDGAT1-SiOLEOSIN* expressions have induced a hallmarked fatty acid distribution as enhanced LA at the expense of ALA in high oil transgenic plants (Vanhercke et al., 2014; Liu et al., 2017). When the *SDP1* retromer complex mediated LD-peroxisome communication during the TAG turnover (Thazar-Poulot et al., 2015) was RNAi suppressed, the fatty acid mobilizations in the HO69-derived super-transformed potato lines may be further impacted, leading to more diversified fatty acid distributions in vegetative tissues.

Starch composition and structure were significantly altered in the mature transgenic potato tubers relative to their parent lines. The decreased amylose content, varied amylopectin CLD and accumulation of GBPs suggested the activity of starch biosynthetic enzymes have been affected in the transgenic potatoes derived from both the WT and high oil genetic backgrounds (Luo et al., 2015), leading to altered starch functionality as indicated by the differed swelling power values (Jane et al., 1999; Srichuwong et al., 2005; Vamadevan and Bertoft, 2015). Amylose is the linear long chain polysaccharide molecule with few branches associated inside the starch granule, the biosynthesis of amylose is directly controlled by the GBSS enzyme, which is also one of the GBPs (Denyer et al., 2001; Vamadevan and Bertoft, 2009). However, the increase of GBSS protein in the transgenic potatoes relative to their parent lines was not consistent with the reduction of amylose content. This suggests the GBSS protein accumulation in transgenic potato starch may be a pleiotropic effect of downregulating *AGPase*, while the altered CLD may be due to the reduction in SSII and SBE proteins. We propose that the suppression of *StAGPase* following variable RNAi effects among different transgenic potato plants may be the dominant factor leading to all these differences, because a limited ADP-glucose provision may cause the substrate competition in starch biosynthesis (Lloyd et al., 1999). The negative feedback regulation on the gene expression involved in the sequential biosynthesis of amylose and amylopectin, as the result of *AGPase* downregulation, could induce the alteration of the amylopectin chain length and branch frequency in the starch granule formation thereafter (Kuipers et al., 1994; Lloyd et al., 1999; Luo et al., 2015). Further, with the reduction of amylose, the proportion of amylopectin may increase, leading to enhanced swelling power in WT-L10 and 69-L3. However, similar impacts were not reflected in WT-L5, which may be partially due to the slight decline in amylopectin chain length between DP12 and DP16 (**Figure 4B**). Such a result was similar with the *SSIIa* mutation in wheat (Konik-Rose et al., 2007).

As further revealed in the microscopic analysis, the LD and starch granule derived from the selected transgenic potato tubers both displayed consistent variation with the biochemical results. Obviously, the changes in the starch composition and the starch granule morphology were indicative for the interactions between *AGPase* and other starch biosynthetic enzymes. Additionally, the significantly increased LDs distribution in WT-L5, and the enlarged size of LDs in 69-L3, might be caused by the fusion of small LDs (Fan et al., 2014; Vanhercke et al., 2017). Although the enhancement of LD formation could be largely owing to the *StSDP1* downregulation, and the suppression of *StAGPase* induced alteration in starch granule morphology, the microscopic results still implicated an underlying correspondence between the LD biogenesis and starch biosynthesis in potato tubers. A further comparison with the individual downregulation of *StAGPase* and *StSDP1*, respectively, in both the WT and high oil genetic potato backgrounds may bring more insights in this respect.

Previous efforts in downregulating *AGPase* alone in potato tubers resulted in the reduction of starch, without increasing the lipid content (Klaus et al., 2004). We demonstrated in this study that the carbon reallocation from starch to fatty acids and lipids may be possible when *StAGPase* and *StSDP1* were simultaneously suppressed. Not only were the contents of starch, lipids, and soluble sugars, but also the fatty acid composition, starch granule properties were significantly altered. The expression of *AtWRI1* transcriptional factor in the HO69-derived super-transformation may be a potential factor limiting the valid RNAi suppression of *StSDP1*, and the "feedback inhibition relationship" between the TAG lipase and LD integral protein *OLEOSIN* may be another one (Vanhercke et al., 2017; Huang 2018). Unlike genome editing, RNAi occurs on the post-transcriptional level (Jagtap et al., 2011; Watanabe, 2011), its effects are largely dependent on the insertion site of the RNAi cassettes into potato genome, which are somewhat unpredictable. Moreover, the significantly enhanced production of membrane lipids, particularly MGDG and DGDG, in the transgenic tubers of WT-L5 and 69-L3, may suggest a possibly reinforced fatty acid and/or lipid biosynthesis within the non-photosynthetic plastid, the amyloplast in potato, which was consistent with our previous report (Liu et al., 2017). Amyloplast usually plays the major role in starch biosynthesis, only to a lesser extent in the rather limited fatty acids and plastidial lipid production in potato (Ferreira et al., 2010; Nazarian-Firouzabadi and Visser, 2017). By comparison, the galactolipids abundantly synthesized in chloroplast are not only actively involved in the maintenance of the cellular homeostasis of green tissues (Chapman et al., 2013; Xu and Shanklin, 2016), but also the responsive machinery tackling various plant abiotic/biotic stresses (Welti et al., 2002; Moellering et al, 2010). In our study, the manipulations towards the endosperm reticulum (ER)-specific Kennedy pathway have induced substantial accumulation

of plastidial galactolipids in tubers. One hypothesis is that the tuber specific B33 promoter controlled expression of *AtWRI1* transcriptional factor, as a critical regulatory gene localized on the upstream of the global lipid metabolic networks (Ma et al., 2013; Ma et al., 2016), may have contributed mostly to the excessive production of *de novo* fatty acids as source for the prokaryotic galactolipid production in potato amyloplast (Liu et al., 2017), which might be also enhanced by the RNAi silencing of *StAGPase* to donate more carbon. However, questions such as how the expression of transgenes affect the amyloplast biogenesis (*e.g.* structure and functionality) in high oil potato tubers, how the transgenes contribute to the plastidial lipids biosynthesis, as well as the interactions among the plastid- and ER-specific genes during the carbon partitioning still remain to be further explored. High throughput characterization methods such as transcriptomics, lipidomics, or metabolomics would be useful to better understand the mechanisms underlying these distinct transgenic phenotypes, while high-resolution microscopic technologies like transmission electron microscopy (TEM) could also be applied to depict the structural dynamics of the intracellular organelles in potato tuber. Further, the overproduction of sugars implies a yet limited enhancement of TAG biosynthesis in the transgenic potatoes. There may still be potential to more efficiently direct the carbon flux into the oil production in potato, for example *via* changes to sucrose metabolism (Vanhercke et al., 2019). The results embodied in this study warrant further exploration of the lipid and carbohydrate interactions in plant non-seed biomass tissues. Also, other important storage components such as protein and fiber need to be taken into account in the metabolic engineering of valuable co-products from plants.

EXPERIMENTAL PROCEDURES

Concurrent Gene Silencing of StAGPase and StSDP1 Through RNAi

Selected DNA fragments derived from *StAGPase* and *StSDP1* genes were fused and constructed into an inverted repeat configuration, which was placed behind the *CaMV-35S* promoter in the pWBVec2 vector (Wang et al., 1998). For amplifying the cDNA fragments for *StAGPase* and *StSDP1* genes, total RNAs were isolated from mid-development potato tubers using RNeasy Mini Kit (QIAGEN, Hilden, Germany). The first strand cDNA was synthesized by reverse transcription using Superscript III RT/ Platinium Taq High fidelity Enzyme Mix kit (Life Technologies, Calsbad, CA) with the following primers which specifically amplified a 500 bp fragment of the two target genes, *StAGPase* sense: 5'-ACAGACATGTCTAGACCCAGATG-3', *StAGPase* antisense: 5'-CACTCTCATCCCAAGTGAAGTTGC-3'; *StSDP1* sense: 5'- CTGAGATGGAAGTGAAGCACAGATG-3', *StSDP1* antisense: 5'-CCATTGTTAGTCCTTTCAGTC-3'. The PCR products were then purified by gel fractionation and ligated into the pGEMT Easy vector (Promega, Madison, WI) which was then transformed into *E. coli* cells for selecting target colonies. After the DNA sequencing verification, the two fragments representing *StAGPase* and *StSDP1* genes, respectively, were fused by the overlapping PCR (Bryksin and Matsumura, 2010), then incorporated into the pKannibal vector to clone the sense and antisense fragments. Restriction sites *Bam*HI and *Hin*dIII were selected for cloning in one orientation and *Kpn*I and *Xho*I for the antisense orientation. Subsequently, the resulting RNAi structure, together with the CaMV-35S promoter and OCS terminator sequence were released from the *Not*I site of pKannibal vector and cloned into a binary vector pWBVec2 with hygromycin as plant selectable marker. This binary vector was further introduced into *A. tumefaciens* AGL1 strain through electroporation for potato transformation. The configuration map the pWBVec2 construct was illustrated in **Supplementary Figure 9**.

Potato Transformation

Aseptic seedlings of the HO69 (Liu et al., 2017) were prepared before tissue culture transformation. The establishment of this donor plant system used the method described by Mohapatra and Batra (2017) (**Supplementary Figure 10**). Both the WT- and super- transformations with the same RNAi construct were carried out as described in Liu et al. (2017), except that sucrose concentration used in the super-transformation was reduced to 15 g/L in all the MS media throughout the entire transformation process. This modification in protocol was to address the sensitivity to sucrose of explants derived from HO69 due to *WRI1* overexpression (Cernac and Benning, 2004). The obtained T_0 plants were maintained in the phytotron glasshouse (24/20°C, 16 h photoperiod) at CSIRO Black Mountain Science and Innovation Park, Canberra. After the molecular verification and selection, several lines with representative transgenic traits were selected to synchronically propagate with WT and HO69 under the same conditions for further characterization. Two developmental stages, the flowering stage (>70% of flowers in one plant are blossoming and developing tubers are visible) and the mature stage (>50% aging leaves and >80% mature tubers are observable) were analyzed.

Genetic Verification of Transgenic Plants and qRT-PCR Analysis of Gene Expressions

The Phire™ Plant Direct PCR Kit (Thermo Fisher Scientific, Waltham, MA) was applied to quickly verify the presence of selectable marker gene hygromycin-B-phosphotransferase (*HPH*) in the DNAs isolated from the leaves and tubers of T_0 potato plants. Primers used for the amplification of a 200 bp region of the hygromycin gene were: sense 5'-GACCTGCCTGAAACCGAACT-3'; antisense 5'-TCGTCCATCACAGTTTGCC-3'. The PCR reaction program was as follows: initial denaturation at 95 °C for 3 min, followed with 40 cycles of 95 °C for 10 s, 60 °C for 30 s, 72 °C for 30 s. The PCR products were visualized on 1% agarose gel to initially verify the transgenic plants.

Total RNA from healthy and fully expanded leaves of WT, HO69, and the selected transgenic potato lines were isolated using the RNeasy Mini Kit (Qiagen) as specified in the manufacture's protocol, and the quantity was measured using a Nanodrop spectrophotometer ND 1000 (Thermo Fisher Scientific). The

total RNA from mature potato tubers were extracted by the cetyl trimethyl ammonium bromide (CTAB) method (Reynolds et al., 2019) and purified using a RNeasy MinElute Cleanup Kit (Qiagen) following manufacturer's instructions. Real-time quantitative reverse transcription polymerase chain reaction (qRT-PCR) was applied to study the gene expression of *StAGPase* and *StSDP1* in potato vegetative tissues, with the *S. tuberosum CYCLOPHILIN (stCYP)* gene as the reference gene. The targeting primers for the *StCYP* gene are sense: 5'-CTCTTCGCCGATACCACTC-3'; antisense: 5'-CACACGGTGGAAGGTTGAG-3'. Primers for *StAGPase* are sense: 5'-CACACAATTCAACTCTGCCTC-3'; antisense: 5'-GCTCCTCAAACAACCACAG-3', and primers for *StSDP1* are sense: 5'-GTTGTCACTCGTGGACTCG-3'; antisense: 5'-CTTGGACAAGATCAGGTGG-3'. The real-time qRT-PCR reaction was developed in a Biorad 96 well PCR machine (BioRad, Hercules, CA) programmed as 95°C for 3 min, 39 cycles of 95°C for 10 s, 56°C for 30 s, and 72°C for 30 s, with the FastStart Universal SYBR Green Master (ROX) kit (Roche, Indianapolis, IN) as the supporting reaction system. Gene expression was calculated by following the $2^{-\Delta\Delta Ct}$ method (Livak and Schmittgen, 2001).

Lipid and Carbohydrate Biochemical Analysis

Healthy potato fully expanded leaves and tubers were freshly sampled at the two developmental stages, and immediately freeze-dried for 72 h. The lipid analysis including TFA, FFA, neutral lipids (*i.e.* TAG, DAG), and polar lipids (*i.e.* PC, MGDG, DGDG, PE and PG) were developed as previously described by Vanhercke et al. (2018) through the TLC and GC analysis and carbohydrates analysis including total starch and total soluble sugars were measured as described by Liu et al. (2017) *via* the Megazyme Total Starch Kit (Megazyme International Ireland, Bray, Ireland) following the manufacturer's instruction.

Starch Property Analysis of Mature Potato Tubers

Potato starch was isolated from mature and healthy tubers sampled at the mature stage as described in Liu et al. (2017). Estimation of the amylose content was made by following the coloration method described in Morrison and Laignelet (1983). The CLD analysis was carried out using the capillary electrophoresis (CE), following starch debranching as described in Luo et al. (2015). The SDS-PAGE analysis of GBPs, with starch content used to standardize the amount was carried out following the method described by Luo et al. (2015). The digital analysis of protein bands intensity on SDS gels was developed on the ImageScanner III machine (GE Healthcare Life Science) via the Totallab Quant Software (Totallab, Newcastle, USA) by following manufacturers' instructions. The swelling power analysis of potato tuber flour was carried out following Konik-Rose et al. (2007).

Microscopic Analysis

Confocal scanning microscopy analysis of LDs was carried out as previously described (Vanhercke et al., 2018). SEM and light microscopy analyses of the potato tuber starch granules were carried out as previously described (Liu et al., 2017).

Statistical Analysis

GenStat 9.0 software was used to calculate the least significant difference (LSD) value of all data for multiple comparisons.

DATA AVAILABILITY STATEMENT

The datasets generated for this study are available on request to the corresponding author.

AUTHOR CONTRIBUTIONS

XX designed the research, performed the experiments and wrote the paper. TV, PS, and SS provided precious guidance all along the research as project supervisors. JL and CK-R assisted the starch experiments. SA and DH assisted the preparation of the transgenic construct. LV assisted the confocal microscopic analysis. LT assisted the glasshouse maintenance. PJS, ZL and QL conceived and designed the project, and improved the manuscript.

FUNDING

This project is supported by CSIRO Agriculture and Food and The University of Sydney.

ACKNOWLEDGMENTS

XX would like to acknowledge the China Scholarship Council for funding him in the doctoral study in Australia.

SUPPLEMENTARY MATERIAL

The Supplementary Material for this article can be found online at: https://www.frontiersin.org/articles/10.3389/fpls.2019.01444/full#supplementary-material

REFERENCES

Baltes, N. J., and Voytas, D. F. (2015). Enabling plant synthetic biology through genome engineering. *Trends Biotechnol.* 33 (2), 120–131. doi: 10.1016/j.tibtech.2014.11.008

Barıs, I., Tuncel, A., Ozber, N., Keskin, O., and Kavakli, I. H. (2009). Investigation of the interaction between the large and small subunits of potato ADP-glucose pyrophosphorylase. *PloS Comput. Biol.* 5 (10), e1000546. doi: 10.1371/journal.pcbi.1000546

Barrell, P. J., Yongjin, S., Cooper, P. A., and Conner, A. J. (2002). Alternative selectable markers for potato transformation using minimal T-DNA vectors. *Plant Cell Tiss. Org.* 70 (1), 61–68. doi: 10.1023/A:1016013426923

Bates, P. D. (2016). Understanding the control of acyl flux through the lipid metabolic network of plant oil biosynthesis. *Biochim. Biophys. Acta* 1861 (9b), 1214–1225. doi: 10.1016/j.bbalip.2016.03.021

Bates, P. D., Durrett, T. P., Ohlrogge, J. B., and Pollard, M. (2009). Analysis of acyl fluxes through multiple pathways of triacylglycerol synthesis in developing soybean embryos. *Plant Physiol.* 150 (1), 55–72. doi: 10.1104/pp.109.137737

Bozhkov, P. V. (2018). Plant autophagy: mechanisms and functions. *J. Exp. Bot.* 69 (6), 1281–1285. doi: 10.1093/jxb/ery070

Bryksin, A. V., and Matsumura, I. (2010). Overlap extension PCR cloning: a simple and reliable way to create recombinant plasmids. *Biotechniques* 48 (6), 463–465. doi: 10.2144/000113418

Cernac, A., and Benning, C. (2004). *Wrinkled1* encodes an AP2/EREB domain protein involved in the control of storage compound biosynthesis in Arabidopsis. *Plant J.* 40 (4), 575–585. doi: 10.1111/j.1365-313X.2004.02235.x

Chapman, K. D., Dyer, J. M., and Mullen, R. T. (2013). Commentary, why don't plant leaves get fat? *Plant Sci.* 207, 128–134. doi: 10.1016/j.plantsci.2013.03.003

Chapman, K. D., and Ohlrogge, J. B. (2012). Compartmentation of triacylglycerol accumulation in plants. *J. Biol. Chem.* 287, 2288–2294. doi: 10.1074/jbc.R111.290072

Clarke, B., Liang, R., Morell, M. K., Bird, A. R., Jenkins, C. L. D., and Li, Z. (2008). Gene expression in a starch synthase IIa mutant of barley: changes in the level of gene transcription and grain composition. *Funct. Integr. Genomic* 8 (3), 211–221. doi: 10.1007/s10142-007-0070-7

D'Andrea, S. (2016). Lipid droplet mobilization: The different ways to loosen the purse strings. *Biochimie.* 120, 17–27. doi: 10.1016/j.biochi.2015.07.010

Denyer, K. A. Y., Johnson, P., Zeeman, S., and Smith, A. M. (2001). The control of amylose synthesis. *J. Plant Physiol.* 158 (4), 479–487. doi: 10.1078/0176-1617-00360

Du, Z., and Benning, C. (2016). "Triacylglycerol accumulation in photosynthetic cells in plants and algae," in *Lipids in Plant and Algae Development*. Eds. Nakamura, Y., and Li-Beisson, Y. (Cham: Springer International Publishing), 179–205. doi: 10.1007/978-3-319-25979-6_8

Eastmond, P. J. (2006). SUGAR-DEPENDENT1 encodes a patatin domain triacylglycerol lipase that initiates storage oil breakdown in germinating Arabidopsis seeds. *Plant Cell.* 18 (3), 665–675. doi: 10.1105/tpc.105.040543

Fan, J., Yan, C., Roston, R., Shanklin, J., and Xu, C. (2014). Arabidopsis lipins, *PDAT1* acyltransferase, and *SDP1* triacylglycerol lipase synergistically direct fatty acids toward β-oxidation, thereby maintaining membrane lipid homeostasis. *Plant Cell.* 26 (10), 4119–4134. doi: 10.1105/tpc.114.130377

Ferreira, S. J., Senning, M., Sonnewald, S., Keßling, P. M., Goldstein, R., and Sonnewald, U. (2010). Comparative transcriptome analysis coupled to X-ray CT reveals sucrose supply and growth velocity as major determinants of potato tuber starch biosynthesis. *BMC Genomics* 11 (1), 93. doi: 10.1186/1471-2164-11-93

Geigenberger, P. (2003). Regulation of sucrose to starch conversion in growing potato tubers. *J. Exp. Bot.* 54 (382), 457–465. doi: 10.1093/jxb/erg074

Grommers, H. E., and van der Krogt, D. A. (2009). "Potato starch: production, modifications and uses," in *Food Science and Technology, Starch*, Eds. BeMiller, J., and Whistler, R. (New York: Academic Press), 511–539. doi: 10.1016/B978-0-12-746275-2.00011-2

Halpin, C. (2005). Gene stacking in transgenic plants –the challenge for 21st century plant biotechnology. *Plant Biotechnol. J.* 3 (2), 141–155. doi: 10.1111/j.1467-7652.2004.00113.x

Hendriks, J. H., Kolbe, A., Gibon, Y., Stitt, M., and Geigenberger, P. (2003). ADP-glucose pyrophosphorylase is activated by posttranslational redox-modification in response to light and to sugars in leaves of Arabidopsis and other plant species. *Plant Physiol.* 133 (2), 838–849. doi: 10.1104/pp.103.024513

Hofvander, P., Ischebeck, T., Turesson, H., Kushwaha, S. K., Feussner, I., Carlsson, A. S., et al. (2016). Potato tuber expression of Arabidopsis *WRINKLED1* increase triacylglycerol and membrane lipids while affecting central carbohydrate metabolism. *Plant Biotechnol. J.* 14, 1883–1898. doi: 10.1111/pbi.12550

Huang, A. H. (2018). Plant lipid droplets and their associated proteins: potential for rapid advances. *Plant Physiol.* 176 (3), 1894–1918. doi: 10.1104/pp.17.01677

Hwang, S. K., Hamada, S., and Okita, T. W. (2007). Catalytic implications of the higher plant ADP-glucose pyrophosphorylase large subunit. *Phytochemistry* 68 (4), 464–477. doi: 10.1016/j.phytochem.2006.11.027

Jagtap, U. B., Gurav, R. G., and Bapat, V. A. (2011). Role of RNA interference in plant improvement. *Naturwissenschaften* 98 (6), 473–492. doi: 10.1007/s00114-011-0798-8

Jane, J. L., Chen, Y., Lee, L., McPherson, A. E., Wong, K. S., Radosavljevic, M., et al. (1999). Effects of amylopectin branch chain length and amylose content on the gelatinization and pasting properties of starch. *Cereal Chem.* 76 (5), 629–637. doi: 10.1094/CCHEM.1999.76.5.629

Jobling, S. A., Westcott, R. J., Tayal, A., Jeffcoat, R., and Schwall, G. P. (2002). Production of a freeze-thaw-stable potato starch by antisense inhibition of three starch synthase genes. *Nat. Biotechnol.* 20 (3), 295–299. doi: 10.1038/nbt0302-295

Jonik, C., Sonnewald, U., Hajirezaei, M. R., Flügge, U. I., and Ludewig, F. (2012). Simultaneous boosting of source and sink capacities doubles tuber starch yield of potato plants. *Plant Biotechnol. J.* 10 (9), 1088–1098. doi: 10.1111/j.1467-7652.2012.00736.x

Kelly, A. A., and Feussner, I. (2016). Oil is on the agenda: lipid turnover in higher plants. *BBA-Mol Cell Biol. l.* 1861 (9), 1253–1268. doi: 10.1016/j.bbalip.2016.04.021

Kelly, A. A., Shaw, E., Powers, S. J., Kurup, S., and Eastmond, P. J. (2013). Suppression of the SUGAR-DEPENDENT1 triacylglycerol lipase family during seed development enhances oil yield in oilseed rape (*Brassica napus* L.). *Plant Biotechnol. J.* 11 (3), 355–361. doi: 10.1111/pbi.12021

Klaus, D., Ohlrogge, J. B., Ekkehard, N. H., and Dormann, P. (2004). Increased fatty acid production in potato by engineering of acetyl-CoA carboxylase. *Planta* 219, 389–396. doi: 10.1007/s00425-004-1236-3

Konik-Rose, C., Thistleton, J., Chanvrier, H., Tan, I., Halley, P., Gidley, M., et al. (2007). Effects of starch synthase IIa gene dosage on grain, protein and starch in endosperm of wheat. *Theor. Appl. Genet.* 115 (8), 1053. doi: 10.1007/s00122-007-0631-0

Kuipers, A. G., Jacobsen, E., and Visser, R. G. (1994). Formation and deposition of amylose in the potato tuber starch granule are affected by the reduction of granule-bound starch synthase gene expression. *Plant Cell* 6 (1), 43–52. doi: 10.2307/3869673

Lee, S. M., Ryu, T. H., Kim, S. I., Okita, T., and Kim, D. (2009). Kinetic and regulatory properties of plant ADP-glucose pyrophosphorylase genetically modified by heterologous expression of potato upreg mutants *in vitro* and. *vivo. Plant Cell Tiss. Org.* 96 (2), 161. doi: 10.1007/s11240-008-9472-z

Levy, D., Coleman, W. K., and Veilleux, R. E. (2013). Adaptation of potato to water shortage: irrigation management and enhancement of tolerance to drought and salinity. *Am. J. Potato Res.* 90 (2), 186–206. doi: 10.1007/s12230-012-9291-y

Li, Y., Han, D., Hu, G., Sommerfeld, M., and Hu, Q. (2010). Inhibition of starch synthesis results in overproduction of lipids in *Chlamydomonas reinhardtii*. *Biotechnol. Bioeng.* 107 (2), 258–268. doi: 10.1002/bit.22807

Li, Z., Li, D., Du, X., Wang, H., Larroque, O., Jenkins, C. L., et al. (2011). The barley amo1 locus is tightly linked to the starch synthase *IIIa* gene and negatively regulates expression of granule-bound starch synthetic genes. *J. Exp. Bot.* 62 (14), 5217–5231. doi: 10.1093/jxb/err239

Liu, Q., Guo, Q., Akbar, S., Zhi, Y., El Tahchy, A., Mitchell, M., et al. (2017). Genetic enhancement of oil content in potato tuber (*Solanum tuberosum* L.) through an integrated metabolic engineering strategy. *Plant Biotechnol. J.* 15, 56–67. doi: 10.1111/pbi.12590

Livak, K. J., and Schmittgen, T. D. (2001). Analysis of relative gene expression data using real-time quantitative PCR and the $2^{-\Delta\Delta CT}$ method. *Methods* 25 (4), 402–408. doi: 10.1006/meth.2001.1262

Lloyd, J. R., Springer, F., Buléon, A., Müller-Röber, B., Willmitzer, L., and Kossmann, J. (1999). The influence of alterations in ADP-glucose pyrophosphorylase activities on starch structure and composition in potato tubers. *Planta* 209 (2), 230–238. doi: 10.1007/s004250050627

Luo, J., Jobling, S. A., Millar, A., Morell, M. K., and Li, Z. (2015). Allelic effects on starch structure and properties of six starch biosynthetic genes in a rice recombinant inbred line population. *Rice* 8 (1), 15. doi: 10.1186/s12284-015-0046-5

Marchive, C., Nikovics, K., To, A., Lepiniec, L., and Baud, S. (2014). Transcriptional regulation of fatty acid production in higher plants: molecular bases and

biotechnological outcomes. *Eur. J. Lipid Sci. Tech.* 116 (10), 1332–1343. doi: 10.1002/ejlt.201400027

Mitchell, M., Pritchard, J., Okada, S., Larroque, O., Yulia, D., Pettolino, F., et al. (2017). Oil accumulation in transgenic potato tubers alters starch quality and nutritional profile. *Front. Plant Sci.* 8, 554. doi: 10.3389/fpls.2017.00554

Mohapatra, P. P., and Batra, V. K. (2017). Tissue culture of potato (Solanum tuberosum L.): A review. *IJCMAS* 6 (4), 489–495. doi: 10.20546/ijcmas.2017.604.058

Morrison, W. R., and Laignelet, B. (1983). An improved colorimetric procedure for determining apparent and total amylose in cereal and other starches. *J. Cereal Sci.* 1 (1), 9–20. doi: 10.1016/S0733-5210(83)80004-6

Matos, A. R., and Pham-Thi, A. T. (2009). Lipid deacylating enzymes in plants: old activities, new genes. *Plant Physiol. Biochem.* 47 (6), 491–503. doi: 10.1016/j.plaphy.2009.02.011

Muller-Rober, B., Sonnewald, U., and Willmitzer, L. (1992). Inhibition of the ADP-glucose pyrophosphorylase in transgenic potatoes leads to sugar-storing tubers and influences tuber formation and expression of tuber storage protein genes. *EMBO J.* 11 (4), 1229–1238. doi: 10.1002/j.1460-2075.1992.tb05167.x

Moellering, E. R., Muthan, B., and Benning, C. (2010). Freezing tolerance in plants requires lipid remodeling at the outer chloroplast membrane. *Science* 330 (6001), 226–228. doi: 10.1126/science.1191803

Ma, W., Kong, Q., Arondel, V., Kilaru, A., Bates, P. D., Thrower, N. A., et al. (2013). Wrinkled1, a ubiquitous regulator in oil accumulating tissues from Arabidopsis embryos to oil palm mesocarp. *PloS One* 8 (7), e68887. doi: 10.1371/journal.pone.0068887

Ma, W., Kong, Q., Mantyla, J. J., Yang, Y., Ohlrogge, J. B., and Benning, C. (2016). 14-3-3 protein mediates plant seed oil biosynthesis through interaction with *AtWRI1*. *Plant J.* 88 (2), 228–235. doi: 10.1111/tpj.13244

Nazarian-Firouzabadi, F., and Visser, R. G. (2017). Potato starch synthases: functions and relationships. *BB Rep.* 10, 7–16. doi: 10.1016/j.bbrep.2017.02.004

O'Leary, M. H. (1988). Carbon isotopes in photosynthesis. *Bioscience* 38 (5), 328–336. doi: 10.2307/1310735

Ohlrogge, J. B., and Jaworski, J. G. (1997). Regulation of fatty acid synthesis. *Annu. Rev. Plant Physiol. Plant Mol. Biol.* 48, 109–136. doi: 10.1146/annurev.arplant.48.1.109

Pinhero, R. G., Waduge, R. N., Liu, Q., Sullivan, J. A., Tsao, R., Bizimungu, B., et al. (2016). Evaluation of nutritional profiles of starch and dry matter from early potato varieties and its estimated glycemic impact. *Food Chem.* 203, 356–366. doi: 10.1016/j.foodchem.2016.02.040

Radakovits, R., Jinkerson, R. E., Darzins, A., and Posewitz, M. C. (2010). Genetic engineering of algae for enhanced biofuel production. *Eukaryot. Cell* 9 (4), 486–501. doi: 10.1128/EC.00364-09

Rahman, M. M., Divi, U. K., Liu, Q., Zhou, X., Surinder, S. P., and Aruna, K. (2016). Oil-rich nonseed tissues for enhancing plant oil production. *CAB Rev.* 11 (021), 1–11. doi: 10.1079/PAVSNNR201611021

Rawsthorne, S. (2002). Carbon flux and fatty acid synthesis in plants. *Prog. Lipid Res.* 41 (2), 182–196. doi: 10.1016/S0163-7827(01)00023-6

Reynolds, K. B., Cullerne, D. P., El Tahchy, A., Rolland, V., Blanchard, C. L., Wood, C. C., et al. (2019). Identification of genes involved in lipid biosynthesis through *de novo* transcriptome assembly from Cocos nucifera developing endosperm. *Plant Cell Physiol.* 60 (5), 945–960. doi: 10.1093/pcp/pcy247

Sanjaya, S., Durrett, T. P., Weise, S. E., and Benning, C. (2011). Increasing the energy density of vegetative tissues by diverting carbon from starch to oil biosynthesis in transgenic Arabidopsis. *Plant Biotechnol. J.* 9, 874–883. doi: 10.1111/j.1467-7652.2011.00599.x

Scherer, G. F., Ryu, S. B., Wang, X., Matos, A. R., and Heitz, T. (2010). Patatin-related phospholipase A: nomenclature, subfamilies and functions in plants. *Trends Plant Sci.* 15 (12), 693–700. doi: 10.1016/j.tplants.2010.09.005

Schwall, G. P., Safford, R., Westcott, R. J., Jeffcoat, R., Tayal, A., Shi, Y., et al. (2000). Production of very-high-amylose potato starch by inhibition of SBE A and B. *Nat. Biotechnol.* 18 (5), 551–554. doi: 10.1038/75427

Siaut, M., Cuine, S., Cagnon, C., Fessler, B., Nguyen, M., Carrier, P., et al. (2011). Oil accumulation in the model green alga *Chlamydomonas reinhardtii*: characterization, variability between common laboratory strains and relationship with starch reserves. *BMC Biotechnol.* 11 (1), 7. doi: 10.1186/1472-6750-11-7

Slocombe, S. P., Cornah, J., Pinfield-Wells, H., Soady, K., Zhang, Q., Gilday, A., et al. (2009). Oil accumulation in leaves directed by modification of fatty acid breakdown and lipid synthesis pathways. *Plant Biotechnol. J.* 7 (7), 694–703. doi: 10.1111/j.1467-7652.2009.00435.x

Srichuwong, S., Sunarti, T. C., Mishima, T., Isono, N., and Hisamatsu, M. (2005). Starches from different botanical sources II: Contribution of starch structure to swelling and pasting properties. *Carbohydr. Polym.* 62 (1), 25–34. doi: 10.1016/j.carbpol.2005.07.003

Stitt, M. (1995). The use of transgenic plants to study the regulation of plant carbohydrate metabolism. *Funct. Plant Biol.* 22 (4), 635–646. doi: 10.1071/PP9950635

Sundar, I. K., and Sakthivel, N. (2008). Advances in selectable marker genes for plant transformation. *J. Plant Physiol.* 165 (16), 1698–1716. doi: 10.1016/j.jplph.2008.08.002

Sweetlove, L. J., Kossmann, J., Riesmeier, J. W., Trethewey, R. N., and Hill, S. A. (1998). The control of source to sink carbon flux during tuber development in potato. *Plant J.* 15 (5), 697–706. doi: 10.1046/j.1365-313x.1998.00247.x

Takahashi, K., Ide, Y., Hayakawa, J., Yoshimitsu, Y., Fukuhara, I., Abe, J., et al. (2018). Lipid productivity in TALEN-induced starchless mutants of the unicellular green alga *Coccomyxa* sp. strain Obi. *Algal Res.* 32, 300–307. doi: 10.1016/j.algal.2018.04.020

Tetlow, I. J., Morell, M. K., and Emes, M. J. (2004). Recent developments in understanding the regulation of starch metabolism in higher plants. *J. Exp. Bot.* 55 (406), 2131–2145. doi: 10.1093/jxb/erh248

Thazar-Poulot, N., Miquel, M., Fobis-Loisy, I., and Gaude, T. (2015). Peroxisome extensions deliver the Arabidopsis *SDP1* lipase to oil bodies. *PNAS* 112 (13), 4158–4163. doi: 10.1073/pnas.1403322112

Tiessen, A., and Padilla-Chacon, D. (2013). Subcellular compartmentation of sugar signaling: links among carbon cellular status, route of sucrolysis, sink-source allocation, and metabolic partitioning. *Front. Plant Sci.* 3, 306. doi: 10.3389/fpls.2012.00306

Tjellström, H., Strawsine, M., and Ohlrogge, J. B. (2015). Tracking synthesis and turnover of triacylglycerol in leaves. *J. Exp. Bot.* 66 (5), 1453–1461. doi: 10.1093/jxb/eru500

Vamadevan, V., and Bertoft, E. (2015). Structure-function relationships of starch components. *Starch-Stärke* 67 (1-2), 55–68. doi: 10.1002/star.201400188

Vanhercke, T., Belide, S., Taylor, M. C., El Tahchy, A., Okada, S., Rolland, V., et al. (2018). Upregulation of lipid biosynthesis pathway increases the oil content in leaves of *Sorghum bicolor*. *Plant Biotechnol. J.* 17 (1), 220–232. doi: 10.1111/pbi.12959

Vanhercke, T., Divi, U. K., El Tahchy, A., Liu, Q., Mitchell, M., Taylor, M. C., et al. (2017). Step changes in leaf oil accumulation *via* iterative metabolic engineering. *Metab. Eng.* 39, 237–246. doi: 10.1016/j.ymben.2016.12.007

Vanhercke, T., Dyer, J. M., Mullen, R. T., Kilaru, A., Rahman, M. M., Petrie, J. R., et al. (2019). Metabolic engineering for enhanced oil in biomass. *Prog. Lipid Res.* 74, 103–129. doi: 10.1016/j.plipres.2019.02.002

Vanhercke, T., El Tahchy, A., Liu, Q., Zhou, X., Shrestha, P., Divi, U. K., et al. (2014). Metabolic engineering of biomass for high energy density, oilseed-like triacylglycerol yields from plant leaves. *Plant Biotechnol. J.* 12 (2), 231–239. doi: 10.1111/pbi.12131

Welti, R., Li, W., Li, M., Sang, Y., Biesiada, H., Zhou, H., et al. (2002). Profiling membrane lipids in plant stress responses role of phospholipase Dα in freezing-induced lipid changes in Arabidopsis. *J. Biol. Chem.* 277 (35), 31994–32002. doi: 10.1074/jbc.M205375200

Walther, T. C., and Farese, R. V. Jr. (2012). Lipid droplets and cellular lipid metabolism. *Annu. Rev. Biochem.* 81, 687–714. doi: 10.1146/annurev-biochem-061009-102430

Wang, M., Li, Z., Matthews, P. R., Upadhyaya, N. M., and Waterhouse, P. M. (1998). Improved vector for *Agrobacterium tumefaciens*-mediated transformation of monocot plants. *Acta Hortic.* 461, 401–407. doi: 10.17660/ActaHortic.1998.461.46

Watanabe, Y. (2011). Overview of plant RNAi. *Methods Mol. Biol.* 744, 1–11. doi: 10.1007/978-1-61779-123-9_1

Xu, C., and Shanklin, J. (2016). Triacylglycerol metabolism, function, and accumulation in plant vegetative tissues. *Annu. Rev. Plant Biol.* 67, 179–206. doi: 10.1146/annurev-arplant-043015-111641

Xu, X., Yang, H., Singh, S. P., Sharp, P. J., and Liu, Q. (2018). Genetic manipulation of non-classic oilseed plants for enhancement of their potential as a biofactory for triacylglycerol production. *Engineering* 4 (4), 523–533. doi: 10.1016/j.eng.2018.07.002

Yu, L., Fan, J., Yan, C., and Xu, C. (2018). Starch deficiency enhances lipid biosynthesis and turnover in leaves. *Plant Physiol.* 178 (1), 118–129. doi: 10.1104/pp.18.00539

Yu, S., Zhao, Q., Miao, X., and Shi, J. (2013). Enhancement of lipid production in low-starch mutants *Chlamydomonas reinhardtii* by adaptive laboratory evolution. *Bioresour. Technol.* 147, 499–507. doi: 10.1016/j.biortech.2013.08.069

Zaheer, K., and Akhtar, M. H. (2016). Potato production, usage, and nutrition-a review. *Crit. Rev. Food Sci. Nutr.* 56 (5), 711–721. doi: 10.1080/10408398.2012.724479

Zale, J., Jung, J. H., Kim, J. Y., Pathak, B., Karan, R., Liu, H., et al. (2016). Metabolic engineering of sugarcane to accumulate energy-dense triacylglycerols in vegetative biomass. *Plant Biotechnol. J.* 14 (2), 661–669. doi: 10.1111/pbi.12411

Zeeman, S. C., Kossmann, J., and Smith, A. M. (2010). Starch: its metabolism, evolution and biotechnological modification in plants. *Annu. Rev. Plant Biol.* 61, 209–234. doi: 10.1146/annurev-arplant-042809-112301

Zhai, Z., Keereetaweep, J., Liu, H., Feil, R., Lunn, J. E., and Shanklin, J. (2018). Trehalose 6-phosphate positively regulates fatty acid synthesis by stabilizing *WRINKLED1*. *Plant Cell* 30 (10), 2616–2627. doi: 10.1105/tpc.18.00521

Zhai, Z., Liu, H., Xu, C., and Shanklin, J. (2017). Sugar potentiation of fatty acid and triacylglycerol accumulation. *Plant Physiol.* 175 (2), 696–707. doi: 10.1104/pp.17.00828

Conflict of Interest: The authors declare that the research was conducted in the absence of any commercial or financial relationships that could be construed as a potential conflict of interest.

frontiers in Plant Science

REVIEW
published: 10 December 2019
doi: 10.3389/fpls.2019.01568

New Insights Into the Role of Seed Oil Body Proteins in Metabolism and Plant Development

Qun Shao, Xiaofan Liu, Tong Su, Changle Ma and Pingping Wang**

Shandong Provincial Key Laboratory of Plant Stress, College of Life Sciences, Shandong Normal University, Jinan, China

Oil bodies (OBs) are ubiquitous dynamic organelles found in plant seeds. They have attracted increasing attention recently because of their important roles in plant physiology. First, the neutral lipids stored within these organelles serve as an initial, essential source of energy and carbon for seed germination and post-germinative growth of the seedlings. Secondly, they are involved in many other cellular processes such as stress responses, lipid metabolism, organ development, and hormone signaling. The biological functions of seed OBs are dependent on structural proteins, principally oleosins, caleosins, and steroleosins, which are embedded in the OB phospholipid monolayer. Oleosin and caleosin proteins are specific to plants and mainly act as OB structural proteins and are important for the biogenesis, stability, and dynamics of the organelle; whereas steroleosin proteins are also present in mammals and play an important role in steroid hormone metabolism and signaling. Significant progress using new genetic, biochemical, and imaging technologies has uncovered the roles of these proteins. Here, we review recent work on the structural or metabolic roles of these proteins in OB biogenesis, stabilization and degradation, lipid homeostasis and mobilization, hormone signal transduction, stress defenses, and various aspects of plant growth and development.

Keywords: oil body intrinsic proteins, lipid metabolism, hormone signaling, stress responses, plant development

OPEN ACCESS

Edited by:
Xue-Rong Zhou, Commonwealth Scientific and Industrial Research Organisation, Australia

Reviewed by:
Ray J. Rose, University of Newcastle, Australia
Jay Shockey, United States Department of Agriculture, United States

****Correspondence:***
Changle Ma
machangle@sdnu.edu.cn
Pingping Wang
pingping.wang@sdnu.edu.cn

Specialty section:
This article was submitted to Plant Metabolism and Chemodiversity, a section of the journal Frontiers in Plant Science

Received: *25 September 2019*
Accepted: *08 November 2019*
Published: *10 December 2019*

Citation:
Shao Q, Liu X, Su T, Ma C and Wang P (2019) New Insights Into the Role of Seed Oil Body Proteins in Metabolism and Plant Development. Front. Plant Sci. 10:1568. doi: 10.3389/fpls.2019.01568

INTRODUCTION

Lipids are essential for all kingdoms of life because they are involved in a remarkably wide variety of cellular functions, including energy homeostasis, membrane remodeling, and cell signaling (Pyc et al., 2017). The cellular mechanisms of assembling, storing, and supplying lipids by forming intracellular lipid particles are relatively conserved in all eukaryotes, including yeast (Leber et al., 1994), insects (Zhang et al., 2010), mammals (Murphy, 2001), and plants (Bao et al., 2018), as well as prokaryotes (Wältermann et al., 2005);. Traditionally, these lipid particles have had a variety of names, including oil bodies (OB), oleosomes, spherosomes, lipid bodies, lipid droplets (LD), or lipid vesicles. In recent years, the terms OB or LD have been adopted by most laboratories. OBs are present in seeds, leaves, pollens, fruits, flowers, and roots of higher plants (angiosperms), the vegetative and reproductive organs of lower plants, the glands and adipose tissues of mammals, as well as in algae, fungi, nematodes, and bacteria (Huang, 2013; Shimada et al., 2018).

These organelles consist of a densely packed hydrophobic core of neutral lipids surrounded by a phospholipid monolayer decorated by three main classes of OB-associated proteins: oleosins, caleosins, and steroleosins. The acyl moieties of the phospholipid molecules face inward with the hydrophobic triacylglycerol (TAG) in the matrix and the hydrophilic phospholipid head groups

in the cytosol (Tzen et al., 1997). OBs in the seeds of plants are generally circular to ovoid with the average diameter of 0.5–2.5 μm, but the diameter of some OBs can be 2–3 times larger than 2.5 μm, such as in legume seeds (Tzen et al., 1993; Song et al., 2017). Recently, 3D reconstruction analysis showed that the volume of most OBs in *Brassica napus* seeds were less than 100 μm^3 (Yin et al., 2018).

OBs are highly dynamic organelles and are actively involved in many diverse physiological processes including membrane biogenesis supporting organelle or cell growth, diurnal regulation process, hormone signaling, and plant growth and development. OBs also act as a "sink" for toxic fatty acids which can be lethal to the cells (Pyc et al., 2017). The decomposition of OBs by proteases and lipases and the subsequent β-oxidation of the released fatty acids can provide carbon and energy during seed germination and post-germinative growth of the seedlings (Huang, 1996). As a result of their importance in plant physiology, seed OBs have been intensively studied in the past few decades, surpassing our knowledge in nonplant organisms.

The functions of OBs are dependent on three classes of OB intrinsic proteins: oleosins, caleosins, and steroleosins. These distinct structural OB proteins are associated with specific biological functions. The structural or metabolic roles of these proteins in the control of lipid store mobilization, OB degradation, hormone signal transduction, and stress defenses are discussed in this review.

OB INTRINSIC PROTEINS

Oleosin, Caleosin, and Steroleosin

OBs in the intact cells of a mature seed never coalesce or aggregate, even after long-term storage, because the entire surface of an OB is covered by proteins (Leprince et al., 1998). The most abundant protein constituents are the structural alkaline proteins termed oleosins. Oleosins are also located in other tissues such as the tapetum and the external surface of pollen grains (Kim et al., 2002). They have a molecular mass of 15–50 kDa, depending on the isoform and plant species in which they occur (Tzen et al., 1990; Jolivet et al., 2009).

The oleosin gene was first cloned from maize (Vance and Huang, 1987). In *Arabidopsis*, 16 oleosin proteins have been identified, including five seed-type oleosins, eight anther-type oleosins, and three seed-and-anther type oleosins (**Table 1**). The most abundant oleosin in *Arabidopsis* seeds is oleosin-1 (OLE1), followed by oleosin-2 (OLE1) (D'Andrea, 2016; Shimada et al., 2008). Seed-type oleosins are involved in regulating both OB size and seed germination. Anther-type oleosins have glycine-rich domains not found in seed-type oleosins and function in stabilizing pollen OBs and forming pollen and the pollen coat (Mayfield et al., 2001; Kim et al., 2002).

Another major group of OB structural proteins are the caleosins. Caleosin was first reported (named as Sopl) as a minor constituent in purified OBs from sesame (*Sesamum indicum*) seeds. Their name arose from their ability to bind calcium and their oleosin-like structures (Chen et al., 1998; 1999). Eight caleosin genes (*AtCLO1-AtCLO8*) have been found in the *Arabidopsis* genome (**Table 1**) (Hanano et al., 2006; Shen et al., 2014). Among them, *AtCLO1* and *AtCLO2* are preferentially expressed in developing embryos and seeds during seed maturation and the first days following germination. *AtCLO5* expression level is low but detectable in buds. *AtCLO3* is mainly expressed in above-ground tissues, whereas *ATCLO4* is expressed in the vascular bundles in all major plant tissues, as well as in guard cells and germinating seeds (Aubert et al., 2010; Kim et al., 2011; Shen et al., 2014). Expression data for the other caleosin genes are still scarce.

In contrast with oleosins, caleosins are present in more primitive species, such as fungi and single-celled algae (Charuchinda et al., 2015), whereas oleosins are only present in more recent higher plant species (Huang et al., 2009). Because of these observations, oleosin may have been derived from caleosin, which may represent a more ancient structural OB protein in plants, and has become more specifically associated with OB formation and maintenance (Jiang and Tzen, 2010).

The earliest identified plant steroleosins were Sop2 and Sop3 from sesame, named steroleosin-A and -B, respectively. They are homologous proteins with sterol-binding and sterol-coupling dehydrogenase activity (Chen et al., 1998; Lin et al., 2002). Later, the homologous steroleosin encoded by At5g50600 was purified from *Arabidopsis* seed OBs (Jolivet et al., 2004). This protein, with a high degree of similarity to Sop2, exhibits hydroxysteroid dehydrogenase (HSD) activity and belongs to the short-chain steroid dehydrogenase reductase superfamily (SDR) which is involved in sterol-regulated signal transduction in diverse organisms. As a result, this protein is named AtHSD1 (d'Andréa et al., 2007). There are eight putative steroleosin homologs in the *Arabidopsis* genome, including two identical copies of *AtHSD1*, two identical copies of *AtHSD4*, and four other homologs. Sequence alignment showed that the promoter, coding sequence, and terminator of two copies of the AtHSD1 gene, and two copies of the AtHSD4 gene are completely identical at the nucleotide level (**Table 1**) (Li et al., 2007).

Unlike oleosin and caleosin proteins which are specific to plants, OB-associated sterol dehydrogenases are also present in mammals. However, phylogenic analysis indicates that plant 17β-HSDs display only 24% identity with those corresponding sequences in mammals. These enzymes have been demonstrated to be important in steroid hormone metabolism and signaling in both plants and mammals (d'Andréa et al., 2007).

Structure of OB-Associated Proteins

All oleosins and caleosins have three regions: a hydrophilic N-terminal domain, a specific and highly conserved hydrophobic central domain and a hydrophilic C-terminal α-helical domain (Tzen and Huang, 1992). The central domain forms a hairpin-like structure composed of antiparallel β strands connected by a proline knot motif and is responsible for OB localization. The N- and C-terminals are exposed to the cytoplasm, and the central domain anchors the protein in the OB membrane (Huang, 1996; Huang and Huang, 2017). In contrast to oleosin, caleosin has a significantly larger N-terminal hydrophilic domain containing an EF-hand calcium binding motif and several potential

TABLE 1 | Three OB-associated proteins in *Arabidopsis thaliana*

TAIR locus	Description	Putative function	Reference
Oleosin			
AT4G25140	OLE1, OLEO1, OLEOSIN 1	Major seed OB protein, involved in seed lipid accumulation and freezing tolerance of seeds.	van Rooijen et al., 1992; Siloto et al, 2006
AT5G40420	OLE2, OLEO2, OLEOSIN 2	Major seed OB protein, involved in seed lipid accumulation and freezing tolerance of seeds.	Zou et al.,1995; Shimada et al,2008
AT3G27660	OLEO3, OLEOSIN3	Seed OB protein, involved in seed lipid accumulation and OB degradation.	Kirik et al., 1996; Deruyffelaere et al., 2015
AT3G01570	Oleosin 4, OLE4	Major seed OB protein, involved in seed lipid accumulation and freezing tolerance of seeds.	Kim et al., 2002; Shimada et al, 2008
AT5G51210	Oleosin 5, OLE5	Minor seed OB oleosin, a possible role for these oleosins in the control of OB dynamics.	Kirik et al., 1996; Deruyffelaere et al., 2015
AT5G07510	ATGRP14, glycine rich protein 14	A pollen coat protein. No report of function.	Mayfield and Preuss, 2000
AT5G07540	ATGRP17, glycine rich protein 17	A pollen coat protein. No report of function.	de Oliveira et al., 1993
AT5G07530	ATGRP17, glycine rich protein 17	A glycine rich protein containing oleosin domain, found on mature pollen coat, have a role in initiating pollination.	Mayfield and Preuss, 2000
AT5G07520	ATGRP18, glycine rich protein 18	A pollen coat protein. No report of function.	de Oliveira et al., 1993
AT5G07550	ATGRP19, glycine rich protein 19	A glycine rich pollen coat protein. No report of function.	de Oliveira et al., 1993
AT5G07560	ATGRP20, glycine rich protein 20	A glycine rich protein expressed specifically in the florets. No report of function.	Mayfield et al., 2001
AT3G18570	Oleosin family protein	A protein expressed in both maturing seeds and florets. No report of function.	Kim et al., 2002
AT2G25890	Oleosin family protein	A protein expressed in both maturing seeds and florets . No report of function.	Kim et al., 2002
AT1G48990	Oleosin family protein	A protein expressed in both maturing seeds and florets. No report of function.	Kim et al., 2002
AT5G07600	Oleosin family protein	A oleosin expressed specifically in the florets (tapetum). No report of function.	Kim et al., 2002
AT5G61610	Oleosin family protein	A oleosin expressed specifically in the florets (tapetum). No report of function.	Kim et al., 2002
Caleosin			
AT4G26740	AtCLO1, ATPXG1, ATS1, CLO1	A caleosin in seed OBs. Catalyze hydroperoxide-dependent mono-oxygenation reactions and sensitive to some hormones.	Naested et al., 2000; Hanano et al., 2006
AT5G55240	AtCLO2, ATS2, ATPXG2	A seed caleosin with peroxygenase activity has roles in dormancy or germination of seeds.	Hanano et al., 2006
AT2G33380	AtCLO3, ATPXG3, RD20	A caleosin expressed in various organs acts as a peroxygenase involved in oxylipin metabolism during stress and sensitive to various stresses.	Aubert et al., 2010; Blée et al., 2014
AT1G70670	AtCLO4, ATPXG4	A stress-responsive and caleosin-like protein mainly expressed in leaf and was sensitive to some stresses in root and cell culture.	Hanano et al., 2006; Kim et al., 2011; Blée et al., 2012
AT1G23240	AtCLO5, ATPXG5	A caleosin was mainly expressed in bud.	Hanano et al., 2006
AT1G70680	AtCLO6	Caleosin family protein. No report of function.	Shen et al., 2014
AT1G23250	AtCLO7	Be without conserved EF-hand and might lost the ability to bind calcium	Shen et al., 2014
AT5G29560	AtCLO8	No report	Shen et al., 2014
Steroleosin			
AT5G50600 / AT5G50700	AtHSD1	A hydroxysteroid dehydrogenase in seed OBs acts as a $NADP^+$-dependent 11β-,17β-hydroxysteroid dehydrogenase/17β-ketosteroid reductase.	Jolivet et al., 2004; d'Andréa et al., 2007
AT3G47350	AtHSD2	A putative hydroxysteroid dehydrogenase (HSD)	Li et al., 2007
AT3G47360	AtHSD3	A putative hydroxysteroid dehydrogenase (HSD).	Li et al., 2007
AT5G50590/ AT5G50690	AtHSD4	A putative hydroxysteroid dehydrogenase (HSD).	Li et al., 2007; Baud et al., 2009
AT4G10020	AtHSD5	A putative hydroxysteroid dehydrogenase (HSD).	Li et al., 2007
AT5G50770	AtHSD6	A putative hydroxysteroid dehydrogenase (HSD).	Li et al., 2007

phosphorylation sites within the C-terminal hydrophilic domain. Both the N- and C-terminal regions of caleosin also contain heme-binding sites with conserved histidine residues that together coordinate the binding of heme prosthetic groups (**Figure 1**) (Hanano et al., 2006; Chapman et al., 2012).

Unlike oleosin and caleosin, steroleosin possesses a distinctive structure containing an N-terminal hydrophobic OB-anchoring segment and a soluble sterol-binding dehydrogenase/reductase domain, located in the cytosol. A unique proline knob motif is in the middle of the steroleosin N-terminus, corresponding

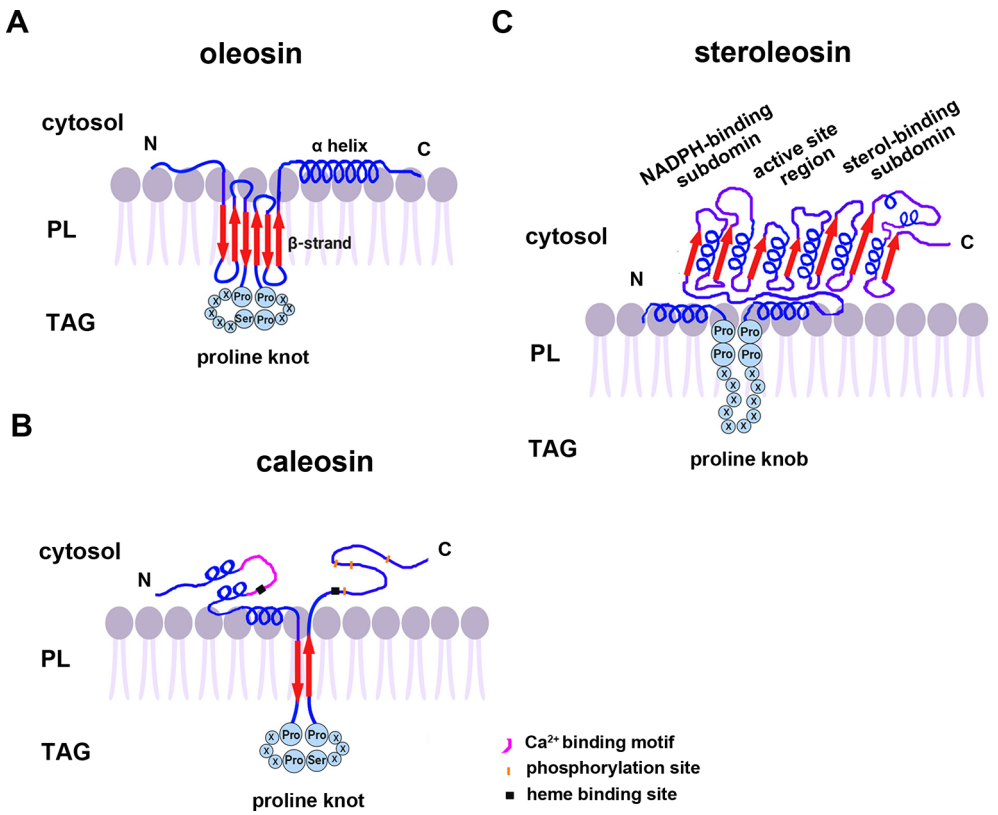

FIGURE 1 | A model of the secondary structure organizations of **(A)** oleosin, **(B)** caleosin, and **(C)** steroleosin on the surface of plant seed oil bodies. Predicted structures of the proline knot or proline knob motif are shown in all three proteins. The model is mainly based on information from Chen et al. (1999); Hanano et al. (2006); d'Andréa et al. (2007), and Tzen (2012). TAG, Triacylglycerol; PL, phospholipid.

to the hydrophobic segment that is presumably responsible for association with the OB phospholipid monolayer. The core structure of the sterol-binding dehydrogenase/reductase domain contains a conserved NADPH-binding subdomain, a NSYK conserved active site region and a divergent sterol-binding subdomain (**Figure 1**) (Lin et al., 2002; d'Andréa et al., 2007).

Cotranslational and posttranslational modifications of OB-associated proteins may elevate their structural stability and prevent ubiquitination and degradation of OBs. Mass spectrum analyses showed that the first methionine in the N-termini of nascent oleosin and caleosin isoforms from sesame seed OBs is removed and the following alanine is acetylated. N-terminal-acetylation is catalyzed by several distinct N-terminal acetyltransferases (NATs) in eukaryotes—NatA-NatF. N-termini with small amino acid residues in the second position (such as Met Ser-, Met Ala-, like oleosin and caleosin, Met Thr-, Met Val-), are mostly processed by methionine aminopeptidase (MAP), and the resulting newly generated N-termini may be acetylated by NatA (Arnesen, 2011; Ree et al., 2018). However, candidates for the proposed acetyltransferase activities that modify the N-termini of oleosins have yet not been reported. Additionally, deamidation of a glutamine residue is also found in the N-terminus of oleosin. Deamidation of glutamine residues have been considered to be the most common post-translational modification occurring in living systems and to be nonenzymatic reactions (Li et al., 2010). This posttranslational modification introduces more negative charges to the protein surface and may reinforce OB stability by preventing aggregation under physiological conditions. Amino acid sequence analysis shows that both steroleosin isoforms (Sop2 and Sop3) possess a free initial methionine residue at their N-termini. They also possess an N-terminal sequence responsible for endoplasmic reticulim (ER) targeting *via* the signal-recognition particle (SRP) dependent pathway which anchors to OBs. No ER targeting signal sequences are present in the N-termini of caleosin or oleosin isoforms. Because of this signal sequence, no posttranslational cleavage or modification occurs in the N-termini of the mature steroleosins (Lin et al., 2005).

OLEOSINS FUNCTION DURING SEED MATURATION AND GERMINATION

Oleosins are only found in plants, including green algae (Huang, 2013). However, in mammals and insects, a different set of abundant OB proteins, such as perilipins (PLINs) (Sztalryd and Kimmel, 2014) that are absent in plants, serve similar functions. Although the lipid bodies in yeast, such as *Saccharomyces*

cerevisiae, are functionally similar to OBs in plant seeds, no oleosin homologs are present (Jacquier et al., 2013).

Oleosins have a variety of confirmed functions. They contribute to the stability and resolubility of OBs during seed (and pollen grain) desiccation, regulate OB size and viability in overwintering seeds, and are important for lipid mobilization during seed germination (**Figure 2**) (Schmidt and Herman, 2008; Shimada et al., 2008; Wu et al., 2010; Miquel et al., 2014).

Oleosins Affect the Stability and Size of OBs

Oleosins stabilize OBs by creating a negative charge on the OB surface which prevents OB coalescence due to steric hindrance and electrical repulsion (Tzen and Huang, 1992). OB reconstitution showed that oleosins are essential to avoid coalescence and important for maintaining the physical stability of OBs (Deleu et al., 2010). Oleosin concentrations have been reported to correlate with OB size in several oil plants including rape, mustard, cotton, flax, maize, peanut, sesame, olive, and avocado (Tzen et al., 1993; Ting et al., 1996). The size of OBs is inversely proportional to the concentration of oleosin: high-oil seeds of maize with relatively low oleosin levels have large OBs, while low-oil seeds of maize with high oleosin levels have small OBs (Ting et al., 1996). Similarly, the avocado mesocarp cell, which does not express oleosin, has only one very large OB (20μm in diameter) (Platt-Aloia and Thompson, 1981). Several studies in *Arabidopsis* and rice have shown that oleosin depletion caused by RNA interference (RNAi) leads to the appearance of unusually large and structurally abnormal OBs (Siloto et al., 2006; Miquel et al., 2014).

In mature *Arabidopsis* seeds, OLE1 and OLE2 accumulate at higher levels than OLE3 and OLE4, whereas OLE5 has the lowest abundance (Siloto et al., 2006; Miquel et al., 2014). Shimada et al. investigated the physiological function of oleosins using an oleosin-deficient mutant series of *A. thaliana* and found that oleosin levels affected germination and the freezing tolerance of seeds. Among the mutants used, the double *Arabidopsis* mutant *ole1 ole2* has the lowest levels of oleosins and hardly germinates under normal conditions. In addition, freezing treatment followed by imbibition at 4°C accelerates the fusion of OBs and generates acentric nuclei (irregularly shaped nuclei found on the periphery of seed cells) leading to seed mortality and inhibition of seed germination in the *ole1 ole2* mutant. Thus, oleosins increase seed viability and maintain seed germination by preventing abnormal fusion of OBs during overwintering (Shimada et al., 2008).

Oleosins Regulate Lipid Metabolization

Oleosins play an important role in regulating the biosynthesis, metabolization, and mobilization of lipids during seed maturation and germination (Parthibane et al., 2012). Increasing evidence suggests oleosins affect the lipid levels of plant organs. In *S. cerevisiae*, phosphatidic acid phosphohydrolase (PAH1) catalyzes the rate-limiting step for TAG formation, the

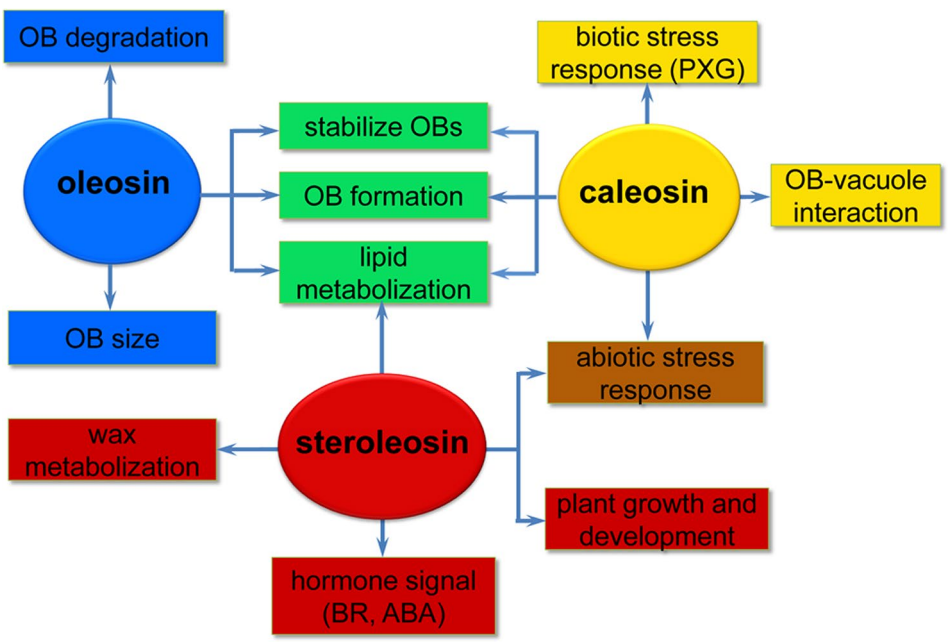

FIGURE 2 | A simplified overview of the putative roles of the three oil body (OB) intrinsic proteins in various processes of plant development. Oleosins (blue) mainly act as structural proteins stabilizing OBs and are involved in lipid metabolization during seed germination and seedling growth. Caleosins (orange) play important roles in biotic and abiotic stress responses through their peroxygenase (PXG) activities. Steroleosins (red) are involved in regulating plant growth and development mainly *via* an unknown mechanism by which the proteins interact with hormones such as brassinosteroids (BRs) and abcisic acid (ABA). Green indicates processes that both oleosin and caleosin are involved in. Brown indicates processes that both caleosin and steroleosin are involved with.

dephosphorylation of phosphatidic acid to diacylglycerol (DAG), which play a direct role in OB biogenesis (Skinner et al., 2009). OB numbers of yeast cells lacking PAH1 (*pah1* mutant) reduce by more than 60%. PAH1, probably working through DAG, controls the formation of OBs (Adeyo et al., 2011). Ectopic expression of *A. thaliana* oleosin1 (OLE1) in *pah1* cells not only increases the levels of newly synthesized neutral lipids including TAG and steryl esters (STE), but also increases OB formation. OBs are formed from membranes enriched in neutral lipids by promoting the sequestration of neutral lipids within the ER bilayer and protecting the TAG pool from hydrolysis by lipases (Jacquier et al., 2013). It is well known that diacylglycerol *O*-acyltransferase (DGAT1) is a critical enzyme involved in TAG synthesis *via* the acyl-CoA-dependent pathway in developing seeds (Chapman and Ohlrogge, 2012). Winichayakul et al. coexpressed *Arabidopsis* DGAT1 and a synthetically stabilized oleosin (cysteine [Cys]-oleosin) from sesame seeds in *Arabidopsis* and *S. cerevisiae*. Both transgenic plants and yeast cells produced significantly increased neutral lipid levels in vegetative organs and yeast cells than in the respective wild type cells or when expressing DGAT1 alone. The increasing neutral lipids then elevates CO_2 levels in the chloroplast, leading to a higher CO_2 fixation rate and an increase in biomass production (Winichayakul et al., 2013). Overexpression of *Arabidopsis* seed OLE1 induces elevated leaf TAG levels in transgenic *Arabidopsis* plants. TAG content is increased up to sevenfold compared to wild type (Fan et al., 2013). Vanhercke et al. also obtained the similar results. They found that simultaneous expression in tobacco of the *A. thaliana* transcription factor WRI1, DGAT, and the *S. indicum OLEOSIN* gene caused TAG levels in tobacco leaves to dramatically increase (more than 15% of the dry weight) without a detrimental effect on plant development or seed viability (Vanhercke et al., 2014). Four *Brassica napus* oleosin genes were overexpressed in *Arabidopsis* increased the linoleic acid content (13.3% at most) and the seed weight. In the meanwhile, the eicosaenoic acid content decreased by 11% in seeds of transgenic lines (Chen et al., 2019). The experimental evidence confirmed that oleosins play important roles in regulating lipid metabolization.

Oleosins Play an Important Role in OB Formation and Degradation

In seeds, oleosins are also involved in OB formation and degradation (Schmidt and Herman, 2008; Quettier and Eastmond, 2009). During OB biogenesis, oleosin is first integrated into the ER membrane before it is targeted to the OBs (Ting et al., 1997; Jacquier et al., 2013).

OBs are structurally and functionally conserved across species. Several studies demonstrated that plant oleosins from maize (*Zea mays* L.), sunflower, and *B. napus* are correctly targeted to endogenous OBs when heterologously expressed in *S. cerevisiae* or mammalian cells (Ting et al., 1997; Beaudoin et al., 2000; Hope et al., 2002). Thus, because of the convenience of using yeast cells, expression of plant oleosins in yeast cells is helpful to investigate the possible function of these proteins in neutral lipid homeostasis and OB biogenesis. In *S. cerevisiae*, four enzymes, including acyl-CoA: sterol acyltransferases (Are1 and Are2) which produce STE, lecithin cholesterol acyltransferase (LCAT)-related protein (Lro1), and acyl-CoA: diacylglycerol acyltransferase (Dga1) which produces TAG, are involved in synthesis of neutral lipids and LD biogenesis (Oelkers et al., 2002; Czabany et al., 2007). In quadruple yeast mutant cells lacking OBs due to the deletion of all four genes, some OB-localized membrane proteins, such as Erg6 (an enzyme of the ergosterol biosynthetic pathway) or Dga1, are mislocalized in the ER bilayer. Induction of neutral lipid synthesis in these mutants leads to the formation of OBs and a concomitant relocalization of the mislocalized OB proteins from the ER onto OBs (Jacquier et al., 2011). Similarly, GFP-tagged versions of OLE1 from *A. thaliana* were expressed in *S. cerevisiae* and showed proper targeting of the protein to OBs. In wild-type yeast cells, GFP-OLE1 induces OB formation, but in yeast mutant cells lacking OBs GFP-OLE1 localizes to the ER membrane and is significantly less stable and rapidly degraded (Jacquier et al., 2013). These observations suggest that oleosins have high affinity for neutral lipids and phospholipids, probably due to the extraordinary architecture of oleosins which is ideal for localization within OBs.

During plant seed germination and seedling growth, oleosins are hydrolyzed by endogenous proteases as the initial step in lipase-induced TAGs mobilization. The hydrolysis of oleosins has been observed in many plant species. To date, the reported enzymes involved in this process include the ubiquitin/proteasome system, the thioredoxin-regulated cysteine protease, and the aspartic protease, among others.

In plants, degradation of most intracellular proteins is *via* ubiquitination of the respective proteins and subsequent digestion by the proteasome (Sorokin et al, 2009). Ubiquitination of oleosins was first reported in young sesame seedlings. Ubiquitinated oleosin and caleosin were detected after seed imbibition by mass spectrometric analyses and further immunological detection using antibodies against ubiquitin (Hsiao and Tzen, 2011). Using proteomic and immunochemical approaches, Deruyffelaere et al. revealed the physiological regulation of oleosin ubiquitination during seed germination and defined the topologies of the ubiquitin attached to oleosins. OLE1-OLE5 are hydrolyzed sequentially by proteases just prior to lipid degradation in germinated seeds, concomitant with several posttranslational modifications of the oleosins. During this process, OLE5 degraded first, followed by OLE2 and OLE4, and then OLE1 and OLE3. The OLE5 and 8 kDa proteolytic fragment of OLE2 are phosphorylated, while OLE1-OLE4 are ubiqutinated at the onset of lipid degradation. The ubiquitination topology of the oleosins is complex and differs for the various oleosins, suggesting distinct specific degradation pathways (Deruyffelaere et al., 2015). Recently, two research teams presented important insights into the mechanism regulating the extraction and turnover of oleosins in plants. Two key components, PUX10 (a member of the plant ubiquitin regulatory X (UBX)-domain containing protein family) and CDC48A (the AAA ATPase, Cell Division Cycle 48) were found. PUX10 localizes to OBs and binds to the ubiquitinated oleosins *via* its hydrophobic domain and interacts with ubiquitin and CDC48A *via* its UBA and UBX domains, respectively. As an adaptor, PUX10 recruits CDC48A to ubiquitinated oleosins, leading to dislocation of oleosins from

OBs *via* the segregase activity of CDC48A (Deruyffelaere et al., 2018; Kretzschmar et al., 2018).

Trx h (thioredoxin h) activates a thiol-protease to degrade the oleosin coat of OBs in sunflower (*Helianthus annuus* L.) seedlings (Babazadeh et al., 2012). In soybean, series analysis of proteases, including analyzing the specificity, optimal pH, and temperature, suggest that OB extrinsic proteins, probably two thiol proteases of the papain family, Bd 30K and P34, originated during seed maturation, are responsible for the hydrolysis of 24 and 18 kDa oleosins (Chen et al., 2014). Similarly, a two-chain (32 and 9 kDa) aspartic protease was identified from the crude extract of peanut OBs. This enzyme shows high affinity for OBs and hydrolyzes both OB intrinsic proteins, such as oleosin, caleosin, steroleosin, and extrinsic proteins (Chen et al., 2018). However, these studies did not provide direct evidence for the interaction between endogenous proteases and oleosins, and the proteases for the oleosin hydrolysis were also not well-known.

Oleosins are involved in several OB functions. In addition to being the main structural protein to maintain OB stability, oleosins are important for the biogenesis and dynamics of the organelle. However, the precise mechanism underlying oleosins' functions, especially in OB degradation, and how oleosins interact with other proteins require further, more extensive research.

CALEOSIN FUNCTIONS IN PLANT

As the OB-associated proteins, besides being confined to the OB surface in plant seeds, caleosins have also been detected in vegetative tissues where they are associated with the endoplasmic reticulum, the vacuole and the envelope of chloroplasts (Hernandez-Pinzon et al., 2001; Carter et al., 2004; Partridge and Murphy, 2009). These diverse localizations suggest that distinct caleosins may fulfill various physiological functions in plant growth, development, and regulation of plant-environment interactions (**Figure 2**).

Caleosins Affect the Stability of OBs and Lipid Metabolization

Caleosins are also considered structural stabilizers of OBs. Analyses of lower plant species such as cycad (*Cycas revoluta*) confirm that OBs from megagametophytes are primarily associated with caleosin, while oleosin is absent (Jiang et al., 2009; Jiang and Tzen, 2010). In another case, stable artificial OBs composed of TAG and phospholipids can be stabilized by the addition of caleosin alone, in the absence of oleosin (Chen et al, 2004). Moreover, knockdown of a 24 kDa oleosin using RNAi in soybean seed OBs is accompanied by an increased caleosin content, reflecting a compensatory mechanism of caleosin to maintain OB integrity (Schmidt and Herman, 2008).

Caleosin is involved in lipid metabolization and biogenesis of OBs. In *Arabidopsis*, AtCLO1 is exclusively expressed during seed development and its expression is not affected by exogenous abcisic acid (ABA) or osmotic stresses in vegetative tissues, indicating its seed-specific roles (Naested et al., 2000). Studies from two *Arabidopsis Atclo1* mutants provide evidence for a role of caleosin in lipid degradation and trafficking in OBs during seed germination. Embryos from germinating *Atclo1* mutant seeds exhibit a significant delay in the breakdown of storage lipid and display distorted vacuole morphology, abnormal internalization of vacuole membranes, and a significant decrease in OB-vacuole interactions. These results indicate that caleosin participates in the interactions between OBs and vacuoles that affect breakdown of OBs during germination (Poxleitner et al., 2006).

Heterologous AtCLO1 expression in yeast causes accumulation of OB neutral lipids, resulting in larger and more abundant OBs containing more fatty acids and steryl esters (Froissard et al., 2009). However, the impact of heterologous expression of caleosin versus oleosin in yeast is distinct, with oleosin expression inducing normal OB formation, and expressed oleosins were properly targeted to OBs (Ting et al., 1997; Jacquier et al., 2013). Thus, caleosin and oleosin play important but non-redundant roles in OB biogenesis.

The Putative Role of Caleosins in Stress Responses

The Ca^{2+}-binding EF-hand motif in the N-terminus of caleosins is indicative of the protein's role in environmental adaptation. Calcium not only serves as a necessary nutrient for plant growth and development but also acts as one of the most important secondary messengers in many processes, such as cell division, apoptosis, polarity formation, photosynthesis, and stress resistance (Yang et al., 2017; Zheng et al., 2017; Jin et al., 2018). AtCLO3 [also designated RESPONSIVE TO DEHYDRATION20 (RD20)], a leaf caleosin isoform with Ca^{2+}-dependent protein kinase activity, is strongly induced by many abiotic stresses such as drought, high salinity, and ABA, suggesting this protein may participate in stress signal transduction (Aubert et al, 2010; Aubert et al., 2011; Blée et al., 2014). Consistent with this idea, *AtCLO3* knock-out plants show enhanced stomatal opening and reduced drought tolerance indicating that AtCLO3 plays an important role in the drought response by controlling stomatal aperture (Aubert et al., 2010). The expression of AtCLO4, another OB-associated caleosin in *Arabidopsis*, is down-regulated by exogenous ABA exposure and salt stress. The *atclo4* mutant is hypersensitive to ABA during seed germination and shows increased drought tolerance in the adult stage. Exogenous ABA treatment in the *atclo4* mutant leads to increased expression of some ABA-dependent regulatory genes, such as *ABF3* and *ABF4*. Experimental data suggest that AtCLO4 functions as a negative regulator in ABA signaling and has important roles in the plant's response to environmental stresses, in addition to its possible roles in seed development and germination in *Arabidopsis* (Kim et al., 2011).

The presence of several heme-binding motifs in caleosin indicates that caleosins can bind heme and possess peroxygenase (PXG) functionality. In plant, peroxygenases catalyze hydroxylation and epoxidations of unsaturated fatty acids by transferring one oxygen atom from a hydroperoxide to the corresponding substrate, thus oxidizing it (Blée et al., 2012). Peroxygenase is also involved in the biosynthesis of plant oxylipins, a large family of oxidized fatty acids and

metabolites originating from polyunsaturated fatty acids (PUFAs). Formation of oxylipins is mainly initiated by α-dioxygenases (α-DOX) or lipoxygenases (LOX) (Lòpez et al., 2011). α-DOX converts PUFAs into highly reactive 2-hydroperoxyoctadecatrienoic acids, which can be converted into the corresponding 2-hydroxyoctadecatrienoic acid or decomposed nonenzymatically into CO_2 and shortened aldehyde derivatives (Hamberg et al., 2003). LOX catalyzes oxygenation of unsaturated fatty acids, yielding the corresponding fatty acid hydroperoxides, which are then reduced by peroxygenases into the corresponding fatty acid hydroxides (FAOH). Such oxylipins play significant roles in plant defense against pests and pathogens by inducing defense genes, regulating cell death or acting directly through their antimicrobial properties (Prost et al., 2005; Lòpez et al., 2011). Some caleosins, such as AtCLO1-4 from *Arabidopsis*, have been identified as calcium-binding heme-oxygenases with peroxygenase activity (Partridge and Murphy 2009; Kim et al., 2011).

Purified PXG (a caleosin from oat seed OBs) and crude extracts of yeast expressing the recombinant AtCLO1, AtCLO2, and EFA27 (a caleosin from rice) proteins were all able to perform co-oxidation reactions typical of peroxygenase, such as oxidizing thiobenzamide to its sulfoxide and oleic acid into 9,10-epoxy-stearate (Hanano et al., 2006).

In addition to induction by abiotic stresses, the expression of AtCLO3 is also enhanced by pathogens, suggesting a role in biotic stress responses as well (Shimada et al., 2014). The recombinant protein obtained from *S. cerevisiae* expressing the peroxygenase AtCLO3 was confirmed to possess hydroperoxide reductase activity, leading to the formation of endogenous FAOH from hydroperoxides of unsaturated fatty acids. Arabidopsis plants overexpressing AtCLO3 also accumulate 13-hydroxy-9,11,15-octadecatrienoic acid, a linolenate-derived hydroxide. These FAOHs confer tolerance to oxidative stress by decreasing the accumulation of reactive oxygen species (ROS) and minimizing cell death (Blée et al., 2014). Microarray analysis in wild type plants showed that AtCLO3 is coexpressed with genes involved in the biosynthesis of very long chain fatty acids (VLCFA), components of seeds, and cuticular waxes. This experiment revealed that, compared to control plants, *Arabidopsis* overexpressing AtCLO3 exhibit an increased proportion of VLCFA in fatty acid composition of the seeds and contain higher amounts of alkanes and aldehydes in leaf cuticular waxes. As a result, altering the levels of these leaf cuticle wax components increases resistance to the fungus *Alternaria brassicicola* (Hanano et al., 2015). Shimada et al. observed that α-DOX1 (a leaf OB protein with α-dioxygenase activity) and AtCLO3 work together to catalyze coupled reactions to produce 2-hydroxyoctadecanoic acid (2-HOT), which has antifungal activity against members of the genus *Colletotrichum*. Infection with *C.higginsianum* induces 2-HOT production and promotes formation of AtCLO3 and α-DOX1-positive OBs in the area around the site of infection. This study provides evidence of leaf OB function in plant defense *via* production of a phytoalexin under pathological conditions (Shimada et al., 2014; Shimada and Hara-Nishimura, 2015). Thus, the peroxygenase activities of these proteins were involved in the oxylipin signaling pathway and plant defense responses.

To date, among the Arabidopsis caleosin-like genes, possible roles have only been reported for AtCLO1, AtCLO3, and AtCLO4. The roles of the other caleosins remain largely uncharacterized.

HSD EXPRESSION AND FUNCTION IN PLANT

Compared with oleosin and caleosin proteins, HSDs are only minor components of OBs in oilseed plants and thus less emphasis has been placed on investigating steroleosins (d'Andréa et al., 2007). Unlike oleosin or caleosin, steroleosin does not play a key role in maintaining the structural stability and integrity of OBs. When stabilized only by recombinant steroleosin fusion proteins (F-steroleosin or DS steroleosin), artificial pine OBs lacking oleosin and caleosin are relatively unstable and larger than native OBs (Pasaribu et al., 2016). However, steroleosins play important roles in plant development and stress responses *via* the enzymatic activity of the HSDs and hormone signaling (**Figure 2**).

Enzyme Activity and Substrate Analysis of HSDs

OBs from different forms of life have been reported to possess HSD activity and to be involved in the metabolism of steroids. However, there have only been a few reports on the presence of active HSDs in plants. Studies suggest that *Arabidopsis* and *S. indicum* seed OBs contain 11β- and 17β-HSD activities carried out by AtHSD1, and Sop2 and Sop3, respectively (Lin and Tzen, 2004; d'Andréa et al., 2007; Li et al., 2007).

Overexpressed Sop2 and Sop3 proteins are capable of oxidizing estradiol and corticosterone, thus exhibiting 17β- and 11β-HSD activities. However, they possess different sterol selectivities and $NADP^+$ specificities. Sop2 exhibits higher dehydrogenase activity to estradiol than to corticosterone in the presence of either $NADP^+$ or NAD^+, and higher activity is detected using $NADP^+$ than NAD^+ as a cofactor when comparing the the same sterol substrate. In contrast, Sop3 is active and shows similar dehydrogenase activities to both examined sterols, but only in the presence of $NADP^+$. Therefore, these two steroleosins may conduct different biological functions during the formation or degradation of seed OBs (Lin and Tzen, 2004).

Either within purified OBs from *A. thaliana* seeds or as a purified bacterially expressed chimeric enzyme *in vitro*, AtHSD1 is capable of catalyzing $NADP^+$-dependent dehydrogenation of 11β- and 17β- hydroxysteroids, including cortisol, corticosterone, and estradiol, indicating 11β- and 17β- HSD activity. Purified OBs also exhibit NADPH-dependent 17β-ketosteroid reductase activity by which estrone is converted into estradiol. $NADP^+$, rather than NAD^+, is the preferred cofactor for AtHSD1 (d'Andréa et al., 2007). OsHSD1 also displays $NADP^+$ and NAD^+-dependent dehydrogenase activity when using either estradiol or corticosterone as substrates, but shows higher dehydrogenase activity with NAD^+ than $NADP^+$ (Zhang et al., 2016). Steroleosin from *P. massoniana* OBs also exhibits sterol dehydrogenase activity with estradiol and corticosterone as substrates in the presence of $NADP^+$ (Pasaribu et al., 2016).

AtHSD1 did not possess 3β-HSD activity as it cannot convert either cholesterol into 4-cholestene-3-one, or dehydroepiandrosterone (DHEA) into 4-androstene-3,17-dione (4AD) under the experimental conditions. Thus, 3β-hydroxysterols are likely not substrates for AtHSD1, suggesting AtHSD1 might belong to the 17β-HSD superfamily (d'Andréa et al., 2007). 3β-HSD activity of HSDs from other plants has also not yet been found.

HSDs' Possible Role in Plant Growth and Development

AtHSD1 expression is tissue specific and is strongly expressed in the above-ground parts of seedlings, especially vascular tissues, and is weakly expressed in root tissues. It has also been observed in the bud and silique pedicels (Li et al., 2007). *AtHSD1* mRNA accumulation dramatically increases during seed and silique maturation, decreasing sharply during late maturation and the early germination process, resulting in full disappearance in fully germinated plantlets and in the vegetative organs and flowers of plants. AtHSD1 protein expression appears to be slightly delayed compared to mRNA accumulation as protein levels remain almost stable during the maturation phase and early germination (Baud et al., 2009). The 5' region of the *AtHSD1* gene contains two RY motifs that are recognized by LEAFY COTYLEDON2 (LEC2) and FUSCA3 (FUS3) B3 domain proteins (Kroj et al., 2003; Braybrook et al., 2006). These proteins are transcriptional regulators that induce the expression of oleosin, caleosin and certain genes encoding key enzymes involved in fatty acid (FA) biosynthesis and oil accumulation in developing leaves and seeds (Guo et al., 2013; Tang et al., 2018). Therefore, *AtHSD1* tissue specific expression seems to be controlled largely at the transcriptional level, with LEC2 being involved in the transcriptional activation of *AtHSD1*.

Both a loss-of-function *hsd* mutant produced by RNAi and transgenic *Arabidopsis* plants overexpressing *AtHSD1* (AOHSD) have been used to analyze the function of *AtHSD1*. Compared to wild type plants, AOHSD plants show a series of phenotypes including reduced seed dormancy, thicker stems and increased growth, branching, flower production, and seed yield. Similarly, the increased growth phenotype found in AOHSD plants is also observed in transgenic *B. napus* plants overexpressing *AtHSD1*. Accordingly, the *AtHSD1* RNAi mutant (*hsd*) shows a semi-dwarfed phenotype. Together, the phenotypes of AOHSD plants and the *hsd* mutant demonstrate that AtHSD1 is involved in regulating growth and development in plants (Li et al., 2007).

The rice OsHSD1 protein is localized to both the ER and the OB surface and has a similar subcellular localization pattern as AtHSD1. It was found to be expressed in all organs tested including roots, culms, leaves, and panicles, with expression levels highest in leaf sheathes (Zhang et al., 2016). In the rice *oshsd1* mutant, in addition to a reduced plant height phenotype, a thin water film is formed on the leaf surface when the leaves are wetted due to a wax deficiency. Deletion of *OsHSD1* is responsible for the wax-deficient phenotype, providing the first evidence that steroleosin is involved in wax metabolism. The cuticles on the surface of the mutant leaf show a reduced amount of epicuticular wax crystals and thicker cuticle membrane compared to wild type. Further analysis of the wax components showed that long-chain fatty acids (C16 and C18) and VLCFAs (C26, C28, and C30), are significantly increased in the leaves of the mutant. This work provides new insights into HSDs involvement in wax and lipid metabolism.

Response of AtHSD to BR, ABA, and Abiotic Stress

Besides the phenotypes mentioned above, AOHSD plants also exhibit hypersensitivity to brassinosteroids (BRs), reduced sensitivity to ABA and increased catabolism of ABA (Li et al., 2007). In addition to these, observations also indicate that HSD may be involved in the stress response of plants.

As a powerful plant hormone, BR regulates some growth-specific processes including cell elongation, the promotion of seed germination and plant growth, vascular differentiation, ammonium uptake, photomorphogenesis, and skotomorphogenesis. BR-deficient mutants display extreme dwarf phenotypes (Noguchi et al., 1999). Experimental evidence confirmed that BR promotes seed germination by directly enhancing the growth potential of the emerging embryo (Leubner-Metzger, 2001). Interestingly, *AtHSD1* expression is significantly induced by treatment with BL (brassinolide, the most active BR) in wild type plants but markedly decreased in BR-deficient mutants under similar treatment (Li et al., 2007). Additionally, the increased seed germination, growth and seed yield phenotypes of AOHSD plants are similar to those of plants that overproduce BRs (Choe et al., 2001), overexpress the BR receptor gene *BRI1* (Nam and Li, 2002) or of wild type plants treated with exogenous BL. AOHSD plants also show increased sensitivity to BRs. Accordingly, the *AtHSD1* RNAi mutant (*hsd*) is relatively insensitive to BRs. About 40 genes are significantly induced in AOHSD plants compared to wild type. The function of several these genes are similar to that of BL-induced genes encoding putative cell elongation or expansion-associated proteins, such as pectinesterase and xyloglucan fucosyltransferase (Li et al., 2007). The AOHSD phenotype appears to be due to enhancement of the effect of endogenous BRs or as a result of elevated BR concentrations; therefore, AtHSD is likely responsible for catalyzing a step in the biosynthesis of BRs or is involved in BR signaling (Li et al., 2007).

AtHSD1 gene expression affects sensitivity to and metabolism of ABA. ABA signaling plays an important role in many biological processes, such as embryo development, seed maturation, dormancy and germination, seedling establishment, vegetative development, root growth, stomatal movement, flowering, pathogen response, senescence, and stress response (Finkelstein, 2013; Wang et al., 2018). After ABA treatment, the levels of all ABA metabolites in AOHSD seeds are much higher than wild type. AOHSD seeds exhibit greatly reduced sensitivity to ABA, while *hsd* mutant seeds are more sensitive to ABA during germination, similar to the BR biosynthetic mutant *det2-1* and the BR-insensitive mutant *bri1-1* (Steber and McCourt, 2001; Li et al., 2007).

Seed germination, plant growth and development are severely affected by various abiotic stresses (Ding et al.,

2018; He et al., 2018). Increasing evidence has accumulated demonstrating the interplay of HSDs and stress tolerance. For example, transgenic seeds of both *Arabidopsis* and canola which overexpress HSD (AOHSD and BOHSD) show increased salt tolerance compared to wild type (Li et al., 2007). The expression level of OsHSD1 is induced by NaCl and cold treatment, but is inhibited by drought treatment. Moreover, it is well known that the plant cuticular wax has many functions, including protection against UV radiation, resistance to pathogens and tolerance to environmental stresses (Bruhn et al., 2014; Sun et al., 2015). Studies have also provided some evidence for the relationship between abiotic stress and fatty acid metabolism (Thomas et al., 2012; Zhou et al., 2016; Wang et al., 2017; Sui et al., 2018). The role of OsHSD1 in wax and lipid metabolism and the fact that its expression is induced by NaCl and cold suggest OsHSD1 may be involved in environmental stress responses. However, the exact regulatory mechanism remains to be elucidated. The canola (*B.napus*) homolog of AtHSD1 also shows a putative role in stress response. The protein exhibits higher relative expression in imbibed seeds under polyethylene glycol (PEG) treatment than under treatment with the ABA analog PBI429, and also exhibits higher relative expression in nongerminating, ABA analog-treated seeds than in germinating seeds (Li et al., 2005).

Together, in *A. thaliana*, AtHSD1 has been reported to be important in regulating growth and development, stress tolerance, and produce BR-like effects. However, the genetic mechanisms of the effects and the role of AtHSD1 in response to BR action have not been established, and other HSD homologs have not yet been studied.

INTERACTIONS BETWEEN OB-ASSOCIATED PROTEINS AND OTHER PROTEINS

To properly understand the mechanisms of lipid storage regulation, it is essential to define the interactome of OB-associated proteins. However, limited experimental evidence regarding the physical interactions of OB-associated proteins has been obtained, primarily due to technical limitations, especially in plants (Tsai et al., 2015; Kolkhof et al., 2017).

Lipid droplet-associated proteins (LDAPs) are abundant components of OBs in non-seed cell types and are critical for the dynamic regulation of neutral lipid compartmentalization during various developmental and stress-related processes such as heat, cold, and drought conditions. LDAP3 is the most highly and ubiquitously expressed *LDAP* gene in *Arabidopsis*, including in seeds (Gidda et al., 2016). Using the LDAP3 isoform as "bait" to screen a yeast two-hybrid library, Pyc et al. identified a new protein At5g16550, which they named LDIP (LDAP-interacting protein). The protein was confirmed to target specifically to the OB surface with further biochemical and cellular experiments. LDIP T-DNA mutants showed enlarged OBs and had increased total neutral lipid content in both leaves and seeds. These data suggest LDIP is a novel regulator in OB biology (Pyc et al., 2017).

Another case of protein-protein interaction during oleosin degradation in *Arabidopsis* germinated seeds has been mentioned above (Deruyffelaere et al., 2015). Ubiquitination of oleosins occurs at the onset of lipid degradation. Three distinct motifs, including monoubiquitin, K48-linked diubiquitin, and K63-linked diubiquitin, are attached to the major oleosins OLE1 and OLE2. These distinct motifs designate oleosins toward different degradation pathways according to the ubiquitination type. Deruyffelaere et al. further confirmed that PUX10 localized to OBs interacts directly with ubiquitinated oleosins and mediates dislocation of oleosins by the AAA ATPase CDC48A (Deruyffelaere et al., 2018; Kretzschmar et al., 2018).

More work needs to be done to uncover the mechanism of interactions between OB associated proteins and other proteins in OB biology.

OUTLOOK AND FUTURE PERSPECTIVES

OB-associated proteins in seeds and the pollen of plants, mainly including oleosin, caleosin, and steroleosin, have been studied extensively in recent years. Although it has been gradually revealed that these proteins possess numerous functions important for cellular physiology, many questions remain.

Regarding OB biogenesis, the mechanisms regulating extraction of OBs to the cytosol and how OBs are recognized and bound by proteins remain incompletely understood. Post-germinative mobilization of neutral lipids stored in seed OBs is preceded by the degradation of OB-anchored proteins. However, the mechanisms underlying the dislocation of these proteins from the OB monolayer are still unknown. It has been known that these proteins are hydrolyzed by endogenous proteases during seed germination and seedling growth. But so far, little information concerning the identity of the endogenous protease has been revealed. In addition to oleosin, caleosin, and steroleosin, several other OB-associated proteins (such as OBAP1 identified in maize scutellum) have been detected recently (López-Ribera et al., 2014; Müller et al., 2017; Kretzschmar et al., 2018; De Chirico et al., 2018). Additionally, distinct populations of OBs have been found to exist in plants, each possessing different proteins, suggesting functional differentiation of OBs in plant seedlings. Further research is needed to study the mechanism of OB dynamics in other plant tissues and to determine what the roles of the newly identified OB-associated proteins in OB biogenesis and turnover may be.

Two OB-associated proteins, caleosin and steroleosin, were confirmed to participate in cellular stress defenses *via* enzymatic activities and hormone signaling, however, the genetic role of these genes in response to stress and hormone action has also not yet been established. For example, AOHSD plants exhibit hypersensitivity to BR, insensitivity to ABA and increased stress tolerance. ABA and BRs have been shown to act antagonistically (Mandava, 1988); thus, it is difficult to reconcile how the BR-like effects of HSD can be associated with enhanced stress tolerance (which is promoted by ABA) (Li et al., 2007). Therefore, the relationship between BR, ABA, and stress tolerance may be more complex and further investigation will be required to define precise mode of action of HSDs in this process.

Moreover, several *CLO* genes or *HSD* genes are closely linked on the chromosomes in *A. thaliana*, so it is difficult to construct

multiple mutants using traditional methods. This likely has limited research into caleosin and steroleosin. Now, the CRISPR system (Liang et al., 2018) and traditional crosses may be used to edit several genes simultaneously and construct multiple mutants in which all members of the *CLO* or *HSD* gene families could be knocked out, allowing for further functional analysis.

In short, continuing advances in analytic techniques and genomics will help to find more OB-associated proteins and further reveal the exact role of these proteins in stress response, lipid and BR metabolism, and OB formation. These studies may also provide novel opportunities for increasing stress resistance, enhancing plant yield or increasing the total TAG content in plant tissues for a variety of industrial applications.

AUTHOR CONTRIBUTIONS

QS, PW, and CM conceived and wrote the manuscript. XL and TS contributed to the revision of the manuscript. All authors read and approved the submitted version.

FUNDING

This study was funded by the Key Technology Research and Development Program of Shandong (2018GSF121037 and 2018GNC113010) and the National Natural Science Foundation of China (31770290 and 31970301).

REFERENCES

Adeyo, O., Horn, P. J., Lee, S., Binns, D. D., Chandrahas, A., Chapman, K. D., et al. (2011). The yeast lipin orthologue Pah1p is important for biogenesis of lipid droplets. *J. Cell Biol.* 192, 1043–1055. doi: 10.1083/jcb.201010111

Arnesen, T. (2011). Towards a functional understanding of protein N terminal acetylation. *PloS Biol.* 9, e1001074. doi: 10.1371/journal.pbio.1001074

Aubert, Y., Vile, D., Pervent, M., Aldon, D., Ranty, B., Simonneau, T., et al. (2010). RD20, a stress-inducible caleosin, participates in stomatal control, transpiration and drought tolerance in *Arabidopsis thaliana*. *Plant Cell Physiol.* 51, 1975–1987. doi: 10.1093/pcp/pcq155

Aubert, Y., Leba, L. J., Cheval, C., Ranty, B., Vavasseur, A., Aldon, D., et al. (2011). Involvement of RD20, a member of caleosin family, in ABA-mediated germination in *Arabidopsis thaliana*. *Plant Signal. Behav.* 6, 538–540. doi: 10.4161/psb.6.4.14836

Babazadeh, N., Poursaadat, M., Sadeghipour, H. R., and Colagar, A. H. Z. (2012). Oil body mobilization in sunflower seedlings is potentially regulated by thioredoxin h. *Plant Physiol. Biochem.* 57, 134–142. doi: 10.1016/j.plaphy.2012.05.013

Bao, B., Chao, H., Wang, H., Zhao, W., Zhang, L., Raboanatahiry, N., et al. (2018). Stable, environmental specific and novel QTL identification as well as genetic dissection of fatty acid metabolism in *Brassica napus*. *Front. Plant Sci.* 9, 1018. doi: 10.3389/fpls.2018.01018

Baud, S., Dichow, N. R., Kelemen, Z., d'Andréa, S., To, A., Berger, N., et al. (2009). Regulation of HSD1 in seeds of *Arabidopsis thaliana*. *Plant Cell Physiol.* 50, 1463–1478. doi: 10.1093/pcp/pcp092

Beaudoin, F., Wikinson, B. M., Stirling, C. J., and Napier, A. (2000). In vivo targeting of a sunflower oil body protein in yeast secretory (*sec*) mutants. *Plant J.* 23, 159–170. doi: 10. 1046/j.1365-313x.2000.00769.x

Blée, E., Flenet, M., Boachon, B., and Fauconnier, M. L. (2012). A non-canonical caleosin from *Arabidopsis* efficiently epoxidizes physiological unsaturated fatty acids with complete stereo selectivity. *FEBS J.* 279, 3981–3995. doi: 10.1111/j.1742-4658.2012.08757.x

Blée, E., Boachon, B., Burcklen, M., Le Guédard, M., Hanano, A., Heintz, D., et al. (2014). The reductase activity of the *Arabidopsis* caleosin RESPONSIVE TO DESSICATION 20 mediates gibberellin-dependent flowering time, abscisic acid sensitivity, and tolerance to oxidative stress. *Plant Physiol.* 166, 109–124. doi: 10.1104/pp.114. 245316

Braybrook, S. A., Stone, S. L., Park, S., Bui, A. Q., Le, B. H., Fischer, R. L., et al. (2006). Genes directly regulated by LEAFY COTYLEDON2 provide insight into the control of embryo maturation and somatic embryogenesis. *Proc. Natl. Acad. Sci. U.S.A.* 103, 3468–3473. doi: 10.1073/pnas.0511331103

Bruhn, D., Mikkelsen, T., Rolsted, M., Egsgaard, H., and Ambus, P. (2014). Leaf surface wax is a source of plant methane formation under UV radiation and in the presence of oxygen. *Plant Biol.* 16, 512–516. doi: 10.1111/plb.12137

Carter, C., Pan, S., Zouhar, J., Avila, E. L., Girke, T., and Raikhel, N. V. (2004). The vegetative vacuole proteome of *Arabidopsis thaliana* reveals predicted and unexpected proteins. *Plant Cell* 16, 3285–3303. doi: 10.1105/tpc.104.027078

Chapman, K. D., and Ohlrogge, J. B. (2012). Compartmentation of triacylglycerol accumulation in plants. *J. Biol. Chem.* 287, 2288–2294. doi: 10.1074/jbc.R111.290072

Chapman, K. D., Dyer, J. M., and Mullen, R. T. (2012). Biogenesis and functions of lipid droplets in plants. Thematic review series: lipid droplet synthesis and metabolism: from yeast to man. *J. Lipid Res.* 53, 215–226. doi: 10.1194/jlr.R021436

Charuchinda, P., Waditee-Sirisattha, R., Kageyama, H., Yamada, D., Sirisattha, S., Tanaka, Y., et al. (2015). Caleosin from *Chlorella vulgaris* TISTR 8580 is salt-induced and heme-containing protein. *Biosci. Biotechnol. Biochem.* 79, 1119–1124. doi: 10.1080/09168451.2015.1010480

Chen, E. C. F., Tai, S. S. K., Peng, C. C., and Tzen, J. T. C. (1998). Identification of three novel unique proteins in seed oil bodies of sesame. *Plant Cell Physiol.* 39, 935–941. doi: 10. 1093/oxfordjournals.pcp.a029457

Chen, C. F., Tsai, C. C. Y., and Tzen, J. T. C. (1999). Cloning and secondary structure analysis of caleosin, a unique calcium-binding protein in oilbodies of plant seeds. *Plant Cell Physiol.* 40, 1079–1086. doi: 10.1093/oxfordjournals.pcp.a029490

Chen, M. C., Chyan, C. L., Lee, T. T., Huang, S. H., and Tzen, J. T. (2004). Constitution of stable artificial oil bodies with triacylglycerol, phospholipid, and caleosin. *J. Agric. Food Chem.* 52, 3982–3987. doi: 10.1021/jf035533g

Chen, Y., Zhao, L., Cao, Y., Kong, X., and Hua, Y. (2014). Oleosins (24 and 18 kDa) are hydrolyzed not only in extracted soybean oil bodies but also in soybean germination. *J. Agric. Food Chem.* 62, 956–965. doi: 10.1021/jf405382w

Chen, Y., Chen, Y., Zhao, L., Kong, X., Yang, Z., and Hua, Y. (2018). A two-chain aspartic protease present in seeds with high affinity for peanut oil bodies. *Food Chem.*, 241, 443–451. doi: 10.1016/j.foodchem.2017.09.020

Chen, K., Yin, Y., Liu, S., Guo, Z., Zhang, K., Liang, Y., et al. (2019). Genome-wide identification and functional analysis of oleosin genes in *Brassica napus* L. *BMC Plant Biol.* 19, 294. doi: 10.1186/s12870-019-1891-y

Choe, S., Fujioka, S., Noguchi, T., Takatsuto, S., Yoshida, S., and Feldmann, K. A. (2001). Overexpression of *DWARF4* in the brassinosteroid biosyntheticpathway results in increased vegetative growth and seed yield in *Arabidopsis*. *Plant J.* 26, 573–582. doi: 10. 1046/j.1365-313x.2001.01055.x

Czabany, T., Athenstaedt, K., and Daum, G. (2007). Synthesis, storage and degradation of neutral lipids in yeast. *Biochim. Biophys. Acta* 1771, 299–309. doi: 10.1016/j.bbalip.2006.07.001

d'Andréa, M., Canonge, A., Beopoulos, P., Jolivet, M. A., Hartmann, M., Miquel, L., et al. (2007). At5g50600 encodes a member of the short-chain dehydrogenase reductase superfamily with 11β- and 17β-hydroxysteroid dehydrogenase activities associated with *Arabidopsis thaliana* seed oil bodies. *Biochimie* 89, 222–229. doi: 10.1016/j.biochi.2006.09.013

D'Andrea, S. (2016). Lipid droplet mobilization: the different ways to loosen the purse strings. *Biochimie* 120, 17–27. doi: 10.1016/j.biochi.2015.07.010

De Chirico, S., di Bari, V., Foster, T., and Gray, D. (2018). Enhancing the recovery of oilseed rape seed oil bodies (oleosomes) using bicarbonate-based soaking and grinding media. *Food Chem.* 241, 419–426. doi: 10.1016/j.foodchem.2017.09.008

de Oliveira, D. E., Franco, L. O., Simoens, C., Seurinck, J., Coppieters, J., Botterman, J., et al. (1993). Inflorescence-specific genes from *Arabidopsis thaliana* encoding glycine-rich proteins. *Plant J.* 3, 495–507. doi: 10.1046/j.1365-313x.1993.03040495.x

Deleu, M., Vaca-Medina, G., Fabre, J., Roiz, J., Valentin, R., and Mouloungui, Z. (2010). Interfacial properties of oleosins and phospholipids from rapeseed for

the stability of oil bodies in aqueous medium. *Colloids Surf. B Biointerfaces* 80, 125–132. doi: 10.1016/j. colsurfb.2010.05.036

Deruyffelaere, C., Bouchez, I., Morin, H., Guillot, A., Miquel, M., Froissard, M., et al. (2015). Ubiquitin-mediated proteasomal degradation of oleosins is involved in oil body mobilization during post-germinative seedling growth in *Arabidopsis*. *Plant Cell Physiol.* 56, 1374–1387. doi: 10.1093/pcp/pcv 056

Deruyffelaere, C., Purkrtova, Z., Bouchez, I., Collet, B., Cacas, J. L., Chardot, T., et al. (2018). PUX10 is a CDC48A adaptor protein that regulates the extraction of ubiquitinated oleosins from seed lipid droplets in *Arabidopsis*. *Plant Cell* 30, 2116–2136. doi: 10.1105/tpc.18. 00275

Ding, T. L., Yang, Z., Wei, X. C., Yuan, F., Yin, S. S., and Wang, B. S. (2018). Evaluation of salt-tolerant germplasm and screening of the salt-tolerance traits of sweet sorghum in the germination stage. *Funct. Plant Biol.* 45, 1073–1081. doi: 10.1071/FP18009

Fan, J., Yan, C., Zhang, X., and Xu, C. (2013). Dual role for phospholipid: diacylglycerol acyltransferase: enhancing fatty acid synthesis and diverting fatty acids from membrane lipids to triacylglycerol in *Arabidopsis* leaves. *Plant Cell* 253506, –3518. doi: 10.1104/pp.113.216820

Finkelstein, R. (2013). Abscisic acid synthesis and response. *Arabidopsis Book* 11, e0166. doi: 10.1199/tab.0166

Froissard, M., D'andréa, S., Boulard, C., and Chardot, T. (2009). Heterologous expression of AtClo1, a plant oil body protein, induces lipid accumulation in yeast. *FEMS Yeast Res.* 9, 428–438. doi: 10.1111/j.1567-1364.2009.00483.x

Gidda, S. K., Park, S., Pyc, M., Yurchenko, O., Cai, Y., Wu, P., et al. (2016). Lipid droplet-associated proteins (LDAPs) are required for the dynamic regulation of neutral lipid compartmentation in plant cells. *Plant Physiol.* 170, 2052–2071. doi: 10.1104/pp.15.01977

Guo, F. D., Liu, C. L., Xia, H., Bi, Y. P., Zhao, C. Z., Zhao, S. Z., et al. (2013). Induced expression of AtLEC1 and AtLEC2 differentially promotes somatic embryogenesis in transgenic tobacco plants. *PloS One* 8, e71714. doi: 10.1371/journal.pone.0071714

Hamberg, M., Sanz, A., Rodriguez, M. J., Calvo, A. P., and Castresana, C. (2003). Activation of the fatty acid alpha-dioxygenase pathway during bacterial infection of tobacco leaves: formation of oxylipins protecting against cell death. *J. Biol. Chem.* 278, 51796–51805. doi: 10.1074/jbc.M310514200

Hanano, A., Burcklen, M., Flenet, M., Ivancich, A., Louwagie, M., Garin, J., et al. (2006). Plant seed peroxygenase is an original heme-oxygenase with an EF-hand calcium binding motif. *J. Biol. Chem.* 281, 33140–33151. doi: 10.1074/jbc.M605395200

Hanano, A., Bessoule, J. J., Heitz, T., and Blée, E. (2015). Involvement of the caleosin/peroxygenase RD20 in the control of cell death during *Arabidopsis* responses to pathogens. *Plant Signal. Behav.* 10, e991574. doi: 10.4161/15592324.2014. 991574

He, M., He, C. Q., and Ding, N. Z. (2018). Abiotic stresses: general defenses of land plants and chances for engineering multistress tolerance. *Front. Plant Sci.* 9, 1771. doi: 10.3389/fpls.2018.01771

Hernandez-Pinzon, I., Patel, K., and Murphy, D. J. (2001). The *Brassica napus* calcium-binding protein caleosin has distinct endoplasmic reticulumand lipid body-associated isoforms. *Plant Physiol. Biochem.* 39, 615–622. doi: 10.1016/S0981-9428(01)01274-8

Hope, R. G., Murphy, D. J., and McLauchlan, J. (2002). The domains required to direct core proteins of hepatitis C virus and GB virus-B to lipid droplets share common features with plant oleosin proteins. *J. Biol. Chem.* 277, 4261–4270. doi: 10.1074/jbc.M108798200

Hsiao, E. S., and Tzen, J. T. (2011). Ubiquitination of oleosin-H and caleosin in sesame oil bodies after seed germination. *Plant Physiol. Biochem.* 49, 77–81. doi: 10.1016/j.plaphy.2010.10.001

Huang, C. Y., and Huang, ,. A. H. C. (2017). Unique motifs and length of hairpin in oleosin target the cytosolic side of endoplasmic reticulum and budding lipid droplet. *Plant Physiol.* 174, 2248–2260. doi: 10.1104/pp.17.00366

Huang, C. Y., Chung, C. I., Lin, Y. C., Hsing, Y. C., and Huang, A. H. C. (2009). Oil bodies and oleosins in *Physcomitrella* possess characteristics representative of early trends in evolution. *Plant Physiol.* 150, 1192–1203. doi: 10.1104/pp.109.138123

Huang, A. H. C. (1996). Oleosin and oil bodies in seeds and other organs. *Plant Physiol.* 110, 1055–1061. doi: 10.1104/pp.110.4.1055

Huang, C. Y. (2013). *Evolution and functions of oleosins and oleosin-coated oil bodies in plants* (Riverside Press: University of California).

Jacquier, N., Choudhary, V., Mari, M., Toulmay, A., Reggiori, F., and Schneiter, R. (2011). Lipid droplets are functionally connected to the endoplasmic reticulum in *Saccharomyces cerevisiae*. *J. Cell Sci.* 124, 2424–2437. doi: 10.1242/jcs.076836

Jacquier, N., Mishra, S., Choudhary, V., and Schneiter, R. (2013). Expression of oleosin and perilipins in yeast promotes formation of lipid droplets from the endoplasmic reticulum. *J. Cell. Sci.* 126, 5198–5209. doi: 10.1242/jcs.131896

Jiang, P. L., and Tzen, J. (2010). Caleosin serves as the major structural protein as efficient as oleosin on the surface of seed oil bodies. *Plant Signal. Behav.* 5, 447–449. doi: 10.4161/psb. 5.4.10874

Jiang, P. L., Chen, J. C., Chiu, S. T., and Tzen, J. T. (2009). Stable oil bodies sheltered by a unique caleosin in cycad megagametophytes. *Plant Physiol. Biochem.* 471009-, 1016. doi: 10.1016/j.plaphy.2009.07.004

Jin, W. W., Long, Y., Fu, C. H., Zhang, L. B., Xiang, Wang, J., et al. (2018). Ca^{2+} imaging and gene expression profiling of *Lonicera Confusa* in response to calcium-rich environment. *Sci. Rep.* 8, 10. doi: 10.1038/s41598-018-25611-5

Jolivet, P., Roux, E., D'Andréa, S., Davanture, M., Negroni, L., Zivy, M., et al. (2004). Protein composition of oil bodies in *Arabidopsis thaliana* ecotype WS. *Plant Physiol. Biochem.* 42, 501–509. doi: 10.1016/j.plaphy.2004.04.006

Jolivet, P., Boulard, C., Bellamy, A., Larré, C., Barre, M., Rogniaux, H., et al. (2009). Protein composition of oil bodies from mature *Brassica napus* seeds. *Proteomics* 9, 3268–3284. doi: 10.1002/pmic.200800449

Kim, H. U., Hsieh, K., Ratnayake, C., and Huang, A. H. C. (2002). A novel group of oleosins is present inside the pollen of *Arabidopsis*. *J. Biol. Chem.* 27722677-, 22684. doi: 10.1074/jbc.M109298200

Kim, Y. Y., Jung, K. W., Yoo, K. S., Jeung, J. U., and Shin, J. S. (2011). A stress-responsive caleosin-like protein, AtCLO4, acts as a negative regulator of ABA responses in *Arabidopsis*. *Plant Cell Physiol.* 52, 874–884. doi: 10.1093/pcp/pcr039

Kirik, V., Kolle, K., Balzr, H., and Baumlein, H. (1996). Two new oleosin isoforms with altered expression patterns in seeds of the *Arabidopsis* mutant *fus3*. *Plant Mol. Biol.* 31, 413–417. doi: 10.1007/bf00021803

Kolkhof, P., Werthebach, M., van de Venn, A., Poschmann, G., Chen, L., Welte, M., et al. (2017). A luciferase-fragment complementation assay to detect lipid droplet-associated protein-protein interactions. *Mol. Cell Proteomics* 16, 329–345. doi: 10.1074/mcp.M116.061499

Kretzschmar, F. K., Mengel, L. F., Müller, A., Schmitt, K., Blersch, K. F., Valerius, O., et al. (2018). PUX10 is a lipid droplet-localized scaffold protein that interacts with CELL DIVISION CYCLE48 and is involved in the degradation of lipid droplet proteins. *Plant Cell* 30, 2137–2160. doi: 10.1105/tpc.18.00276

Kroj, T., Savino, G., Valon, C., Giraudat, J., and Parcy, F. (2003). Regulation of storage protein gene expression in *Arabidopsis*. *Development* 130, 6065–6073. doi: 10.1242/dev.00814

López-Ribera, I., Paz, J. L. L., Repiso, C., García, N., Miquel, M., Hernández, M. L., et al. (2014). The evolutionary conserved oil body associated protein OBAP1 participates in the regulation of oil body size. *Plant Physiol.* 164, 1237–1249. doi: 10.1104/pp.113.233221

Lòpez, M. A., Vicente, J., Kulaserakan, S., Vellosillo, T., Martinez, M., Irigoyen, M. I., et al. (2011). Antagonistic role of 9-lipoxygenase-derived oxylipins and ethylene in the control of oxidative stress, lipid peroxidation and plant defence. *Plant J.* 67, 447–458. doi: 10.1111/j.1365-313X.2011.04608.x

Leber, R., Zinser, E., Paltauf, F., Daum, G., and Zellnig, G. (1994). Characterization of lipid particles of the yeast, *Saccharomyces cerevisiae*. *Yeast* 10, 1421–1428. doi: 10.1002/yea.320101105

Leprince, O., van Aelst, A. C., Pritchard, H. W., and Murphy, D. J. (1998). Oleosins prevent oil-body coalescence during seed imbibition as suggested by a low-temperature scanning electron microscope study of desiccation-tolerant and -sensitive oilseeds. *Planta* 204, 109–119. doi: 10.1007/s004250050236

Leubner-Metzger, G. (2001). Brassinosteroids and gibberellins promote tobacco seed germination by distinct pathways. *Planta*. 213, 758–763. doi: 10.1007/s004250100542

Li, F., Wu, X. Z., Tsang, E., and Cutler, A. J. (2005). Transcriptional profiling of imbibed *Brassica napus* seed. *Genomics.* 86, 718–730. doi: 10.1016/j.ygeno.2005.07.006

Li, F., Asami, T., Wu, X., Tsang, E. W., and Cutler, A. J. (2007). A putative hydroxysteroid dehydrogenase involved in regulating plant growth and development. *Plant Physiol.* 145, 87–97. doi: 10.1104/pp.107.100560

Li, X., Lin, C., and O'Connor, P. B. (2010). Glutamine deamidation: differentiation of glutamic acid and gamma-glutamic acid in peptides by electron capture dissociation. *Anal. Chem.* 82, 3606–3615. doi: 10.1021/ac9028467

Liang, Z., Chen, K., Yan, Y., Zhang, Y., and Gao, C. (2018). Genotyping genome-edited mutations in plants using CRISPR ribonucleoprotein complexes. *Plant Biotechnol. J.* 12, 2053–2062. doi: 10.1111/pbi.12938

Lin, L. J., and Tzen, J. T. C. (2004). Two distinct steroleosins are present in seed oil bodies. *Plant Physiol. Biochem.* 42, 601–608. doi: 10.1016/j.plaphy.2004.06.006

Lin, L. J., Tai, S. S., Peng, C. C., and Tzen, J. T. (2002). Steroleosin, a sterol-binding dehydrogenase in seed oil bodies. *Plant Physiol.* 128, 1200–1211. doi: 10.1104/pp.010928

Lin, L. J., Liao, P. C., Yang, H. H., and Tzen, J. T. (2005). Determination and analyses of the N-termini of oil-body proteins, steroleosin, caleosin and oleosin. *Plant Physiol. Biochem.*, 43, 770–776. doi: 10.1016/j.plaphy.2005.07.008

Müller, A. O., Blersch, K. F., Gippert, A. L., and Ischebeck, T. (2017). Tobacco pollen tubes -a fast and easy tool for studying lipid droplet association of plant proteins. *Plant J.* 89, 1055–1064. doi: 10.1111/tpj.13441

Mandava, N. B. (1988). Plant growth-promoting brassinosteroids. *Annu. Rev. Plant Physiol. Plant Mol. Biol.* 39, 23–52. doi: 10.1146/annurev.pp.39.060188.000323

Mayfield, J. A., and Preuss, D. (2000). Rapid initiation of *Arabidopsis* pollination requires the oleosin-domain protein GRP17. *Nat. Cell Biol.* 2, 128–130. doi: 10.1038/35000084

Mayfield, J. A., Fiebig, A., Johnstone, S. E., and Preuss, D. (2001). Gene families from the *Arabidopsis thaliana* pollen coat proteome. *Science* 292, 2482–2485. doi: 10.1126/science.1060972

Miquel, M., Trigui, G., d'Andréa, S., Kelemen, Z., Baud, S., Berger, A., et al. (2014). Specialization of oleosins in oil body dynamics during seed development in *Arabidopsis* seeds. *Plant Physiol.* 164, 1866–1878. doi: 10.1104/pp.113.233262

Murphy, D. J. (2001). The biogenesis and functions of lipid bodies in animals, plants and microorganisms. *Prog. Lipid Res.* 40, 325–438. doi: 10.1016/S0163- 7827(01)00013-3

Naested, H., Frandsen, G. I., Jauh, G. Y., Hernandez-Pinzon, I., Nielsen, H. B., Murphy, D. J., et al. (2000). Caleosins: Ca^{2+}-binding proteins associated with lipid bodies. *Plant Mol. Biol.* 44, 463–476. doi: 10.1023/A:1026564411918

Nam, K. H., and Li, J. (2002). BRI1/BAK1, a receptor kinase pair mediating brassinosteroid singaling. *Cell* 110, 203–212. doi: 10.1016/s0092-8674(02)00814- 0

Noguchi, T., Fujioka, S., Choe, S., Takatsuto, S., Yoshida, S., Yuan, H., et al. (1999). Brassinosteroid-insensitive dwarf mutants of *Arabidopsis* accumulate brassinosteroids. *Plant Physiol.* 121, 743–752. doi: 10.1104/pp.121.3.743

Oelkers, P., Cromley, D., Padamsee, M., Billheimer, J. T., and Sturley, S. L. (2002). The DGA1 gene determines a second triglyceride synthetic pathway in yeast. *J. Biol. Chem.* 277, 8877–8881. doi: 10.1074/jbc.M111646200

Parthibane, V., Rajakumari, S., Venkateshwari, V., Iyappan, R., and Rajasekharan, R. (2012). Oleosin is bifunctional enzyme that has both monoacylglycerol acyltransferase and phospholipase activities. *J. Biol. Chem.* 287, 1946–1954. doi: 10.1074/jbc.M111.309955

Partridge, M., and Murphy, D. J. (2009). Roles of a membrane-bound caleosin and putative peroxygenase in biotic and abiotic stress responses in *Arabidopsis*. *Plant Physiol. Biochem.* 47, 796–806. doi: 10.1016/j.plaphy.2009.04.005

Pasaribu, B., Chung, T. Y., Chen, C. S., Jiang, P. L., and Tzen, J. T. C. (2016). Identification of steroleosin in oil bodies of pine megagametophytes. *Plant Physiol. Biochem.* 101, 173–181. doi: 10.1016/j.plaphy.2016.02.008

Platt-Aloia, K. A., and Thompson, W. W. (1981). Ultrastructure of the mesocarp of mature avocado fruit and changes associated with ripening. *Ann. Bot.* 48, 451–465. doi: 10.1093/oxfordjournals.aob.a086149

Poxleitner, M., Rogers, S. W., Lacey Samuels, ,. A., Browse, J., and Rogers, J. C. (2006). A role for caleosin in degradation of oil-body storage lipid during seed germination. *Plant J.* 47, 917–933. doi: 10.1111/j.1365-313X.2006.02845.x

Prost, I., Dhondt, S., Rothe, G., Vicente, J., Rodriguez, M. J., Kift, N., et al. (2005). Evaluation of the antimicrobial activities of plant oxylipins support their involvement in defense against pathogens. *Plant Physiol.* 139, 1902–1913. doi: 10.1104/pp.105.066274

Pyc, M., Cai, Y., Greer, M. S., Yurchenko, O., Chapman, K. D., Dyer, J. M., et al. (2017). Turning over a new leaf in lipid droplet biology. *Trends Plant Sci.* 22, 596–609. doi: 10.1016/j.tplants.2017.03.012

Quettier, A. L., and Eastmond, P. J. (2009). Storage oil hydrolysis during early seedling growth. *Plant Physiol. Biochem.* 47, 485–490. doi: 10.1016/j.plaphy.2008.12.005

Ree, R., Varland, S., and Arnesen, T. (2018). Spotlight on protein N-terminal acetylation. *Exp. Mol. Med.* 50, 90. doi: 10.1038/s12276-018-0116-z

Schmidt, M. A., and Herman, E. M. (2008). Suppression of soybean oleosin produces micro-oil bodies that aggregate into oil body/ER complexes. *Mol. Plant* 1, 910–924. doi: 10.1093/mp/ssn049

Shen, Y., Xie, J., Liu, R. D., Ni, X. F., Wang, X. H., Li, Z. X., et al. (2014). Genomic analysis and expression investigation of caleosin gene family in *Arabidopsis*. *Biochem. Biophys. Res. Commun.* 448, 365–371. doi: 10.1016/j.bbrc

Shimada, T. L., and Hara-Nishimura, I. (2015). Leaf oil bodies are subcellular factories producing antifungal oxylipins. *Curr. Opin. Plant Biol.* 25, 145–150. doi: 10.1016/j.pbi.2015.05.019

Shimada, T. L., Shimada, H., Takahashi, H., and Fukao, Y. (2008). A novel role of oleosins in freezing tolerance of oilseeds in Arabidopsis thaliana. *Plant J.* 55, 798–809. doi: 10.1111/j.1365-313X.2008.03553.x

Shimada, T. L., Takano, Y., Shimada, T., Fujiwara., M., Fukao, Y., Mori, M., et al. (2014). Leaf oil body functions as a subcellular factory for the production of a phytoalexin in *Arabidopsis*. *Plant Physiol.* 164, 105–118. doi: 10.1104/pp.113.230185

Shimada, T. L., Hayashi, M., and Hara-Nishimura, I. (2018). Membrane dynamics and multiple functions of oil bodies in seeds and leaves. *Plant Physiol.* 176, 199–207. doi: 10.1104/pp.17.01522

Siloto, R. M. P., Findlay, K., Lopez-Villabos, A., Yeung, E. C., Nykiforuk, C. L., and Moloney, M. M. (2006). The accumulation of oleosins determines the size of seed oil bodies in *Arabidopsis*. *Plant Cell.* 18, 1961–1974. doi: 10.1105/tpc.106.041269

Skinner, J. R., Shew, T. M., Schwartz, D. M., Tzekov, A., Lepus, C. M., Abumrad, N. A., et al. (2009). Diacylglycerol enrichment of endoplasmic reticulum or lipid droplets recruits perilipin 3/TIP47 during lipid storage and mobilization. *J. Biol. Chem.* 284, 30941–30948. doi: 10.1074/jbc.M109.013995

Song, Y. H., Wang, X. D., and Rose, R. J. (2017). Oil body biogenesis and biotechnology in legume seeds. *Plant Cell Rep.* 36, 1519–1532. doi: 10.1007/s00299-017-2201-5

Sorokin, A. V., Kim, E. R., and Ovchinnikov, L. P. (2009). Proteasome system of protein degradation and processing. *Biochem. (Mosc)* 74, 1411–1442. doi: 10.1134/S000629790913001X

Steber, C. M., and McCourt, P. (2001). A role for brassinosteroids in germination in *Arabidopsis*. *Plant Physiol.* 125, 763–769. doi: 10.1104/pp.125.2.763

Sui, N., Wang, Y., Liu, S. S., Yang, Z., Wang, F., and Wan, S. B. (2018). Transcriptomic and physiological evidence for the relationship between unsaturated fatty acid and salt stress in peanut. *Front. Plant Sci.* 9, 7. doi: 10.3389/fpls.2018.00007

Sun, W., Li, Y., Zhao, Y. X., and Zhang, H. (2015). The TsnsLTP4, a nonspecific lipid transfer protein involved in wax deposition and stress tolerance. *Plant Mol. Biol. Rep.* 33, 962–974. doi: 10.1007/s11105-014-0798-x

Sztalryd, C., and Kimmel, A. R. (2014). Perilipins: lipid droplet coat proteins adapted for tissue-specific energy storage and utilization, and lipid cytoprotection. *Biochimie* 96, 96–101. doi: 10.1016/j.biochi.2013.08.026

Tang, G. Y., Xu, P. L., Ma, W. H., Wang, F., Liu, Z. J., Wan, S. B., et al. (2018). Seed-specific expression of AtLEC1 increased oil content and altered fatty acid composition in seeds of pPeanut (*Arachis hypogaea* L.). *Front. Plant Sci.* 9, 260. doi: 10.3389/fpls.2018.00260

Thomas, D., Patrick, G., Zuther, E., Bettina, S., Hincha, D. K., and Willmitzer, L. (2012). Differential remodeling of the lipidome during cold acclimation in natural accessions of *Arabidopsis thaliana*. *Plant J. Cell. Mol. Biol.* 72, 972–982. doi: 10.1111/tpj.12007

Ting, J. T., Lee, K., Ratnayake, C., Platt, K. A., Balsamo, R. A., and Huang, A. H. (1996). Oleosin genes in maize kernels having diverse oil contents are constitutively expressed independent of oil contents. *Planta* 199, 158–165. doi: 10.1007/bf001968924

Ting, J. T. L., Balsamo, R. A., Ratnayake, C., and Huang, A. H. C. (1997). Oleosin of plant seed oil bodies is correctly targeted to the lipid bodies in transformed yeast. *J. Biol. Chem.* 272, 3699–3706. doi: 10.1074/jbc.272.6.3699

Tsai, C. H., Zienkiewicz, K., Amstutz, C. L., Brink, B. G., Warakanont, J., Roston, R., et al. (2015). Dynamics of protein and polar lipid recruitment during lipid droplet assembly in *Chlamydomonas reinhardtii*. *Plant J.* 83, 650–660. doi: 10.1111/tpj.12917

Tzen, J. T. C., and Huang, A. H. C. (1992). Surface structure and properties of plant seed oil bodies. *J. Cell Biol.* 117, 327–335. doi: 10.1083/jcb.117.2.327

Tzen, J. T. C., Lai, Y. K., Chan, K. L., and Huang, A. H. C. (1990). Oleosin isoforms of high and low molecular weights are present in the oil bodies of diverse seed species. *Plant Physiol.* 94, 1282–1289. doi: 10.1104/pp.94.3.1282

Tzen, J. T. C., Cao, Y. Z., Laurent, P., Ratnayake, C., and Huang, A. H. C. (1993). Lipids, proteins, and structure of seed oilbodies from diverse species. *Plant Physiol.* 101, 267–276. doi: 10.1104/pp.101.1.267

Tzen, J. T. C., Peng, C. C., Cheng, D. J., Chen, E. C. F., and Chiu, J. M. H. (1997). A new method for seed oil body purification and examination of oil body integrity following germination. *J. Biochem.* 121, 762–768. doi: 10.1093/oxfordjournals.jbchem.a021651

Tzen, J. T. (2012). Integral proteins in plant oil bodies. *ISRN Bot.* 2012, 1–16. doi: 10.5402/2012/173954

van Rooijen, G. J. H., Terning, L. I., and Moloney, M. M. (1992). Nucleotide sequence of an *Arabidopsis thaliana* oleosin gene. *Plant Mol. Biol.* 18, 1177–1179. doi: 10.1007/bf00047721

Vance, V. B., and Huang, A. H. (1987). The major protein from lipid bodies of maize. Characterization and structure based on cDNA cloning. *J. Biol. Chem.* 262, 11275–11279.

Vanhercke, T., El Tahchy, A., Liu, Q., Zhou, X. R., Shrestha, P., Divi, U. K., et al. (2014). Metabolic engineering of biomass for high energy density: oilseed-like triacylglycerol yields from plant leaves. *Plant Biotechnol. J.* 12, 231–239. doi: 10.1111/pbi.12131

Wältermann, M., Hinz, A., Robenek, H., Troyer, D., Reichelt, R., Malkus, U., et al. (2005). Mechanism of lipid-body formation in prokaryotes: how bacteria fatten up. *Mol. Microbiol.* 55, 750–763. doi: 10.1111/j.1365-2958.2004.04441.x

Wang, J. S., Zhang, Q., Cui, F., Hou, L., Zhao, S. Z., Xia, H., et al. (2017). Genome-wide analysis of gene expression provides new insights into cold responses in *Thellungiella salsuginea*. *Front. Plant Sci.* 8, 713. doi: 10.3389/fpls.2017.00713

Wang, K., He, J. N., Zhao, Y., Wu, T., Zhou, X. F., Ding, Y. L., et al. (2018). EAR1 negatively regulates ABA signaling by enhancing 2C protein phosphatase activity. *Plant Cell* 30, 815–834. doi: 10.1105/tpc.17.00875

Winichayakul, S., Scott, R. W., Roldan, M., Hatier, J. H., Livingston, S., Cookson, R., et al. (2013). in Vivo Packaging of Triacylglycerols Enhances *Arabidopsis* Leaf Biomass and Energy Density. *Plant Physiol.* 162, 626–639. doi: 10.1104/Pp.113.216820

Wu, Y. Y., Chou, Y. R., Wang, C. S., Tseng, T. H., Chen, L. J., and Tzen, J. T. (2010). Different effects on triacylglycerol packaging to oil bodies in transgenic rice seeds by specifically eliminating one of their two oleosin isoforms. *Plant Physiol. Biochem.* 48, 81–89. doi: 10.1016/j.plaphy.2009.12.004

Yang, S., Li, L., Zhang, J. L., Geng, Y., Guo, F., Wang, J. G., et al. (2017). Transcriptome and differential expression profiling analysis of the mechanism of Ca^{2+} regulation in peanut (*Arachis hypogaea*) pod development. *Front. Plant Sci.* 8, 1609. doi: 10.3389/fpls.2017.01609

Yin, Y. T., Guo, L. X., Chen, K., Guo, Z. Y., Chao, H. B., Wang, B. S., et al. (2018). 3D Reconstruction of lipid droplets in the seed of *Brassica napus*. *Sci. Rep.* 8, 6560. doi: 10.1038/s41598-018-24812-2

Zhang, S. O., Box, A. C., Xu, N., Le Men, J., Yu, J., Guo, F., et al. (2010). Genetic and dietary regulation of lipid droplet expansion in *Caenorhabditis elegans*. *Proc. Natl. Acad. Sci. U.S.A.* 107, 4640–4645. doi: 10.1073/pnas.09123081 07

Zhang, Z., Cheng, Z. J., Gan, L., Zhang, H., Wu, F. Q., Lin, Q. B., et al. (2016). OsHSD1, a hydroxysteroid dehydrogenase, is involved in cuticle formation and lipid homeostasis in rice. *Plant Sci.* 249, 35–45. doi: 10.1016/j.plantsci.2016.05.005

Zheng, Y., Liao, C., Zhao, S., Wang, C., and Guo, Y. (2017). The glycosyltransferase QUA1 regulates chloroplast-associated calcium signaling during salt and drought stress in *Arabidopsis*. *Plant Cell Physiol.* 58, 329–341. doi: 10.1093/pcp/pcw192

Zhou, J. C., Fu, T. T., Sui, N., Guo, J. R., Feng, G., Fan, J. L., et al. (2016). The role of salinity in seed maturation of the euhalophyte *Suaeda salsa*. *Plant Biosyst.* 150, 83–90. doi: doi.10.1080/11263504.2014.976294

Zou, J. T., Abrams, G. D., Barton, D. L., Taylor, D. C., Pomeroy, M. K., and Abrams, S. R. (1995). Induction of lipid and oleosin biosynthesis by (+)- abscisic acid and its metabolites in microspore-derived embryos of *Brassica napus* L.cv reston (biological responses in the presence of 8[prime]-hydroxyabscisic acid). *Plant Physiol.* 108, 563–571. doi: 10.1104/pp.108.2.563

Conflict of Interest: The authors declare that the research was conducted in the absence of any commercial or financial relationships that could be construed as a potential conflict of interest.

frontiers in Plant Science

ORIGINAL RESEARCH
published: 29 January 2020
doi: 10.3389/fpls.2019.01744

Heterogeneous Distribution of Erucic Acid in *Brassica napus* Seeds

Shaoping Lu[1†], *Mina Aziz*[2,3†], *Drew Sturtevant*[2,3,4], *Kent D. Chapman*[2,3*] *and Liang Guo*[1*]

[1] National Key Laboratory of Crop Genetic Improvement, Huazhong Agricultural University, Wuhan, China, [2] Center for Plant Lipid Research and Department of Biological Sciences, University of North Texas, Denton, TX, United States, [3] BioDiscovery Institute, University of North Texas, Denton, TX, United States, [4] University of Texas Southwestern Medical Center, Dallas, TX, United States

Brassica napus (*B. napus*) is the world's most widely grown temperate oilseed crop. Although breeding for human consumption has led to removal of erucic acid from refined canola oils, there is renewed interest in the industrial uses of erucic acid derived from *B. napus*, and there is a rich germplasm available for use. Here, low- and high-erucic acid accessions of *B. napus* seeds were examined for the distribution of erucic acid-containing lipids and the gene transcripts encoding the enzymes involved in pathways for its incorporation into triacylglycerols (TAGs) across the major tissues of the seeds. In general, the results indicate that a heterogeneous distribution of erucic acid across *B. napus* seed tissues was contributed by two isoforms (out of six) of *FATTY ACYL COA ELONGASE* (*FAE1*) and a combination of phospholipid:diacylglycerol acyltransferase (PDAT)- and diacylglycerol acyltransferase (DGAT)-mediated incorporation of erucic acid into TAGs in cotyledonary tissues. An absence of the expression of these two *FAE1* isoforms accounted for the absence of erucic acid in the TAGs of the low-erucic accession.

Keywords: *Brassica napus*, canola, erucic acid, spatial distribution, matrix assisted laser desorption/ionization-mass spectrometry imaging

OPEN ACCESS

Edited by:
Xue-Rong Zhou, Commonwealth Scientific and Industrial Research Organization, Australia

Reviewed by:
Guanqun (Gavin) Chen, University of Alberta, Canada
Cunmin Qu, Southwest University, China

***Correspondence:**
Kent D. Chapman
chapman@unt.edu
Liang Guo
guoliang@mail.hzau.edu.cn

[†]*These authors have contributed equally to this work*

Specialty section:
This article was submitted to Plant Metabolism and Chemodiversity, a section of the journal Frontiers in Plant Science

Received: *20 October 2019*
Accepted: *11 December 2019*
Published: *29 January 2020*

Citation:
Lu S, Aziz M, Sturtevant D, Chapman KD and Guo L (2020) Heterogeneous Distribution of Erucic Acid in Brassica napus Seeds. Front. Plant Sci. 10:1744. doi: 10.3389/fpls.2019.01744

INTRODUCTION

Brassica napus (AACC, 2n = 38) is an allotetraploid oilseed plant species formed by the hybridization of two diploid species of *Brassica rapa* (AA, 2n = 20) and *Brassica oleracea* (CC, 2n = 18) about 7,500 years ago (Chalhoub et al., 2014; An et al., 2019). It is the third largest oil crop in the world and accounts for approximately 15% of the vegetable oil used for human consumption (Wells et al., 2014; Liu et al., 2016; Carruthers et al., 2017; Kaur et al., 2019). Like most oilseeds, triacylglycerols (TAGs) comprise 95% of *B. napus* seed oil which are composed of a glycerol backbone esterified with three fatty acyl chains (Ai et al., 2014; Guan et al., 2016). These fatty acids vary in levels of saturation and carbon lengths and can contain mono/polyunsaturated fatty acids such as oleic (C18:1), linoleic (C18:2), linolenic (C18:3) and erucic (C22:1) acids, and/or saturated fatty acids such as palmitic acid (C16:0) and stearic acid (C18:0) (Zhao et al., 2007; Lu et al., 2016; Zhao et al., 2019).

There are two major seed-oil types of *B. napus*, low-erucic acid type and high-erucic acid type. Low erucic acid content (< 2%) is a major evaluation index for edible rapeseed cultivars (Hristov et al., 2011; Yan et al., 2015), and reducing erucic acid content has been a major goal for rapeseed

breeding programs (Yan et al., 2015; Zhao et al., 2019). Alternatively, cultivars of *B. napus* containing high erucic acid are an important resource for industrial applications (Hristov et al., 2011). Recently, with the increasing demand for biodegradable and environmentally safe oil products such as biodiesel, lubricants, surfactants, pharmaceuticals, cosmetics, soaps, rubber and nylon, there has been renewed demand for erucic acid from high-erucic acid rapeseed (Hristov et al., 2011; Li et al., 2012; Konkol et al., 2019). In fact, *B. napus* cultivars were naturally high in erucic acid before the canola cultivar was bred for human consumption in 1974 (Hristov et al., 2011).

Although *de novo* fatty acid synthesis occurs in the plastids, long-chain monounsaturated fatty acids are formed in the cytoplasm by a membrane-bound FATTY ACYL COA ELONGASE (FAE) complex on the endoplasmic reticulum (ER) (Katavic et al., 2002). The plastid-produced oleic acid (C18:1) is the initial substrate for the FAE complex to generate erucic acid (C22:1) in *B. napus*, through two cycles of elongation. Each round of elongation involves four reactions catalyzed by the FAE complex. The first step involves a condensation of the C18:1-CoA with malonyl-CoA to generate the corresponding 3-ketoacyl-CoA. This 3-ketoacyl-CoA is then reduced to a 3-hydroxyacyl-CoA derivative that undergoes sequential dehydration and reduction to generate the elongated acyl-CoA final product (Katavic et al., 2002). FAE1 is the condensing enzyme that catalyzes the first of four reactions of the FAE complex, and is the rate-limiting enzyme that controls erucic acid accumulation in *B. napus* (Millar and Kunst, 1997). In *B. napus*, there are six paralogs encoding FAE1 proteins (Qiu et al., 2006; Wu et al., 2008; Cao et al., 2010). *BnaA8.FAE1* and *BnaC3.FAE1* are the two major genes responsible for erucic acid synthesis in *B. napus* seeds and they elongate 18:1-CoA to 20:1-CoA, and then 20:1-CoA to 22:1-CoA (Furmanek et al., 2014; Kaur et al., 2019). These two genes are highly expressed in the seeds of high-erucic acid varieties and are minimally expressed in low- erucic acid varieties (Qiu et al., 2006; Cao et al., 2010). After the formation of 22:1-CoA, it can be acylated to the glycerol backbone by enzymes in either the canonical Kennedy or Lands pathways to ultimately form TAG (Chapman and Ohlrogge, 2012; Furmanek et al., 2014).

In oilseeds, TAGs are primarily stored in the embryo, which consists of outer cotyledons (OC), inner cotyledons (IC), and an embryonic axis (EA) (Borisjuk et al., 2013; Woodfield et al., 2017; Lu et al., 2018). Previous studies of *B. napus* seeds with low erucic acid content have shown that total lipids and lipid molecular species are differentially distributed across its seed tissues (Borisjuk et al., 2013; Woodfield et al., 2017; Lu et al., 2018). Although the metabolism of erucic acid is understood, the spatial distribution of lipids containing erucic acid has not been explored. Matrix assisted laser desorption/ionization-mass spectrometry imaging (MALDI-MSI) is a mass spectrometry visualization platform for imaging metabolites *in situ* and has been an important tool for mapping the spatial distributions of glycerolipids in oilseeds, especially phosphatidylcholine (PC) and TAG (Horn and Chapman, 2014a; Sturtevant et al., 2015). Currently, MADLI-MSI has been used to analyze the spatial distribution of lipid metabolites in many oilseeds including cotton, castor, *Camelina*, *Arabidopsis* and low-erucic varieties of *B. napus* seeds (Horn et al., 2012; Horn et al., 2013; Horn et al., 2014; Horn and Chapman, 2014a; Sturtevant et al., 2016; Woodfield et al., 2017; Lu et al., 2018; Sturtevant et al., 2019). Here, two *B. napus* accessions, WH3401 (high-erucic) and WY20 (low-erucic), were comprehensively analyzed to compare their lipid distributions as well as gene expression profiles of *FAE1* and other related lipid biosynthesis genes. Results presented here will help elucidate the mechanisms for controlling the heterogeneous deposition of erucic acid in *B. napus* seed tissues.

MATERIALS AND METHODS

Plant Seed Collection and Analysis

B. napus accessions, WH3401 and WY20, are part of a collection of natural and breeder-developed accessions that have been planted in Wuhan, China for many years. The agronomic traits of both accessions are stable. Mature seeds of field-grown plants were collected to measure oil content, using near infrared spectroscopy, and to determine erucic acid content. Seed weight (1,000-seed weight) and seed diameter were also measured. For developing seeds, flowers were labelled after bud opening and were bagged for seed selfing. Developing seeds were collected from 5–6 individual plants grown in the field on the campus of Huazhong Agricultural University. Seeds were collected from siliques 18, 23, 28, 33, 38, 43, 48, and 53 days after flowering (DAF), and were flash-frozen in liquid nitrogen for the analysis of seed dry weight, fatty acid composition, and TAG content, as well as for RNA extractions. Mature desiccated seeds were used for gas chromatography-flame ionization detector (GC-FID), MALDI-MSI and electrospray ionization-mass spectrometry (ESI-MS) analysis.

Mature desiccated seeds from 5-6 individual plants were dissected, and OC, IC, EA, and SC were separated under stereoscopic microscope and weighed as described previously (Lu et al., 2018). Fatty acid composition of dissected seed tissues, developing and mature seeds was quantified as methyl esters using a GC-FID (based on the internal standard heptadecanoic acid, C17:0, added at the time of extraction), following the method described by Lu et al. (2016).

Tissue Preparation and Lipid Distribution Analysis by MALDI-MS Imaging

Mature desiccated seeds of two accessions were embedded in a 10% gelatin solution, frozen and cryo-sectioned as described previously (Sturtevant et al., 2015). Tissue sections were coated with 2, 5-dihydroxybenzoic acid (DHB; 98%, Sigma-Aldrich) by sublimation, following the method adapted from Hankin et al. (2007). Coated seed sections were analyzed by a hybrid MALDI-linear ion trap-Orbitrap mass spectrometer (MALDI-LTQ-Orbitrap XL; Thermo Scientific, San Jose, CA, USA) as described by Lu et al. (2018). MALDI-MSI data analysis and images processing were performed according to the method described by Horn and Chapman (2014b).

ESI-MS Analysis of TAG and PC of Whole Seeds

Lipids were extracted from mature seeds as described by Chapman and Moore (1993) using hot-isopropanol to inactivate phospholipases. TAG (tri-17:0) and PC (di-14:0) (Sigma-Aldrich) were added into the extraction solution as internal standards. Crude lipid extracts were purified and neutral and polar lipids were separated and eluted as described previously (Lu et al., 2018). The neutral and polar lipid fractions were analyzed on an API 3000 mass spectrometer (SCIEX, https://sciex.com) to determine TAG and PC species and content. Instrument conditions were set as described by Welti et al. (2002) and Li et al. (2014). The molecular compositions of TAG and PC were determined from full MS scans and precursor ion fragment of the head group at *m/z* of 184.07, respectively. Data analysis used an open source software, LipidomeDB Data as described by Zhou et al. (2011).

RNA Extraction and Real-Time PCR

Developing seeds collected from 3 individual plants were used for RNA extraction for real-time qPCR analysis. The RNA was extracted from 18, 23, 28, 33, 38, 43, 48, 53 DAF seeds and OC, IC, EA of 43 DAF seeds using RNAprep pure plant kit (DP432, http://www.tiangen.com/). The RNA extracts were used to synthesize the first-strand cDNA using an EasyScript RT Kit (AE311-03). Quantitative PCR (qPCR) was done using the BIO-RAD CFX96 qPCR detection system (Bio-Rad, http://www.bio-rad.com) with SYBR green to monitor dsDNA accumulation. The primers of *FAE1s* were designed to test the total expression of *FAE1b* and *f*, as well as *FAE1a* and *e* because they have highly similar sequences, respectively. All primers used for qPCR were listed in **Table S1**. The qPCR conditions were the same as described previously (Lu et al., 2018). Gene expression levels estimated by real-time qPCR were normalized to the levels of *BnACTIN*.

RESULTS AND DISCUSSION

Comparative Analysis of Two *B. napus* Seeds Differing in Erucic Acid Content

In the current study, two natural *B. napus* accessions that differ in their erucic acid content were selected, WH3401 (high-erucic), which contains ca. 34% erucic acid, and WY20 (low-erucic) with almost no erucic acid content. The two accessions had different general and storage characteristics as summarized in **Table 1**. Compared to WH3401, WY20 had larger seed size and weight, but lower seed oil content. The seed oil content was measured by near-infrared spectrometry, and the average seed oil content over a three-year period was 54 and 42% in WH3401 and WY20, respectively (**Table 1**). Moreover, the fatty acid (FA) composition of the seeds was determined by GC-FID, and the two accessions exhibited different fatty acid profiles. The C18:1, C20:1, and C22:1 species constituted ca. 20, 15, and 40%, respectively, of the total fatty acid pool in the high-erucic accession. While in the low-erucic seeds, C18:1 was the major fatty acid, representing ca. 70% of the total fatty acid content, with only traces of C20:1 and C22:1 detected. The levels of the other fatty acids were similar between the two accessions (**Figure 1A**).

TABLE 1 | The characteristics of high- and low-erucic acid rapeseed (*Brassica napus* L.).

Name	Seed oil content (%)	Erucic acid content (%)	Weight /1,000 seed (g)	Diameter (mm)
WH3401	54.52 ± 2.00	34.05 ± 0.26	3.31 ± 0.10	1.84 ± 0.04
WY20	42.60 ± 0.97**	0.20 ± 0.25**	4.00 ± 0.07**	1.99 ± 0.06**

*Two inbreed accessions were naturalized in Hubei for many years, the agronomic traits trend to be stable. The data of seed oil content, erucic acid content and seed weight are the average value of 3 years. Open-pollen seeds were analyzed by near infrared spectrometer and 5 plants were analyzed for each accession every year. ** denotes significant difference at* $P < 0.01$ *using student t-test.*

The different seed tissues of the two accessions, including the outer cotyledon (OC), inner cotyledon (IC), embryonic axis (EA), and seed coat (SC) were dissected, and separately analyzed for weight, fatty acid composition, and oil content (**Figure 1**); a representative image of the different seed tissues under bright-field microscope is shown (**Figure 1B**). The weight percentage of each of the four tissues per seed was similar between the two accessions with the OC having the highest proportion among the different tissues (**Figure 1C**). However, it seems that WH3401 has a relatively thicker seed coat, where the SC represents 30% of the seed weight, versus 20% in WY20 (**Figure 1C**). This difference in the seed coat was associated with a decrease in the proportion of the OC in WH3401 (35%) compared to WY20 (44%) (**Figure 1C**). Not surprisingly, the fatty acid composition in the four seed tissues does reflect that of the whole seeds for both accessions (**Figure 1D**). In WH3401, the C22:1 had the highest percentage (ca. 45%) in the outer and inner cotyledons, while in EA and SC tissues, C18:1, C18:2, and C22:1 nearly had equal proportions (ca. 25% each) of the total fatty acids. By contrast, in WY20, the C18:1 species was the most abundant in all the four seed tissues, it was ca. 62, 64, 48, and 53% in OC, IC, EA, and SC (**Figure 1D**). As with the whole-seed oil content, each of the dissected seed tissues had higher oil content in WH3401, relative to WY20, with the SC has the lowest oil content among all tissues in both accessions (**Figure 1E**).

Furthermore, water content, dry weight and FA accumulation were measured at different time points during seed development, spanning 18-53 DAF (**Figure 2**). Water content and dry weight mass were comparable between WH3401 and WY20 throughout seed development (**Figure 2A**). For FA accumulation, a difference was observed between the two accessions as early as 33 DAF, but it became more pronounced at later stages (**Figure 2B**). As expected, the accumulation of C20:1 and C22:1 fatty acid was greater in WH3401 than WY20, while opposite pattern was observed for the other fatty acids, especially the C16:0, C18:0, C18:1, and C18:2 species (**Figure 2B**).

Spatial Distribution of TAG and PC in *B. napus* Seeds *in situ*

To get insights into the tissue distribution of TAGs and the metabolic precursors, PCs, seeds of both accessions were cryo-

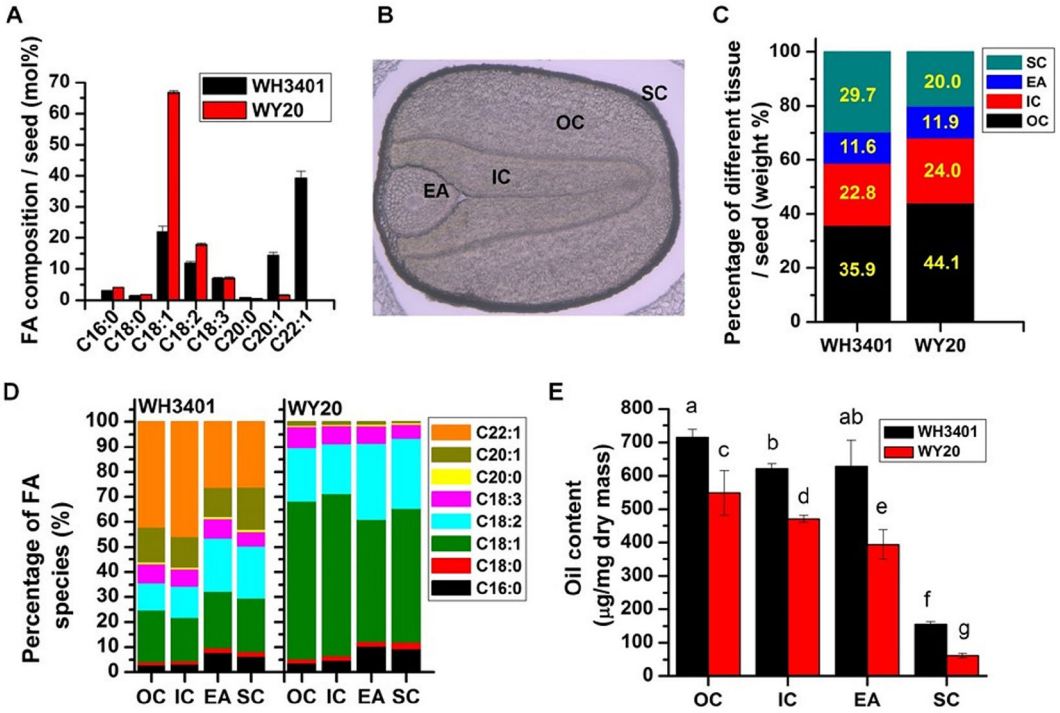

FIGURE 1 | Oil content and fatty acid composition in dissected seed tissues. **(A)** Fatty acid composition in whole seeds (means ± SD, n = 6). **(B)** Seed structure under bright-field microscope. **(C)** Percentage of different tissues in whole seeds. **(D)** Fatty acid composition of different seed tissues. **(E)** Oil content of different seed tissues (means ± SD, n = 5–6). Letters denote significant difference at $P < 0.05$ using ANOVA analysis. FA, fatty acid; EA, embryonic axis; IC, inner cotyledon; OC, outer cotyledon; SC, seed coat.

sectioned and analyzed with MALDI-MSI (Horn and Chapman, 2014a; Horn and Chapman, 2014b; Sturtevant et al., 2015; Woodfield et al., 2017) (**Figures. S1**, **S2** and **3**). High-resolution mass spectra were collected at each location on the tissue sections at 40-micron step size, and the data were analyzed by Metabolite Imager software (Horn and Chapman, 2014b). The ion intensities for TAG and PC molecular species were converted to mol%, and then plotted as false-color images on a green (minimum) to red (maximum) scale representing the ion intensity corresponding to each *m/z*, with the scale adjusted individually to visualize the distribution of each molecular species across the seeds. Moreover, the relative levels of TAG and PC molecular species analyzed by MALDI-MSI (calculated as mol% from the ion intensities summed over the entire tissue section) were compared to those determined quantitatively in whole-seed extracts by ESI-MS. Both methods showed consistency in the measured average mol% for most of the determined molecular species (**Figure 4**).

For TAGs, the 50C and 52C series had similar distribution pattern between both accessions, and heterogeneity was mainly observed between the cotyledonary tissues and embryonic axis, where these species were preferentially localized to the embryonic axis (**Figure S1**). Since the 18C fatty acids (especially C18:1) were the major fatty acids in the low-erucic accession (WY20), the corresponding 54C TAGs, mainly TAG-54:3, TAG-54:4, and TAG-54:5, were the most abundant TAG species in this accession (**Figure 4A**), and they were either more enriched in the cotyledons (e.g. TAG-54:3) or evenly distributed throughout the seed tissues (e.g. TAG-54:4 and TAG-54:5) (**Figure S1**). The other, minor 54C TAGs in WY20 were mainly localized in the embryonic axis (**Figure S1**). Conversely, in WH3401 (high-erucic), the 54C TAGs were significantly less abundant (**Figure 4A**), and were almost exclusively localized to the embryonic axis (**Figure S1**). Another major difference between both accessions is in the relative abundance of the high-molecular weight TAGs such as the 58C, 60C, and 62C series. These TAGs were the most abundant TAG molecular species in the high-erucic accession (**Figure 4A**), which is consistent with the high abundance of the C20:1 and C22:1 fatty acids in this accession, while they were barely detectable in the low-erucic accession that lacks the C20:1 and C22:1 fatty acids (**Figures 3A** and **4A**). In the high-erucic accession (WH3401), these high-molecular weight TAGs were more enriched in the cotyledonary tissues (**Figure 3A**).

For PCs, the 34C PC species were mainly localized to the embryonic axis in both accessions, except for PC34:1 which was localized to both cotyledons and the embryonic axis (**Figure S2**). The 36C PCs, mainly PC-36:2, PC-36:3, and PC-36:4, were the

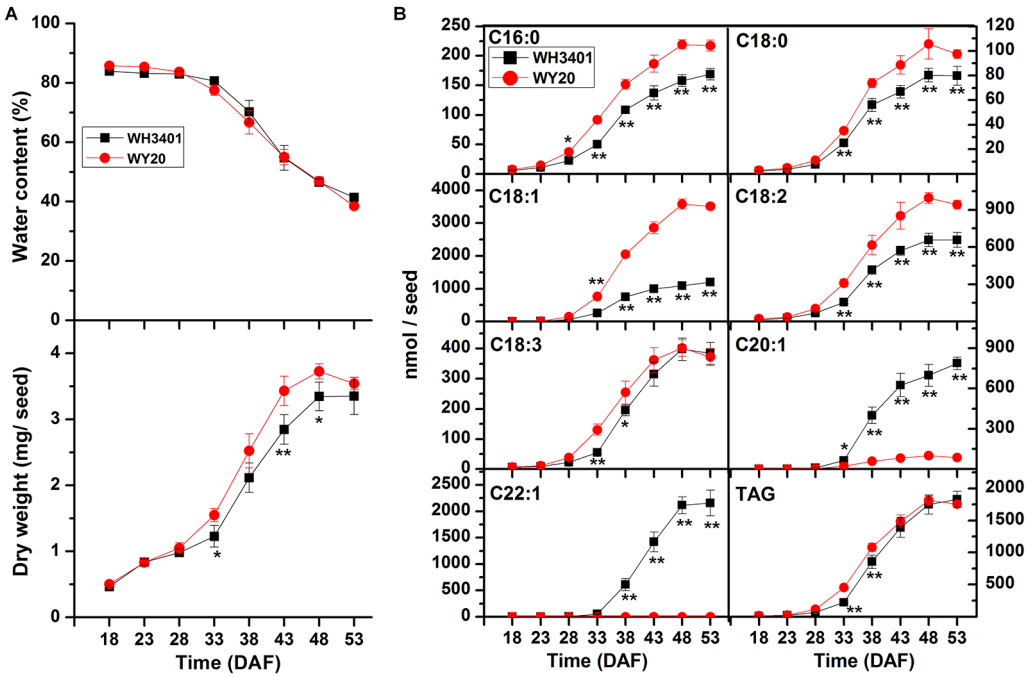

FIGURE 2 | Characterization of seed development of WH3401 and WY20. **(A)** Water content and seed weight (dry weight) during seed development. Data of seed water content and seed weight are the means ± SD of 5 individual plants. **(B)** Fatty acid accumulation during seed development. Data of fatty acid content are the means ± SD of 6 individual plants. DAF, days after flowering. * and ** denote significant difference at $P < 0.05$ and $P < 0.01$, respectively, based on Student's *t* test.

major PC species in both accessions (**Figure 4B**). These molecular species also had similar distribution patterns in both WY20 and WH3401, where PC-36:2 (the most abundant PC) was localized to the cotyledons, while PC-36:4 had a preferential localization in the embryonic axis, and PC-36:3 was uniformly distributed throughout the seed tissues (**Figure 3B**). The main difference in PC distribution between both accessions is the presence of 38C and 40C species in the high-erucic seeds, which were more enriched in the cotyledonary tissues, while these molecular species were absent in the low-erucic seeds (**Figure 3**). However, based on overall mol%, these very long chain PCs (38C and 40C) represented a relatively minor contribution to the PC pool in the high-erucic accession (WH3401; e.g., see scales are mostly less than 2 mol%). The observed distribution patterns of TAG and PC molecular species were consistent in three different biological replicates (**Figure S3**).

Gene Expression in Seed Tissues of the High- and Low-Erucic Accessions

Phylogenetic analysis of *FAE1* in *B. napus* revealed that there are 6 different *FAE1* genes (Chalhoub et al., 2014), denoted as *FAE1a-f* (**Figure S4A**). Analysis of the amino acid sequences of the 6 isoforms of FAE1 protein indicated that both FAE1a and FAE1e, as well as FAE1b and FAE1f, are more closely related to each other (**Figure S4B**). Analysis of *FAE1* expression in whole-seeds of both accessions during development showed that only the b and f isoforms were expressed in WH3401 seeds, with the highest expression detected at 43 DAF, while no *FAE1* expression was detected in WY20 at any of the selected time points (**Figure 5A**). Therefore, 43 DAF time point was selected to perform comprehensive transcriptomic analysis in dissected seed tissues of both accessions (**Figure 5B**).

FAE1 expression in the dissected seed tissues showed that *FAE1* was highly expressed in the outer and inner cotyledons of WH3401, relative to the EA, and as expected, it was barely expressed in all tissues of WY20 (**Figure 5B**). The expression pattern of *FAE1* in WH3401 was consistent with the fatty acid composition analysis showing that erucic acid (C22:1) was the most abundant FA species in the outer and inner cotyledons. It is also consistent with the MALDI-MSI results, where the erucic acid-containing TAGs (e.g. the 58C, 60C, and 62C series) were more enriched in the cotyledonary tissues than the EA.

The expression levels of the different genes involved in TAG biosynthesis in the ER were compared among the different seed tissues of the high- and low-erucic accessions (**Figure 5B**). There are two possible routes that can lead to TAG assembly in the ER. One route is through the conventional Kennedy pathway, which utilizes glycerol-3-phosphate as initial substrate and includes four sequential enzymes, glycerol-3-phosphate acyltransferase 9 (GPAT9), 1-acylglycerol-3-phosphate acyltransferase (LPAAT), phosphatidic acid phosphatase (PAP) and diacylglycerol acyltransferase (DGAT) (Chapman and Ohlrogge, 2012). In

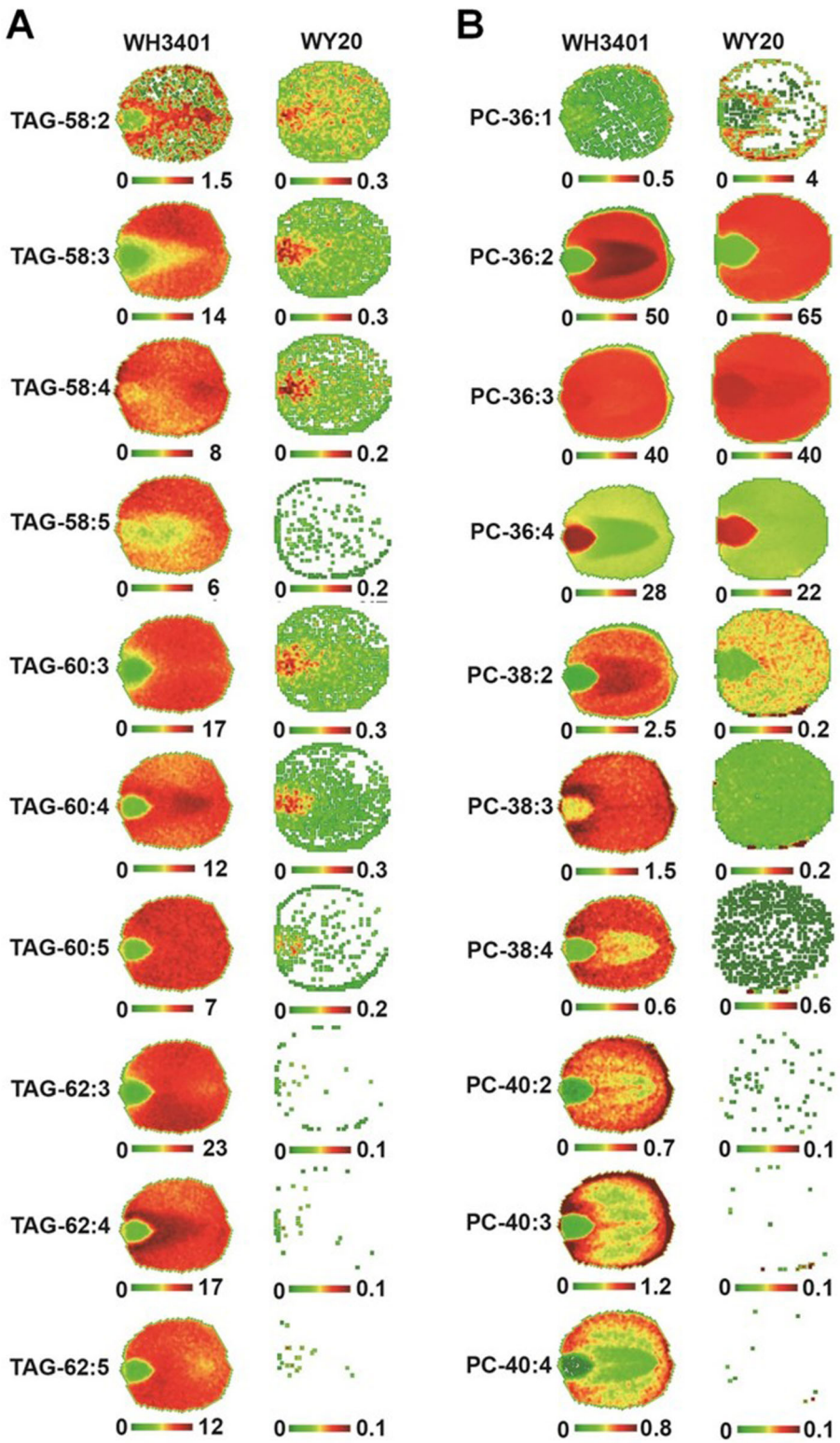

FIGURE 3 | Spatial distribution of triacylglycerol (TAG) and phosphatidylcholine (PC) species in mature seeds. False-colored images of embryo cross sections showing the spatial distribution of selected TAG **(A)** and PC **(B)** species in WH3401 and WY20 seeds. Three biological replicates with consistent results have been analyzed (**Figure S3**).

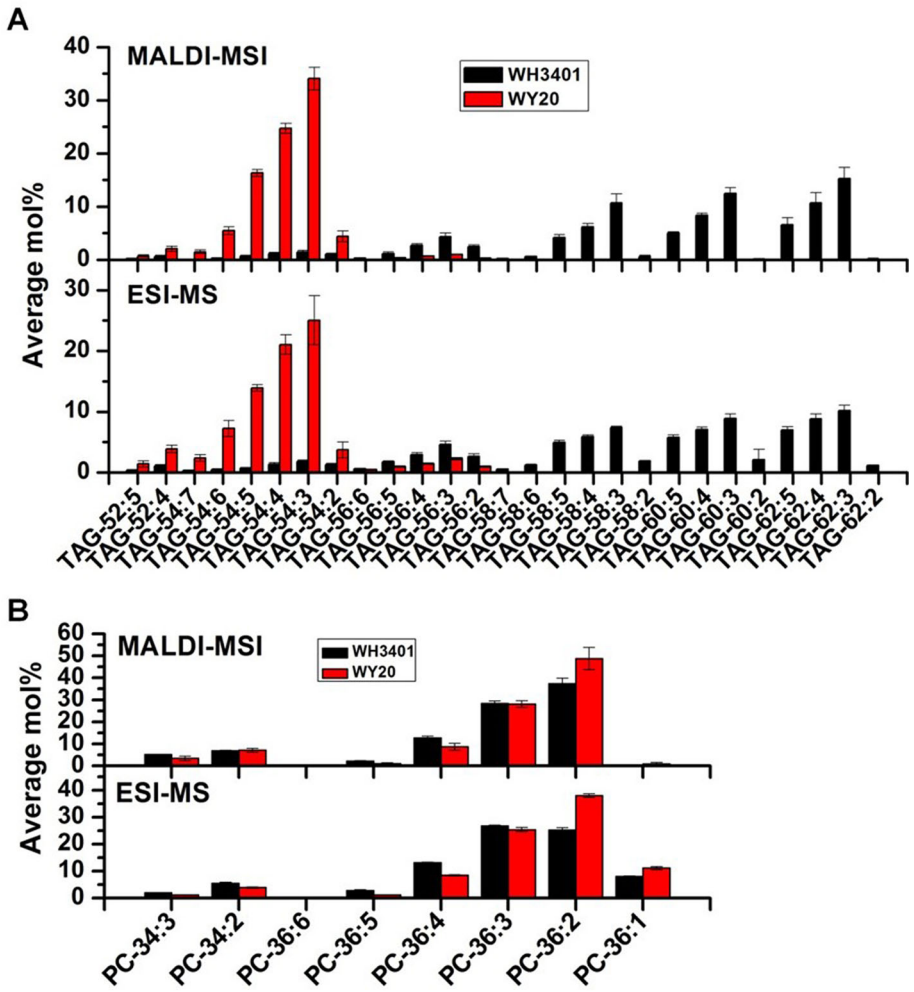

FIGURE 4 | Comparison of the relative levels of triacylglycerol (TAG) and phosphatidylcholine (PC) species in mature seeds measured by MADLI-MSI (mol% from ion intensities summed over the entire section) and ESI-MS of whole-seed extracts using tri-17:0 TAG and di-14:0 PC as a quantitative standard. **(A)** TAG species. **(B)** PC species. Data are the means ± SD of 3 biological replicates.

WH3401, *GPAT9* had the highest expression in the OC, while in WY20, it was relatively more expressed in the EA than the cotyledonary tissues. For *LPAAT*, it was highly expressed in the OC of WH3401, relative to all the other tissues of both accessions. In WH3401, *DGAT* was expressed to higher levels in the IC than the other two tissues, while in WY20, it was expressed in EA > IC > OC (**Figure 5B**). The other pathway of TAG assembly involves the transfer of an acyl chain from the acyl-CoA pool to lysophosphatidylcholine (LPC) to form PC, and then from PC to diacylglycerol (DAG) to form TAG, *via* the action of two enzymes, lysophosphatidylcholine acyltransferase (LPCAT) and phospholipid:diacylglycerol acyltransferase (PDAT), respectively (Chapman and Ohlrogge, 2012). In WH3401, *LPCAT* was more expressed in the cotyledonary tissue than the EA, while opposite pattern was observed in WY20. *PDAT* had a similar expression pattern to that of *LPAAT*, where the highest expression level was observed in the OC of WH3401 compared to all the other tissues of both accessions (**Figure 5**). Based on these results, it seems that both pathways could be contributing to the assembly of erucic acid-containing TAGs in WH3401, since the expression pattern of almost all the genes of both the TAG biosynthesis pathways suggests a more enrichment in the cotyledonary tissues, relative to the EA, which is consistent with the observed cotyledonary localization of erucic acid-containing TAGs in this accession. However, the affinity of native lysophosphatidic acid acyltransferase (LPAAT) is poor for fatty acyl chains with more than 18 carbons, implying C22:1 is difficult to incorporate into the *sn-2* position of lipids by the Kennedy pathway (Lassner et al., 1996; Furmanek et al., 2014; Kaur et al., 2019) (**Figure 5**). This may suggest that LPCAT and PDAT help to compensate for this deficiency of LPAAT by introducing erucic acid into the *sn*-2 position of TAGs. Further positional analysis of PC and glycerolipid molecular species will be necessary to confirm this speculation. In any case, it seems that there is a complex and heterogeneous distribution of TAG

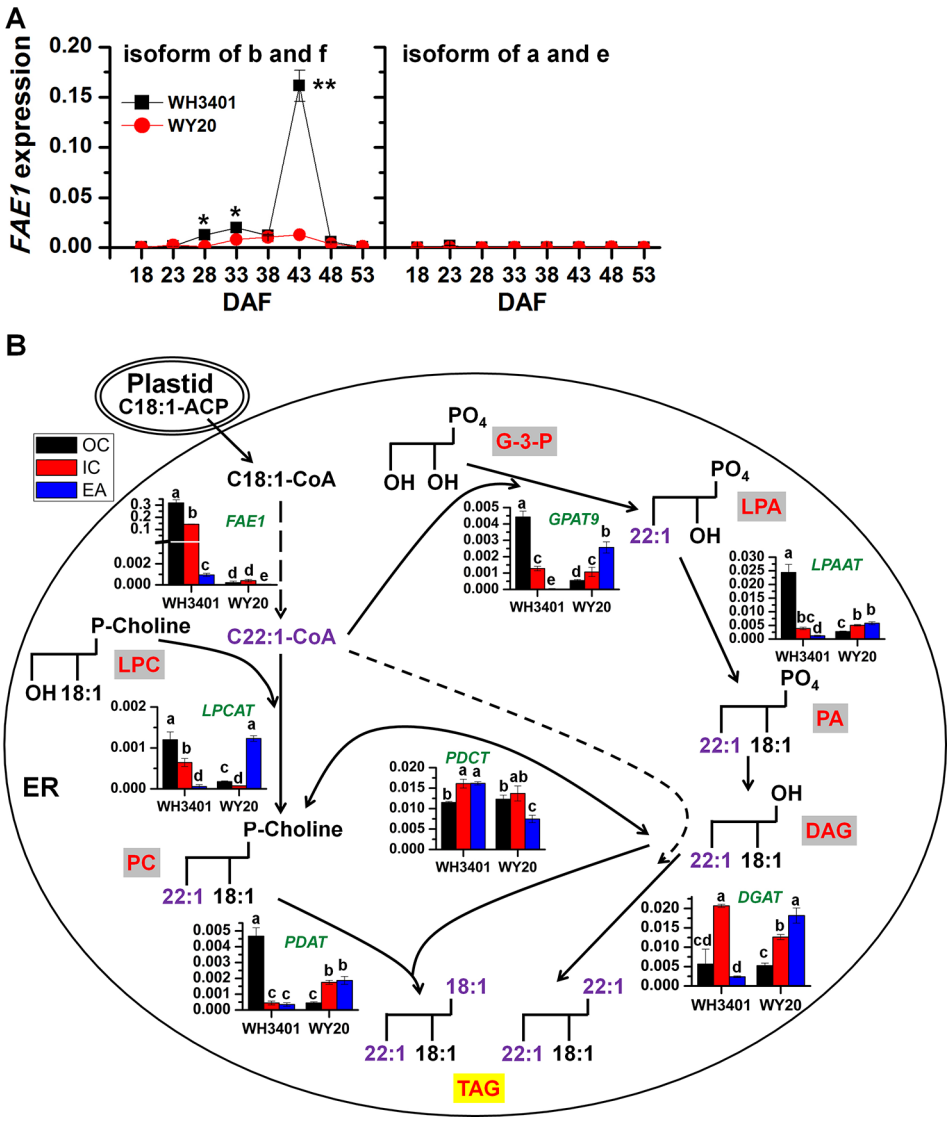

FIGURE 5 | The gene expression change of *FAE1s* in developing seeds and a model of TAG accumulation explaining C22:1 flux into TAG (means ± SD, n = 3). **(A)** Total expression level of the b and f isoforms, as well as the a and e isoforms of *FAE1* in the whole seeds during seed development. * and ** denote significant difference at $P < 0.05$ and $P < 0.01$, respectively, based on Student's *t* test. **(B)** Gene expression levels in the different tissues of 43-day-old seeds mapped to the TAG biosynthesis pathway. Data represent the average of gene expression level of 3 biological replicates. Letters denote significant difference at $P < 0.05$ using ANOVA analysis. Green italic letter denotes gene names, while red letter with gray or yellow background frame denotes lipid classes. EA, embryonic axis; IC, inner cotyledon; OC, outer cotyledon; G-3-P, glycerol-3-phosphate; GPAT9, glycerol-3-phosphate acyltransferase 9; LPA, lysophosphatidic acid; LPAAT, lysophosphatidic acid acyltransferase; PA, phosphatidic acid; DAG, diacylglycerol; DGAT, diacylglycerol acyltransferase; TAG, triacylglycerol; FAE1, fatty acid elongase 1; LPC, lysophosphatidylcholine; LPCAT, lysophosphatidylcholine acyltransferase; PC, phosphatidylcholine; PDCT, phosphatidylcholine:diacylglycerol cholinephosphotransferase; PDAT, phospholipid:diacylglycerol acyltransferase.

pathways that contributes to the enrichment of erucic acid in TAG in cotyledons.

CONCLUSION

Here, the distribution of the erucic acid in *B. napus* seeds, and the transcripts encoding the elongation enzymes primarily responsible for its synthesis, were identified. As expected, the distribution of the *FAE1* transcripts were associated with the distributions of total erucic acid in seed parts analyzed by GC-FID, or in TAGs analyzed by ESI-MS (in extracts) or by MALDI-MSI (*in situ* in seed sections). The pathways for TAG assembly of erucic acid-containing TAGs could be through either DGAT or PDAT based on expression patterns and pathway analysis. Overall, these studies shed light on the spatial complexity of TAG assembly in *B. napus* seeds, especially for erucic acid-containing TAGs.

DATA AVAILABILITY STATEMENT

The datasets generated for this study are available on request to the corresponding authors.

AUTHOR CONTRIBUTIONS

LG, KC, and SL designed and supervised the study. SL, MA, and DS performed the experiments and data analysis. SL and MA prepared the manuscript. LG, KC, and DS revised the manuscript. All the authors read and approved the manuscript.

FUNDING

This work was supported by National Natural Science Foundation of China (31701458, 31871658) and a grant from the U.S. Department of Energy, Biological and Environmental Research (BER) program under contract # DE-SC0020325.

SUPPLEMENTARY MATERIAL

The Supplementary Material for this article can be found online at: https://www.frontiersin.org/articles/10.3389/fpls.2019.01744/full#supplementary-material

REFERENCES

Ai, F. F., Bin, J., Zhang, Z. M., Huang, J. H., Wang, J. B., Liang, Y. Z., et al. (2014). Application of random forests to select premium quality vegetable oils by their fatty acid composition. *Food Chem.* 143, 472–478. doi: 10.1016/j.foodchem.2013.08.013

An, H., Qi, X., Gaynor, M. L., Hao, Y., Gebken, S. C., Mabry, M. E., et al. (2019). Transcriptome and organellar sequencing highlights the complex origin and diversification of allotetraploid Brassica napus. *Nat. Commun.* 10, 2878. doi: 10.1038/s41467-019-10757-1

Borisjuk, L., Neuberger, T., Schwender, J., Heinzel, N., Sunderhaus, S., Fuchs, J., et al. (2013). Seed architecture shapes embryo metabolism in oilseed rape. *Plant Cell* 25, 1625–1640. doi: 10.1105/tpc.113.111740

Cao, Z., Tian, F., Wang, N., Jiang, C., Lin, B., Xia, W., et al. (2010). Analysis of QTLs for erucic acid and oil content in seeds on A8 chromosome and the linkage drag between the alleles for the two traits in Brassica napus. *J. Genet. Genomics* 37, 231–240. doi: 10.1016/S1673-8527(09)60041-2

Carruthers, J. M., Cook, S. M., Wright, G. A., Osborne, J. L., Clark, S. J., Swain, J. L., et al. (2017). Oilseed rape (Brassica napus) as a resource for farmland insect pollinators: quantifying floral traits in conventional varieties and breeding systems. *Glob Change Biol. Bioenergy* 9, 1370–1379. doi: 10.1111/gcbb.12438

Chalhoub, B., Deboeud, F., Liu, S. Y., Parkin, I. A. P., Tang, H. B., Wang, X. Y., et al. (2014). Early allopolyploid evolution in the post-Neolithic Brassica napus oilseed genome. *Science* 345, 950–953. doi: 10.1126/science.1253435

Chapman, K. D., and Moore, T. S. (1993). N-acylphosphatidylethanolamine synthesis in plants: occurrence, molecular composition, and phospholipid origin. *Arch. Biochem. Biophys.* 301, 21–33. doi: 10.1006/abbi.1993.1110

Chapman, K. D., and Ohlrogge, J. B. (2012). Compartmentation of triacylglycerol accumulation in plants. *J. Biol. Chem.* 287, 2288–2294. doi: 10.1074/jbc.R111.290072

Furmanek, T., Demski, K., Banas, W., Haslam, R., Napier, J., Stymne, S., et al. (2014). The utilization of the acyl-CoA and the involvement PDAT and DGAT in the biosynthesis of erucic acid-rich triacylglycerols in Crambe seed oil. *Lipids* 49, 327–333. doi: 10.1007/s11745-014-3886-7

Guan, M., Chen, H., Xiong, X., Lu, X., Li, X., Huang, F., et al. (2016). A study on triacylglycerol composition and the structure of high-oleic rapeseed oil. *Engineering* 2, 258–262. doi: 10.1016/J.Eng.2016.02.004

Hankin, J. A., Barkley, R. M., and Murphy, R. C. (2007). Sublimation as a method of matrix application for mass spectrometric imaging. *J. Am. Soc. Mass Spectrom* 18, 1646–1652. doi: 10.1016/j.jasms.2007.06.010

Horn, P. J., and Chapman, K. D. (2014a). Lipidomics in situ: insights into plant lipid metabolism from high resolution spatial maps of metabolites. *Prog. Lipid Res.* 54, 32–52. doi: 10.1016/j.plipres.2014.01.003

Horn, P. J., and Chapman, K. D. (2014b). Metabolite Imager: customized spatial analysis of metabolite distributions in mass spectrometry imaging. *Metabolomics* 10, 337–348. doi: 10.1007/s11306-013-0575-0

Horn, P. J., Korte, A. R., Neogi, P. B., Love, E., Fuchs, J., Strupat, K., et al. (2012). Spatial mapping of lipids at cellular resolution in embryos of cotton. *Plant Cell* 24, 622–636. doi: 10.1105/tpc.111.094581

Horn, P. J., Silva, J. E., Anderson, D., Fuchs, J., Borisjuk, L., Nazarenus, T. J., et al. (2013). Imaging heterogeneity of membrane and storage lipids in transgenic Camelina sativa seeds with altered fatty acid profiles. *Plant J.* 76, 138–150. doi: 10.1111/tpj.12278

Horn, P. J., Sturtevant, D., and Chapman, K. D. (2014). Modified oleic cottonseeds show altered content, composition and tissue-specific distribution of triacylglycerol molecular species. *Biochimie* 96, 28–36. doi: 10.1016/j.biochi.2013.08.010

Hristov, A. N., Domitrovich, C., Wachter, A., Cassidy, T., Lee, C., Shingfield, K. J., et al. (2011). Effect of replacing solvent-extracted canola meal with high-oil traditional canola, high-oleic acid canola, or high-erucic acid rapeseed meals on rumen fermentation, digestibility, milk production, and milk fatty acid composition in lactating dairy cows. *J. Dairy Sci.* 94, 4057–4074. doi: 10.3168/jds.2011-4283

Katavic, V., Mietkiewska, E., Barton, D. L., Giblin, E. M., Reed, D. W., and Taylor, D. C. (2002). Restoring enzyme activity in nonfunctional low erucic acid Brassica napus fatty acid elongase 1 by a single amino acid substitution. *FEBS J.* 269, 5625–5631. doi: 10.1046/j.1432-1033.2002.03270.x

Kaur, H., Wang, L., Stawniak, N., Sloan, R., Van Erp, H., Eastmond, P., et al. (2019). The impact of reducing fatty acid desaturation on the composition and thermal stability of rapeseed oil. *Plant Biotechnol. J.* doi: 10.1111/pbi.13263

Konkol, D., Szmigiel, I., Domzal-Kedzia, M., Kulazynski, M., Krasowska, A., Opalinski, S., et al. (2019). Biotransformation of rapeseed meal leading to production of polymers, biosurfactants, and fodder. *Bioorg Chem.* 93. doi: 10.1016/j.bioorg.2019.03.039

Lassner, M., Lardizabal, K. D., and Metz, J. G. (1996). A jojoba beta-Ketoacyl-CoA synthase cDNA complements the canola fatty acid elongation mutation in transgenic plants. *Plant Cell* 8, 281–292. doi: 10.1105/tpc.8.2.281

Li, X., Van Loo, E. N., Gruber, J., Fan, J., Guan, R., Frentzen, M., et al. (2012). Development of ultra-high erucic acid oil in the industrial oil crop Crambe abyssinica. *Plant Biotechnol. J.* 10, 862–870. doi: 10.1111/j.1467-7652.2012.00709.x

Li, M., Baughman, E., Roth, M. R., Han, X., Welti, R., and Wang, X. (2014). Quantitative profiling and pattern analysis of triacylglycerol species in *Arabidopsis* seeds by electrospray ionization mass spectrometry. *Plant J.* 77, 160–172. doi: 10.1111/tpj.12365

Liu, S., Fan, C., Li, J., Cai, G., Yang, Q., Wu, J., et al. (2016). A genome-wide association study reveals novel elite allelic variations in seed oil content of Brassica napus. *Theor. Appl. Genet.* 129, 1203–1215. doi: 10.1007/s00122-016-2697-z

Lu, S., Yao, S., Wang, G., Guo, L., Zhou, Y., Hong, Y., et al. (2016). Phospholipase Depsilon enhances Braasca napus growth and seed production in response to nitrogen availability. *Plant Biotechnol. J.* 14, 926–937. doi: 10.1111/pbi.12446

Lu, S., Sturtevant, D., Aziz, M., Jin, C., Li, Q., Chapman, K. D., et al. (2018). Spatial analysis of lipid metabolites and expressed genes reveals tissue-specific heterogeneity of lipid metabolism in high- and low-oil *Brassica napus* L. seeds. *Plant J.* 94, 915–932. doi: 10.1111/tpj.13959

Millar, A. A., and Kunst, L. (1997). Very-long-chain fatty acid biosynthesis is controlled through the expression and specificity of the condensing enzyme. *Plant J.* 12, 121–131. doi: 10.1046/j.1365-313X.1997.12010121.x

Qiu, D., Morgan, C., Shi, J., Long, Y., Liu, J., Li, R., et al. (2006). A comparative linkage map of oilseed rape and its use for QTL analysis of seed oil and erucic acid content. *Theor. Appl. Genet.* 114, 67–80. doi: 10.1007/s00122-006-0411-2

Sturtevant, D., Lee, Y. J., and Chapman, K. D. (2015). Matrix assisted laser desorption/ionization-mass spectrometry imaging (MALDI-MSI) for direct visualization of plant metabolites in situ. *Curr. Opin. Biotechnol.* 37, 53–60. doi: 10.1016/j.copbio.2015.10.004

Sturtevant, D., Duenas, M. E., Lee, Y. J., and Chapman, K. D. (2016). Three-dimensional visualization of membrane phospholipid distributions in Arabidopsis thaliana seeds: a spatial perspective of molecular heterogeneity. *Biochim. Biophys. Acta* 1862, 268–281. doi: 10.1016/j.bbalip.2016.11.012

Sturtevant, D., Romsdahl, T. B., Yu, X.-H., Burks, D. J., Azad, R. K., Shanklin, J., et al. (2019). Tissue-specific differences in metabolites and transcripts contribute to the heterogeneity of ricinoleic acid accumulation in Ricinus communis L. (castor) seeds. *Metabolomics* 15. doi: 10.1007/s11306-018-1464-3

Wells, R., Trick, M., Soumpourou, E., Clissold, L., Morgan, C., Werner, P., et al. (2014). The control of seed oil polyunsaturate content in the polyploid crop species Brassica napus. *Mol. Breed* 33, 349–362. 10.1007/s11032-013-9954-5

Welti, R., Li, W., Li, M., Sang, Y., Biesiada, H., Zhou, H. E., et al. (2002). Profiling membrane lipids in plant stress responses. Role of phospholipase D alpha in freezing-induced lipid changes in *Arabidopsis*. *J. Biol. Chem.* 277, 31994–32002. doi: 10.1074/jbc.M205375200

Woodfield, H. K., Sturtevant, D., Borisjuk, L., Munz, E., Guschina, I. A., Chapman, K., et al. (2017). Spatial and temporal mapping of key lipid species in Brassica napus seeds. *Plant Physiol.* 173, 1998–2009. doi: 10.1104/pp.16.01705

Wu, G., Wu, Y., Xiao, L., Li, X., and Lu, C. (2008). Zero erucic acid trait of rapeseed (Brassica napus L.) results from a deletion of four base pairs in the fatty acid elongase 1 gene. *Theor. Appl. Genet.* 116, 491–499. doi: 10.1007/s00122-007-0685-z

Yan, G., Li, D., Cai, M., Gao, G., Chen, B., Xu, K., et al. (2015). Characterization of FAE1 in the zero erucic acid germplasm of Brassica rapa L. *Breed Sci.* 65, 257–264. doi: 10.1270/jsbbs.65.257

Zhao, J., Dimov, Z., Becker, H. C., Ecke, W., and Möllers, C. (2007). Mapping QTL controlling fatty acid composition in a doubled haploid rapeseed population segregating for oil content. *Mol. Breed.* 21, 115–125. doi: 10.1007/s11032-007-9113-y

Zhao, Q., Wu, J., Cai, G., Yang, Q., Shahid, M., Fan, C., et al. (2019). A novel quantitative trait locus on chromosome A9 controlling oleic acid content in Brassica napus. *Plant Biotechnol. J.* 17, 2313–2324. doi: 10.1111/pbi.13142

Zhou, Z., Marepally, S. R., Nune, D. S., Pallakollu, P., Ragan, G., Roth, M. R., et al. (2011). LipidomeDB data calculation environment: online processing of direct-infusion mass spectral data for lipid profiles. *Lipids* 46, 879–884. doi: 10.1007/s11745-011-3575-8

Conflict of Interest: The authors declare that the research was conducted in the absence of any commercial or financial relationships that could be construed as a potential conflict of interest.

frontiers in Plant Science

MINI REVIEW
published: 04 February 2020
doi: 10.3389/fpls.2020.00024

Molecular Basis of Plant Oil Biosynthesis: Insights Gained From Studying the WRINKLED1 Transcription Factor

Que Kong[1], *Yuzhou Yang*[1], *Liang Guo*[2], *Ling Yuan*[3] *and Wei Ma*[1]*

[1] School of Biological Sciences, Nanyang Technological University, Singapore, Singapore, [2] National Key Laboratory of Crop Genetic Improvement, Huazhong Agricultural University, Wuhan, China, [3] Department of Plant and Soil Sciences, Kentucky Tobacco Research and Development Center, University of Kentucky, Lexington, KY, United States

Most plant species generate and store triacylglycerol (TAG) in their seeds, serving as a core supply of carbon and energy to support seedling development. Plant seed oils have a wide variety of applications, from being essential for human diets to serving as industrial renewable feedstock. WRINKLED1 (WRI1) transcription factor plays a central role in the transcriptional regulation of plant fatty acid biosynthesis. Since the discovery of *Arabidopsis WRI1* gene (*AtWRI1*) in 2004, the function of WRI1 in plant oil biosynthesis has been studied intensively. In recent years, the identification of WRI1 co-regulators and deeper investigations of the structural features and molecular functions of WRI1 have advanced our understanding of the mechanism of the transcriptional regulation of plant oil biosynthesis. These advances also help pave the way for novel approaches that will better utilize WRI1 for bioengineering oil production in crops.

Keywords: WRI1, transcription factor, plant oil biosynthesis, intrinsically disordered region, post-translational modifications, protein stability, protein–protein interaction

OPEN ACCESS

Edited by:
Xue-Rong Zhou, Commonwealth Scientific and Industrial Research Organisation, Australia

Reviewed by:
Enrique Martinez Force, Instituto de la Grasa (IG), Spain
Aruna Kilaru, East Tennessee State University, United States

***Correspondence:**
Wei Ma
weima@ntu.edu.sg

Specialty section:
This article was submitted to Plant Metabolism and Chemodiversity, a section of the journal Frontiers in Plant Science

Received: *03 November 2019*
Accepted: *10 January 2020*
Published: *04 February 2020*

Citation:
Kong Q, Yang Y, Guo L, Yuan L and Ma W (2020) Molecular Basis of Plant Oil Biosynthesis: Insights Gained From Studying the WRINKLED1 Transcription Factor. Front. Plant Sci. 11:24. doi: 10.3389/fpls.2020.00024

INTRODUCTION

Plants biosynthesize and store fatty acids mostly as triacylglycerol (TAG) in their seeds to support seedling development as carbon and energy resource. TAG (often familiar to many people as vegetable oils) is a highly energy-rich natural resource, as it has higher energy compared to carbohydrates and proteins. Vegetable oils are not only vital for the human diet, but also have other important applications such as the production of detergents and lubricants. Vegetable oils are also used to produce biodiesel. The global demand for plant oils is rapidly increasing, and is estimated to double by 2030 (Chapman and Ohlrogge, 2012). The growing demand for vegetable oil increases the need for higher plant oil production.

TAG biosynthesis consists of two major steps, fatty acid biosynthesis and TAG assembly, requiring the collaboration between cellular compartment plastids and the endoplasmic reticulum (ER) (Ohlrogge and Chapman, 2011). Fatty acids are first synthesized in the plastids and then exported to ER to complete the TAG assembly. Fatty acid biosynthesis initiates with acetyl-CoA carboxylase (ACC) that catalyzes the carboxylation to convert acetyl-CoA and bicarbonate into malonyl-CoA. Fatty acids are next elongated by the fatty acid synthase (FAS) complex, with two

carbon increments. Upon completion of fatty acids assembly, mediated by FAS, the synthesized fatty acids are exported from plastids to ER, in forms of acyl-CoA. The subsequent TAG synthesis in ER mainly occurs through the eukaryotic phospholipid biosynthetic pathway (Bates et al., 2009). In the last step of TAG synthesis, diacylglycerol (DAG) is converted to TAG (either using acyl-CoA or phospholipids), which is catalyzed by diacylglycerol acyltransferase (DGAT) or phosphatidylcholine:diacylglycerol acyltransferase (PDAT) (Zou et al., 1999; Dahlqvist et al., 2000; Zhang et al., 2009). TAG biosynthesis is sophisticated and not fully understood; therefore, investigation of regulatory mechanisms of TAG biosynthesis is essential, not only for advancing the basic research of plant lipids, but also for bioengineering novel oil crops with increased oil content.

CRUCIAL ROLE OF WRI1 IN TRANSCRIPTIONAL CONTROL OF PLANT OIL BIOSYNTHESIS

Numerous studies have shown that WRINKLED1 (WRI1) is vital for transcriptional control of plant oil biosynthesis. The discovery of *wri1-1* mutant (the *Arabidopsis* loss-of-function mutant of *AtWRI1*) was reported in 1998, leading to subsequent characterization of AtWRI1. Compared to the wild-type (WT), seed oil content in *wri1-1* is reduced by 80% (Focks and Benning, 1998). The *WRI1* gene encodes a transcription factor which belongs to the APETALA2 (AP2) transcription factor family (**Figure 1A**) (Cernac and Benning, 2004; Masaki et al., 2005). Transcriptomic (microarray) analysis of WT and *wri1-1* using developing seeds found that the majority of genes with reduced expression level in the *wri1-1* mutant encode enzymes in late glycolysis and fatty acid biosynthesis (Ruuska et al., 2002). Subsequent studies confirmed that a number of genes in late glycolysis and fatty acid biosynthesis are indeed AtWRI1 targets (Baud et al., 2007; Maeo et al., 2009). The AW-box ([CnTnG](n)$_7$[CG]) was characterized as an AtWRI1 binding element (Maeo et al., 2009). WRI1 was hence considered a "master regulator" in transcriptional control of TAG biosynthesis (Chapman and Ohlrogge, 2012).

REGULATORS CONTROLLING THE EXPRESSION OF *WRI1*

Two central seed developmental regulators, LEAFY COTYLEDON1 (LEC1) and LEAFY COTYLEDON2 (LEC2), were hypothesized as essential transcriptional regulators which regulate *AtWRI1* expression (**Figure 1B**). Expression of *AtWRI1* is increased in the *LEC1* gain-of-function mutant, *tnp* (Casson and Lindsey, 2006). In addition, expression of *AtWRI1* is elevated in transgenic plants overexpressing *LEC1* (Mu et al., 2008), suggesting LEC1 is possibly an upstream transcriptional regulator which activates the expression of *AtWRI1* (Santos-Mendoza et al., 2008; Marchive et al., 2014). Induction of *LEC2* in inducible *LEC2*-overexpression lines leads to the activation of *AtWRI1*, whereas *AtWRI1* expression is decreased in *lec2* mutant compared to WT plants (Baud et al., 2007). Therefore, the genetic and molecular evidence indicates that LEC2 functions as another transcriptional regulator controlling *AtWRI1*. In addition, transgenic maize overexpressing maize *LEC1* (*ZmLEC1*) results in increased expression of maize *WRI1* (*ZmWRI1*). ZmLEC1 is also shown to increase the *GUS* expression of $_{promoter}$*ZmWRI1:GUS* in maize cell culture (Shen et al., 2010). Transgenic soybean plants overexpressing soybean *LEC2* (*GmLEC2*) results in elevated expression of soybean *WRI1* (*GmWRI1*) (Manan et al., 2017). The evidence suggested a conserved mechanism controlling *WRI1* expression *via* LEC1 and LEC2 in different plant species. How LEC1 or LEC2 binds the AtWRI1 promoter has not been determined (Santos-Mendoza et al., 2008; Marchive et al., 2014). Importantly, recent ChIP followed by DNA microarray (ChIP-chip) experiments demonstrated that *AtWRI1* is a direct target gene of LEC1 (Pelletier et al., 2017).

FUSCA3 (FUS3) is another transcriptional regulator which mediates the expression of *AtWRI1* (**Figure 1B**). Comparative transcriptome analysis using microarray showed that expression of *AtWRI1* is reduced in a *fus3* mutant (Yamamoto et al., 2010). FUS3 has been speculated to regulate the expression of *AtWRI1* similar to LEC2, creating the functional redundancy between FUS3 and LEC2 (Yamamoto et al., 2010). Recent ChIP-Chip evidence confirmed that *AtWRI1* is a direct target of FUS3 (Wang and Perry, 2013). Sucrose treatment induced *AtWRI1* expression (Masaki et al., 2005). Expression of some sugar-responsive genes is stimulated by AtWRI1, suggesting the potential role of WRI1 in sugar signaling from carbon flow to oil production (Masaki et al., 2005). FUS3 does not affect *LEC1/LEC2* expression, suggesting that activation of *AtWRI1* by sucrose is *via* FUS3 instead of LEC1/LEC2 (Zhang et al., 2016a).

In addition to the transcriptional regulators LEC1, LEC2, and FUS3, other plants species may have alternative upstream regulators which contribute to mediating the expression of *WRI1*. In oil palm mesocarp, where most palm oil is derived from and *EgWRI1* displays high expression, the inability to detect expression of key regulator genes, such as *EgLEC1*, *EgLEC2*, and *EgFUS3*, suggests that expression of *EgWRI1* involves additional fruit-specific upstream regulators (Bourgis et al., 2011). EgNF-YA3, EgNF-YC2, and EgABI5 have been recently found to be capable of binding to the promoter region and activate the expression of *EgWRI1* (Yeap et al., 2017).

Arabidopsis transcription factor MYB89 is a newly identified transcriptional repressor of *AtWRI1* (**Figure 1B**). Transgenic plants overexpressing *MYB89* shows decreased *AtWRI1* expression, and a *myb89* loss-of-function mutant displays elevated *AtWRI1* expression compared to WT (Li et al., 2017a). ChIP experiments also showed that MYB89 binds to the *AtWRI1* promoter directly, suggesting that *AtWRI1* is a direct target gene of MYB89 (Li et al., 2017a).

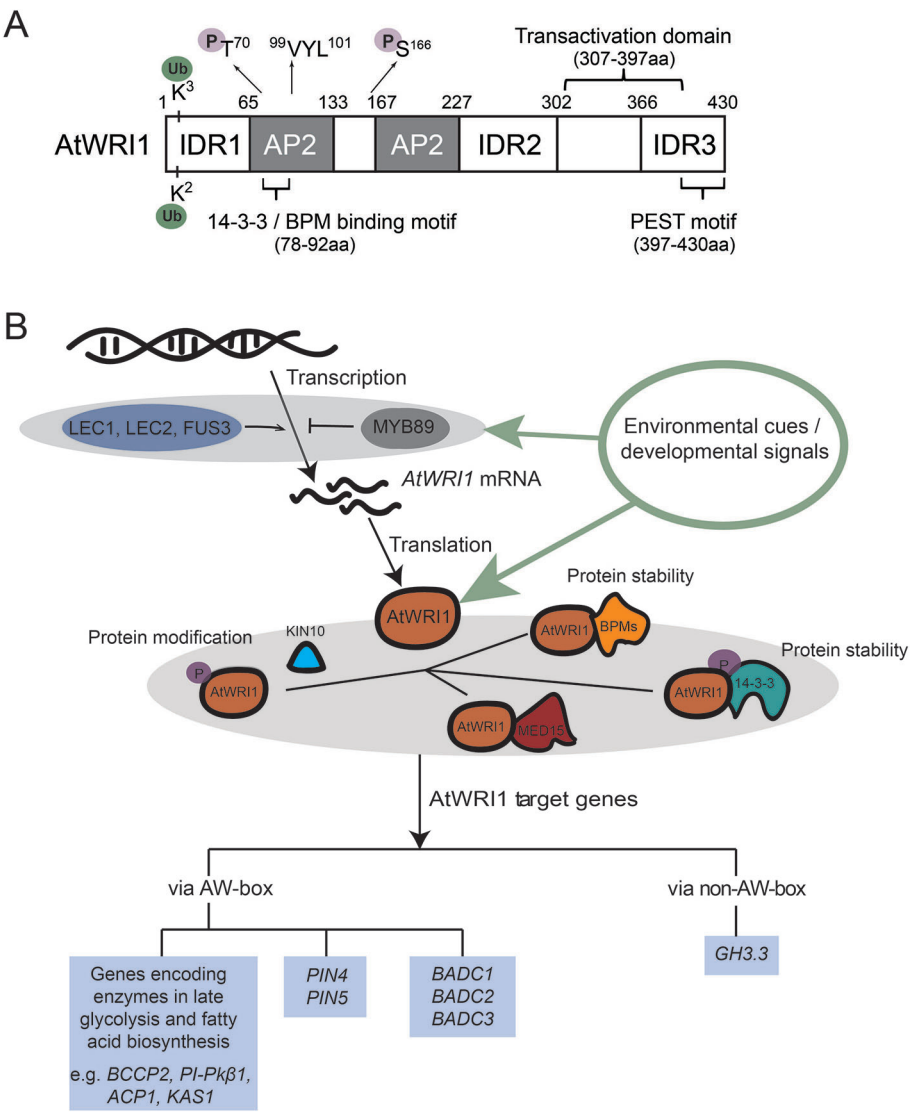

FIGURE 1 | AtWRI1 structural characteristics and molecular mechanism of AtWRI1-regulated gene expression. **(A)** Schematic diagram of AtWRI1. AtWRI1 protein comprises of two AP2 domains, three intrinsically disordered regions (IDRs), a functional motif of "VYL", the transactivation domain (TAD), the 14-3-3 and E3 ligase adaptor (BPM) binding motifs, the PEST motif, the ubiquitination sites, and the KIN10 phosphorylation sites. **(B)** Regulatory mechanism of AtWRI1 target genes. LEC1, LEC2, and FUS3 are positive regulators which mediate *AtWRI1* expression. MYB89 acts as a negative regulator of *AtWRI1* expression. At the protein level, AtWRI1 is regulated by post-translational modifications (such as phosphorylation and ubiquitination) and AtWRI1-interacting regulators, such as 14-3-3s, mediator subunit 15 (MED15), BPMs, and kinase KIN10. In the perception of environmental or developmental signals, the regulators fine-tune the protein stability and transcriptional activity of AtWRI1, through protein complex assembly and modifications, leading to mediation of the expression of AtWRI1 target genes.

REGULATORY MECHANISMS MEDIATING WRI1 PROTEIN STABILITY AND ACTIVITY

WRI1 activity is vital for oil biosynthesis as well as some developmental processes, such as seed germination and seedling establishment (Focks and Benning, 1998; Cernac and Benning, 2004; Cernac et al., 2006). Hence, it is not surprising that recent work uncovered several regulatory mechanisms that modulate WRI1 activity at different levels.

To prevent hyper-activation of key biological processes, the activities of transcription factors controlling metabolic pathways are often fine-tuned through protein-interacting regulators (Mouchiroud et al., 2014; Pireyre and Burow, 2015; Hafner et al., 2019). The interaction of AtWRI1 with CULLIN3-based E3 ligase adaptor BTB/POZMATH 1 (BPM1) in yeast-two-hybrid (Y2H) screening identified BPM1 as an AtWRI1-interacting partner (Chen et al., 2013). It is also demonstrated that AtWRI1 physically interacts with other BPM proteins. AtWRI1 assembles with E3 ligase adaptor BPMs, which mediates the degradation of AtWRI1 *via* 26S proteasome (Chen et al., 2013), connecting E3 ligase with plant oil production through the mediation of WRI1 protein stability.

Many proteins lack fixed three-dimensional structures, and intrinsic disordered regions (IDRs) have been found in eukaryotic proteins (Dyson and Wright, 2005; Kragelund et al., 2012; Valsecchi et al., 2013). IDRs tend to facilitate different confirmation requirements for varied specificities that are often regulated by post-translational modifications. Recent *in silico* analysis predicted three IDRs in the AtWRI1 protein (Ma et al., 2015). Functional analysis led to the characterization of an IDR3-located PEST motif (related to proteolysis), and a transactivation domain (TAD). Both TAD and IDR3-PEST motif are in the C-terminal region of AtWRI1, although not overlapping (**Figure 1A**). AtWRI1 variants, including IDR3-PEST deletion and mutations in putative phosphorylation residues of the IDR3-PEST motif, display enhanced protein stability and the expression of these variants elevated oil biosynthesis compared to that of AtWRI1 WT (Ma et al., 2015); therefore, phosphorylation is speculated to regulate AtWRI1 stability and activity (Ma et al., 2015).

In recent years, new AtWRI1-interacting regulators have been identified, expanding our understanding of the AtWRI1 regulatory network (summarized in **Figure 1B**). AtWRI1 physically interacts with 14-3-3 proteins in yeast and plant cells (Ma et al., 2016). 14-3-3 proteins are phosphopeptide-binding factors that are involved in various biological and physiological processes, such as metabolism, membrane transport, signal transduction, and protein modification (Jaspert et al., 2011; Paul et al., 2012; de Boer et al., 2013). Overexpression of *14-3-3* elevated oil production by increasing transcriptional activity and protein stability of AtWRI1 (Ma et al., 2016). Subsequent functional analysis identified overlapping 14-3-3- and BPM- binding motifs in AtWRI1. A hypothetical model suggests the interaction between AtWRI1 and 14-3-3 hinders either BPMs binding to AtWRI1 or the detachment of BPMs from AtWRI1. The AtWRI1–14-3-3 complex possesses elevated stability and transcriptional activity (Ma et al., 2016; Kong and Ma, 2018a).

It is often the case that plant gene regulation does not require *de novo* synthesis of transcription factor proteins; rather, it is mediated by post-transcriptional modification pathways. Among such pathways, protein phosphorylation mediated by kinases is perhaps the best studied process. KIN10 is an SNF1-related protein kinase which serves as a central regulator in transcriptional control of plant energy signal transduction pathways (Baena-Gonzalez et al., 2007). Recently, KIN10 has been shown to physically interact with and phosphorylate AtWRI1, leading to AtWRI1 degradation (Zhai et al., 2017). Phosphorylation deficient mutations at two residues in AtWRI1 (T70 and S166) impair KIN10-mediated phosphorylation and increase the AtWRI1 stability. 14-3-3 binding motif and KIN10 phosphorylation sites in AtWRI1 are neighboring, suggesting the possibility that the two may have overlapping proteasome-mediated protein degradation pathways (Zhai et al., 2017). In addition, trehalose 6-phosphate (T6P) was found to contribute to WRI1 stabilization and increase the generation of fatty acids *via* suppression of KIN10 activity (Zhai et al., 2018).

Recruitment of mediator complexes by transcription factors to accomplish their functions is a conserved mechanism of transcriptional regulation in eukaryotes (Taatjes, 2010). Physical interaction of Arabidopsis mediator complex MED15 subunit with AtWRI1 was demonstrated *in vivo* and *in vitro* (Kim et al., 2016). Transgenic Arabidopsis plants overexpressing *MED15* displayed increased expression levels of oil biosynthetic genes targeted by AtWRI1. ChIP assays revealed that MED15 is capable of binding to promoters of AtWRI1 targets (Kim et al., 2016). However, the elevated expression of these AtWRI1 target genes in transgenic *wri1* plants overexpressing *MED15* suggested that MED15 interacts with other transcriptional regulators to regulate the gene expression of AtWRI1 targets (Kim et al., 2016).

FUNCTIONAL CONSERVATION OF WRI1 IN DIFFERENT PLANT SPECIES

A high degree of cross-species conservation is a hallmark of important master transcriptional regulators. A number of *WRI1* orthologs have been found in various monocot and dicot plant species, including *Brassica napus* (Liu et al., 2010), *Brachypodium distachyon* (Yang et al., 2015), *Camelina sativa* (An et al., 2017), *Zea mays* (Shen et al., 2010; Pouvreau et al., 2011), *Elaeis guineensis* (Bourgis et al., 2011; Ma et al., 2013), *Glycine max* (Manan et al., 2017; Zhang et al., 2017; Chen et al., 2020), *Ricinus communis* (Tajima et al., 2013; Ji et al., 2018), *Avena sativa* (Grimberg et al., 2015), *Cocos nucifera* (Sun et al., 2017), *Cyperus esculentus* (Grimberg et al., 2015), *Gossypium spp* (Qu et al., 2012), *Jatropha curcas* (Ye et al., 2018), *Persea americana* (Kilaru et al., 2015), *Solanum tuberosum* (Grimberg et al., 2015), and *Oryza sativa* (Mano et al., 2019). Expressing *AtWRI1* or *WRI1* orthologs in *wri1* loss-of-function mutants complemented the decreased seed oil phenotype of *wri1* (Cernac and Benning, 2004; Pouvreau et al., 2011; Ma et al., 2013; An et al., 2017; Ye et al., 2018; Chen et al., 2020). Numerous *WRI1* orthologs display high expression levels in developing seeds, correlating closely to the *AtWRI1* expression patterns. Nonetheless, some *WRI1s* have been found to show high expression in non-seed tissues. For example, the expression of oil palm *WRI1* (*EgWRI1*) is high in mesocarp and substantially increases in the ripening processes of fruits (Bourgis et al., 2011). In addition, *PaWRI1* and *CeWRI1* exhibit high expression levels in avocado mesocarp and nutsedge stem tubers, respectively (Grimberg et al., 2015; Kilaru et al., 2015). Structural features and functional domains/motifs, which have been identified in the AtWRI1 protein, including "VYL" (Ma et al., 2013), IDR (Ma et al., 2015), and the PEST motif (Ma et al., 2015), are conserved in other WRI1 proteins (Ma et al., 2013; Ma et al., 2015; Yang et al., 2015; An et al., 2017; Kong and Ma, 2018b; Ye et al., 2018; Chen et al., 2020; Kong et al., 2019; Snell et al., 2019; Tang et al., 2019). *WRI1* orthologs identified in *Ricinus connunis and Oryza sativa* encode WRI1 proteins lacking a "VYL" motif but still trigger oil biosynthesis *in planta* by activating the expression of WRI1 target genes (Ji et al., 2018; Mano et al., 2019). Recent work on RcWRI1-B and OsWRI1-1 suggested that "VYL" might not

be important for some WRI1s (Ji et al., 2018; Mano et al., 2019), despite its conservation in numerous WRI1s and its functional importance in both AtWRI1 (Ma et al., 2013) and Arabidopsis AP2 transcription factor, ANT (Krizek, 2003).

WRI1 TARGET GENES WHICH ARE NOT INVOLVED IN OIL BIOSYNTHESIS

In addition to its role as a transcriptional regulator controlling expression of genes in late glycolysis and oil biosynthesis, WRI1 has been found to target genes in pathways other than oil biosynthesis. AtWRI1 is not only able to bind to the promoters of *PINs* (*PIN-FORMEDs*) through the AW-box, but also binds to the promoter of *GH3.3* (a gene involved in auxin degradation) *via* a non-AW-box element, suggesting a role in modifying auxin homeostasis (Kong et al., 2017) (also see **Figure 1B**). The altered expression of auxin-related genes was also found in roots of soybean *GmWRI1s*-overexpressing plants or *GmWRI1s*-RNAi plants compared to WT control (Chen et al., 2020). Furthermore, *AtWRI1* is a homolog of *CitAP2.10* (encoding a *Citrus sinensis* AP2 transcription factor which is in charge of (+)-valencene biosynthesis), and AtWRI1 is capable of transactivating the *C. sinensis terpene synthase* 1 (*CsTPS1*) promoter in a dual-luciferase assay (Shen et al., 2016). How regulation of the AtWRI1 targets is linked to plant growth and development, such as root growth (Kong et al., 2017), is currently under investigation. It is important to consider the alternative targets when utilizing WRI1 to bioengineer crops for plant oil production. However, convincing evidence exists demonstrating *WRI1* as one of the most effective genes for plant oil bioengineering.

IMPORTANCE OF WRI1 FOR PLANT OIL PRODUCTION

Transgenic plants overexpressing *AtWRI1* or *WRI1* orthologs show significantly increased seed oil content in a number of studies (Cernac and Benning, 2004; Liu et al., 2010; Shen et al., 2010; An and Suh, 2015; Yang et al., 2015; Sun et al., 2017; Ye et al., 2018). Transgenic Arabidopsis and Brachypodium seedlings, overexpressing *AtWRI1* and *BdWRI1* respectively, have increased oil content in vegetative tissues (Sanjaya et al., 2011; Yang et al., 2015). Selection of proper promoters to drive *WRI1* expression is also critical for oil bioengineering. For instance, significantly increased oil content in seeds was observed in transgenic maize with embryo-preferred *OLEOSIN* (*OLE*) promoter driven *ZmWRI1*, but there was no distinguishable oil increase in transgenic maize with the starch endosperm-specific *19 KD ZEIN* promoter driven *ZmWRI1* (Shen et al., 2010). Another example is transgenic Arabidopsis transformed by a vector that confers *FUS3* promoter driven *AtWRI1* expression, which turns out to be effective in increasing seed oil production due to an extension of oil biosynthesis during the mid-phase seed developmental process (Kanai et al., 2016).

Ectopic expression of *AtWRI1* or *WRI1* orthologs in a transient tobacco expression system is also able to productively trigger TAG accumulation in tobacco leaves (Vanhercke et al., 2013; Grimberg et al., 2015; Ma et al., 2015). Transient co-expression of *AtWRI1* and *DGAT1* in tobacco leaves has led to considerably augmented oil content compared to expression of *WRI1* alone, which suggests a synergistic effect between these two genes (Vanhercke et al., 2013). Transient overexpression of engineered *AtWRI1* variants in tobacco leaves, either deletion of IDR3-PEST motif or phosphorylation deficient mutations in the IDR3-PEST motif, resulted in production of stabilized WRI1 proteins and enhanced oil production (Ma et al., 2015). Transient co-expression of *AtWRI1* and *14-3-3* in tobacco leaves resulted in increased stability of AtWRI1 and enhanced oil production (Ma et al., 2016). The AtWRI1^{K2RK3R} variant, with mutations in two ubiquitination residues, resulted in increased protein stability and oil biosynthesis using a tobacco transient expression system (Zhai et al., 2017). In metabolic engineering to enhance oil production in vegetative tissues, the strategy of "push, pull, package, and protect" is to upregulate (push) the *de novo* fatty acid pathway using a key transcription factor, combined with pulling the precursors toward the end products using rate-limiting enzymes, packaging TAG in oil bodies, and protecting TAG from degradation. *WRI1* overexpression has been shown to be pivotal in such designed strategy (Vanhercke et al., 2019).

Transgenic plants, overexpressing transcription factors which can upregulate *WRI1* expression, also display elevated seed oil content. For instance, transgenic Arabidopsis plants that overexpress *GmZF351* or *GmDREBL* have increased oil content in seeds. Both soybean transcription factors are capable of binding to the *AtWRI1* promoter and activate *AtWRI1* expression (Zhang et al., 2016b; Li et al., 2017b). Overexpression of *ZmLEC1* (an activator of *WRI1*) also effectively increases seed oil in various plants species including Arabidopsis, Camelina, and maize (Shen et al., 2010; Zhu et al., 2018).

Unusual fatty acids, such hydroxy fatty acids (HFAs), have high value for industrial applications because of their distinctive physical and chemical properties. Nonetheless, transgenic Arabidopsis plants which overexpress a hydroxylase gene only yield low amount of HFA with reduction of total seed oil (Bates and Browse, 2011; Bates et al., 2014). A feedback inhibition of fatty acid biosynthesis was believed to be the main reason for the decreased seed oil content (Bates et al., 2014). In order to overcome this bottleneck, Adhikari et al. attempted to generate Arabidopsis transgenic plants which co-express *AtWRI1* with *RcFAH12* (encoding a castor fatty acid hydroxylase). The resulting transgenic Arabidopsis plants have significantly elevated proportions of HFA and entire seed oil content, demonstrating WRI1's role for effective circumventing feedback inhibition of fatty acid synthesis when ectopic expressing a hydroxylase gene (Adhikari et al., 2016).

Aberrant growth or cell death was observed in some transgenic plants which overexpress *WRI1* (Cernac and Benning, 2004; Marchive et al., 2014; Yang et al., 2015). Choosing suitable

promoters for certain plant species hence becomes a necessary consideration for the development of oil crops.

PERSPECTIVES

Since the discovery of the *wri1-1* mutant, multiple studies have established the central role of WRI1 in transcriptional regulation of plant oil biosynthesis. However, key questions remain, including what are the upstream regulators of WRI1 and how do the master regulators of seed development, such as LEC1, LEC2, and FUS3, mediate the expression of *WRI1*? Alternative transcriptional regulators could play important roles in controlling *WRI1* expression in response to various developmental or environmental cues. Several transcriptional regulators of *EgWRI1* have been recently identified in oil palm (Yeap et al., 2017). Whether the newly expanded regulatory network in oil palm is conserved in other plant species is unclear. More detailed analyses of the *WRI1* promoters from various plant species may allow us to generalize the conserved nature of combinatorial WRI1 transcriptional regulation.

AtWRI3 and AtWRI4 are WRI1-like proteins identified in Arabidopsis. Seed-specific overexpression of *AtWRI3* or *AtWRI4* in the *wri1* mutant complemented the low seed-oil phenotype (To et al., 2012). AtWRI3 and AtWRI4 seem to share overlapping function with AtWRI1 in providing acyl precursors for cutin biosynthesis in floral tissues; however, their roles in seed oil biosynthesis are less certain as they are predominantly expressed in non-seed tissues such as stems and flowers (To et al., 2012). It should be noted that the *wri1 wri3 wri4* triple mutant displayed no apparent changes in vegetative growth, raising the speculation of the involvement of other unidentified transcriptional regulators that control fatty acid biosynthesis in vegetative tissues (To et al., 2012; Marchive et al., 2014). Investigation of the unique and overlapping functions of WRI1-like factors will shed light on the complex transcriptional control of fatty acid biosynthesis, especially in vegetative tissues.

Structural analyses of WRI1 variants and orthologs have revealed that the IDR3-PEST motif, binding motifs of E3 ligase adaptor BPMs and 14-3-3s, and phosphorylation residues (T70/S166) are relevant for AtWRI1 stability and transcriptional activity, consequently affecting plant oil production (Ma et al., 2013; Ma et al., 2015; Ma et al., 2016; Zhai et al., 2017). Recent studies on the missing "VYL" motif of RcWRI1-B and OsWRI1-1 also open the discussion about the importance of "VYL" in WRI1 proteins (Ji et al., 2018; Mano et al., 2019). Generation of the three-dimensional structure, in combination of computer modeling, will further advance our understanding of WRI1 function.

The emerging picture shows crosstalk between the WRI1-interacting regulators which are also post-translationally regulated, highlighting the cooperative activity of the WRI1 transcriptional machinery (**Figure 1**). Phosphorylation has been proposed to play dual roles in mediating AtWRI1 protein stability during embryo development (Ma et al., 2016; Kong and Ma, 2018a). Therefore, one possible mechanism to fine-tune WRI1 activity is through phosphorylation and dephosphorylation by various kinases and phosphatases in response to different developmental and environmental cues. Recent progress in WRI1 interactome facilitates the identification of novel WRI-interacting factors; however, the molecular mechanisms mediating the interplay among these regulators remain to be elucidated.

Key questions also remain regarding WRI1 protein stability. Why do plants degrade WRI1? Understanding of the control mechanism of WRI1 degradation, particularly under different developmental stages and environmental conditions, will help address the biological questions of "when" and "how" the endogenous degradation system activates to degrade WRI1. The answers to these questions may ultimately be used to guide our efforts to increase plant oil production.

AtWRI1 activates the expression of several *BIOTIN ATTACHMENT DOMAIN-CONTAINING* (*BADC*) genes that inhibit fatty acid biosynthesis (Liu et al., 2019), suggesting an additional layer of regulation of WRI1-mediated fatty acid biosynthesis. In summary, while the recent insights on WRI1 significantly advance our understanding of the molecular mechanisms governing plant oil biosynthesis, our knowledge of the complex regulatory system is far from complete.

AUTHOR CONTRIBUTIONS

QK, YY, and WM conceived the ideas, prepared the figures and wrote the first draft. LG, LY, and WM reviewed and edited the figures and manuscript. All authors read and approved the final version of the manuscript.

FUNDING

This work was supported by a Nanyang Technological University Startup grant and a Ministry of Education (MOE) of Singapore Tier 1 to WM (2018-T1-002-019).

ACKNOWLEDGMENTS

We apologize to all authors whose important work is not cited due to space limitations.

REFERENCES

Adhikari, N. D., Bates, P. D., and Browse, J. (2016). WRINKLED1 rescues feedback inhibition of fatty acid synthesis in hydroxylase-expressing seeds. *Plant Physiol.* 171 (1), 179–191. doi: 10.1104/pp.15.01906

An, D., and Suh, M. C. (2015). Overexpression of Arabidopsis WRI1 enhanced seed mass and storage oil content in Camelina sativa. *Plant Biotechnol. Rep.* 9, 137–148. doi: 10.1007/s11816-015-0351-x

An, D., Kim, H., Ju, S., Go, Y. S., Kim, H. U., and Suh, M. C. (2017). Expression of Camelina WRINKLED1 Isoforms rescue the seed phenotype of the arabidopsis wri1 mutant and increase the triacylglycerol content in tobacco leaves. *Front. Plant Sci.* 8, 34. doi: 10.3389/fpls.2017.00034

Baena-Gonzalez, E., Rolland, F., Thevelein, J. M., and Sheen, J. (2007). A central integrator of transcription networks in plant stress and energy signalling. *Nature* 448 (7156), 938–942. doi: 10.1038/nature06069

Bates, P. D., and Browse, J. (2011). The pathway of triacylglycerol synthesis through phosphatidylcholine in Arabidopsis produces a bottleneck for the accumulation of unusual fatty acids in transgenic seeds. *Plant J.* 68 (3), 387–399. doi: 10.1111/j.1365-313X.2011.04693.x

Bates, P. D., Durrett, T. P., Ohlrogge, J. B., and Pollard, M. (2009). Analysis of acyl fluxes through multiple pathways of triacylglycerol synthesis in developing soybean embryos. *Plant Physiol.* 150 (1), 55–72. doi: 10.1104/pp.109.137737

Bates, P. D., Johnson, S. R., Cao, X., Li, J., Nam, J. W., Jaworski, J. G., et al. (2014). Fatty acid synthesis is inhibited by inefficient utilization of unusual fatty acids for glycerolipid assembly. *Proc. Natl. Acad. Sci. U. S. A* 111 (3), 1204–1209. doi: 10.1073/pnas.1318511111

Baud, S., Mendoza, M. S., To, A., Harscoet, E., Lepiniec, L., and Dubreucq, B. (2007). WRINKLED1 specifies the regulatory action of LEAFY COTYLEDON2 towards fatty acid metabolism during seed maturation in Arabidopsis. *Plant J.* 50 (5), 825–838. doi: 10.1111/j.1365-313X.2007.03092.x

Bourgis, F., Kilaru, A., Cao, X., Ngando-Ebongue, G. F., Drira, N., Ohlrogge, J. B., et al. (2011). Comparative transcriptome and metabolite analysis of oil palm and date palm mesocarp that differ dramatically in carbon partitioning. *Proc. Natl. Acad. Sci. U. S. A* 108 (30), 12527–12532. doi: 10.1073/pnas.1106502108

Casson, S. A., and Lindsey, K. (2006). The turnip mutant of Arabidopsis reveals that LEAFY COTYLEDON1 expression mediates the effects of auxin and sugars to promote embryonic cell identity. *Plant Physiol.* 142 (2), 526–541. doi: 10.1104/pp.106.080895

Cernac, A., and Benning, C. (2004). WRINKLED1 encodes an AP2/EREB domain protein involved in the control of storage compound biosynthesis in Arabidopsis. *Plant J.* 40 (4), 575–585. doi: 10.1111/j.1365-313X.2004.02235.x

Cernac, A., Andre, C., Hoffmann-Benning, S., and Benning, C. (2006). WRI1 is required for seed germination and seedling establishment. *Plant Physiol.* 141 (2), 745–757. doi: 10.1104/pp.106.079574

Chapman, K. D., and Ohlrogge, J. B. (2012). Compartmentation of triacylglycerol accumulation in plants. *J. Biol. Chem.* 287 (4), 2288–2294. doi: 10.1074/jbc.R111.290072

Chen, L., Lee, J. H., Weber, H., Tohge, T., Witt, S., Roje, S., et al. (2013). Arabidopsis BPM proteins function as substrate adaptors to a CULLIN3-based E3 ligase to affect fatty acid metabolism in plants. *Plant Cell* 25 (6), 2253–2264. doi: 10.1105/tpc.112.107292

Chen, B., Zhang, G., Li, P., Yang, J., Guo, L., Benning, C., et al. (2020). Multiple GmWRI1s are redundantly involved in seed filling and nodulation by regulating plastidic glycolysis, lipid biosynthesis and hormone signalling in soybean (Glycine max). *Plant Biotechnol. J.* 18 (1), 155 –171. doi: 10.1111/pbi.13183

Dahlqvist, A., Stahl, U., Lenman, M., Banas, A., Lee, M., Sandager, L., et al. (2000). Phospholipid:diacylglycerol acyltransferase: an enzyme that catalyzes the acyl-CoA-independent formation of triacylglycerol in yeast and plants. *Proc. Natl. Acad. Sci. U. S. A* 97 (12), 6487–6492. doi: 10.1073/pnas.120067297

de Boer, A. H., van Kleeff, P. J., and Gao, J. (2013). Plant 14-3-3 proteins as spiders in a web of phosphorylation. *Protoplasma* 250 (2), 425–440. doi: 10.1007/s00709-012-0437-z

Dyson, H. J., and Wright, P. E. (2005). Intrinsically unstructured proteins and their functions. *Nat. Rev. Mol. Cell Biol.* 6 (3), 197–208. doi: 10.1038/nrm1589

Focks, N., and Benning, C. (1998). wrinkled1: a novel, low-seed-oil mutant of Arabidopsis with a deficiency in the seed-specific regulation of carbohydrate metabolism. *Plant Physiol.* 118 (1), 91–101. doi: 10.1104/pp.118.1.91

Grimberg, A., Carlsson, A. S., Marttila, S., Bhalerao, R., and Hofvander, P. (2015). Transcriptional transitions in Nicotiana benthamiana leaves upon induction of oil synthesis by WRINKLED1 homologs from diverse species and tissues. *BMC Plant Biol.* 15, 192. doi: 10.1186/s12870-015-0579-1

Hafner, A., Bulyk, M. L., Jambhekar, A., and Lahav, G. (2019). The multiple mechanisms that regulate p53 activity and cell fate. *Nat. Rev. Mol. Cell Biol.* 20 (4), 199–210. doi: 10.1038/s41580-019-0110-x

Jaspert, N., Throm, C., and Oecking, C. (2011). Arabidopsis 14-3-3 proteins: fascinating and less fascinating aspects. *Front. Plant Sci.* 2, 96. doi: 10.3389/fpls.2011.00096

Ji, X. J., Mao, X., Hao, Q. T., Liu, B. L., Xue, J. A., and Li, R. Z. (2018). Splice variants of the castor WRI1 gene upregulate fatty acid and oil biosynthesis when expressed in tobacco leaves. *Int. J. Mol. Sci.* 19 (1), 146. doi: 10.3390/ijms19010146

Kanai, M., Mano, S., Kondo, M., Hayashi, M., and Nishimura, M. (2016). Extension of oil biosynthesis during the mid-phase of seed development enhances oil content in Arabidopsis seeds. *Plant Biotechnol. J.* 14 (5), 1241–1250. doi: 10.1111/pbi.12489

Kilaru, A., Cao, X., Dabbs, P. B., Sung, H. J., Rahman, M. M., Thrower, N., et al. (2015). Oil biosynthesis in a basal angiosperm: transcriptome analysis of Persea Americana mesocarp. *BMC Plant Biol.* 15, 203. doi: 10.1186/s12870-015-0586-2

Kim, M. J., Jang, I. C., and Chua, N. H. (2016). The mediator complex MED15 subunit mediates activation of downstream lipid-related genes by the WRINKLED1 transcription factor. *Plant Physiol.* 171 (3), 1951–1964. doi: 10.1104/pp.16.00664

Kong, Q., and Ma, W. (2018a). WRINKLED1 as a novel 14-3-3 client: function of 14-3-3 proteins in plant lipid metabolism. *Plant Signal Behav.* 13, e1482176. doi: 10.1080/15592324.2018.1482176

Kong, Q., and Ma, W. (2018b). WRINKLED1 transcription factor: how much do we know about its regulatory mechanism? *Plant Sci.* 272, 153–156. doi: 10.1016/j.plantsci.2018.04.013

Kong, Q., Ma, W., Yang, H., Ma, G., Mantyla, J. J., and Benning, C. (2017). The Arabidopsis WRINKLED1 transcription factor affects auxin homeostasis in roots. *J. Exp. Bot.* 68, 4627–4634. doi: 10.1093/jxb/erx275

Kong, Q., Yuan, L., and Ma, W. (2019). WRINKLED1, a "Master Regulator" in transcriptional control of plant oil biosynthesis. *Plants (Basel)* 8 (7), 238. doi: 10.3390/plants8070238

Kragelund, B. B., Jensen, M. K., and Skriver, K. (2012). Order by disorder in plant signaling. *Trends Plant Sci.* 17 (11), 625–632. doi: 10.1016/j.tplants.2012.06.010

Krizek, B. A. (2003). AINTEGUMENTA utilizes a mode of DNA recognition distinct from that used by proteins containing a single AP2 domain. *Nucleic Acids Res.* 31 (7), 1859–1868. doi: 10.1093/nar/gkg292

Li, D., Jin, C., Duan, S., Zhu, Y., Qi, S., Liu, K., et al. (2017a). MYB89 transcription factor represses seed oil accumulation. *Plant Physiol.* 173 (2), 1211–1225. doi: 10.1104/pp.16.01634

Li, Q. T., Lu, X., Song, Q. X., Chen, H. W., Wei, W., Tao, J. J., et al. (2017b). Selection for a Zinc-finger protein contributes to seed oil increase during soybean domestication. *Plant Physiol.* 173 (4), 2208–2224. doi: 10.1104/pp.16.01610

Liu, J., Hua, W., Zhan, G., Wei, F., Wang, X., Liu, G., et al. (2010). Increasing seed mass and oil content in transgenic Arabidopsis by the overexpression of wri1-like gene from Brassica napus. *Plant Physiol. Biochem.* 48 (1), 9–15. doi: 10.1016/j.plaphy.2009.09.007

Liu, H., Zhai, Z., Kuczynski, K., Keereetaweep, J., Schwender, J., and Shanklin, J. (2019). WRINKLED1 regulates biotin attachment domain-containing proteins that inhibit fatty acid synthesis. *Plant Physiol.* 181 (1), 55–62. doi: 10.1104/pp.19.00587

Ma, W., Kong, Q., Arondel, V., Kilaru, A., Bates, P. D., Thrower, N. A., et al. (2013). Wrinkled1, a ubiquitous regulator in oil accumulating tissues from Arabidopsis embryos to oil palm mesocarp. *PloS One* 8 (7), e68887. doi: 10.1371/journal.pone.0068887

Ma, W., Kong, Q., Grix, M., Mantyla, J. J., Yang, Y., Benning, C., et al. (2015). Deletion of a C-terminal intrinsically disordered region of WRINKLED1 affects its stability and enhances oil accumulation in Arabidopsis. *Plant J.* 83 (5), 864–874. doi: 10.1111/tpj.12933

Ma, W., Kong, Q., Mantyla, J. J., Yang, Y., Ohlrogge, J. B., and Benning, C. (2016). 14-3-3 protein mediates plant seed oil biosynthesis through interaction with AtWRI1. *Plant J.* 88 (2), 228–235. doi: 10.1111/tpj.13244

Maeo, K., Tokuda, T., Ayame, A., Mitsui, N., Kawai, T., Tsukagoshi, H., et al. (2009). An AP2-type transcription factor, WRINKLED1, of Arabidopsis

thaliana binds to the AW-box sequence conserved among proximal upstream regions of genes involved in fatty acid synthesis. *Plant J.* 60 (3), 476–487. doi: 10.1111/j.1365-313X.2009.03967.x

Manan, S., Ahmad, M. Z., Zhang, G., Chen, B., Haq, B. U., Yang, J., et al. (2017). Soybean LEC2 regulates subsets of genes involved in controlling the biosynthesis and catabolism of seed storage substances and seed development. *Front. Plant Sci.* 8, 1604. doi: 10.3389/fpls.2017.01604

Mano, F., Aoyanagi, T., and Kozaki, A. (2019). Atypical splicing accompanied by skipping conserved micro-exons produces unique WRINKLED1, an AP2 domain transcription factor in rice plants. *Plants (Basel)* 8 (7), 207. doi: 10.3390/plants8070207

Marchive, C., Nikovics, K., To, A., Lepiniec, L., and Baud, S. (2014). Transcriptional regulation of fatty acid production in higher plants: molecular bases and biotechnological outcomes. *Eur. J. Lipid Sci. Technol.* 116, 1332–1343. doi: 10.1002/ejlt.201400027

Masaki, T., Mitsui, N., Tsukagoshi, H., Nishii, T., Morikami, A., and Nakamura, K. (2005). ACTIVATOR of Spomin::LUC1/WRINKLED1 of Arabidopsis thaliana transactivates sugar-inducible promoters. *Plant Cell Physiol.* 46 (4), 547–556. doi: 10.1093/pcp/pci072

Mouchiroud, L., Eichner, L. J., Shaw, R. J., and Auwerx, J. (2014). Transcriptional coregulators: fine-tuning metabolism. *Cell Metab.* 20 (1), 26–40. doi: 10.1016/j.cmet.2014.03.027

Mu, J., Tan, H., Zheng, Q., Fu, F., Liang, Y., Zhang, J., et al. (2008). LEAFY COTYLEDON1 is a key regulator of fatty acid biosynthesis in Arabidopsis. *Plant Physiol.* 148 (2), 1042–1054. doi: 10.1104/pp.108.126342

Ohlrogge, J. B., and Chapman, K. D. (2011). The seeds of green energy: expanding the contribution of plant oils as biofuels. *Biochemist. (Lond.)* 33, 34–38. doi: 10.1042/BIO03302034

Paul, A. L., Denison, F. C., Schultz, E. R., Zupanska, A. K., and Ferl, R. J. (2012). 14-3-3 phosphoprotein interaction networks - does isoform diversity present functional interaction specification? *Front. Plant Sci.* 3, 190. doi: 10.3389/fpls.2012.00190

Pelletier, J. M., Kwong, R. W., Park, S., Le, B. H., Baden, R., Cagliari, A., et al. (2017). LEC1 sequentially regulates the transcription of genes involved in diverse developmental processes during seed development. *Proc. Natl. Acad. Sci. U. S. A* 114 (32), E6710–E6719. doi: 10.1073/pnas.1707957114

Pireyre, M., and Burow, M. (2015). Regulation of MYB and bHLH transcription factors: a glance at the protein level. *Mol. Plant* 8 (3), 378–388. doi: 10.1016/j.molp.2014.11.022

Pouvreau, B., Baud, S., Vernoud, V., Morin, V., Py, C., Gendrot, G., et al. (2011). Duplicate maize Wrinkled1 transcription factors activate target genes involved in seed oil biosynthesis. *Plant Physiol.* 156 (2), 674–686. doi: 10.1104/pp.111.173641

Qu, J., Ye, J., Geng, Y. F., Sun, Y. W., Gao, S. Q., Zhang, B. P., et al. (2012). Dissecting functions of KATANIN and WRINKLED1 in cotton fiber development by virus-induced gene silencing. *Plant Physiol.* 160 (2), 738–748. doi: 10.1104/pp.112.198564

Ruuska, S. A., Girke, T., Benning, C., and Ohlrogge, J. B. (2002). Contrapuntal networks of gene expression during Arabidopsis seed filling. *Plant Cell* 14 (6), 1191–1206. doi: 10.1105/tpc.000877

Sanjaya, Durrett, T. P., Weise, S. E., Benning, C. (2011). Increasing the energy density of vegetative tissues by diverting carbon from starch to oil biosynthesis in transgenic Arabidopsis. *Plant Biotechnol. J.* 9 (8), 874–883. doi: 10.1111/j.1467-7652.2011.00599.x

Santos-Mendoza, M., Dubreucq, B., Baud, S., Parcy, F., Caboche, M., and Lepiniec, L. (2008). Deciphering gene regulatory networks that control seed development and maturation in Arabidopsis. *Plant J.* 54 (4), 608–620. doi: 10.1111/j.1365-313X.2008.03461.x

Shen, B., Allen, W. B., Zheng, P., Li, C., Glassman, K., Ranch, J., et al. (2010). Expression of ZmLEC1 and ZmWRI1 increases seed oil production in maize. *Plant Physiol.* 153 (3), 980–987. doi: 10.1104/pp.110.157537

Shen, S. L., Yin, X. R., Zhang, B., Xie, X. L., Jiang, Q., Grierson, D., et al. (2016). CitAP2.10 activation of the terpene synthase CsTPS1 is associated with the synthesis of (+)-valencene in 'Newhall' orange. *J. Exp. Bot.* 67 (14), 4105–4115. doi: 10.1093/jxb/erw189

Snell, P., Grimberg, A., Carlsson, A. S., and Hofvander, P. (2019). WRINKLED1 is subject to evolutionary conserved negative autoregulation. *Front. Plant Sci.* 10, 387. doi: 10.3389/fpls.2019.00387

Sun, R., Ye, R., Gao, L., Zhang, L., Wang, R., Mao, T., et al. (2017). Characterization and ectopic expression of CoWRI1, an AP2/EREBP domain-containing transcription factor from coconut (Cocos nucifera L.) Endosperm, changes the seeds oil content in transgenic arabidopsis thaliana and rice (Oryza sativa L.). *Front. Plant Sci.* 8, 63. doi: 10.3389/fpls.2017.00063

Taatjes, D. J. (2010). The human mediator complex: a versatile, genome-wide regulator of transcription. *Trends Biochem. Sci.* 35 (6), 315–322. doi: 10.1016/j.tibs.2010.02.004

Tajima, D., Kaneko, A., Sakamoto, M., Ito, Y., Hue, N. T., Miyazaki, M., et al. (2013). Wrinkled 1 (WRI1) Homologs, AP2-type transcription factors involving master regulation of seed storage oil Synthesis in Castor Bean (Ricinus communis L.). *Am. J. Plant Sci.* 4, 333–339. doi: 10.4236/ajps.2013.42044

Tang, T., Du, C., Song, H., Aziz, U., Wang, L., Zhao, C., et al. (2019). Genome-wide analysis reveals the evolution and structural features of WRINKLED1 in plants. *Mol. Genet. Genomics* 294 (2), 329–341. doi: 10.1007/s00438-018-1512-8

To, A., Joubes, J., Barthole, G., Lecureuil, A., Scagnelli, A., Jasinski, S., et al. (2012). WRINKLED transcription factors orchestrate tissue-specific regulation of fatty acid biosynthesis in Arabidopsis. *Plant Cell* 24 (12), 5007–5023. doi: 10.1105/tpc.112.106120

Valsecchi, I., Guittard-Crilat, E., Maldiney, R., Habricot, Y., Lignon, S., Lebrun, R., et al. (2013). The intrinsically disordered C-terminal region of Arabidopsis thaliana TCP8 transcription factor acts both as a transactivation and self-assembly domain. *Mol. Biosyst.* 9 (9), 2282–2295. doi: 10.1039/c3mb70128j

Vanhercke, T., El Tahchy, A., Shrestha, P., Zhou, X. R., Singh, S. P., and Petrie, J. R. (2013). Synergistic effect of WRI1 and DGAT1 coexpression on triacylglycerol biosynthesis in plants. *FEBS Lett.* 587 (4), 364–369. doi: 10.1016/j.febslet.2012.12.018

Vanhercke, T., Dyer, J. M., Mullen, R. T., Kilaru, A., Rahman, M. M., Petrie, J. R., et al. (2019). Metabolic engineering for enhanced oil in biomass. *Prog. Lipid Res.* 74, 103–129. doi: 10.1016/j.plipres.2019.02.002

Wang, F., and Perry, S. E. (2013). Identification of direct targets of FUSCA3, a key regulator of Arabidopsis seed development. *Plant Physiol.* 161 (3), 1251–1264. doi: 10.1104/pp.112.212282

Yamamoto, A., Kagaya, Y., Usui, H., Hobo, T., Takeda, S., and Hattori, T. (2010). Diverse roles and mechanisms of gene regulation by the Arabidopsis seed maturation master regulator FUS3 revealed by microarray analysis. *Plant Cell Physiol.* 51 (12), 2031–2046. doi: 10.1093/pcp/pcq162

Yang, Y., Munz, J., Cass, C., Zienkiewicz, A., Kong, Q., Ma, W., et al. (2015). Ectopic Expression of WRINKLED1 affects fatty acid homeostasis in brachypodium distachyon vegetative tissues. *Plant Physiol.* 169 (3), 1836–1847. doi: 10.1104/pp.15.01236

Ye, J., Wang, C., Sun, Y., Qu, J., Mao, H., and Chua, N. H. (2018). Overexpression of a transcription factor increases lipid content in a woody Perennial Jatropha curcas. *Front. Plant Sci.* 9, 1479. doi: 10.3389/fpls.2018.01479

Yeap, W. C., Lee, F. C., Shabari Shan, D. K., Musa, H., Appleton, D. R., and Kulaveerasingam, H. (2017). WRI1-1, ABI5, NF-YA3 and NF-YC2 increase oil biosynthesis in coordination with hormonal signaling during fruit development in oil palm. *Plant J.* 91 (1), 97–113. doi: 10.1111/tpj.13549

Zhai, Z., Liu, H., and Shanklin, J. (2017). Phosphorylation of WRINKLED1 by KIN10 results in its proteasomal degradation, providing a link between energy homeostasis and lipid biosynthesis. *Plant Cell* 29 (4), 871–889. doi: 10.1105/tpc.17.00019

Zhai, Z., Keereetaweep, J., Liu, H., Feil, R., Lunn, J. E., and Shanklin, J. (2018). Trehalose 6-Phosphate positively regulates fatty acid synthesis by stabilizing WRINKLED1. *Plant Cell* 30 (10), 2616–2627. doi: 10.1105/tpc.18.00521

Zhang, M., Fan, J., Taylor, D. C., and Ohlrogge, J. B. (2009). DGAT1 and PDAT1 acyltransferases have overlapping functions in Arabidopsis triacylglycerol biosynthesis and are essential for normal pollen and seed development. *Plant Cell* 21 (12), 3885–3901. doi: 10.1105/tpc.109.071795

Zhang, M., Cao, X., Jia, Q., and Ohlrogge, J. (2016a). FUSCA3 activates triacylglycerol accumulation in Arabidopsis seedlings and tobacco BY2 cells. *Plant J.* 88 (1), 95–107. doi: 10.1111/tpj.13233

Zhang, Y. Q., Lu, X., Zhao, F. Y., Li, Q. T., Niu, S. L., Wei, W., et al. (2016b). Soybean GmDREBL increases lipid content in seeds of transgenic Arabidopsis. *Sci. Rep.* 6, 34307. doi: 10.1038/srep34307

Zhang, D., Zhao, M., Li, S., Sun, L., Wang, W., Cai, C., et al. (2017). Plasticity and innovation of regulatory mechanisms underlying seed oil content mediated by duplicated genes in the palaeopolyploid soybean. *Plant J.* 90 (6), 1120–1133. doi: 10.1111/tpj.13533

Zhu, Y., Xie, L., Chen, G. Q., Lee, M. Y., Loque, D., and Scheller, H. V. (2018). A transgene design for enhancing oil content in Arabidopsis and Camelina seeds. *Biotechnol. Biofuels* 11, 46. doi: 10.1186/s13068-018-1049-4

Zou, J., Wei, Y., Jako, C., Kumar, A., Selvaraj, G., and Taylor, D. C. (1999). The Arabidopsis thaliana TAG1 mutant has a mutation in a diacylglycerol acyltransferase gene. *Plant J.* 19 (6), 645–653. doi: 10.1046/j.1365-313x.1999.00555.x

Conflict of Interest: The authors declare that the research was conducted in the absence of any commercial or financial relationships that could be construed as a potential conflict of interest.

frontiers in Plant Science

ORIGINAL RESEARCH
published: 04 February 2020
doi: 10.3389/fpls.2020.00001

Insights Into Oxidized Lipid Modification in Barley Roots as an Adaptation Mechanism to Salinity Stress

*Dingyi Yu[1,2], Berin A. Boughton[3], Camilla B. Hill[4], Ivo Feussner[5,6], Ute Roessner[1,3] and Thusitha W. T. Rupasinghe[3]**

[1] School of BioSciences, University of Melbourne, Parkville, VIC, Australia, [2] St. Vincent's Institute of Medical Research, University of Melbourne, Fitzroy, VIC, Australia, [3] Metabolomics Australia, Bio21 Institute, University of Melbourne, Parkville, VIC, Australia, [4] School of Veterinary and Life Sciences, Murdoch University, Perth, WA, Australia, [5] Albrecht-von-Haller-Institute for Plant Sciences, Department of Plant Biochemistry, University of Goettingen, Goettingen, Germany, [6] Goettingen Center for Molecular Biosciences, Department of Plant Biochemistry, University of Goettingen, Goettingen, Germany

OPEN ACCESS

Edited by:
Ikuo Nishida, Saitama University, Japan

Reviewed by:
Thierry Heitz, Université de Strasbourg, France
Luisa Hernandez, University of Seville, Spain

***Correspondence:**
Thusitha W. T. Rupasinghe
tru@unimelb.edu.au

Specialty section:
This article was submitted to Plant Metabolism and Chemodiversity, a section of the journal Frontiers in Plant Science

Received: *09 October 2019*
Accepted: *01 January 2020*
Published: *04 February 2020*

Citation:
Yu D, Boughton BA, Hill CB, Feussner I, Roessner U and Rupasinghe TWT (2020) Insights Into Oxidized Lipid Modification in Barley Roots as an Adaptation Mechanism to Salinity Stress. Front. Plant Sci. 11:1. doi: 10.3389/fpls.2020.00001

Lipidomics is an emerging technology, which aims at the global characterization and quantification of lipids within biological matrices including biofluids, cells, whole organs and tissues. The changes in individual lipid molecular species in stress treated plant species and different cultivars can indicate the functions of genes affecting lipid metabolism or lipid signaling. Mass spectrometry–based lipid profiling has been used to track the changes of lipid levels and related metabolites in response to salinity stress. We have developed a comprehensive lipidomics platform for the identification and direct qualification and/or quantification of individual lipid species, including oxidized lipids, which enables a more systematic investigation of peroxidation of individual lipid species in barley roots under salinity stress. This new lipidomics approach has improved with an advantage of analyzing the composition of acyl chains at the molecular level, which facilitates to profile precisely the 18:3-containing diacyl-glycerophosphates and allowed individual comparison of lipids across varieties. Our findings revealed a general decrease in most of the galactolipids in plastid membranes, and an increase of glycerophospholipids and acylated steryl glycosides, which indicate that plastidial and extraplastidial membranes in barley roots ubiquitously tend to form a hexagonal II (HII) phase under salinity stress. In addition, salt-tolerant and salt-sensitive cultivars showed contrasting changes in the levels of oxidized membrane lipids. These results support the hypothesis that salt-induced oxidative damage to membrane lipids can be used as an indication of salt stress tolerance in barley.

Keywords: oxidized lipids, salt stress, barley roots, mass spectrometry, lipid modification, *Hordeum vulgare*, oxylipins

INTRODUCTION

Plants have evolved complex strategies to cope with salinity stress, including the compartmentation and exclusion of Na^+ and Cl^-, biosynthesis of compatible solutes, and maintenance of membrane integrity and fluidity by lipid rearrangement (Allakhverdiev et al., 1999; Wu et al., 2005; Salama et al., 2007; Upchurch, 2008; Sarabia et al., 2018). In recent years, lipidomics has emerged as an effective tool to understand the diversity of membrane lipid compositions and unravel the roles of lipids in plant adaptation and tolerance to abiotic stresses (Welti et al., 2007; Natera et al., 2016; Tenenboim et al., 2016). Lipids and their related metabolites can now be readily detected from cultured cells or tissue extracts, identified and quantified on a large scale with high sensitivity using the latest techniques in lipidomics (Horn and Chapman, 2012; Köfeler et al., 2012; Haslam and Feussner, 2017; Yu et al., 2018). The detected changes in individual lipid species in stress-treated varieties can indicate the functions of lipids and related proteins or genes affecting lipid metabolism or lipid signaling (Welti et al., 2007). Previous studies on lipid composition alterations in response to various plant abiotic stresses, including drought, wounding, freezing, salinity, and nutrient deficiency, have uncovered diverse roles of membrane lipids and associated genes (Horn and Chapman, 2012; Vu et al., 2014; Tarazona et al., 2015; Narayanan et al., 2016; Natera et al., 2016; Sarabia et al., 2018; Tawaraya et al., 2018; Yu et al., 2018).

Cell membranes serve as semi-permeable barriers and gatekeepers that harbor proteins to regulate the influx of sodium ions and osmolytes (Upchurch, 2008). The adjustment of membrane fluidity partially relies on alterations of the unsaturation degree of polar glycerol-based membrane lipids (Murata and Los, 1997; Sui and Han, 2014). To maintain the stable structure of chloroplast or plastidic membranes in saline environments, plants alter their monogalactosyl diacylglycerol (MGDG) to digalactosyl diacylglycerol (DGDG) ratios; this alteration is associated with a membrane phase transition between bilayer phases and other less mobile non-bilayer phases (De Vries et al., 2004; Narayanan et al., 2016).

Salt stress can induce oxidation of vital molecules including glycerol-based membrane lipids (Mosblech et al., 2009) through the enhanced production of reactive oxygen species (ROS). Excessive ROS can react with cellular lipids and induce lipid peroxidation, which produces either esterified or free oxidized fatty acids (FAs) called oxylipins, which are considered biochemical markers of oxidative stress in plants (Howe and Schilmiller, 2002; De Azevedo Neto et al., 2006; Przybyla et al., 2008; Mosblech et al., 2009; Vu et al., 2012). The resultant oxylipins that are esterified in complex polar lipids localized in cell membranes can lead to a deterioration of membrane permeability or even cause cell death (Liu and Huang, 2000; Mosblech et al., 2009).

In addition to glycerol-based lipids, lipid remodeling of sphingolipids (SLs) and sterols (STs) under stress is gaining more attention (Michaelson et al., 2016). SLs are reported essential to basic cellular functions as well as having central roles in the signaling for programmed cell death (PCD) (Michaelson et al., 2016). Compositional changes of ceramides (Cer), hexosylceramides (HexCer), and conjugated STs have been observed under different abiotic stresses (Tarazona et al., 2015; Michaelson et al., 2016; Ferrer et al., 2017). However, the exact roles of these lipids in plant responses to stress are yet to be fully elucidated.

Recent studies have also drawn attention to cardiolipin (CL) accumulation as a response to osmotic stress (Pineau et al., 2013; Pan et al., 2014). CLs are a class of dimeric glycerophospholipids (GPs), and primarily localized in the inner membrane of mitochondria, where they account for around 10% of the total lipid content (Ardail et al., 1990; Schwarzländer and Fuchs, 2017). CLs not only contribute greatly to the permeability of the mitochondrial membranes, but also recruit soluble proteins to the membranes to stabilize respiratory chain supercomplexes (Mårtensson et al., 2017). Studies in various bacterial species, including *Escherichia coli*, *Bacillus subtilis*, and *Staphylococcus aureus*, provide evidence that an increase in CL content is a key factor in osmotic stress adaptation (Romantsov et al., 2008; Romantsov et al., 2009). To date, knowledge on the role of CL in eukaryotes, and in plants in particular, is scarce.

In this study, we present a high-throughput and high-sensitivity mass spectrometry–based lipidomics platform for comprehensive characterization of membrane lipid responses that also captures a range of oxidized lipids. Previously reported workflows for structural annotation and quantification of oxidized lipids in wheat seeds have been based on accurate mass and MS/MS spectra required extensive computation to process the data (Riewe et al., 2017). Our new approach is based on accurate mass combined with scheduled Multiple Reaction Monitoring (sMRM); the resulting data allow structural identification based on accurate mass of the precursor, observed product ions for oxidized lipids with retention time (RT) followed by a simple data processing workflow (Yu et al., 2018). We applied this method to profile oxidized lipids in roots of four Australian barley cultivars (two feed varieties Mundah and Keel which are salt-tolerant; and two malting varieties Gairdner and Vlamingh which are salt-sensitive) in response to salt stress (Coventry et al., 2008; Yu et al., 2018). Barley (*Hordeum vulgare* L.) is an excellent model plant for investigating salt stress, as it is the most salt-tolerant cereal (Munns and Tester, 2008) and different varieties of barley vary

Abbreviations: PBQC, pooled biological quality control; ASG, acylated sterol glucoside; CDS, calibrant delivery system; CE, collision energy; Cer: ceramide; CL, cardiolipin; DAG, diacylglycerol; DGDG, digalactosyl diacylglycerol; DGMG, digalactosyl monoacylglycerol; GIPC, glycosyl inositol phosphorylceramide; GL, glycerolipid; GlcADG, glucuronosyl diacylglycerol; GlcCer, glycosylceramide; GluCer, glucosylceramide; GP, glycerolphospholipid; HexCer, monohexosyl ceramide; IPC, inositol phosphoryl ceramide; MGDG, monogalactosyl diacylglycerol; MGMG, monogalactosyl monoacylglycerol; PC, phosphatidylcholine; PE, phosphatidylethanolamine; PG, phosphatidylglycerol; PI, phosphatidylinositol; PS, phosphatidylserine; SG, sterol glycoside; SL, sphingolipid; SQDG, sulfoquinovosyl diacylglycerol; SQMG, sulfoquinovosyl monoacylglycerol.

in their response to salinity stress (Shelden et al., 2013). Recent studies on two barley varieties (Clipper vs. Sahara) with contrasting response to salt stress have displayed a diversity of lipid alterations using lipidomics approaches (Natera et al., 2016). Spatial lipidomics based on imaging mass spectrometry (IMS) has also revealed differential lipid profiles under salt stress in barley roots and seeds (Sarabia et al., 2018; Gupta et al., 2019; Sarabia et al., 2019) The investigation of lipid profiles across different genotypes with contrasting salinity tolerance levels will lead to a better understanding of existing genetic diversity in current crop germplasm and shed more light into so-far unexplored functions of lipids in salinity tolerance. Our results deliver new insights into the impact of salt stress on the oxidized membrane lipids of barley roots and possible mechanisms of salt adaption of cereal crops.

MATERIAL AND METHODS

Growth Condition, Salt Treatments, and Biomass Measurements

Four varieties of barley were selected based on their importance for crop production, commercially relevant traits, and known difference in germination phenology and salinity tolerance (Tavakkoli et al., 2012; Kamboj et al., 2015; Sarabia et al., 2018; Yu et al., 2018). This selection comprised of two Australian barley feed (Mundah, Keel) and two malting genotypes (Gairdner, Vlamingh). Seeds of four Australian barley (*H. vulgare* L.) cultivars Mundah, Vlamingh, Keel, and Gairdner were provided by the University of Adelaide (SA, Australia). Cultivars were selected based on prior knowledge of their contrasting responses to salinity stress (Coventry et al., 2008; Cao et al., 2017; Yu et al., 2018). Barley seedlings (20 plants per variety and treatment) were grown in hydroponics for 5 weeks as previously described (Cao et al., 2017; Yu et al., 2018). Seeds were imbibed in deionized water with aeration for 16 h and then transferred to moistened filter paper for vernalization at 4°C. After 2 days, seeds were transferred to a plant growth chamber (Fitotron, Weiss Gallenkamp, UK) with 16 h light and 8 h dark for 4 days with the temperature set to constant 17°C. After germination, seedlings were transplanted into a hydroponic system as previously described (Shavrukov et al., 2012). Seedlings were distributed randomly to avoid systematic errors. The nutrient solution was a modified Hoagland's solution with pH adjusted to 6.5 (Hoagland and Arnon, 1950) and replaced weekly to reduce microbial contamination and to avoid nutrient depletion. Salt treatment was initiated 7 days after germination (when the third leaves had just emerged) and was carried out in four 25 mM NaCl increments per day until a concentration of 250 mM NaCl. This was reached by adding 25 mM NaCl into the growth chamber every 6 h in each day over 2.5 days.

A supplement of 6.4 mM $CaCl_2$ was added to the nutrient solution to maintain free Ca^{2+} levels for salt-treated plants (Tester and Davenport, 2003). Control and salt-treated plants were harvested on a single day after a 5-week growth period. Plants were divided into two groups: the first group comprised 40 plants which were used for biomass measurement (five replicates per variety and treatment); the second group consisted of 80 plants from which the roots were harvested for lipid analysis (five replicates per variety and treatment and two random plants per biological replicates).

Barley roots from both groups were quickly separated from shoots with sterilized scissors, gently washed with distilled water to remove remaining hydroponics solution, and blotted dry. Fresh weight (FW) of roots from the first group was immediately measured using an electronic balance (BW 420H, Shimadzu Corporation, Japan). Roots were placed into paper bags and oven-dried at 70°C for 48 h for dry weight (DW) measurements. Roots from the second group were immediately snap-frozen in liquid nitrogen and stored at −80°C until extraction.

Chemicals and Lipid Standards

Methanol (LC-MS grade) was purchased from Fisher Scientific (Scoresby, VIC, Australia); Hexane (LC grade) was from Honeywell (Taren Point, NSW, Australia), and 2-propanol (LC-MS grade) was from RCI Labscan (Bangkok, Thailand). Deionized water was produced by a Millipore Milli-Q system (Billerica, MA, USA). Standards of PE(12:0/12:0) and Cer(d18:1/12:0) were purchased from Avanti Polar Lipids (Alabaster, Alabama, US). A mixture of the two lipid standards was prepared as a stock solution at a concentration of 1 mM in methanol/chloroform 1:1 (v/v) and stored at −20°C. All other chemicals were purchased from Sigma-Aldrich (Castle Hill, NSW, Australia).

Lipid Extraction

For lipid extraction, frozen roots were homogenized into a fine powder using a mortar and pestle and liquid nitrogen. Lipids were extracted according to the procedure previously described for sphingolipid extraction in plant tissues (Markham et al., 2006). Homogenized frozen barley root powder (250–300 mg, exact weight of each sample was recorded) was quickly resuspended with a monophasic mixture of 2-propanol/hexane/water 60:26:14 (v/v/v, 6 ml) and incubated at 60°C for 30 min in an Eppendorf Thermomixer Comfort (Hamburg, Germany) mixing the solutions at 500 rpm. Samples were vortexed for 10 s and sonicated for 1 min every 10 min during incubation. The extracts were centrifuged at 2,000 g for 20 min at room temperature. The supernatant was transferred to a new tube, evaporated to dryness under a stream of nitrogen, then reconstituted in 500 µl of 2-propanol/methanol/water 4:4:1 (v/v/v) and stored at −20°C. A total of five biological replicates with each replicate combining two random plants were prepared. In order to compensate for variations in sample preparation and ionization efficiency, a total of 10 µl of an internal standard mixture, consisting of 100 µM of PE(12:0/12:0) and Cer(d18:1/12:0), was spiked into each replicate prior to extraction. A pooled biological quality control (PBQC) sample was produced by collecting 150 µl from each replicate as described previously (Hill et al., 2014). PBQC samples were used to monitor the reproducibility within and between different sample batches.

HPLC-ESI-QqTOF Conditions

Chromatographic separation of all lipid species was carried out using an Agilent Poroshell column EC-C18 (100 × 2.1 mm, 2.7 µm) at a flow rate of 0.40 ml/min at 50°C. Three linear gradients based on two mobile phases—mobile phase A, methanol/20 mM ammonium acetate 3:7 (v/v); and mobile phase B, 2-propanol/methanol/20 mM ammonium acetate 6:3:1 (v/v/v)—were applied for different lipid classes as published earlier (Yu et al., 2018). The eluted lipids were detected using a SCIEX TripleTOF™ 6600 QqTOF mass spectrometer (Framingham, Massachusetts, USA). The 6600 TripleTOF™ was equipped with a Turbo V™ dual-ion source (ESI and APCI) and an automated calibrant delivery system (CDS). Three HPLC-ESI-QqTOF based PRM assays established as described were applied to profile all lipid species however, in addition oxidized lipids were analyzed based on precursor-product ion transitions (Yu et al., 2018).

The 6600 TripleTOF™ was calibrated automatically every 10 samples *via* the CDS delivering APCI calibration solution (Foster City, CA, USA). CDS injected either positive or negative APCI calibration solution depending on the polarity of ESI and was used to calibrate the mass accuracy of the 6600 TripleTOF™ system in both ionization modes including TOF-MS (MS1 scan) and high-sensitivity MS/MS. With calibration, the mass resolution for precursor ions in MS1 spectra was ∼35,000 FWHM, while the resolution for the resulting fragments in high sensitivity MS/MS scans (PRM transitions) was ∼20,000. Actual mass accuracy was below 5 ppm in MS1 spectra and 10 ppm in MS/MS spectra.

Five biological replicates per treatment per variety were prepared and analyzed in the same LC-MS batch. As a result, 423 of 517 targeted lipids were detected with CV values of PBQC samples below 25% and used for further analysis. Most of the remaining 84 compounds with CVs above 25% were of low abundance and were not included in further analysis. Median CV values of the 423 compounds as an indicator for analytical reproducibility was 9%, which is well within acceptable limits for lipidomics. Detailed 423 lipid species profiles for all treatments and varieties have been included in **Supplementary Data File S1**.

Data Processing

Mass Feature Extraction From MS1 Data

MarkerView software (Version 1.2, SCIEX, Framingham, Massachusetts, USA) was used to extract mass features from both positive and negative ion mode MS1 data. Mass features were extracted for ions with an *m/z* range between 100 and 1,600 and eluting between 0.5 and 16 min. Noise threshold was set at 300. RT and *m/z* alignment of the mass features were performed with tolerances of 5% and 0.01 Da, respectively. Intensities were normalized by a manual scale factor, which was calculated from an internal standard intensity and sample weight. Only features that were detected in at least three samples of each group were extracted. Only features which contained an isotopic partner were selected for further data analysis. RTs were aligned using internal standards.

Peak Picking for Lipid Profiling Based on MS/MS Data

Lipid profiling using MS/MS data in PRM assays was based on the total peak area of extracted ion count chromatogram (EICC) for one or multiple fragment ions in MultiQuant (Version 3.0.2). For glycerol-based monoacyl (GLP) and diacyl lipids (GP), such as phosphatidylcholine (PC), phosphatidylethanolamine (PE), phosphatidylglycerol (PG), phosphatidylinositol (PI), and phosphatidylserine (PS), as well as CLs performed in negative ion mode, peak area of all negatively charged FA fragments were summed as published earlier (Yu et al., 2018); while for diacylglycerols (DAGs) detected in positive ion mode, the total peak area of all fragments resulting from neutral loss of a FA chain was used. For SPs, the sum of peak area of positively charged long chain bases (LCBs) and their dehydrates from up to three dehydration processes were used for profiling HexCer and Cer species. For STs, the dehydrated ST backbone was the only fragment chosen. Peak picking for fragment ions was finally set to 100 ppm width. Integration settings were as follows: noise percentage, 40%; Gaussian smooth width, 2 points. Peak areas were normalized based on the intensity of internal standards and sample weight.

Statistical Analysis

Tukey's multiple comparison test was employed for FW and DW comparisons across all four cultivars using Prism Version 7.00 (GraphPad Software Inc., San Diego, CA, USA).

For both targeted and untargeted lipid analysis, intensities of compounds/features in each sample (control and salt-treated) were acquired and normalized to the value equivalent to 250 mg fresh sample weight. Student's *t*-tests were conducted on each compound/feature to test for significance (*p*-value) between control and salt-treated samples in each variety using GraphPad Prism 7.00. Adjusted *p*-values were obtained with Benjamini–Hochberg false discovery rate (FDR) correction using MetaboAnalyst (Version 3.0). Panel bar plots and heat maps based on lipid data were created using the R software environment 3.5.0 (http://cran.r-project.org/).

RESULTS

Impact of Salinity on Root Biomass Accumulation

Root FW and DW decreased significantly for all cultivars in response to 5 weeks of salinity stress (**Figure 1**). Under control conditions, Gairdner had the highest root FW and DW, followed by Mundah, Vlamingh, and Keel, which had much lower root FW and DW compared to the other cultivars. As roots are the primary site of salt contact, the ability of roots to maintain FW/DW was shown to be an important indicator of the degree of salinity tolerance (Cao et al., 2017). A comparison of the ratios of values of salt to control (salt/control ratio) was used to evaluate the maintenance of biomass between different varieties. After the 250 mM salt treatment, Keel maintained the highest FW, and also had the highest salt/control FW ratio of above 0.5. Vlamingh

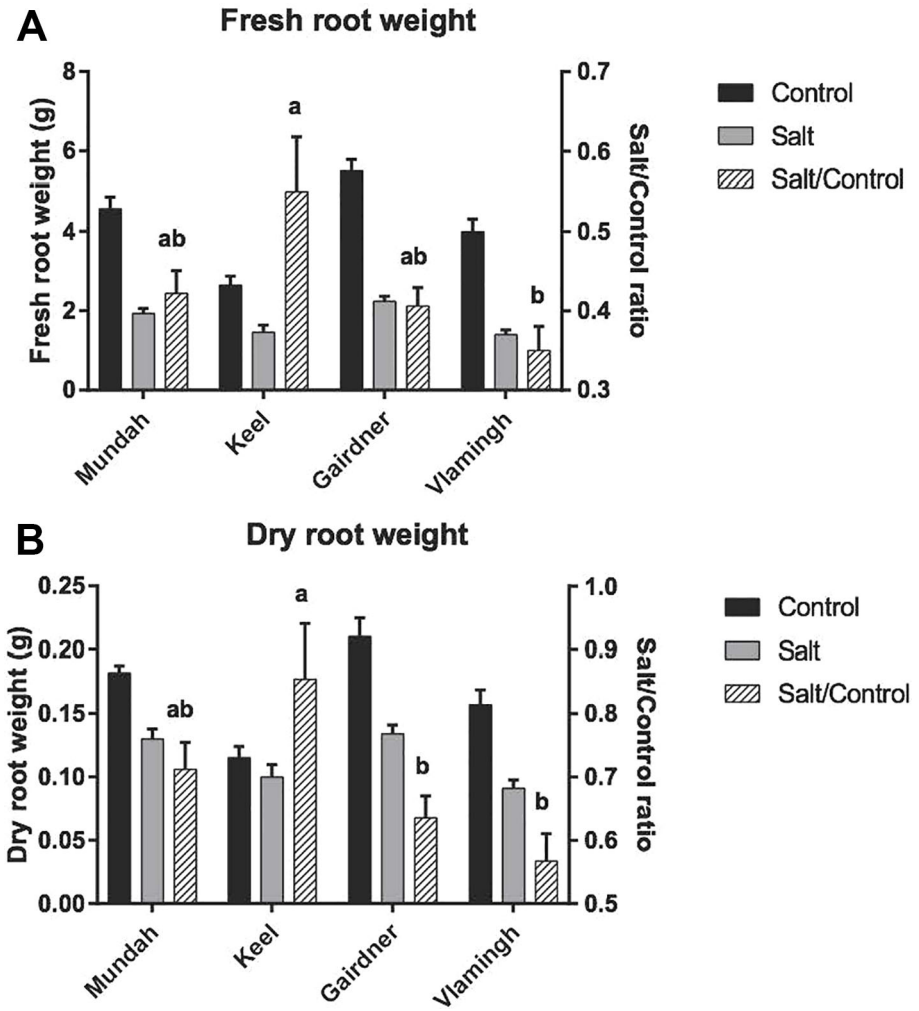

FIGURE 1 | Fresh root weight **(A)** and dry root weight **(B)** of control and salt-treated barley roots across four varieties. Letters above the error bars denote significant differences between salt/control ratio of varieties (Tukey's multiple comparison test; $p < 0.05$, $n = 4$; mean ± SD). Mundah and Keel are salt-tolerant barley cultivars; Vlamingh is salt-sensitive; the salt tolerance ability of Vlamingh is between Mundah and Gairdner.

showed a significant lower salt/control FW ratio than Keel ($p < 0.05$). The ability of Mundah and Gairdner to maintain FW was between that of Keel and Vlamingh. Salt-tolerant varieties showed a distinctly higher ability to maintain DW than salt-sensitive varieties. Keel was shown to be the most tolerant variety in maintaining root DW followed by Mundah. Vlamingh and Gairdner as salt-sensitive varieties have significantly lower root salt/control DW ratios.

Profiling of Oxidized Diacyl-Membrane Lipids From Extracted MS1 Features

To monitor the dynamics of oxidized lipids, we extended the lipidomics workflow established previously (Yu et al., 2018) to include the measurement of oxidized diacyl-lipids. Overall, 38 oxylipin-containing diacyl-GPs (PC, PE, PG, PI and PS) and -GLs (MGDG, DGDG) were detected and profiled using the extended workflow. Due to low abundance of some lipid classes present in the samples, oxidized lyso lipids and triacyl GLs were not detected.

To identify oxidized diacyl-lipids, we first generated a theoretical list of potential oxidized lipids containing five types of 18-carbon oxidized FAs and then manually verified the presence in our samples according to precursor *m/z* match, RT pattern, and MS/MS spectra. The five types of oxylipins including 18:2-O ($C_{18}H_{31}O_3$), 18:3-O ($C_{18}H_{29}O_3$), 18:4-O ($C_{18}H_{27}O_3$), 18:2-2O ($C_{18}H_{31}O_4$), and 18:3-2O ($C_{18}H_{29}O_4$) were selected based on their occurrence in previous studies (Ibrahim et al., 2011; Vu et al., 2012; Riewe et al., 2017). Oxidized lipids in the list either carry one of the three most abundant normal-FAs (16:0, 18:2, 18:3) with one oxylipin, or carry both oxidized fatty acyl chains. The total number of oxygen atoms in acyl chains of listed lipids range from one to four. Notably, each type of oxylipin might refer to one or several structures, which cannot be accurately identified by the mass

spectrometry approach used in this study. As previously summarized, 18:4-O can identify as: oxo-phytodienoic acid (OPDA) 18:3-O, and can refer to two possible lipid structures: a keto FA and a hydroxy FA; 18:2-O and 18:2-2O are either hydroxy or dihydroxy FA acids, respectively; and 18:3-2O is possibly derived from ketols, FA hydroperoxides, or dihydroxy FAs or their mixtures (Mosblech et al., 2009; Vu et al., 2012).

Using a mobile phase containing ammonium acetate, most ox-GPs and ox-GLs will be observed as negatively charged $[M+OAc]^-$ or $[M-H]^-$ anions or both, which is analogous to normal diacyl species. Collision-induced dissociation (CID) of negatively charged precursors in MS/MS experiments induced cleavage of two acyl chains into carboxylate anions. The *m/z* values of carboxylate anions for different oxylipin chains are listed in **Table 1**. Specifically, fragments of oxidized FA18:3-2O and 18:2-2O were detected as 18:4-O and 18:3-O anions, respectively, due to a dehydration process. Apart from the precursor ions and fatty acyl fragments, some other characteristic fragments related to the polar head of lipids can also be observed as important indicators. Lipid separation on reversed-phase columns is largely dependent on FA composition. Elution patterns of lipid species within a lipid class is another

TABLE 1 | Detected oxidized diacyl glycerolipids and glycerophospholipids using HPLC-ESI-QqTOF. Detected/theoretical precursor ions, acyl fragments detected from MS/MS spectra, RTs, and mass deviations are listed.

No.	Class	Species	Detected Precursor	Theoretical Precursor	Ox-FA Fragment	FA Fragment	RT	Mass Error on Precursor
1	ox-PC	PC(34:3)-O	830.555	830.557	293.212	255.232	6.96	1.81
2	ox-PC	PC(34:4)-O	828.539	828.533	291.196	255.232	6.27	–7.12
3a	ox-PC	PC(36:5)-O	854.555	854.551	293.212	279.232	6.57	–4.21
3b	ox-PC	PC(36:5)-O	854.555	854.551	295.227	277.216	6.57	–4.21
4	ox-PC	PC(36:6)-O	852.539	852.536	293.216	277.216	5.83	–3.40
5	ox-PE	PE(34:2)-2O	746.497	746.490	293.216	255.232	7.06	–8.98
6	ox-PE	PE(34:3)-2O	744.482	744.486	291.196	255.232	6.22	4.97
7	ox-PE	PE(34:3)-O	728.487	728.483	293.212	255.232	7.16	–5.49
8	ox-PE	PE(34:4)-O	726.471	726.474	291.196	255.232	6.52	4.13
9	ox-PE	PE(36:4)-2O	770.497	770.500	293.212	279.232	6.51	3.50
10	ox-PE	PE(36:4)-O	754.502	754.500	295.227	279.232	7.3	–3.31
11a	ox-PE	PE(36:5)-2O	768.482	768.485	291.196	279.232	5.73	3.64
11b	ox-PE	PE(36:5)-2O	768.482	768.485	293.216	277.216	5.73	3.64
12a	ox-PE	PE(36:5)-O	752.487	752.488	293.212	279.232	6.62	1.59
12b	ox-PE	PE(36:5)-O	752.487	752.488	295.227	277.216	6.62	1.59
13	ox-PE	PE(36:6)-2O	766.466	766.466	291.196	277.216	4.75	0.00
14	ox-PE	PE(36:6)-O	750.471	750.472	293.212	277.216	5.98	1.20
15	ox-PG	PG(34:2)-O	761.496	761.499	295.227	255.232	6.37	3.81
16	ox-PG	PG(34:3)-O	759.481	759.474	293.212	255.232	5.64	–9.35
17	ox-PG	PG(34:4)-O	757.465	757.471	291.196	255.232	5.09	8.05
18	ox-PI	PI(34:3)-O	847.497	847.492	293.212	255.232	5.34	–6.49
19	ox-PI	PI(34:4)-O	845.482	845.479	295.227	255.232	4.76	–2.84
20	ox-PI	PI(36:4)-O	873.513	873.515	295.227	279.232	5.59	2.29
21a	ox-PI	PI(36:5)-O	871.487	871.487	293.212	279.232	4.96	0.01
21b	ox-PI	PI(36:5)-O	871.487	871.487	295.227	277.216	4.96	0.01
22	ox-PI	PI(36:6)-O	869.481	869.479	293.212	277.215	4.26	–1.96
23	ox-PS	PS(34:3)-2O	701.439	701.440	291.196	255.232	5.04	1.71
24	ox-PS	PS(34:3)-O	685.444	685.438	293.212	255.232	5.93	–8.75
25	ox-PS	PS(34:4)-O	683.429	683.424	291.196	255.232	5.24	–7.48
26	ox-PS	PS(34:4)-2O	699.424	699.421	291.196	255.232	4.21	–3.32
27	ox-PS	PS(36:4)-2O	727.455	727.452	293.216	279.232	5.34	–4.81
28	ox-PS	PS(36:4)-O	711.460	711.463	295.227	279.232	6.08	4.50
29a	ox-PS	PS(36:5)-2O	725.439	725.435	291.196	279.232	4.45	–5.24
29b	ox-PS	PS(36:5)-2O	725.439	725.435	293.216	277.216	4.45	–5.24
30a	ox-PS	PS(36:5)-O	709.444	709.440	293.212	279.232	5.44	–6.06
30b	ox-PS	PS(36:5)-O	709.444	709.440	295.227	277.216	5.44	–6.06
31	ox-PS	PS(36:6)-O	707.429	707.423	293.212	277.216	4.81	–8.91
32	ox-MGDG	MGDG(34:4)-O	825.536	825.528	291.196	255.232	7.29	–9.21
33a	ox-MGDG	MGDG(36:5)-O	851.552	851.558	293.212	279.232	7.21	7.52
33b	ox-MGDG	MGDG(36:5)-O	851.552	851.558	295.227	277.216	7.21	7.52
34	ox-MGDG	MGDG(36:6)-O	849.536	849.535	293.212	277.216	6.47	–0.82
35	ox-DGDG	DGDG(34:3)-O	989.605	989.607	293.212	277.216	6.82	2.02
36	ox-DGDG	DGDG(36:4)-O	1015.620	1015.624	295.227	279.232	7.06	3.64
37a	ox-DGDG	DGDG(36:5)-O	1013.605	1013.608	293.212	279.232	6.32	3.16
37b	ox-DGDG	DGDG(36:5)-O	1013.605	1013.608	295.227	277.216	6.32	3.16
38	ox-DGDG	DGDG(36:6)-O	1011.589	1011.591	293.212	277.216	5.54	2.17

RT, retention time; FA, fatty acid; PC, phosphatidylcholine.

important criterion to remove false IDs. Shorter acyl chains and higher unsaturation degree result in an earlier elution time for similar lipids (Patton et al., 1982). Oxidized lipids elute earlier than their parent non-oxidized lipids due to presence of more hydrophilic oxidized acyl chains, and RTs of oxidized lipids differing in carbon length and number of double bonds display similar pattern as their parent non-oxidized lipids (**Figure 2**).

Following this workflow, 38 ox-lipids were confirmed in this study, including 4 ox-PC, 10 ox-PE, 3 ox-PG, 5 ox-PI, 9 ox-PS, 3 ox-MGDG, and 4 ox-DGDG species. Molecular formula, acyl-chain fragments, RTs, and mass deviations of precursor ions in MS1 spectra of these lipids are listed in **Table 1**. Each detected ox-GP or GL molecular species consists of a normal-FA chain, 16:0, 18:3, or 18:2, in combination with an oxidized chain from 18:3-O, 18:3-2O, 18:2-O, and 18:2-2O. Representative MS/MS spectra of PE(36:5-O) and PE(36:5-2O) are shown in **Figures 3A, B**, respectively.

Lipid Composition of Barley Roots Is Significantly Altered After Salinity Stress in All Four Varieties

The focus of this study was to investigate salt-induced alterations of membrane lipids, including GPs, GLs, ox-GPs, ox-GLs, SPs, and STs. We also included lipid species which are usually not present in membrane bilayers but potentially provide a source of backbones and acyl chains in membrane lipid synthesis, or act as signaling intermediates associated with membrane activities, such as DAGs, lyso (monoacyl)-GPs/GLs (Okazaki and Saito, 2014; Tarazona et al., 2015). The most abundant lipid profile of barley roots has been reported.

To provide a global visualization of the lipidome alterations, the lipid data were presented as log fold change (FC) of total lipid content after salinity stress in each lipid classes for all four cultivars (**Figure 4**). FC of the total lipid content per each lipid class was calculated using the log ratio of the lipid response in salt-treated to control barley roots. The log FC of the total lipid profile for each class shows distinct profiles between control and salt-treated samples for all four cultivars, which exemplifies that the barley root lipidome is significantly altered by salt treatment (**Figure 4**). Upon salt treatment, the root lipidome of the four varieties become more similar to each other than under control conditions for several lipid classes, such as GPs, GLs, lyso-GPs, and SLs, while oxidized lipids show a significant difference between the salt stress sensitive and tolerant varieties. The FC of the total lipid content of PC, PE, PG, PI, PS, CL, and Glc-ST show a significant increase, while lysophosphatidylcholine (LPC), lysophosphatidylethanolamine (LPE), lysophosphatidylglycerol (LPG), MGDG, monogalactosyl monoacylglycerol (MGMG), DGDG, digalactosyl monoacylglycerol (DGMG), sulfoquinovosyl diacylglycerol (SQDG), glucuronosyl diacylglycerol (GlcADG), and Cer show significant decreases following salt treatment. The most significant lipid profile changes based on the varieties which are tolerant to salt stress compared to those being sensitive to salt tolerance were observed in the oxidized lipids as shown in **Figure 4**. The total oxidized lipid profile showed little increase or no change for the two salt-tolerant cultivars Mundah and Keel, whereas the salt-sensitive cultivars Gairdner and Vlamingh show significant decreases in response to salt stress. Overall, the total lipid profile of all the lipid classes clearly showed that both treatment and genotype contribute to the diversity of the barley root lipidome.

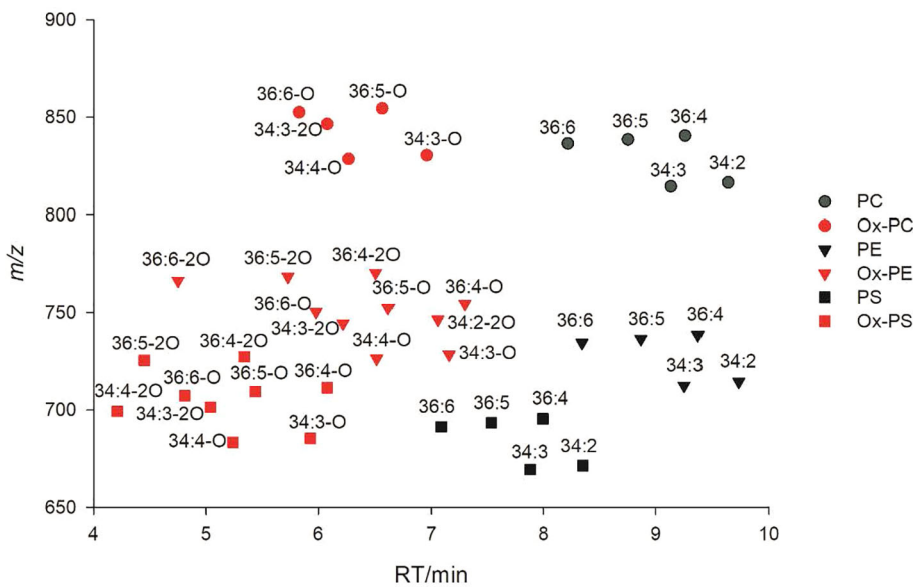

FIGURE 2 | 2D LC-MS plot of oxidized phosphatidylcholine (PC)/phosphatidylethanolamine (PE)/phosphatidylserine (PS) and their parent non-oxidized lipids.

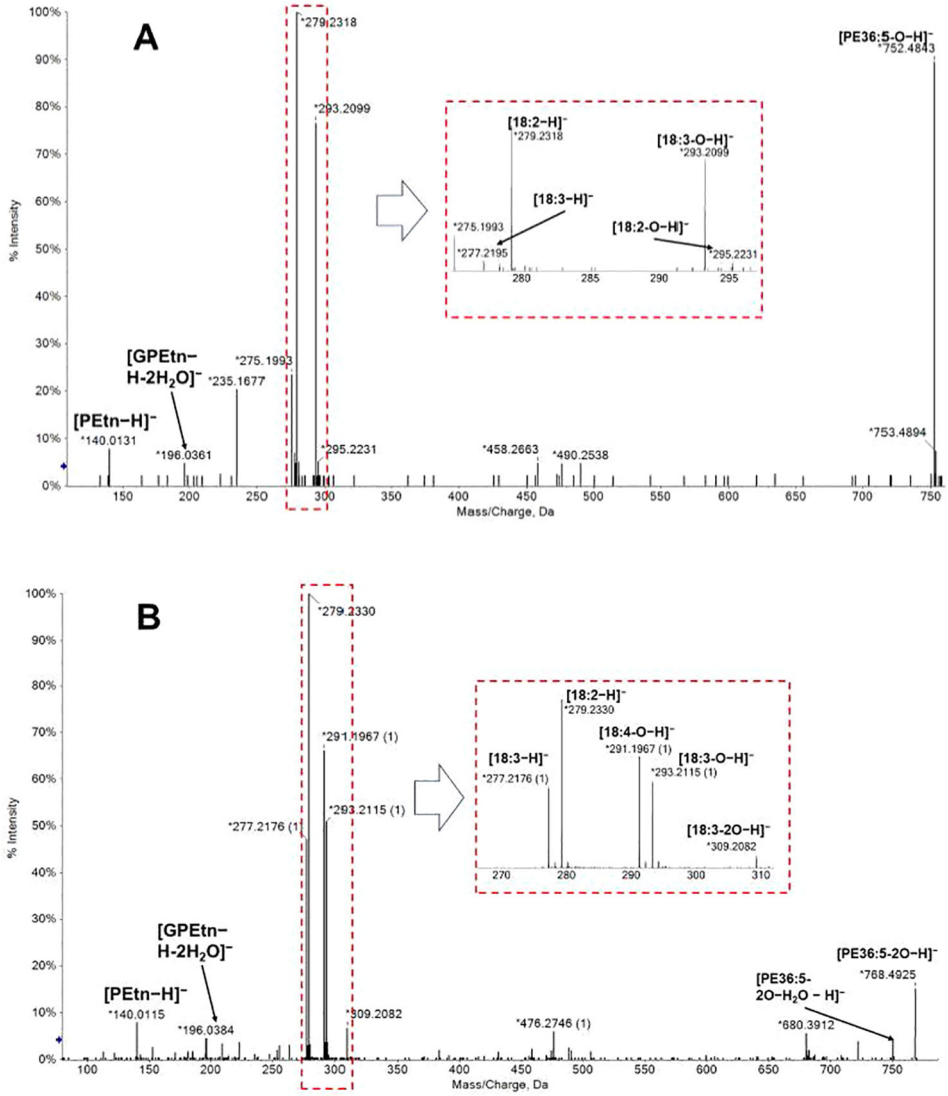

FIGURE 3 | MS/MS spectra of [M–H]– precursors of PE(36:5-O) **(A)** and PE(36:5-2O) **(B)**. Acyl chains can be partially resolved in negative ion mode MS/MS spectra. PE(36:5-O) were a mixture of PE(18:2-O/18:3) and PE(18:3-O/18:2); PE(36:5-2O) were a mixture of PE(18:2-2O/18:3) and PE(18:3-2O/18:2). GPEtn: glycerophosphorylethanolamine; PEtn, phosphorylethanolamine.

Linolenic Acid Levels Increase in the Majority of Structural Diacyl GPs Containing Medium to Long Fatty Acyl Chains (C14~18) in Response to Salinity Stress

To further investigate how treatment modified individual lipid species levels and if there are distinct differences in the lipid levels based on genotype, pairwise Student's *t*-test and FC analysis of GPs were carried out on the 423 GP species (including 34 oxdized lipids) between control and salt-treated samples (**Figure S1**).

GPs are considered as major structural components of plant plasma membranes and intracellular membranes. Among them, PC and PE are the two predominant structural GPs; the other GPs are mainly PG, PI, and PS species (Furt et al., 2011). One distinct feature for structural GPs observed in salt-treated roots of all four barley varieties was the increased amount of linolenic acid (18:3) across several numbers of GP species. This is reflected by the substantial accumulation of diacyl-GPs containing a linolenic acid (18:3) and a medium to long chain FA (14:0, 16:0, 16:1, 18:0, 18:1, 18:2, and 18:3), resulting in combined FA chain lengths as 32, 34, and 36 with a high number of double bonds, as they account for more than 90% of total diacyl-GPs (**Figure S1**). Our previous work provided insight of the lipid abundance in barley roots and most lipids belongs to diacyl-GPs and GIPCs in the salt-treated group were present with higher

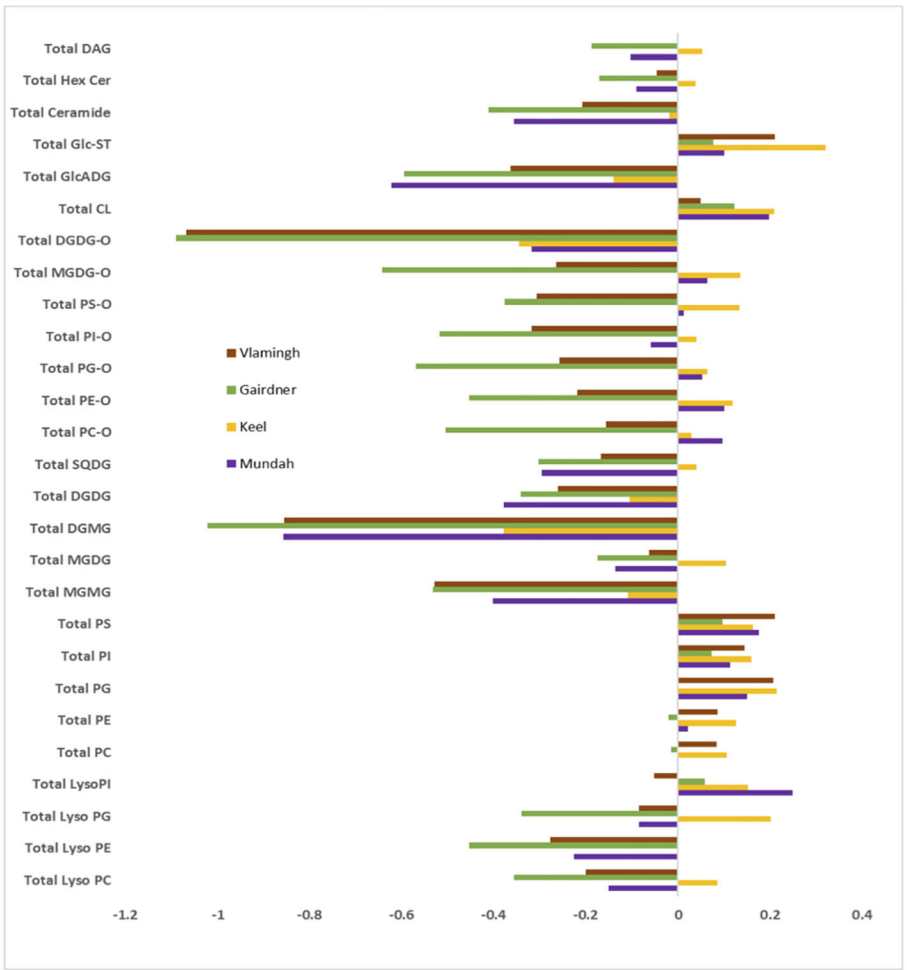

FIGURE 4 | Log2 fold change (FC) of total lipids per each class after salt treatment in four barley varieties: Gairdner, Vlamingh, Mundah, and Keel.

abundance than control, while more lyso-species and diacyl-GLs (except DAG) were observed to be present in higher amounts in control sample (Yu et al., 2018). Different varieties show different magnitudes in the increase of these lipids. Based on the results of the pairwise *t*-tests between control and salt-treated samples in each variety, 27, 23, and 25 out of 31 linolenic acid–containing diacyl-GPs were significantly increased (adjusted $p < 0.05$) in Keel, Mundah, and Vlamingh respectively; while only 9 species were significantly increased in Gairdner.

Contrasting trends were observed in other structural diacyl-GPs containing a C18:3 combined with a very long chain FA (VLCFA, C20~26) across different varieties (**Figure S1**). Different patterns were observed for the 22 lipids monitored across the four varieties. Gairdner showed a substantial decrease in most of these lipids with 20 lipids decreased and 15 that were statistically significant. Vlamingh also held an overall decrease (18 lipids) but to a lesser extent than Gairdner and only 4 being statistically significant. In the two salt-tolerant varieties Mundah and Keel, almost equal numbers of lipids decreased (12 in Mundah and 10 in Keel) and increased (10 in Mundah and 12 in Keel). In Mundah and Keel, only five and two lipids showed statistically significant decreases; three and four lipids showed statistically significant increases, respectively.

DAGs, which are critical precursors for the synthesis of PCs and PEs, did not always show concurrent trends as their corresponding PC and PEs. DAGs containing a linolenic acid (18:3), such as DAG (18:2_18:3), DAG(18:3_18:2), and DAG(16:0_18:3), increased in Keel and Vlamingh but decreased in the other two varieties.

Regarding the fate of a class of potential signaling lipids—lyso-GPs, a general decrease was observed in most of LysoPCs and LysoPEs in all four varieties with statistically significance based on Student's ***t***-test and one-way analysis of variance (ANOVA). FDR (Hochberg and Benjamini, 1990) was used to reduce type I errors in multiple comparisons. However, several major unsaturated species are an exception with contrasting alterations across the different cultivars. For example, LysoPC (18:2) and LysoPC(18:3) in salt-treated samples showed significant increases with more than 1.40-fold in Keel, while a slight increase for LysoPC(18:2) and LysoPC(18:3) with 1.03-fold and 1.20-fold, respectively, in Mundah compared to the control

samples. Conversely, a significant decrease of LysoPC(18:2) and a slight decrease of LysoPC(18:3) was detected in the two salt-sensitive varieties, Gairdner (reduced to 72% and 95% in salt-treated samples respectively), and Vlamingh (reduced to 70% and 90% in salt-treated samples respectively) in response to salinity stress.

Decrease of Plastidial Glycerolipids in Response to Salinity Stress

GL including MGDGs/MGMGs, DGDGs/DGMGs, SQDGs, and GlcADGs are synthesized and mainly present in plastidial membranes (Dörmann, 2013; Okazaki et al., 2013). Compositional changes of these plastidial glycerolipids occur in

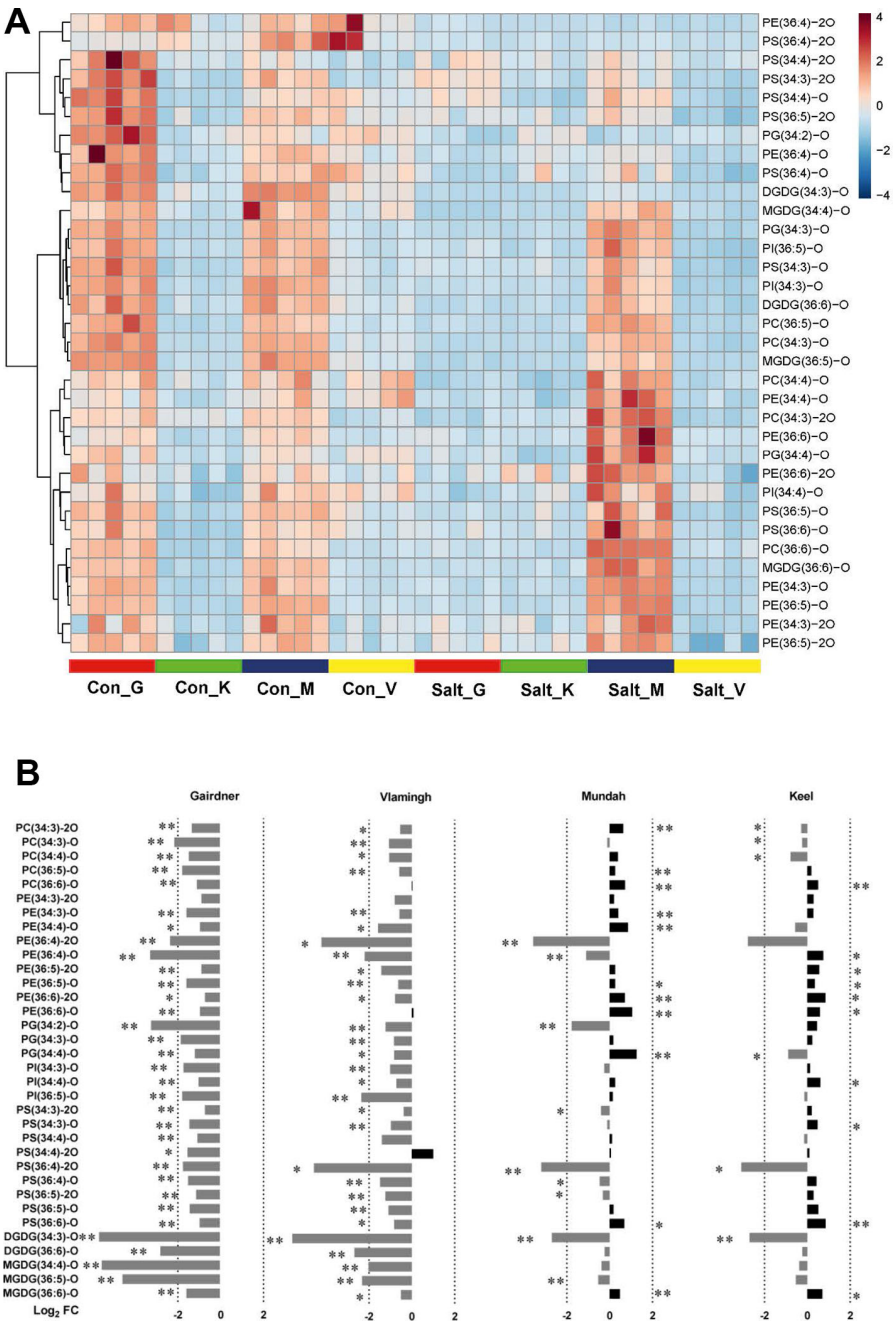

FIGURE 5 | (A) Heat map of 34 oxidized lipids in control (con) and salt-treated (salt) samples (n = 5) in four barley varieties: Gairdner (G), Keel (K), Mundah (M), and Vlamingh (V). **(B)** Histogram displaying log2 FC of 34 oxidized lipids after salt treatment in the four barley varieties.

response to drought, cold, freezing, and salinity, all of which can induce osmotic stress (Moellering et al., 2010; Tarazona et al., 2015).

In our experiments, the majority of the 111 detected GL species decreased in Gairdner (103 of the 111 species decreased of which 93 were $p < 0.05$), Mundah (103 of the 111 species decreased of which 88 were statistically significant), and Vlamingh (93 of the 111 species decreased of which 68 were statistically significant) under salinity compared to control; while a much smaller number of GL species (68 out of 111 detected of which only 34 were statistically significant) decreased in salt-treated Keel roots (**Figure S2**). On the other hand, Keel has the most species (14 species out of the 111 detected) exhibiting significant increases; while in Gairdner, Mundah, and Vlamingh only 2, 4 and 8 out of 111 detected significantly increased, respectively.

Compared to DGDGs, MGDGs showed a lesser degree of reduction in relative concentration across the four varieties (**Figure 5A**). For example, MGDG(16:0_18:2) reduced to 58%, 56%, and 68% in Gairdner, Mundah, and Vlamingh in salt-treated samples compared to control samples, respectively, and remained unchanged in Keel; while the level of DGDG(16:0_18:2) decreased to 28%, 20%, 19%, and 58% in Gairdner, Mundah, Vlamingh, and Keel, respectively (**Figures S2A, S2B**). The relatively smaller degree of decrease in MGDGs compared to DGDGs leads to an increase in the calculated value of the MGDG/DGDG ratio after salt stress in barley roots.

Among the four diacyl-GL classes (MGDG, DGDG, SQDG, and GlcADG), DGDGs showed the most pronounced overall decrease (**Figure S2B**). Twenty-nine out of 30 analyzed DGDG species in each of Gairdner, Mundah, and Vlamingh, as well as 24 DGDG species in Keel, decreased of which 25 species were statistically significantly decreased in Gairdner and Mundah, 20 in Vlamingh, and only 14 in Keel when compared to their respective controls. These results indicate that Keel appears to sustain the levels of DGDGs after salt treatment. However, the most abundant DGDG species, such as DGDG(16:0_18:2), DGDG(16:0_18:3), and DGDG(18:2_18:3), were still significantly decreased across all four varieties.

SQDGs and GlcADGs were observed with similar patterns in response to salinity as MGDGs and DGDGs (**Figure S2C**). Most SQDGs and GlcADGs exhibited a drastic decrease in Gairdner, Mundah, and Vlamingh; while Keel maintained levels as in control samples. Unlike structural diacyl-GPs, no obvious distinction was observed among GLs with different unsaturation degrees. Also, no obvious correlation was observed between the length of fatty acyl chains and GL modification. For example, MGDGs and DGDGs containing VLCFA did not show substantial reduction compared to those containing shorter FAs (≤ C18) (**Figure S2C**).

Monoacyl GLs including MGMG and DGMG were overall more susceptible to salt stress than diaycl-GLs. Nearly all detected DGMG and MGMG species were significantly decreased after salt treatment across all varieties, except DGMG(26:1) (**Figure S2**). In Gairdner, Mundah, and Vlamingh, all 10 species in salt-treated samples decreased to less than 30% compared to control samples; two species, DGMG (16:0) and DGMG(20:1), even dropped to below 10% in salt-treated samples. Keel again stood out with much smaller reductions of DGMG ranging between 45% and 81%.

Salinity-Induced Accumulation of the Mitochondrial Specific Lipid Class CL

Strong accumulation was observed for the unique mitochondrial lipid class of CL in this study. In barley roots, the five most abundant CLs are CL(72:8), CL(72:9), CL(72:10), CL(72:11), and CL(72:12) (Zhou et al., 2016). After salt treatment, all five CLs showed substantial increases in Gairdner, Keel, and Mundah, where most increases being statistically significant (**Figure S3**). Specifically, CL(72:10) significantly increased 1.37-fold in Gairdner, 1.60-fold in Keel, and 1.51-fold in Mundah, while CL(72:11) significantly increased 1.76-fold in Gairdner, 1.67-fold in Keel, and 1.84-fold in Mundah (**Figure S3**). CL(72:8) increased significantly only in Gairdner (1.36-fold) and Mundah (1.63-fold). Interestingly, CL(72:9) had a significant increase only in Keel (1.78-fold). CL(72:10), CL(72:11), and CL (72:12) were also observed to be increased in Vlamingh but only CL(72:11) was statistically significant (1.35-fold) (**Figure S3**). Plant CLs are synthesized by CARDIOLIPIN SYNTHASE (CLS) transferring a phosphatidyl group from cytidine diphosphate–diacylglycerol (CDP-DAG) to a PG molecule (Nowicki et al., 2005). Based on the results from previously published studies (Zhou et al., 2016), fatty acyl chains of the five major CLs are predominantly 18:2 and 18:3. Thus, these CLs are most likely synthesized from three PGs: PG(18:2_18:2), PG(18:2_18:3), and PG(18:3_18:3). Levels of the three PGs were also significantly elevated under salt stress in Keel (1.75-fold, 1.74-fold, and 1.89-fold, respectively), Mundah (1.34-fold, 1.45-fold, and 1.61-fold, respectively), and Vlamingh (1.58-fold, 1.57-fold, and 1.57-fold, respectively) (**Figure S3**).

Contrasting Responses of Oxidized Lipids in Response to Salinity Between Tolerance and Sensitive Barley Cultivars

Heat maps were utilized to visualize the compositional differences of oxidized lipids between treatments and across different varieties (**Figure 5A**). One distinct feature of oxidized lipids is that large variations exist among the four varieties even before and after salinity treatment. In non-treated barley roots, oxidized lipids were at higher levels in roots of Gairdner and Mundah relative to those of Keel and Vlamingh. When the varieties were exposed to salt stress, contrasting alterations to the oxidized lipid ratios were observed across the different cultivars (**Figure 5B**). In the salt-sensitive cultivar Gairdner, all of the oxidized lipids exhibited dramatic decreases after salt stress; 33 out of 34 detected species decreased significantly (adjusted $p < 0.05$); among them, 29 species decreased by more than half. In the other salt-sensitive variety Vlamingh, most of the oxidized lipids were also decreased compared to control samples but to a lesser extent than Gairdner with only 29 species out of 34 being statistically significant (**Figure 5B**). However, a general tendency of increased responses was observed in oxidized lipids in the two salt-tolerant varieties, especially in the oxidized diacyl-GP species. Twenty out of 29 detected oxidized diacyl-GPs in Mundah showed a relative increase; 10 of the 20 lipids increased with statistical significance.

In Keel, 19 of 29 oxidized diacyl-GPs were also increased but to a lesser extent, with 9 of the 20 lipids exhibiting statistical significance (**Figure 5**).

DISCUSSION

Root Biomass Is a Good Indicator of Salt Tolerance in Barley

High salinity (250 mM) caused significant inhibition to root growth and significantly decreased fresh and DW accumulation in all four barley varieties. The degree of decrease in both FW and DW was smaller in the salt-tolerant varieties Mundah and Keel compared to the salt-sensitive varieties Gairdner and Vlamingh. This is in agreement with previous investigations where Mundah and Keel were found to have greater salt tolerance than Gairdner and Vlamingh, as determined by maintaining their growth (Coventry et al., 2008; Cao et al., 2017).

Although both Mundah and Keel showed a strong ability to maintain root biomass, they are very likely to utilize different salt tolerant mechanisms. Mundah has been demonstrated to maintain higher Na^+ and K^+ concentration in roots compared to Keel (Shelden et al., 2013), which suggests that Mundah may have a greater tissue tolerance to sodium ions, while Keel may primarily rely on other mechanisms such as sodium exclusion. It has been reported that the ionic stress stage is much less evident in Mundah than in Keel, which is most likely owing to the higher ionic tolerance in Mundah (Harris et al., 2010). The distinct membrane lipid composition observed between Mundah and Keel both before and after treatment provides support for this hypothesis (**Figure 5A**). As the lipid layers in root plasma and intracellular membranes play critical roles in regulating flux of Na^+ and K^+ ions across membranes, the different lipid compositions may relate to different activities in the cross-membrane ion transport (Parida and Das, 2005).

Both Unsaturation Degree and Carbon Length Distribution of GPs Are Important in Plasma Membranes Adapting to Salinity Stress

Diacyl-GPs, which are core components of plasma membrane bilayers, have been the major focus in previous abiotic stress studies (Los and Murata, 2004). The degree of unsaturation of these lipids was considered as a decisive factor in maintaining plasma membrane fluidity during stress (Upchurch, 2008). Higher concentrations of unsaturated fatty acyl chains can lead to stronger steric hindrance between diacyl-GPs, and therefore generate increased molecular disorder within a membrane bilayer (Los and Murata, 2004). Our results in the present study show that all four barley varieties increased the levels of linolenic acid (18:3)–containing diacyl-GP species, thereby increasing membrane fluidity in response to salinity. These results are in accordance with previous studies that show that the ability to maintain or increase unsaturated lipids correlates with a high level of salinity tolerance (Lin and Wu, 1996; López-Pérez et al., 2009; Mansour et al., 2015). The increase of linolenic acid in plasma membranes was also reported under salt stress in roots of other barley varieties (Yu et al., 1999; Natera et al., 2016). Therefore, we can regard it as a common salt-responsive strategy adopted in barley.

One advantage of the lipidomics method used in this study is that the composition of acyl chains at the molecular level was determined. This enabled us to precisely profile the 18:3-containing diacyl-GPs and allowed individual comparison of lipids across varieties. By taking advantage of this, we found that the increase of 18:3 was biased in favor of diacyl-GP species containing medium to long chain FAs (C14 ~ 18); while when 18:3 was found in combination with VLCFAs, contrasting alterations were observed. This suggests that there are possibly different roles of VLCFAs and medium to long chain FAs in their ability to modify the membrane biophysical properties in response to salinity. The difference may result from the higher steric hindrance and higher hydrophobicity generated by VLCFAs compared to medium to long FAs. A higher concentration of VLCFAs can lead to lower membrane fluidity (Bach and Faure, 2010). Another possible reason for the preference for a combination of 18:3 with medium to long FA is the more complex biosynthetic pathway of VLCFA which requires more biosynthetic steps, more enzymes, and energy, thus being energetically more costly for the plant (Millar et al., 2000).

Increase of MGDG/DGDG Ratio and ASG Concentrations Suggests That Salinity May Induce the Formation of a Hexagonal II Phase in Plastid and Plasma Membranes

Compared to plasma membranes, plastid membranes seem to be less well-maintained. All four barley varieties showed a remarkable reduction in MGDG/MGMG, DGDG/DGMG, SQDG, and GlcADG amounts in response to salinity stress. This suggests a possible inhibition or even degradation of plastid membranes upon salinity. The decrease of these plastidial lipids and inhibition of galactosyl transferases combined with impairment of plastid/chloroplast membranes has been reported for salt stress before (Müller and Santarius, 1978; Shu et al., 2013; Bejaoui et al., 2016). The MGDG/DGDG ratio is associated with the physical state of plastid envelope membranes, and a higher MGDG/DGDG ratio suggests that a proportion of liquid-crystalline membranes are transformed into a hexagonal II (HII) non-bilayer phase (Dörmann and Benning, 2002; Dörmann, 2013). Lipids in the HII non-bilayer phase are organized into inverted micelles with the polar head groups on the inside and the hydrophobic tails on the outside (Jouhet, 2013). We observed a similar increase in the ratios and interpreted that this may be a possible protective mechanism of plastid membranes to maintain function under salinity stress. As previously reported, activities of plastidial enzymes such as violaxanthin de-epoxidase (VDE) require a lipid inverted hexagonal structure to operate efficiently in chloroplast membranes (Jouhet, 2013) and the VDE was also demonstrated to be expressed in wheat roots under salt stress (Zhang et al., 2003; Remorini et al., 2009).

SGs and ASGs are two classes of ST conjugates located mainly in the plasma membrane. STs and their conjugates were proposed to play a prominent role in regulating membrane acyl chain ordering and permeability (Schuler et al., 1991). Similar to MGDGs in the plastid membrane, ASGs and SGs can also induce the plasma membrane and the tonoplast to form an HII phase under freezing

stress and cold acclimation (Webb et al., 1995). In the present study, The combination of the increased ASG content, MGDG/DGDG ratio, and the increased amount of ASG indicate that plastidial and extra-plastidial membranes in barley roots are shifted towards favorable conditions to form an hexagonal II phase to maintain membrane functions under salinity stress. Compared to ASGs, SGs showed fewer changes in all four barley varieties. Previously, an increase of SGs was observed in heat and freeze induced osmotic stress in *Arabidopsis* and wheat (Tarazona et al., 2015; Narayanan et al., 2016; Tamura et al., 2016). It is suggested that ASG species are much more effective in promoting the phase transition than SGs and free STs (Grille et al., 2010). Thus, the bias of favoring increasing ASG rather than increasing SG in response to salt stress might be an indicator of salt tolerance in plants. However, the specific roles of ASGs and SGs in salinity response remain to be further elucidated.

Accumulation of CL Might Be Associated With an Altered Morphology of Mitochondria During Salt Stress

CLs, which are enriched in the inner membranes of mitochondria, were highly salinity-responsive in all barley varieties showing a remarkable increase in the present study. It appears that salinity induces the synthesis of CLs in barley roots, as their synthetic precursors, the PGs, were also observed to significantly increase.

Mitochondria are the main site of respiration, and they play crucial roles in a plant's response to abiotic stresses, such as providing energy and reductants for stress resistance, regulating the production and removal of ROS, and serving as a source of metabolic intermediates (Millar et al., 2011). In high saline environments, the ultrastructure of mitochondria has been observed to have an enlarged and swollen appearance in the roots of *Zea mays* (maize) (Nir et al., 1970). Further experiments on *Saccharomyces cerevisiae* (baker's yeast) demonstrated that the ability of yeast to resist the swelling under osmotic stress greatly depends on CLs found in the mitochondrial membrane (Koshkin and Greenberg, 2002). Thus, the increased CL synthesis in the present study is most likely associated with altered morphology of mitochondria during salt stress. However, further evidence for potential modifications of the ultrastructure of barley root mitochondria under salt stress is needed to demonstrate whether levels of CLs are correlated with the ability to resist the mitochondria swelling in barley roots.

Another possible mechanism underlying the increased CL synthesis may be due to induced PCD under salinity induced hyperosmotic stress as shown in yeast (Koshkin and Greenberg, 2002). Enhanced interactions between CLs and certain mitochondrial proteins can promote mitochondrial scission and breakdown of mitochondrial outer membranes, thus promoting the process of PCD (Gonzalvez and Gottlieb, 2007).

Increased Oxidized Glycerolipids May Relate to Higher Oxidation Tolerance in Salt-Tolerant Varieties

Salinity stress can trigger ROS production in plastids, apoplasts, cytoplasm, and mitochondria and the ability to both regulate ROS production and detoxification is crucial in salt-tolerant varieties (Miller et al., 2010). Oxidized membrane lipids are an indicator of oxidation that may have occurred on membranes (Berger et al., 2001; Przybyla et al., 2008). In the present study, the levels of most of the detected oxidized diacyl-GPs showed significant increases in the salt-tolerant varieties Keel and Mundah under salt stress. MS/MS spectra of these oxidized diacyl-GPs showed that oxidized fatty acyl chains were derived from the two most abundant unsaturated FAs 18:2 and 18:3. Thus, the induced synthesis of 18:3 may not only contribute to the increase of 18:3-containing diacyl-GPs in plasma membranes to adjust fluidity, but it also may act as substrates to scavenge ROS levels and prevent oxidization of other cell components in salt-tolerant varieties. Contrastingly, the salt-sensitive varieties Vlamingh and Gairdner exhibited decreases in the concentrations of most of the oxidized diacyl-GPs. This is supported by recent studies that demonstrated that certain degrees of oxidation of membrane lipids can prevent or retard oxidative impairment to other components of the cell (Vu et al., 2012). Further, unsaturated FAs and especially FA 18:3 in membrane lipids can serve as a sink for ROS (Vu et al., 2012; Mène-Saffrané et al., 2009). They can immediately scavenge ROS through non-enzymatic reactions without activating gene or signaling pathways thus providing a fast mechanism for ROS scavenging (Mène-Saffrané et al., 2009). Thus, the alteration of oxidized lipids could be a potential indicator that differentiate salt-tolerant and salt-sensitive barley varieties.

CONCLUSIONS

High salinity (250 mM NaCl) leads to significant alterations in the profiles of GPs, GLs, SLs, and ST derivatives in roots of four hydroponically grown barley varieties (Keel, Mundah, Gairdner, and Vlamingh). All four varieties responded to high salinity stress by remodeling of lipids in plasma membranes and intracellular membranes. In plasma membranes, the increased proportions of 18:3-containing diacyl-GPs were substantial; further, short to medium chain FAs (C14~18) had distinct responses as compared to VLCFAs. In plastid membranes, a general decrease in most of MGDGs/MGMGs, DGDGs/DGMGs, SQDGs, and GlcADGs was observed. The combination of the increased MGDG/DGDG ratio and an increased amount of ASG suggest that plastidial and extraplastidial membranes in barley roots ubiquitously tend to form an HII phase under salinity stress. Accumulation of CLs occurred in mitochondrial membranes, suggesting for a potential role of CLs in maintaining the morphology of mitochondria under salinity. In addition, salt-tolerant and salt-sensitive cultivars showed contrasting trends in the levels of most of the detected oxidized membrane lipids. Further studies need to investigate whether the behavior of these oxidized lipids can present an indication of salt tolerance levels in barley. These findings could be further investigated by future experiments to

discover the insight into the biological system. In summary, our studies demonstrated new evidence on diverse alteration of lipids of cell membranes in barley roots under salinity stress, which provides promising avenues for future research to decipher the exact roles of these lipids under salt stress.

DATA AVAILABILITY STATEMENT

All datasets generated for this study are included in the article/ **Supplementary Material**.

AUTHOR CONTRIBUTIONS

TR, BB, CH, and UR designed and planned the experiments. DY ran the experiment and collected data. TR, BB, CH, DY, UR, and IF performed data interpretation and wrote the manuscript.

ACKNOWLEDGMENTS

The authors would like to thank A/Prof. Stuart Roy (University of Adelaide) for providing the barley seeds. LC-MS analysis was carried out at Metabolomics Australia which is supported by funds from the Australian Government's National Collaborative Research Infrastructure Scheme (NCRIS) administered through Bioplatforms Australia (BPA) Ltd. TR gratefully acknowledges the Dyson Fellowship (The University of Melbourne) for collaboration opportunity with IF. UR has been funded through an Australian Research Council Future Fellowship (FT130100326).

SUPPLEMENTARY MATERIAL

The Supplementary Material for this article can be found online at: https://www.frontiersin.org/articles/10.3389/fpls.2020.00001/full#supplementary-material

REFERENCES

Allakhverdiev, S. I., Nishiyama, Y., Suzuki, I., Tasaka, Y., and Murata, N. (1999). Genetic engineering of the unsaturation of fatty acids in membrane lipids alters the tolerance of Synechocystis to salt stress. *Proc. Natl. Acad. Sci.* 96 (10), 5862–5867. doi: 10.1073/pnas.96.10.5862

Ardail, D., Privat, J., Egret-Charlier, M., Levrat, C., Lerme, F., and Louisot, P. (1990). Mitochondrial contact sites. *Lipid Compos. Dyn. J. Biol. Chem.* 265 (31), 18797–18802.

Bach, L., and Faure, J. D. (2010). Role of very-long-chain fatty acids in plant development, when chain length does matter. *Comptes Rendus Biol.* 333 (4), 361–370. doi: 10.1016/j.crvi.2010.01.014

Bejaoui, F., Salas, J. J., Nouairi, I., Smaoui, A., Abdelly, C., Martínez-Force, E., et al. (2016). Changes in chloroplast lipid contents and chloroplast ultrastructure in Sulla carnosa and Sulla coronaria leaves under salt stress. *J. Plant Physiol.* 198, 32–38, 8. doi: 10.1016/j.jplph.2016.03.018

Berger, S., Weichert, H., Porzel, A., Wasternack, C., Kühn, H., and Feussner, I. (2001). Enzymatic and non-enzymatic lipid peroxi-dation in leaf development. *Biochem. Biophys. Acta* 1533, 266–276. doi: 10.1016/S1388-1981(01)00161-5

Cao, D., Lutz, A., Hill, C. B., Callahan, D. L., and Roessner, U. (2017). A quantitative profiling method of phytohormones and other metabolites applied to barley roots subjected to salinity stress. *Front. In Plant Sci.* 7, 2070. doi: 10.3389/fpls.2016.02070

Coventry, S., Smith, D., McKay, A., Eckermann, P., and Eglinton, J. (2008). in: Investigating root architecture in barley and responses to salinity and high boron. Proceedings of the 10th International Barley Genetics Symposium. Alexandria, Egypt, ICARDA, 5-10 Apr 2008..

Dörmann, P., and Benning, C. (2002). Galactolipids rule in seed plants. *Trends In Plant Sci.* 7 (3), 112–118. doi: 10.1016/S1360-1385(01)02216-6

Dörmann, P. (2013). Galactolipids in plant membranes. *eLS*, doi: 10.1002/9780470015902.a0020100.pub2

De Azevedo Neto, A. D., Prisco, J. T., Enéas-Filho, J., De Abreu, C. E. B., and Gomes-Filho, E. (2006). Effect of salt stress on antioxidative enzymes and lipid peroxidation in leaves and roots of salt-tolerant and salt-sensitive maize genotypes. *Environ. Exp. Bot.* 56 (1), 87–94. doi: 10.1016/j.envexpbot.2005.01.008

De Vries, A. H., Mark, A. E., and Marrink, S. J. (2004). The binary mixing behavior of phospholipids in a bilayer: a molecular dynamics study. *J. Phys. Chem. B.* 108 (7), 2454–2463. doi: 10.1021/jp0366926

Ferrer, A., Altabella, T., Arró, M., and Boronat, A. (2017). Emerging roles for conjugated sterols in plants. *Prog. In Lipid Res.* 67, 27–37. doi: 10.1016/j.plipres.2017.06.002

Furt, F., Simon-Plas, F., and Mongrand, S. (2011). "Lipids of the plant plasma membrane," *Plant Cell Mono.* (Springer), 19, 3–30. doi: 10.1007/978-3-642-13431-9_1

Gonzalvez, F., and Gottlieb, E. (2007). Cardiolipin: setting the beat of apoptosis. *Apoptosis* 12 (5), 877–885. doi: 10.1007/s10495-007-0718-8

Grille, S., Zaslawski, A., Thiele, S., Plat, J., and Warnecke, D. (2010). The functions of steryl glycosides come to those who wait: recent advances in plants, fungi, bacteria and animals. *Prog. In Lipid Res.* 49 (3), 262–288. doi: 10.1016/j.plipres.2010.02.001

Gupta, S. V. K., Rupasinghe, T. W. T., Callahan, D. L., Natera, S. H. N., Smith, P. M., Hill, C. B., et al. (2019). Spatio-Temporal Metabolite and Elemental Profiling of Salt Stressed Barley Seeds During Initial Stages of Germination by MALDI-MSI and μ-XRF Spectrometry. *Front. Plant Sci.* 10, 1139. doi: 10.3389/fpls.2019.01139

Harris, B. N., Sadras, V. O., and Tester, M. (2010). A water-centred framework to assess the effects of salinity on the growth and yield of wheat and barley. *Plant Soil* 336 (1-2), 377–389. doi: 10.1007/s11104-010-0489-9

Haslam, R. P., and Feussner, I. (2017). Green light for lipid fingerprinting. *Biochim. Biophys. Acta* 1862, 782–785. doi: 10.1016/j.bbalip.2017.04.005

Hill, C. B., Bacic, A., and Roessner, U. (2014). LC-MS profiling to link metabolic and phenotypic diversity in plant mapping populations. *Mass Spectrom. In Metabol.: Methods Protoc.*1198, 29–41. doi: 10.1007/978-1-4939-1258-2_3

Hoagland, D. R., and Arnon, D. I. (1950). "The water-culture method for growing plants without soil," in *Circular* (California Agricultural Experiment Station 347), 32.

Hochberg, Y., and Benjamin, Y. (1990). More powerful procedures for multiple significance testing. *Stat. Med.* 9, 811–818. doi: 10.1002/sim.4780090710

Horn, P. J., and Chapman, K. D. (2012). Lipidomics in tissues, cells and sub-cellular compartments. *Plant J.* 70 (1), 69–80. doi: 10.1111/j.1365-313X.2011.04868.x

Howe, G. A., and Schilmiller, A. L. (2002). Oxylipin metabolism in response to stress. *Curr. Opin. In Plant Biol.* 5 (3), 230–236. doi: 10.1016/S1369-5266(02)00250-9

Ibrahim, A., Schütz, A. L., Galano, J. M., Herrfurth, C., Feussner, K., Durand, T., et al. (2011). The alphabet of galactolipids in Arabidopsis thaliana. *Front. In Plant Sci.* 2, 95. doi: 10.3389/fpls.2011.00095

Jouhet, J. (2013). Importance of the hexagonal lipid phase in biological membrane organization. *Front. In Plant Sci.* 4 (494). doi: 10.3389/fpls.2013.00494

Kamboj, A., Ziemann, M., and Have, M. (2015). Identification of salt-tolerant barley varieties by a consolidated physiological and molecular approach. *Acta Physiologiae Plantarum* 37 (1716). doi: 10.1007/s11738-014-1716-4

Köfeler, H. C., Fauland, A., Rechberger, G. N., and Trötzmüller, M. (2012). Mass spectrometry based lipidomics: an overview of technological platforms. *Metabolites* 2 (1), 19–38. doi: 10.3390/metabo2010019

Koshkin, V., and Greenberg, M. L. (2002). Cardiolipin prevents rate-dependent uncoupling and provides osmotic stability in yeast mitochondria. *Biochem. J.* 364 (1), 317–322. doi: 10.1042/bj3640317

López-Pérez, L., Del Carmen Martínez-Ballesta, M., Maurel, C., and Carvajal, M. (2009). Changes in plasma membrane lipids, aquaporins and proton pump of

broccoli roots, as an adaptation mechanism to salinity. *Phytochemistry* 70 (4), 492–500. doi: 10.1016/j.phytochem.2009.01.014

Lin, H., and Wu, L. (1996). Effects of salt stress on root plasma membrane characteristics of salt-tolerant and salt-sensitive buffalograss clones. *Environ. Exp. Bot.* 36 (3), 239–254. doi: 10.1016/0098-8472(96)01025-8

Liu, X., and Huang, B. (2000). Heat stress injury in relation to membrane lipid peroxidation in creeping bentgrass. *Crop Sci.* 40 (2), 503–510. doi: 10.2135/cropsci2000.402503x

Los, D. A., and Murata, N. (2004). Membrane fluidity and its roles in the perception of environmental signals. *Biochim. Biophys. Acta (BBA) - Biomembr.* 1666 (1), 142–157. doi: 10.1016/j.bbamem.2004.08.002

Mårtensson, C. U., Doan, K. N., and Becker, T. (2017). Effects of lipids on mitochondrial functions. *Biochim. Biophys. Acta (BBA)-Mol. Cell Biol. Lipids* 1862 (1), 102–113. doi: 10.1016/j.bbalip.2016.06.015

Mène-Saffrané, L., Dubugnon, L., Chételat, A., Stolz, S., Gouhier-Darimont, C., and Farmer, E. E. (2009). Nonenzymatic oxidation of trienoic fatty acids contributes to reactive oxygen species management in *Arabidopsis*. *J. Biol. Chem.* 284 (3), 1702–8 doi: 10.1074/jbc.M807114200

Müller, M., and Santarius, K. A. (1978). Changes in chloroplast membrane lipids during adaptation of barley to extreme salinity. *Plant Physiol.* 62 (3), 326–329. doi: 10.1104/pp.62.3.326

Mansour, M. M. F., Salama, K. H. A., and Allam, H. Y. H. (2015). Role of the plasma membrane in saline conditions: lipids and proteins. *Bot. Rev.* 81 (4), 416–451. doi: 10.1007/s12229-015-9156-4

Markham, J. E., Li, J., Cahoon, E. B., and Jaworski, J. G. (2006). Separation and identification of major plant sphingolipid classes from leaves. *J. Biol. Chem.* 281, 22684–22694. doi: 10.1074/jbc.M604050200

Michaelson, L. V., Napier, J. A., Molino, D., and Faure, J.-D. (2016). Plant sphingolipids: their importance in cellular organization and adaption. *Biochim. Biophys. Acta (BBA) - Mol. Cell Biol. Lipids* 1861 (9), 1329–1335. doi: 10.1016/j.bbalip.2016.04.003

Millar, A. A., Smith, M. A., and Kunst, L. (2000). All fatty acids are not equal: discrimination in plant membrane lipids. *Trends In Plant Sci.* 5 (3), 95–101. doi: 10.1016/S1360-1385(00)01566-1

Millar, A. H., Whelan, J., Soole, K. L., and Day, D. A. (2011). Organization and regulation of mitochondrial respiration in plants. *Annu. Rev. Plant Biol.* 62, 79–104. doi: 10.1146/annurev-arplant-042110-103857

Miller, G., Suzuki, N., Ciftci-Yilmaz, S., and Mittler, R. (2010). Reactive oxygen species homeostasis and signalling during drought and salinity stresses. *Plant Cell Environ.* 33 (4), 453–467. doi: 10.1111/j.1365-3040.2009.02041.x

Moellering, E. R., Muthan, B., and Benning, C. (2010). Freezing tolerance in plants requires lipid remodeling at the outer chloroplast membrane. *Science* 330 (6001), 226–228. doi: 10.1126/science.1191803

Mosblech, A., Feussner, I., and Heilmann, I. (2009). Oxylipins: structurally diverse metabolites from fatty acid oxidation. *Plant Physiol. Biochem.* 47 (6), 511–517. doi: 10.1016/j.plaphy.2008.12.011

Munns, R., and Tester, M. (2008). Mechanisms of salinity tolerance. *Annu. Rev. Plant Biol.* 59, 651–681. doi: 10.1146/annurev.arplant.59.032607.092911

Murata, N., and Los, D. A. (1997). Membrane fluidity and temperature perception. *Plant Physiol.* 115 (3), 875. doi: 10.1104/pp.115.3.875

Narayanan, S., Prasad, P. V., and Welti, R. (2016). Wheat leaf lipids during heat stress: II. Lipids experiencing coordinated metabolism are detected by analysis of lipid co-occurrence. *Plant Cell Rnvironment* 39 (3), 608–617. doi: 10.1111/pce.12648

Narayanan, S., Tamura, P. J., Roth, M. R., Prasad, P. V., and Welti, R. (2016). Wheat leaf lipids during heat stress: I. High day and night temperatures result in major lipid alterations. *Plant Cell Environ.* 39 (4), 787–803. doi: 10.1111/pce.12649

Natera, S. H., Hill, C. B., Rupasinghe, T. W., and Roessner, U. (2016). Salt-stress induced alterations in the root lipidome of two barley genotypes with contrasting responses to salinity. *Funct. Plant Biol.* doi: 10.1071/FP15253

Nir, I., Klein, S., and Poljakoff-Mayber, A. (1970). Changes in fine structure of root cells from maize seedlings exposed to water stress. *Aust. J. Biol. Sci.* 23 (2), 489–492. doi: 10.1071/BI9700489

Nowicki, M., Müller, F., and Frentzen, M. (2005). Cardiolipin synthase of Arabidopsis thaliana. *FEBS Lett.* 579 (10), 2161–2165. doi: 10.1016/j.febslet.2005.03.007

Okazaki, Y., and Saito, K. (2014). Roles of lipids as signaling molecules and mitigators during stress response in plants. *Plant J.* (4), 584–596. doi: 10.1111/tpj.12556

Okazaki, Y., Otsuki, H., Narisawa, T., Kobayashi, M., Sawai, S., Kamide, Y., et al. (2013).). A new class of plant lipid is essential for protection against phosphorus depletion. *Nat. Commun.* 4, 1510. doi: 10.1038/ncomms2512

Pan, R., Jones, A. D., and Hu, J. (2014). Cardiolipin-mediated mitochondrial dynamics and stress response in Arabidopsis. *Plant Cell* 26 (1), 391–409. doi: 10.1105/tpc.113.121095

Parida, A. K., and Das, A. B. (2005). Salt tolerance and salinity effects on plants: a review. *Ecotoxicol. Environ. Saf.* 60 (3), 324–349. doi: 10.1016/j.ecoenv.2004.06.010

Patton, G., Fasulo, J., and Robins, S. (1982). Separation of phospholipids and individual molecular species of phospholipids by high-performance liquid chromatography. *J. Lipid Res.* 23 (1), 190–196.

Pineau, B., Bourge, M., Marion, J., Mauve, C., Gilard, F., Maneta-Peyret, L., et al. (2013). The importance of cardiolipin synthase for mitochondrial ultrastructure, respiratory function, plant development, and stress responses in Arabidopsis. *Plant Cell* 25 (10), 4195–4208. doi: 10.1105/tpc.113.118018

Przybyla, D., Göbel, C., Imboden, A., Hamberg, M., Feussner, I., and Apel, K. (2008). Enzymatic, but not non-enzymatic, 1O2-mediated peroxidation of polyunsaturated fatty acids forms part of the EXECUTER1-dependent stress response program in the flu mutant of Arabidopsis thaliana. *Plant J.* 54, 236–248. doi: 10.1111/j.1365-313X.2008.03409.x

Remorini, D., Melgar, J. C., Guidi, L., Degl'Innocenti, E., Castelli, S., Traversi, M. L., et al. (2009). Interaction effects of root-zone salinity and solar irradiance on the physiology and biochemistry of Olea europaea. *Environ. Exp. Bot.* 65 (2-3), 210–219. doi: 10.1016/j.envexpbot.2008.12.004

Riewe, D., Wiebach, J., and Altmann, T. (2017). Structure annotation and quantification of wheat seed oxidized lipids by high resolution LC-MS/MS. *Plant Physiol.* 175 (2), 600–618. doi: 10.1104/pp.17.00470

Romantsov, T., Guan, Z., and Wood, J. M. (2009). Cardiolipin and the osmotic stress responses of bacteria. *Biochim. Biophys. Acta (BBA)-Biomembr.* 1788 (10), 2092–2100. doi: 10.1016/j.bbamem.2009.06.010

Salama, K. H., Mansour, M. M. F., Ali, F. Z., and Abou-Hadid, A. F. (2007). NaCl-induced changes in plasma membrane lipids and proteins of Zea mays L. cultivars differing in their response to salinity. *Acta Physiol. Plant.* 29 (4), 351–359. doi: 10.1007/s11738-007-0044-3

Sarabia, L. D., Boughton, B., Rupasinghe, T., Allison, M. L., Van de Meene, A. M. L., Callahan, D. L., et al. (2018). High-mass-resolution MALDI mass spectrometry imaging reveals detailed spatial distribution of metabolites and lipids in roots of barley seedlings in response to salinity stress. *Metabolomics* 14 (5), 63. doi: 10.1007/s11306-018-1359-3

Sarabia, L., Boughton, B., Rupasinghe, T., Callahan, D., Hill, C., and Roessner, U. (2019). Comparative spatial lipidomics analysis reveals cellular lipid remodelling in different developmental zones of barley roots in response to salinity. *Plant Cell Environ.* 43, 327–343. doi: 10.1111/pce.13653

Schuler, I., Milon, A., Nakatani, Y., Ourisson, G., Albrecht, A. M., Benveniste, P., et al. (1991). Differential effects of plant sterols on water permeability and on acyl chain ordering of soybean phosphatidylcholine bilayers. *Proc. Natl. Acad. Sci.* 88 (16), 6926–6930. doi: 10.1073/pnas.88.16.6926

Schwarzländer, M., and Fuchs, P. (2017). Plant mitochondrial membranes: adding structure and new functions to respiratory physiology. *Curr. Opin. In Plant Biol.* 40, 147–157. doi: 10.1016/j.pbi.2017.09.002

Shavrukov, Y., Genc, Y., and Hayes, J. (2012). The use of hydroponics in abiotic stress tolerance research. Hydroponics: a standard methodology for plant biological researches, InTech. 40–66. doi: 10.5772/35206

Shelden, M. C., Roessner, U., Sharp, R. E., Tester, M., and Bacic, A. (2013). Genetic variation in the root growth response of barley genotypes to salinity stress. *Funct. Plant Biol.* 40 (5), 516–530. doi: 10.1071/FP12290

Shu, S., Yuan, L. Y., Guo, S. R., and Sun J.and Yuan, Y. H. (2013). Effects of exogenous spermine on chlorophyll fluorescence, antioxidant system and ultrastructure of chloroplasts in Cucumis sativus L. under salt stress. *Plant Physiol. Biochem.* 63, 209–216. doi: 10.1016/j.plaphy.2012.11.028

Sui, N., and Han, G. (2014). Salt-induced photoinhibition of PSII is alleviated in halophyte Thellungiella halophila by increases of unsaturated fatty acids in membrane lipids. *Acta Physiol. Plant.* 36 (4), 983–992. doi: 10.1007/s11738-013-1477-5

Tarazona, P., Feussner, K., and Feussner I, I. (2015). An enhanced plant lipidomics method based on multiplexed liquid chromatography–mass spectrometry

reveals additional insights into cold-and drought-induced membrane remodeling. *Plant J.* 84 (3), 621–633. doi: 10.1111/tpj.13013

Tavakkoli, E., Faehi, F., Rengasamy, P., and McDonald, G. (2012). A comparison of hydroponic and soil-based screening methods to identify salt tolerance in the field in barley. *J. Exp. Bot.* 63 (10), 3853–3867 doi: 10.1093/jxb/ers085

Tawaraya, K., Honda, S., Cheng, W., Chuba, M., Okazaki, Y., Saito, K., et al. (2018). Ancient rice cultivar extensively replaces phospholipids with non-phosphorus glycolipid under phosphorus deficiency. *Physiol. Plant.* 163:297–305. doi: 10.1111/ppl.12699

Tenenboim, H., Burgos, A., Willmitzer, L., and Brotman, Y. (2016). Using lipidomics for expanding the knowledge on lipid metabolism in plants. *Biochimie* 130, 91–96. doi: 10.1016/j.biochi.2016.06.004

Tester, M., and Davenport, R. (2003). Na^+ tolerance and Na^+ transport in higher plants. *Ann. Bot.* 91 (5), 503–527. doi: 10.1093/aob/mcg058

Upchurch, R. G. (2008). Fatty acid unsaturation, mobilization, and regulation in the response of plants to stress. *Biotechnol. Lett.* 30 (6), 967–977. doi: 10.1007/s10529-008-9639-z

Vu, H. S., Tamura, P., Galeva, N. A., Chaturvedi, R., Roth, M. R., Williams, T. D., et al. (2012). Direct infusion mass spectrometry of oxylipin-containing Arabidopsis membrane lipids reveals varied patterns in different stress responses. *Plant Physiol.* 158 (1), 324–339. doi: 10.1104/pp.111.190280

Vu, H. S., Shiva, S., Roth, M. R., Tamura, P., Zheng, L., Li, M., et al. (2014). Lipid changes after leaf wounding in Arabidopsis thaliana: expanded lipidomic data form the basis for lipid co-occurrence analysis. *Plant J.* 80 (4), 728–743. doi: 10.1111/tpj.12659

Webb, M. S., Irving, T. C., and Steponkus, P. L. (1995). Effects of plant sterols on the hydration and phase behavior of DOPE/DOPC mixtures. *Biochim. Biophys. Acta (BBA)-Biomembr.* 1239 (2), 226–238. doi: 10.1016/0005-2736(95)00147-U

Welti, R., Shah J., J., Li, W., Li, M., Chen, J., Burke, J. J., et al. (2007). Plant lipidomics: discerning biological function by profiling plant complex lipids using mass spectrometry. *Front. In Biosci.* 12, 2494–2506. doi: 10.2741/2250

Wu, J., Seliskar, D. M., and Gallagher, J. L. (2005). The response of plasma membrane lipid composition in callus of the halophyte Spartina patens (Poaceae) to salinity stress. *Am. J. Bot.* 92 (5), 852–858. doi: 10.3732/ajb.92.5.852

Yu, B. J., Gong, H. M., and Liu, Y. L. (1999). Effects of exogenous fatty acids on h +-atpase activity and lipid composition of plasma membrane vesicles isolated from roots of barley seedlings under salt stress. *J. Plant Physiol.* 155 (4), 646–651. doi: 10.1016/S0176-1617(99)80067-4

Yu, D., Rupasinghe, T. W. T., Boughton, B. A., Natera, S. H., Hill, C. B., Tarazona, P., et al. (2018). A high-resolution HPLC-QqTOF platform using parallel reaction monitoring for in-depth lipid discovery and rapid profiling. *Anal. Chim. Acta* 1026, 87–100. doi: 10.1016/j.aca.2018.03.062

Zhang, J., Ying, J., Chang, S., Li, B., and Li, Z. (2003). Cloning and expression analysis of violaxanthin de–epoxidase (VDE) cDNA in wheat. *Acta Botanica Sin.* 45 (8), 981–985.

Zhou, Y., Peisker, H., and Dörmann, P. (2016). Molecular species composition of plant cardiolipin determined by liquid chromatography mass spectrometry. *J. Lipid Res.* 57 (7), 1308–1321. doi: 10.1194/jlr.D068429

Conflict of Interest: The authors declare that the research was conducted in the absence of any commercial or financial relationships that could be construed as a potential conflict of interest.

frontiers in Plant Science

ORIGINAL RESEARCH
published: 07 February 2020
doi: 10.3389/fpls.2020.00030

Producing Cyclopropane Fatty Acid in Plant Leafy Biomass *via* Expression of Bacterial and Plant Cyclopropane Fatty Acid Synthases

Shoko Okada[1*], *Matthew Taylor*[1], *Xue-Rong Zhou*[2], *Fatima Naim*[3], *David Marshall*[4], *Stephen J. Blanksby*[4], *Surinder P. Singh*[2] *and Craig C. Wood*[2]

[1] CSIRO Land and Water, Canberra, ACT, Australia, [2] CSIRO Agriculture and Food, Canberra, ACT, Australia, [3] Center for Crop Disease Management, Faculty of Science and Engineering, School of Molecular and Life Sciences, Curtin University, Perth, WA, Australia, [4] Central Analytical Research Facility, Institute for Future Environments, Queensland University of Technology, Brisbane, QLD, Australia

OPEN ACCESS

Edited by:
Joachim Hermann Schiemann, Julius Kühn-Institut, Germany

Reviewed by:
Shiu Cheung Lung, The University of Hong Kong, Hong Kong
Georg Hölzl, University of Bonn, Germany

***Correspondence:**
Shoko Okada
shoko.okada@csiro.au

Specialty section:
This article was submitted to Plant Biotechnology, a section of the journal Frontiers in Plant Science

Received: 01 November 2019
Accepted: 13 January 2020
Published: 07 February 2020

Citation:
Okada S, Taylor M, Zhou X-R, Naim F, Marshall D, Blanksby SJ, Singh SP and Wood CC (2020) Producing Cyclopropane Fatty Acid in Plant Leafy Biomass via Expression of Bacterial and Plant Cyclopropane Fatty Acid Synthases. Front. Plant Sci. 11:30. doi: 10.3389/fpls.2020.00030

Saturated mid-chain branched fatty acids (SMCBFAs) are widely used in the petrochemical industry for their high oxidative stability and low melting temperature. Dihydrosterculic acid (DHSA) is a cyclopropane fatty acid (CPA) that can be converted to SMCBFA *via* hydrogenation, and therefore oils rich in DHSA are a potential feedstock for SMCBFA. Recent attempts to produce DHSA in seed oil by recombinant expression of cyclopropane fatty acid synthases (CPFASes) resulted in decreased oil content and poor germination or low DHSA accumulation. Here we explored the potential for plant vegetative tissue to produce DHSA by transiently expressing CPFAS enzymes in leaf. When CPFASes from plant and bacterial origin were transiently expressed in *Nicotiana benthamiana* leaf, it accumulated up to 1 and 3.7% DHSA in total fatty acid methyl ester (FAME), respectively, which increased up to 4.8 and 11.8%, respectively, when the *N. benthamiana* endogenous oleoyl desaturase was silenced using RNA interference (RNAi). Bacterial CPFAS expression produced a novel fatty acid with a cyclopropane ring and two carbon-carbon double bonds, which was not seen with plant CPFAS expression. We also observed a small but significant additive effect on DHSA accumulation when both plant and bacterial CPFASes were co-expressed, possibly due to activity upon different oleoyl substrates within the plant cell. Lipidomics analyses found that CPFAS expression increased triacylglycerol (TAG) accumulation relative to controls and that DHSA was distributed across a range of lipid species, including diacylglycerol and galactolipids. DHSA and the novel CPA were present in phosphatidylethanolamine when bacterial CPFAS was expressed in leaf. Finally, when plant diacylglycerol acyltransferase was coexpressed with the CPFASes DHSA accumulated up to 15% in TAG. This study shows that leaves can readily produce and accumulate DHSA in leaf oil. Our findings are discussed in line with current knowledge in leaf oil production for a possible route to DHSA production in vegetative tissue.

Keywords: dihydrosterculic acid, oleochemical, branched chain fatty acid, cyclopropane fatty acid synthase, *Nicotiana benthamiana*, triacylglycerol

INTRODUCTION

Saturated mid-chain branched fatty acids (SMCBFAs) offer unique properties that combine the benefits of saturated and unsaturated fatty acids and are thus an important component of the oleochemical industry (Kinsman, 1979; Biermann and Metzger, 2008). SMCBFA have no carbon-carbon bonds, and therefore are less susceptible to free radical attack that provides high oxidative stability compared to unsaturated fatty acids [e.g. oxidative stability at 110°C for soybean oil fatty acid methyl ester (FAME) = 3.1 h, purified saturated branched-chain FAME = 64 h; (Ngo et al., 2011)]. On the other hand, the mid-chain methyl groups confer a lower melting point over saturated fatty acids of similar chain lengths (e.g. stearic acid Tm = 69.3°C, tuberculostearic acid Tm = 20–26°C; Schmidt and Shirley, 1949; Haynes, 2016; **Figure 1**). Compared to either monounsaturated fatty acids or saturated fatty acids, SMCBFAs have high oxidative stability with lubricity at low temperatures, features that are sought after in many oleochemicals (Kinsman, 1979; Zhang et al., 2004; Ngo et al., 2011; Hasselberg and Behr, 2016). One such example of SMCBFA is tuberculostearic acid, where the methyl group is found midway along the fatty acyl chain (**Figure 1**). Currently isostearic acids such as tuberculostearic acid are chemically synthesized using purified fatty acids (Kinsman, 1979; Biermann and Metzger, 2008), however such chemical synthesis methods are expensive and require extra steps of purification to remove undesired isomers (Lou et al., 2004) or are relatively inefficient (Palko et al., 2013).

A potentially elegant and alternative method of synthesis of mid-chain branched fatty acids is *via* the *in planta* production of cyclopropane oils that can be extracted and hydrogenated in post-harvest processing to yield SMCBFA products (**Figure 1**). Cyclopropane fatty acids are widely found in bacteria, trypanosomatids, Myriapoda, and higher plants (reviewed in Oudejans et al., 1971; Fish et al., 1981; Sebedio and Grandgirard, 1989; Grogan and Cronan, 1997), and in this report we focus on the production of dihydrosterculic acid (DHSA), a naturally occurring fatty acid with a mid-chain cyclopropane ring across the C9–C10 carbons (cis-9,10-methyleneoctadecanoic acid; DHSA; **Figure 1B**). The biochemical and molecular bases for the biosynthesis of cyclopropane fatty acids has been elucidated in various higher plants (Bao et al., 2002; Yu et al., 2011) and bacteria (Wang et al., 1992). The biological function of cyclopropane fatty acids is proposed to be one related to stress response and adaptation of membranes to changes in pH, salt, drought, and high temperature stress (reviewed in Knivett and Cullen, 1965; Kuiper and Stuiver, 1972; Grogan and Cronan, 1997; Shabala and Ross, 2008). The general class of cyclopropane fatty acid synthases (CPFASes) operate on monounsaturated acyl chains on phospholipids to produce cyclopropane rings. The *Escherichia coli* (Ec) CPFAS is proposed to cyclopropanate C16:1 and C18:1 that are predominantly esterified to the sn-2 position of phospholipids (Hildebrand and Law, 1964), whereas in plants the CPFAS cyclopropanates the oleoyl chain on the *sn*-1 position of phosphatidylcholine (PC, Bao et al., 2003).

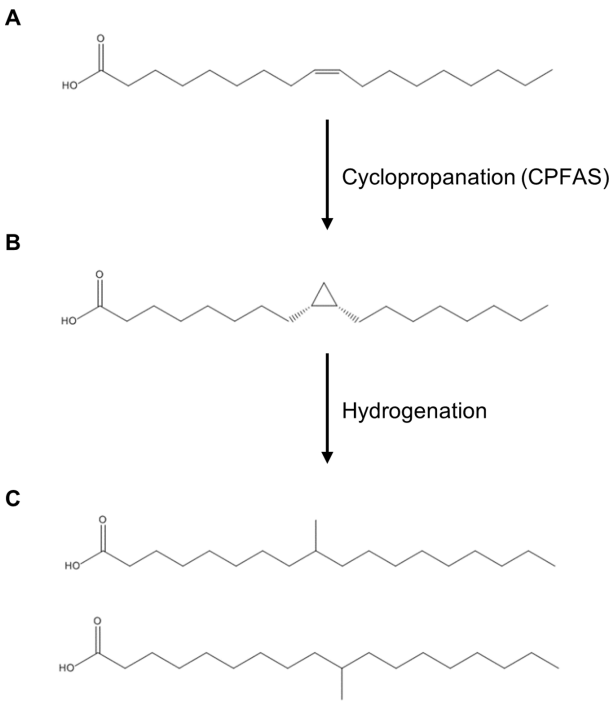

FIGURE 1 | Chemical structures of fatty acids and corresponding reactions relevant to this study. **(A)** oleic acid; **(B)** dihydrosterculic acid; **(C)** isostearic acid isomers.

There are limited reports of transgenic expression of CPFAS in plants. Expression of EcCPFAS produced DHSA in tobacco leaf calli accumulating up to approximately 3% of total fatty acids (Schmid, 1995). Tobacco suspension cells were used for the expression of *Sterculia foetida* CPFAS demonstrating accumulation of 4% DHSA in total fatty acids (Bao et al., 2002). In seeds the cotton (Gh) CPFAS expressed in a high oleic background of *fad2/fae1 Arabidopsis* accumulated approximately 1% DHSA in mature seed lipids, despite having potential access to a high level of oleic acid as substrate (Yu et al., 2011). In contrast EcCPFAS in the same seed context produced up to 9% DHSA, and up to 35% with additional expression of *S. foetida* lysophosphatidic acid acyltransferase (Yu et al., 2014; Yu et al., 2018), suggesting that one barrier to DHSA synthesis and accumulation in transgenic seed oil may be due to differences in the site of synthesis on PC. Despite the relatively high accumulation of DHSA in these developing *Arabidopsis* seeds it was found that seeds with greater than 9% DHSA suffered poor germination rates, and over 40% of the DHSA was found to

Abbreviations: At, *Arabidopsis thaliana*; CPA, cyclopropane fatty acid; CPFAS, cyclopropane fatty acid synthase; DAG, diacylglycerol; DGDG, digalactosyldiacylglycerol; DGAT1, diacylglycerol acyltransferase 1; DHSA, dihydrosterculic acid; Ec, *Escherichia coli*; FAD2, fatty acid desaturase 2; FAME, fatty acid methyl ester; GC, gas chromatography; Gh, *Gossypium hirsutum*; LC, liquid chromatography; MGDG, monogalactosyldiacylglycerol; MS, mass spectrometry; Nb, *Nicotiana benthamiana*; PC, phosphatidylcholine; PE, phosphatidylethanolamine; SMCBFA, saturated mid-chain branched fatty acid; TAG, triacylglycerol; TLC, thin layer chromatography.

accumulate on PC. When EcCPFAS was coexpressed with a lipid handling enzyme in *Camelina* seed, DHSA accumulated only up to 6% and still over 30% of DHSA remained in polar lipids (Yu et al., 2019). Collectively these results indicate that DHSA is produced on polar lipids in developing seeds, however the channeling of DHSA from polar lipids into seed oil is not efficient (Yu et al., 2018), or it affects seed quality and successive germination in higher amounts of DHSA (Yu et al., 2014). Like DHSA production in transgenic seed, similar problems with unusual fatty acids being accumulated on membrane lipids and adversely affecting oil content and germination has been found in transgenic seed engineered to produce ricinoleic acid (van Erp et al., 2011) and epoxy fatty acid (Li et al., 2012).

Although oilseeds are generally considered the major source of food oils and feedstocks for oleochemical industries, recent advances in metabolic engineering have opened the possibility of producing high levels of oil in leaf biomass (reviewed in Vanhercke et al., 2019). These advances have seen leaves produce over 30% of dry weight as triacylglycerol (Vanhercke et al., 2017). Given the difficulties in generating commercially viable levels of unusual fatty acids in seeds while avoiding impacts on seed viability and germination, it has been proposed that metabolically engineered oils could be produced in leafy biomass (Wood, 2014). For engineering oils into leaves, transient leaf assays using *Nicotiana benthamiana* have proven helpful in rapidly combining multiple genes into functional pathways (Wood et al., 2009; Vanhercke et al., 2013; Reynolds et al., 2015). The endogenous fluxes of lipids in transient assays have also been modified using endogene silencing techniques that allow improved fluxes of critical substrates into introduced metabolic pathways (Naim et al., 2012).

Here we explore the production and accumulation of DHSA in a transient leaf expression system and monitor the placement of this unusual fatty acid on a range of lipid species including those in membranes and oils. In order to achieve higher DHSA production we rely upon the silencing of endogenous oleoyl desaturases to raise oleic levels in leaves using an RNA silencing technique that does not interfere with transgene expression (Naim et al., 2012). Although both plant and bacterial CPFASes produce DHSA that accumulates into leaf oil we found that both genes were capable of accumulating DHSA in oil to a maximum of 15%. Furthermore, we also found that expression of EcCPFAS increased the relative oil content in leaves. Based on the findings from this study we discuss possible implications for the production and accumulation of DHSA in plant vegetative tissue.

RESULTS

Cotton and *Escherichia coli* Cyclopropane Fatty Acid Synthases Expressed in *Nicotiana benthamiana* Leaf Produce Dihydrosterculic Acid

We first explored the feasibility of producing dihydrosterculic acid in plant leaf using the *N. benthamiana* leaf transient expression system (Wood et al., 2009). Two CPFASes from *E. coli* (EcCPFAS) and cotton (GhCPFAS) were tested, which produced 3.7 ± 0.4% (n = 7) and 0.9 ± 0.1% (n = 6) DHSA in total FAME, respectively (**Figure 2**). The DHSA peak was confirmed by gas chromatography-mass spectrometry (GC-MS) against a reference standard dihydrosterculic (DHS) methyl ester. We then increased the oleic acid content in *N. benthamiana* to see if increased substrate availability would assist in higher levels of DHSA production. To do this we used a hairpin construct to silence the endogenous oleoyl desaturase (NbFAD2) *via* RNA interference (RNAi), herein termed *hpNbFAD2.1*, which was previously shown to increase total oleic acid content in the leaf transient expression system by six-fold compared to the control when tomato yellow leaf curl virus suppressor protein V2 was coexpressed (Naim et al., 2012). When *hpNbFAD2.1* was coexpressed with Ec- or GhCPFAS production of DHSA significantly increased three- and five-

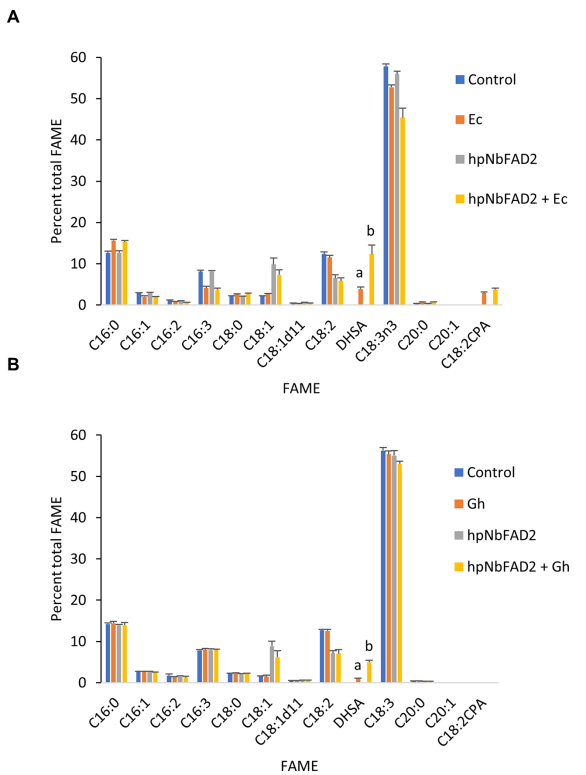

FIGURE 2 | Cyclopropane fatty acid (CPA) production in *Nicotiana benthamiana* leaf transiently expressing cyclopropane fatty acid synthase and increasing oleic acid by silencing the endogenous oleoyl desaturase (NbFAD2) increases CPA accumulation. **(A)** Total fatty acid methyl ester (FAME) profile of *N. benthamiana* leaf total lipid extracts expressing cotton cyclopropane fatty acid synthase (GhCPFAS), tomato yellow leaf curl virus suppressor protein V2, green fluorescent protein (GFP), and *hpNbFAD2.1*. **(B)** FAME profile of *N. benthamiana* leaf total lipid extracts expressing *Escherichia coli* cyclopropane fatty acid synthase (EcCPFAS), V2, GFP, and *hpNbFAD2.1*. Error bars are standard deviations of six and seven biological replicates for the GhCPFAS and EcCPFAS set, respectively. Different letters above the bars indicate significant differences ($p < 0.01$). V2, tomato yellow leaf curl virus viral suppressor; GFP, green fluorescent protein; hp, hairpin.

fold to 11.8 ± 2.1% (n = 7, T test t(7) = −9.9, p < 0.01) and 4.8 ± 0.4% (n = 6, T test t(6) = −18.9, p < 0.01) in total FAME, respectively, compared to when the CPFASes were expressed without *hpNbFAD2.1* (**Figure 2**).

Next, we expressed Ec- and GhCPFAS individually and in combination in the hpNbFAD2.1 background to see the effect of co-expressing the two CPFASes on DHSA accumulation in *N. benthamiana* leaf (**Figure 3**). In this particular experiment Gh- or EcCPFAS expression alone produced 4.2 ± 0.7% (n = 6) and 8.0 ± 1.3% (n = 6) DHSA in total FAME, respectively, however when these two CPFASes were co-expressed there was a small but significant increase in DHSA accumulation to 10.7 ± 0.9% DHSA compared to EcCPFAS expression alone (n = 6, T test t (10) = −3.9, p < 0.01).

Structural Investigation of a Novel Cyclopropane Fatty Acid Produced by *Escherichia coli* Cyclopropane Fatty Acid Synthase Expression

EcCPFAS expression in *N. benthamiana* leaf generated an unidentified compound that was not detected with GhCPFAS expression or in the negative control (**Figure 4**). This compound migrated at 13.879 min in GC analysis of FAMEs of the triacylglycerol (TAG) fraction (1–2%; **Figure 4C**). GC-MS analysis indicated that this compound was a 19-carbon fatty acid containing a cyclopropane ring, with two degrees of unsaturation based on the retention time and *m/z* fragmentation pattern. To determine if EcCPFAS can cyclopropanate C18:3Δ9Z,12Z,15Z we expressed the gene in *Saccharomyces cerevisiae* and exogenously supplied it with C18:3. Subsequently, the same compound produced in *N. benthamiana* was detected in the GC trace (**Supplementary Figure 1**). Further GC-MS analysis of this compound with 4,4-dimethyloxazoline, 3-pyridylcarbinol, and pyrrolidine derivatives also agreed with the FAME analysis (**Figures 4D–F**), as having a cyclopropane ring and two degrees of unsaturation. There was evidence from the mass spectra of these derivatives to suggest the location of the carbon-carbon double bonds being Δ12 and Δ15. While a characteristic odd mass (*m/z* 247) was observed with the 3-pyridylcarbinol ester indicative of a cyclopropane ring on Δ9-10, the lack of mass abundance and inconsistencies with the characteristic 12 unit mass difference between Δ9 and Δ10 formed during fragmentation of the cyclopropane ring (Zhang et al., 1987) did not allow us to absolutely determine the position of the cyclopropane ring. Similarly, ozone-induced dissociation (OzID; Thomas et al., 2008) analysis tentatively identified this fatty acid to have the cyclopropane ring on Δ9-10, though again this position was not definitive. While further investigation of the structure of this compound is ongoing, we will refer to it as C18:2CPA for the remainder of this paper.

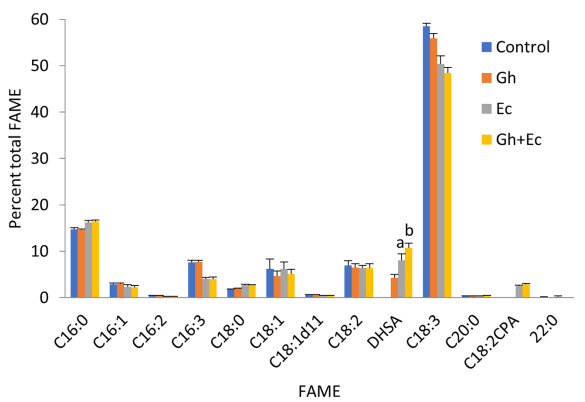

FIGURE 3 | Coexpressing cotton and *Escherichia coli* cyclopropane fatty acid synthases (CPFASes) shows additive effect on DHSA accumulation. Total fatty acid methyl ester (FAME) profile of *Nicotiana benthamiana* leaf total lipid extracts expressing cyclopropane fatty acid synthases separately (Gh, Ec) or together (Gh+Ec), each set coexpressed with tomato yellow leaf curl virus suppressor protein V2, green fluorescent protein (GFP), and *hpNbFAD2.1*. The control expression contained V2, GFP, and *hpNbFAD2.1*. Error bars are standard deviations of six biological replicates. Different letters above the bars indicate significant differences (p < 0.01). Gh, cotton CPFAS; Ec, *E. coli* CPFAS.

Lipid Class Analysis of Cyclopropane Fatty Acid-Containing Species

A more extensive analysis of the fluxes of cyclopropane fatty acids in transient leaf assays was conducted using a combination of GC analysis of thin layer chromatography (TLC) fractions and liquid chromatography-tandem mass spectrometry (LC-MSMS) of total lipid extracts from leaves expressing either Gh- or EcCPFAS, *hpNbFAD2.1*, green fluorescent protein (GFP), and V2.

Phosphatidylcholine

Total lipids extracted from leaves expressing either Gh- or EcCPFAS were subjected to TLC for GC analysis of the PC fraction. Both Gh- or EcCPFAS expression resulted in 25–27% accumulation of DHSA in the PC fraction as determined by GC analysis (**Figure 5**). LC-MSMS analysis showed an increase predominantly in the odd chain species PC 35:1, 35:3, 37:2, and 37:4 and also to a lesser extent PC 37:3 and the even numbered PC 38:2 (**Figure 6**). The structural composition of PC species of *N. benthamiana* leaves expressing EcCPFAS were more thoroughly investigated using OzID to elucidate positions of unsaturation, as well as composite tandem mass spectrometry methods employing both collision- and ozone-induced dissociation to identify the fatty acyl chains at each *sn*-position (Thomas et al., 2008; Pham et al., 2014). For the odd-chain PCs of composition PC 35:1 and PC 35:3, OzID mass spectra revealed that these predominantly comprised structures with a C16:0 fatty acid at the *sn*-1 position with either a DHSA or C18:2CPA occupying the *sn*-2 position, respectively. Interestingly, PC 36:2 contained roughly equivalent proportions of C18:1 Δ9 and Δ11. The only other PC species observed to contain C18:1 Δ11 was PC 37:2, which comprised C18:1 and DHSA with no specificity for the *sn*-position. PC 38:2 comprised two DHSA moieties. PC 37:4

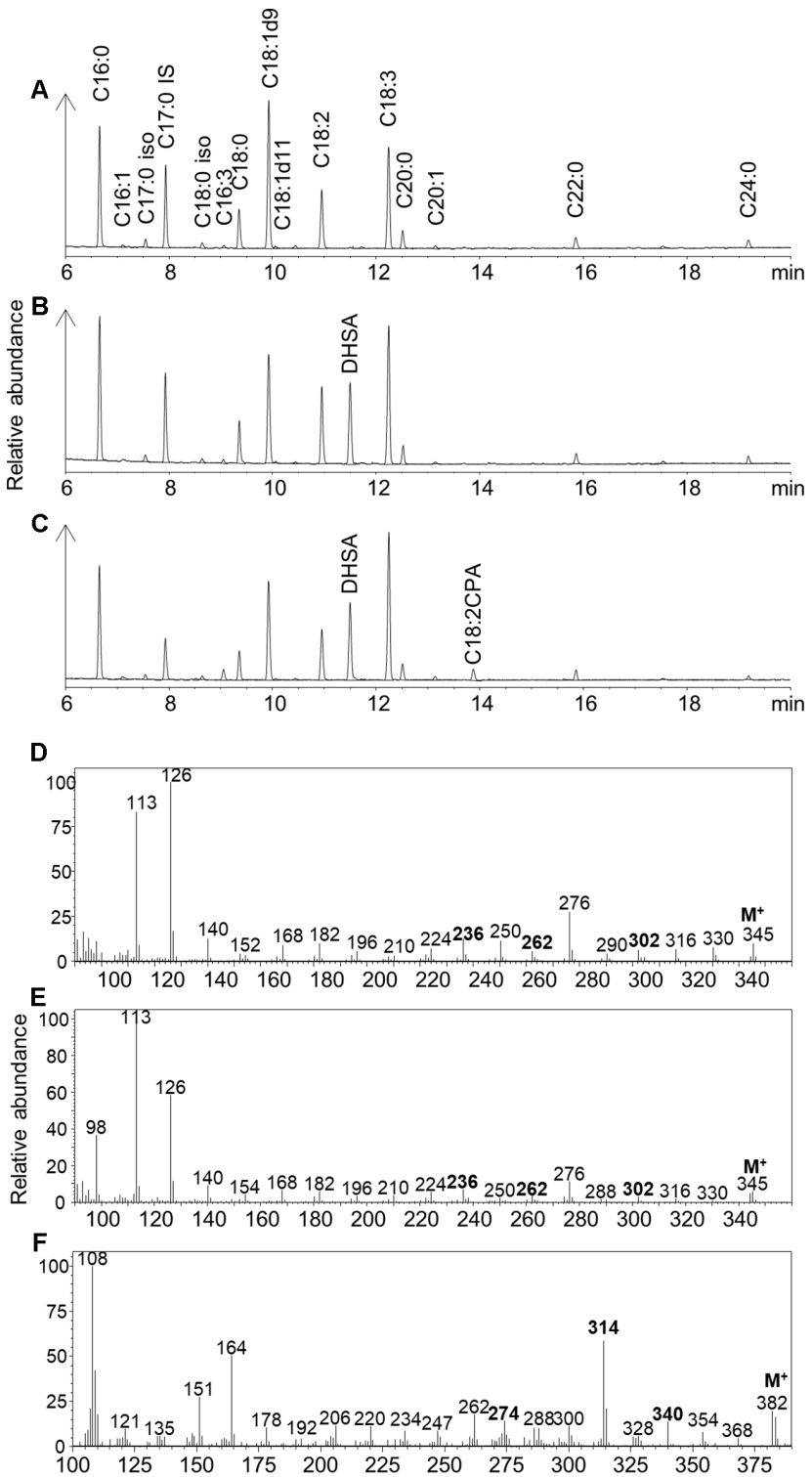

FIGURE 4 | Gas chromatography traces of **(A)** Fatty acid methyl esters (FAMEs) of the triacylglycerol (TAG) fraction of *Nicotiana benthamiana* leaf total lipid extracts expressing tomato yellow leaf curl virus suppressor protein V2, green fluorescent protein (GFP), *hpNbFAD2.1*, and *Arabidopsis thaliana* diacylglycerol acyltransferase (AtDGAT1); iso, isomer; IS, internal standard C17:0. **(B)** FAMEs of the TAG fraction of *N. benthamiana* leaf total lipid extracts expressing tomato yellow leaf curl virus suppressor protein V2, GFP, *hpNbFAD2.1*, AtDGAT1, and cotton cyclopropane fatty acid synthase (GhCPFAS); **(C)** FAMEs of the TAG fraction of *N. benthamiana* leaf total lipid extracts expressing tomato yellow leaf curl virus suppressor protein V2, GFP, *hpNbFAD2.1*, AtDGAT1, and *Escherichia coli* cyclopropane fatty acid synthase (EcCPFAS); **(D)** 4,4-dimethyloxazoline derivative of C18:2CPA; **(E)** pyrrolidine derivative of C18:2CPA; **(F)** 3-pyridylcarbinol derivative of C18:2CPA.

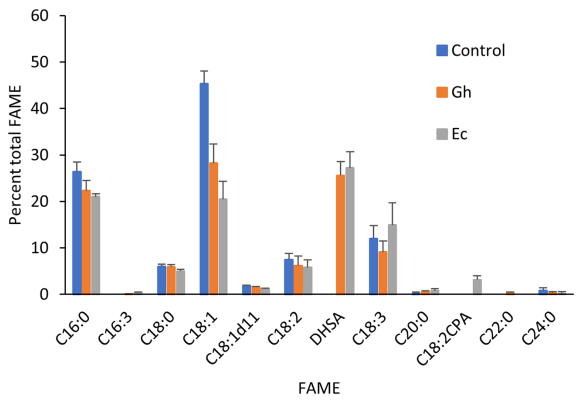

FIGURE 5 | Fatty acid methyl ester (FAME) profile of phosphatidylcholine fraction in *Nicotiana benthamiana* leaf total lipid extracts expressing cotton or *Escherichia coli* cyclopropane fatty acid synthase (CPFAS). Each CPFAS was coexpressed with tomato yellow leaf curl virus suppressor protein V2, green fluorescent protein (GFP), and *hpNbFAD2.1*. The control contained V2, GFP, and *hpNbFAD2.1*. Error bars are standard deviations of six biological replicates. Gh, cotton CPFAS; Ec, *E. coli* CPFAS.

contained both *sn*-positional isomers of C18:3/DHSA, however C18:2CPA was not observed in this species (*i.e.*, PC C18:1/C18:2CPA). Similar to PC 37:2, PC 37:6 was found to contain C18:2CPA on either *sn*-position.

Phosphatidylethanolamine

Because EcCPFAS is known to cyclopropanate unsaturated acyl chains bound to phosphatidylethanolamine (PE, Grogan and Cronan, 1997) we investigated the acyl chain composition of PE using LC-MSMS upon Ec- or GhCPFAS expression in *N. benthamiana* leaf (**Figure 7**). Noticeable differences between Ec- and GhCPFAS expression were decrease in PE 34:2 (C16:0/C18:2), PE 34:3 (C16:0/C18:3), PE 36:4 (C18:1/C18:3 and C18:2/C18:2), and PE 36:5 (C18:2/C18:3), and increase in PE 35:1 (C16:0/DHSA), PE 37:3 (C18:2/DHSA), PE 37:4 (C18:3/DHSA and C18:2/C18:2CPA), PE 37:5 (C18:2/C18:2CPA), and PE 37:6 (C18:3/C18:2CPA) when EcCPFAS was expressed (both with or without GhCPFAS) relative to the negative control and GhCPFAS expression. GhCPFAS also produced minor amounts of PE 37:3 and PE 37:4, however EcCPFAS produced relatively more DHSA as well as C18:2CPA-containing PE species. PE 38:4 (DHSA/C18:2CPA) was also detected in leaf expressing EcCPFAS.

Diacylglycerol and Triacylglycerol

Diacylglycerol (DAG) and TAG species were analyzed by LC-MSMS to investigate the acyl chain combinations containing DHSA. While many DHSA- containing DAG and TAG species were commonly shared between the two CPFAS-expressing leaf lipid extracts, extracts expressing EcCPFAS contained quantitatively more compared to those with GhCPFAS expression based on the response factors. The most abundant DAG species in *N. benthamiana* transiently expressing either Gh- or EcCPFAS were DAG 34:3 (C16:0/C18:3), DAG 36:6 (C18:3/C18:3), DAG 37:4 (DHSA/C18:3), DAG 36:4 (C18:3/C18:1), and DAG 36:5 (C18:2/C18:3) (**Figure 8**). While other DHSA-containing DAG species were observed [namely, DAG 35:1 (C16:0/DHSA), DAG 37:1 (C18:0/DHSA), and DAG 37:3 (C18:2/DHSA)], DAG 37:4 was approximately 12% of the total DAG species with both Gh- or EcCPFAS expression.

The percent distribution of TAG species shows that the most abundant species upregulated with expression of CPFASes are: TAG 53:4, TAG 55:7, TAG 56:5 followed by lower levels of TAG 53:2&3 and TAG 55:4-6. The overall distribution of acyl chains on different TAG species was assessed on triple-quadrupole LC-MS (LC-MS QQQ) by the neutral loss of each acyl chain. The most abundant DHSA- containing TAG species were TAG 53:2 (C16:0/C18:1/DHSA), TAG 53:3 (C16:0/C18:2/DHSA), TAG 53:4 (C16:0/C18:3/DHSA), TAG 55:4 (C18:0/C18:3/DHSA), TAG 55:5 (C18:1/C18:3/DHSA), TAG 55:6 (C18:2/C18:3/DHSA), TAG 55:7 (C18:3/C18:3/DHSA), and TAG 56:5 (DHSA/DHSA/C18:3) (**Figure 9**).

We observed a relative increase in neutral lipids DAG and TAG in total lipids extracted from *N. benthamiana* expressing EcCPFAS, with or without GhCPFAS, compared to those without EcCPFAS expression (**Supplementary Figure 2**).

Galactolipids

LC-MSMS detected only minor amounts of DHSA- containing galactolipid species with CPFAS expression, which were coupled with C18:1, C18:2, or C18:3. The four most common galactolipid species, monogalactosyldiacylglycerol (MGDG) 36:6 (C18:3/C18:3), MGDG 34:6 (C16:3/C18:3), digalactosyldiacylglycerol (DGDG) 34:3 (C16:0/C18:3), and DGDG 36:6 (C18:3/C18:3) accounted for over 80% of each galactolipid species in *N. benthamiana* expressing V2, GFP, and *hpNbFAD2.1*. There was a noticeable decrease in DGDG 34:3 (C16:0/C18:3), DGDG 36:6 (C18:3/C18:3), MGDG 34:6 (C16:3/C18:3), and MGDG 36:6 (C18:3/C18:3) in leaf lipid extracts expressing EcCPFAS, but not those with GhCPFAS (MGDG, **Figure 10**; DGDG, **Figure 11**). With the expression of EcCPFAS MGDG 34:6 was reduced to about 20% of the total MGDG pool. There was a corresponding increase in MGDG 37:4 (DHSA/C18:3) accounting for 15% of the MGDG with the coexpression of both CPFASes, with minor accumulation of MGDG 35:1(C16:0/DHSA), 35:3(C16:0/C18:2CPA), 35:4(C16:3/DHSA), and 38:2(DHSA/DHSA) species.

Cotton and *Escherichia coli* Cyclopropane Fatty Acid Synthase Expressed in *Nicotiana benthamiana* Leaf Accumulates Dihydrosterculic Acid in Triacylglycerol

As previously described, it is possible to increase the oil content in transient leaf assays with the expression of *Arabidopsis thaliana* diacylglycerol acyltransferase (AtDGAT1) (Wood et al., 2009). TAG is the lipid class that is currently being used widely throughout the fossil fuel industry as a feedstock for oleochemicals that could be replaced with more sustainable sources of plant oils (Carlsson et al., 2011). TAG can also provide a neutral storage solution for fatty acids such as DHSA that are synthesized on polar lipids such as PC and PE (Yu et al., 2014; Yu et al., 2018; Yu et al., 2019). We coexpressed Gh- or

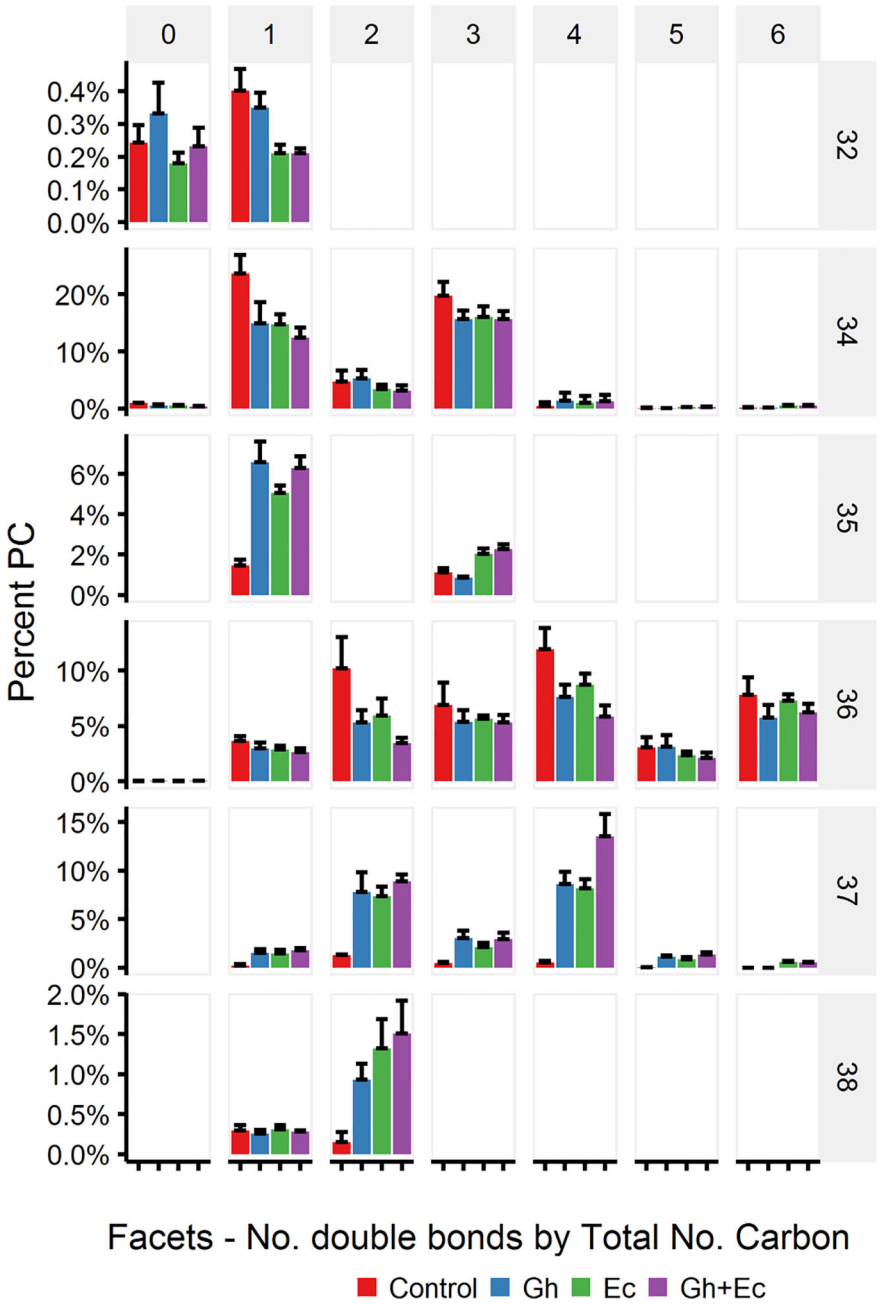

FIGURE 6 | Phosphatidylcholine (PC) species in total lipid extracts of *Nicotiana benthamiana* leaf expressing cotton and/or *Escherichia coli* cyclopropane fatty acid synthase (CPFAS), tomato yellow leaf curl virus suppressor protein V2, green fluorescent protein (GFP), and *hpNbFAD2.1* identified by liquid chromatography-tandem mass spectrometry (LC-MSMS). The control contained V2, GFP, and *hpNbFAD2.1*. Error bars are standard deviations of six biological replicates. Ec, *E. coli* CPFAS; Gh, cotton CPFAS.

EcCPFAS along with *hpNbFAD2.1*, V2, and AtDGAT1 to see if DHSA could be accumulated in the TAG fraction (**Figure 12B**). In this particular experiment Gh- and EcCPFAS produced DHSA at 4.5 ± 0.7% (n = 6) and 7.5 ± 0.4% (n = 6) in total FAME, respectively (**Figure 12A**), indicating that coexpressing AtDGAT1 with CPFAS did not increase overall DHSA accumulation in *N. benthamiana* leaf.

The FAME profile of TAG fractions from leaf total lipid extracts separated by thin layer chromatography showed that DHSA produced from both Gh- and EcCPFAS accumulated equally in TAG, at approximately 15.8% (GhCPFAS, 15.8 ± 1.3%; EcCPFAS, 15.8 ± 1.1%; n = 6; **Figure 12B**). In all extractions an equal amount of C17:0 TAG (triheptadecanoin) was included to allow monitoring of total TAG content throughout the analysis. Comparison of the

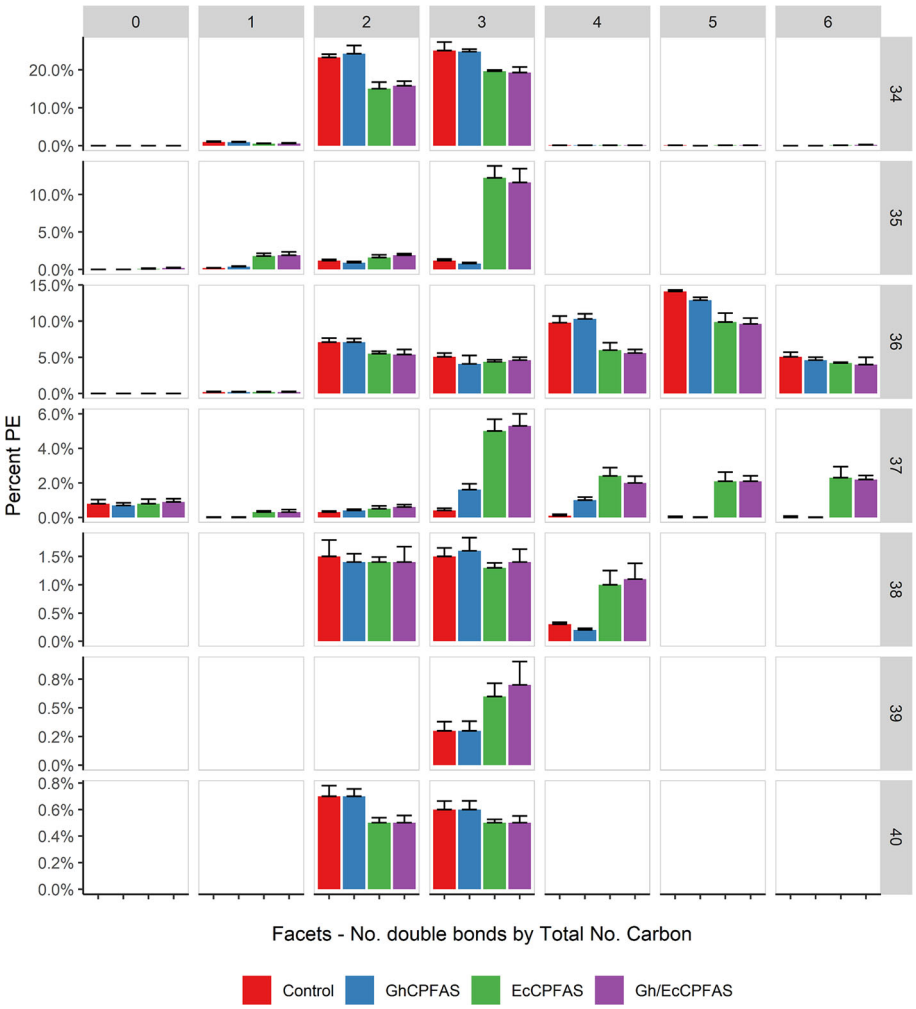

FIGURE 7 | Phosphatidylethanolamine (PE) species in total lipid extracts of *Nicotiana benthamiana* leaf expressing cotton and/or *Escherichia coli* cyclopropane fatty acid synthase (CPFAS), tomato yellow leaf curl virus suppressor protein V2, green fluorescent protein (GFP), and *hpNbFAD2.1* identified by liquid chromatography-tandem mass spectrometry (LC-MSMS). The control contained V2, GFP, and *hpNbFAD2.1*. Error bars are standard deviations of six biological replicates. Ec, *E. coli*; Gh, cotton.

relative amount of C17:0 FAME showed that TAG content increased to 1.0 ± 0.2 and 1.5 ± 0.3% leaf dry weight with Gh- and EcCPFAS expression compared to the control without CPFAS expression at 0.7 ± 0.2%, respectively (**Figure 12B**).

DISCUSSION

One major advantage of transient leaf assays is the ability to rapidly test combinations of different genes and make robust side-by-side comparisons in the context of plant expression. We compared the metabolic flux of DHSA produced by plant- and bacterial-derived CPFAS genes. When expressed individually both enzymes performed similarly in terms of the accumulation of DHSA in TAG. This can be contrasted with similar comparisons in oilseeds where the bacterial CPFAS produced more than five times as much DHSA compared to the plant CPFAS (Yu et al., 2011; Yu et al., 2014). We boosted the oleic acid content of leaves using simultaneous suppression of the endogenous *N. benthamiana FAD2*, although this only results in approximately 10% oleic acid in total lipid. Despite this relatively modest level of substrate, both plant and bacterial CPFASes were capable of a metabolic flux accumulating DHSA to approximately 15% in leaf oils. In comparison developing seed of the *fad2/fae1 Arabidopsis* mutant had close to 80% oleic acid in the polar lipids, yet only accumulated up to 10% CPA in TAG when EcCPFAS was expressed (Yu et al., 2014).

The leaf transient assay format also allowed a streamlined method to combine both the plant and bacterial CPFASes to see if we could further increase DHSA production in leaf. Co-expression of Ec- and

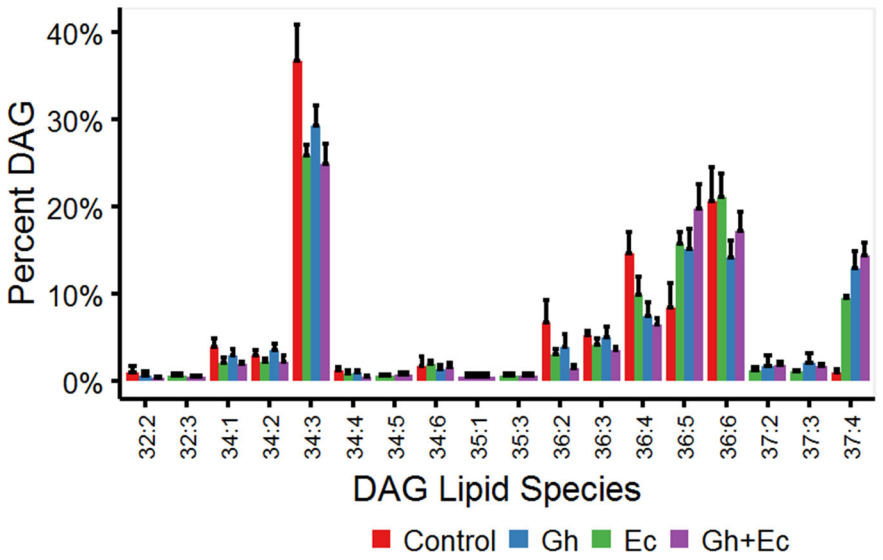

FIGURE 8 | Diacylglycerol (DAG) species in total lipid extracts of *Nicotiana benthamiana* leaf expressing cotton and/or *Escherichia coli* cyclopropane fatty acid synthase (CPFAS), tomato yellow leaf curl virus suppressor protein V2, green fluorescent protein (GFP), and *hpNbFAD2.1* identified by liquid chromatography-tandem mass spectrometry (LC-MSMS). The control contained V2, GFP, and *hpNbFAD2.1*. Error bars are standard deviations of six biological replicates. Ec, *E. coli* CPFAS; Gh, cotton CPFAS.

GhCPFAS gave the surprising results of a partially additive effect on DHSA accumulation. This result suggests that the CPFAS enzymes are capable of catalyzing different oleoyl substrates. Such a result is consistent with *E. coli* CPFAS acting on oleoyl substrates on both *sn*-1 and -2 positions of PC, and the plant CPFAS operating on the oleoyl chain on the *sn*-1 position of PC (Hildebrand and Law, 1964; Bao et al., 2003; Yu et al., 2014), as well as *E. coli* CPFAS being able to access the oleoyl chain on PE more effectively due to it being the natural substrate in the bacteria (this study; Grogan and Cronan, 1997; Yu et al., 2018). In terms of the variation in the level of DHSA accumulation seen between different experimental sets a review on *N. benthamiana* transient expression by Sheludko (2008) illustrates the large variation in protein expression using this system. This variation seems to occur for many reasons, such as batch-to-batch differences in the physiological state and age of the plants and condition of *Agrobacterium* upon infiltration and during expression, as well as the position of the leaf within an individual plant that is used for expression. In our study, and in other studies looking at modification of fatty acids *via* expression of a lipid modification enzyme there is another layer of variation in the lipid composition between plant batches (commented in Vanhercke et al., 2019), which may also contribute to the variation seen in the level of DHSA accumulation between infiltration sets. Despite this variation we still did observe a consistent increase in DHSA accumulation within batches when the bacterial and cotton CPFASes were coexpressed.

The movement of DHSA from the site of synthesis (PC) into DHSA rich oils can be boosted by the addition of specific DHSA handling enzymes. In plant seed the flux of oleic acid into DHSA could be significantly boosted by the further addition of a DHSA-specific lysophosphatidic acid acyltransferase (SfLPAT2, Yu et al., 2014), or phosphatidylcholine:diacylglycerol cholinephosphotransferase (Yu et al., 2019). We tested co-expression of EcCPFAS and SfLPAT2 to see if leaf tissue could benefit from DHSA channeling to the sn-2 position of polar and neutral lipids, however we did not observe any increase in DHSA accumulation. Our result is in contrast with that reported in *Arabidopsis* seed coexpressing EcCPFAS and SfLPAT2 (**Supplementary Figure 3**; Yu et al., 2014). Further investigation on lipid handling enzymes that will increase DHSA accumulation into leaf oil is currently underway.

Lipidomic analysis of leaves expressing CPFASes found an increase in TAG species that were composed of acyl chains that were derived from thylakoid galactolipid species. Transfer of galactolipids into TAG in leaves has also been observed in senescing leaves of *A. thaliana* (Kaup et al., 2002), ozone-fumigated spinach leaves (Sakaki et al., 1990a), and drought-stressed cotton leaves (El-Hafid et al., 1989). Much of this acyl chain transfer is thought to occur *via* transfer of acyl chains from MGDG to TAG *via* various intermediates such as acyl-CoA and DAG (Sakaki et al., 1990a; Sakaki et al., 1990b; Xiao et al., 2010). As production of DHSA from CPFAS expression resulted in the transfer of galactolipids into TAG, it is possible that DHSA induces a stress response, which in turn induces transfer of the fatty acid into a neutral environment for the leaf in the form of oil. In terms of the recipient DAG species for TAG assembly with DHSA the increase in DAG 36:5 percentage seems to be mainly offset by a decrease in DAG 34:3 percentage in CPFAS expression lines. DAG 34:3 seems to be preferentially used by the endogenous TAG assembly machinery in combination with

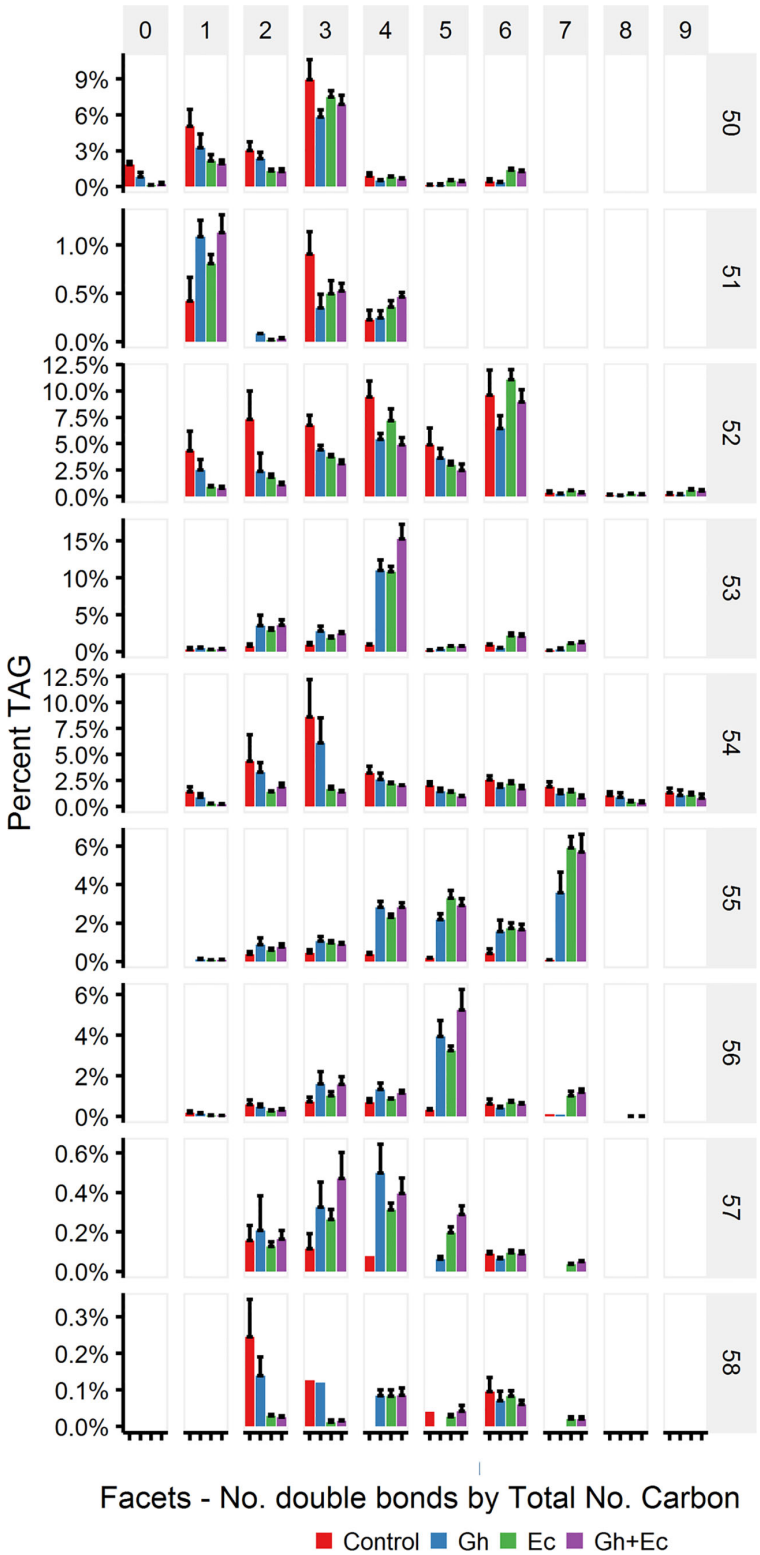

FIGURE 9 | Abundant triacylglycerol (TAG) species containing cyclopropane fatty acids in total lipid extracts of *Nicotiana benthamiana* leaf expressing cotton and/or *Escherichia coli* cyclopropane fatty acid synthase (CPFAS), tomato yellow leaf curl virus suppressor protein V2, green fluorescent protein (GFP), and *hpNbFAD2.1* identified by liquid chromatography-tandem mass spectrometry (LC-MSMS). The control contained V2, GFP, and *hpNbFAD2.1*. Error bars are standard deviations of six biological replicates. Ec, *E. coli* CPFAS; Gh, cotton CPFAS.

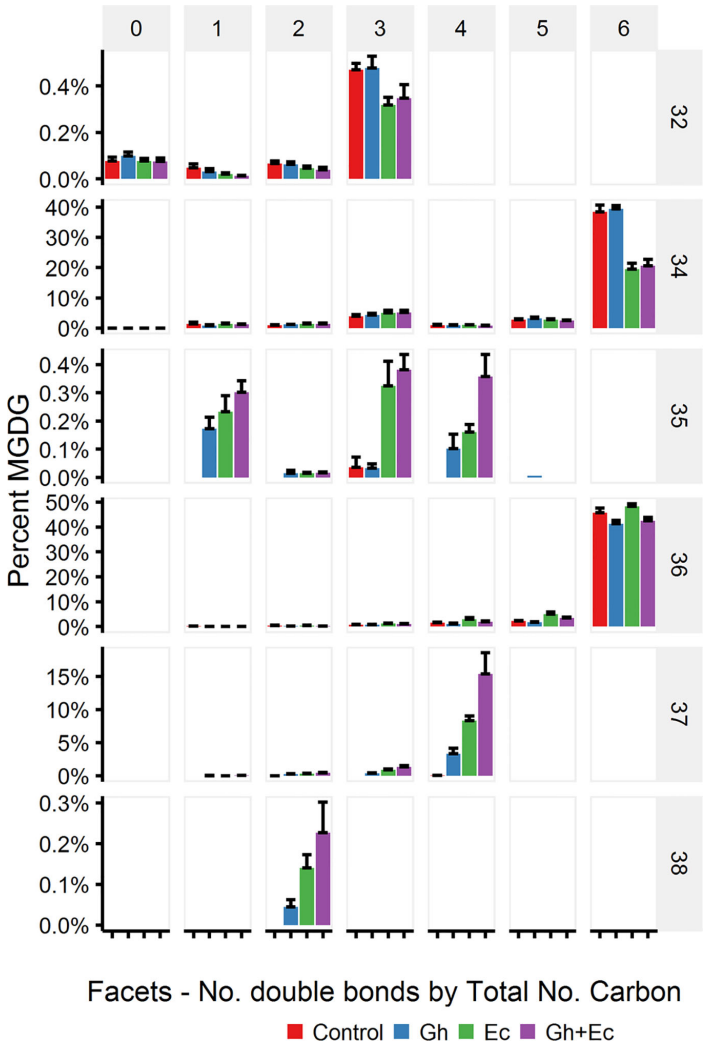

FIGURE 10 | Monogalactosyldiacylglycerol (MGDG) species in total lipid extracts of *Nicotiana benthamiana* leaf expressing cotton and/or *Escherichia coli* cyclopropane fatty acid synthase (CPFAS), tomato yellow leaf curl virus suppressor protein V2, green fluorescent protein (GFP), and *hpNbFAD2.1* identified by liquid chromatography-tandem mass spectrometry (LC-MSMS). The control contained V2, GFP, and *hpNbFAD2.1*. Error bars are standard deviations of six biological replicates. Ec, *E. coli* CPFAS; Gh, cotton CPFAS.

DHSA (TAG 53:4) when compared to that of DAG 36:5 (TAG 55:6). Therefore, if the ratio of assembly of the different DAG species is consistent but usage as substrate for TAG assembly is different with DHSA then it could possibly explain the relative increase in DAG 36:5 and simultaneous decrease in DAG 34:3.

Interestingly we identified for the first time a novel lipid compound generated by *E. coli* CPFAS, C18:2CPA, which is possibly generated from α-linolenic acid as substrate. We attempted to identify the structure of C18:2CPA using three different derivatization methods for GC-MS analysis, as well as OzID analysis. While we confirmed the positions of the two double bonds on Δ12 and Δ15 from all of the above analyzes, the position of the cyclopropane ring could not be conclusively determined. Like DHSA, C18:2CPA is capable of being hydrogenated to form SMCBFA, and therefore its production is noteworthy from an oleochemical feedstock point of view. This catalytic plasticity of *E. coli* CPFAS (that was not seen in the cotton CPFAS) has the potential to provide various forms of cyclopropane fatty acid as substrates for production of a wide range of SMCBFAs. Another interesting observation to note is the lack of lactobacillic acid (11R,12S-methylene-octadecanoic acid) that could potentially be produced by *E. coli* CPFAS expression in these transient leaf assays. OzID analysis of PC species detected C18:1Δ11 as an acyl chain, which is the endogenous substrate for CPFAS in *E. coli*, from which lactobacillic acid is produced (Grogan and Cronan, 1984). We

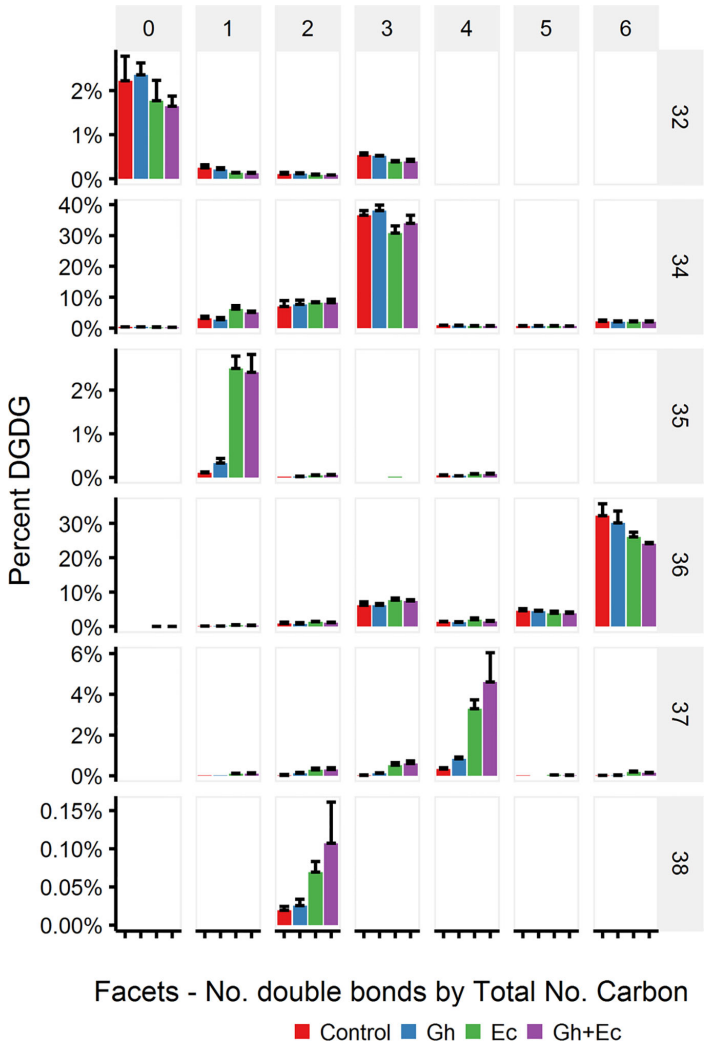

FIGURE 11 | Digalactosyldiacylglycerol (DGDG) species in total lipid extracts of *Nicotiana benthamiana* leaf expressing cotton and/or *Escherichia coli* cyclopropane fatty acid synthase (CPFAS), tomato yellow leaf curl virus suppressor protein V2, green fluorescent protein (GFP), and *hpNbFAD2.1* identified by liquid chromatography-tandem mass spectrometry (LC-MSMS). The control contained V2, GFP, and *hpNbFAD2.1*. Error bars are standard deviations of six biological replicates. Ec, *E. coli* CPFAS; Gh, cotton CPFAS.

did not detect any lactobacillic acid in any of our lipid analyzes, which suggests that the C18:1Δ11 is not available to the recombinant *E. coli* CPFAS for cyclopropanation. C18:1Δ11 is proposed to be synthesized by elongation of C16:1Δ9 in the plastid (Xue et al., 2013), and therefore most of it may be on PC in the plastid where it is not accessible to *E. coli* CPFAS.

In transient leaf assays the expression of *E. coli* CPFAS, and presumably the production of DHSA, increased the relative amount of TAG. This is in contrast with oilseed production systems, in which it is commonly reported that production of high levels of unusual fatty acids has negative impacts on the total amount of TAG, including DHSA (Yu et al., 2014), ricinoleic acid (van Erp et al., 2011), and gamma linolenic acid in safflower (Nykiforuk et al., 2012). In oilseeds these bottlenecks in flux can be ascribed to the accumulation of the unusual fatty acid in the cell membranes such as in PC lipids. In our analyses we found that DHSA was present in PC at approximately 25%, which also could benefit from additional lipid handling enzymes that preferentially transfers cyclopropane fatty acids from polar lipids to neutral lipids, i.e. TAG. The sensing of fatty acids in plant cells is a little-known area, however it has been hypothesized that oleic acid is a signaling molecule (Andre et al., 2012). Perhaps accumulation of DHSA at the expense of oleic acid in the tissue interrupts this signaling process allowing more oil to accumulate than is otherwise possible with common fatty acids. Vanhercke et al. (2017) saw a trade-off between

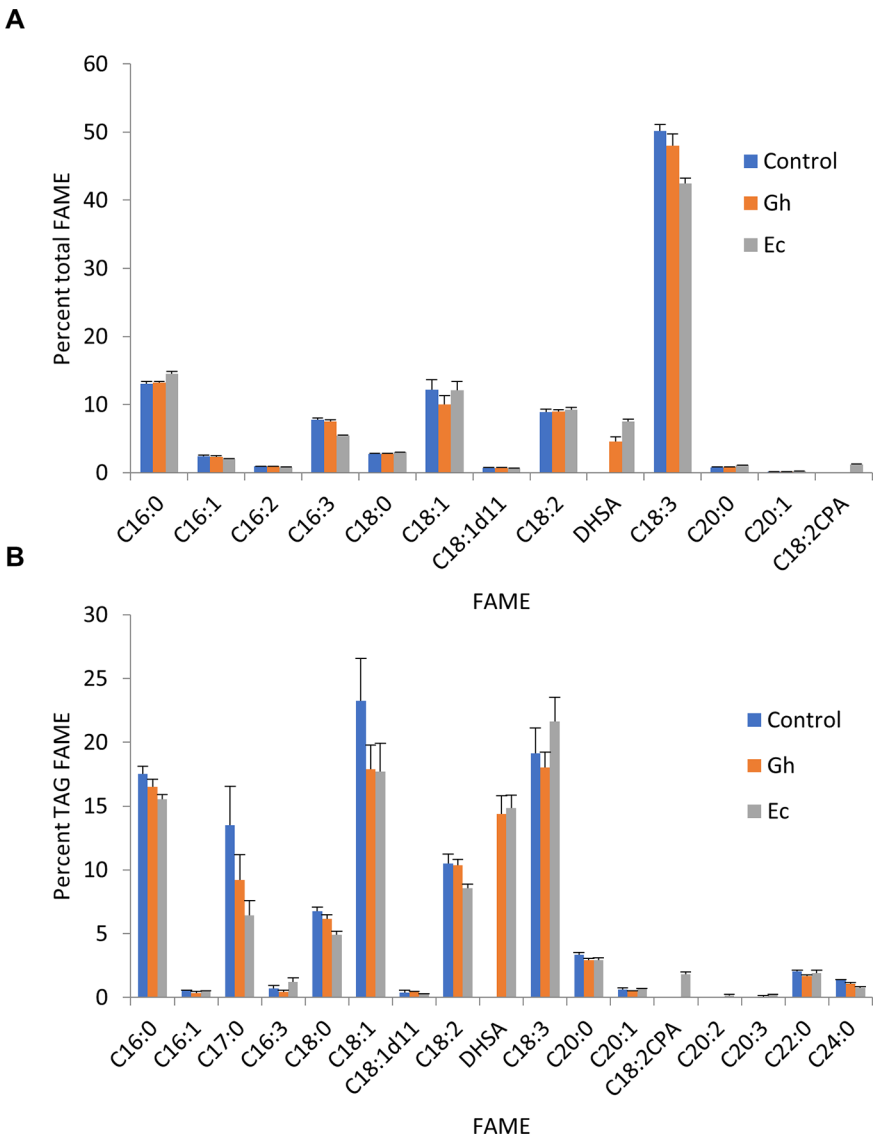

FIGURE 12 | Cyclopropane fatty acid (CPA) accumulates in the triacylglycerol (TAG) fraction in *Nicotiana benthamiana* leaf total lipid extracts expressing cyclopropane fatty acid synthase (CPFAS). **(A)** Total fatty acid methyl ester (FAME) profile of *N. benthamiana* leaf expressing cotton or *Escherichia coli* CPFAS, tomato yellow leaf curl virus suppressor protein V2, green fluorescent protein (GFP), *hpNbFAD2.1*, and *Arabidopsis* diacylglycerol acyltransferase 1 (AtDGAT1). The control contained V2, GFP, *hpNbFAD2.1*, and AtDGAT1. Error bars are standard deviations of six biological replicates. **(B)** FAME profile of the TAG fraction in *N. benthamiana* leaf total lipid extracts expressing cotton or *E. coli* CPFAS, tomato yellow leaf curl virus suppressor protein V2, GFP, *hpNbFAD2.1*, and AtDGAT1. The control contained V2, GFP, *hpNbFAD2.1*, and AtDGAT1. C17:0 FAME was an internal standard added as triheptadecanoin per dry leaf weight prior to extraction. Error bars are standard deviations of six biological replicates. Ec, *E. coli* CPFAS; Gh, cotton CPFAS.

carbohydrate (i.e. starch and soluble sugars) and TAG accumulation when genes involved in seed oil synthesis were expressed in *Nicotiana tabacum* leaf. However, the level of PC did not change with TAG accumulation when two of the seed oil synthesis genes were transiently expressed in *N. benthamiana* (Vanhercke et al., 2013). It would be of interest to see where the carbon for increased DHSA accumulation is coming from in our study, which will guide future efforts in generating stable transformants. More detailed investigations will be needed to investigate the molecular basis of TAG increase upon expression of *E. coli* CPFAS in leaf tissue. In conclusion the production of cyclopropane fatty acids in plants could provide a potential feedstock for the production of saturated mid-chain branched fatty acids that are in demand for oleochemical products. Focus

on improved movement of DHSA from PC into neutral lipids in further investigations could improve upon the yields achieved thus far. We are currently exploring the combination of DHSA accumulation pathways with the latest iterations of platforms producing high oil in vegetative tissue (Vanhercke et al., 2014).

MATERIAL AND METHODS

Escherichia coli Cyclopropane Fatty Acid Synthase

The full-length gene coding for EcCPFAS was amplified from DH10B genomic DNA. The nucleotide sequence was 100% identical to accession M98330.

Cotton Cyclopropane Fatty Acid Synthase

The full-length gene coding for GhCPFAS (accession AY574036) was synthesized (Thermo Fisher Scientific, MA, US) with two silent nucleotide substitutions G2043A and G2551A from the published sequence to remove XhoI restriction sites.

Construction of 35S Cyclopropane Fatty Acid Synthase Vectors for Plant Expression

pENTR11 (Thermo Fisher Scientific, MA, US) was digested with NcoI, overhangs removed with DNA polymerase I, Large (Klenow) fragment, and re-ligated to generate pENTR-NcoI. *E. coli* and cotton CPFAS genes were cloned into pENTR-NcoI *via* two EcoRI restriction sites and EcoRI and XhoI restriction sites respectively, and subsequently cloned into a cauliflower mosaic virus (CaMV) 35S promoter-driven over-expression vector pXZP393 (Zhou et al., 2013a) using LR Clonase™ II enzyme mix (Thermo Fisher Scientific, MA, US) according to the manufacturer's instructions. Resulting plasmids containing the two CPFASes were used to transform *Agrobacterium tumefaciens* strain AGL1 for *N. benthamiana* leaf transient expression.

Nicotiana benthamiana Leaf Transient Expression

Recombinant AGL1 containing *35S::EcCPFAS* and *35S::GhCPFAS*, viral suppressor *35S::V2*, visual expression marker *35S::GFP*, *N. benthamiana* microsomal oleate desaturase silencer *35S::hpNbFAD2.1*, and *A. thaliana* diacylglycerol acyltransferase *35S::AtDGAT1* (Naim et al., 2012) were grown in Luria-Bertani (LB) broth with appropriate antibiotics for 2 days at 28°C with shaking. On the third day of incubation acetosyringone was added to the cultures to a final concentration of 100 µM and further incubated for 2–3 h, after which the cultures were collected by centrifugation at 2000*g* for 10 min, and resuspended in infiltration buffer (5 mM 2-(*N*-morpholino) ethanesulfonic acid (MES), 5 mM $MgSO_4$, 500 µM acetosyringone). Infiltration mixes were prepared with each AGL1 at 0.3 OD600 units and infiltrated using a syringe on the underside of 5–6-week-old *N. benthamiana* leaves. Biological replicates of each experiment were produced by individual agroinfiltration spots on different leaves across different plants. Infiltrated plants were left at 24°C with 10:14 light:dark cycle for 5 days. On the fifth day expression of the infiltrated region was confirmed by presence of the GFP signal, which was harvested, freeze dried overnight, weight recorded, and stored in −80°C until analysis.

Fatty Acid Methyl Ester Analysis

Total lipid was extracted from leaf tissue as previously described (Naim et al., 2012), with triheptadecanoin (1 µg/mg dry leaf weight, Nu-Chek Prep Inc., MN, US) added to each sample prior to extraction. Lipid extractions equivalent to approximately 2.5 mg dry leaf weight were transmethylated with 0.1 M sodium methoxide in methanol:chloroform = 9:1 at 95°C for 60 min to prepare FAMEs and extracted with hexane. For triacylglycerol analysis extractions equivalent to approximately 10 mg dry leaf weight were separated by TLC on pre-coated silica gel aluminum foils (Fluka, Sigma Aldrich, MO, US) with hexane:diethyl ether: acetic acid = 70:30:1 (vol:vol:vol) as the separation solvent. The TLC foil was briefly stained with iodine and corresponding fractions parallel to the triolein standard were collected, and FAMEs prepared as described above. Total lipid fractionation for phosphatidylcholine analysis was performed according to Wood et al. (2009). GC was performed as previously described (Zhou et al., 2011) using an Agilent 6890N GC (Agilent Technologies, CA, US) equipped with a SGE BPX70 column (Trajan Scientific and Medical Pty Ltd, VIC, Australia, 30 m x 0.25 mm i.d., 0.25 µm film thickness), a flame ionization detector, a split/splitless injector, and an Agilent Technologies 7683 Series autosampler and injector using helium as the carrier gas. Peak responses were calibrated against FAMEs of authentic Nu-Chek gas–liquid chromatography (GLC) standard-411 (Nu-Chek Prep Inc, MN, US), which contains equal-weight amounts of 31 different FAMEs, with added additional equal-weight amount of methyl dihydrosterculate (Matreya LLC, PA, US). FAME peaks were integrated using the Agilent ChemStation software (Agilent Technologies, CA, US), and the percentage was calculated with responses normalized against the corresponding weight of each FAME peak. TAG content as % per dry leaf weight was calculated as per Vanhercke et al., 2013.

GC-MS was performed to confirm the identity of FAMEs not present in the base control infiltration and was carried out on a Shimadzu GC-MS QP2010 Plus ion-trap fitted with on-column injection (Shimadzu Corp., Kyoto, Japan) as previously described (Zhou et al., 2013b), equipped with a SGE BPX70 column (Trajan Scientific and Medical Pty Ltd, VIC, Australia, 30 m x 0.25 mm i.d., 0.25 µm film thickness). Pyrrolidine derivatives were prepared from FAME according to Andersson and Holman (1974). Picolinyl derivatives were prepared directly from FAME according to the method of Destaillats and Angers (2002). 4,4-dimethyloxazoline, pyrrolidine, and picolinyl derivatives were analyzed on the GC-MS as per Zhou et al. (2013b), except for pyrrolidine and picolinyl derivatives, for which an extension of the final holding temperature at 240°C was employed, resulting

in a total run time of 35 min. Mass spectra were acquired and processed with GC-MS solution software version 2.61 (Shimadzu Corp., Kyoto, Japan).

Lipid Class Analysis

LC-MSMS analysis of total lipid extracts was conducted based on previously described methods (Reynolds et al., 2015). Briefly, total lipid extracts were analyzed on an Agilent 6490 triple quadrupole mass spectrometer with jetstream and ion funnel technology (Agilent Technologies, CA, US). Lipid species were separated by liquid chromatography on a Waters (MA, US) BEH C8 (100 mm × 2.1 mm × 2.7 μm) column using an Agilent 1290 LC system (Agilent Technologies, CA, US). Solvents used for the separation of lipid species were mobile phase A (acetonitrile:water, 9:1, with 10 mM ammonium acetate and 0.2% acetic acid) and B (2-isopropanol: acetonitrile:water, 80:15:5, with 10 mM ammonium acetate and 0.2% acetic acid) with a flow rate of 0.2 ml/min. An initial gradient of 1% B was held for 2 min, then raised to 20% B over 3 min to elute PC, PE, DAG, DGDG, and MGDG species followed by a sharp increase to 60% B over 3 min and slowly increased to 70% B for separation of the TAG species over 4 min before re-equilibration at 1% B. The mass spectrometer gas temperature and flow were set to 250°C and 14 L/min and 250°C at 11 L/min for the sheath gas, nebulizer at 45 psi, capillary voltage at 3000 V, and nozzle voltage at 1000 V. The ammonium adducts of MGDG, DGDG, DAG, and TAG species were analyzed by the neutral loss of fatty acid C16 to C20, and the pronated PCs and PEs were identified by a characteristic fragment ion at *m/z* 184 or neutral loss of m/z 141, respectively. Multiple reaction monitoring lists were based on the loss of observed fatty acids using a collision of 28 V for all lipid species except DAG where 14 V was used. Chromatograms were integrated using Agilent Quantitative Analysis software version 6.0 (Agilent Technologies, CA, US). Statistical and graphical analysis was conducted using R (R Core Team, 2014) and data packages dplyr and tidyr (Wickham, 2014) and the graphical interpretation using ggplot2 (Wickham, 2010) using Rstudio (www.rstudio.com).

Ozone-Induced Dissociation Analysis of Total Lipid Extracts of *Nicotiana benthamiana* Expressing *Escherichia coli* Cyclopropane Fatty Acid Synthase

Total lipid extracts of *N. benthamiana* expressing *35S::EcCPFAS*, *35S::V2*, *35S::GFP*, *35S::hpNbFAD2.1*, and *35S::AtDGAT1* were subjected to OzID analysis (Thomas et al., 2008) and composite collision-induced dissociation (CID) and OzID (Marshall et al., 2016) on a modified LTQ XL ion trap mass spectrometer (Thermo Fisher Scientific, MA, US). PC species were separated on a Waters (MA, US) C18 CSH (100 mm × 2.1 mm × 1.7 μm) column, using an initial mobile phase of 12:5% A (water) with 87.5% B (60:40 methanol:acetonitrile) at a flow rate of 0.2 ml/min for 2 min, before ramping to 100% B over 15 min. The post-column eluent was combined by tee infusion with a 0.5 mM solution of sodium acetate or lithium acetate to facilitate the exclusive formation of sodium (or lithium) adduct ions by electrospray ionization. PC metal adduct ions were held in the ion trap in the presence of ozone for 100–1000 ms.

Saccharomyces cerevisiae Expression of *Escherichia coli* Cyclopropane Fatty Acid Synthase

EcCPFAS in pENTR-NcoI was used to transfer EcCPFAS into pYES-DEST52 (Thermo Fisher Scientific, MA, US) using LR Clonase™ II enzyme mix (Thermo Fisher Scientific, MA, US) according to the manufacturer's instructions. The resulting plasmid was used to transform *S. cerevisiae* strain INVSc1 (Thermo Fisher Scientific, MA, US) with the Yeast Transformation Kit (Sigma Aldrich, MO, US). Exogenous feeding of yeast, FAME preparation, and GC-MS analysis followed the methods of Zhou et al. (2013b).

DATA AVAILABILITY STATEMENT

The raw data supporting the conclusions of this article will be made available by the authors, without undue reservation, to any qualified researcher.

AUTHOR CONTRIBUTIONS

SO, SS, and CW conceived the project and designed the experiments. SO, MT, X-RZ, FN, DM, and SB conducted the experiments. All authors contributed to writing the manuscript.

FUNDING

This project was co-funded by CSIRO and Grains Research and Development Corporation. Access to the Central Analytical Research Facility, operated by the Institute for Future Environments, Queensland University of Technology, was supported by generous funding from the QUT Science and Engineering Faculty.

ACKNOWLEDGMENTS

We thank Cheryl Blundell, Katherine Damcevski, Bei Dong, and Annette Kasprzak for their outstanding technical assistance. We would also like to acknowledge Andrew Warden and Anna El Tahchy for their critical reviews of this article.

SUPPLEMENTARY MATERIAL

The Supplementary Material for this article can be found online at: https://www.frontiersin.org/articles/10.3389/fpls.2020.00030/full#supplementary-material

REFERENCES

Andersson, B. A., and Holman, R. T. (1974). Pyrrolidides for mass spectrometric determination of the position of the double bond in monounsaturated fatty acids. *Lipids* 9, 185–190. doi: 10.1007/BF02532690

Andre, C., Haslam, R. P., and Shanklin, J. (2012). Feedback regulation of plastidic acetyl-CoA carboxylase by 18:1-acyl carrier protein in Brassica napus. *Proc. Nat. Acad. Sci. U.S.A.* 109, 10107–10112. doi: 10.1073/pnas.1204604109

Bao, X., Katz, S., Pollard, M., and Ohlrogge, J. (2002). Carbocyclic fatty acids in plants: Biochemical and molecular genetic characterization of cyclopropane fatty acid synthesis of Sterculia foetida. *Proc. Natl. Acad. Sci. U.S.A.* 99, 7172–7177. doi: 10.1073/pnas.092152999

Bao, X., Thelen, J. J., Bonaventure, G., and Ohlrogge, J. B. (2003). Characterization of cyclopropane fatty-acid synthase from Sterculia foetida. *J. Biol. Chem.* 278, 12846–12853. doi: 10.1074/jbc.M212464200

Biermann, U., and Metzger, J. O. (2008). Synthesis of alkyl-branched fatty acids. *Eur. J. Lipid Sci. Tech.* 110, 805–811. doi: 10.1002/ejlt.200800033

Carlsson, A. S., Yilmaz, J. L., Green, A. G., Stymne, S., and Hofvander, P. (2011). Replacing fossil oil with fresh oil – with what and for what? *Eur. J. Lipid Sci. Tech.* 113, 812–831. doi: 10.1002/ejlt.201100032

Destaillats, F., and Angers, P. (2002). One-step methodology for the synthesis of FA picolinyl esters from intact lipids. *J. Am. Oil Chem. Soc.* 79, 253–256. doi: 10.1007/s11746-002-0469-7

El-Hafid, L., Pham, A. T., Zuily-Fodil, Y., and da Silva, J. V. (1989). Enzymatic breakdown of polar lipids in cotton leaves under water stress: I. Degradation of monogalactosyl-diacylglycerol. *Plant Physiol. Biochem.* 27, 495–502.

Fish, W. R., Holz, G. G., Beach, D. H., Owen, E., and Anekwe, G. E. (1981). The cyclopropane fatty-acid of trypanosomatids. *Mol. Biochem. Parasitol.* 3, 103–115. doi: 10.1016/0166-6851(81)90010-4

Grogan, D. W., and Cronan, Jr., J. E. (1984). Cloning and manipulation of the Escherichia coli cyclopropane fatty acid synthase gene: physiological aspects of enzyme overproduction. *J. Bacteriol.* 158, 286–295. doi: 10.1128/JB.158.1.286-295.1984

Grogan, D. W., and Cronan, Jr., J. E. (1997). Cyclopropane ring formation in membrane lipids of bacteria. *Microbiol. Mol. Biol. Rev.* 61, 429–441. doi: 10.1128/.61.4.429-441.1997

Hasselberg, J., and Behr, A. (2016). Saturated branched fatty compounds: proven industrial processes and new alternatives. *Eur. J. Lipid Sci. Technol.* 118, 36–46. doi: 10.1002/ejlt.201500461

Haynes W. M. (Eds.) (2016). *CRC Handbook of Chemistry and Physics 97th ed* (Cleveland, Ohio: CRC Press). doi: 10.1201/9781315380476

Hildebrand, J. G., and Law, J. H. (1964). Fatty acid distribution in bacterial phospholipids. The specificity of the cyclopropane synthetase reaction. *Biochemistry* 3, 1304–1308. doi: 10.1021/bi00897a020

Kaup, M. T., Froese, C. D., and Thompson, J. E. (2002). A role for diacylglycerol acyltransferase during leaf senescence. *Plant Physiol.* 129, 1616–1626. doi: 10.1104/pp.003087

Kinsman, D. V. (1979). Isostearic and other branched acids. *J. Am. Oil Chem. Soc.* 56, A823–A827. doi: 10.1007/BF02667455

Knivett, V. A., and Cullen, J. (1965). Some factors affecting cyclopropane acid formation in Escherichia coli. *Biochem. J.* 96, 771–776. doi: 10.1042/bj0960771

Kuiper, P. J., and Stuiver, B. (1972). Cyclopropane fatty acids in relation to earliness in spring and drought tolerance in plants. *Plant Physiol.* 49, 307–309. doi: 10.1104/pp.49.3.307

Li, R., Yu, K., Wu, Y., Tateno, M., Hatanaka, T., and Hildebrand, D. F. (2012). Vernonia DGATs can complement the disrupted oil and protein metabolism in epoxygenase-expressing soybean seeds. *Metab. Eng.* 14, 29–38. doi: 10.1016/j.ymben.2011.11.004

Lou, Y., Horikawa, M., Kloster, R. A., Hawryluk, N. A., and Corey, E. J. (2004). A new chiral Rh(II) catalyst for enantioselective [2 + 1]-cycloaddition. Mechanistic implications and applications. *J. Am. Chem. Soc.* 126, 8916–8918. doi: 10.1021/ja047064k

Marshall, D. L., Pham, H. T., Bhujel, M., Chin, J. S. R., Yew, J. Y., Mori, K., et al. (2016). Sequential collision- and ozone-induced dissociation enables assignment of relative acyl chain position in triacylglycerols. *Anal. Chem.* 88, 2685–2692. doi: 10.1021/acs.analchem.5b04001

Naim, F., Nakasugi, K., Crowhurst, R. N., Hilario, E., Zwart, A. B., Hellens, R. P., et al. (2012). Advanced engineering of lipid metabolism in Nicotiana benthamiana using a draft genome and the V2 viral silencing-suppressor protein. *PloS One* 7, e52717. doi: 10.1371/journal.pone.0052717

Ngo, H. L., Dunn, R. O., Sharma, B., and Foglia, T. A. (2011). Synthesis and physical properties of isostearic acids and their esters. *Eur. J. Lipid Sci. Tech.* 113, 180–188. doi: 10.1002/ejlt.201000335

Nykiforuk, C. L., Shewmaker, C., Harry, I., Yurchenko, O. P., Zhang, M., Reed, C., et al. (2012). High level accumulation of gamma linolenic acid (C18:3Δ6,9,12 cis) in transgenic safflower (Carthamus tinctorius) seeds. *Transgenic Res.* 21, 367–381. doi: 10.1007/s11248-011-9543-5

Oudejans, R. C., Vanderho, D. J., and Vandonge, J. P. (1971). Isolation and identification of cyclopropane fatty acids from millipede Graphidostreptus tumuliporus (Karsch) (Myriapoda-diplopoda). *Biochemistry* 10, 4938–4941. doi: 10.1021/bi00802a016

Palko, J. W., Buist, P. H., and Manthorpe, J. M. (2013). A flexible and modular stereoselective synthesis of (9R,10S)-dihydrosterculic acid. *Tetrahedron: Asymmetry* 24, 165–168. doi: 10.1016/j.tetasy.2013.01.003

Pham, H. T., Maccarone, A. T., Thomas, M. C., Campbell, J. L., Mitchell, T. W., and Blanksby, S. J. (2014). Structural characterization of glycerophospholipids by combinations of ozone- and collision-induced dissociation mass spectrometry: the next step towards "top-down" lipidomics. *Analyst* 139, 204–214. doi: 10.1039/C3AN01712E

R Core Team. (2014). R: A language and environment for statistical computing. (Vienna, Austria: R Foundation for Statistical Computing)

Reynolds, K. B., Taylor, M. C., Zhou, X.-R., Vanhercke, T., Wood, C. C., Blanchard, C. L., et al. (2015). Metabolic engineering of medium-chain fatty acid biosynthesis in Nicotiana benthamiana plant leaf lipids. *Front. Plant Sci.* 24, 164. doi: 10.3389/fpls.2015.00164

Sakaki, T., Kondo, N., and Yamada, M. (1990a). Pathway for the synthesis of triacylglycerols from monogalactosyldiacylglycerols in ozone-fumigated spinach leaves. *Plant Physiol.* 94, 773–780. doi: 10.1104/pp.94.2.773

Sakaki, T., Saito, K., Kawaguchi, A., Kondo, N., and Yamada, M. (1990b). Conversion of monogalactosyldiacylglycerols to triacylglycerols in ozone-fumigated spinach leaves. *Plant Physiol.* 94, 766–772. doi: 10.1104/pp.94.2.766

Schmid, K. M. (1995). "Dihydrosterculate in tobacco transformed with bacterial cyclopropane fatty acid synthase," in *Plant Lipid Metabolism*. J.-C. Kader and P. Mazliak Eds. (Kluwer Academic Publishers), 108–110. doi: 10.1007/978-94-015-8394-7_31

Schmidt, G. A., and Shirley, D. A. (1949). A new synthesis of tuberculostearic acid. *J. Amer Chem. Soc.* (Dordrecht, Netherlands: Springer) 71, 3804–3806. doi: 10.1021/ja01179a064

Sebedio, J. L., and Grandgirard, A. (1989). Cyclic fatty acids: natural sources, formation during heat treatment, synthesis and biological properties. *Prog. Lipid Res.* 28, 303–336. doi: 10.1016/0163-7827(89)90003-9

Shabala, L., and Ross, T. (2008). Cyclopropane fatty acids improve Escherichia coli survival in acidified minimal media by reducing membrane permeability to H+ and enhanced ability to extrude H+. *Res. Microbiol.* 159, 458–461. doi: 10.1016/j.resmic.2008.04.011

Sheludko, Y. V. (2008). Agrobacterium-mediated transient expression as an approach to production of recombinant proteins in plants. *Recent Pat. Biotechnol.* 2, 198–208. doi: 10.2174/187220808786241033

Thomas, M. C., Mitchell, T. W., Harman, D. G., Deeley, J. M., Nealon, J. R., and Blanksby, S. J. (2008). Ozone-induced dissociation: elucidation of double bond position within mass-selected lipid ions. *Anal. Chem.* 80, 303–311. doi: 10.1021/ac7017684

van Erp, H., Bates, P. D., Burgal, J., Shockey, J., and Browse, J. (2011). Castor phospholipid:diacylglycerol acyltransferase facilitates efficient metabolism of hydroxy fatty acids in transgenic Arabidopsis. *Plant Physiol.* 155, 683–693. doi: 10.1104/pp.110.167239

Vanhercke, T., El Tahchy, A., Shrestha, P., Zhou, X.-R., Singh, S. P., and Petrie, J. R. (2013). Synergistic effect of WRI1 and DGAT1 coexpression on triacylglycerol biosynthesis in plants. *FEBS Lett.* 587, 364–369. doi: 10.1016/j.febslet.2012.12.018

Vanhercke, T., El Tahchy, A., Liu, Q., Zhou, X.-R., Shrestha, P., Divi, U. K., et al. (2014). Metabolic engineering of biomass for high energy density: oilseed-like triacylglycerol yields from plant leaves. *Plant Biotech. J.* 12, 231–239. doi: 10.1111/pbi.12131

Vanhercke, T., Divi, U. K., El Tahchy, A., Liu, Q., Mitchell, M., Taylor, M. C., et al. (2017). Step changes in leaf oil accumulation via iterative metabolic engineering. *Metab. Eng.* 39, 237–346. doi: 10.1016/j.ymben.2016.12.007

Vanhercke, T., Dyer, J. M., Mullen, R. T., Kilaru, A., Rahman, M. M., Petrie, J. R., et al. (2019). Metabolic engineering for enhanced oil in biomass. *Prog. Lipid Res.* 74, 103–129. doi: 10.1016/j.plipres.2019.02.002

Wang, A.-Y., Grogan, D. W., and Cronan, Jr., J. E. (1992). Cyclopropane fatty acid synthase of Escherichia coli: deduced amino acid sequence, purification, and studies of the enzyme active site. *Biochemistry* 31, 11020–11028. doi: 10.1021/bi00160a011

Wickham, H. (2010). A layered grammar of graphics. *J. Comp. Graph Stat.* 19, 3–28. doi: 10.1198/jcgs.2009.07098

Wickham, H. (2014). Tidy data. *J. Stat. Softw.* 59, 1–23. doi: 10.18637/jss.v059.i10

Wood, C. C., Petrie, J. R., Shrestha, P., Mansour, M. P., Nichols, P. D., Green, A. G., et al. (2009). A leaf-based assay using interchangeable design principles to rapidly assemble multistep recombinant pathways. *Plant Biotech. J.* 7, 914–924. doi: 10.1111/j.1467-7652.2009.00453.x

Wood, C. C. (2014). Leafy biofactories: producing industrial oils in non-seed biomass. *EMBO Rep.* 15, 201–202. doi: 10.1002/embr.201338132

Xiao, S., Gao, W., Chen, Q. F., Chan, S. W., Zheng, S. X., Ma, J. Y., et al. (2010). Overexpression of Arabidopsis acyl-CoA binding protein ACBP3 promotes starvation-induced and age-dependent leaf senescence. *Plant Cell* 22, 1463–1482. doi: 10.1105/tpc.110.075333

Xue, J.-A., Mao, X., Yang, Z.-R., Wu, Y. M., Jia, X.-Y., Zhang, L., et al. (2013). Expression of yeast acyl-CoA-Δ9 desaturase leads to accumulation of unusual monounsaturated fatty acids in soybean seeds. *Biotechnol. Lett.* 35, 951–959. doi: 10.1007/s10529-013-1149-y

Yu, X.-H., Rawat, R., and Shanklin, J. (2011). Characterization and analysis of the cotton cyclopropane fatty acid synthase family and their contribution to cyclopropane fatty acid synthesis. *BMC Plant Biol.* 11, 97. doi: 10.1186/1471-2229-11-97

Yu, X.-H., Prakash, R. R., Sweet, M., and Shanklin, J. (2014). Coexpressing Escherichia coli cyclopropane synthase with Sterculia foetida lysophosphatidic acid acyltransferase enhances cyclopropane fatty acid accumulation. *Plant Physiol.* 164, 455–465. doi: 10.1104/pp.113.230953

Yu, X.-H., Cahoon, R. E., Horn, P. J., Shi, H., Prakash, R. R., Cai, Y., et al. (2018). Identification of bottlenecks in the accumulation of cyclic fatty acids in camelina seed oil. *Plant Biotech. J.* 16, 926–938. doi: 10.1111/pbi.12839

Yu, X.-H., Cai, Y., Chai, J., Schwender, J., and Shanklin, J. (2019). Expression of a lychee phosphatidylcholine : diacylglycerol cholinephosphotransferase with an Escherichia coli cyclopropane fatty acid synthase enhances cyclopropane fatty acid accumulation in camelina seeds. *Plant Physiol.* 180, 1351–1361. doi: 10.1104/pp.19.00396

Zhang, J. Y., Yu, Q. T., and Huang, Z. H. (1987). 2-Substituted 4, 4-dimethyloxazolines as useful derivatives for the localization of cyclopropane rings in long-chain fatty acids. *Mass Spectros* 35, 23–30. doi: 10.5702/massspec.35.23

Zhang, Z. C. C., Dery, M., Zhang, S. G., and Steichen, D. (2004). New process for the production of branched-chain fatty acids. *J. Surfactants Deterg.* 7, 211–215. doi: 10.1007/s11743-004-0306-x

Zhou, X.-R., Singh, S. P., and Green, A. G. (2011). Caenorhabditis elegans Δ12-Desaturase FAT-2 is a bifunctional desaturase able to desaturate a diverse range of fatty acid substrates at the Δ12 and Δ15 positions. *J. Biol. Chem.* 286, 43644–43650. doi: 10.1074/jbc.M111.266114

Zhou, X.-R., Shrestha, P., Yin, F., Petrie, J. R., and Singh, S. P. (2013a). AtDGAT2 is a functional acyl-CoA: diacylglycerol acyltransferase and displays different acyl-CoA substrate preferences than AtDGAT1. *FEBS Lett.* 587, 2371–2376. doi: 10.1016/j.febslet.2013.06.003

Zhou, X.-R., Singh, S. P., and Green, A. G. (2013b). Characterization of the FAD2 gene family from Hiptage benghalensis: a ricinoleic acid accumulating plant. *Phytochemistry* 92, 42–48. doi: 10.1016/j.phytochem.2013.05.006

Conflict of Interest: The authors declare that the research was conducted in the absence of any commercial or financial relationships that could be construed as a potential conflict of interest.

frontiers in Plant Science

ORIGINAL RESEARCH
published: 20 February 2020
doi: 10.3389/fpls.2020.00097

Single Nucleotide Mutagenesis of the *TaCHLI* Gene Suppressed Chlorophyll and Fatty Acid Biosynthesis in Common Wheat Seedlings

Chaojie Wang[1,2†], Lili Zhang[1†], Yingzhuang Li[1], Zeeshan Ali Buttar[1], Na Wang[1], Yanzhou Xie[1,2] and Chengshe Wang[1,2]*

[1] College of Agronomy, Northwest A&F University, Yangling, China, [2] State Key Laboratory of Crop Stress Biology for Arid Areas, Northwest A&F University, Yangling, China

OPEN ACCESS

Edited by:
Xue-Rong Zhou, Agriculture & Food, Commonwealth Scientific and Industrial Research Organisation (CSIRO), Australia

Reviewed by:
Huiru Peng, China Agricultural University (CAU), China
Hisashi Ito, Hokkaido University, Japan

***Correspondence:**
Chengshe Wang
wangcs2008@126.com

[†]*These authors have contributed equally to this work*

Specialty section:
This article was submitted to Plant Metabolism and Chemodiversity, a section of the journal Frontiers in Plant Science

Received: *18 October 2019*
Accepted: *22 January 2020*
Published: *20 February 2020*

Citation:
Wang C, Zhang L, Li Y, Ali Buttar Z, Wang N, Xie Y and Wang C (2020) Single Nucleotide Mutagenesis of the TaCHLI Gene Suppressed Chlorophyll and Fatty Acid Biosynthesis in Common Wheat Seedlings. Front. Plant Sci. 11:97. doi: 10.3389/fpls.2020.00097

Wheat (*Triticum aestivum* L.) is one of the most important crops in the world. Chlorophyll plays a vital role in plant development and crop improvement and further determines the crop productivity to a certain extent. The biosynthesis of chlorophyll remains a complex metabolic process, and fundamental biochemical discoveries have resulted from studies of plant mutants with altered leaf color. In this study, we identified a chlorophyll-deficiency mutant, referred to as *chli*, from the wheat cultivar Shaannong33 that exhibited an obvious pale-green leaf phenotype at the seedling stage, with significantly decreased accumulation of chlorophyll and its precursors, protoporphyrin IX and Mg-protoporphyrin IX. Interestingly, a higher protoporphyrin IX to Mg-protoporphyrin IX ratio was observed in *chli*. Lipid biosynthesis in *chli* leaves and seeds was also affected, with the mutant displaying significantly reduced total lipid content relative to Shaanong33. Genetic analysis indicated that the pale-green leaf phenotype was controlled by a single pair of recessive nuclear genes. Furthermore, sequence alignment revealed a single-nucleotide mutation (G664A) in the gene TraesCS7A01G480700.1, which encodes subunit I of the Mg-chelatase in plants. This single-nucleotide mutation resulted in an amino acid substitution (D221N) in the highly conserved domain of subunit I. As a result, mutant protein Tachli-7A lost the ability to interact with the normal protein TaCHLI-7A, as assessed by yeast two-hybrid assay. Meanwhile, *Tachli-7A* could not recover the chlorophyll deficiency phenotype of the *Arabidopsis thaliana* SALK_050029 mutant. Furthermore, we found that in Shaannong33, the protoporphyrin IX to Mg-protoporphyrin IX ratio was growth state-dependent and insensitive to environmental change. Overall, the mutation in Tachli-7A impaired the function of Mg-chelatase and blocked the conversion of protoporphyrin IX to Mg- protoporphyrin IX. Based on our results, the *chli* mutant represents a potentially useful resource for better understanding chlorophyll and lipid biosynthetic pathways in common wheat.

Keywords: common wheat, pale-green mutant, gene clone, *CHLI*, protoporphyrin IX, lipid

INTRODUCTION

Wheat (*Triticum aestivum* L.) is one of the most important crops in the world. Nearly 35% of the human population obtains substantial caloric intake from wheat-derived food (Paux et al., 2008). As such, enhancing wheat yield remains a major goal of crop breeding (Emamgholizadeh et al., 2015). Photosynthesis plays a critical role in crop productivity and is therefore a target for plant improvement (Nasyrov, 1978). During photosynthesis, chlorophyll (Chl) pigments play key roles in light absorption (Fromme et al., 2003). It is generally believed that higher levels of solar energy conversion to chemical energy may result in a certain degree of enhanced crop biomass accumulation (Chen and Blankenship, 2011). During photosynthesis, Chl absorbs light energy, representing the first step in the conversion of light energy into chemical D:\Application Data\Microsoft\Local Settings\Application Data\youdao\dict\Application\7.5.2.0\resultui\dict\energy. Therefore, leaf Chl content is an important indicator of plant photosynthetic activity (Li et al., 2019). For example, in modern maize breeding, most grain yield increases have been primarily due to improved chloroplast structure and increased solar energy absorption by Chl (Li C. et al., 2015). Hence, Chl content is generally considered one of the major factors limiting photosynthetic efficiency (Hotta et al., 1997; Zhang et al., 2018). Solar energy capture by Chl has been known since as early as 1935 (Chlorophyll, 1935). However, gaps remain in the knowledge of Chl biosynthesis and the underlying genes in wheat. Hence, it is necessary to study the molecular basis of Chl biosynthesis in wheat to provide useful insight for improving photosynthetic efficiency. Further, Chl biogenesis is highly integrated with several critical metabolic networks, such as *de novo* fatty acid biosynthesis in the chloroplast (Wang and Benning, 2012), which not only influences plant cellular homeostasis but also impacts carbon fixation, assimilation, and distribution (Hölzl and Dörmann, 2019). Chl biosynthesis is also thought to take place upstream of a number of anabolic processes that regulate plant development, overall productivity, and adaptability to environmental change (Tripathy and Pattanayak, 2012).

Previous studies have found that Chl biosynthesis is a complex biological process involving at least 15 enzymatic reactions in Arabidopsis (*Arabidopsis thaliana*) (Tanaka and Tanaka, 2007). Specifically, a variety of enzymes and metabolites are involved in sequential reactions, which begin with glutamate formation and generate Chl a and Chl b as the end products (Beale, 2005; Tanaka and Tanaka, 2007). All genes involved in this process have been identified in Arabidopsis (Nasyrov et al., 1975; Tanaka and Tanaka, 2007). The insertion of metal ions (either Mg^{2+} or Fe^{2+}) into Proto IX is not only the major branch point in the biosynthesis of Chl- and heme-derived pigments, but it is an important regulatory step in the Chl biosynthesis pathway (**Figure 1A**) (Tanaka and Tanaka, 2007). Insertion of Mg^{2+} into Proto IX is catalyzed by magnesium chelatase (Mg-chelatase) (Jensen et al., 1996a), which is an ATP-dependent reaction (Pardo et al., 1980; Lake et al., 2004). Mg-chelatase is a heterotrimeric enzyme complex that is composed of three subunits (i.e., I, D, and H) in photosynthetic bacteria (Bollivar et al., 1994) and plants (Nakayama et al., 1995). In particular, the CHLI subunit has been classified into the AAA^+ (ATPases Associated with diverse cellular Activities) protein family according to its protein sequence and three-dimensional structure (Fodje et al., 2001; Lake et al., 2004). The CHLD subunit, which has an incomplete ATPase domain compared to CHLI, relies on the formation of an I-D complex through its interaction with CHLI to be stabilized (Hansson et al., 1999).

It is well known that the insertion of Mg^{2+} into protoporphyrin IX (Proto IX) is the most important step affecting Chl biosynthesis. Blocking this process may result in lowered Chl content and a green deficiency phenotype (Willows and Hansson, 2003). Chl deficient mutants have previously been reported in rice (Jung et al., 2003), cucumber (Gao et al., 2016), and maize (Sawers et al., 2006), all of which featured significantly decreased Chl content and pale-green leaves. The Mg-chelatase has been studied in these mutants. Particularly in rice, the mutant protein Oschli failed to interact with protein CHLD, which disrupted the biosynthesis of Mg-Proto IX. As a consequence, the Oschli mutant exhibited a yellow leaf phenotype with less Chl than wild-type Nipponbare (Zhang et al., 2015). Similarly, in cucumber C528, an amino acid substitution (G269R) occurred in subunit I protein CsChlI, which reduced Mg-chelatase enzymatic activity and resulted in a lower level of Chl and a golden-colored leaf phenotype (Gao et al., 2016). Similar mutants have also been described in barley (Jensen et al., 1996b). Presently, genes encoding subunits of Mg-chelatase have been characterized in a number of plants, but this complex remains to be further investigated in common wheat. The first observation of an albino wheat strain was made as early as 1929 (Smith and Harrington, 1929), but no genes related to leaf color have been identified to date. For example, wheat mutants ygld1, ygld2 (Li et al., 2013), and Ygm (Zhang et al., 2017) were only recently mapped to chromosomes. Not surprisingly therefore, Chl metabolism in common wheat is still unclear.

In this study, we explored the molecular mechanism underlying the wheat Chl-deficient mutant wheat *chli*, which had an amino acid mutation in the TaCHLI-7A protein (subunit I of the wheat Mg-chelatase) that resulted in decreased Chl content at the one-leaf stage and a pale-green leaf phenotype. Genetic analysis and yeast two-hybrid experiments were carried out to determine the differences between *chli* and wild-type Shaannong33 (SN33) in terms of Chl and lipid biosynthesis during wheat development. Previous studies have suggested that under saturating light conditions, photosynthetic rates in the modern wheat cultivar are associated with higher flag-leaf relative Chl content as compared with the landraces (Gaju et al., 2016). Moreover, Chl content can act as a proxy for leaf photosynthetic capacity (Inoue et al., 2016; Croft et al., 2017) and is intimately related to fatty acid biosynthesis, which is likely to influence wheat seedling development strongly. As a major regulatory point of Chl biogenesis, Mg-chelatase represents an important target for the improvement of photosynthetic efficiency (Zhang et al., 2018). Hence, our studies on *chli* open the door to a better understanding of Chl metabolism, photosynthetic regulation, and variety improvement in common wheat.

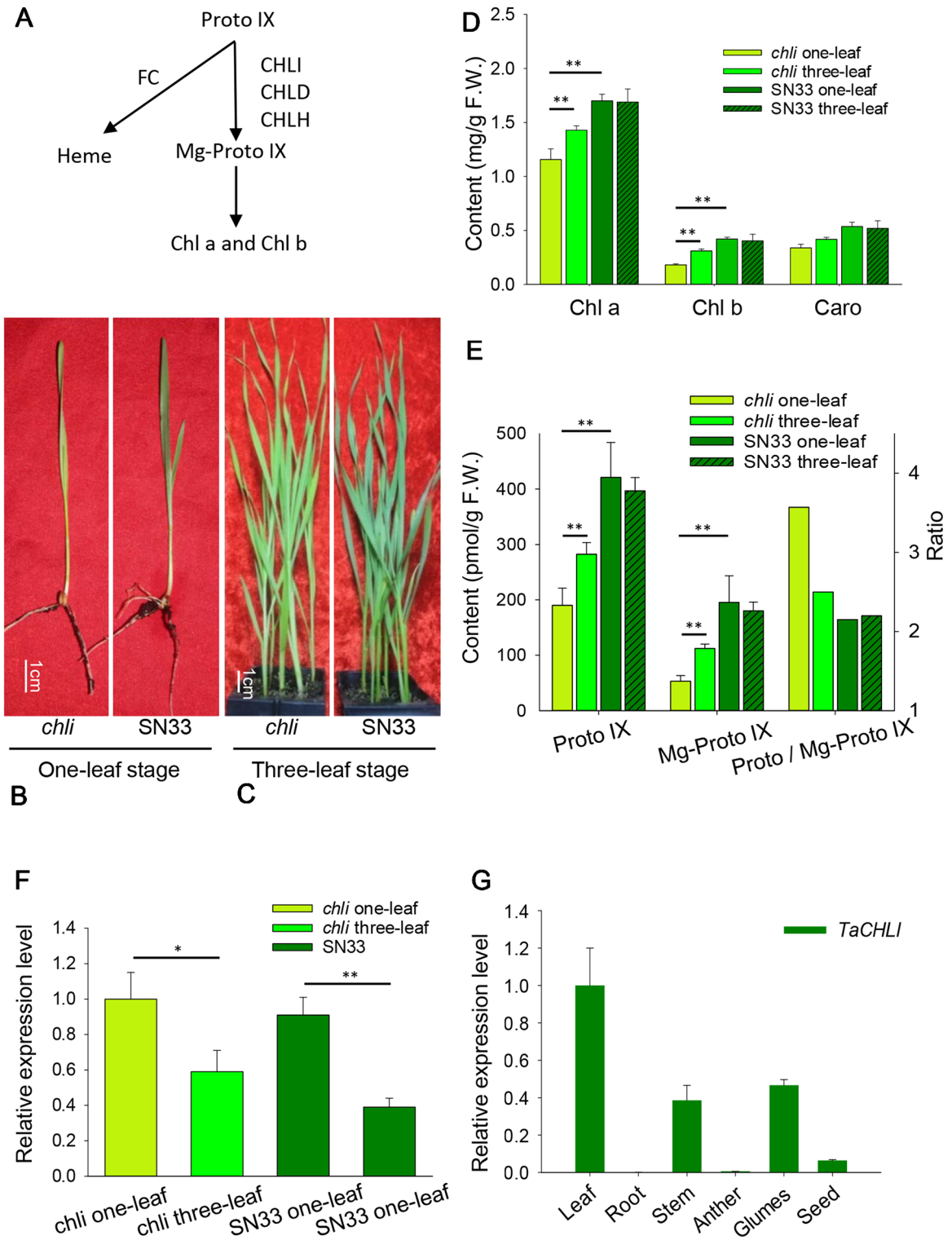

FIGURE 1 | Characterization of *chli* and SN33. **(A)** Mg-Proto IX biosynthesis in chloroplasts. FC: protoporphyrin IX ferrochelatase. **(B)** Phenotype at the one-leaf stage. **(C)** Phenotype at the three-leaf stage. **(D)** Contents of Chl a, Chl b,and Caro at the one-leaf and three-leaf stages. **(E)** Content of Proto IX and Mg- Proto IX and the Proto IX to Mg-Proto IX ratio. **(F)** Relative expression of gene *TaCHLI* in *chli* and SN33. **(G)** Relative expression of gene *TaCHLI* in different tissues. Stem was from the green part; developing seed was from 20 days after pollination. Means and standard deviations were obtained from three independent replicates with three technical replicates. F.W.: fresh weight. ** indicates significant differences at $p < 0.01$. * indicates significant differences at $p < 0.05$.

MATERIALS AND METHODS

Plant Materials and Growth Conditions

The pale-green leaf mutant *chli* was selected from bread wheat cultivar Shannnong33 (SN33, dark green used as wild type) mutant library (Li M. et al., 2015) and self-crossed until F5. For genetic analysis, two $F_{2:3}$ populations were produced from crossing *chli* × Zhongmai895 (ZM895, dark green) and ZM895 × *chli*, resulting in 190 and 211 individual lines. SN33, *chli*, and F2:3 populations were grown in plant incubator under a 16/8 h (day/night) cycle at a constant temperature of 22°C. Thirty seeds of each of the SN33, *chli*, and $F_{2:3}$ lines were seeded in a 10 cm × 10 cm pot for phenotype observation. In the heading stage of SN33, flag leaves were cut and collected at 6:00, 7:00, 8:00, 9:00, 11:00, 13:00, 15:00, and 19:00 (temperature, degrees centigrade: 18, 20, 22, 24, 27, 24, 22, and 20, respectively; light and humidity was not controlled) from a greenhouse (a glass greenhouse with light from the sun to simulate field conditions) and kept in liquid nitrogen for further analysis.

Content Measurement of Chl A, Chl B, Caro, Proto IX, and Mg-Proto IX

Chl pigments were measured at the one-leaf and three-leaf stage. Fully expanded leaf samples (0.2 g) were weighed into a 5-mL tube and ground into powder in liquid nitrogen, and 3 mL of 80% extraction buffer (water-acetone, 2:8, v/v) was then added. Each sample was soaked for 1 h in the dark. After extraction, the samples were centrifuged for 10 min at 12000 rpm. The supernatant was then filtered with 0.22-μm syringe filters (Organic-system, Sangon, China). We detected the absorbance value at wavelengths of 470, 645, and 663 nm using a spectrophotometer (SpectraMax M3; Molecular Devices, USA). The Chl and Caro contents were determined according to the equation of Lichtenthaler (Lichtenthaler, 1987). Agilent HPLC (High-Performance Liquid Chromatography) systems (Agilent 1260 Infinity II, USA) were used to determine the content of Proto IX and Mg-Proto IX (Mochizuki et al., 2008; Scharfenberg et al., 2015).

Fatty Acid Measurement

The fatty acid was measured following Gas Chromatography (GC) measurement as described previously (Li et al., 2006; Yang et al., 2019). About 10 mg dry tissue powder was esterified in 2 mL methanol with 2.5% (v/v) H_2SO_4, and 50 μg triheptadecanoin was used as internal standard. The tube was then incubated at 80°C for 120 min. Thereafter, 1 mL of hexane and 2 mL 0.9% NaCl (w/v) were added to extract fatty acid methyl esters (FAMEs). FAMEs were quantified by GC as follows: 50°C for 1 min and ramped to 175°C at 35°C/min with a 1-min temperature hold, followed by a ramp to 230°C at 4°C/min, with a final 5-min temperature hold.

DNA, RNA Extraction, and cDNA Synthesis

DNA of parent and individual lines was extracted by the CTAB method (Murray and Thompson, 1980), and total RNA was isolated by the TRIzol method (Couto et al., 2015). After extraction, the quality of the DNA and RNA was determined by gel electrophoresis using 1% agarose gel, and the concentration was measured with a spectrophotometer (SpectraMax M3; Molecular Devices, USA). gDNA-free RNA was reverse-transcribed to cDNA using the PrimeScript II 1st strand cDNA Synthesis Kit (Takara, Japan) according to the manufacturer's protocol.

Gene Mapping

The mutant gene was found to be located on chromosome 7A by using the wheat 660K SNP chip. To increase the accuracy and shorten the interval of the physical region, two DNA pools were made with the DNA from F_2 (B23×ZM895), while individuals and phenotypic evaluation were from $F_{2:3}$ lines. The DNA pool with recessive plants was composed of equal amounts of DNA from 40 homozygote pale-green plant samples. In contrast, the DNA pool with dominant plants was composed of equal amounts of DNA from 40 homozygote dark-green plant samples. The DNA of parental lines and two DNA pools were genotyped by using the 660K SNP wheat chip array. SNPs were processed with the Illumina Genome Studio Polyploid Clustering tool (v1.0) and mapped to the Chinese Spring wheat physical map (Appels et al., 2018). The distribution frequencies of polymorphisms (SNPs) on chromosomes were analyzed after SNP filtration using the following method: i. deleting the SNPs that were not detected in the Chinese Spring wheat physical map; ii. deleting the SNPs that were missing in one of two DNA pools; iii. deleting the SNPs that showed no polymorphism between parental DNA or the two DNA pools. The SNP distribution frequency ratio (polymorphism SNP numbers/total SNPs mapped to the wheat physical map) on the wheat chromosome physical map was calculated at 10 Mb physical intervals.

Primer Design and Gene Cloning

In the high-frequency distribution region of polymorphism SNPs on a chromosome, candidate genes were predicted according to the open reading frame annotation from IWGSC RefSeq v1.0 (https://wheat-urgi.versailles.inra.fr/Seq-Repository/Annotations). Potential genes were selected according to the gene annotation and previous studies, such as genes related to chlorophyll synthesis, phytochrome et al. The full-length coding sequences of *TaCHLI-7A* and *Tachli-7A* were amplified using the primer pair CHLI-F/R (**Table 1**) from leaf cDNA of SN33 and *chli,* respectively. The PCR reactions were performed by using Pfu DNA polymerase (Sangon Biotech, China),

TABLE 1 | Primers used for PCR and qPCR.

Name	Sequence (5'-3')
CHLI-F	GTGTCTCCCAATCCCTCTC
CHLI-R	ACCTCGAGAGTAATCTAGCCA
dCHLI-F	TGTCCTGCCTACAATGCGGTA
dCHLI-R	ACCTCGAGAGTAATCTAGCCA
qCHLI-F	TCACCACCACCAAGATCACCA
qCHLI-R	CTCGAACGCCTTGACACCTTC
TaActin-F	TCAGCCATACTGTGCCAATC
TaActin-R	CTTCATGCTGCTTGGTGC
Kan-F	ACGGAAGGAATGTCTCCTGCTA
Kan-R	TCCTTCCAGCCATAGCATCATGT

and then PCR products were separated by 1% agarose gel electrophoresis. The DNA fragments were then cloned into a sequencing vector for sequencing after the DNA was recovered from the agarose gel. A Cleaved Amplified Polymorphic (CAP) primer pair, dCHLI-F/R, was designed according to the mutant site in Tachli-7A (dCHLI-F can only bind to the *TaCHLI-7A* DNA sequence specifically but not to *TaCHLI-7B* and *TaCHLI-7D*) (**Figure S1**). After PCR amplification using Pfu DNA polymerase (Sangon Biotech, China), the products were digested using restriction endonuclease Tth111I (NEB) and separated by 1% agarose gel electrophoresis. The PCR reaction was run as follows: 95°C for 90 s, followed by 32 cycles of 94°C for 30 s, 58-62°C (depending on primers) for 30 s, and 72°C for 3 min.

Yeast Two-Hybrid Assay

Yeast two-hybrid analysis was performed using the GAL4 Two-Hybrid System according to the manufacturer's instructions (Matchmaker; Clontech, USA). The full-length cDNA of *TaCHLI-7A* and *Tachli-7A* were cloned into the bait vector pGBKT7 and the prey vector pGADT7, respectively. Pairs of the plasmids BD and AD were co-transformed into yeast strain AH109 according to the manufacturer's instructions. Transformants were first selected on plates containing a double-dropout SD medium (lacking Leu and Trp) and then tested on selective SD medium (lacking Leu, Trp, His, and Ade).

Gene Transformation in *Arabidopsis* Mutant and Transgenic Plant Screening

In order to confirm whether *Tachli-7A* has normal function *in vivo*, the full-length coding sequences of *TaCHLI-7A* and *Tachli-7A* were cloned into pCambia1302 vector. The recombinant vectors pCambia1302-35s*::TaCHLI-7A* and pCambia 1302-35s*:: Tachli-7A* were then transformed into the *Agrobacterium* strain GV3101. The GV3101-containing recombinant vector was then used to transform the *Arabidopsis* (Col-0) Chl-deficiency mutant (SALK_050029) homozygous lines through *Agrobacterium*-mediated transformation (Zhang X. et al., 2006). *Arabidopsis* Chl deficiency mutant SALK_050029 contains an insertion fragment at position 10203378 of chromosome 4 and shows pale-green leaves (https://abrc.osu.edu/stocks/number/SALK_050029). Transgenic lines were screened on 1/2 MS (Murashige and Skoog, 1962) plates supplemented with 25 mg L^{-1} hygromycin. In the presence of hygromycin screening medium, the positive transgenic plants exhibit roots and extend well on selective medium. By contrast, non-transgenic plants exhibit repressed root (Bent, 2006). Homozygous T_2 plants of *TaCHLI-7A* were obtained, but transgenic plants, which contained wheat mutant gene *Tachli-7A*, did not recover the Chl in leaf, had weak growth (**Figure S10 A**), and could not survive in soil after two-week selection by hygromycin. Thus, no homozygous T_2 plants of *Tachli-7A* were obtained. Multiple PCR was used to confirm the T_2 transgenic plants. The PCR reaction contained 10 μM each of primers followed the manual of Pfu DNA polymerase (Sangon Biotech, China). The primer dCAP-F/R was used to confirm the transgenic *Arabidopsis*. Kan-F/R (**Table 1**), designed for aminoglycoside phosphotransferase (Kanamycin$^+$ selection marker for bacteria, in plasmid but outside of the T-DNA region), was used to detect whether there was contamination of *Agrobacterium* that contained target plasmid. A plant tissue direct PCR Kit (OMEGA, USA) was used to confirm T_0 *Tachli-7A* transgenic plants. The normal and mutant *Arabidopsis* used in the experiment were Col-0 type.

Real-Time PCR Analysis

For Real-Time PCR analysis, primary cDNA was diluted 10 times, and 1 μl was used in a 20 μl Real-Time PCR reaction. PCR reaction and data collection were performed by using Applied Biosystems® QuantStudio® 3 (USA) with 2X SG Fast qPCR Master Mix (Low Rox) (Sangon Biotech, China). Relative gene expression levels were calculated by using the $2^{-\Delta\Delta CT}$ method with three replicates (Miao et al., 2017). All data were normalized against the expression level of the wheat actin gene. All Real-Time PCR had three replicates with three technological replicates. Melting curves and the amplification efficiency of primers used for RT-qPCR (**Figures S2**–**S5**) were tested before the experiment. An 8-fold dilution of cDNA was made to measure Ct values and to generate standard curves. The slope, R^2, and amplification efficiency were calculated by using SPSS (v17.0) (Zeng et al., 2017). For the *TaCHLI-7A* expression analysis of transgenic *Arabidopsis*, the primer pair actin-F/R from the ACTIN2 gene in *Arabidopsis* was used as the control gene (Lung et al., 2018).

Statistical Analyses

The result for each sample is shown as mean ± standard deviation (SD) from three replicates. Two-tailed Student's t-test was used to analyze the significance of differences between samples by using SPSS. P-value < 0.05 (*) and P-value < 0.01 (**) are regarded as significant.

RESULTS

Phenotypic Characterization

Under plant incubator conditions, the wild type (SN33) showed dark green leaves (**Figures 1B, C**). In contrast, the mutant *chli* expressed pale-green leaves (**Figures 1B, C**). The F_2 segregation of leaf color of crosses *chli* × Zhongmai895 and ZM895 × *chli* and also in the cross SN33 × *chli* is 3:1 (green: pale-green) (**Table 2**, **Figure S7** and **S8**). In order to explore the mechanism responsible for the pale-green leaves, pigment content was measured. Specifically, we compared SN33 and *chli* at the one-leaf stage and the three-leaf stage. Compared with SN33, the contents of Chl a, Chl b, and carotenoid (Caro) in *chli* were significantly lower, accumulating to 68.2%, 43.2%, and 62.5% of the levels observed in SN33 at the one-leaf stage, respectively (**Figure 1D**). At the three-leaf stage, the levels of Chl a, Chl b, and Caro in *chli* were 84.6%, 76.6%, and 80.4% of those in SN33, respectively. From the one-leaf stage to the three-leaf stage, increases in Proto IX and Mg-Proto IX were observed in both *chli* and SN33. In particular, a significant increase was observed in *chli*, with increases of 74.7% and 218.9% in Proto IX and Mg-

TABLE 2 | Genetic analysis of leaf color in progenies derived from the crossings *chli*×ZM895 and ZM895×*chli* at the seedling stage in greenhouse.

Crossing	Parents and generations	No. of plants			Expected ratio	χ^2	P
		YG.	Seg.	DG.			
chli×ZM895	*chli*	5		0			
	ZM895	0		5			
	F_1	0		20			
	F_2	43		168	1:3	0.051	0.82
	$F_{2:3}$	40	111	54	1:2:1	0.075	0.96
ZM895×*chli*	*chli*	5		0			
	ZM895	0		5			
	F_1	0		20			
	F_2	53		180	1:3	0.011	0.92
	$F_{2:3}$	47	96	53	1:2:1	0.009	0.99
SN33×*chli*	*chli*	5		0			
	SN33	0		5			
	F_1	0		30			
	F_2	35		86	1:3	0.029	0.86

YG, yellow-green; DG, dark-green; Seg, segregation; $F_{2:3}$: from individual of F_2; $\chi_{20.01}(1)=6.63$; $\chi_{20.01}(2)=9.21$.

Proto IX content, respectively. In contrast, Proto IX and Mg-Proto IX increased by 4.7% and -7.5% in SN33, respectively, from the one-leaf stage to the three-leaf stage. As shown in **Figure 3B**, Proto IX and Mg-Proto IX contents were consistently lower in *chli* than in SN33. At the one-leaf stage, Proto IX content in *chli* was only 32.8% of that in SN33, increasing to 60.0% at the three-leaf stage. For Mg-Proto IX, it was only 17.9% and 61.9%, respectively, at the one-leaf stage and the three-leaf stage. In SN33, the Proto IX to Mg-Proto ratio showed stable levels of 2.15 and 2.20 in the one-leaf and three-leaf stages. In contrast, the ratio was higher in *chli* in both stages but decreased from 3.75 to 2.50 from the one-leaf stage to the three-leaf stage (**Figure 1E**).

Meanwhile, we also explored the content of Proto IX and Mg-Proto IX and the Proto IX to Mg-Proto IX ratio in SN33 under simulated natural field conditions in a glass greenhouse during the flowering period. Interestingly, the content of Proto IX and Mg-Proto IX and the Proto IX to Mg-Proto ratio showed stable levels in response to changes in solar intensity, temperature, and humidity during the daytime. As shown in **Figure 6A**, under simulated field conditions, the contents of Proto IX and Mg-Proto IX between 6:00 to 19:00 were 1356 ± 102 pmol and 432 ± 29 pmol, respectively. The Proto IX to Mg-Proto IX ratio was 3.14 ± 0.08 under the same conditions. Furthermore, the contents of Proto IX and Mg-Proto IX and the Proto IX to Mg-Proto IX ratio were stable and climate-independent (**Figure 6A**). These values were, however, growth state-dependent. For example, under plant incubator conditions, the Proto IX to Mg-Proto IX ratio in SN33 was 2.16, but under simulated field conditions during daytime, the ratio was 3.14 on average.

Altered Fatty Acid Biosynthesis in Leaves and Seeds

We next sought to explore the relationship between Chl deficiency and fatty acid content in leaves and seeds. The differences in total fatty acid content in leaves and seeds are shown in **Figure 8A**. At the one-leaf stage and three-leaf stage in both leaves and seeds, the total fatty acid content was significantly lower in *chli* than in SN33. Total fatty acid content in SN33 was 4.50 (% dry weight), 4.50, and 4.65 in seeds, leaves at the one-leaf stage, and leaves at the three-leaf stage, respectively. In *chli*, these values were 3.80, 3.71, and 3.61 (% dry weight). Remarkably, the fatty acid proportion was not significantly different between *chli* and SN33 (**Figures 8B–D**).

Candidate Gene Isolation

For genetic analysis, two $F_{2:3}$ populations were generated by crossing *chli* × ZM895 and ZM895 × *chli*, which resulted in 190 and 211 individual lines (**Table 2**), respectively. Isolated DNA was hybridized on the wheat 660 K SNP chip array. After filtration, a total of 2010 polymorphic SNP probes were identified from two DNA pools and confirmed in the parental DNA. Those 2010 polymorphic SNP probes covered all 21 wheat chromosomes. Next, those 2010 polymorphic SNPs were mapped on the Chinese Spring wheat chromosomes based on IWGSC RefSeq v1.0 (**Figure 2A**).

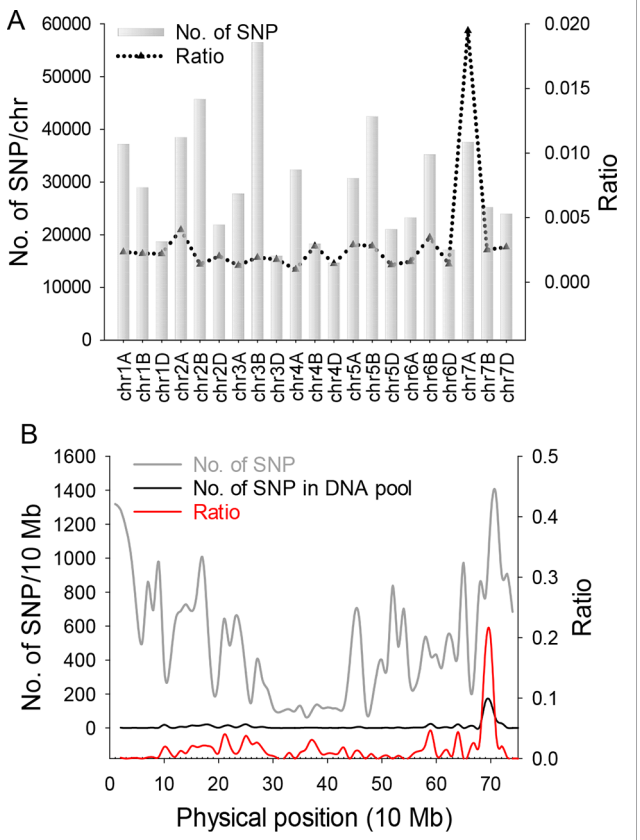

FIGURE 2 | SNP distribution calculation and statistical analysis. **(A)** SNP distribution in 21 wheat chromosomes. Gray bars indicate the total number of SNPs on 21 wheat chromosomes from the SNP chip. Black triangles indicate the ratio value (polymorphism SNP numbers)/(total SNP numbers from chip). **(B)** Gray line represents the total number of SNPs from the wheat chip on chromosome 7A. Black line indicates the number of polymorphism SNPs on 7A from two DNA pools. Red line is the ratio value (polymorphism SNP numbers)/(total SNP numbers from chip) of 7A.

A total of 732 of the 2010 polymorphic SNPs were mapped on chromosome 7AL (**Figure 2B**). This distribution frequency of polymorphic SNPs indicated that the mutant gene was located on chromosome 7AL of Chinese Spring wheat. Meanwhile, the polymorphic SNP density distribution limited the mutant gene to a ~10 Mb region in the interval 670-680 Mb between SNP probes XA-111499939 and XA-109363735 (**Figure 2B**) (based on the Chinese Spring RefSeq v1.0 sequence) (**Figure 2B**). A total of 184 putative genes were predicted in this interval, from which the candidate gene TraesCS7A01G480700.1 (chr7A:672872418-672874726) was identified (**Table S1**). Potential candidate genes were selected on the basis of the gene annotation and previous studies, such as the genes that related to chlorophyll synthesis, phytochrome, et al. Interestingly, TraesCS7A01G480700.1-encoded protein CHLI in common wheat was found in this interval, which is a major subunit of Mg-chelatase, is involved in the biosynthesis of chlorophyll, and may correspond to the mutant gene of *chli*. Thereafter, TraesCS7A01G480700.1 was referred to as *TaCHLI-7A* and selected as a potential candidate gene for further analysis.

Gene Sequencing and Marker Design

Based on the sequence of gene TraesCS7A02G480700.1 (**Figure S6**), the primer pair CHLI-seqF/R (**Table 1**) was designed to amplify the full-length cDNA of *TaCHLI* from SN33 and *chli*. As shown in **Figure 3A**, a 1266 bp-length cDNA sequence was obtained. Simultaneously, the sequencing results also revealed one single nucleotide substitution in *TaCHLI-7A* between SN33 and *chli* (**Figure 4A**). The nucleotide G in SN33 at position 664 was replaced by A in *chli*, which resulted in a single amino acid substitution (D221N) (**Figure 4B**). In parallel, it was found that this mutation did not occur in other normal wheat cultivars. All of the tested homozygote pale-green plants of F_2 contained an A at this nucleotide site. In contrast, the tested homozygote green plants of F_2 had a G while heterozygote green plants of F_2 had an A:G genotype. The primer pair dCHLI-F/R (**Table 1**) was then used to amplify part of the gene sequence of *TaCHLI-7A* and *Tachli-7A* specifically. Meanwhile, *TaCHLI-7B* on chromosome 7B and *TaCHLI-7D* on chromosome 7D were not amplified by dCHLI-F/R. Sequencing analysis of *TaCHLI-7A* revealed a Tth111I recognition site (GACNNNGTC) in the PCR products of SN33 (5′-GACNNNGTC-3′). However, the Tth111I recognition site in the PCR products of mutant *chli* (5′-AACNNNGTC-3′) was impaired by the nucleotide replacement from G (SN33) to A (*chli*) at position 664. Following the PCR amplification, the product was digested using the restriction endonucleases Tth111I (NEB). The PCR product from SN33 (GACNNNGTC) could be digested, while the product from *chli* (AACNNNGTC) could not (**Figure 3B**). Therefore, the primer pair dCHLI-F/R can be used to easily distinguish the genotype of *chli* from that of the wild type.

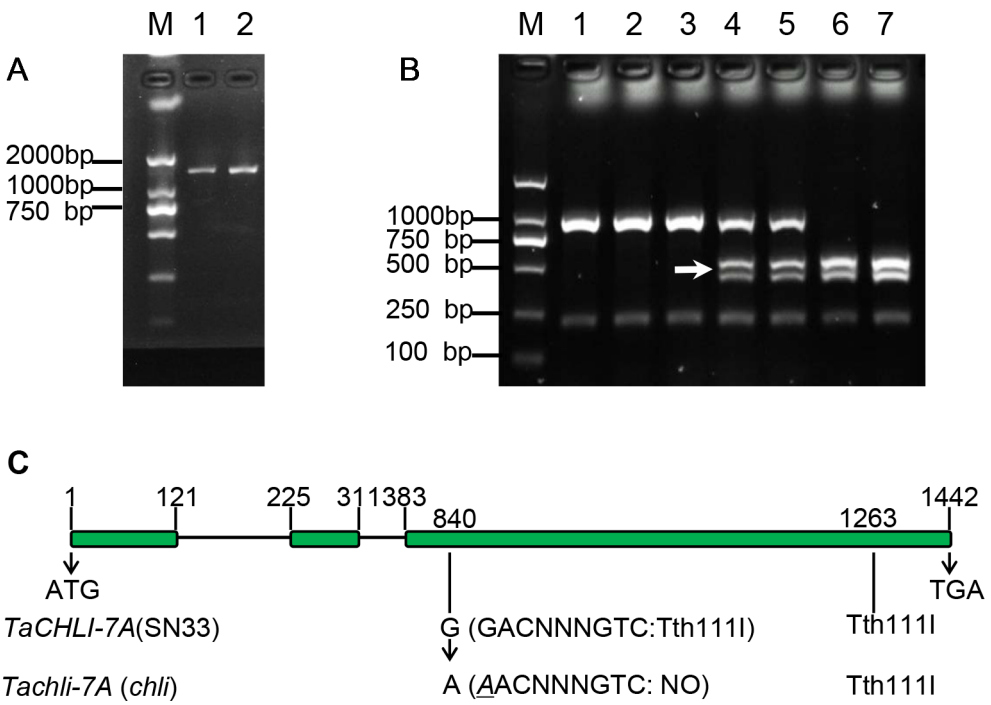

FIGURE 3 | Characterization of gene *TaCHLI* of SN33 and *chli*. **(A)** Full-length cDNA production of *TaCHLI*. M: marker; 1: SN33 cDNA; 2: *chli* cDNA. **(B)** Discrimination by CAPS marker. M: DNA marker; 1: *chli*; 2 and 3: homozygotes (yellow-green leaf) from the F_2 population; 4 and 5: heterozygotes (dark-green leaf) from the F_2 population; 6: homozygotes (dark-green leaf) from the F_2 population; 7: SN33. Arrow shows the restriction endonucleases cleavage site in *TaCHLI-7A*. **(C)** Structure and variations of *TaCHLI*. Electrophoresis was performed using 1% agarose gels.

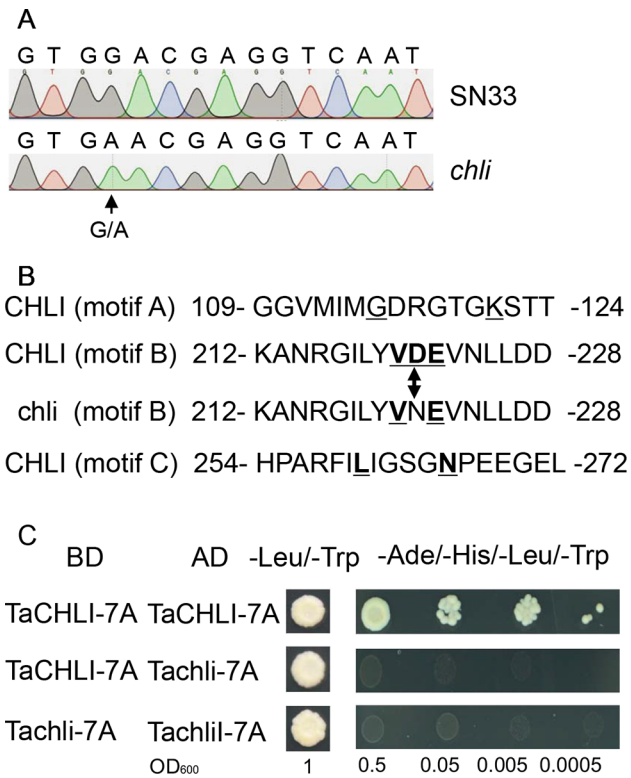

FIGURE 4 | Sequencing results and amino acid residues. **(A)** Sequencing results of *TaCHLI-7A* and *Tachli-7A*. Black arrow indicates single-nucleotide variations. **(B)** Three conserved ATPase-binding motifs of TaCHLI. Bold and underlined letters indicate the conserved residues of CHLI in SN33. Double arrow indicates conserved substitutions from D (SN33) to N (*chli*). **(C)** Yeast two-hybrid assay between TaCHLI-7A and Tachli-7A. BD: pGBKT7; AD: pGADT7; -Leu/-Trp: SD medium lacking amino acids Leu and Trp. -Ade/-His/-Leu/-Trp: SD medium lacking amino acids Ade, His, Leu, and Trp.

Yeast Two-Hybrid Assay and Transformation of the *Arabidopsis CHLI* Mutant

We cloned *TaCHLI-7A* and *Tachli-7A* into bait vector pGBKT7 and prey vector pGADT7, respectively, and the yeast two-hybrid system was used to test the interaction between them. The results showed that yeast cells that contained vector pGBKT7-*TaCHLI-7A* and pGADT7-*TaCHLI-7A* could not only grow on medium SD (-Leu/-Trp) but also on medium SD (-Ade/-His/-Leu/-Trp), which suggested that protein TaCHLI-7A could interact with itself (**Figure 4C**). However, yeast cells that contained vector pGBKT7-*TaCHLI-7A* and pGADT7-*Tachli-7A* could not grow normally on medium SD (-Ade/-His/-Leu/-Trp) (**Figure 4C**). Furthermore, yeast cells with vector pGBKT7-*Tachli-7A* and pGADT7-*Tachli-7A* did not grow normally on medium SD (-Ade/-His/-Leu/-Trp) (**Figure 4C**). In general, normal TaCHLI-7A protein could interact with itself, but it could not interact with mutant protein Tachli-7A. In addition, mutant protein Tachli-7A could not interact with itself. As shown in **Figure S10A**, the *Arabidopsis* mutant SALK_050029, which contains a mutation in the *CHLI* gene, exhibited pale-green leaves. We next transformed *35s::TaCHLI-7A* and *35s::Tachli-7A* constructs in this *Arabidopsis* mutant to confirm the function of the wheat genes. At the T_2 generation, the SALK_050029 mutant carrying *35s::TaCHLI-7A* showed a green leaf phenotype (**Figures 5C–F**) to varying degrees. In contrast, SALK_050029 carrying *35s::Tachli-7A* showed a pale-green phenotype (**Figure S10A**) and could not survive in soil after selection by hygromycin. In the T_2 generation, the content of Chl in homozygous transgenic plants was significantly higher than that in *Arabidopsis* SALK_050029 mutant (**Figure S9**), which suggested that the specific mutation in Tachli-7A impaired Mg-chelatase activity.

Expression Pattern of *TaCHLI*

We next explored the expression pattern of *TaCHLI* by using RT-qPCR. Melting curve analysis of the real-time PCR products revealed a single peak (**Figures S2** and **S4**), which confirmed the specificity of the primers. In addition, the efficiency of the primer qCHLI-F/R was 96.8%, with an R^2 is 0.99 (**Figure S3**). For *TaActin*, the primer efficiency was 99.7%, with an R^2 is 0.99 (**Figure S5**). High specificity and amplification efficiency indicated that reliable results could be obtained from this experiment. As shown in **Figure 1G**, mRNAs were most abundant in green tissues (e.g., leaves, glumes, and stems). As expected, few mRNAs could be detected in anthers and roots, which lack chloroplasts. In developing seeds, the expression level was higher than that in anthers and roots but lower than that in green tissues. These results suggested that *TaCHLI* was mainly expressed in green tissues. Therefore, we chose to only examine the expression pattern of *TaCHLI* in leaves of SN33 and *chli*. As shown in **Figure 1F**, the expression level of *TaCHLI* in *chli* was higher at the one-leaf stage than that at the three-leaf stage. A similar expression pattern was observed in SN33. Flag leaves of SN33 were collected during the flowering period in order to assess the expression pattern under field conditions. Meanwhile, we found that the expression of *CHLI* in SN33 was quite stable during the daytime (**Figure 6B**).

DISCUSSION

Previous studies have identified various leaf color mutants in common wheat (Williams et al., 1985; Zhang et al., 2017). However, only a few genes have been characterized, especially in common wheat, to date (Zhang et al., 2017). In this study, we identified a pale-green leaf mutant with Chl deficiency in the seedling stage. Genetic analysis indicated that the pale-green leaf phenotype was linked to a pair of recessive nuclear genes (**Table 2**), which is consistent with the previous reports that most of the Chl deficiency genes are recessive (Willows and Hansson, 2003). The 660K wheat SNP chip, which is generally accepted as an efficient tool for gene mapping (Wu et al., 2018), was used to localize the mutant gene to a 670-680 Mb region of wheat chromosome 7AL. In this region (**Figure 2B**), gene TraesCS7A02G480700.1 was predicted as the candidate gene and was named *TaCHLI-7A*. Interestingly, this gene shared high

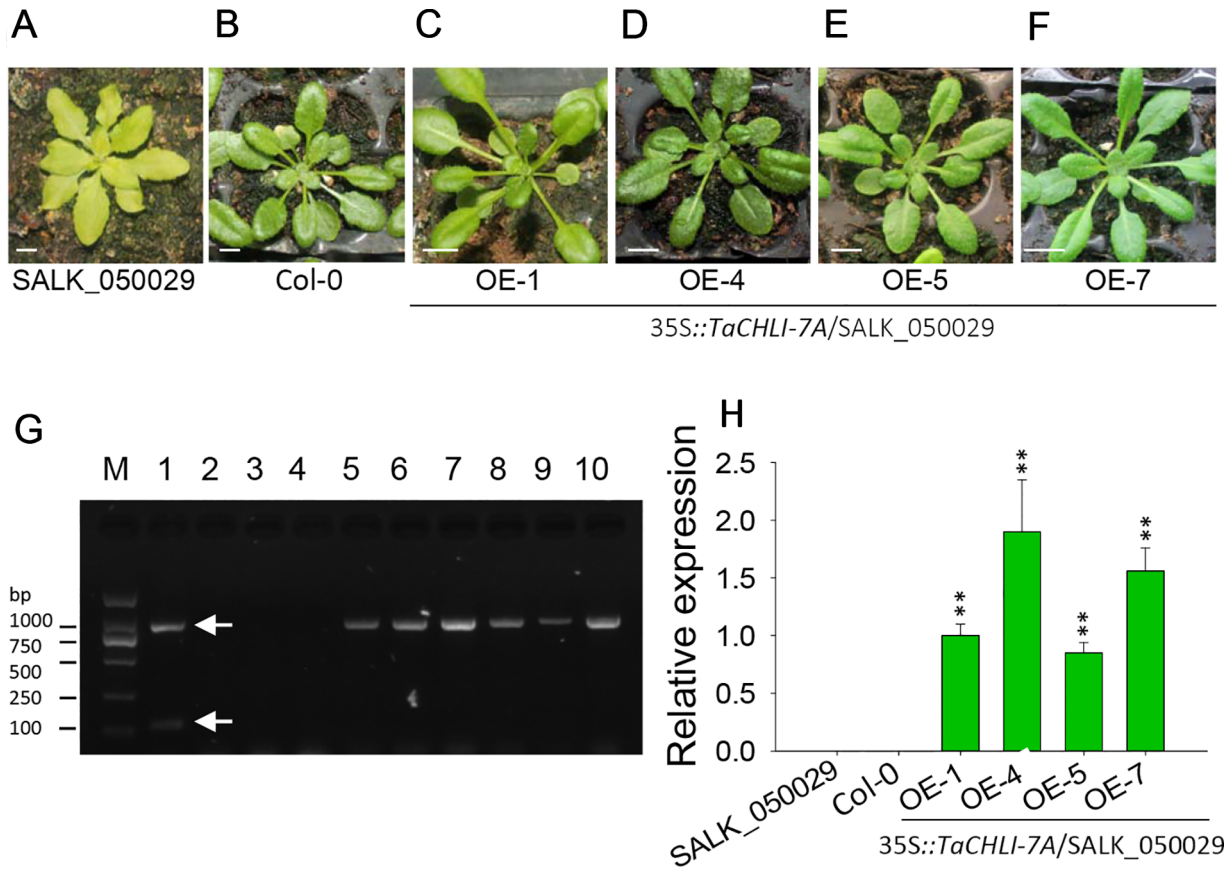

FIGURE 5 | Phenotype of homozygous T_2 transgenic plants of *Arabidopsis* SALK_050029 mutant. **(A)** 3-week-old mutant SALK_050029. **(B)** 3-week-old *Arabidopsis* (Col-0). **(C–F)** 3-week-old homozygous T_2 of 35S::*TaCHLI-7A* transgenic SALK_050029 mutant plant. **(G)** PCR results of transgenic SALK_050029 of 35S::*TaCHLI-7A* gene. M: DNA Marker; PCR templates of Lane 1-4: plasmid of 35S::*TaCHLI-7A*, water, DNA of SALK_050029, DNA of Col-0; 5 and 6: tissue of T_0 of 35S::*TaCHLI-7A* transgenic SALK_050029; 7-10: DNA of OE-1, OE-4, OE-5, OE-7 respectively. **(H)** Relative expression level of gene *TaCHLI-7A* in SALK_050029, Col-0 and transgenic *TaCHLI-7A* SALK_050029. Significant differences of the expression level were calculated by comparing WT, OE-1, OE-4, OE-5, and OE-7 with the expression level value of SALK_050029 (the value was marked as 0), calculating the expression level of OE-1 as 1. OE is overexpression. Means and standard deviations were obtained from three independent replicates with three technical replicates. ** indicates significant differences at $p < 0.01$. Bars: 1 cm. Higher white arrow in G indicates the PCR product of dCAP-F/R; lower white arrow in E indicates the PCR product of Kan-F/R.

homology with the *Arabidopsis* gene *CHLI* 1 (Apchelimov et al., 2007; Kim et al., 2009) (**Figure 7**). Sequence analysis further revealed a single-nucleotide mutation in *TaCHLI-7A* at position 664, which changed G (in SN33) to A (in *chli*) (**Figure 4A**).

CHLI is a highly conserved protein in plants (Zhang et al., 2018). As shown in the phylogenetic tree (**Figure 7**), CHLI from dicots tended to cluster together, which was also observed for monocots. Being highly conserved in protein implies that protein CHLI plays a crucial role in the determining of the Mg-chelatase activity. Previous studies indicated that CHLI belongs to a superfamily of putative DNA-dependent ATPases and contains three highly conserved motifs (i.e., motifs A, B, and D) (Walker and Willows, 1997). In mutant *chli*, the aspartic acid (D) in SN33 at position 221 was replaced by asparagine (N), which occurred on motif B of the CHLI (**Figure 4B**). Gao et al. found that the mutation in amino acid of CHLI in Cucumber resulted in Chl deficiency in plant leaves (Gao et al., 2016). This was confirmed in rice mutant *chlorina-9* (Zhang H. et al., 2006), maize mutant *Oy1* (Sawers et al., 2006), soybean mutant *yll* (Campbell et al., 2015). In short, amino acid substitution in the conserved motif may impair the enzyme activity of Mg-chelatase and then block the biosynthesis of Chl a and Chl b. This result was confirmed by an *Arabidopsis* leaf Chl-deficiency recovery experiment that showed that TaCHLI-7A could recover leaf Chl deficiency to a normal green leaf phenotype but that Tachli-7A did not function in leaf Chl-deficiency mutant SALK_050029. Meanwhile, *chli* is the first mutant in which the mutation occurred on the conserved amino acid residue in motif B.

Fatty acids play an important role in plant development, not only as one of the major constituents of cellular membranes but also as signal transductors in plant responses to various abiotic/biotic stresses (Zhang et al., 2005; Upchurch, 2008). Despite the fact that many studies have been carried out to identify factors that affect fatty acid biosynthesis in plants (Williams et al., 1988;

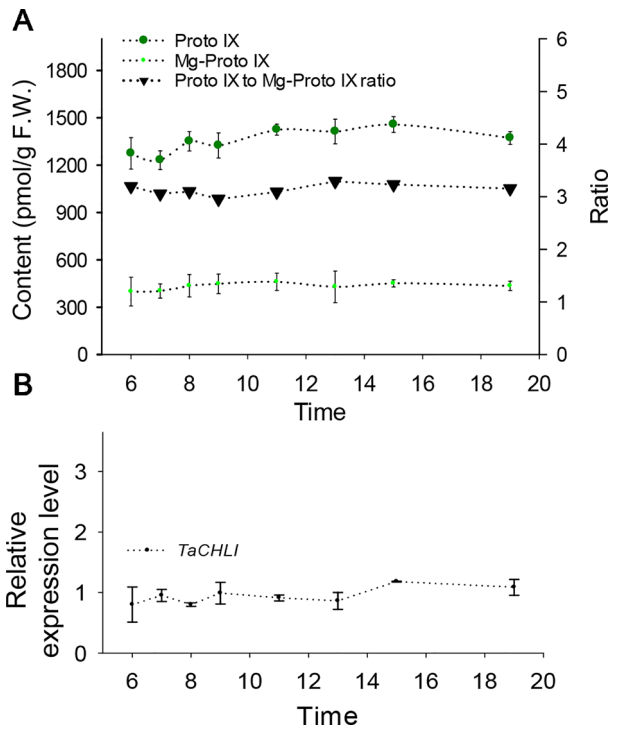

FIGURE 6 | Contents of Proto IX and Mg-Proto IX, Proto IX to Mg-Proto IX ratio, and expression level of *TaCHLI* in SN33 under simulated field conditions. **(A)** Contents of Proto IX and Mg-Proto IX and Proto IX to Mg-Proto IX ratio. **(B)** *TaCHLI* expression levels under simulated field conditions from 6:00 to 19:00. Means and standard deviations were obtained from three independent replicates with three technical replicates. F.W.: fresh weight.

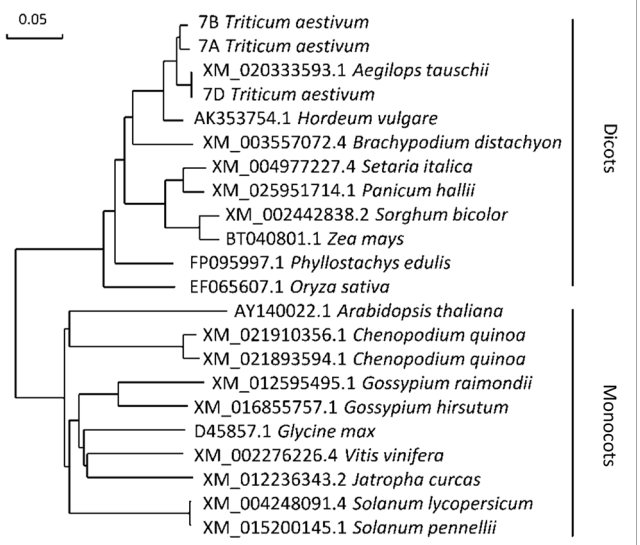

FIGURE 7 | Molecular phylogenetic analysis of gene *CHLI*. The number before the Latin name represents the accession number from the National Center for Biotechnology Information (NCBI). 7A, 7B, and 7D represent the cDNA sequences from Chinese spring wheat. Phylogenetic analysis of gene *CHLI* conducted by using the maximum likelihood method and bootstrap confidence values exceeding 80% from 1000 replicates.

Baud and Lepiniec, 2009; Luisa Hernandez et al., 2011), little is known about the relationship between Chl synthesis and fatty acid biosynthesis. Our study demonstrated that the total lipid content of both leaves and seeds (**Figure 8A**) was significantly lower in mutant *chli* than that in SN33. As plastids are the dominant site for the anabolic production of nascent lipids (Hölzl and Dörmann, 2019), large amounts of acetyl-CoA are needed (Lichtenthaler, 1999). Meanwhile, phytol, part of the Chl structure, shares a common biosynthetic precursor substrate with lipids in biosynthesis (Lichtenthaler, 1999). Additionally, photosynthesis in chloroplasts generates the ATP for fatty acid biosynthesis (Slabas and Fawcett, 1992). Hence, Chl deficiency in mutant *chli* may restrict the efficient production of ATP, thereby altering fatty acid production. Further exploration is necessary to better understand the relationship between Chl and fatty acid biogenesis, which may ultimately provide insight for improving wheat breeding and enhancing wheat grain quality (Wang et al., 2011).

Chl biosynthesis is a complex process that requires a series of enzymes. Mg-chelatase-catalyzed insertion of Mg^{2+} into Chl biosynthesis is the branching point in the biosynthesis of Chl and heme as well as being a putative critical step in Chl biosynthesis (**Figure 1A**) (Moulin and Smith, 2005). For example, rice Chl-deficiency mutant *ell* (CHLI mutant in rice) exhibited a 4.7 times higher Proto IX to Mg-Proto IX ratio than wild-type plants (Zhang et al., 2015). In our study, this ratio in *chli* (3.37 and 2.50 at the one-leaf and three-leaf stages, respectively) was higher than that in SN33 (2.15 and 2.20 at the one-leaf and three-leaf stages, respectively) (**Figure 1E**). The higher ratio of Proto IX to Mg-Proto in *chli* demonstrated that metabolic substrate conversion efficiency was blocked in *chli*. These results further confirmed that the function of Tachli-7A was impaired in *chli*. It should be noted that the content of Proto IX was lower than that in SN33. This result is different from *ell*, which showed higher levels of Proto IX content than wild type (Zhang H. et al., 2006). Interestingly, some reports have indicated that mutants blocked at CHLI do not show detectable increases in Chl intermediates (Papenbrock et al., 2000). Meanwhile, we also found that the ratio of Proto IX to Mg-Proto in SN33 was leaf development-independent (2.15 and 2.20 at the one-leaf and three-leaf stages, respectively) (**Figure 1E**), as well as being steady at around 3.14 under simulated field conditions during the daytime (**Figure 6A**). Taken together, these results demonstrated that mutation of CHLI blocked the conversion of Proto IX to Mg-Proto IX in plants. Meanwhile, different molecular mechanisms may operate in different plants to regulate Mg-chelatase activity and balance the Proto IX to Mg-proto IX ratio. More attention should be paid to this subject.

Previous studies on the self-assembly of CHLI demonstrated that the aggregated CHLI protein complex contains 6-8 CHLI subunits (Jensen et al., 1998). In the initial step of Mg-chelatase activation, the CHLI protein complex interacts with one

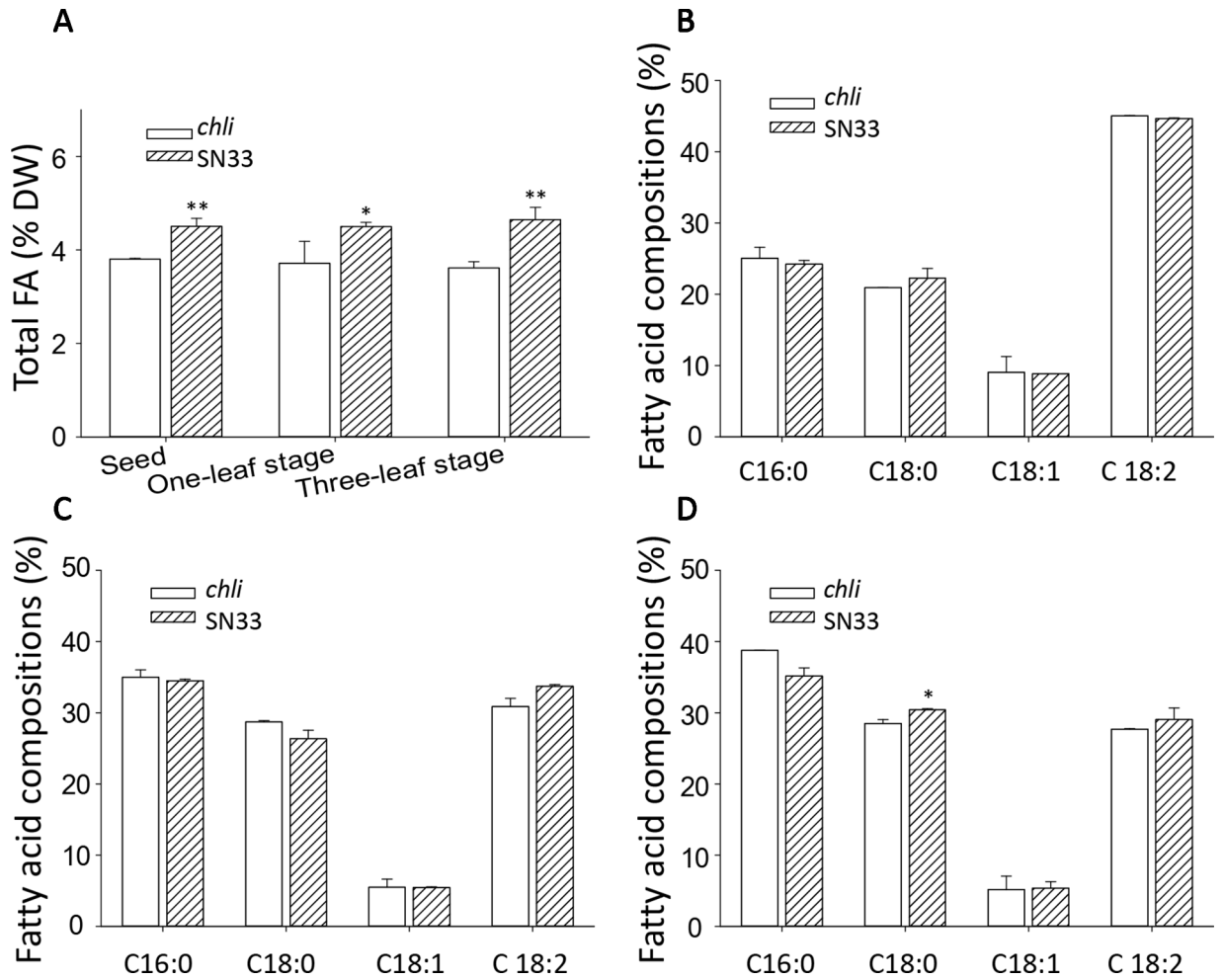

FIGURE 8 | Fatty acid content of wheat. **(A)** Total fatty acid content of seeds and leaves. **(B)** Fatty acid compositions of leaves at the one-leaf stage. **(C)** Fatty acid compositions of leaves at the three-leaf stage. **(D)** Fatty acid compositions of seeds. FA: fatty acid. SN33/*chli*: ratio of average content of SN33 to *chli*. Means and standard deviations were obtained from three independent replicates with three technical replicates. ** indicates significant differences at $p < 0.01$. * indicates significant differences at $p < 0.05$.

D subunit initially (Walker and Willows, 1997), which suggests that CHLI self-assembly is one necessary step for the Mg-chelatase. Therefore, analyzing the ability to form the CHLI protein complex provides a potential way to confirm the function of CHLI. Yeast two-hybrid assay demonstrated that the mutant protein Tachli-7A may not be able to form the protein complex, at least in the yeast two-hybrid system. Furthermore, Tachli-7A may lose the ability to interact with the D subunit. A similar result was found in the etiolated leaf and lethal mutant *ell* of rice, where the malfunctioned protein OSchli lost the ability to interact with OsCHLD, further leading to reduced contents of Mg-Proto IX and Chl (Zhang et al., 2015). It is consistent with our results that normal TaCHLI-7A protein can restore the Chl deficiency in mutant SALK_050029 (**Figure 5A**) but Tachli-7A cannot (**Figure S10A**). Hence, we infer that mutation on Tachli-7A is an important potential contributor to pale leaf formation in *chli*.

A clear expression pattern of *TaCHLI* contributes to an improved understanding of the characteristics of Chl biosynthesis. Our results indicated that the expression of *TaCHLI* showed the highest levels in leaves, was lower in developing seeds and stems, and was negligible in roots and anthers of SN33 (**Figure 1G**). This is consistent with previous studies in cucumber (Gao et al., 2016) and soybean (Zhang et al., 2018). As a major staple food (Paux et al., 2008), the growth of wheat under field conditions is influenced by many factors, such as light and temperature. Hence, it is necessary to determine how climate factors influence TaCHLI expression, as well as the content of Proto IX and Mg-Proto IX. The results (**Figure 6B**) suggested that the expression level of *TaCHLI* and the Proto IX to Mg-Proto ratio in SN33 was steady in the daytime, but interestingly, the Proto IX to Mg-Proto ratio was higher under simulated field conditions (3.14) than in a plant incubator (2.16). These results indicated that the conversion efficiency from Proto

IX to Mg-Proto is also growth-state dependent and was not affected by climate factors to a certain extent. More studies should be done to clarify the unknown mechanism behind it.

DATA AVAILABILITY STATEMENT

The raw data supporting the conclusions of this article will be made available by the authors, without undue reservation, to any qualified researcher.

AUTHOR CONTRIBUTIONS

CSW conceived the original research. CJW performed most of the experiments and wrote the article with LZ. CJW and LZ contributed equally. YL, YX, and NW prepared the plant materials and measured the phenotype. ZB modified the manuscript.

FUNDING

This project was partially supported by the National Key Research and Development Program of China (Project: 2016YFD0102101) and by the Construction Project of Nanyang Wheat Experimental Demonstration Station of Northwest A&F University (Project: A289021417).

ACKNOWLEDGMENTS

We are grateful to Mingfei Li for the creation and preservation of the original material. Dr. Zheng Yang helped us measure the fatty acids in the experiment. Dr. Xiaoyu Xu helped modified the manuscript. This study was supported by Dr. Luxiang Liu (Chinese Academy of Agricultural Sciences, CAAS) and funding from the National Key Research and Development Program of China (Project: 2016YFD0102101) and Construction Project of Nanyang Wheat Experimental Demonstration Station of Northwest A&F University (Project:A289021417).

SUPPLEMENTARY MATERIAL

The Supplementary Material for this article can be found online at: https://www.frontiersin.org/articles/10.3389/fpls.2020.00097/full#supplementary-material

REFERENCES

(1935). Chlorophyll. *Nature* 135, 275.

Apchelimov, A. A., Soldatova, O. P., Ezhova, T. A., Grimm, B., and Shestakov, S. V. (2007). The analysis of the ChlI 1 and ChlI 2 genes using acifluorfen-resistant mutant of Arabidopsis thaliana. *Planta* 225, 935–943. doi: 10.1007/s00425-006-0390-1

Appels, R., Eversole, K., Feuillet, C., Keller, B., Rogers, J., et al. (2018). Shifting the limits in wheat research and breeding using a fully annotated reference genome. *Sci. (New York N.Y.)* 361, eaar7191. doi: 10.1126/science.aar7191

Baud, S., and Lepiniec, L. (2009). Regulation of *de novo* fatty acid synthesis in maturing oilseeds of Arabidopsis. *Plant Physiol. Biochem.* 47, 448–455. doi: 10.1016/j.plaphy.2008.12.006

Beale, S. I. (2005). Green genes gleaned. *Trends Plant Sci.* 10, 309–312. doi: 10.1016/j.tplants.2005.05.005

Bent, A. (2006). "Arabidopsis thaliana floral dip transformation method" in Agrobacterium protocols. (Totowa: Humana Press), 87–104.

Bollivar, D. W., Suzuki, J. Y., Beatty, J. T., Dobrowolski, J. M., and Bauer, C. E. (1994). Directed mutational analysis of bacteriochlorophyll a biosynthesis in Rhodobacter capsulatus. *J. Mol. Biol.* 237, 622–640. doi: 10.1006/jmbi.1994.1260

Campbell, B. W., Mani, D., Curtin, S. J., Slattery, R. A., Michno, J., et al. (2015). Identical substitutions in magnesium chelatase paralogs result in Chlorophyll-Deficient soybean mutants. *G3: Genes|Genomes|Genetics* 5, 123. doi: 10.1534/g3.114.015255

Chen, M., and Blankenship, R. E. (2011). Expanding the solar spectrum used by photosynthesis. *Trends In Plant Sci.* 16, 427–431. doi: 10.1016/j.tplants.2011.03.011

Couto, D., Stransfeld, L., Arruabarrena, A., Zipfel, C., and Lozano-Duran, R. (2015). Broad application of a simple and affordable protocol for isolating plant RNA. *BMC Res. Notes* 8, 154. doi: 10.1186/s13104-015-1119-7

Croft, H., Chen, J. M., Luo, X., Bartlett, P., Chen, B., et al. (2017). Leaf chlorophyll content as a proxy for leaf photosynthetic capacity. *Global Change Biol.* 23, 3513–3524. doi: 10.1111/gcb.13599

Emamgholizadeh, S., Parsaeian, M., and Baradaran, M. (2015). Seed yield prediction of sesame using artificial neural network. *Eur. J. Agron.* 68, 89–96. doi: 10.1016/j.eja.2015.04.010

Fodje, M. N., Hansson, A., Hansson, M., Olsen, J. G., Gough, S., et al. (2001). Interplay between an AAA module and an integrin I domain may regulate the function of magnesium chelatase. *J. Mol. Biol.* 311, 111–122. doi: 10.1006/jmbi.2001.4834

Fromme, P., Melkozernov, A., Jordan, P., and Krauss, N. (2003). Structure and function of photosystem I: Interaction with its soluble electron carriers and external antenna systems. *FEBS Lett.* 555, 40–44doi.org/10.1016/S0014-5793(03)01124-4.

Gaju, O., DeSilva, J., Carvalho, P., Hawkesford, M. J., Griffiths, S., et al. (2016). Leaf photosynthesis and associations with grain yield, biomass and nitrogen-use efficiency in landraces, synthetic-derived lines and cultivars in wheat. *Field Crops Res.* 193, 1–15. doi: 10.1016/j.fcr.2016.04.018

Gao, M., Hu, L., Li, Y., and Weng, Y. (2016). The chlorophyll-deficient golden leaf mutation in cucumber is due to a single nucleotide substitution in CsChlI for magnesium chelatase I subunit. *Theor. Appl. Genet.* 129, 1961–1973. doi: 10.1007/s00122-016-2752-9

Hansson, A., Kannangara, C. G., von Wettstein, D., and Hansson, M. (1999). Molecular basis for semidominance of missense mutations in the XANTHA-H (42-kDa) subunit of magnesium chelatase. *Proc. Natl. Acad. Sci. U.S.A* 96, 1744–1749. doi: 10.1073/pnas.96.4.1744

Hölzl, G., and Dörmann, P. (2019). *Chloroplast lipids and their biosynthesis. Annual Review of Plant Biology* 70, 51–58. doi: 10.1146/annurev-arplant-050718-100202

Hotta, Y., Tanaka, T., Takaoka, H., Takeuchi, Y., and Konnai, M. (1997). Promotive effects of 5-aminolevulinic acid on the yield of several crops. *Plant Growth Regul.* 22, 109–114. doi: 10.1023/A:1005883930727

Inoue, Y., Guérif, M., Baret, F., Skidmore, A., Gitelson, A., et al. (2016). Simple and robust methods for remote sensing of canopy chlorophyll content: a comparative analysis of hyperspectral data for different types of vegetation. *Plant Cell Environ.* 39, 2609–2623. doi: 10.1111/pce.12815

Jensen, P. E., Gibson, L. C., Henningsen, K. W., and Hunter, C. N. (1996a). Expression of the chlI, chlD, and chlH genes from the Cyanobacterium synechocystis PCC6803 in Escherichia coli and demonstration that the three cognate proteins are required for magnesium-protoporphyrin chelatase activity. *J. Biol. Chem.* 271, 16662–16667. doi: 10.1074/jbc.271.28.16662

Jensen, P. E., Willows, R. D., Petersen, B. L., Vothknecht, U. C., Stummann, B. M., et al. (1996b). Structural genes for Mg-chelatase subunits in barley: Xantha-f, -g and -h. *Mol. Gen. Genet.* 250, 383–394. doi: 10.1007/bf02174026

Jensen, P. E., Gibson, L. C., and Hunter, C. N. (1998). Determinants of catalytic activity with the use of purified I, D and H subunits of the magnesium protoporphyrin IX chelatase from Synechocystis PCC6803. *Biochem. J.* 334 (Pt 2), 335–344. doi: 10.1042/bj3340335

Jung, K. H., Hur, J., Ryu, C. H., Choi, Y., Chung, Y. Y., et al. (2003). Characterization of a rice chlorophyll-deficient mutant using the T-DNA gene-trap system. *Plant Cell Physiol.* 44, 463–472. doi: 10.1093/pcp/pcg064

Kim, E., Li, X., Razeghifard, R., Anderson, J. M., Niyogi, K. K., et al. (2009). The multiple roles of light-harvesting chlorophyll a/b-protein complexes define structure and optimize function of Arabidopsis chloroplasts: a study using two chlorophyll b-less mutants. *Biochim. Et Biophys. Acta (BBA) - Bioenerg.* 1787, 973–984. doi: 10.1016/j.bbabio.2009.04.009

Lake, V., Olsson, U., Willows, R. D., and Hansson, M. (2004). ATPase activity of magnesium chelatase subunit I is required to maintain subunit D *in vivo*. *Eur. J. Biochem.* 271, 2182–2188. doi: 10.1111/j.1432-1033.2004.04143.x

Li, Y., Beisson, F., Pollard, M., and Ohlrogge, J. (2006). Oil content of Arabidopsis seeds: the influence of seed anatomy, light and plant-to-plant variation. *Phytochemistry* 67, 904–915. doi: 10.1016/j.phytochem.2006.02.015

Li, N., Jia, J., Xia, C., Liu, X., and Kong, X. (2013). Characterization and mapping of novel chlorophyll deficient mutant genes in durum wheat. *Breed. Sci.* 63, 169–175. doi: 10.1270/jsbbs.63.169

Li, C., Tao, Z., Liu, P., Zhang, J., Zhuang, K., et al. (2015). Increased grain yield with improved photosynthetic characters in modern maize parental lines. *J. Integr. Agric.* 14, 1735–1744. doi: 10.1016/S2095-3119(14)60959-X

Li, M., Xie, Y., Liu, L., Wang, C., Xu, X., et al. (2015). Construction and preliminary assessment of a mutant library of common wheat cultivar Shaannong 33 mutated with Sodium Azide. *J. Triticeae Crops* 35, 22–29. doi: 10.7606/j.issn.1009-1041.2015.01.04

Li, D., Tian, L., Wan, Z., Jia, M., Yao, X., et al. (2019). Assessment of unified models for estimating leaf chlorophyll content across directional-hemispherical reflectance and bidirectional reflectance spectra. *Remote Sens. Environ.* 231, 111240. doi: 10.1016/j.rse.2019.111240

Lichtenthaler, H. K. (1987). *Chlorophylls and carotenoids: Pigments of photosynthetic biomembranes* (Cambridge, Massachusetts: Academic Press), 350–382.

Lichtenthaler, H. K. (1999). The 1-deoxy-D-xylulose-5-phosphate pathway of isoprenoid biosynthesis in plants. *Annu. Rev. Plant Physiol. Plant Mol. Biol.* 50, 47–65. doi: 10.1146/annurev.arplant.50.1.47

Luisa Hernandez, M., Padilla, M. N., Dolores Sicardo, M., Mancha, M., and Martinez-Rivas, J. M. (2011). Effect of different environmental stresses on the expression of oleate desaturase genes and fatty acid composition in olive fruit. *Phytochemistry* 72, 178–187. doi: 10.1016/j.phytochem.2010.11.026

Lung, S., Liao, P., Yeung, E. C., Hsiao, A., Xue, Y., et al. (2018). Arabidopsis ACYL-COA-BINDING PROTEIN1 interacts with STEROL C4-METHYL OXIDASE1-2 to modulate gene expression of homeodomain-leucine zipper IV transcription factors. *New Phytol.* 218, 183–200. doi: 10.1111/nph.14965

Miao, Q., Deng, P., Saha, S., Jenkins, J. N., Hsu, C., et al. (2017). Transcriptome analysis of Ten-DPA fiber in an upland cotton (*Gossypium hirsutum*); line with improved fiber traits from Phytochrome A1 RNAi Plants. *Am. J. Plant Sci.* 08, 2530–2553. doi: 10.4236/ajps.2017.810172

Mochizuki, N., Tanaka, R., Tanaka, A., Masuda, T., and Nagatani, A. (2008). The steady-state level of Mg-protoporphyrin IX is not a determinant of plastid-to-nucleus signaling in *Arabidopsis*. *Proc. Natl. Acad. Sci. U.S.A* 105, 15184–15189. doi: 10.1073/pnas.0803245105

Moulin, M., and Smith, A. G. (2005). Regulation of tetrapyrrole biosynthesis in higher plants. *Biochem. Soc. Trans.* 33, 737–742. doi: 10.1042/BST0330737

Murashige, T., and Skoog, F. (1962). A revised medium for rapid growth and bio assays with tobacco tissue cultures. *Physiol. Plant.* 15, 473–497. doi: 10.1111/j.1399-3054.1962.tb08052.x

Murray, M. G., and Thompson, W. F. (1980). Rapid isolation of high molecular weight plant DNA. *Nucleic Acids Res.* 8, 4321–4325doi.org/10.1093/nar/8.19.4321.

Nakayama, M., Masuda, T., Sato, N., Yamagata, H., Bowler, C., et al. (1995). Cloning, subcellular localization and expression of CHL1, a subunit of magnesium-chelatase in soybean. *Biochem. Biophys. Res. Commun.* 215, 422–428. doi: 10.1006/bbrc.1995.2481

Nasyrov, Y. S., Giller, Y. E., and Usmanov, P. D. (1975). *Genetic control of chlorophyll biosynthesis and formation of its forms in vivo*. Eds. Y. S. Nasyrov and Z. Šesták (Dordrecht: Springer Netherlands), 133–145.

Nasyrov, Y. S. (1978). Genetic control of photosynthesis and improving of crop productivity. *Annu. Rev. Plant Physiol.* 29, 215–237. doi: 10.1146/annurev.pp.29.060178.001243

Papenbrock, J., Pfundel, E., Mock, H. P., and Grimm, B. (2000). Decreased and increased expression of the subunit CHL I diminishes Mg chelatase activity and reduces chlorophyll synthesis in transgenic tobacco plants. *Plant J.* 22, 155–164. doi: 10.1046/j.1365-313x.2000.00724.x

Pardo, A. D., Chereskin, B. M., Castelfranco, P. A., Franceschi, V. R., and Wezelman, B. E. (1980). ATP requirement for mg chelatase in developing chloroplasts. *Plant Physiol.* 65, 956–960doi.org/10.1104/pp.65.5.956.

Paux, E., Sourdille, P., Salse, J., Saintenac, C., Choulet, F., et al. (2008). A physical map of the 1-gigabase bread wheat chromosome 3B. *Science* 322, 101–104. doi: 10.1126/science.1161847

Sawers, R. J. H., Viney, J., Farmer, P. R., Bussey, R. R., Olsefski, G., et al. (2006). The maize oil yellow1 (Oy1) gene encodes the i subunit of magnesium chelatase. *Plant Mol. Biol.* 60, 95–106. doi: 10.1007/s11103-005-2880-0

Scharfenberg, M., Mittermayr, L., von Roepenack-Lahaye, E., Schlicke, H., Grimm, B., et al. (2015). Functional characterization of the two ferrochelatases in Arabidopsis thaliana. *Plant Cell Environ.* 38, 280–298. doi: 10.1111/pce.12248

Slabas, A. R., and Fawcett, T. (1992). The biochemistry and molecular biology of plant lipid biosynthesis. *Plant Mol. Biol.* 19, 169–191. doi: 10.1007/BF00015613

Smith, W. K., and Harrington, J. B. (1929). Wheat albinos. *J. Heredity* 20, 19–22. doi: 10.1093/oxfordjournals.jhered.a103091

Tanaka, R., and Tanaka, A. (2007). Tetrapyrrole Biosynthesis in Higher Plants. *Annual Review of Plant Biology*, 58 (1), 321–346. doi: 10.1146/annurev.arplant.57.032905.105448

Tripathy, B. C., and Pattanayak, G. K. (2012). *Chlorophyll biosynthesis in higher plants*. Eds. J. J. Eaton-Rye, B. C. Tripathy and T. D. Sharkey (Dordrecht: Springer Netherlands), 63–94.

Upchurch, R. G. (2008). Fatty acid unsaturation, mobilization, and regulation in the response of plants to stress. *Biotechnol. Lett.* 30, 967–977. doi: 10.1007/s10529-008-9639-z

Walker, C. J., and Willows, R. D. (1997). Mechanism and regulation of Mg-chelatase. *Biochem. J.* 327 (Pt 2), 321–333doi.org/10.1042/bj3270321.

Wang, Z., and Benning, C. (2012). Chloroplast lipid synthesis and lipid trafficking through ER-plastid membrane contact sites. *Biochem. Soc. Trans.* 40, 457–463. doi: 10.1042/BST20110752

Wang, Y., Sun, X., Zhao, Y., Kong, F., Guo, Y., et al. (2011). Enrichment of a common wheat genetic map and QTL mapping for fatty acid content in grain. *Plant Sci.* 181, 65–75. doi: 10.1016/j.plantsci.2011.03.020

Williams, N. D., Joppa, L. R., Duysen, M. E., and Freeman, T. P. (1985). Inheritance of three Chlorophyll-Deficient mutants of common wheat. *Crop Sci.* 25, 1023–1025. doi: 10.2135/cropsci1985.0011183X002500060030x

Williams, J. P., Khan, M. U., Mitchell, K., and Johnson, G. (1988). The effect of temperature on the level and biosynthesis of unsaturated fatty acids in Diacylglycerols of em *Brassica napus* em leaves. *Plant Physiol.* 87, 904. doi: 10.1104/pp.87.4.904

Willows, R. D., and Hansson, M. (2003). "Mechanism, structure, and regulation of magnesium chelatase,". In K. M. Kadish, K. M. Smith and R. Guilard (Eds.), *The porphyrin handbook: chlorophylls and bilins: biosynthesis, synthesis and degradation*. (San Diego: Elsevier), 1–47. doi: 10.1016/B978-0-08-092387-1.50007-2

Wu, J., Liu, S., Wang, Q., Zeng, Q., Mu, J., et al. (2018). Rapid identification of an adult plant stripe rust resistance gene in hexaploid wheat by high-throughput SNP array genotyping of pooled extremes. *Theor. Appl. Genet.* 131, 43–58. doi: 10.1007/s00122-017-2984-3

Yang, Z., Liu, X., Li, N., Du, C., Wang, K., et al. (2019). WRINKLED1 homologs highly and functionally express in oil-rich endosperms of oat and castor. *Plant Sci.* 287, 110193. doi: 10.1016/j.plantsci.2019.110193

Zeng, L., Zhu, T., Gao, Y., Wang, Y., Ning, C., et al. (2017). Effects of Ca addition on the uptake, translocation, and distribution of Cd in Arabidopsis thaliana. *Ecotoxicol. Environ. Saf.* 139, 228–237. doi: 10.1016/j.ecoenv.2017.01.023

Zhang, M., Barg, R., Yin, M., Gueta-Dahan, Y., Leikin-Frenkel, A., et al. (2005). Modulated fatty acid desaturation *via* overexpression of two distinct ω-3 desaturases differentially alters tolerance to various abiotic stresses in transgenic tobacco cells and plants. *Plant J.* 44, 361–371. doi: 10.1111/j.1365-313X.2005.02536.x

Zhang, H., Li, J., Yoo, J., Yoo, S., Cho, S., et al. (2006). Rice Chlorina-1 and Chlorina-9 encode ChlD and ChlI subunits of Mg-chelatase, a key enzyme for chlorophyll synthesis and chloroplast development. *Plant Mol. Biol.* 62, 325–337. doi: 10.1007/s11103-006-9024-z

Zhang, X., Henriques, R., Lin, S., Niu, Q., and Chua, N. (2006). Agrobacterium-mediated transformation of Arabidopsis thaliana using the floral dip method. *Nat. Protoc.* 1, 641–646. doi: 10.1038/nprot.2006.97

Zhang, H., Liu, L., Cai, M., Zhu, S., Zhao, J., et al. (2015). A point mutation of magnesium chelatase OsCHLI gene dampens the interaction between CHLI and CHLD subunits in rice. *Plant Mol. Biol. Rep.* 33, 1975–1987. doi: 10.1007/s11105-015-0889-3

Zhang, L., Liu, C., An, X., Wu, H., Feng, Y., et al. (2017). Identification and genetic mapping of a novel incompletely dominant yellow leaf color gene, Y1718, on chromosome 2BS in wheat. *Euphytica* 213, 141. doi: 10.1007/s10681-017-1894-4

Zhang, D., Chang, E., Yu, X., Chen, Y., Yang, Q., et al. (2018). Molecular characterization of Magnesium Chelatase in soybean [Glycine max (L.) Merr.]. *Front. In Plant Sci.* 9, 720. doi: 10.3389/fpls.2018.00720

Conflict of Interest: The authors declare that the research was conducted in the absence of any commercial or financial relationships that could be construed as a potential conflict of interest.

frontiers in Plant Science

ORIGINAL RESEARCH
published: 06 March 2020
doi: 10.3389/fpls.2020.00215

A Synergistic Genetic Engineering Strategy Induced Triacylglycerol Accumulation in Potato (*Solanum tuberosum*) Leaf

Xiao-yu Xu[1,2], Sehrish Akbar[1], Pushkar Shrestha[1], Lauren Venugoban[1], Rosangela Devilla[1], Dawar Hussain[1], Jiwon Lee[3], Melanie Rug[3], Lijun Tian[1], Thomas Vanhercke[1], Surinder P. Singh[1], Zhongyi Li[1], Peter J. Sharp[2]* and Qing Liu[1]**

[1] CSIRO Agriculture and Food, Canberra, ACT, Australia, [2] Plant Breeding Institute and Sydney Institute of Agriculture, School of Life and Environmental Sciences, The University of Sydney, Camperdown, NSW, Australia, [3] Center for Advanced Microscopy, The Australian National University, Canberra, ACT, Australia

OPEN ACCESS

Edited by:
Zeng-Yu Wang,
Qingdao Agricultural University, China

Reviewed by:
Hugh S. Mason,
Arizona State University, United States
Enrique Martinez Force,
Instituto de la Grasa (IG), Spain

***Correspondence:**
Qing Liu
qing.liu@csiro.au
Zhongyi Li
zhongyi.li@csiro.au
Peter J. Sharp
peter.sharp@sydney.edu.au

Specialty section:
This article was submitted to Plant Biotechnology, a section of the journal Frontiers in Plant Science

Received: 19 September 2019
Accepted: 12 February 2020
Published: 06 March 2020

Citation:
Xu X, Akbar S, Shrestha P, Venugoban L, Devilla R, Hussain D, Lee J, Rug M, Tian L, Vanhercke T, Singh SP, Li Z, Sharp PJ and Liu Q (2020) A Synergistic Genetic Engineering Strategy Induced Triacylglycerol Accumulation in Potato (Solanum tuberosum) Leaf. Front. Plant Sci. 11:215. doi: 10.3389/fpls.2020.00215

Potato is the 4th largest staple food in the world currently. As a high biomass crop, potato harbors excellent potential to produce energy-rich compounds such as triacylglycerol as a valuable co-product. We have previously reported that transgenic potato tubers overexpressing *WRINKLED1*, *DIACYLGLYCEROL ACYLTRANSFERASE 1,* and *OLEOSIN* genes produced considerable levels of triacylglycerol. In this study, the same genetic engineering strategy was employed on potato leaves. The overexpression of *Arabidopsis thaliana WRINKED1* under the transcriptional control of a senescence-inducible promoter together with *Arabidopsis thaliana DIACYLGLYCEROL ACYLTRANSFERASE 1* and *Sesamum indicum OLEOSIN* driven by the *Cauliflower Mosaic Virus 35S* promoter and small subunit of Rubisco promoter respectively, resulted in an approximately 30- fold enhancement of triacylglycerols in the senescent transgenic potato leaves compared to the wild type. The increase of triacylglycerol in the transgenic potato leaves was accompanied by perturbations of carbohydrate accumulation, apparent in a reduction in starch content and increased total soluble sugars, as well as changes of polar membrane lipids at different developmental stages. Microscopic and biochemical analysis further indicated that triacylglycerols and lipid droplets could not be produced in chloroplasts, despite the increase and enlargement of plastoglobuli at the senescent stage. Possibly enhanced accumulation of fatty acid phytyl esters in the plastoglobuli were reflected in transgenic potato leaves relative to wild type. It is likely that the plastoglobuli may have hijacked some of the carbon as the result of *WRINKED1* expression, which could be a potential factor restricting the effective accumulation of triacylglycerols in potato leaves. Increased lipid production was also observed in potato tubers, which may have affected the tuberization to a certain extent. The expression of transgenes in potato leaf not only altered the carbon partitioning in the photosynthetic source tissue, but also the underground sink organs which highly relies on the leaves in development and energy deposition.

Keywords: potato, *Solanum tuberosum*, lipids, triacylglycerol, lipid droplets, plastoglobuli

INTRODUCTION

Plant vegetative tissues such as leaves are usually viewed as 'source organs,' within which a matrix of assimilative photosynthetic activities and metabolite transport proceeds. Other tissues like seeds, fruits and tubers are considered as 'sink organs' because of their predominant functions in nutrient and energy storage (Fischer and Weber, 2002). The storage substances reserved in the sink organs are important to seed germination or sprouting and subsequent seedling establishment, whilst serving as the major economic products in agricultural production (Poxleitner et al., 2006; Graham, 2008; Yang et al., 2009; Kelly et al., 2011). Conventionally, following harvesting, the leftover vegetative biomass is either used as livestock fodder or bio-fertilizer, if not wasted. Recently the possibility to take further advantage of high biomass plants as a source of biodiesel was suggested (Vanhercke et al., 2013, 2019), as manipulation of plant metabolic networks through genetic engineering approaches has provided the insight that some non-sink plant vegetative tissues may be reprogrammed to store energy-dense compounds such as oil (Chapman et al., 2013; Xu and Shanklin, 2016).

Triacylglycerols (TAG), as the major form of oil in plants, store higher levels of energy compared to starch and cellulose and have long been regarded as the most applicable alternative feedstock of fossil fuels (Durrett et al., 2008; Carlsson et al., 2011; Chapman and Ohlrogge, 2012). Oil palm (*Elaeis guineensis*) and oilseed crops including soybean (*Glycine max*), rapeseed (*Brassica napus*) and sunflower (*Helianthus annuus*) are the current main production platforms of vegetable oils (Xu et al., 2018; Vanhercke et al., 2019). However, the ratio of oil-bearing seeds to the whole plant biomass is often small in such crops, suggesting a possibly viable value in engineering the vegetative biomass plant parts for TAG production. Presently, the functional annotations of many genes involved in lipid metabolism have been made available in model plant *Arabidopsis thaliana* and several oil-rich plant species (Costa et al., 2010; Bourgis et al., 2011; Brown et al., 2012; Nguyen et al., 2013; Higashi et al., 2015). With the increased knowledge of TAG biosynthesis and turnover, it has become possible to genetically modify oil production and accumulation in plant vegetative tissues. Whilst the current understanding of plant TAG metabolism is mostly derived from studies on oilseeds, the biochemical pathways and their regulatory mechanisms are relatively conserved between seed and vegetative plant tissues (Xu and Shanklin, 2016).

As a result, a suite of key genes regulating TAG metabolism has been identified and tested in model plants as well as some potential platform plants, showing that a multigene-based pathway manipulation of oil production in plant vegetative tissues could be feasible. Up to 15% TAG in leaf dry weight (DW) was accumulated in transgenic tobacco (*Nicotiana tabacum*) through the simultaneous overexpression of *A. thaliana WRINKLED1* (*AtWRI1*), *A. thaliana diacylglycerol acyltransferase1* (*AtDGAT1*) and sesame (*Sesamum indicum*) *OLEOSIN1* (*SiOLEOSIN1*) genes (Vanhercke et al., 2014a), coined the 'Push, Pull and Protect' synergistic strategy for oil increase (Vanhercke et al., 2014b). In addition, the C_4 plant sorghum (*Sorghum bicolor*) was recently reported to produce between 3 and 8.4% of TAG by DW in vegetative tissues following co-expression of *Zea mays WRI1, Umbelopsis ramanniana DGAT2a,* and *SiOLEOSIN* (Vanhercke et al., 2018). Further enhancement of TAG accumulation was achieved by downregulating the TAG-specific lipase sugar-dependent 1 (*SDP1*) gene, which resulted in doubled TAG production (30% of DW) in transgenic tobacco leaf (Vanhercke et al., 2017), while sugarcane (*Saccharum officinarum*) engineered with the similar methodology also displayed a 95- fold enhancement of TAG content in vegetative tissues (Zale et al., 2016).

Potato is traditionally regarded as a vegetable food rich in starch. With a global production of 388 million tonnes in 2017, potato is currently the 4^{th} largest staple food in the world (Zaheer and Akhtar, 2016). There is no doubt that the exploration of new opportunities to add value to the potato crop would be of potential benefit. We have previously applied the 'Push, Pull and Protect' strategy in potato through tuber-specific expression of *AtWRI1* driven by the patatin promoter, together with *AtDGAT1* and *SiOLEOSIN1* which led to an almost 100-fold increase in TAG levels in tuber tissues (Liu et al., 2017a). TAG increase to a lesser extent in potato tuber has also been observed when *AtWRI1* was overexpressed alone under transcriptional control of an alternative tuber-specific promoter derived from the granule bound starch synthase (*GBSS*) gene (Hofvander et al., 2016). A rather moderate increase in TAG in potato tuber was displayed through the overexpression of *A. thaliana* acetyl-CoA carboxylase (*ACCase*) (Klaus et al., 2004). As a source organ, potato leaf represents the greatest proportion of the aerial vegetative tissues, and primarily provides apoplastic sucrose to support the underground tuber growth (Fernie and Willmitzer, 2001; Hastilestari et al., 2018). Earlier research results on potato leaf molecular biology/biochemistry were mostly focused on pest control (Douches et al., 2001; Dita Rodriguez et al., 2006; Peiman and Xie, 2006; Athanikar and Badar, 2016) and photosynthetic regulation (Fleisher et al., 2006; Timlin et al., 2006; Rolando et al., 2015; Paradiso et al., 2018). The potential of potato leaves as a biofactory for TAG production is highly attractive considering the size of the aboveground biomass as a byproduct of potato production. However, earlier attempts failed to enhance TAG accumulation in potato leaf by transforming the 'Push, Pull, Protect' construct which was successfully used in generating high oil tobacco leaf (Vanhercke et al., 2014a), likely due to the strong pleiotropic effects of *AtWRI1* expression driven by the green tissue active promoter derived from the small subunit of Rubisco (*SSU*) gene (Qing Liu, unpublished data).

In this study, a senescence-inducible promoter, the Senescence Associated Gene 12 (*SAG12*) derived from *A. thaliana* (Noh and Amasino, 1999), was utilized to regulate the expression of *AtWRI1* in combination with *AtDGAT1* controlled by *CaMV-35S* promoter and *SiOLEOSIN1* controlled by *SSU* promoter. The employment of a senescence-inducible promoter in driving *AtWRI1* is anticipated to minimize the potentially undesirable pleiotropic effects of overexpressing *WRI1* on the selection of transgenic cells and subsequent growth and development of transgenic plants (Yang et al., 2015; Kong and Ma, 2018). We were able to increase TAG in potato leaf, and the effects of transgenes on other carbohydrates, mainly total starch/sugars are evaluated.

The potential factors limiting the effective accumulation of TAG in transgenic potato leaves were fundamentally explored. Further, the impacts of transgene expression on tuber constituents, morphology and production have also been assessed.

RESULTS

Validation and Assessment of Transgene Expressions in Potato Leaf and the Selection of Representative Lines for Further Analysis

A total of 17 independent primary transgenic lines were selected *via* the transformation of pOIL076 construct into potato (*Solanum tuberosum* cv Atlantic) on the kanamycin-containing media. The transgenic status of these plants was verified by polymerase chain reaction (PCR) of each of the three transgenes being overexpressed, including *AtWRI1*, *AtDGAT1* and *SiOLEOSIN1* from genomic DNA (data not shown). The analysis of the total fatty acid (TFA) contents of senescent leaves of the 17 independent T_0 transgenic potatoes showed a significant variation between 2.6 and 4.5% of leaf DW, compared to 2.4% in the wild type (WT) (**Figure 1A**). Among these transgenic lines, L3 and L5, which contained relatively high levels of TFA, 4.11 and 4.46% respectively, were selected for further analysis. Potato plants are typically propagated vegetatively by tuber-cutting. Consequently the transgenes in transgenic potato plants remain in their heterozygous status without segregation. In order to obtain synchronized growth and physiological status of potato plants for analysis, WT, L3 and L5 transgenic lines were propagated by tuber-cutting and grown under the controlled glasshouse conditions and sampled at three developmental stages including flowering, mature and senescent stages.

Transgene expression assessment was carried out through real-time quantitative reverse transcription polymerase chain reaction (qRT-PCR). The expressions of *AtWRI1*, *AtDGAT1* and *SiOLEOSIN* were not detected in WT, but showed variable expression patterns in the two selected transgenic lines during plant development, relative to the reference gene *S. tuberosum* cyclophilin (*stCYP*) (**Figures 1B,C**). *AtWRI1* displayed low yet consistent expression in both transgenic lines at the flowering stage, and was significantly increased afterward, particularly at the senescent stage in L3 (**Figure 1B**). *AtDGAT1* constantly exhibited the highest expression among the three transgenes, which peaked at the senescent stage in both L3 and L5. The expression of *SiOLEOSIN* was relatively consistent over the three developmental stages in L3 (**Figure 1B**), in contrast to L5 in which the highest expression was observed at the flowering stage (**Figure 1C**).

Characterization of Lipids and Carbohydrate Accumulations in Transgenic Lines During Plant Development

Total fatty acid contents of both L3 and L5 showed consistently significant increases compared with WT over the three developmental stages, and reached the maximum level at the mature stage as 6.19 and 7.05% of leaf DW respectively (**Figure 2B**), but reduced thereafter. There were significant variations in the contents of starch and the total soluble sugars between transgenic lines and WT. Specifically, the contents of the total soluble sugars in L3 and L5 showed about 1.4-fold reduction at the flowering stage (**Figure 2A**), but were significantly increased at the mature and senescent stages relative to WT (**Figure 2C**). The starch contents of L3 and L5 were consistently lower than WT over the entire growth period. For example, the starch content in L3 was reduced drastically to as low as 3.12% (DW) at the senescent stage, which is a 2.6-fold drop compared to 7.96% in WT (**Figure 2C**). At the mature stage, starch content in WT reached as high as 14.91% of leaf DW, in contrast to transgenic lines with rather low starch accumulations (8.77% in L3 and 4% in L5, respectively) (**Figure 2B**).

In comparison to the rather moderate increases in TFA, TAG accumulation in both L3 and L5 was much more evident over the three developmental stages (**Figure 3A**). The highest TAG contents in L3 and L5 were recorded at the senescent stage as 0.84 and 0.82% of leaf DW respectively, which was nearly 30-fold increase compared to 0.03% in WT. TAG was clearly the predominant neutral lipid across the three developmental stages in L3 and L5, peaking at the senescent stage (**Figure 3B**). The accumulation of the two galactolipids, monogalactosyldiacylglycerol (MGDG) and digalactosyldiaclglycerol (DGDG), in transgenic leaves rose significantly at the flowering stage, with L5 displaying the highest MGDG content as 1.38% (DW), which was increased nearly 2-fold compared to WT (**Figure 3C**), but subsequently dropped to a lower level in the senescent stage (**Figure 3E**). DGDG accumulation showed a similar trend of change with MGDG during the development. Phospholipids including phosphotidylcholine (PC), phosphatidylethanolamine (PE), and phosphatidylglycerol (PG) were also correspondingly varied in L3 and L5, particularly at the flowering and senescent stages. Compared to WT, contents of PC were significantly increased in the two transgenic lines at the flowering stage, and PE and PG contents in L5 were nearly doubled (**Figure 3C**). At the senescent stage, only PC remained the higher level than WT, particularly in L3 (0.36% of DW), whereas PG was barely detectable (**Figure 3E**). Despite the highest production of TFA, no significant variation was observed in polar membrane lipids between WT and transgenic plants at mature stage (**Figure 3D**).

The variation in TAG and polar membrane lipids in transgenic lines was accompanied by the alteration of fatty acid composition relative to WT (**Figures 4**, **5**). The significant reduction in the level of α-linolenic acid (ALA, C18:$3^{\Delta 9,12,15}$) in TAG and PC represented the major fatty acid change in transgenic potatoes compared to WT. Correspondingly, palmitoleic acid (C16:$1^{\Delta 9}$), oleic acid (C18:$1^{\Delta 9}$) and linoleic acid (LA, C18:$2^{\Delta 9,12}$), as well as the long chain fatty acids (LCFAs) including arachidic acid (C20:0) and the others, were all increased, particularly in TAG at the flowering and mature stages (**Figures 4A,B**). However, a significant reduction in palmitic acid (C16:0) in TAG was observed in L3 and L5 at the senescent stage, and a 3-fold increase in stearic acid (C18:0) was particularly reflected in

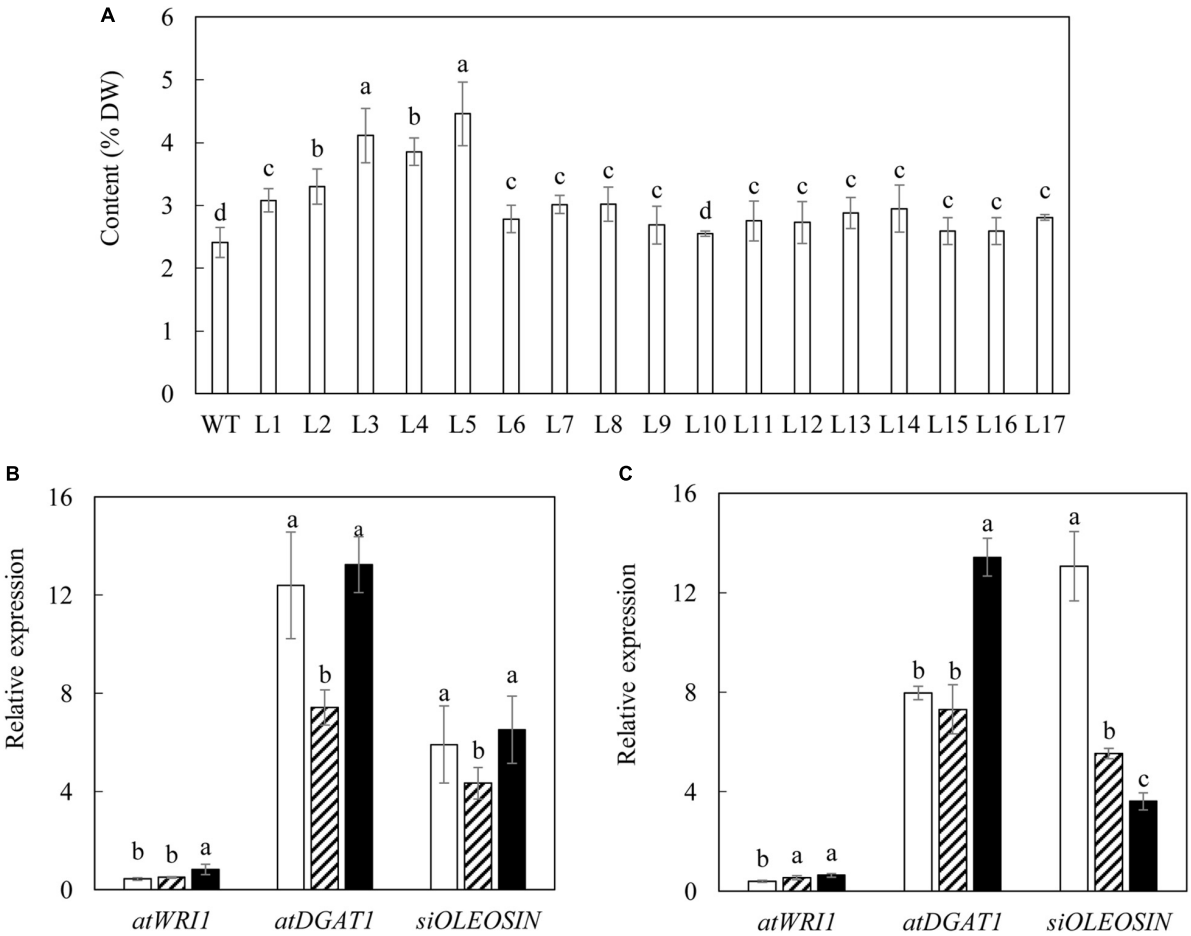

FIGURE 1 | Selection of transgenic potato plants. **(A)** TFA content in the senescent leaves of WT and seventeen selected transgenic potato lines at T_0 generation. **(B,C)** Real-time qRT-PCR analysis of gene expressions in the leaves of two selected transgenic lines, L3 **(B)** and L5 **(C)**, at the three developmental stages: flowering stage (open bar), mature stage (bar with upward diagonal) and senescent stage (black bar). The data represent the mean values ± standard deviation (SD) of three biological replicates. Letters (a, b, c, and d) above the bars are based on LSD, bars marked with different letters are statistically significantly different at $P < 0.05$.

L3 (**Figure 4C**). By comparison, such distinct fluctuations in the levels of saturated fatty acids and monounsaturated fatty acids (MUFA) were not reflected in PC throughout the leaf development (**Figures 4D–F**). In galactolipids, the fatty acid composition of transgenic lines was mainly featured by the significantly increased hexadecatrienoic acid (C16:3) in MGDG at the flowering stage (**Figure 5A**), and enhanced LA in both galactolipids at all stages, relative to WT (**Figure 5**).

Microscopic Observation of Potato Leaves Displayed Enlarged Cytosolic Lipid Droplets in Transgenic Lines and Plastoglobuli in Chloroplasts Throughout the Development

In parallel with the biochemical analysis, microscopic analysis of leaves sampled at the three developmental stages was undertaken. Both LD and plastoglobuli were observed in the mesophyll cells of potato leaves with the transmission electron microscopy (TEM) (**Figure 6**). LDs were found in the cytosol in all three samples: WT, L3 and L5, with proximity to chloroplast and mitochondria, and plastoglobuli were found inside the chloroplasts. Under the two-dimensional (2D) horizon, both LD and plastoglobuli spheres were visualized as irregular round shapes. The average diameters were therefore compared in order to reflect the possible variation in the morphology. In WT, LDs did not appear to vary significantly with the aging of the leaf, but plastoglobuli enlarged as leaves developed, the average diameter increasing more than ten times from less than 0.1 μm at the flowering stage to 1 μm in the senescent stage (**Figures 6A,D,G**). A similar observation in terms of plastoglobuli size increase was also made in L3 and L5. But, in addition to the expanding plastoglobuli, the transgenic mesophyll cells were featured with dramatically enlarged LDs often with irregular shapes. Particularly, at the flowering stage, the diameter of LDs in L3 and L5 were approximately 3 and 5 μm respectively, which was in sharp contrast to merely 1.5 μm in WT. At the senescent stage, LDs of the two transgenic lines had enlarged dramatically to about 10 μm in diameter (**Figures 6H,I**). However, the number of LDs did not show significant variation in L3 and L5 from WT when the scale bars were normalized to

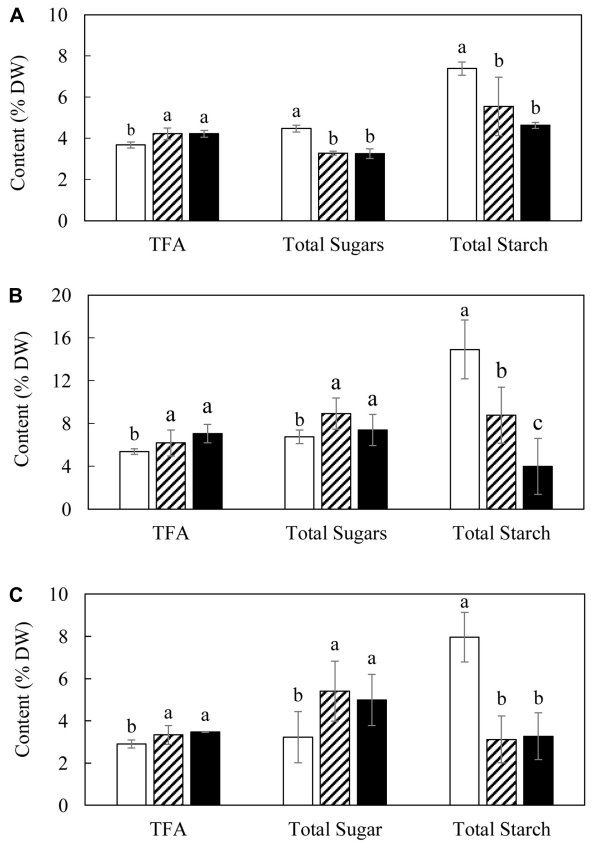

FIGURE 2 | Contents of TFA and total carbohydrate in potato leaves at the three developmental stages in WT (open bar), L3 (bar with upward diagonal) and L5 (black bar). **(A)** Flowering stage; **(B)** Mature stage; **(C)** Senescent stage. The data represent the mean values ± SD of three biological replicates. Letters (a, b, c, and d) above the bars are based on LSD, bars marked with different letters are statistically significantly different at $P < 0.05$.

1 μm in all the photographs. Starch granules were observed in abundance in all chloroplasts imaged. But compared to WT, L3 and L5 seemed to exhibit decreased numbers of starch granules and potential alteration in granule shapes (**Figures 6E,F,H**).

Acyl Distribution in TAG and Galactolipids in the Senescent Potato Leaves and Lipid Compartmentalization

In order to explore the potential factors impacting TAG production in transgenic potato leaves, characterization of the positional distribution of fatty acids in lipids specifically distributed into chloroplast and cytosol was carried out, together with the fundamental analysis of the intracellular TFA allocation and identification of one of the major components, fatty acid phytyl ester, in plastoglobuli of plant chloroplasts at the senescent stage (Rottet et al., 2015). These experiments aimed at initially exploring the potential variation in lipid compartmentalization and plastoglobuli biogenesis in potato leaves.

TAG purified from the senescent leaves of WT and two transgenic lines were digested with the *Rhizopus arrhizus* lipase, which preferentially cleaves fatty acids bonded to the outer positions (*sn*-1 and *sn*-3) of the glycerol backbone of a TAG molecule, resulting in the production of
hboxtextitsn-2 MAG and *sn*-1/3 FFA. Thus, the fatty acids in *sn*-2 MAG represent the fatty acids of *sn*-2 position of TAG and FFA molecules reflecting the acyl components of *sn*-1/3 positions. As displayed in **Table 1**, the relatively higher preference to outer positions by saturated fatty acids was observed in both WT and the transgenic lines, while unsaturated fatty acids, mainly the C18 polyunsaturated fatty acids (PUFA), showed a clear preference to the *sn*-2 position. The increase in LA largely at the expense of ALA in transgenic plants was also reflected on the *sn*-2 position. MGDG and DGDG were digested with the same lipase to yield lyso-MGDG and lyso-DGDG retaining the *sn*-2 acyl chain and releasing FFAs from the *sn*-1 position (**Tables 2**, **3**). Similar to TAG, the unsaturated fatty acids, represented by C16:3, LA and ALA, showed preference to *sn*-2 position while saturated fatty acids, mostly palmitic acid and stearic acid, were enriched at *sn*-1 position.

Confocal scanning microscopy was applied to visualize the distribution of neutral lipids in potato leaves at the senescent stage. The presence of neutral lipids mainly in the form of LD and plastoglobuli was visualized following Bodipy staining which is specific to neutral lipids (**Figure 7**). Compared with WT, significantly more abundant LDs were observed in L3 (**Figures 7C,D**) and L5 (**Figures 7E,F**). Plastoglobuli were associated with chloroplasts and appeared to be visually smaller than LD in cytosol. Such an observation was consistent with the TEM analysis. As being particularly exemplified in L5 with a further magnification, plastoglobuli, as a type of neutral lipids storage structure, were found to be overlapping with chloroplast, whereas LDs which incorporate TAG as the predominant component were found in cytosol (**Figures 7G,H**).

The acyl fatty acids derived from chloroplast and cytosol were then compared (**Figure 8**). After normalizing based on the amount of chlorophyll, the cytosolic TFA contents in potato leaves showed higher accumulation compared to the chloroplasts. Relative to WT, L3 and L5 showed a significant increase in the amount of TFA in chloroplasts but significant reduction in cytosols (**Figure 8A**). The fatty acid compositions of chloroplast and leaf were both featured by significantly increased LA at the expense of ALA in transgenic plants relative to WT, but the production of LCFAs was only identified in the leaf fatty acids (**Figure 8C**). Fatty acid phytyl esters, as one of the major components of plastoglobuli, were obtained by TLC fractionation, but slightly co-migrated with the wax ester components. At the flowering stage, significant deposition of the fatty acid phytyl esters was identified in both L3 and L5, in sharp contrast to WT in which the bands representing fatty acid phytyl esters were barely detectable on the TLC plate (**Figure 8D**), but became visible at the leaf senescent stage (**Figure 8E**).

Effects of Transgene Expressions on Mature Potato Tubers

Mature potato tubers were sampled at the leaf senescent stage in parallel with leaves for analysis. Real-time PCR indicated

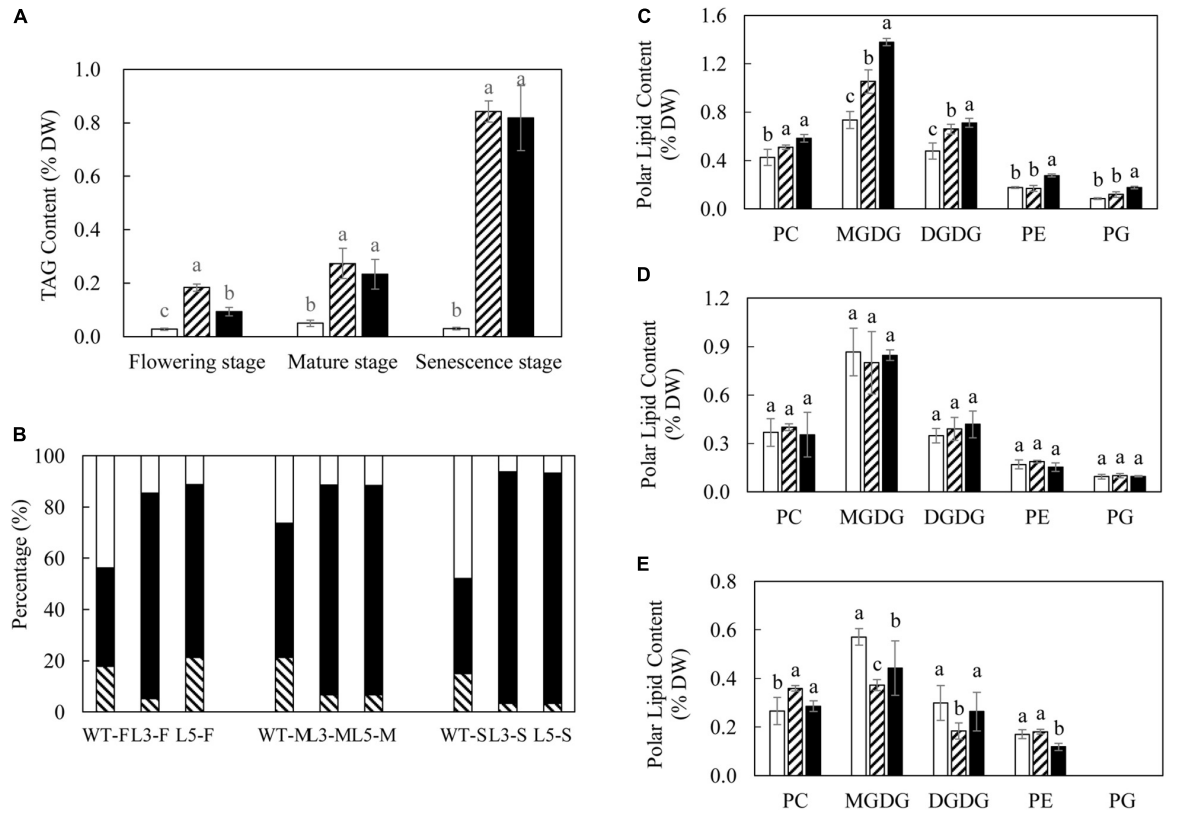

FIGURE 3 | Lipid dynamics in potato leaves at the three developmental stages. **(A)** TAG content in WT (open bar), L3 (bar with upward diagonal) and L5 (black bar); **(B)** Proportional variations of DAG (bar with downward diagonal), TAG (black bar) and FFA (open bar) at the flowering (F), mature (M), and senescent (S) stages. **(C)** Polar lipids content at the flowering stage in WT (open bar), L3 (bar with upward diagonal) and L5 (black bar); **(D)** Polar lipids content at the mature stage in WT (open bar), L3 (bar with upward diagonal) and L5 (black bar); **(E)** Polar lipids content at the senescent stage in WT (open bar), L3 (bar with upward diagonal) and L5 (black bar). The data represent the mean values ± SD of three biological replicates. Letters (a, b, c, and d) above the bars are based on LSD, bars marked with different letters are statistically significantly different at $P < 0.05$.

that the transgenes of *AtDGAT1* and *SiOLEOSIN* also showed considerable levels of expression in the tubers of L3 and L5, whereas the expression of *AtWRI1* was barely identified (**Figure 9A**). Generally, the L5 tuber displayed the highest expression levels of the two transgenes relative to L3, with *SiOLEOSIN* being the most highly expressed. As a result, significant alteration in the contents of lipids and carbohydrates was observed. In particular, TFA content of L5 was doubled and TAG increased 5-fold compared to WT (**Figure 9B**). Similarly in L3, the TAG content increased by 2-fold. The total polar lipids which accounted for the major part of tuber TFA also increased significantly in both L3 and L5 relative to WT. Interestingly, in terms of the total carbohydrate variation, L3 showed significant increase in starch content and reduction in the total soluble sugars compared to WT, but not in L5 (**Figure 9B**). The fatty acid compositions of TAG (**Figure 9C**) and total polar lipids (**Figure 9D**) in the transgenic tubers were generally consistent with the transgenic leaves, except that L3 showed enhanced ALA in polar lipids relative to WT.

The preliminary assessment of several agronomic traits of potato tubers including density, yield, water content, the number of tubers per plant, and tuber size were tabulated in **Supplementary Table 1**, with photographs recorded of the mature and healthy tubers harvested from individual plants (**Supplementary Figure 1**). Significantly, tuber density and tuber water content of L3 and L5 were both reduced compared to WT, accompanied by relatively increased tuber yields (recorded as total fresh tuber weight). However, the number of tubers produced per plant, as well as the tuber size, has been significantly reduced in L3. Tubers were divided into four size groups (Size A, B, C, D) from the large size to small size by the maximum tuber length per potato. Tubers clustered in Size C (3 cm < tuber length < 6 cm) represented the largest proportion in WT and L5 (51.26 and 40.65%, respectively), while the Size A (tuber length > 9 cm) represented the largest proportion in L3 (34.38%). Accordingly, L3 showed the highest average weight of a single tuber, compared to WT and L5.

DISCUSSION

Plant leaves are the predominant source organ supporting high plant biomass establishment (Badeck et al., 2005; Ainsworth and Bush, 2011; Yaseen et al., 2013). Previous

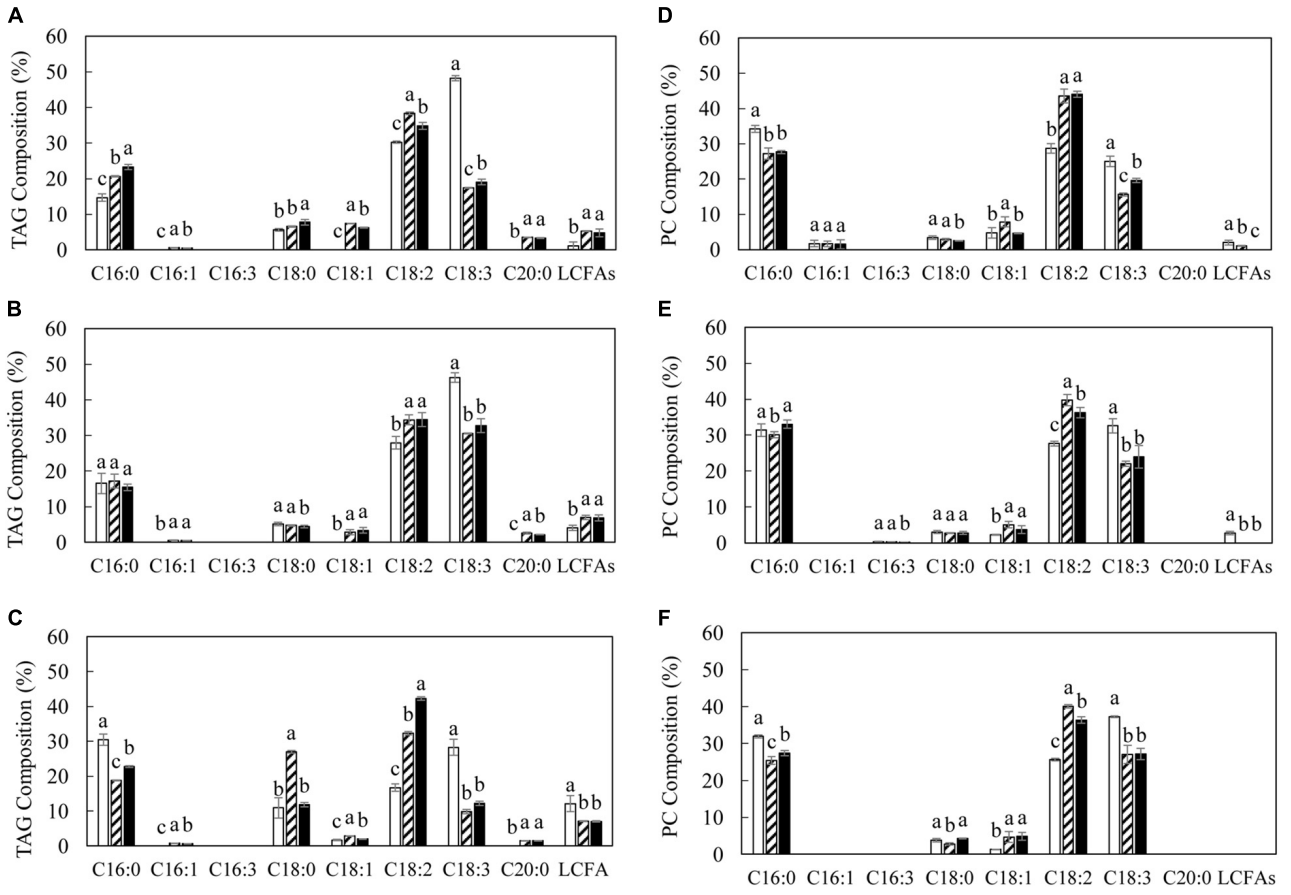

FIGURE 4 | Fatty acid compositions of TAG and PC in potato leaves at the three developmental stages in WT (open bar), L3 (bar with upward diagonal) and L5 (black bar). **(A–C)** TAG at the flowering, mature, senescent stages respectively; **(D–F)** PC at the flowering, mature, senescent stages respectively. The data represent the mean values ± SD of three biological replicates. Letters (a, b, c, and d) above the bars are based on LSD, bars marked with different letters are statistically significantly different at $P < 0.05$.

research on metabolic engineering of TAG in plant vegetative tissues were carried out in both model plants such as Arabidopsis (Fan et al., 2013, 2014) and tobacco (Vanhercke et al., 2014a, 2017), and high biomass crops such as sugarcane (Zale et al., 2016), potato tuber (Hofvander et al., 2016; Liu et al., 2017a), and sorghum (Vanhercke et al., 2018). This study applied the previously reported 'Push, Pull and Protect' genetic engineering strategy in potato leaf using the senescence-inducible promoter *SAG12* to drive the *AtWRI1* transcriptional factor, to minimize the undesirable effects of excessive expression of *WRI1* on plant development as most of the critical biological processes have been completed at the plant senescent stage (Gregersen et al., 2013; Avila-Ospina et al., 2014; Yang et al., 2015). The *CaMV-35S* promoter driving for constitutive gene expression was able to maintain a high level of *AtDGAT1* expression without causing substantial disturbance to plant development (Bouvier-Navé et al., 2000; Vanhercke et al., 2014a). *SSU* promoter is highly active in plant green tissues (Reiss et al., 1987) and used to control expression of the LD integral protein *SiOLEOSIN1* to assist in TAG packaging within the leaves.

Consistent with the observations made in transgenic tobacco leaf producing high levels of TAG (Vanhercke et al., 2014a, 2017), enhanced TAG accumulation in potato leaves was accompanied by total starch reduction and increase in soluble sugars, followed by varied equilibrium between neutral and polar lipids as well as altered fatty acid compositions. However, the increment of TAG varied significantly between these two *Solanaceae* species. The transgenic tobacco displayed 15% TAG of leaf DW (Vanhercke et al., 2014a), whereas in the transgenic potato leaves TAG was limited to just 0.8% of leaf DW (**Figure 3A**). In the high oil transgenic tobacco leaf, abundant LDs with large and irregular shapes were accumulated in the cytosol (Vanhercke et al., 2014a). However, in transgenic potato leaf, in addition to the significantly enlarged cytosolic LDs relative to WT under the 2D horizon, the increases in the number and size of plastoglobuli were also observed, which was in contrast to the observation made in transgenic tobacco leaf. Such discrepancies suggested that the three transgenes functioned in a similar pattern as in tobacco leaf, but clearly less effective in potato leaf. Although we could not rule out the possibility of insertion loci of transgene cassettes into a relatively inactive

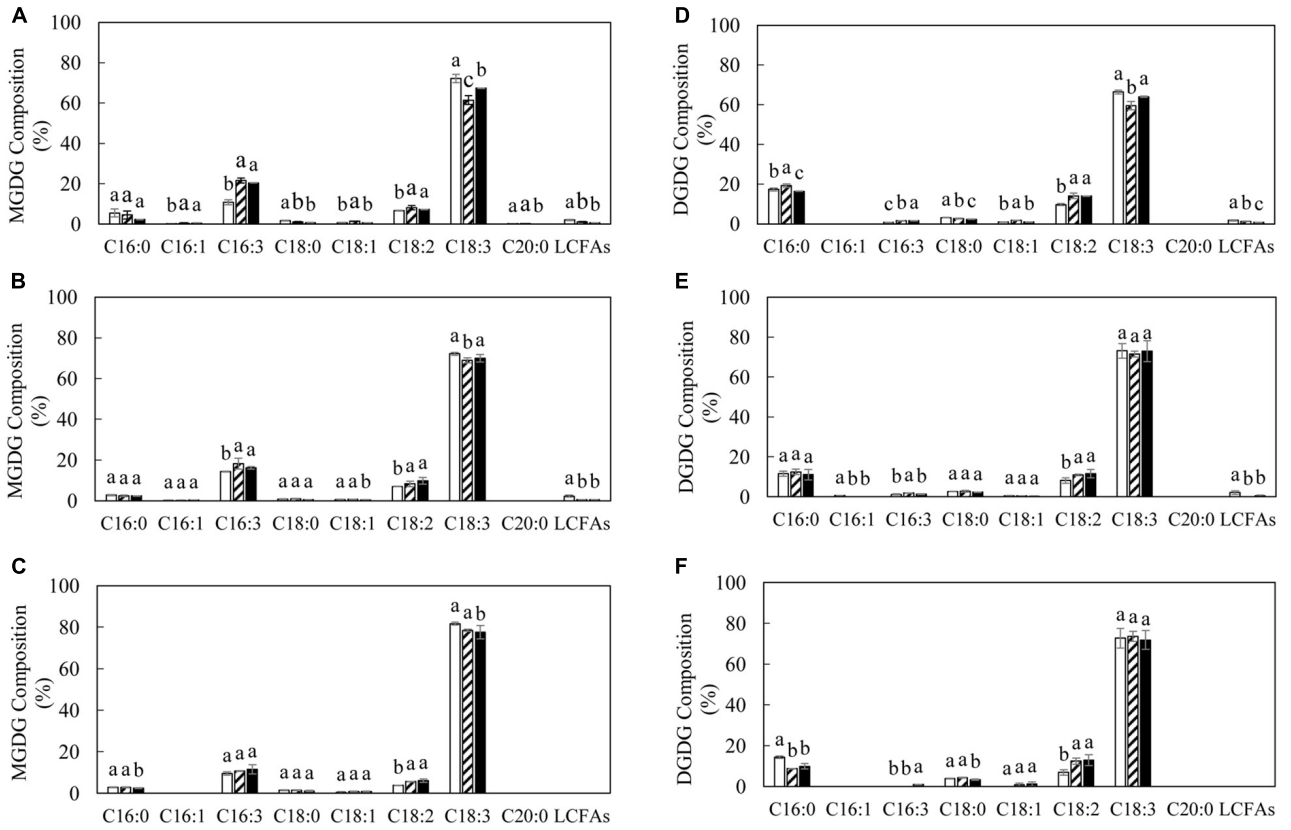

FIGURE 5 | Fatty acid compositions of MGDG and DGDG in potato leaves at the three developmental stages in WT (open bar), L3 (bar with upward diagonal) and L5 (black bar). **(A–C)** MGDG at the flowering, mature, senescent stages respectively; **(D–F)** DGDG at the flowering, mature, senescent stages respectively. The data represent the mean values ± SD of three biological replicates. Letters (a, b, c, and d) above the bars are based on LSD, bars marked with different letters are statistically significantly different at $P < 0.05$.

region of chromosome (Finnegan and McElroy, 1994; Kumar and Fladung, 2002; Bradford et al., 2005), it is more likely that the metabolic differences between tobacco and potato leaves is attributable to a certain extent. Potato leaves have evolved a system for rapid and efficient transfer of metabolites to stolon to support the underground tuber development (Fernie et al., 2002; Geigenberger, 2003; Roessner-Tunali et al., 2003). This is distinctive from tobacco leaf which has been selected as a highly productive organ (Vanhercke et al., 2014a).

Expression of the three transgenes has been discussed in transgenic potato tuber (Liu et al., 2017a) and tobacco leaf (Vanhercke et al., 2014a). In particular, *AtDGAT1* under the control of *CaMV-35S* promoter was the most highly expressed transgene, which has been viewed as a critical rate-limiting enzyme in TAG biosynthesis (Chapman et al., 2013; Xu and Shanklin, 2016). In this study, at the flowering stage, L3 had a significantly higher expression level of *AtDGAT1* than in L5 (**Figure 1B**), which was coincidental to a 2-fold higher TAG accumulation in L3 relative to L5 (**Figure 2A**). However, a significant boost of TAG synthesis in both transgenic lines was observed in the senescent stage, when the expression of *AtWRI1* was significantly increased. Despite the inconsistent expression levels of *SiOLEOSIN* (**Figure 1B**), similar levels of TAG accumulation were found at the senescent stage in both transgenic lines. The poor correlation between *SiOLEOSIN1* gene expression and TAG accumulation may suggest that the TAG production in transgenic potato leaves depends highly on the expression of *AtWRI1* and *AtDGAT1* transgenes, while *SiOLEOSIN* may not function as a major contributor. Further, the possibly enlarged size of LDs could have resulted from LD fusion and represented instability and vulnerability of LDs for degradation (Vanhercke et al., 2014a). The rapid rise in TAG accumulation in the senescent stage demonstrated the functionality of *AtWRI1* as a key gene in upregulating TAG biosynthesis with even lower expression levels relative to other transgenes (Maeo et al., 2009; Baud et al., 2009; To et al., 2012; Ma et al., 2015).

The alteration in leaf fatty acid compositions in L3 and L5 was consistent with the high oil transgenic tobacco leaf and potato tuber. The increase in LA and LCFAs and the reduction in ALA remained a hallmark of the 'Push, Pull and Protect' strategy, likely as the result of *AtWRI1* expression which impacts on the expression of fatty acid desaturases and fatty acid elongases (To et al., 2012; Liu et al., 2017a), from which other fatty acids such as the MUFA were affected. The expression of *SiOLEOSIN* may

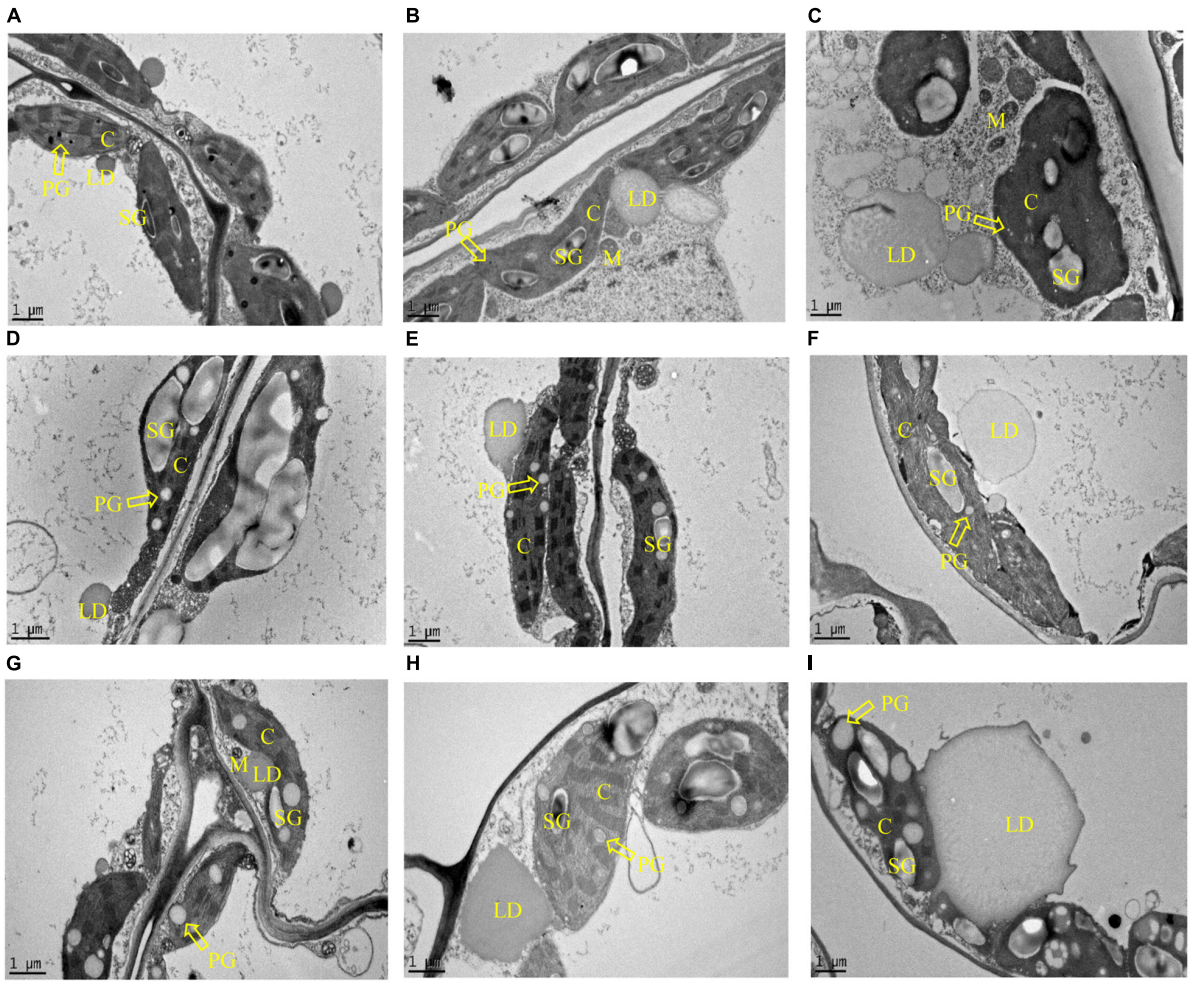

FIGURE 6 | TEM imaging of the intracellular structures in potato leaves in the three developmental stages. Lipid droplet (LD), plastoglobuli (PG), chloroplast (C), starch granule (SG), and mitochondria (M) can be clearly visualized. The arrowheads point at PG. **(A–C)** Sections of leaf cells in WT, L3, and L5, respectively at the flowering stage; **(D–F)** Sections of leaf cells in WT, L3, and L5, respectively at the mature stage; **(G–I)** Sections of leaf cells in WT, L3, and L5, respectively at the senescent stage. PGs were observed in the chloroplast and LDs in the cytosol. L3 and L5 seem to display enlarged size but irregular morphology of LDs compared to WT, while PGs showed a similar trend of enlargement with LDs in plant development in both WT and the two transgenic lines. The scale bars correspond to 1 μm.

TABLE 1 | Positional distribution of fatty acids in TAG of potato senescent leaves.

Sample	Position	C16:0	C16:1	C16:3	C18:0	C18:1$^{\Delta 9}$	C18:1$^{\Delta 11}$	C18:2	C18:3	C20:0	C20:2	C22:0	C24:0
WT	Original	34.7	0.0	0.0	12.4	1.9	0.0	19.0	32.0	0.0	0.0	0.0	0.0
	sn-2	27.0	0.0	0.0	16.7	0.0	0.0	28.8	27.4	0.0	0.0	0.0	0.0
	sn-1/3	38.5	0.0	0.0	10.2	2.9	0.0	14.0	34.3	0.0	0.0	0.0	0.0
L3	Original	20.2	0.8	0.0	29.1	3.0	0.0	34.8	10.5	1.6	0.0	0.0	0.0
	sn-2	19.0	0.0	0.0	14.9	3.0	0.0	35.7	27.4	0.0	0.0	0.0	0.0
	sn-1/3	20.8	1.1	0.0	36.1	3.0	0.0	34.3	2.1	2.4	0.0	0.0	0.0
L5	Original	24.5	0.6	0.0	12.7	2.2	0.0	45.4	13.0	1.6	0.0	0.0	0.0
	sn-2	11.5	0.0	0.0	8.5	3.5	0.0	41.3	35.2	0.0	0.0	0.0	0.0
	sn-1/3	31.0	1.0	0.0	14.8	1.5	0.0	47.4	1.9	2.4	0.0	0.0	0.0

partially affect the membrane lipid constitution, for example PC, which is a major component of the phospholipids coating LDs (Chapman et al., 2012; Liu et al., 2017a). In transgenic potato lines, MGDG and DGDG were increased significantly at the flowering stage, but drastically reduced at the subsequent senescent stage. This could be due to the natural disintegration of the cellular membrane and chlorophyll catabolism which led to the degradation of photosynthetic membrane lipids, and

TABLE 2 | Positional distribution of fatty acids in MGDG of potato senescent leaves.

Sample	Position	C16:0	C16:1	C16:3	C18:0	C18:1$^{\Delta 9}$	C18:1$^{\Delta 11}$	C18:2	C18:3	C20:0	C20:2	C22:0	C22:2	C24:0
WT	Original	2.8	0.0	9.5	1.5	0.7	0.0	3.8	81.7	0.0	0.0	0.0	0.0	0.0
	sn-1	16.5	0.0	0.0	19.1	0.0	0.0	5.0	59.4	0.0	0.0	0.0	0.0	0.0
	sn-2	6.8	0.0	19.1	8.6	0.0	0.0	5.7	59.8	0.0	0.0	0.0	0.0	0.0
L3	Original	2.8	0.0	10.6	1.4	0.9	0.0	5.6	78.7	0.0	0.0	0.0	0.0	0.0
	sn-1	18.5	0.0	0.0	23.8	1.2	0.0	8.2	48.3	0.0	0.0	0.0	0.0	0.0
	sn-2	9.8	0.0	24.0	13.2	0.0	0.0	10.2	42.8	0.0	0.0	0.0	0.0	0.0
L5	Original	2.4	0.0	11.6	1.5	0.8	0.0	6.1	77.6	0.0	0.0	0.0	0.0	0.0
	sn-1	13.8	0.0	0.0	14.2	1.2	0.0	9.2	59.8	1.0	0.0	0.8	0.0	0.0
	sn-2	7.2	0.0	26.0	10.3	0.9	0.0	10.1	45.5	0.0	0.0	0.0	0.0	0.0

TABLE 3 | Positional distribution of fatty acids in DGDG of potato senescent leaves.

Sample	Position	C16:0	C16:1	C16:3	C18:0	C18:1$^{\Delta 9}$	C18:1$^{\Delta 11}$	C18:2	C18:3	C20:0	C20:2	C22:0	C22:2	C24:0
WT	Original	14.3	0.0	0.0	3.8	0.0	0.0	6.9	75	0.0	0.0	0.0	0.0	0.0
	sn-1	32.8	0.0	0.0	15.5	0.0	0.0	6.9	44.8	0.0	0.0	0.0	0.0	0.0
	sn-2	22.2	0.0	0.0	2.6	0.0	0.0	13.7	61.5	0.0	0.0	0.0	0.0	0.0
L3	Original	8.7	0.0	0.0	4.3	0.9	0.0	12.4	73.7	0.0	0.0	0.0	0.0	0.0
	sn-1	31.8	0.0	0.0	16.0	2.1	0.0	8.2	41.9	0.0	0.0	0.0	0.0	0.0
	sn-2	19.4	0.0	0.0	3.2	0.0	0.0	11.8	65.6	0.0	0.0	0.0	0.0	0.0
L5	Original	9.8	0.0	0.9	3.3	1.3	0.0	12.9	71.8	0.0	0.0	0.0	0.0	0.0
	sn-1	30.1	0.0	0.0	14.4	2.4	0.0	8.5	44.6	0.0	0.0	0.0	0.0	0.0
	sn-2	22.6	0.0	0.0	8.7	2.5	0.0	11.3	54.9	0.0	0.0	0.0	0.0	0.0

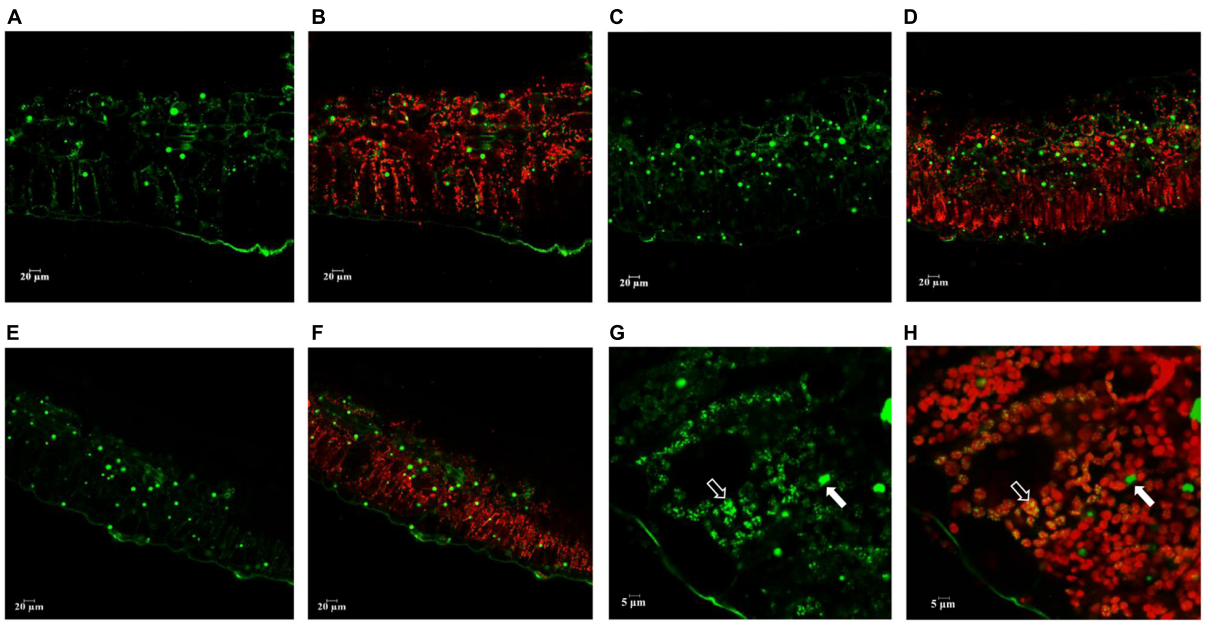

FIGURE 7 | Confocal microscopy analysis of the neutral lipid droplets distribution in the senescent potato leaves. Neutral lipid droplets were stained with Bodipy (green), and the autofluorescence of chloroplasts was visualized in red. **(A,B)** Fresh leaf sections of WT; **(C,D)** Fresh leaf sections of L3; **(E,F)** Fresh leaf sections of L5; **(G,H)** Magnified leaf sections of L5 as an example. Plastoglobuli (marked in white open arrow head) and LD (marked in closed open arrow head) showed exclusive distribution in the cellular compartments, with plastoglobuli highly attached with the chloroplast and LD accumulated in the cytosol. The scale bars are located in the lower left corner for each photograph, images **(A–F)** (20 μm), images **(G,H)** (5 μm).

further impact on the reallocation of plastidial acyl flux (Hölzl and Dörmann, 2019). The perturbation of membrane lipids not only affects to the compartmentalization of lipid metabolism, but also the biogenesis of plastoglobuli which are a class of unique lipoprotein organelle exclusively existing inside the chloroplast (Rey et al., 2000).

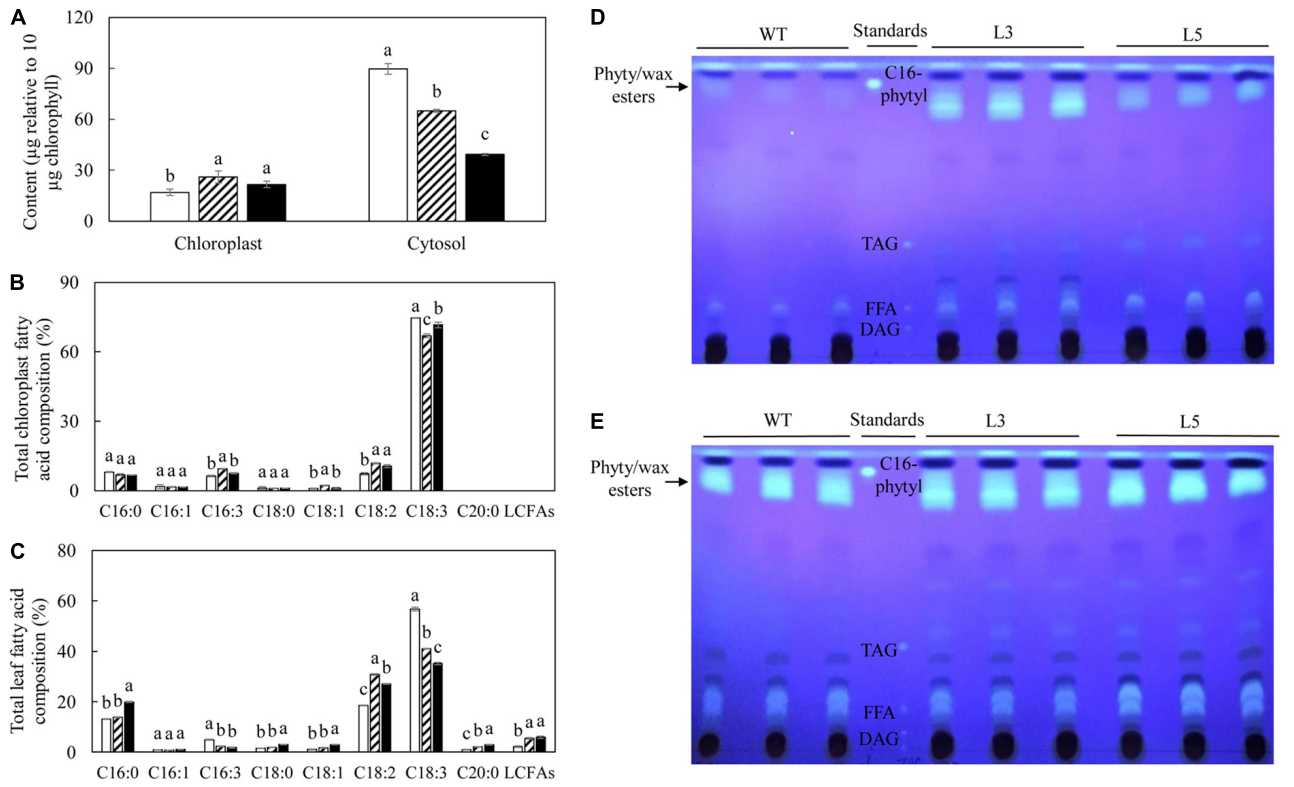

FIGURE 8 | Acyl distribution analysis in the potato senescent leaves of WT (open bar), L3 (bar with upward diagonal) and L5 (black bar). **(A)** TFA contents normalized for the same amount of chlorophyll; **(B)** Total chloroplast fatty acid composition; **(C)** Total leaf fatty acid composition; **(D)** TLC fractionation of fatty acid phytyl esters at the flowering stage; **(E)** TLC fractionation of fatty acid phytyl esters at the senescent stage. TFA content in cytosol was calculated via subtracting the TFA of chloroplast from the TFA content in leaf; the palmitoyl hexadecanoate was synthesized as C16- phytyl standard to indicate the probable location of phytyl esters band on TLC, the wax ester was slightly mingled with the phytyl ester bands. The data represent the mean values ± SD of three biological replicates. Letters (a, b, c, and d) above the bars are based on LSD, bars marked with different letters are statistically significantly different at $P < 0.05$.

Plastoglobuli have been generally considered as a functional neutral lipids storage organelle which assists coordinating the lipid molecule exchanges between plastidial and extraplastidial envelopes of the chloroplast (Bréhélin and Kessler, 2008; Besagni and Kessler, 2013). A variety of neutral lipids can be synthesized in plastoglobuli, such as fatty acid phytyl esters, tocopherols, prenylquione, as well as TAG in some reports (Rottet et al., 2015; van Wijk and Kessler, 2017). The biogenesis of plastoglobuli was reported to be highly sensitive to various biotic/abiotic factors (Munné-Bosch et al., 2001; Munne-Bosch, 2005; Evans et al., 2010; Shao et al., 2016), and displayed a very similar structural morphology to the cytosolic LD (van Wijk and Kessler, 2017). The two transgenic potato lines, L3 and L5, have both displayed plastoglobuli in the chloroplast at the three developmental stages as observed by TEM, which was not observed in the high oil transgenic tobacco and sorghum leaves (Vanhercke et al., 2014a, 2017, 2018), despite some previous research on plastoglobuli on tobacco (Hurkman and Kennedy, 1975; Tevini and Steinmüller, 1985; Synková et al., 2006). Such a difference may therefore imply the potential particularity of potato leaf in terms of the lipid metabolism. Also, considering the similarity between plastoglobuli and LD, it has long been controversial whether chloroplasts harbor the capability to produce TAG directly or not (Fan et al., 2011; Moriyama et al., 2018). As in some microalga, for instance Chlamydomonas (*Chlamydomonas reinhardtii*), it was reported that TAG could accumulate in the chloroplast under some extreme conditions such as nitrogen starvation (Wang et al., 2009; Goodson et al., 2011; Simionato et al., 2013; Scranton et al., 2015).

However, according to the experimental results from the positional fatty acids distribution analysis (**Tables 1–3**), it was reflected that the positional fatty acid distribution pattern remained generally consistent among WT and the two transgenic plants, demonstrating that the TAG synthesis is dominated by the eukaryotic pathway, while the galactolipids were produced through the prokaryotic pathway (Kunst et al., 1989; Bates et al., 2009; Wang and Benning, 2012). As further reflected in the images of confocal microscopy (**Figure 7H**), it was obvious that the cellular distributions of LD and plastoglobuli were highly compartmentalized (Austin et al., 2006; Rottet et al., 2015; van Wijk and Kessler, 2017). Therefore, the incorporation of TAG within chloroplasts as neutral lipid droplets similar to plastoglobuli would be unlikely in potato leaves. Taken together, these results suggested that the biogenesis of plastoglobuli and LD in potato leaf is evidently differentiated. Nevertheless, possible competition of acyl flux may exist as suggested by

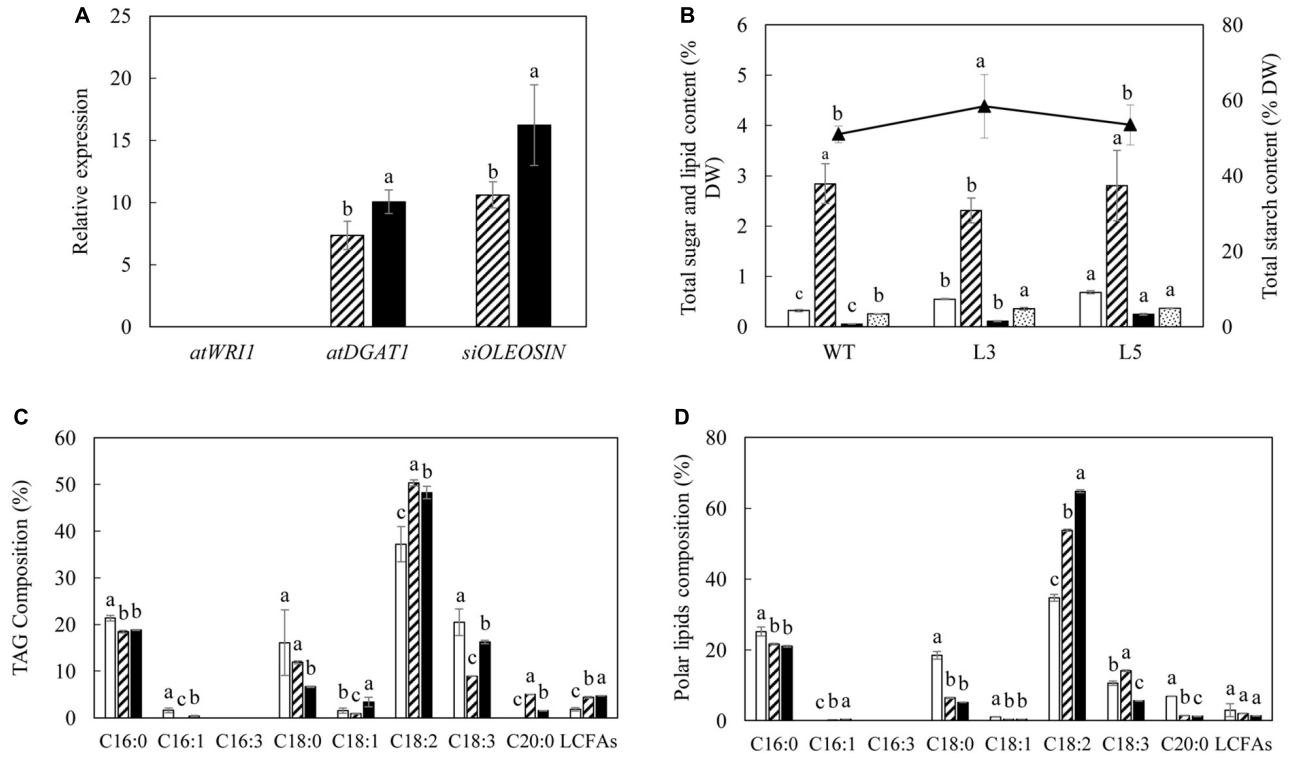

FIGURE 9 | Lipid and carbohydrate analysis in the mature potato tubers. **(A)** Real-time qRT-PCR analysis of the transgene expressions in L3 (bar with upward diagonal) and L5 (black bar); **(B)** Contents of TFA (open bar), total soluble sugars (bar with upward diagonal), total starch (triangle marker), TAG (black bar) and total polar lipid (bar with small confetti); **(C)** Fatty acid composition of TAG in WT (open bar), L3 (bar with upward diagonal) and L5 (black bar); **(D)** Fatty acid composition of total polar lipids in WT (open bar), L3 (bar with upward diagonal) and L5 (black bar). The data represent the mean values ± SD of three biological replicates. Letters (a, b, c, and d) above the bars are based on LSD, bars marked with different letters are statistically significantly different at $P < 0.05$.

the comparative fatty acid analysis between chloroplast and cytosol (**Figure 8B**), which may be mainly associated with the spatial regulation of different lipid gene expressions (Cernac and Benning, 2004; Shockey et al., 2006; Baud et al., 2009; Chapman and Ohlrogge, 2012). But the reduced fatty acids allocation in the cytosol of L3 and L5 could be the direct result of the carbon reallocation into plastoglobuli for fatty acid phytyl esters biosynthesis as displayed in the TLC fractionation (**Figures 8D,E**), possibly resulted from the enhanced expression of phytyl ester synthase (Lippold et al., 2012) as a result of the exogenous upregulation of *AtWRI1*.

Enhanced expressions of *AtDGAT1* and *SiOLEOSIN* as the result of transgene expression were also detected in mature transgenic potato tubers. However, the increase in TAG accumulation in L3 and L5 tubers did not show comparable values as reported in the high oil transgenic tubers regulated by a tuber-specific promoter (Liu et al., 2017a). We hypothesized that the lower level of TAG accumulation in transgenic tubers may be largely due to the invalid expression of *AtWRI1* with limited promoter function in tuber, but could be correlated with the *CaMV-35S* constitutive promoter controlled *AtDGAT1* expression (**Figure 9A**). By contrast, the *SiOLEOSIN* which was transcriptionally controlled by the *SSU* promoter and displayed the highest expression levels may not contribute to the TAG enhancement in tubers, which warrants for further investigation. Interestingly, L3 produced larger tubers with significantly increased starch content and reduced soluble sugars, in contrast to L5 in which the total carbohydrate content remained consistent with WT. Moreover, the reductions in tuber density and tuber water content compared to WT were observed in L3 and L5 (**Supplementary Table 1**), suggesting that the transgenes may have also potentially changed the tuber development to a certain extent, which could be largely due to the altered carbon partitioning in the source organ leaf (Sonnewald et al., 1997; Chincinska et al., 2008; Jonik et al., 2012; Katoh et al., 2015).

Plant lipid metabolism is highly regulated by a series of enzymatic steps and metabolic nodes, through the compartmentalization of different intracellular structures, the fatty acids produced from plastids are progressively and effectively distributed (Xu and Shanklin, 2016; Lavell and Benning, 2019). Genetic manipulation of the TAG metabolism thus requires great understanding on not only the carbon partitioning, but also how different lipid metabolic systems are orchestrated. Compared with other plant species, potato particularly reserves carbon in the underground tuber in which tuberization is a physiological process highly dependent on leaf (Fernie and Willmitzer, 2001; Timlin et al., 2006). In addition,

concerning that the photosynthetic efficiency of chloroplast in senescent plant tissues may be weakened (Hensel et al., 1993; Paul and Pellny, 2003; Thomas, 2013), which could lead to the expansion of plastoglobuli, as well as the reduced capability of *de novo* fatty acids biosynthesis (Troncoso-Ponce et al., 2013; Rottet et al., 2015; van Wijk and Kessler, 2017; Hasan et al., 2019). Even though it has been known that TAG accumulation could be achieved in relatively higher level in the senescent leaf (Troncoso-Ponce et al., 2013), it was not typically reflected in the potato leaf in this study. Future studies could therefore be devoted to exploring the interrelationship between plastoglobuli and LDs in potato leaf cells as a model, as well as the carbon metabolic regulation between leaf and tuber in potato, in order to rationally design novel approaches for genetic enhancement of TAG accumulation in potato vegetative tissues.

Experimental Procedures

Binary Plasmid Construct pOIL076

The binary plasmid construct pOIL076, which contains three transgene expression cassettes as *SAG12:AtWRI1*, *35S:AtDGAT1* and *SSU:SiOLEOSIN*, was designed by modification of our previously reported construct pJp3502 (Vanhercke et al., 2014a), by replacing the *SSU* promoter which controls *AtWRI1* with the *SAG12* promoter derived from Arabidopsis. Structure of the transgene cassettes in pOIL076 construct is summarized in **Supplementary Figure 2**.

Potato Transformation and Verification

Potato transformation was conducted following the method described in Liu et al. (2017a). The Phire plant direct PCR kit (Thermo Fisher Scientific, Waltham, MA, United States) was applied to quickly verify the presence of three transgenes in T_0 potato leaves by following the manufacturer's instructions. Primers used for the amplification of *AtWRI1* were: sense 5′-GCTTCCCATCTTCCGTTATG-3′, antisense 5′-GCAGAGG GTGACCAAAGAAG-3′; primers for *AtDGAT1* were: sense 5′-GGCGATTTTGGATTCTGCTGGC-3′, antisense 5′-GGAA CCAGAGAGAAGAAGTC-3′; and primers for *SiOLEOSIN* were: sense 5′-CAGCAGCAACAAACACGTG-3′, antisense 5′-GAGAAGATCACCAGGAGAG-3′. PCR reaction program included initial denaturation at 95°C for 3 min, followed with 40 cycles of 95°C for 10 s, 60°C for 30 s, 72°C for 30 s, which was carried out on a PCR machine (Thermo Fisher Scientific).

Selection of Representative Transgenic Lines for Characterization

A total of 17 transgenic plants were selected and grown alongside WT potato in a glasshouse (24/20°C, 16 h photoperiod). Potato leaves sampled at the senescent stage from the T_0 transgenic population were screened for the TFA content, and two lines named L3 and L5 showing the most significantly increased TFA were selected for further analysis and synchronically propagated with WT under the same glasshouse environment for characterization. Samples for biochemical and molecular analysis were harvested at three potato developmental stages, starting from opening of its first flower as the flowering stage (>70% of flowers in one plant were blossoming), followed by mature (>80% of flowers in one plant were withered) and senescent (>50% aging leaves in one plant were visible) stages. Healthy and fully expanded leaves with the typical features of each developmental stage were collected from three randomly arranged and biologically replicated plants. Mature tubers were only sampled at the plant senescent stage. Samples were immediately freeze-dried for 72 h prior to extraction of lipids or RNA.

Lipid Classes Characterization

The extraction of total lipids, lipid fractionation and quantification were carried out following the methods previously described by Liu et al. (2017a). Neutral lipids and free fatty acids (FFAs) were separated in the solvent system of hexane: diethyl ether: acetic acid (70: 30: 1, by volume) on TLC. Polar lipids including PC, MGDG, DGDG, PE, and PG were separated using the solvent system consisting of chloroform: methanol: acetic acid: distilled water (30: 5: 3: 1, by volume).

Positional distribution of fatty acids in TAG, MGDG and DGDG was investigated *via* lipase digestion. The *Rhizopus arrhizus* lipase (Fluka, Buchs, Switzerland) was utilized to digest TAG, MGDG and DGDG respectively. TAG, MGDG or DGDG were isolated from the total lipids of potato leaf at the senescent stage by TLC fractionation, and further purified using chloroform: methanol (2: 1, by volume). The treatment of each lipid digestion and subsequent fractionation were performed as described in Liu et al. (2017b). Fatty acid methyl esters (FAME) analysis was carried out using the samples prepared from the TLC purified *sn*-2 MAG from TAG, and the *sn*-1 FFA and *sn*-2 lyso-MGDG/DGDG from galactolipids by GC analysis. It should be noted that the fatty acid composition of the *sn*-1/3 FFA released from TAG was calculated as previously described in Christie et al. (1984). The digestion of galactolipids using the same methods as the TAG was previously reported by Yongmanitchai and Ward (1993).

Fatty acid phytyl esters were fractionated from the total leaf lipids on TLC using a solvent system hexane: diethyl ether: acetic acid (85: 15: 1, by volume) as described in Ischebeck et al. (2006). To indicate the probable position of fatty acid phytyl esters, the palmitoyl hexadecanoate was synthesized for use as the C16- phytyl standard in TLC analysis (Pereira et al., 2002).

Total Starch and Soluble Sugars Measurement

Three phases were visibly separated in the chloroform/methanol/0.1M KCl based lipid extraction after centrifugation. The upper phase contains soluble sugars and proteins whereas the insoluble substances such as starch and fiber remain in the interphase and the lower phase containing the lipids dissolved in chloroform, which were used for analysis of total soluble sugars, starch and lipids, respectively. The total soluble sugars was analyzed according to the anthrone coloration method. Briefly, 5–10 μL of supernatant obtained from the lipid extraction was isolated and boiled for 10 min

in 500 μL anthrone solution (0.2% anthrone in 70% H_2SO_4), and measured under 630 nm for absorbance. Total starch content was measured by boiling the sample for 30 min in 0.2 M NaOH and neutralized with 4 μL glacial acetic acid prior to be analyzed with the Megazyme Total Starch Kit (Megazyme International Ireland, Bray, Ireland) following the manufacturer's instruction.

RNA Extraction and qRT-PCR Analysis of Transgene Expression

Total RNAs from potato leaf tissues at different developmental stages were extracted using the RNeasy Mini Kit (Qiagen, Hilden, Germany), followed by quality check on a Nanodrop spectrophotometer ND 1000 (Thermo Fisher Scientific) and in an ethidium bromide-stained 1% agarose gel electrophoresis. The total RNA from mature potato tubers were extracted by the cetyl trimethyl ammonium bromide (CTAB) method (Reynolds et al., 2019) and purified using a RNeasy MinElute Cleanup Kit (Qiagen) following manufacturer's instructions.

Expression of transgenes was analyzed using the qRT-PCR in triplicate biological samples, each with two technical replicates. Reverse transcription of total RNAs into cDNA was performed with a SuperScript^{TM} IV First-Strand Synthesis System kit (Thermo Fisher Scientific, Waltham, MA, United States). The oligo nucleotide sequence used for each transgene was as same as described in the PCR verification of the T_0 transgenic potato plants. The reference gene and its corresponding primers selected to calibrate the expression analysis was the *S. tuberosum CYCLOPHILIN* (*stCYP*), as previously described in Liu et al. (2017a). The FastStart Universal SYBR Green Master (ROX) kit (Roche, Indianapolis, IN) was utilized to conduct the real-time qRT-PCR reaction, with the reaction program as 95°C for 3 min, 39 cycles of 95°C for 10 s, 58°C for 30 s and 72°C for 30 s using a Biorad 96 well PCR machine (Bio-Rad, Hercules, CA, United States). Calculation was made by following the $2^{-\Delta\ \Delta\ Ct}$ method (Livak and Schmittgen, 2001).

Chloroplast Isolation, Purification and Fatty Acids Analysis

Chloroplasts were isolated from the senescent potato leaves following the method described in Hosaka and Hanneman (1987), the collected chloroplast pellets were gathered for the subsequent purification by using a sugar-gradient centrifuging method (Elias and Givan, 1978), through which intact potato chloroplasts were well separated and stored in 4 mL stock buffer (0.33 M sucrose in extraction buffer C) under 4°C. The integrity and quality of chloroplast was checked by light microscopy using Leica-DMR (Leica Microsystems, Wetzlar, Germany) (**Supplementary Figure 3**).

For the TFA extraction, 1.5 mL stock buffer containing purified chloroplasts on ice was first mixed with 0.5 mL 1M KCl solution, then 6 mL chloroform: methanol (2: 1, by volume) was added following 5 min vortex and 5 min centrifugation at 1,700 rpm. The lower phase was collected and evaporated under nitrogen, then dissolved in 200 μL chloroform as stock under −20°C. As chloroplast cannot be accurately quantified as leaf DW, the amount of chlorophyll was used as the reference standard for normalization. Chlorophyll from chloroplast and leaf lipid solutions was measured via the spectrometric method described in Warren (2008). FAME analysis of TFA were then proceeded using GC. The TFA in cytosol was calculated via subtracting the TFA of chloroplast from the TFA content in leaf.

Microscopy Observation of Lipid Droplet

Transmission Electron Microscopy was applied to visualize the cellular distribution and morphology of LDs in potato leaf tissues. Dissected tissues were submerged in fixative 2.5% glutaraldehyde and 4% paraformaldehyde in 0.1 M phosphate buffer, and post fixed with 1% osmium tetroxide for 2 h. Fixed samples were infiltrated and embedded in LR white resin after gradual ethanol dehydration. 70 nm ultrathin sections were prepared with a Leica EM UC6 Ultramicrotome (Leica Microsystems). Each section was stained with 2% UA for 15 and 5 min with lead citrate. The sections were examined with a Hitachi H7100 transmission electron microscope (Hitachi, Tokyo, Japan) at 75 kV accelerating voltage. Confocal scanning microscopy analysis was processed by using freshly sampled potato leaf at the senescent stage, as described in Vanhercke et al. (2018).

Basic Tuber Physiology Analysis

For the basic tuber physiological trait analysis, three healthy independent potato plants as biological replicates of WT, L3 and L5 respectively were measured. After harvesting all the mature tubers from an individual plant, the maximum tuber length was measured and divided into four groups according to the size (Size A, tuber length $>$ 9 cm; Size B, 6 cm $<$ tuber length $<$ 9 cm; Size C, 3 cm $<$ tuber length $<$ 6 cm; Size D, tuber length $<$ 3 cm). From each group, an intact tuber was selected then analyzed with the tuber water percentage (tuber water content/tuber fresh weight) and tuber density (fresh tuber weight/tuber volume). The tuber water content was calculated with the oven-drying method, and the tuber volume with the dewatering method.

Statistical Analysis

GenStat 9.0 software was used to calculate the least significant difference (LSD) value of all data for multiple comparison.

DATA AVAILABILITY STATEMENT

The datasets generated for this study are available on request to the corresponding author.

AUTHOR CONTRIBUTIONS

XX designed the research, performed the experiments, and wrote the manuscript. SA and DH assisted the preparation of the

transgenic construct and the tissue culture transformation. PS assisted the fatty acid positional distribution analysis. RD assisted the fatty acid phytyl ester analysis. LV assisted the confocal microscopic analysis. JL and MR assisted the TEM analysis. LT assisted the glasshouse maintenance. TV and SS provided precious guidance all along the research as project supervisors. PJS, ZL, and QL conceived and designed the project, and improved the manuscript.

FUNDING

This project was supported by CSIRO Agriculture and Food and The University of Sydney.

ACKNOWLEDGMENTS

XX would like to acknowledge the China Scholarship Council for funding him in the doctoral study in Australia. The authors would like to acknowledge the facilities of Microscopy Australia at the Advanced Imaging Precinct, The Australian National University, a facility funded by the University and the Federal Government.

SUPPLEMENTARY MATERIAL

The Supplementary Material for this article can be found online at: https://www.frontiersin.org/articles/10.3389/fpls.2020.00215/full#supplementary-material

REFERENCES

Ainsworth, E. A., and Bush, D. R. (2011). Carbohydrate export from the leaf: a highly regulated process and target to enhance photosynthesis and productivity. *Plant Physiol.* 155, 64–69. doi: 10.1104/pp.110.167684

Athanikar, G., and Badar, P. (2016). Potato leaf diseases detection and classification system. *IJCSMC* 5, 76–88.

Austin, J. R., Frost, E., Vidi, P. A., Kessler, F., and Staehelin, L. A. (2006). Plastoglobules are lipoprotein subcompartments of the chloroplast that are permanently coupled to thylakoid membranes and contain biosynthetic enzymes. *Plant Cell* 18, 1693–1703. doi: 10.1105/tpc.105.039859

Avila-Ospina, L., Moison, M., Yoshimoto, K., and Masclaux-Daubresse, C. (2014). Autophagy, plant senescence, and nutrient recycling. *J. Exp. Bot.* 65, 3799–3811. doi: 10.1093/jxb/eru039

Badeck, F. W., Tcherkez, G., Nogues, S., Piel, C., and Ghashghaie, J. (2005). Post-photosynthetic fractionation of stable carbon isotopes between plant organs - a widespread phenomenon. *Rapid Commun. Mass Spectrom.* 19, 1381–1391. doi: 10.1002/rcm.1912

Bates, P. D., Durrett, T. P., Ohlrogge, J. B., and Pollard, M. (2009). Analysis of acyl fluxes through multiple pathways of triacylglycerol synthesis in developing soybean embryos. *Plant Physiol.* 150, 55–72. doi: 10.1104/pp.109.137737

Baud, S., Wuillème, S., To, A., Rochat, C., and Lepiniec, L. (2009). Role of *WRINKLED1* in the transcriptional regulation of glycolytic and fatty acid biosynthetic genes in *Arabidopsis*. *Plant J.* 60, 933–947. doi: 10.1111/j.1365-313X.2009.04011.x

Besagni, C., and Kessler, F. (2013). A mechanism implicating plastoglobules in thylakoid disassembly during senescence and nitrogen starvation. *Planta* 237, 463–470. doi: 10.1007/s00425-012-1813-9

Bourgis, F., Kilaru, A., Cao, X., Ngando-Ebongue, G. F., Drira, N., Ohlrogge, J. B., et al. (2011). Comparative transcriptome and metabolite analysis of oil palm and date palm mesocarp that differ dramatically in carbon partitioning. *Proc. Natl. Acad. Sci. U.S.A.* 108, 12527–12532. doi: 10.1073/pnas.1106502108

Bouvier-Navé, P., Benveniste, P., Oelkers, P., Sturley, S. L., and Schaller, H. (2000). Expression in yeast and tobacco of plant cDNAs encoding acyl CoA: diacylglycerol acyltransferase. *Eur. J. Biochem.* 267, 85–96. doi: 10.1046/j.1432-1327.2000.00961.x

Bradford, K. J., Van Deynze, A., Gutterson, N., Parrott, W., and Strauss, S. H. (2005). Regulating transgenic crops sensibly: lessons from plant breeding, biotechnology and genomics. *Nat. Biotechnol.* 23, 439–444. doi: 10.1038/nbt1084

Bréhélin, C., and Kessler, F. (2008). The plastoglobule: a bag full of lipid biochemistry tricks. *J. Photochem. Photobiol.* 84, 1388–1394. doi: 10.1111/j.1751-1097.2008.00459.x

Brown, A. P., Kroon, J. T., Swarbreck, D., Febrer, M., Larson, T. R., Graham, I. A., et al. (2012). Tissue-specific whole transcriptome sequencing in castor, directed at understanding triacylglycerol lipid biosynthetic pathways. *PLoS One* 7:e30100. doi: 10.1371/journal.pone.0030100

Carlsson, A. S., Yilmaz, J. L., Green, A. G., Stymne, S., and Hofvander, P. (2011). Replacing fossil oil with fresh oil - with what and for what? *Eur. J. Lipid Sci. Technol.* 113, 812–831. doi: 10.1002/ejlt.201100032

Cernac, A., and Benning, C. (2004). Wrinkled1 encodes an AP2/EREB domain protein involved in the control of storage compound biosynthesis in *Arabidopsis*. *Plant J.* 40, 575–585. doi: 10.1111/j.1365-313x.2004.02235.x

Chapman, K. D., Dyer, J. M., and Mullen, R. T. (2012). Biogenesis and functions of lipid droplets in plants thematic review series: lipid droplet synthesis and metabolism: from yeast to man. *J. Lipid Res.* 53, 215–226. doi: 10.1194/jlr.R021436

Chapman, K. D., Dyer, J. M., and Mullen, R. T. (2013). Commentary, why don't plant leaves get fat? *Plant Sci.* 207, 128–134. doi: 10.1016/j.plantsci.2013.03.003

Chapman, K. D., and Ohlrogge, J. B. (2012). Compartmentation of triacylglycerol accumulation in plants. *J. Biol. Chem.* 287, 2288–2294. doi: 10.1074/jbc.R111.290072

Chincinska, I. A., Liesche, J., Krügel, U., Michalska, J., Geigenberger, P., Grimm, B., et al. (2008). Sucrose transporter *StSUT4* from potato affects flowering, tuberization, and shade avoidance response. *Plant Physiol.* 146, 515–528. doi: 10.1104/pp.107.112334

Christie, W. W., Clegg, R. A., Calvert, D. T., and Noble, R. C. (1984). The positional distributions of fatty acids in the triacylglycerols and phosphatidylcholines of the intestinal and popliteal lymph and plasma of sheep. *Lipids* 19, 982–986. doi: 10.1007/bf02534739

Costa, G. G., Del Cardoso, K. C., Bem, L. E., Lima, A. C., Cunha, M. A., de Campos-Leite, L., et al. (2010). Transcriptome analysis of the oil-rich seed of the bioenergy crop *Jatropha curcas* L. *BMC Genome* 11:462. doi: 10.1186/1471-2164-11-462

Dita Rodriguez, M. A., Brommonschenkel, S. H., Matsuoka, K., and Mizubuti, E. S. G. (2006). Components of resistance to early blight in four potato cultivars: effect of leaf position. *J. Phytopathol.* 154, 230–235. doi: 10.1111/j.1439-0434.2006.01089.x

Douches, D. S., Kisha, T. J., Coombs, J. J., Li, W., Pett, W. L., and Grafius, E. J. (2001). Effectiveness of natural and engineered host plant resistance in potato to the Colorado potato beetle. *Hortscience* 36, 967–970. doi: 10.21273/hortsci.36.5.967

Durrett, T. P., Benning, C., and Ohlrogge, J. B. (2008). Plant triacylglycerols as feedstocks for the production of biofuels. *Plant J.* 54, 593–607. doi: 10.1111/j.1365-313X.2008.03442.x

Elias, B. A., and Givan, C. V. (1978). Density gradient and differential centrifugation methods for chloroplast purification and enzyme localization in leaf tissue. *Planta* 142, 317–320. doi: 10.1007/BF00385083

Evans, I. M., Rus, A. M., Belanger, E. M., Kimoto, M., and Brusslan, J. A. (2010). Dismantling of *Arabidopsis thaliana* mesophyll cell chloroplasts during natural leaf senescence. *Plant Biol.* 12, 1–12. doi: 10.1111/j.1438-8677.2009.00206.x

Fan, J., Andre, C., and Xu, C. (2011). A chloroplast pathway for the de novo biosynthesis of triacylglycerol in *Chlamydomonas reinhardtii*. *FEBS Lett.* 585, 1985–1991. doi: 10.1016/j.febslet.2011.05.018

Fan, J., Yan, C., Roston, R., Shanklin, J., and Xu, C. (2014). Arabidopsis lipins, *PDAT1* acyltransferase, and *SDP1* triacylglycerol lipase synergistically direct fatty acids toward β-oxidation, thereby maintaining membrane lipid homeostasis. *Plant Cell* 26, 4119–4134. doi: 10.1105/tpc.114.130377

Fan, J., Yan, C., Zhang, X., and Xu, C. (2013). Dual role for phospholipid: diacylglycerol acyltransferase: enhancing fatty acid synthesis and diverting fatty acids from membrane lipids to triacylglycerol in *Arabidopsis* leaves. *Plant Cell* 25, 3506–3518. doi: 10.1105/tpc.113.117358

Fernie, A. R., Tiessen, A., Stitt, M., Willmitzer, L., and Geigenberger, P. (2002). Altered metabolic fluxes result from shifts in metabolite levels in sucrose phosphorylase - expressing potato tubers. *Plant Cell Environ.* 25, 1219–1232. doi: 10.1046/j.1365-3040.2002.00918.x

Fernie, A. R., and Willmitzer, L. (2001). Molecular and biochemical triggers of potato tuber development. *Plant Physiol.* 127, 1459–1465. doi: 10.1104/pp.010764

Finnegan, J., and McElroy, D. (1994). Transgene inactivation: plants fight back! *Nat. Biotechnol.* 12, 883–888. doi: 10.1038/nbt0994-883

Fischer, K., and Weber, A. (2002). Transport of carbon in non-green plastids. *Trends Plant Sci.* 7, 345–351. doi: 10.1016/s1360-1385(02)02291-4

Fleisher, D. H., Timlin, D. J., and Reddy, V. R. (2006). Temperature influence on potato leaf and branch distribution and on canopy photosynthetic rate. *Agron. J.* 98, 1442–1452. doi: 10.2134/agronj2005.0322

Geigenberger, P. (2003). Regulation of sucrose to starch conversion in growing potato tubers. *J. Exp. Bot.* 54, 457–465. doi: 10.1093/jxb/erg074

Goodson, C., Roth, R., Wang, Z. T., and Goodenough, U. (2011). Structural correlates of cytoplasmic and chloroplast lipid body synthesis in *Chlamydomonas reinhardtii* and stimulation of lipid body production with acetate boost. *Eukaryot. Cell* 10, 1592–1606. doi: 10.1128/EC.05242-11

Graham, I. A. (2008). Seed storage oil mobilization. *Annu. Rev. Plant Biol.* 59, 115–142. doi: 10.1146/annurev.arplant.59.032607.092938

Gregersen, P. L., Culetic, A., Boschian, L., and Krupinska, K. (2013). Plant senescence and crop productivity. *Plant Mol. Biol.* 82, 603–622. doi: 10.1007/s11103-013-0013-8

Hasan, M. M., Sharmeen, I. A., Hakeem, K. R., Alharby, H. F., and Hajar, A. S. (2019). "The physiology and molecular biology of stress-induced senescence," in *Senescence Signaling and Control in Plants*, 1st Edn, eds M. Sarwat, and N. Tuteja, (Cambridge, MA: Academic Press), 1–14. doi: 10.1016/b978-0-12-813187-9.00001-9

Hastilestari, B. R., Lorenz, J., Reid, S., Hofmann, J., Pscheidt, D., Sonnewald, U., et al. (2018). Deciphering source and sink responses of potato plants (*Solanum tuberosum* L.) to elevated temperatures. *Plant Cell Environ.* 41, 2600–2616. doi: 10.1111/pce.13366

Hensel, L. L., Grbić, V., Baumgarten, D. A., and Bleecker, A. B. (1993). Developmental and age-related processes that influence the longevity and senescence of photosynthetic tissues in *Arabidopsis*. *Plant Cell* 5, 553–564. doi: 10.1105/tpc.5.5.553

Higashi, Y., Okazaki, Y., Myouga, F., Shinozaki, K., and Saito, K. (2015). Landscape of the lipidome and transcriptome under heat stress in *Arabidopsis thaliana*. *Sci. Rep.* 5:10533. doi: 10.1038/srep10533

Hofvander, P., Ischebeck, T., Turesson, H., Kushwaha, S. K., Feussner, I., Carlsson, A. S., et al. (2016). Potato tuber expression of *Arabidopsis WRINKLED1* increase triacylglycerol and membrane lipids while affecting central carbohydrate metabolism. *Plant Biotechnol. J.* 14, 1883–1898. doi: 10.1111/pbi.12550

Hölzl, G., and Dörmann, P. (2019). Chloroplast lipids and their biosynthesis. *Annu. Rev. Plant Biol.* 70, 51–81. doi: 10.1146/annurev-arplant-050718-100202

Hosaka, K., and Hanneman, R. E. (1987). A rapid and simple method for determination of potato chloroplast DNA type. *Am. Potato J.* 64, 345–353. doi: 10.1007/bf02853596

Hurkman, W. J., and Kennedy, G. S. (1975). Ultrastructural changes of chloroplasts in aging tobacco leaves. *Proc. Indiana Acad. Sci.* 85, 89–95.

Ischebeck, T., Zbierzak, A. M., Kanwischer, M., and Dörmann, P. (2006). A salvage pathway for phytol metabolism in *Arabidopsis*. *J. Biol. Chem.* 281, 2470–2477. doi: 10.1074/jbc.m509222200

Jonik, C., Sonnewald, U., Hajirezaei, M. R., Flügge, U. I., and Ludewig, F. (2012). Simultaneous boosting of source and sink capacities doubles tuber starch yield of potato plants. *Plant Biotechnol. J.* 10, 1088–1098. doi: 10.1111/j.1467-7652.2012.00736.x

Katoh, A., Ashida, H., Kasajima, I., Shigeoka, S., and Yokota, A. (2015). Potato yield enhancement through intensification of sink and source performances. *Breed. Sci.* 65, 77–84. doi: 10.1270/jsbbs.65.77

Kelly, A. A., Quettier, A. L., Shaw, E., and Eastmond, P. J. (2011). Seed storage oil mobilization is important but not essential for germination or seedling establishment in *Arabidopsis*. *Plant Physiol.* 157, 866–875. doi: 10.1104/pp.111.181784

Klaus, D., Ohlrogge, J. B., Ekkehard Neuhaus, H., and Dormann, P. (2004). Increased fatty acid production in potato by engineering of acetyl-CoA carboxylase. *Planta* 219, 389–396.

Kong, Q., and Ma, W. (2018). WRINKLED1 transcription factor: how much do we know about its regulatory mechanism? *Plant Sci.* 272, 153–156. doi: 10.1016/j.plantsci.2018.04.013

Kumar, S., and Fladung, M. (2002). Transgene integration in aspen: structures of integration sites and mechanism of T-DNA integration. *Plant J.* 31, 543–551. doi: 10.1046/j.1365-313x.2002.01368.x

Kunst, L., Browse, J., and Somerville, C. (1989). Altered chloroplast structure and function in a mutant of *Arabidopsis* deficient in plastid glycerol-3-phosphate acyltransferase activity. *Plant Physiol.* 90, 846–853. doi: 10.1104/pp.90.3.846

Lavell, A. A., and Benning, C. (2019). Cellular organization and regulation of plant glycerolipid metabolism. *Plant Cell Physiol.* 60, 1176–1183. doi: 10.1093/pcp/pcz016

Lippold, F., vom Dorp, K., Abraham, M., Hölzl, G., Wewer, V., Yilmaz, J. L., et al. (2012). Fatty acid phytyl ester synthesis in chloroplasts of *Arabidopsis*. *Plant Cell* 24, 2001–2014. doi: 10.1105/tpc.112.095588

Liu, Q., Guo, Q., Akbar, S., Zhi, Y., El Tahchy, A., Mitchell, M., et al. (2017a). Genetic enhancement of oil content in potato tuber (*Solanum tuberosum* L.) through an integrated metabolic engineering strategy. *Plant Biotechnol. J.* 15, 56–67. doi: 10.1111/pbi.12590

Liu, Q., Wu, M., Zhang, B., Shrestha, P., Petrie, J. R., Green, A. G., et al. (2017b). Genetic enhancement of palmitic acid accumulation in cotton seed oil through RNAi down-regulation of ghKAS2 encoding β-ketoacyl-ACP synthase II (KASII). *Plant Biotechnol. J.* 15, 132–143. doi: 10.1111/pbi.12598

Livak, K. J., and Schmittgen, T. D. (2001). Analysis of relative gene expression data using real-time quantitative PCR and the 2 -Δ ΔCT method. *Methods* 25, 402–408. doi: 10.1006/meth.2001.1262

Ma, W., Kong, Q., Grix, M., Mantyla, J. J., Yang, Y., Benning, C., et al. (2015). Deletion of a C-terminal intrinsically disordered region of WRINKLED 1 affects its stability and enhances oil accumulation in *Arabidopsis*. *Plant J.* 83, 864–874. doi: 10.1111/tpj.12933

Maeo, K., Tokuda, T., Ayame, A., Mitsui, N., Kawai, T., Tsukagoshi, H., et al. (2009). An AP2-type transcription factor, WRINKLED1, of *Arabidopsis thaliana* binds to the AW-box sequence conserved among proximal upstream regions of genes involved in fatty acid synthesis. *Plant J.* 60, 476–487. doi: 10.1111/j.1365-313X.2009.03967.x

Moriyama, T., Toyoshima, M., Saito, M., Wada, H., and Sato, N. (2018). Revisiting the algal "chloroplast lipid droplet": the absence of an entity that is unlikely to exist. *Plant Physiol.* 176, 1519–1530. doi: 10.1104/pp.17.01512

Munne-Bosch, S. (2005). The role of α-tocopherol in plant stress tolerance. *J. Plant Physiol.* 162, 743–748. doi: 10.1016/j.jplph.2005.04.022

Munné-Bosch, S., Jubany-Mari, T., and Alegre, L. (2001). Drought-induced senescence is characterized by a loss of antioxidant defenses in chloroplasts. *Plant Cell Environ.* 24, 1319–1327. doi: 10.1046/j.1365-3040.2001.00794.x

Nguyen, H. T., Silva, J. E., Podicheti, R., Macrander, J., Yang, W., Nazarenus, T. J., et al. (2013). Camelina seed transcriptome: a tool for meal and oil improvement and translational research. *Plant Biotechnol. J.* 11, 759–769. doi: 10.1111/pbi.12068

Noh, Y. S., and Amasino, R. M. (1999). Identification of a promoter region responsible for the senescence-specific expression of SAG12. *Plant Mol. Biol.* 41, 181–194.

Paradiso, R., Arena, C., Rouphael, Y., d'Aquino, L., Makris, K., Vitaglione, P., et al. (2018). Growth, photosynthetic activity and tuber quality of two potato cultivars in controlled environment as affected by light source. *Plant Biosyst.* 153, 725–735. doi: 10.1080/11263504.2018.1549603

Paul, M. J., and Pellny, T. K. (2003). Carbon metabolite feedback regulation of leaf photosynthesis and development. *J. Exp. Bot.* 54, 539–547. doi: 10.1093/jxb/erg052

Peiman, M., and Xie, C. (2006). Sensitive detection of potato viruses, PVX, PLRV and PVS, by RT-PCR in potato leaf and tuber. *Aust. Plant Dis. Notes* 1, 41–46. doi: 10.1016/j.jviromet.2009.06.027

Pereira, A. S., Siqueira, D. S., Elias, V. O., Simoneit, B. R., Cabral, J. A., and Neto, F. R. A. (2002). Three series of high molecular weight alkanoates found in

Amazonian plants. *Phytochemistry* 61, 711–719. doi: 10.1016/s0031-9422(02)00348-5

Poxleitner, M., Rogers, S. W., Lacey Samuels, A., Browse, J., and Rogers, J. C. (2006). A role for caleosin in degradation of oil-body storage lipid during seed germination. *Plant J.* 47, 917–933. doi: 10.1111/j.1365-313x.2006.02845.x

Reiss, B., Wasmann, C. C., and Bohnert, H. J. (1987). Regions in the transit peptide of SSU essential for transport into chloroplasts. *Mol. Genet. Genomics* 209, 116–121. doi: 10.1007/bf00329845

Rey, P., Gillet, B., Römer, S., Eymery, F., Massimino, J., Peltier, G., et al. (2000). Over-expression of a pepper plastid lipid-associated protein in tobacco leads to changes in plastid ultrastructure and plant development upon stress. *Plant J.* 21, 483–494. doi: 10.1046/j.1365-313x.2000.00699.x

Reynolds, K. B., Cullerne, D. P., El Tahchy, A., Rolland, V., Blanchard, C. L., Wood, C. C., et al. (2019). Identification of genes involved in lipid biosynthesis through *de novo* transcriptome assembly from *Cocos nucifera* developing endosperm. *Plant Cell Physiol.* 60, 945–960. doi: 10.1093/pcp/pcy247

Roessner-Tunali, U., Urbanczyk-Wochniak, E., Czechowski, T., Kolbe, A., Willmitzer, L., and Fernie, A. R. (2003). *De novo* amino acid biosynthesis in potato tubers is regulated by sucrose levels. *Plant Physiol.* 133, 683–692. doi: 10.1104/pp.103.024802

Rolando, J. L., Ramírez, D. A., Yactayo, W., Monneveux, P., and Quiroz, R. (2015). Leaf greenness as a drought tolerance related trait in potato (*Solanum tuberosum* L.). *Environ. Exp. Bot.* 110, 27–35. doi: 10.1016/j.envexpbot.2014.09.006

Rottet, S., Besagni, C., and Kessler, F. (2015). The role of plastoglobules in thylakoid lipid remodeling during plant development. *Biochim. Biophys. Acta* 1847, 889–899. doi: 10.1016/j.bbabio.2015.02.002

Scranton, M. A., Ostrand, J. T., Fields, F. J., and Mayfield, S. P. (2015). Chlamydomonas as a model for biofuels and bio-products production. *Plant J.* 82, 523–531. doi: 10.1111/tpj.12780

Shao, R., Xin, L., Zheng, H., Li, L., Ran, W., Mao, J., et al. (2016). Changes in chloroplast ultrastructure in leaves of drought-stressed maize inbred lines. *Photosynthetica* 54, 74–80. doi: 10.1007/s11099-015-0158-6

Shockey, J. M., Gidda, S. K., Chapital, D. C., Kuan, J. C., Dhanoa, P. K., Bland, J. M., et al. (2006). Tung tree *DGAT1* and *DGAT2* have nonredundant functions in triacylglycerol biosynthesis and are localized to different subdomains of the endoplasmic reticulum. *Plant Cell* 18, 2294–2313. doi: 10.1105/tpc.106.043695

Simionato, D., Block, M. A., La Rocca, N., Jouhet, J., Maréchal, E., Finazzi, G., et al. (2013). The response of *Nannochloropsis gaditana* to nitrogen starvation includes de novo biosynthesis of triacylglycerols, a decrease of chloroplast galactolipids, and reorganization of the photosynthetic apparatus. *Eukaryot. Cell* 12, 665–676. doi: 10.1128/EC.00363-12

Sonnewald, U., Hajirezaei, M. R., Kossmann, J., Heyer, A., Trethewey, R. N., and Willmitzer, L. (1997). Increased potato tuber size resulting from apoplastic expression of a yeast invertase. *Nat. Biotechnol.* 15, 794–797. doi: 10.1038/nbt0897-794

Synková, H., Schnablová, R., Polanská, L., Hušák, M., Šiffel, P., Vácha, F., et al. (2006). Three-dimensional reconstruction of anomalous chloroplasts in transgenic ipt tobacco. *Planta* 223, 659–671. doi: 10.1007/s00425-005-0119-6

Tevini, M., and Steinmüller, D. (1985). Composition and function of plastoglobuli. *Planta* 163, 91–96. doi: 10.1007/BF00395902

Thomas, H. (2013). Senescence, ageing and death of the whole plant. *New Phytol.* 197, 696–711. doi: 10.1111/nph.12047

Timlin, D., Lutfor Rahman, S. M., Baker, J., Reddy, V. R., Fleisher, D., and Quebedeaux, B. (2006). Whole plant photosynthesis, development, and carbon partitioning in potato as a function of temperature. *Agron. J.* 98, 1195–1203. doi: 10.2134/agronj2005.0260

To, A., Joubès, J., Barthole, G., Lécureuil, A., Scagnelli, A., Jasinski, S., et al. (2012). WRINKLED transcription factors orchestrate tissue-specific regulation of fatty acid biosynthesis in *Arabidopsis*. *Plant Cell* 24, 5007–5023. doi: 10.1105/tpc.112.106120

Troncoso-Ponce, M. A., Cao, X., Yang, Z., and Ohlrogge, J. B. (2013). Lipid turnover during senescence. *Plant Sci.* 205-206, 13–19. doi: 10.1016/j.plantsci.2013.01.004

van Wijk, K. J., and Kessler, F. (2017). Plastoglobuli: plastid microcompartments with integrated functions in metabolism, plastid developmental transitions, and environmental adaptation. *Annu. Rev. Plant Biol.* 68, 253–289. doi: 10.1146/annurev-arplant-043015-111737

Vanhercke, T., Belide, S., Taylor, M. C., El Tahchy, A., Okada, S., Rolland, V., et al. (2018). Upregulation of lipid biosynthesis pathway increases the oil content in leaves of *Sorghum bicolor*. *Plant Biotechnol. J.* 17, 220–232. doi: 10.1111/pbi.12959

Vanhercke, T., Divi, U. K., El Tahchy, A., Liu, Q., Mitchell, M., Taylor, M. C., et al. (2017). Step changes in leaf oil accumulation via iterative metabolic engineering. *Metab. Eng.* 39, 237–246. doi: 10.1016/j.ymben.2016.12.007

Vanhercke, T., Dyer, J. M., Mullen, R. T., Kilaru, A., Rahman, M. M., Petrie, J. R., et al. (2019). Metabolic engineering for enhanced oil in biomass. *Prog. Lipid Res.* 74, 103–129. doi: 10.1016/j.plipres.2019.02.002

Vanhercke, T., El Tahchy, A., Liu, Q., Zhou, X., Shrestha, P., Divi, U. K., et al. (2014a). Metabolic engineering of biomass for high energy density, oilseed-like triacylglycerol yields from plant leaves. *Plant Biotechnol. J.* 12, 231–239. doi: 10.1111/pbi.12131

Vanhercke, T., El Tahchy, A., Shrestha, P., Zhou, X., Singh, S. P., and Petrie, J. R. (2013). Synergistic effect of *WRI1* and *DGAT1* coexpression on triacylglycerol biosynthesis in plants. *FEBS Lett.* 587, 364–369. doi: 10.1016/j.febslet.2012.12.018

Vanhercke, T., Petrie, J. R., and Singh, S. P. (2014b). Energy densification in vegetative biomass through metabolic engineering. *Biocatal. Agric. Biotechnol.* 3, 75–80. doi: 10.1016/j.bcab.2013.11.010

Wang, Z., and Benning, C. (2012). Chloroplast lipid synthesis and lipid trafficking through ER-plastid membrane contact sites. *Biochem. Soc. Trans.* 40, 457–463. doi: 10.1042/BST20110752

Wang, Z., Ullrich, N., Joo, S., Waffenschmidt, S., and Goodenough, U. (2009). Algal lipid bodies: stress induction, purification, and biochemical characterization in wild-type and starchless *Chlamydomonas reinhardtii*. *Eukaryot. Cell* 8, 1856–1868. doi: 10.1128/EC.00272-09

Warren, C. R. (2008). Rapid measurement of chlorophylls with a microplate reader. *J. Plant Nutr.* 31, 1321–1332. doi: 10.1080/01904160802135092

Xu, C., and Shanklin, J. (2016). Triacylglycerol metabolism, function, and accumulation in plant vegetative tissues. *Annu. Rev. Plant Biol.* 67, 179–206. doi: 10.1146/annurev-arplant-043015-111641

Xu, X., Yang, H., Singh, S. P., Sharp, P. J., and Liu, Q. (2018). Genetic manipulation of non-classic oilseed plants for enhancement of their potential as a biofactory for triacylglycerol production. *Engineering* 4, 523–533. doi: 10.1016/j.eng.2018.07.002

Yang, M. F., Liu, Y. J., Liu, Y., Chen, H., Chen, F., and Shen, S. H. (2009). Proteomic analysis of oil mobilization in seed germination and postgermination development of *Jatropha curcas*. *J. Proteome Res.* 8, 1441–1451. doi: 10.1021/pr800799s

Yang, Y., Munz, J., Cass, C., Zienkiewicz, A., Kong, Q., Ma, W., et al. (2015). Ectopic expression of *WRI1* affects fatty acid homeostasis in *Brachypodium distachyon* vegetative tissues. *Plant Physiol.* 169, 1836–1847. doi: 10.1104/pp.15.01236

Yaseen, M., Ahmad, T., Sablok, G., Standardi, A., and Hafiz, I. A. (2013). Role of carbon sources for *in vitro* plant growth and development. *Mol. Biol. Rep.* 40, 2837–2849. doi: 10.1007/s11033-012-2299-z

Yongmanitchai, W., and Ward, O. P. (1993). Positional distribution of fatty acids, and molecular species of polar lipids, in the diatom *Phaeodactylum tricornutum*. *Microbiology* 139, 465–472. doi: 10.1099/00221287-139-3-465

Zaheer, K., and Akhtar, M. H. (2016). Potato production, usage, and nutrition - a review. *Crit. Rev. Food Sci. Nutr.* 56, 711–721. doi: 10.1080/10408398.2012.724479

Zale, J., Jung, J. H., Kim, J. Y., Pathak, B., Karan, R., Liu, H., et al. (2016). Metabolic engineering of sugarcane to accumulate energy-dense triacylglycerols in vegetative biomass. *Plant Biotechnol. J.* 14, 661–669. doi: 10.1111/pbi.12411

Conflict of Interest: The authors declare that the research was conducted in the absence of any commercial or financial relationships that could be construed as a potential conflict of interest.

frontiers in Plant Science

ORIGINAL RESEARCH
published: 17 March 2020
doi: 10.3389/fpls.2020.00288

A Versatile High Throughput Screening Platform for Plant Metabolic Engineering Highlights the Major Role of *ABI3* in Lipid Metabolism Regulation

Benjamin Pouvreau[1,2], Cheryl Blundell[1,2], Harpreet Vohra[3], Alexander B. Zwart[4], Taj Arndell[1], Surinder Singh[1] and Thomas Vanhercke[1]*

[1] Agriculture and Food, CSIRO, Canberra, ACT, Australia, [2] Synthetic Biology Future Science Platform, CSIRO, Canberra, ACT, Australia, [3] The John Curtin School of Medical Research, Australian National University College of Health and Medicine, Canberra, ACT, Australia, [4] Data61, CSIRO, Canberra, ACT, Australia

OPEN ACCESS

Edited by:
John Sedbrook, Illinois State University, United States

Reviewed by:
Timothy Patrick Durrett, Kansas State University, United States
Michael Marks, University of Minnesota Twin Cities, United States

***Correspondence:**
Benjamin Pouvreau
benjamin_pouvreau@yahoo.fr

Specialty section:
This article was submitted to Plant Metabolism and Chemodiversity, a section of the journal Frontiers in Plant Science

Received: *27 October 2019*
Accepted: *26 February 2020*
Published: *17 March 2020*

Citation:
Pouvreau B, Blundell C, Vohra H, Zwart AB, Arndell T, Singh S and Vanhercke T (2020) A Versatile High Throughput Screening Platform for Plant Metabolic Engineering Highlights the Major Role of ABI3 in Lipid Metabolism Regulation. Front. Plant Sci. 11:288. doi: 10.3389/fpls.2020.00288

Traditional functional genetic studies in crops are time consuming, complicated and cannot be readily scaled up. The reason is that mutant or transformed crops need to be generated to study the effect of gene modifications on specific traits of interest. However, many crop species have a complex genome and a long generation time. As a result, it usually takes several months to over a year to obtain desired mutants or transgenic plants, which represents a significant bottleneck in the development of new crop varieties. To overcome this major issue, we are currently establishing a versatile plant genetic screening platform, amenable to high throughput screening in almost any crop species, with a unique workflow. This platform combines protoplast transformation and fluorescence activated cell sorting. Here we show that tobacco protoplasts can accumulate high levels of lipid if transiently transformed with genes involved in lipid biosynthesis and can be sorted based on lipid content. Hence, protoplasts can be used as a predictive tool for plant lipid engineering. Using this newly established strategy, we demonstrate the major role of *ABI3* in plant lipid accumulation. We anticipate that this workflow can be applied to numerous highly valuable metabolic traits other than storage lipid accumulation. This new strategy represents a significant step toward screening complex genetic libraries, in a single experiment and in a matter of days, as opposed to years by conventional means.

Keywords: high throughput screening, protoplast, metabolic engineering, lipid accumulation, fluorescence activated cell sorting

INTRODUCTION

Modern societies have slowly transitioned, over the past couple of centuries, from a bio-based economy to a petrol-based economy. Agriculture consequently transitioned to a food/feed focus whereas it used to meet all demands for energy and materials too. Driven by the threat of climate change and a need for more sustainability, re-establishing a bio-based economy is currently a

major global challenge. To compete with established petrochemical industries, crops need to be re-engineered to have new traits or produce new compounds. However, current crop metabolic engineering approaches are slow and difficult, and this creates a significant bottleneck in the development of new crop varieties that are tailored to meet future agricultural needs in an ever changing environment.

As reflected by the late Richard Feynman's statement: "What I cannot create, I do not understand," the major challenge in crop metabolic engineering is to find the right set of genetic components necessary to obtain a desired trait. This is particularly due to traditional functional genetic studies in crops being time consuming, complicated and not usually compatible with high throughput. Indeed, it usually takes several months to over a year to obtain desired mutants or transgenic plants (Ishida et al., 2007; Yadava et al., 2017) necessary to study the effect of single genetic components on specific traits of interest. The testing of complex metabolic or genetic circuits thus seems like a herculean task. The use of model plants, such as *Arabidopsis thaliana*, with fully annotated genomes and much faster and cheaper gene delivery systems (Clough and Bent, 1998), had an undeniable impact on crop improvement (Provart et al., 2016), but still has limitations regarding time, scale and technology transfer between species.

While more promising, few transient transformation systems have been developed to test genetic components for crop re-engineering strategies. Currently, the most widely used transient transformation system for rapid gene testing is agroinfiltration of *Nicotiana benthamiana* leaves (Yang et al., 2000), which allows for the delivery of one or multiple genetic components to test multigene circuits in a few days (Wood et al., 2009). Pioneering studies have already demonstrated the power of such efficient transient transformation systems. For example, the "Leaf Oil" platform technology, which allows plants to accumulate oil in all vegetative organs (Vanhercke et al., 2017) with yields potentially exceeding those of canola and oil palm, was quickly developed thanks to an extensive number of design-built-test-learn cycles (Vanhercke et al., 2013, 2014; El Tahchy et al., 2017) that strongly relied on an efficient use of the agroinfiltration-based system. The technology is continuously being upgraded by further cycles to create tailor-made products for biofuel applications (Reynolds et al., 2015; Reynolds et al., 2017), and is also being transferred to a range of major crops such as sugarcane (Zale et al., 2016), maize (Alameldin et al., 2017) and *Sorghum bicolor* (Vanhercke et al., 2019). Such high biomass crops have the potential to become a future sustainable and abundant supply of plant oils for food, feed, biofuel and oleo-chemical applications (Rahman et al., 2016; Weselake, 2016). This type of assay is not limited to studying leaf specific metabolic pathways. Petrie et al. (2010) demonstrated that co-infiltration of the tested components in combination with the *A. thaliana LEAFY COTYLEDON2* (*LEC2*) gene results in a leaf with a seed-like gene regulation profile, thus allowing for the testing of seed-specific components. A modified version of this assay was also developed in transgenic *LEC2* induced *Brassica napus* somatic embryos for testing seed-specific components with increased reliability to predict seed traits (Belide et al., 2013). These assays allowed for the rapid gene testing and assembly of the ω3 fish-like oil synthetic seed biosynthesis pathway that was first deployed in *A. thaliana* as proof of concept (Petrie et al., 2012), and then in oilseed crops such as *Camelina sativa* (Petrie et al., 2014) and canola (Walsh et al., 2016), with ω3 production at industrially relevant levels. Nevertheless, these transient transformation systems are still limited in terms of scale, species and tissue specificity, and other transient assays are required to overcome these limitations.

Another type of transient system based on protoplast transfection has been available for more than 50 years, and now represents a very promising system for rapid testing of genetic components in most plants, and for several reasons. First, protoplasts can be isolated from almost any tissue of any crop (Burris et al., 2016), thus allowing better predictability through more species-targeted approaches than the agroinfiltration-based system that is established only in tobacco and few other species. Second, protoplasts are single cells, thus allowing more precise studies than multicellular systems to address tissue and cell-type specific questions. Thirdly, a very large number of protoplasts can be isolated from one preparation, allowing testing of many variables simultaneously in one assay. Finally, protoplast transformation is now well established (Yoo et al., 2007), with a higher efficiency than any other plant transformation system (Jiang et al., 2013), and is therefore very well suited for high throughput platforms. The use of protoplast-based systems also allows access to other types of high throughput approaches, such as flow cytometry and cell sorting, which open a wide new range of screening possibilities. Protoplasts have long been extensively used with fluorescence activated cell sorting for several different applications. Such methods were developed from the early 1980s for applications such as protoplast viral infection level monitoring (van Klaveren et al., 1983) and chlorophyll content and size distribution characterization (Galbraith et al., 1988). More recently, similar approaches have been used for more complex studies such as protein accumulation detection (Cronjé et al., 2004), overexpression analyses (Bargmann and Birnbaum, 2009), sorting of particular cell types for RNA isolation and transcriptome-wide analyses (Birnbaum et al., 2005; Bargmann and Birnbaum, 2010), or to study cell-type specific expression during both development and stress (Grønlund et al., 2012). Such techniques allow for the direct screening of millions of variants in a very short amount of time, and ongoing improvements (You et al., 2014) allow for the development of increasingly powerful high throughput screening methods. For example, recently, cell sorting based on the lipid content of thousands of mutant lines of a green unicellular algae was achieved in a few hours, followed by a few additional days for cellular multiplication and additional lipid analyses to confirm the phenotype (Terashima et al., 2015), representing one of the most powerful mutant screens ever reported for green vegetal cells. While random mutagenesis is not available for protoplasts, transient transformation is very efficient, and transformation of expression libraries could be carried out to generate large numbers of transformed cells for rapid trait evaluation by flow cytometry. However, sorting of plant protoplasts based on a high value trait, such as lipid accumulation, has not yet been reported.

The regulation of lipid biosynthesis and storage in plants has been extensively studied. The highly conserved plant transcription factors ABSCISIC ACID INSENSITIVE 3 (ABI3) (Giraudat et al., 1992), FUSCA3 (FUS3) (Luerssen et al., 1998), LEAFY COTYLEDON1 (LEC1) (Meinke et al., 1994; West et al., 1994), and LEC2 (Chen et al., 1997) are the major master regulators that control the gene regulation networks governing most seed developmental mechanisms (Suzuki et al., 2003; Braybrook et al., 2006; To et al., 2006; North et al., 2010; Wang and Perry, 2013). The *abi3*, *fus3*, *lec1*, and *lec2* mutants share common phenotypes such as reduced storage protein accumulation and anthocyanin accumulation (To et al., 2006). FUS3, LEC1, and LEC2 also have been reported to trigger triacylglycerol accumulation in seeds, leaves and liquid cell culture (Lotan et al., 1998; Zhang et al., 2002, 2016; Santos Mendoza et al., 2005; Tan et al., 2011; Vanhercke et al., 2017). The major action of LEC1, LEC2, and FUS3 on lipid accumulation is mostly through regulating directly or indirectly the expression of the Wrinkled1 (WRI1) transcription factor (Casson and Lindsey, 2006; Baud et al., 2007; Santos-Mendoza et al., 2008; Yamamoto et al., 2010; Wang and Perry, 2013; Marchive et al., 2014), but the complete picture of *WRI1* regulation is still unclear (Kim et al., 2016). *WRI1* function is highly conserved amongst plants. *WRI1* is a node acting at the interplay between these master regulatory elements and fatty acid metabolism. *WRI1* directly regulates the transcription level of many genes essential for fatty acid synthesis to trigger seed oil production (Baud et al., 2007; Pouvreau et al., 2011). After it was demonstrated that *WRI1* overexpression increases oil accumulation without undesirable side effects (Shen et al., 2010; Pouvreau et al., 2011), *WRI1* became a major target of metabolic engineering approaches to increase oil content (Vanhercke et al., 2013, 2014, 2017). By contrast, even though many of ABI3 targeted genes are known to function in seed oil storage (Wang et al., 2007; Monke et al., 2012), to date, little is known about the direct effect of *ABI3* on lipid content in plants.

In this study, we demonstrate that protoplasts from 15-day-old tobacco leaf can accumulate high levels of lipid if transiently transformed with genes involved in lipid biosynthesis. We observed a direct correlation between protoplast lipid content and protoplast fluorescence intensity after lipid-specific fluorescent staining. Furthermore, we show that protoplasts can be sorted based on lipid content and further used for downstream processing and analyses. Transient gene expression in protoplasts produced metabolic results similar to those reported for stably transformed plants, in terms of lipid accumulation. We demonstrate that combinatorial gene testing is possible in protoplasts and we observed a similar synergistic effect of the genes *WRI1* and *DGAT1* on increasing lipid accumulation in protoplasts, compared with previously published studies conducted in transiently and stably transformed leaves (Vanhercke et al., 2013, 2014). Taken together, our results demonstrate that tobacco leaf protoplasts are a reliable model for plant lipid engineering. This platform constitutes a new high throughput tool to develop plant lipid engineering strategies, but also an alternative strategy to study plant lipid metabolism in general, such as the relative effects of major known elicitors of lipid accumulation in plants. We compared the effect of *ABI3*, *FUS3*, *LEC1*, and *LEC2* on lipid accumulation in protoplasts. Our results confirm that *ABI3* is an important regulator of oil accumulation and demonstrate for the first time the direct correlation between *ABI3* overexpression and increased lipid content in plants. These results also suggest that *ABI3* might trigger lipid accumulation partly through pathways independent from *WRI1* and *LEC2* regulation.

MATERIALS AND METHODS

Plant Material and Growth Conditions

Plants used in this study all originated from the *Nicotiana tabacum* cultivar Wisconsin 38, including wild-type (WT) and a T4 generation *WRI1-DGAT1-OLEOSIN* transgenic line, referred to as High Oil (HO), for the high levels of triglycerides accumulating in its leaves (Vanhercke et al., 2014). Seeds were surface-sterilized by 2 min incubation in 70% ethanol, followed by 10 min incubation in 1.8% bleach and five washes in sterile water, all with frequent agitation. Seeds were sown on half MS media, supplemented with 3% sucrose, in petri dishes and placed in the dark at 4°C for 4 days. Plants were grown in a growth cabinet under 16 h day/8 h night light conditions (100 μmol m^{-2} s^{-1}) at 22°C/18°C, respectively.

Plasmids DNA Construction and Preparation

Vectors were designed as minimal plant expression constructs for production in large quantity in *Escherichia coli* and strong transient expression in tobacco protoplasts. A modified pENTR11 vector (Invitrogen) was used as a minimal backbone after removal of the ccdB operon, conserving only kanamycin resistance and the *E. coli* origin of replication. The chemically synthesized (GeneArt) *CaMV35S* promoter, coding sequence (*A. thaliana* WRI1, DGAT1, ABI3, FUS3, LEC1, or LEC2, respectively AT3G54320.1, AT2G19450.1, AT3G24650.1, AT3G26790.1, AT1G21970.1, or AT1G28300, codon optimized for tobacco) and NOS terminator were ligated in this minimal vector. For protoplast transient transformation, plasmid DNA was prepared using the NucleoBond Xtra Midi Kit (MACHEREY-NAGEL, Germany) according to the manufacturer's recommended protocol, and resuspended in ultrapure DNAse/RNAse-free distilled water (Invitrogen) at 1 μg/μl.

Protoplasts Preparation, Transient Transformation and Staining

The whole procedure was conducted under sterile conditions. Plants were collected 15 days after germination. Leaf tissues were harvested and thinly sliced in protoplast buffer (400 mM mannitol, 10 mM MES hydrate, 20 mM KCl, 20 mM CaCl2, 2 mM MgCl2, pH 5.7, 0.1% bovine serum albumin). Leaf strips were rinsed with fresh protoplast buffer, placed in enzyme solution (protoplast buffer supplemented with 1.2% cellulase Onozuka

R-10, 0.6% cellulase Onozuka RS, and 0.4% macerozyme R-10), subjected to vacuum for 10 min and incubated in enzyme solution for 16 h in the dark at 22°C. After incubation, protoplasts were released with 5 min agitation on a rotating plate at 50 rpm, filtered through a 40 μm cell strainer, washed twice with fresh protoplast buffer, counted on a hemocytometer, and then resuspended in fresh protoplast buffer at 0.25 M cells per ml. For transformation, protoplast samples were incubated for 1 h on ice, the buffer was then removed, pelleted protoplasts were resuspended in an identical volume of MMg solution (0.4 M mannitol, 15 mM MgCl2, 4 mM MES, pH 5.6), supplemented with 25 μg/ml of each plasmid and then mixed with an identical volume of PEG solution (40% PEG4000, 0.2 M mannitol, 300 mM CaCl2). After 5 min incubation, protoplasts were washed twice with fresh protoplast buffer, resuspended in fresh protoplast buffer at 0.25 M cells per ml, placed in culture plates and incubated in a growth cabinet under constant light conditions (150 μmol m^{-2} s^{-1}) at 22°C. For lipid staining, protoplasts in protoplast buffer at 0.25 M cells per ml were supplemented with 1 μg/ml BODIPY^{TM} 493/503, incubated for 15 min at room temperature in the dark, spun down (300 × g for 5 min) and resuspended in the same volume of fresh protoplast buffer.

Lipid Extractions and Analyses

For total lipid extractions, fresh leaves were cut as for protoplast isolation and freeze-dried whereas freshly isolated protoplasts were spun down (for 5 min) to remove all buffer and then snap-frozen in liquid nitrogen. Samples were ground with a ball bearing in TissuLyser II (QIAGEN, Germany) and homogenized in 36% methanol, 36% chloroform, 20 mM acetic acid, 1 mM EDTA. Total lipid fraction (lower phase) was separated by 2 min centrifugation at 4000 × g, dried under nitrogen and resuspended in chloroform. Total lipid extracts were fractionated by thin layer chromatography fractionation as previously described (El Tahchy et al., 2017), followed by fatty acid methyl ester quantification and analysis by gas chromatography, also conducted as previously described (Vanhercke et al., 2013; El Tahchy et al., 2017). Unless otherwise stated, analyses were conducted on a minimum of three individual samples for each genotype, condition or cell population.

Cell Imaging by Microscopy

Glass slides were prepared by placing four drops of petroleum jelly in a square arrangement and 50 μl of protoplasts at 1 M cells per ml in protoplast buffer within that square. A coverslip was then gently pressed down on the solution and jelly drops. Protoplasts were captured (**Figure 3A**) using a 40× objective on a Zeiss Axio Imager M1 fluorescence compound microscope fitted with an AxioCam HR Rev3 camera (Carl Zeiss Microscopy GmbH, Germany), with bright field and no filter or with UV light and a Filter Set 38 HE (Excitation filter BP 450–490 nm, Beam splitter FT 495 HE, emission BP 500–550 nm) to visualize lipid bodies stained with BODIPY^{TM} 493/503. Images were acquired using the Zeiss Zen imaging software (blue edition, Carl Zeiss Microscopy GmbH, Germany).

Protoplast Flow Cytometry and Fluorescence Activated Cell Sorting

Cell sorting was performed on a BD FACS Aria III (BDIS, San Jose) with a 100 μm nozzle and data were acquired and analyzed using the DIVA 8.0 software. Protoplasts suspended in the protoplast buffer at a concentration of 1 million/ml were acquired at an approximate flow rate of 10 μl/min with mild agitation. Data were acquired for 30,000 particles and after exclusion of doublets, the samples were analyzed for BODIPY^{TM} 493/503 (Excitation 488 nm, Emission 530/30 nm) and chlorophyll auto fluorescence (Excitation 640 nm, Emission 670/30 nm). Cells were sorted based on BODIPY/chlorophyll signal ratio. For each gated population, three independent samples of 0.25 M cells were collected in protoplast buffer.

Flow cytometric analyses were conducted on an Invitrogen Attune NxT Flow Cytometer and analyzed with Invitrogen Attune NxT Software. Cells suspended in the protoplast buffer at a concentration of 0.25 M cells per ml were analyzed at a flow rate of 250 μl/min and data were acquired for 300 μl. BODIPY^{TM} 493/503 fluorescence was excited with a 488-nm laser and emission was captured by a 530/30-nm bandpass filter. Unless otherwise stated, analyses were conducted on a minimum of three individual samples for each condition.

Statistical Analysis

For the statistical analysis presented in **Figure 5**, data were analyzed via a linear mixed model fitted using the "lmer" linear mixed modeling function from the "lme4" package (Bates et al., 2015) of the R statistical software system (R Core Team., 2014). This allowed the analysis to properly account for the impacts of the grouping of processed samples together on plates (via a factor "Plate"), and also recognize that the full dataset is formed from two individual repeats of the same experiment (via a factor "Experiment"). Hence, the model incorporated a (random effects) "blocking" structure consisting of "Sample", nested within Plate, nested within "Experiment". Treatment (fixed effects) structure was modeled as a two-way factorial, *WRI1* crossed with *DGAT1*, where factors *WRI1* (having levels WRI1+ and WRI1−) and *DGAT1* (levels DGAT1+ and DGAT1−) represent the presence/absence of the corresponding genes in the samples. Hence, the WT treatment corresponds to the combination "WRI1−:DGAT1−" and the samples transformed with *DGAT*1, *WRI1*, or both, correspond to "WRI1−:DGAT1+," "WRI1+:DGAT1−" and "WRI1+:DGAT1+," respectively. The model allows to test for the "main effect" of *WRI1* (the average effect of *WRI1* status, regardless of *DGAT1* status), the main effect of *DGAT1* (the average effect of *DGAT1* status, regardless of *WRI1* status), and the interaction effect between *WRI1* and *DGAT1* (the combined effects of *WRI1* and *DGAT1* after having removed effects of the two main effects terms).

In fitting any statistical model, it is important to assess various residual diagnostic plots to ensure that the assumptions underlying the model are met and that predictions and tests derived from the model are reliable. Residual diagnostic plots from the fit of the model to the raw data suggested that the random scatter in the data increases as the mean of the data

increases; a common property of such assay data. To model the data appropriately, a log10 (log to base 10) transformation of the data was required to ensure that the model assumption of constant variance was met. The statistical model was therefore applied to the log10 transformed data, and predicted means were back-transformed as required to obtain predictions on the original data scale. Treatment predicted means and associated statistics were obtained using the R "predictmeans" package (Luo et al., 2018). Tests for the statistical significance of terms in the factorial treatment structure were obtained using the R "lmerTest" (Kuznetsova et al., 2017) package.

The errors bars and *P*-values presented in **Figures 2**, **3**, **4** and **6** correspond to the standard deviation and a two-tailed t-test with unequal variance.

RESULTS

Protoplasts Can Be Used as a Predictive Tool for Plant Lipid Engineering

To confirm that protoplasts can be used as a predictive tool for plant lipid engineering, we tested if the HO phenotype of a previously established stably transformed line could be reproduced with protoplasts isolated from the same line. The surprising lack of studies regarding lipid accumulation in protoplasts to date suggested that such approaches might not be possible to be conducted. We previously reported the establishment of a HO line of tobacco (henceforth referred to as HO) accumulating in its leaves up to 24 times more total lipid, and particularly 76 times more triglycerides, at maturity, compared to WT (Vanhercke et al., 2014). We also reported that this increased lipid accumulation was gradual during development, thus potentially making it difficult to measure the increase in very young tissue. Leaf tissues from 15 days old WT and HO plants were harvested and partly used for protoplast isolation. The remaining leaf tissues as well as protoplasts isolated from the same leaf samples were then analyzed for their triglycerides and total lipid content (**Figure 2**). The analysis revealed that at this early developmental stage and under the specific growth conditions of this assay, HO plantlets had accumulated about two times more total lipid and almost 90 times more triglycerides than WT, while HO protoplasts had accumulated about 25% more total lipid and more than two times more triglycerides than WT. Thus, despite some variation in intensity, the analysis confirmed that the increase can still be measured at the protoplast level. We also confirmed that even though the variation between the HO line and WT would be easier to measure by focusing on the triglycerides level, it is still quite feasible to measure it at the total lipid level. This will allow for the use of generalist neutral lipid stains, which stain any neutral lipid and not only triglycerides, to measure the variation in oil content.

We can observe a disparity at 15 days between the lipid contents of fresh tissues and protoplasts, indicating that the variation between HO and WT is reduced in the protoplast samples. One reason could be that fresh tissue samples are mostly constituted of fibres, which contains no lipid, and are not present in the protoplast sample. Another explanation is that the total leaf sample contains multiple types of cells, whereas protoplasts isolation methods are notorious to mostly enrich mesophyll cells.

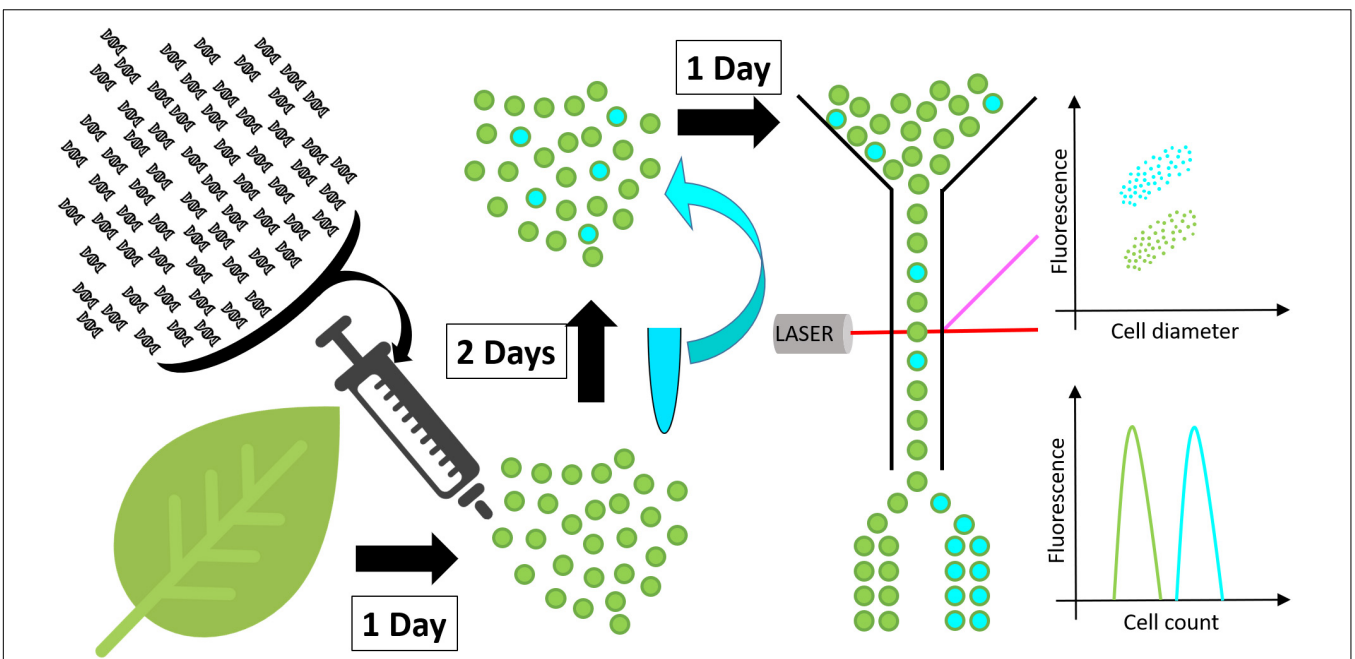

FIGURE 1 | Schematic representation of the high throughput screen developed in this work. Protoplasts (green spheres) are isolated from a leaf and transformed with DNA constructs. After 48 h incubation, to allow for transgene expression and metabolite accumulation, protoplasts are stained with a neutral lipid specific fluorescent stain and screened for fluorescence by flow cytometry or fluorescence activated cell sorting.

It could be that mesophyll cell contains more TAG than other types of leaf cells, but this was not tested in this study. This could explain why the WT protoplast sample appears to have a richer lipid composition than the fresh tissue it was prepared from, because it concentrates a certain type of cells only. Finally, a recent study demonstrated that the protoplast isolation itself could trigger the accumulation of some lipid species (Barnes et al., 2019), which could also explain why the WT protoplast sample appears to have a richer lipid composition than the WT leaf tissue sample.

A New and Rapid Method for Testing DNA Constructs for Plant Lipid Engineering

The new protoplast-based platform for high throughput plant lipid engineering presented in this study allows for the testing of DNA constructs in regard to their ability to induce lipid accumulation in plant cells within only 72 h. Using BODIPY^{TM} 493/503, a fluorescent neutral lipid stain, lipid quantity in protoplasts is evaluated by measuring cell fluorescence by flow cytometry or alternatively by fluorescence activated cell sorting if specific cell populations need to be separated for further analyses (**Figure 1**). Protoplasts with high lipid accumulation consequently exhibit higher fluorescence and can be identified and eventually sorted based on the relative intensity of the fluorescent stain per cell.

Tobacco Leaf Protoplasts Can Be Sorted Based on Lipid Content

In the previous part, we demonstrated that we can measure variation in protoplast oil accumulation by conducting the analysis at the total lipid level instead of focusing on triglyceride accumulation only, which should allow for the use of a generalist neutral lipid stain, which stains triglycerides and all other neutral lipid, to measure the variation in oil content. We next sought to confirm that protoplasts can be sorted based on storage lipid content. Protoplasts were isolated from the leaves of 15-day-old WT and HO plantlets as described above, and stained with BODIPY^{TM} 493/503, a generalist neutral lipid stain, prior to microscopy (**Figure 3A**) or flow cytometric analysis (**Figure 3B**). WT and HO stained protoplasts were consecutively sorted, based on their intensity of BODIPY^{TM} 493/503 fluorescence relative to chlorophyll auto-fluorescence. Previous iterations of sorting coupled with microscopy allowed us to determine where the intact green cells are situated in the graph generated during cell sorting (data not shown). Two distinct populations of intact green cells were gated, with P1 defined as the most intensively stained cells and P2 as the rest of the intact green cells (**Figure 3B**). Average stain fluorescence per cell was calculated for each population (**Figure 3C** left). For each population, three samples of 250,000 cells were collected and then subjected to the same total lipid analysis as described above (**Figure 3C** right). This was not done for the WT-P1 population because it was not possible to retrieve enough cells to conduct the analysis. Several conclusions could be drawn for this assay.

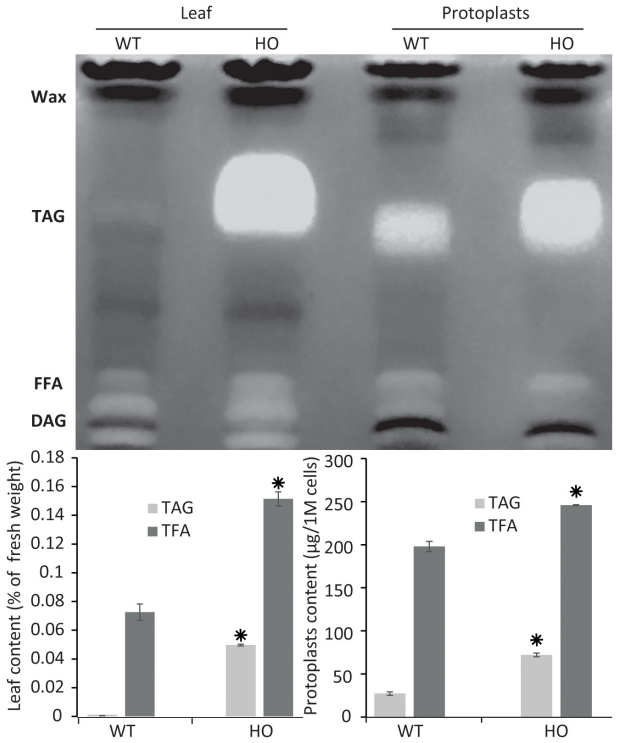

FIGURE 2 | Protoplast lipid quantification results mimic total tissue lipid analysis results. Thin layer chromatography plate separation of total fatty acids (TFA) extracted from leaves or from isolated protoplasts of WT or HO lines and total lipid and triacylglycerol (TAG) quantification of the same samples quantified by gas chromatography. Concentrations are given in percent relative to leaf fresh weight or in micrograms per million cells. Bars represent standard deviation. Stars indicate statistically relevant variation compared to WT (P-values < 0.05). FFA, free fatty acids; DAG, diacylglycerol. See **Supplementary Figure S1** for standards run next to samples.

First, we confirmed that BODIPY^{TM} 493/503 staining allows for measuring of the oil content difference that we previously measured between WT and HO protoplasts. The whole HO sample had a higher average protoplast stain fluorescence intensity than the whole WT sample (blue bars in **Figure 3C** left). This correlates with the results presented in the previous part demonstrating that HO protoplasts accumulate more total lipid than WT and illustrates the direct correlation between lipid content and BODIPY^{TM} 493/503 fluorescence intensity.

Secondly, the flow cytometric analysis showed that the HO sample had a distinct P1 population that segregated from the rest of the cells, while the WT cells attributed to the P1 population corresponded to the top cells of the P2 population rather than being a distinct cell population (**Figure 3B**). For both WT and HO samples, cells of the P1 population exhibited higher average stain fluorescence intensity compared to cells of the P2 population (**Figure 3C** left). Lipid analysis revealed that the HO-P2 population was significantly more lipid-rich than the WT-P2 population and that the HO-P1 population was significantly more lipid-rich than both the HO-P2 and WT-P2 populations (**Figure 3C** right). The variation in total lipid quantified in the

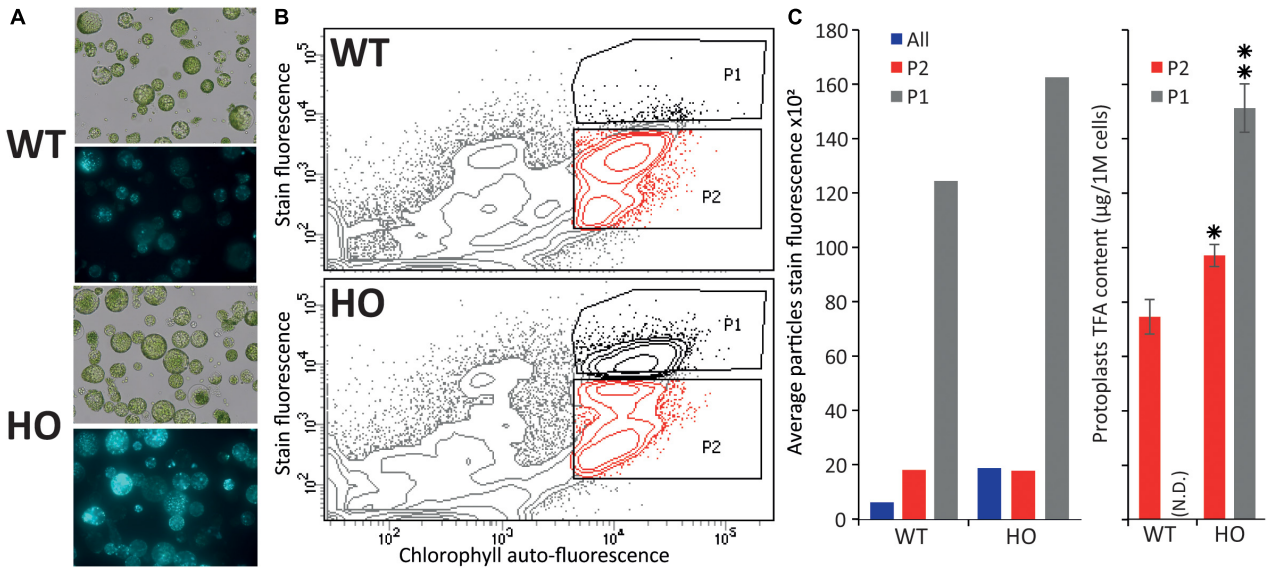

FIGURE 3 | Fluorescence activated cell sorting of lipid rich tobacco leaf protoplasts. **(A)** Microscopy images of protoplasts extracted from WT or HO (line with high leaf oil content) tobacco leaves in bright field (top) and their lipid content (bottom), visualized under fluorescent light after BODIPY^{TM} 493/503 staining. **(B)** Cell sorting of the same protoplast samples, with the P1 population defined as the protoplasts with the highest stain fluorescence to chlorophyll auto-fluorescence ratio, and P2 defined as the remainder of the intact cells (based on previous data not show). **(C)** Average stain fluorescence (left) and lipid content (right) for each sorted population. Average stain fluorescence of each whole sample is also indicated (blue bars). Where N.D. is in brackets, this indicates not determined. Error bars represent the standard deviation. Asterisks represent statistically significant differences (P-value < 0.05) compared with WT (one asterisk) or with both WT and HO P2 population (two asterisks).

HO-P2 and WT-P2 populations, while these two populations present a very similar level of fluorescence can be explained by the strong disparity between the ratios of different lipid species present in WT and in HO samples (**Supplementary Table S1**). It is possible that BODIPY^{TM} 493/503 has different affinity depending on lipid species, which was not investigated in this study but could explain why the HO-P2 and WT-P2 populations present an identical fluorescence intensity after staining, while containing a slightly different amount of total lipid. Additionally, BODIPY^{TM} 493/503, while being the most appropriate lipophilic dye available for this study, only binds to neutral lipid, while the total lipid quantification would quantify a much larger spectra of lipid species.

Overall, this assay confirmed that protoplasts can be sorted based on lipid content and that measuring the whole sample BODIPY^{TM} 493/503 fluorescence signal (green bars in **Figure 3C** left) is enough to evaluate the effect of a gene combination on the overall lipid content in protoplasts. We also note that the variation measured between the WT and HO sample is amplified when using BODIPY^{TM} 493/503 staining coupled with flow cytometry (compared with lipid analysis methods), suggesting that this alternative screening strategy could be more powerful than traditional ones.

Transiently Transformed Tobacco Leaf Protoplasts Can Accumulate Lipid

We have established that leaf protoplasts from a stable transgenic line that accumulates more oil in its leaves than WT also accumulates on average more oil per protoplast compared to WT and that the difference can be measured by traditional lipid analysis or measured by flow cytometry after protoplast isolation and appropriate staining. However, to date, it was unclear if and how leaf protoplasts would produce an increased quantity of oil compared to WT, after isolation and transient transformation, reflected by the absence of any similar study in the literature.

The stable transgenic line used in the study over-expresses a combination of genes coding for the *A. thaliana* WRI1 transcription factor, a regulator of the late glycolysis and *de novo* fatty acid biosynthesis pathways, the *A. thaliana* DGAT1 acyl-CoA: diacylglycerol acyltransferase, a major lipid metabolism enzyme, and an OLEOSIN oil body protein from *Sesamum indicum*, which coats oil droplets and protects them from degradation. The reasoning for including OLEOSIN was that achieving greater oil accumulation in leaves in a long gene-expression-window (stable expression) might have required reducing oil degradation in this non-seed tissue. However, we previously demonstrated that the combined transient overexpression of *WRI1* and *DGAT1* only in *N. benthamiana* leaves was enough to produce a measurable and significant synergistic effect on leaf oil content (Vanhercke et al., 2013).

Based on the results presented above, next we tested transient transformation of leaf protoplasts with genetic constructs carrying expression cassettes for *WRI1* or *DGAT1* or both and measured the difference in protoplast total neutral lipid content, using BODIPY^{TM} 493/503 staining and flow cytometry recording

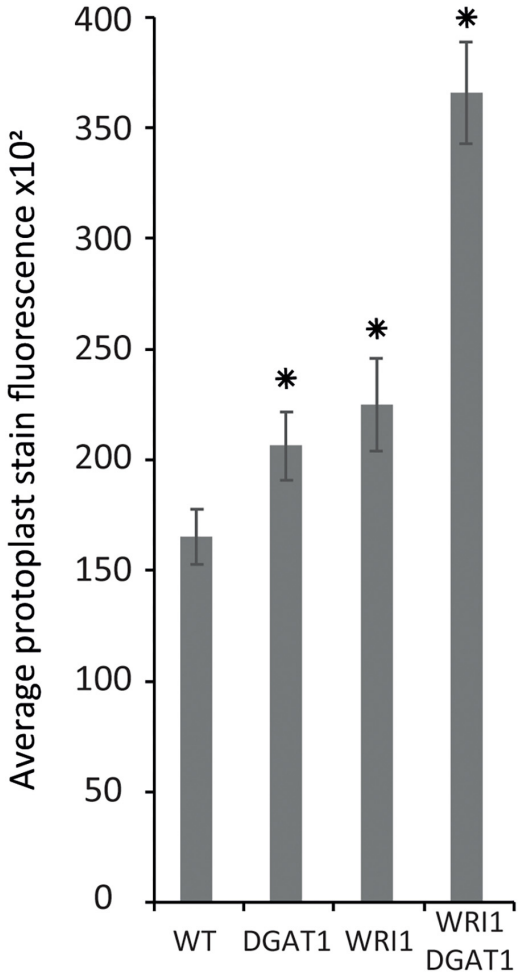

FIGURE 4 | Lipid accumulation in tobacco leaf transiently transformed protoplasts. Lipid accumulation in WT tobacco leaf protoplasts compared to WT protoplasts transiently transformed with WRI1 or DGAT1 or both, was measured with BODIPY^{TM} staining and flow cytometry recording of the average particle stain fluorescence for the whole sample. Error bars represent the standard deviation. Asterisks represent statistically significant differences (*P*-value < 0.05) compared with WT.

of the average protoplast stain fluorescence for the whole sample (**Figure 4**). Compared to the non-transformed control, leaf protoplasts transiently transformed with *WRI1* or *DGAT1* or both exhibited increased average stain fluorescence, indicating an increase in total neutral lipid content.

We also observed that when co-transformed, the combined effect of *WRI1* and *DGAT1* on lipid accumulation is greater than the additive effect of each individual transformations, illustrating a synergistic effect of *WRI1* and *DGAT1* (**Figure 4**) toward lipid accumulation in *N. tabacum* leaf protoplast, consistent with previous reports from *N. benthamiana* leaf transient assay (Vanhercke et al., 2013) and stably transformed *N. tabacum* plants (Vanhercke et al., 2014). The significance of this observation was accessed by a statistical analysis, which is further discussed below.

Combinatorial Gene Testing in Protoplasts Mimics Results Obtained With Leaf Transient Assay

The statistical analysis of the data confirms the statistical significance of the synergistic effect, with a *P*-value for the interaction effect on the log10-transformed scale of $p < 5e\text{-}6$. An interaction plot of the WRI1 by DGAT1 predicted means is given in **Figure 5A**. The significant *P*-value confirms that the lack of parallelism of the lines (and hence the presence of the synergistic effect) joining the pairs of means is genuine. **Figure 5B** plots the predicted means back-transformed to the scale of the data, with associated back-transformed 95% confidence interval limits for the means indicated by the error bars.

Overall our results confirm that protoplast systems are robust models that can be used to predict and inform plant phenotype and are compatible with combinatorial gene testing. This finding is particularly important for coupling transient protoplast expression with high throughput combinatorial gene screening.

ABI3 Induces Lipid Accumulation in Tobacco Leaf Protoplasts

Our new screening strategy constitutes a new high throughput tool to fast-track plant lipid engineering strategies and offers an alternative method to study plant lipid metabolism. We therefore wanted to use this newly developed strategy to investigate the relative effect of the major known seed specific developmental regulators. ABI3, FUS3, LEC1, and LEC2 are master regulators that control the gene regulation networks governing most seed developmental mechanisms. FUS3, LEC1, and LEC2 also have been reported to trigger oil accumulation through regulation of *WRI1*, which controls the expression of many genes essential for fatty acid synthesis. However, while many targets of ABI3 were identified to function in seed oil storage, the direct effect of *ABI3* on lipid content in plants remained undocumented.

Tobacco leaf protoplasts were transiently transformed with *WRI1* and *DGAT1* only or with one of the master regulators, being *ABI3*, *FUS3*, *LEC1*, or *LEC2*. The effect on protoplast total neutral lipid content was then measured and compared as described above (**Figure 6A**). This first assay indicated that in addition to the combined effect of *WRI1* and *DGAT1*, only co-expression with *FUS3* and *ABI3* significantly (*P*-value < 0.05) further increased protoplast total neutral lipid content. This was particularly surprising due to the lack of a previously reported direct effect of *ABI3* overexpression on plant lipid accumulation. To date, the most efficient gene combination reported for lipid accumulation enhancement involved *WRI1* with *DGAT1* and *LEC2* or *SDP1* silencing (Vanhercke et al., 2017). Therefore, in a second similar analysis we investigated in more detail the individual effect of individual genes (*WRI1*, *DGAT1*, *LEC2*, and *ABI3*) and of several related combinations on total neutral lipid content in transiently transformed protoplasts (**Figure 6B**). This second assay confirmed that *ABI3* overexpression alone resulted in the highest accumulation of total neutral lipid in protoplasts. In addition, unlike *LEC2*, co-expression with *ABI3* further increased the lipid content of protoplasts transiently transformed with *WRI1* and *DGAT1*. This difference supports

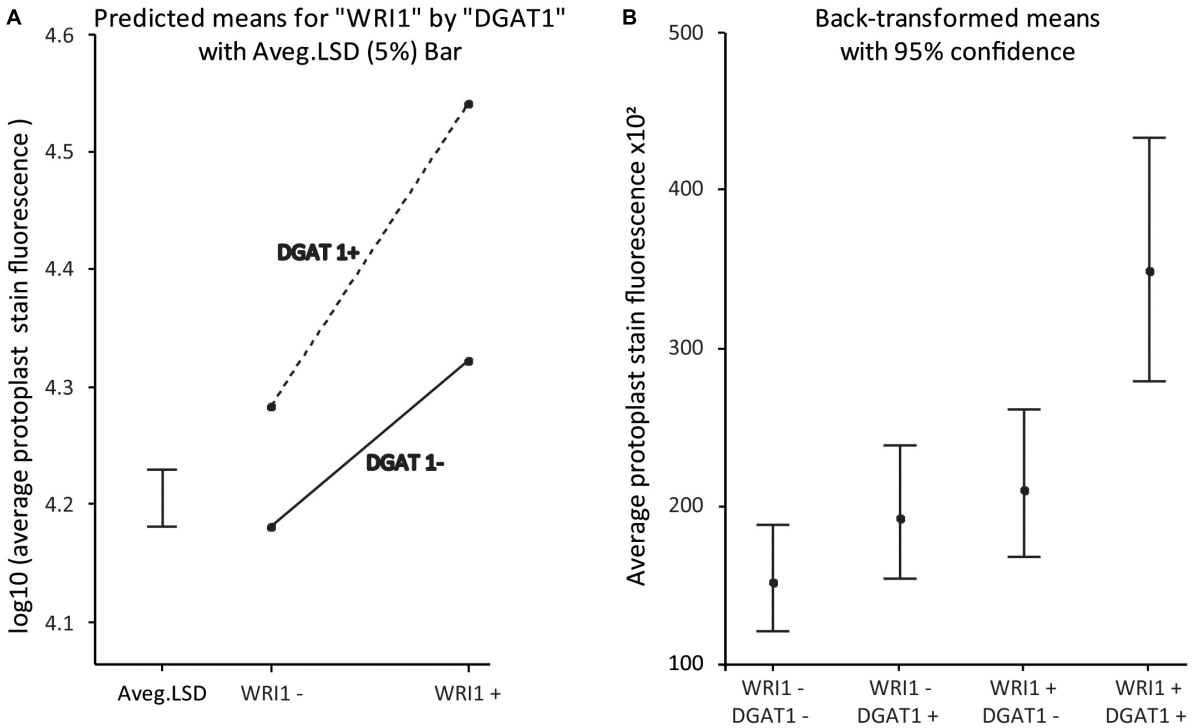

FIGURE 5 | *WRI1* and *DGAT1* have a synergistic positive effect on protoplast lipid biosynthesis. **(A)** Interaction plot of predicted treatment means with 5% Least Significant Difference (LSD) bar on the log10-transformed scale and **(B)** Plot of the back-transformed predicted means (with back-transformed 95% confidence interval limits) from the analysis of the data previously presented in **Figure 4B**. WT corresponds to "WRI1−:DGAT1−" and the samples transformed with *DGAT1*, *WRI1* and both, correspond to WRI1−:DGAT1+, **"**WRI1+:DGAT1−**"** and **"**WRI1+:DGAT1+**,"** respectively.

the previous reports that *LEC2* regulates fatty acid biosynthesis mainly through the regulation of *WRI1* (Baud et al., 2007; Santos-Mendoza et al., 2008). Thus, the addition of *LEC2* might be ineffective due to the expression level of exogenous *WRI1* in the co-transformed protoplasts being already so high that triggering the expression of native *WRI1* would make a negligible effect on the overall *WRI1* expression levels in protoplasts. Overall, our results suggest that *ABI3* control over plant lipid metabolism and storage might involve mechanisms that act independently from the previously described *LEC2* and *WRI1* regulation networks. Our new screening approach also suggests that *ABI3* could be an important factor triggering oil accumulation in plants and suppose that *ABI3* should be of prime interest in future plant lipid engineering approaches.

DISCUSSION

Transient Protoplast Transformation as an Alternative Predictive Tool for Plant Lipid Engineering

In this study, we demonstrated that protoplasts from 15-day-old tobacco leaves are a reliable model to study plant lipid engineering. This protoplast-based screening assay takes about three days to complete, as compared to the minimum of two weeks required for a traditional transient leaf transformation assays based on agroinfiltration and GC analysis. We confirmed the direct correlation between protoplast lipid content and protoplast fluorescence intensity after lipid specific fluorescent staining. Furthermore, we show that protoplasts can be sorted based on lipid content and further used for downstream processing and lipid or molecular analyses. Our results demonstrate that transient gene expression in protoplasts produces lipid accumulation results similar to those obtained in stably transformed plants. We confirm that combinatorial gene testing is possible in protoplasts, with synergistic effect of the genes *WRI1* and *DGAT1* on increasing lipid accumulation in protoplasts, comparable to previously published studies conducted in transiently and stably transformed leaves (Vanhercke et al., 2013, 2014).

ABI3 Is a Major Regulator of Lipid Accumulation in Plant Cell

Using our newly developed workflow, we demonstrated that *ABI3* has a significant effect on protoplast total neutral lipid content. *ABI3* super-transformation significantly further increased the lipid content of protoplasts transiently transformed with *WRI1* and *DGAT1*, to a higher level than other known major effectors.

This result suggests that *ABI3* control over plant lipid metabolism and storage might at least partially involve mechanisms that are independent from the previously described *LEC2* and *WRI1* regulation networks. Our new approach also suggests that *ABI3* is a major regulator of oil accumulation in

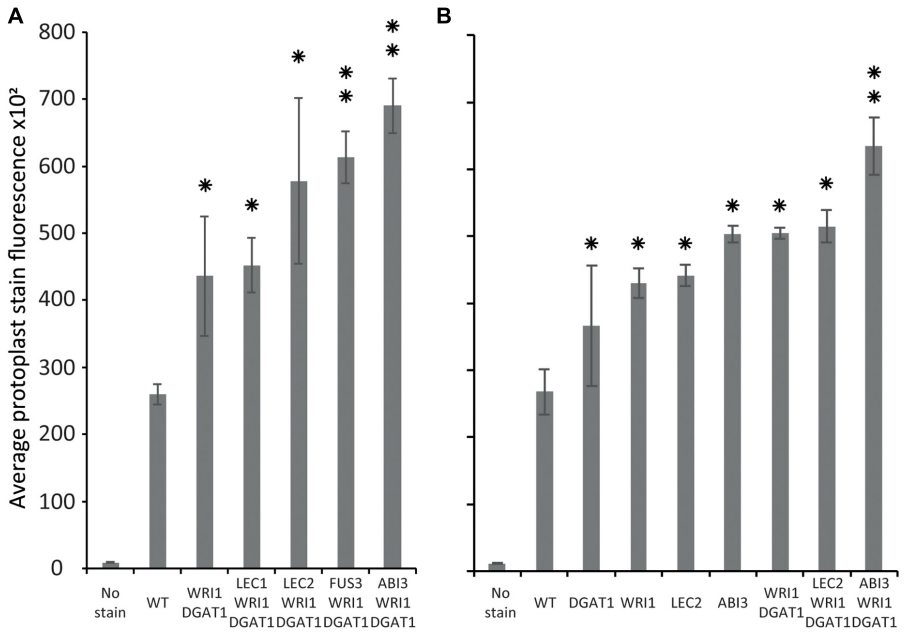

FIGURE 6 | Comparison of the relative effect of various transiently transformed effectors on lipid accumulation in tobacco leaf protoplasts. Lipid accumulation, compared to WT, in tobacco leaf protoplasts transiently transformed with WRI1, DGAT1, ABI3, FUS3, LEC1, or LEC2 and various combinations of these constructs, was measured by flow cytometry and based on the average particle stain fluorescence for the whole sample following BODIPY^{TM} staining. Bars represent standard deviation. **(A)** Comparative additional effect of ABI3, FUS3, LEC1, or LEC2 on lipid content in protoplasts co-transformed with WRI1 and DGAT1. **(B)** Individual effect of WRI1, DGAT1, ABI3, LEC2 and of various combinations of these constructs on lipid content in co-transformed protoplasts. A single star represents statistically significant difference (P-value < 0.05) compared with WT, while the double stars represent additional statistically significant difference (P-value < 0.05) compared with WRI1 and DGAT1 combination (shown for samples with significant increase only).

plants and reveal ABI3 as a new target for future plant lipid engineering approaches.

A New High Throughput Platform for Gene Function and Plant Metabolic Engineering Study

The protoplast-based workflow presented in this study is very versatile and should be compatible with many crop species and for a wide range of future output traits. Indeed, protoplasts can nowadays be isolated from almost any plants and any tissue. A profusion of methods were developed during the 1970s and 1980s for many major crops and model plants, including tobacco (*N. tabacum*) (Takebe and Otsuki, 1969; Guerche et al., 1987a), cowpea (*Vigna unguiculata*) (Hibi et al., 1975), tomato (*Solanum lycopersicum*) (Motoyoshi and Oshima, 1979), turnip (*Brassica rapa*) (Howell and Hull, 1978), barley (*Hordeum vulgare*) (Loesch-Fries and Hall, 1980), cucumber (*Cucumis sativus*) (Maule et al., 1980) great millet (*Sorghum bicolor*), rice (*Oryza sativa*), wheat (*Triticum monococcum*) (Ou-Lee et al., 1986; Bart et al., 2006), canola (*B. napus*) (Guerche et al., 1987b), *A. thaliana* (Damm et al., 1989), and maize (*Zea mays*) (Sheen, 1990). Such approaches then fell into disuse probably due to the very high technical skills required to perform high quality protoplast isolation, transformation and culture. However, new methods were sporadically released for other crops of interest, such as carrot (*Daucus carota*) (Liu et al., 1994). Recently, in the wake of a multitude of new high throughput cutting-edge technologies becoming easily accessible, protoplast-based systems have regained in their popularity and a profusion of improved methods have been released. Protoplast systems are the most suited for rapid screening of gene silencing (siRNA and miRNA) and genome editing (e.g., CRISPR) targets (Zhai et al., 2009; Cao et al., 2014; Maćkowska et al., 2014; You et al., 2014; Schapire and Lois, 2016). In addition, protoplast-based systems are now available for almost any plant of commercial interest, including lettuce (*Lactuca sativa*) (Sasamoto and Ashihara, 2014), grape (*Vitis vinifera*) (Wang et al., 2015) and bean (*Phaseolus vulgaris*) (Nanjareddy et al., 2016) and even the less expected, such as oil palm (*Elaeis guineensis*) (Masani et al., 2014), poplar (*Populus euphratica*) (Guo et al., 2015) and switchgrass (*Panicum virgatum*) (Burris et al., 2016).

In addition, our strategy should allow similar approaches for a broad variety of other metabolic traits since many fluorescent dyes, specific to particular metabolites are available. In the absence of a specific stain, genetic switches or biosensors can be developed for the specific detection of small molecules such as toluene (Behzadian et al., 2011), metabolites (Liu et al., 2017), and even specific proteins of interest (Abe et al., 2011; Wongso et al., 2017). For example, a new phosphatidic acid (PA) biosensor was recently developed to track PA cellular concentration and dynamics (Li et al., 2019). PA is the precursor of most phospholipid and triglyceride and represents around 1% of all lipid. PA acts as a key signaling lipid that predominantly

accumulates at the plasma membrane. This biosensor was based on the use of Förster resonance energy transfer (FRET) and was used to study the spatio-temporal complexity of PA accumulation in plant tissues and its contribution to mediate plant response to salt stress. Numerous other biosensors have been also developed based on FRET to study protein-protein, protein-DNA or DNA-DNA interactions (Lymperopoulos et al., 2010; Crawford et al., 2012). Alternatively, riboswitches have been engineered as nucleotide-based biosensors with great potential (Hallberg et al., 2017; Villa et al., 2018).

The new screening strategy presented in this study constitute the first step toward high throughput screening of complex genetic libraries in a plant system by using transient protoplast transformation and rapid cell sorting based on a fluorescent signal that is linked to a trait of interest. The workflow can be completed as a single experiment in a matter of days as opposed to several years that are needed by conventional means. Such novel synthetic biology inspired high throughput screens are paving the way for rapid identification of new unreported genes or gene combinations that significantly improve traits of interest in crops and thereby greatly improve the timelines associated with crop improvement (Zhang et al., 2019).

DATA AVAILABILITY STATEMENT

All datasets generated for this study are included in the article/**Supplementary Material**, excepted raw flow cytometry data.

AUTHOR CONTRIBUTIONS

BP, TV, and SS conceived the study. BP and CB performed the experimental work with assistance from HV for fluorescence activated cell sorting. BP analyzed the data with assistance from AZ for statistical analysis. BP wrote the manuscript with contributions from all other authors.

FUNDING

This work was partly funded through the CSIRO Synthetic Biology Future Science Platform and the CSIRO Research Office CERC Postdoctoral Fellowship scheme.

ACKNOWLEDGMENTS

Thanks to Nathalie Niesner for cloning the *DGAT1* fragment into the "CaMV35S promoter/NOS terminator" expression cassette of the modified pENTR11 vector. Thanks also to Lauren Venugoban for aiding with microscopy.

SUPPLEMENTARY MATERIAL

The Supplementary Material for this article can be found online at: https://www.frontiersin.org/articles/10.3389/fpls.2020.00288/full#supplementary-material

FIGURE S1 | Repeat of thin layer chromatography plate presented in **Figure 2**. Thin layer chromatography plate separation of total fatty acids (TFA) extracted from leaves or from isolated protoplasts of WT or HO lines. STD stands for standards run in parallel of the samples to validate the location of the lipid.

TABLE S1 | Raw data for lipid quantifications presented in **Figures 2**, **3**. Note: TAG/TFA content in tobacco leaf is presented in % of fresh weight leaf and in protoplasts in μg/1 M cells.

REFERENCES

Abe, R., Ohashi, H., Iijima, I., Ihara, M., Takagi, H., Hohsaka, T., et al. (2011). "Quenchbodies": quench-based antibody probes that show antigen-dependent fluorescence. *J. Am. Chem. Soc.* 133, 17386–17394. doi: 10.1021/ja205925j

Alameldin, H., Izadi-Darbandi, A., Smith, S. A., Balan, V., Jones, A. D., and Sticklen, M. (2017). Production of seed-like storage lipids and increase in oil bodies in corn (Maize; *Zea mays* L.) vegetative biomass. *Ind. Crops Products* 108, 526–534. doi: 10.1016/j.indcrop.2017.07.021

Bargmann, B. O., and Birnbaum, K. D. (2009). Positive fluorescent selection permits precise, rapid, and in-depth overexpression analysis in plant protoplasts. *Plant Physiol.* 149, 1231–1239. doi: 10.1104/pp.108.133975

Bargmann, B. O., and Birnbaum, K. D. (2010). Fluorescence activated cell sorting of plant protoplasts. *J. Vis. Exp.* 18:1673.

Barnes, A. C., Elowsky, C. G., and Roston, R. L. (2019). An *Arabidopsis* protoplast isolation method reduces cytosolic acidification and activation of the chloroplast stress sensor SENSITIVE TO FREEZING 2. *Plant Signal. Behav.* 14:1629270. doi: 10.1080/15592324.2019.1629270

Bart, R., Chern, M., Park, C.-J., Bartley, L., and Ronald, P. C. (2006). A novel system for gene silencing using siRNAs in rice leaf and stem-derived protoplasts. *Plant Methods* 2:13.

Bates, D., Mächler, M., Bolker, B., and Walker, S. (2015). Fitting linear mixed-effects models using lme4. 67:48.

Baud, S., Mendoza, M. S., To, A., Harscoet, E., Lepiniec, L., and Dubreucq, B. (2007). WRINKLED1 specifies the regulatory action of LEAFY COTYLEDON2 towards fatty acid metabolism during seed maturation in *Arabidopsis*. *Plant J.* 50, 825–838. doi: 10.1111/j.1365-313x.2007.03092.x

Behzadian, F., Barjeste, H., Hosseinkhani, S., and Zarei, A. R. (2011). Construction and characterization of *Escherichia coli* whole-cell biosensors for toluene and related compounds. *Curr. Microbiol.* 62, 690–696. doi: 10.1007/s00284-010-9764-5

Belide, S., Zhou, X.-R., Kennedy, Y., Lester, G., Shrestha, P., Petrie, J. R., et al. (2013). Rapid expression and validation of seed-specific constructs in transgenic LEC2 induced somatic embryos of *Brassica napus*. *Plant Cell Tissue Organ Culture (PCTOC)* 113, 543–553. doi: 10.1007/s11240-013-0295-1

Birnbaum, K., Jung, J. W., Wang, J. Y., Lambert, G. M., Hirst, J. A., Galbraith, D. W., et al. (2005). Cell type–specific expression profiling in plants via cell sorting of protoplasts from fluorescent reporter lines. *Nat. Method* 2, 615–619. doi: 10.1038/nmeth0805-615

Braybrook, S. A., Stone, S. L., Park, S., Bui, A. Q., Le, B. H., Fischer, R. L., et al. (2006). Genes directly regulated by LEAFY COTYLEDON2 provide insight into the control of embryo maturation and somatic embryogenesis. *Proc. Natl. Acad. Sci. U.S.A.* 103, 3468–3473. doi: 10.1073/pnas.0511331103

Burris, K. P., Dlugosz, E. M., Collins, A. G., Stewart, C. N., and Lenaghan, S. C. (2016). Development of a rapid, low-cost protoplast transfection system for switchgrass (*Panicum virgatum* L.). *Plant Cell Rep.* 35, 693–704. doi: 10.1007/s00299-015-1913-7

Cao, J., Yao, D., Lin, F., and Jiang, M. (2014). PEG-mediated transient gene expression and silencing system in maize mesophyll protoplasts: a valuable

tool for signal transduction study in maize. *Acta Physiol. Plant* 36, 1271–1281. doi: 10.1007/s11738-014-1508-x

Casson, S. A., and Lindsey, K. (2006). The turnip mutant of *Arabidopsis* reveals that LEAFY COTYLEDON1 expression mediates the effects of auxin and sugars to promote embryonic cell identity. *Plant Physiol.* 142, 526–541. doi: 10.1104/pp.106.080895

Chen, D., Kini, R. M., Yuen, R., and Khoo, H. E. (1997). Haemolytic activity of stonustoxin from stonefish (*Synanceja horrida*) venom: pore formation and the role of cationic amino acid residues. *Biochem. J.* 325, 685–691. doi: 10.1042/bj3250685

Clough, S. J., and Bent, A. F. (1998). Floral dip: a simplified method for *Agrobacterium*-mediated transformation of *Arabidopsis thaliana*. *Plant J.* 16, 735–743. doi: 10.1046/j.1365-313x.1998.00343.x

Crawford, R., Kelly, D. J., and Kapanidis, A. N. (2012). A protein biosensor that relies on bending of single DNA molecules. *Chemphyschem* 13, 918–922. doi: 10.1002/cphc.201100881

Cronjé, M. J., Snyman, M., Bornman, L., and Weir, I. E. (2004). A rapid and reliable flow cytometric method for determining Hsp70 levels in tobacco protoplasts. *Methods Cell Sci.* 25, 237–246. doi: 10.1007/s11022-004-2878-z

Damm, B., Schmidt, R., and Willmitzer, L. (1989). Efficient transformation of *Arabidopsis thaliana* using direct gene transfer to protoplasts. *Molec. Gen. Genet.* 217, 6–12. doi: 10.1007/bf00330935

El Tahchy, A., Reynolds, K. B., Petrie, J. R., Singh, S. P., and Vanhercke, T. (2017). Thioesterase overexpression in Nicotiana benthamiana leaf increases the fatty acid flux into triacylgycerol. *FEBS Lett.* 591, 448–456. doi: 10.1002/1873-3468.12539

Galbraith, D. W., Harkins, K. R., and Jefferson, R. A. (1988). Flow cytometric characterization of the chlorophyll contents and size distributions of plant protoplasts. *Cytometry* 9, 75–83. doi: 10.1002/cyto.990090112

Giraudat, J., Hauge, B. M., Valon, C., Smalle, J., Parcy, F., and Goodman, H. M. (1992). Isolation of the *Arabidopsis* ABI3 gene by positional cloning. *Plant Cell* 4, 1251–1261. doi: 10.1105/tpc.4.10.1251

Grønlund, J. T., Eyres, A., Kumar, S., Buchanan-Wollaston, V., and Gifford, M. L. (2012). Cell specific analysis of *Arabidopsis* leaves using fluorescence activated cell sorting. *J. Visual. Exp.* 68:4214.

Guerche, P., Bellini, C., Le Moullec, J. M., and Caboche, M. (1987a). Use of a transient expression assay for the optimization of direct gene transfer into tobacco mesophyll protoplasts by electroporation. *Biochimie* 69, 621–628. doi: 10.1016/0300-9084(87)90181-7

Guerche, P., Charbonnier, M., Jouanin, L., Tourneur, C., Paszkowski, J., and Pelletier, G. (1987b). Direct gene transfer by electroporation in *Brassica napus*. *Plant Sci.* 52, 111–116. doi: 10.1016/0168-9452(87)90112-9

Guo, Y., Song, X., Zhao, S., Lv, J., and Lu, M. (2015). A transient gene expression system in *Populus euphratica* Oliv. Protoplasts prepared from suspension cultured cells. *Acta Physiol. Plant* 37:160.

Hallberg, Z. F., Su, Y., Kitto, R. Z., and Hammond, M. C. (2017). Engineering and in vivo applications of riboswitches. *Annu. Rev. Biochem.* 86, 515–539. doi: 10.1146/annurev-biochem-060815-014628

Hibi, T., Rezelman, G., and Van Kammen, A. (1975). Infection of cowpea mesophyll protoplasts with cowpea mosaic virus. *Virology* 64, 308–318. doi: 10.1016/0042-6822(75)90107-5

Howell, S. H., and Hull, R. (1978). Replication of cauliflower mosaic virus and transcription of its genome in turnip leaf protoplasts. *Virology* 86, 468–481. doi: 10.1016/0042-6822(78)90086-7

Ishida, Y., Hiei, Y., and Komari, T. (2007). Agrobacterium-mediated transformation of maize. *Nat. Protoc.* 2, 1614–1621. doi: 10.1038/nprot.2007.241

Jiang, F., Zhu, J., and Liu, H. L. (2013). Protoplasts: a useful research system for plant cell biology, especially dedifferentiation. *Protoplasma* 250, 1231–1238. doi: 10.1007/s00709-013-0513-z

Kim, M. J., Jang, I. C., and Chua, N. H. (2016). The mediator complex MED15 subunit mediates activation of downstream lipid-related genes by the WRINKLED1 transcription factor. *Plant Physiol.* 171, 1951–1964. doi: 10.1104/pp.16.00664

Kuznetsova, A., Brockhoff, P. B., and Christensen, R. H. B. (2017). lmerTest package: tests in linear mixed effects models. 82:26.

Li, W., Song, T., Wallrad, L., Kudla, J., Wang, X., and Zhang, W. (2019). Tissue-specific accumulation of pH-sensing phosphatidic acid determines plant stress tolerance. *Nat. Plants* 5, 1012–1021. doi: 10.1038/s41477-019-0497-6

Liu, Y., Liu, Y., and Wang, M. (2017). Design, optimization and application of small molecule biosensor in metabolic engineering. *Front. Microbiol.* 8:2012. doi: 10.3389/fmicb.2017.02012

Liu, Z. B., Ulmasov, T., Shi, X., Hagen, G., and Guilfoyle, T. J. (1994). Soybean GH3 promoter contains multiple auxin-inducible elements. *Plant Cell* 6, 645–657. doi: 10.1105/tpc.6.5.645

Loesch-Fries, L. S., and Hall, T. C. (1980). Synthesis, accumulation and encapsidation of individual brome mosaic virus RNA components in barley protoplasts. *J. Gen. Virol.* 47, 323–332. doi: 10.1099/0022-1317-47-2-323

Lotan, T., Ohto, M., Yee, K. M., West, M. A., Lo, R., Kwong, R. W., et al. (1998). *Arabidopsis* LEAFY COTYLEDON1 is sufficient to induce embryo development in vegetative cells. *Cell* 93, 1195–1205. doi: 10.1016/s0092-8674(00)81463-4

Luerssen, H., Kirik, V., Herrmann, P., and Misera, S. (1998). FUSCA3 encodes a protein with a conserved VP1/AB13-like B3 domain which is of functional importance for the regulation of seed maturation in *Arabidopsis thaliana*. *Plant J.* 15, 755–764. doi: 10.1046/j.1365-313x.1998.00259.x

Luo, D., Ganesh, S., and Koolaard, J. (2018). *Predictmeans: Calculate Predicted Means for Linear Models. R package version 1.0.1*. Available online at: https://CRANR-projectorg/package=predictmeans.

Lymperopoulos, K., Crawford, R., Torella, J. P., Heilemann, M., Hwang, L. C., Holden, S. J., et al. (2010). Single-molecule DNA biosensors for protein and ligand detection. *Angew. Chem. Int. Ed.* 49, 1316–1320. doi: 10.1002/anie.200904597

Maćkowska, K., Jarosz, A., and Grzebelus, E. (2014). Plant regeneration from leaf-derived protoplasts within the Daucus genus: effect of different conditions in alginate embedding and phytosulfokine application. *Plant Cell Tissue Organ Culture (PCTOC)* 117, 241–252. doi: 10.1007/s11240-014-0436-1

Marchive, C., Nikovics, K., To, A., Lepiniec, L., and Baud, S. (2014). Transcriptional regulation of fatty acid production in higher plants: molecular bases and biotechnological outcomes. *Eur. J. Lipid Sci. Technol.* 116, 1332–1343. doi: 10.1002/ejlt.201400027

Masani, M. Y., Noll, G. A., Parveez, G. K., Sambanthamurthi, R., and Prufer, D. (2014). Efficient transformation of oil palm protoplasts by PEG-mediated transfection and DNA microinjection. *PLoS One* 9:e96831. doi: 10.1371/journal.pone.0096831

Maule, A. J., Boulton, M. I., Edmunds, C., and Wood, K. R. (1980). Polyethylene glycol-mediated infection of cucumber protoplasts by cucumber mosaic virus and virus RNA. *J. Gen. Virol.* 47, 199–203. doi: 10.1099/0022-1317-47-1-199

Meinke, D. W., Franzmann, L. H., Nickle, T. C., and Yeung, E. C. (1994). Leafy cotyledon mutants of *Arabidopsis*. *Plant Cell* 6, 1049–1064. doi: 10.1105/tpc.6.8.1049

Monke, G., Seifert, M., Keilwagen, J., Mohr, M., Grosse, I., Hahnel, U., et al. (2012). Toward the identification and regulation of the *Arabidopsis thaliana* ABI3 regulon. *Nucleic Acids Res.* 40, 8240–8254. doi: 10.1093/nar/gks594

Motoyoshi, F., and Oshima, N. (1979). Standardization in inoculation procedure and effect of a resistance gene on infection of tomato protoplasts with tobacco mosaic virus RNA. *J. Gen. Virol.* 44, 801–806. doi: 10.1099/0022-1317-44-3-801

Nanjareddy, K., Arthikala, M. K., Blanco, L., Arellano, E. S., and Lara, M. (2016). Protoplast isolation, transient transformation of leaf mesophyll protoplasts and improved Agrobacterium-mediated leaf disc infiltration of *Phaseolus vulgaris*: tools for rapid gene expression analysis. *BMC Biotechnol.* 16:53. doi: 10.1186/s12896-016-0283-8

North, H., Baud, S., Debeaujon, I., Dubos, C., Dubreucq, B., Grappin, P., et al. (2010). *Arabidopsis* seed secrets unravelled after a decade of genetic and omics-driven research. *Plant J.* 61, 971–981. doi: 10.1111/j.1365-313x.2009.04095.x

Ou-Lee, T. M., Turgeon, R., and Wu, R. (1986). Expression of a foreign gene linked to either a plant-virus or a *Drosophila promoter*, after electroporation of protoplasts of rice, wheat, and sorghum. *Proc. Natl. Acad. Sci. U.S.A.* 83, 6815–6819. doi: 10.1073/pnas.83.18.6815

Petrie, J. R., Shrestha, P., Belide, S., Kennedy, Y., Lester, G., Liu, Q., et al. (2014). Metabolic engineering camelina sativa with fish oil-like levels of DHA. *PLoS ONE* 9:e85061. doi: 10.1371/journal.pone.0085061

Petrie, J. R., Shrestha, P., Liu, Q., Mansour, M. P., Wood, C. C., Zhou, X. R., et al. (2010). Rapid expression of transgenes driven by seed-specific constructs in leaf tissue: DHA production. *Plant Methods* 6:8. doi: 10.1186/1746-4811-6-8

Petrie, J. R., Shrestha, P., Zhou, X. R., Mansour, M. P., Liu, Q., Belide, S., et al. (2012). Metabolic engineering plant seeds with fish oil-like levels of DHA. *PLoS ONE* 7:e49165. doi: 10.1371/journal.pone.0049165

Pouvreau, B., Baud, S., Vernoud, V., Morin, V., Py, C., Gendrot, G., et al. (2011). Duplicate maize Wrinkled1 transcription factors activate target genes involved in seed oil biosynthesis. *Plant Physiol.* 156, 674–686. doi: 10.1104/pp.111.173641

Provart, N. J., Alonso, J., Assmann, S. M., Bergmann, D., Brady, S. M., Brkljacic, J., et al. (2016). 50 years of *Arabidopsis* research: highlights and future directions. *New Phytol.* 209, 921–944. doi: 10.1111/nph.13687

R Core Team. (2014). *R: A Language and Environment for Statistical Computing*. Vienna: R Foundation for Statistical Computing.

Rahman, M. M., Divi, U. K., Liu, Q., Zhou, X., Surinder, S., and Aruna, K. (2016). Oil-rich nonseed tissues for enhancing plant oil production. *CAB Rev.* 11, 1–11.

Reynolds, K. B., Taylor, M. C., Cullerne, D. P., Blanchard, C. L., Wood, C. C., Singh, S. P., et al. (2017). A reconfigured Kennedy pathway which promotes efficient accumulation of medium-chain fatty acids in leaf oils. *Plant Biotechnol. J.* 15, 1397–1408. doi: 10.1111/pbi.12724

Reynolds, K. B., Taylor, M. C., Zhou, X.-R., Vanhercke, T., Wood, C. C., Blanchard, C. L., et al. (2015). Metabolic engineering of medium-chain fatty acid biosynthesis in *Nicotiana benthamiana* plant leaf lipids. *Front. Plant Sci.* 6:164. doi: 10.3389/fpls.2015.00164

Santos Mendoza, M., Dubreucq, B., Miquel, M., Caboche, M., and Lepiniec, L. (2005). LEAFY COTYLEDON 2 activation is sufficient to trigger the accumulation of oil and seed specific mRNAs in *Arabidopsis* leaves. *FEBS Lett.* 579, 4666–4670. doi: 10.1016/j.febslet.2005.07.037

Santos-Mendoza, M., Dubreucq, B., Baud, S., Parcy, F., Caboche, M., and Lepiniec, L. (2008). Deciphering gene regulatory networks that control seed development and maturation in *Arabidopsis*. *Plant J.* 54, 608–620. doi: 10.1111/j.1365-313x.2008.03461.x

Sasamoto, H., and Ashihara, H. (2014). Effect of nicotinic acid, nicotinamide and trigonelline on the proliferation of lettuce cells derived from protoplasts. *Phytochem. Lett.* 7, 38–41. doi: 10.1016/j.phytol.2013.09.008

Schapire, A. L., and Lois, L. M. (2016). A simplified and rapid method for the isolation and transfection of *Arabidopsis* leaf mesophyll protoplasts for large-scale applications. *Methods Mol. Biol.* 1363, 79–88. doi: 10.1007/978-1-4939-3115-6_8

Sheen, J. (1990). Metabolic repression of transcription in higher plants. *Plant Cell* 2, 1027–1038. doi: 10.1105/tpc.2.10.1027

Shen, B., Allen, W. B., Zheng, P., Li, C., Glassman, K., Ranch, J., et al. (2010). Expression of ZmLEC1 and ZmWRI1 increases seed oil production in maize. *Plant Physiol.* 153, 980–987. doi: 10.1104/pp.110.157537

Suzuki, M., Ketterling, M. G., Li, Q.-B., and McCarty, D. R. (2003). Viviparous1 alters global gene expression patterns through regulation of abscisic acid signaling. *Plant Physiol.* 132, 1664–1677. doi: 10.1104/pp.103.022475

Takebe, I., and Otsuki, Y. (1969). Infection of tobacco mesophyll protoplasts by tobacco mosaic virus. *Proc. Natl. Acad. Sci. U.S.A.* 64, 843–848. doi: 10.1073/pnas.64.3.843

Tan, H., Yang, X., Zhang, F., Zheng, X., Qu, C., Mu, J., et al. (2011). Enhanced seed oil production in canola by conditional expression of *Brassica napus* LEAFY COTYLEDON1 and LEC1-LIKE in developing seeds. *Plant Physiol.* 156, 1577–1588. doi: 10.1104/pp.111.175000

Terashima, M., Freeman, E. S., Jinkerson, R. E., and Jonikas, M. C. (2015). A fluorescence-activated cell sorting-based strategy for rapid isolation of high-lipid *Chlamydomonas mutants*. *Plant J.* 81, 147–159. doi: 10.1111/tpj.12682

To, A., Valon, C., Savino, G., Guilleminot, J., Devic, M., Giraudat, J., et al. (2006). A network of local and redundant gene regulation governs arabidopsis seed maturation. *Plant Cell* 18, 1642–1651. doi: 10.1105/tpc.105.039925

van Klaveren, P., Slats, J., Roosien, J., and van Vloten-Doting, L. (1983). Flow cytometric analysis of tobacco and cowpea protoplasts infected in vivo and in vitro with alfalfa mosaic virus. *Plant Mol. Biol.* 2, 19–25. doi: 10.1007/bf00187572

Vanhercke, T., Belide, S., Taylor, M. C., El Tahchy, A., Okada, S., Rolland, V., et al. (2019). Up-regulation of lipid biosynthesis increases the oil content in leaves of Sorghum bicolor. *Plant Biotechnol. J.* 17, 220–232. doi: 10.1111/pbi.12959

Vanhercke, T., Divi, U. K., El Tahchy, A., Liu, Q., Mitchell, M., Taylor, M. C., et al. (2017). Step changes in leaf oil accumulation via iterative metabolic engineering. *Metabol. Eng.* 39, 237–246. doi: 10.1016/j.ymben.2016.12.007

Vanhercke, T., El Tahchy, A., Liu, Q., Zhou, X. R., Shrestha, P., Divi, U. K., et al. (2014). Metabolic engineering of biomass for high energy density: oilseed-like triacylglycerol yields from plant leaves. *Plant Biotechnol. J* 12, 231–239. doi: 10.1111/pbi.12131

Vanhercke, T., El Tahchy, A., Shrestha, P., Zhou, X.-R., Singh, S. P., and Petrie, J. R. (2013). Synergistic effect of WRI1 and DGAT1 coexpression on triacylglycerol biosynthesis in plants. *FEBS Lett.* 587, 364–369. doi: 10.1016/j.febslet.2012.12.018

Villa, J. K., Su, Y., Contreras, L. M., and Hammond, M. C. (2018). Synthetic biology of small RNAs and riboswitches. *Microbiol. Spectr.* 6. doi: 10.1128/microbiolspec.RWR-0007-2017

Walsh, T. A., Bevan, S. A., Gachotte, D. J., Larsen, C. M., Moskal, W. A., Merlo, P. A., et al. (2016). Canola engineered with a microalgal polyketide synthase-like system produces oil enriched in docosahexaenoic acid. *Nat. Biotechnol.* 34, 881–887. doi: 10.1038/nbt.3585

Wang, F., and Perry, S. E. (2013). Identification of direct targets of FUSCA3, a key regulator of *Arabidopsis* seed development. *Plant Physiol.* 161, 1251–1264. doi: 10.1104/pp.112.212282

Wang, H., Guo, J., Lambert, K. N., and Lin, Y. (2007). Developmental control of *Arabidopsis* seed oil biosynthesis. *Planta* 226, 773–783. doi: 10.1007/s00425-007-0524-0

Wang, H., Wang, W., Zhan, J., Huang, W., and Xu, H. (2015). An efficient PEG-mediated transient gene expression system in grape protoplasts and its application in subcellular localization studies of flavonoids biosynthesis enzymes. *Sci. Horticult.* 191, 82–89. doi: 10.1016/j.scienta.2015.04.039

Weselake, R. J. (2016). "Chapter 15 – engineering oil accumulation in vegetative tissue," in *Industrial Oil Crops*, eds T. McKeon, D. Hayes, D. Hildebrand, and R. Weselake (Urbana, IL: AOCS Press), 413–434. doi: 10.1016/b978-1-893997-98-1.00015-4

West, M., Yee, K. M., Danao, J., Zimmerman, J. L., Fischer, R. L., Goldberg, R. B., et al. (1994). LEAFY COTYLEDON1 is an essential regulator of late embryogenesis and cotyledon identity in *Arabidopsis*. *Plant Cell* 6, 1731–1745. doi: 10.1105/tpc.6.12.1731

Wongso, D., Dong, J., Ueda, H., and Kitaguchi, T. (2017). Flashbody: a next generation fluobody with fluorescence intensity enhanced by antigen binding. *Anal. Chem.* 89, 6719–6725. doi: 10.1021/acs.analchem.7b00959

Wood, C. C., Petrie, J. R., Shrestha, P., Mansour, M. P., Nichols, P. D., Green, A. G., et al. (2009). A leaf-based assay using interchangeable design principles to rapidly assemble multistep recombinant pathways. *Plant Biotechnol. J.* 7, 914–924. doi: 10.1111/j.1467-7652.2009.00453.x

Yadava, P., Abhishek, A., Singh, R., Singh, I., Kaul, T., Pattanayak, A., et al. (2017). Advances in maize transformation technologies and development of transgenic maize. *Front. Plant Sci.* 7:1949. doi: 10.3389/fpls.2016.01949

Yamamoto, A., Kagaya, Y., Usui, H., Hobo, T., Takeda, S., and Hattori, T. (2010). Diverse roles and mechanisms of gene regulation by the *Arabidopsis* seed maturation master regulator FUS3 revealed by microarray analysis. *Plant Cell Physiol.* 51, 2031–2046. doi: 10.1093/pcp/pcq162

Yang, Y., Li, R., and Qi, M. (2000). In vivo analysis of plant promoters and transcription factors by agroinfiltration of tobacco leaves. *Plant J.* 22, 543–551. doi: 10.1046/j.1365-313x.2000.00760.x

Yoo, S. D., Cho, Y. H., and Sheen, J. (2007). *Arabidopsis* mesophyll protoplasts: a versatile cell system for transient gene expression analysis. *Nat. Protoc.* 2, 1565–1572. doi: 10.1038/nprot.2007.199

You, M. K., Lim, S. H., Kim, M. J., Jeong, Y. S., Lee, M. G., and Ha, S. H. (2014). Improvement of the fluorescence intensity during a flow cytometric analysis for rice protoplasts by localization of a green fluorescent protein into chloroplasts. *Int. J. Mol. Sci.* 16, 788–804. doi: 10.3390/ijms16010788

Zale, J., Jung, J. H., Kim, J. Y., Pathak, B., Karan, R., Liu, H., et al. (2016). Metabolic engineering of sugarcane to accumulate energy-dense triacylglycerols in vegetative biomass. *Plant Biotechnol. J.* 14, 661–669. doi: 10.1111/pbi.12411

Zhai, Z., Jung, H. I., and Vatamaniuk, O. K. (2009). Isolation of protoplasts from tissues of 14-day-old seedlings of *Arabidopsis thaliana*. *J. Vis. Exp.* 1149.

Zhang, M., Cao, X., Jia, Q., and Ohlrogge, J. (2016). FUSCA3 activates triacylglycerol accumulation in *Arabidopsis* seedlings and tobacco BY2 cells. *Plant J.* 88, 95–107. doi: 10.1111/tpj.13233

Zhang, S., Wong, L., Meng, L., and Lemaux, P. G. (2002). Similarity of expression patterns of knotted1 and ZmLEC1 during somatic and zygotic embryogenesis in maize (*Zea mays* L.). *Planta* 215, 191–194. doi: 10.1007/s00425-002-0735-3

Zhang, Y., Malzahn, A. A., Sretenovic, S., and Qi, Y. (2019). The emerging and uncultivated potential of CRISPR technology in plant science. *Nat. Plants* 5, 778–794. doi: 10.1038/s41477-019-0461-5

Conflict of Interest: The authors declare that the research was conducted in the absence of any commercial or financial relationships that could be construed as a potential conflict of interest.

frontiers in Plant Science

ORIGINAL RESEARCH
published: 07 May 2020
doi: 10.3389/fpls.2020.00406

Genome-Wide Identification of Peanut *KCS* Genes Reveals That *AhKCS1* and *AhKCS28* Are Involved in Regulating VLCFA Contents in Seeds

Dongxin Huai[1], Xiaomeng Xue[1], Yang Li[2], Peng Wang[3,4], Jianguo Li[1], Liying Yan[1], Yuning Chen[1], Xin Wang[1], Nian Liu[1], Yanping Kang[1], Zhihui Wang[1], Yi Huang[1], Huifang Jiang[1], Yong Lei[1] and Boshou Liao[1]**

[1] Key Laboratory of Biology and Genetic Improvement of Oil Crops, Ministry of Agriculture and Rural Affairs, Oil Crops Research Institute of Chinese Academy of Agricultural Sciences, Wuhan, China, [2] College of Life Sciences, Henan Agricultural University, Zhengzhou, China, [3] Key Laboratory of Crop Gene Resources and Germplasm Enhancement in Southern China, Ministry of Agriculture and Rural Affairs, Danzhou, China, [4] Tropical Crops Genetic Resources Institute, Chinese Academy of Tropical Agricultural Sciences, Danzhou, China

OPEN ACCESS

Edited by:
Xue-Rong Zhou,
Agriculture and Food, Commonwealth Scientific and Industrial Research Organisation (CSIRO), Australia

Reviewed by:
Joaquín J. Salas,
Instituto de la Grasa (IG), Spain
Benjamin Pouvreau,
Commonwealth Scientific and Industrial Research Organisation (CSIRO), Australia

***Correspondence:**
Yong Lei
leiyong@caas.cn
Boshou Liao
lboshou@hotmail.com

Specialty section:
This article was submitted to Plant Metabolism and Chemodiversity, a section of the journal Frontiers in Plant Science

Received: 15 November 2019
Accepted: 20 March 2020
Published: 07 May 2020

Citation:
Huai D, Xue X, Li Y, Wang P, Li J, Yan L, Chen Y, Wang X, Liu N, Kang Y, Wang Z, Huang Y, Jiang H, Lei Y and Liao B (2020) Genome-Wide Identification of Peanut KCS Genes Reveals That AhKCS1 and AhKCS28 Are Involved in Regulating VLCFA Contents in Seeds. Front. Plant Sci. 11:406. doi: 10.3389/fpls.2020.00406

The peanut (*Arachis hypogaea* L.) is an important oilseed crop worldwide. Compared to other common edible vegetable oils, peanut oil contains a higher content of saturated fatty acids (SFAs), approximately 20–40% of which are very long chain fatty acids (VLCFAs). To understand the basis for this oil profile, we interrogated genes for peanut β-ketoacyl-CoA synthase (KCS), which is known to be a key enzyme in VLCFA biosynthesis. A total of 30 *AhKCS* genes were identified in the assembled genome of the peanut. Based on transcriptome data, nine *AhKCS* genes with high expression levels in developing seeds were cloned and expressed in yeast. All these AhKCSs could produce VLCFAs but result in different profiles, indicating that the AhKCSs catalyzed fatty acid elongation with different substrate specificities. Expression level analysis of these nine *AhKCS* genes was performed in developing seeds from six peanut germplasm lines with different VLCFA contents. Among these genes, the expression levels of *AhKCS1* or *AhKCS28* were, 4–10-fold higher than that of any other *AhKCS*. However, only the expression levels of *AhKCS1* and *AhKCS28* were significantly and positively correlated with the VLCFA content, suggesting that AhKCS1 and AhKCS28 were involved in the regulation of VLCFA content in the peanut seed. Further subcellular localization analysis indicated that AhKCS1 and AhKCS28 were located at the endoplasmic reticulum (ER). Overexpression of *AhKCS1* or *AhKCS28* in *Arabidopsis* increased the contents of VLCFAs in the seed, especially for very long chain saturated fatty acids (VLCSFAs). Taken together, this study suggests that *AhKCS1* and *AhKCS28* could be key genes in regulating VLCFA biosynthesis in the seed, which could be applied to improve the health-promoting and nutritional qualities of the peanut.

Keywords: peanut, β-ketoacyl-CoA synthase (KCS), very long chain fatty acid (VLCFA) biosynthesis, expression profiling, function analysis

INTRODUCTION

The peanut (*Arachis hypogaea* L.) is a widely cultivated oilseed crop in tropical and subtropical regions, which provides a significant source of protein, folate, tocopherol, phytosterols, polyphenolics such as resveratrol, fiber, and edible oil (Bertioli et al., 2015; Han, 2016; Bertioli et al., 2019). Fatty acid composition is the main factor in determining the nutritional value and application purpose of vegetable oil (Napier and Graham, 2010; Napier et al., 2014). Peanut oil contains ∼20% saturated fatty acids (SFAs), which is higher than that in many commercial vegetable oils (Wang et al., 2013; Giakoumis, 2018). Limiting the intake of dietary SFAs is recommended by most dietary guidelines, because SFAs promote increasing undesirable low-density lipoprotein (LDL) cholesterol in the blood, leading to a high risk of cardiovascular disease (List, 2004; USDA, 2010; Briggs et al., 2017). In the peanut, SFAs are enriched in VLCSFAs, including arachidic acid (C20:0), behenic acid (C22:0), and lignoceric acid (C24:0) (Wang et al., 2013; Giakoumis, 2018). VLCFAs are fatty acids longer than 18 atoms (Haslam and Kunst, 2013; Giakoumis, 2018). Hence, reducing VLCFA content in the peanut is a prime target to improve the nutritional value of peanuts and peanut oil.

In plants, it has been proved that VLCFA biosynthesis is controlled by a condensing enzyme: β-ketoacyl-CoA synthase (KCS) (Todd et al., 1999; Sassa and Kihara, 2014; Huai et al., 2015; Usher et al., 2017). KCS catalyzes the first step of elongation with the substrate and tissue specificities (Blacklock and Jaworski, 2002, 2006; Haslam and Kunst, 2013; Huai et al., 2015). The expression level and substrate preference of KCS determine the ultimate chain length and contents of VLCFAs (James et al., 1995; Katavic et al., 2001; Denic and Weissman, 2007; Sun et al., 2013; Huai et al., 2015; Shi et al., 2017; Ozseyhan et al., 2018). For example, the *KCS* from *Lunaria annua* has been introduced into camelina (*Camelina sativa*) to produce nervonic acid (C24:1) (Guo et al., 2009; Huai et al., 2015). The *fatty acid elongation 1* (*FAE1*) from *Brassica napus* is overexpressed in the rapeseed to increase the content of erucic acid (C22:1) (Nath et al., 2009; Li et al., 2012). In contrast, the silencing of *FAE1* is used to decrease the contents of VLCFAs (Wang et al., 2010; Shi et al., 2017; Ozseyhan et al., 2018).

According to sequence similarity, *KCS* genes in higher plants are divided into two gene families, namely FAE1-type and elongation-type (ELO-type) (Haslam and Kunst, 2013; Guo et al., 2016). A total of 21 FAE1-type KCSs were identified in the *Arabidopsis* genome (Joubes et al., 2008). As the expression patterns and substrate specificities of KCSs are different, they are assigned to play different roles in seed oil biosynthesis (FAE1/KCS18) (James and Dooner, 1990; Lemieux et al., 1990; Kunst et al., 1992; James et al., 1995), development of epidermis (FDH/KCS10, HIC/KCS13) (Gray et al., 2000; Pruitt et al., 2000), suberin metabolism (KCS2/DAISY, KCS9, KCS20) (Franke et al., 2009; Lee et al., 2009; Kim J. et al., 2013), and cuticular lipid metabolism (CER6/CUT1/KCS6, KCS1, KCS16) (Todd et al., 1999; Fiebig et al., 2000; Hegebarth et al., 2017). The ELO-type family is homologous to animal condensing enzymes but shares little homology with the plant KCS enzymes (Leonard et al., 2004; Haslam and Kunst, 2013). Four ELO genes are characterized in *Arabidopsis* (Quist et al., 2009). Only HOS3 is reported to be involved in the biosynthesis of sphingolipid (Quist et al., 2009), while the functions of other plant ELO homologs remain to be investigated (Haslam and Kunst, 2013).

To reduce the contents of VLCFAs in the peanut, it is necessary to identify which *KCS* genes contribute to this trait. In this report, we identified *AhKCS* genes in the peanut, and investigated the expression profiles of these genes. The coding sequences (CDS) and expression levels of *AhKCS* genes in developing seeds were analyzed in peanut lines with different VLCFA contents. Correlation analysis between the *AhKCS* gene expression and VLCFA content identified the major genes contributing to VLCFA content. The identified genes were heterologously expressed in yeast and *Arabidopsis* to confirm their function and substrate specificities. Finally, the candidate AhKCSs for the seed VLCFA content were identified which could be applied in the improvement of peanut oil.

MATERIALS AND METHODS

Plant Materials and Growth Conditions

Peanut (*Arachis hypogaea* L.) cultivar Zhonghua16, germplasm lines C-34, C-119, C-140, C-178, C-224, and C-296 were maintained in our lab. Peanut plants were sowed in the Oil Crops Research Institute of the Chinese Academy of Agricultural Sciences (OCRI-CAAS) experimental field in Wuhan, China. Plants were grown under field conditions in a randomized block experimental design with three replications.

Arabidopsis (*Arabidopsis thaliana*) double mutant *fae1/fad2* (Smith et al., 2003) was obtained from Dr. Edgar Cahoon's Lab at the University of Nebraska-Lincoln, United States. *Arabidopsis* plants were grown in controlled-environment chambers with 16 h light (21°), 8 h dark (18°) cycle, 100 mE light intensity, and 60% relative humidity. Double mutant *fae1/fad2* as control plants were included in each flat area to minimize any spatial aspects of the growth chamber.

Identification of *AhKCS* Genes

Datasets of the genome sequence were downloaded from the following sources. *Arachis hypogaea*: PeanutBase[1] (Bertioli et al., 2019); *Arabidopsis thaliana*: TAIR[2] (Lamesch et al., 2011).

Arabidopsis KCS genes were downloaded in TAIR, whose Pfam domains were retrieved from Pfam Database[3]. Standalone similarity searches for peptide sequences were performed through BLASTP under BLAST + executable suite (Camacho et al., 2009). In addition, an HMM search was performed with the "trusted cutoff" as the threshold for detecting the domains. The results of the two rounds of searches were merged, which was subject to another search against a library of Pfam-A families.

[1]https://peanutbase.org/
[2]https://www.arabidopsis.org/
[3]https://sanger.ac.uk/

Genomic Distribution of AhKCSs

The chromosomal location and syntenic gene pairs information of *KCS* genes were downloaded from PeanutBase. The syntenic diagram illustrating the detailed genomic distribution of *KCS* genes was created by Circos[4] (Krzywinski et al., 2009).

Alignment and Phylogeny Inference

Multiple sequence alignments were performed using the Clustal W program (Thompson et al., 1994). A phylogenetic tree was constructed using the neighbor-joining (NJ) method in the MEGA X software with 1,000 bootstrap replicates (Kumar et al., 2018).

Transcriptomic Analysis

Raw transcriptome data of 22 different tissues collected from cultivated peanut cv. Tifrunner were downloaded from NCBI (BioSample IDs: SAMN03944933-SAMN03944990) (Clevenger et al., 2016). Reads were mapped to the assembled genome of *A. hypogaea* which were deposited in-house. Read mapping and calculation of fragments per kilobase per million reads mapped (FPKM) were performed using TopHat2 (Kim D. et al., 2013). A heatmap was generated using pheatmap, an R package[5].

RNA Extraction

For investigation of the expression profile in developing seeds, seeds of Zhonghua 16 from five specific stages were collected without pericarp: I – white and flat embryo [approximately 20 days after pollination (DAP)]; II – white and teardrop-shaped embryo (30 DAP); III – white and torpedo to round shaped embryo (40 DAP); IV – light pink and round embryo (50 DAP); V – dark pink, large and round embryo (60 DAP). For association analysis between *KCS* expression level and VLCFA contents, developing seeds were harvested at stage III from germplasm lines C-34, C-119, C-140, C-178, C-224, and C-296. Total RNA was extracted using TRIzol reagent (Sigma)[6] according to the manufacturer's instructions. Reverse transcription was performed using SuperScript IV First-Strand Synthesis System as described by the manufacturer (Invitrogen)[7].

Quantitative Real-Time PCR (qRT-PCR) Analysis

Primers for qRT-PCR were designed using the IDT DNA Real Time PCR primer design tool[8] (**Supplementary Table S1**). Real-time PCRs were performed using paired samples with three technical replicates on a Bio-Rad CFX96 Real-Time system (Bio-Rad)[9] and DBI Bioscience Bestar-Real Time PCR Master Mix kit following the manufacturer's instructions. The data were analyzed with LINREG as previously described (Huai et al., 2015). The experiment was repeated using at least three independent biological replicates, with three technical replicates for each biological sample.

Expression of *AhKCS* Genes in Yeast

The nine *AhKCS* genes were individually amplified by PCR from sequenced TA-clones using the primers in **Supplementary Table S2**, with different restriction sites. The PCR products were digested with corresponding restriction enzymes to the added sites in primers, respectively. The digested fragments were ligated into the vector pYX242, respectively (**Supplementary Figure S1**). Based on the inserted gene, the resulting plasmids were designated as pYX242-AhKCS1, pYX242-AhKCS4, pYX242-AhKCS10, pYX242-AhKCS13, pYX242-AhKCS17, pYX242-AhKCS23, pYX242-AhKCS25, pYX242-AhyKCS28, and pYX242-AhKCS29.

The vectors with *AhKCS* genes were introduced into *Saccharomyces cerevisiae* strain INVSc1 (Invitrogen) using the S.c. EasyComp ^{TM} transformation Kit (Invitrogen). Yeast cells transformed with a pYX242 empty vector were used as the control. The transformed yeast cells were selected on minimal agar plates lacking leucine. Transformants were first grown in SC-Leu (synthetic complete minus leucine) medium at 28°C overnight, suspended in SC-Leu medium and grown at 28°C for 2 days; then the transformants were selected and grown as described previously (Guo et al., 2009).

Yeast cells were grown in 50 ml SC-Leu medium at 28°C overnight to OD_{600} of 1.4, the cells were spun to form a pellet and used for biochemical analysis. Cell pellets were lyophilized and then transferred into glass tubes. Fatty acid methyl esters (FAMEs) were prepared with 2.5% (v/v) sulfuric acid/methanol for gas-chromatography analysis as previously described (Huai et al., 2015).

Cloning of *AhKCS* Genes From Peanut Plants

The *AhKCS* genes were cloned from developing seeds at stage III of peanut germplasm lines C-34, C-119, C-140, C-178, C-224, and C-296. Primers were designed based on the sequences of *Arahy.IFJ1V3*, *Arahy.T9PLK1*, *Arahy.1FMC3R*, *Arahy.WQ1I1V*, *Arahy.TIY3DH*, *Arahy.3ATP19, Arahy.XI5WK7*, *Arahy.BGR17W*, and *Arahy.YW30D2*. All the cloning primers are listed in **Supplementary Table S3**.

Subcellular Localization of *AhKCS* Genes

The *AhKCS1* and *AhKCS28* genes without a stop codon were amplified by PCR from sequenced TA-clones using the following primers: 5′- CATGGGTACCATGGCTGATGCAAAAGCA-3′ (*Kpn*I) and 5′-CATGGGATCCTGATGGCAGATACCCTTGGA-3′ (*Bam*HI) (the added restriction sites are underlined). The PCR products were digested with *Kpn*I and *Bam*HI, and the digested fragments were separately ligated into the vector pHBT (GenBank accession No. EF090408). As a result, *AhKCS* genes were inserted between the cauliflower mosaic virus (CaMV) 35S promoter and the green fluorescent protein (GFP) gene. The resulting plasmids were designated as pHBT-AhKCS1-GFP and pHBT-AhKCS28-GFP. The empty vector pHBT-GFP

[4]http://circos.ca/

[5]https://www.r-project.org/

[6]http://www.sigmaaldrich.com/

[7]http://www.invitrogen.com/

[8]http://www.idtdna.com/scitools/Applications/RealTimePCR

[9]http://www.bio-rad.com

was analyzed as a control. The *BnaA.FAE1* from rapeseed was fused with the red fluorescent protein (RFP) gene. The *p35S*:BnaA.FAE1-RFP construct was used as an endoplasmic reticulum (ER) marker (Wang et al., 2010; Haslam and Kunst, 2013).

The pHBT-GFP, pHBT-AhKCS1-GFP, and pHBT-AhKCS28-GFP were each transiently co-expressed with the ER marker in *Arabidopsis* protoplasts by PEG transformation, respectively (Nelson et al., 2007). The protoplast cells were isolated from 15-days-old seedlings of wild-type *Arabidopsis*. The leaf tissues were incubated in a solution containing 1.5% cellulase and 0.75% macerozyme for 4 h with gentle agitation. The protoplasts were collected by centrifuging at 100 g at 4°C for 2 min and resuspended in a solution of 0.4 M mannitol, 15 mM $MgCl_2$, and 4 mM MES (pH 5.7). Then, 100 μl of the protoplast solution with 10 μg plasmid DNA was used for PEG-mediated transformation. After 10 h of incubation in the dark, fluorescence was examined under a laser-scanning confocal microscope (Olympus FV10-ASW).

Expression of *AhKCS* Genes in Arabidopsis

The *AhKCS1* and *AhKCS28* genes were amplified by PCR from sequenced TA-clones using the following primers with added *Not*I restriction sites: 5′-CATGGCGGCCGCATGGCTGATGCAAAAGCA-3′ and 5′-CATGGCGGCCGCTCAGATGGCAGATACCCTTGGA-3′ (the added restriction sites are underlined). The *Not*I digested fragments were separately inserted into the vector pKMS2 (Huai et al., 2015) between the seed-specific soybean oleosin-1 promoter and 3′UTR, to create pKMS2-AhKCS1 and pKMS2-AhKCS28. The cassettes comprising the oleosin promoter and 3′UTR flanking AhKCS1 or AhKCS28 gene were excised using *Asc*I and respectively inserted into the binary vector pBinGlyRed2 containing a DsRed marker gene (Huai et al., 2015) to generate pBinGlyRed2-AhKCS1 and pBinGlyRed2-AhKCS28 (**Supplementary Figure S2**).

The constructs pBinGlyRed2-AhKCS1 and pBinGlyRed2-AhKCS28 were introduced into *Agrobacterium tumefaciens* GV3101 by electro-transformation. The *Arabidopsis fae1/fad2* mutant was transformed according to the previously described method (Zhang et al., 2015). DsRed-positive seeds were identified using a green LED flashlight with a red camera filter lens (Huai et al., 2015).

Gas Chromatographic Analysis of Fatty Acid Compositions

For *Arabidopsis*, the DsRed positive mature seeds from each line were analyzed as a sample. For mature peanut seeds, 20 seeds from each line were collected and grinded as a sample. For developing peanut seeds, 5–10 seeds from each line were collected, lyophilized and grinded as a sample.

FAMEs were prepared from 25 mg finely grounded seeds with 2.5% (v/v) sulfuric acid/methanol as previously described (Huai et al., 2015). Fatty acids were transmethylated at 90°C for 1 h. After cooling to room temperature, 1 ml of aqueous 0.9% NaCl was added, and FAMEs were recovered by three sequential extractions with 1 ml of hexane. FAMEs were analyzed using an Agilent 7890B gas chromatograph with flame ionization detection and the DB-23 column. Fatty acids were identified by retention time according to previous studies (Huai et al., 2018; Liu et al., 2019).

Statistical Analysis

For correlation analysis on expression levels of *AhKCS* genes and VLCFA contents, the expression level data of each *AhKCS* gene and the contents of VLCFAs were collected at the same developing stage. For association analysis between *AhKCS* expression level and VLCFA content in different lines, the expression level data of each *AhKCS* gene at stage III was correlated with the VLCFA content in mature seeds. Correlation coefficients were estimated using the IBM SPSS Statistics software. For the comparison of multiple means, the test for statistical significance was performed with ANOVA and Fisher's least significant difference (LSD) multiple-comparison test, using the same software. In all the analyses, only $P < 0.05$ was considered to be significant.

RESULTS

Identification of *AhKCS* Gene Family Members in the Peanut Genome

To identify all the *AhKCS* genes in the genome of the peanut, HMMER and BLAST searches were performed using 21 *AtKCS* genes from *Arabidopsis* as the query (**Supplementary Table S4**). A total of 30 putative AhKCSs were identified in the peanut, and were numbered based on their chromosomal locations, respectively (**Table 1**). None of these putative *AhKCSs* showed significant homology to *AtELO* genes (**Supplementary Table S5**), indicating that all the identified *AhKCS* genes were FAE1-type. All AhKCSs contained two domains, a 3-Oxoacyl-[acyl-carrier-protein (ACP)] synthase III C terminal domain (ACP_syn_III_C) and a FAE1/Type III polyketide synthase-like protein domain (FAE1_CUT1_RppA) (**Figure 1**). The putative *AhKCS* genes encoded proteins ranging from 432 amino acids to 619 amino acids. Most of these genes contained less than four introns, while seven *AhKCS* genes harbored no intron throughout their whole open reading frames. The alternatively spliced transcripts were identified in *AhKCS14* and *AhKCS22* genes (**Table 1**), implying that different isoforms may play different roles in the development of the peanut.

AhKCS genes were widely distributed throughout genomes but were uneven among chromosomes. There were 14 *AhKCS* genes (*AhKCS1* – *AhKCS14*) located on nine chromosomes in subgenome A, and 16 *AhKCS* genes (*AhKCS15-AhKCS30*) on six chromosomes in subgenome B (**Table 1** and **Figure 2**). No *AhKCS* gene was detected on chromosome 08 in subgenome A, as well as chromosomes 11, 14, 15, and 17 in subgenome B (**Table 1** and **Figure 2**). More than two *AhKCS* genes were identified on chromosomes 10 (3), 13 (3), 18 (4), 19 (3), and 20 (4) (**Table 1** and **Figure 2**). Three chromosomes, 03, 07, and 09 each harbored

two *AhKCS* genes, while seven chromosomes, 01, 02, 04, 05, 06, 12, and 16 each had just one *AhKCS* gene (**Table 1** and **Figure 2**).

Syntenic gene pairs are illustrated with a Circos diagram (**Figure 2**). Twelve *AhKCS* genes in subgenome A were paired with *AhKCS* genes in subgenome B and shared over 90% homology (**Figure 2**). *AhKCS* genes on chromosomes 02, 03, 06, 09, and 10 were syntenic to *AhKCS* genes on corresponding chromosomes 12, 13, 16, 19, and 20. However, *AhKCS1* on chromosome 01 was paired with *AhKCS28* on chromosome 20. Similarly, *AhKCS8* and *AhKCS9* on chromosome 07 were paired with *AhKCS21* and *AhKCS22* on chromosome 18 (**Figure 2**). *AhKCS5* and *AhKCS6* in subgenome A were not paired, as well as four *AhKCS* genes in subgenome B (*AhKCS18*, *AhKCS20*, *AhKCS23,* and *AhKCS24*) (**Figure 2**).

Phylogenetic Analysis of AhKCSs From Peanut Plants

An un-rooted phylogenetic tree was constructed in MEGA X based on the protein sequences of AhKCSs from the peanut, plus the *Arabidopsis* AtKCSs. The KCS proteins were divided into nine groups: α, β, γ, δ, ε, ζ, η, θ, and ι. No AhKCS was classified into Group ε, η, and ι, while no AtKCS was detected in Group α (**Figure 3**). These results indicate that *AhKCS* genes in the peanut might have undergone gene duplication and ensuing sub-functionalization and/or neo-functionalization, generating more complicated functions in the peanut than in *Arabidopsis*.

Group α contained eight AhKCSs: AhKCS8, AhKCS9, AhKCS11, AhKCS14, AhKCS21, AhKCS22, AhKCS26, and AhKCS30, which were not grouped with any AtKCS. Group β harbored five AhKCSs (AhKCS1, AhKCS6, AhKCS10, AhKCS25, and AhKCS28) and three AtKCSs including the AtKCS2/DAISY AtKCS11 and AtKCS20. There were four AhKCSs (AhKCS2, AhKCS7, AhKCS15, and AhKCS19) and three AtKCSs (AtKCS1, AtKCS13, and AtKCS14) in Group γ. Five AhKCSs (AhKCS4, AhKCS5, AhKCS17, AhKCS18, and AhKCS24) and three AtKCSs (AtKCS4, AtKCS9, and AtKCS17) were classified into Group δ. In Group ζ, 4 AhKCSs (AhKCS3, AhKCS16, AhKCS20, and AhKCS23) were grouped with three AtKCSs (AtKCS3, AtKCS12, and AtKCS19). In Group θ, four AhKCSs (AhKCS12, AhKCS13, AhKCS27, and AhKCS29) were closely related to AtKCS10/FDH and AtKCS15 (**Figure 3**).

TABLE 1 | *AhKCS* genes identified in the peanut genome.

ID	Accession	Chr.*	No. of introns	CDS length (bp)	AA
AhKCS1	Arahy.IFJ1V3	01	0	1533	510
AhKCS2	Arahy.AYAJ7Z	02	2	1626	541
AhKCS3	Arahy.DFH8S5	03	1	1437	478
AhKCS4	Arahy.T9PLK1	03	0	1536	511
AhKCS5	Arahy.0744GE	04	4	1563	521
AhKCS6	Arahy.T43VF5	05	1	1473	490
AhKCS7	Arahy.LACR9M	06	0	1566	521
AhKCS8	Arahy.BRB394	07	2	1293	430
AhKCS9	Arahy.LP0WMI	07	1	1449	482
AhKCS10	Arahy.1FMC3R	09	1	1587	528
AhKCS11	Arahy.A9ZVJV	09	1	1416	471
AhKCS12	Arahy.N2G1VT	10	2	1497	498
AhKCS13	Arahy.WQ1I1V	10	2	1617	538
AhKCS14	Arahy.UB51SX	10	4 or 2	1686	561
AhKCS15	Arahy.06CD8W	12	2	1626	541
AhKCS16	Arahy.PB1D04	13	1	1509	502
AhKCS17	Arahy.TIY3DH	13	0	1536	511
AhKCS18	Arahy.V2BP3N	13	2	1860	619
AhKCS19	Arahy.V6AFRQ	16	0	1566	521
AhKCS20	Arahy.F7NA0C	18	0	1458	485
AhKCS21	Arahy.MXV0CY	18	1	1449	482
AhKCS22	Arahy.JWBY7T	18	2 or 1	1389	462
AhKCS23	Arahy.3ATP19	18	2	1431	476
AhKCS24	Arahy.7AH051	19	2	1299	432
AhKCS25	Arahy.XI5WK7	19	1	1587	528
AhKCS26	Arahy.VJNQ2E	19	1	1422	473
AhKCS27	Arahy.X66CUM	20	2	1515	504
AhKCS28	Arahy.BGR17W	20	0	1533	510
AhKCS29	Arahy.YW30D2	20	2	1617	538
AhKCS30	Arahy.A9N57E	20	2	1464	488

**Chromosomes 01–10 belong to the A subgenome; chromosomes 11–20 belong to the B subgenome.*

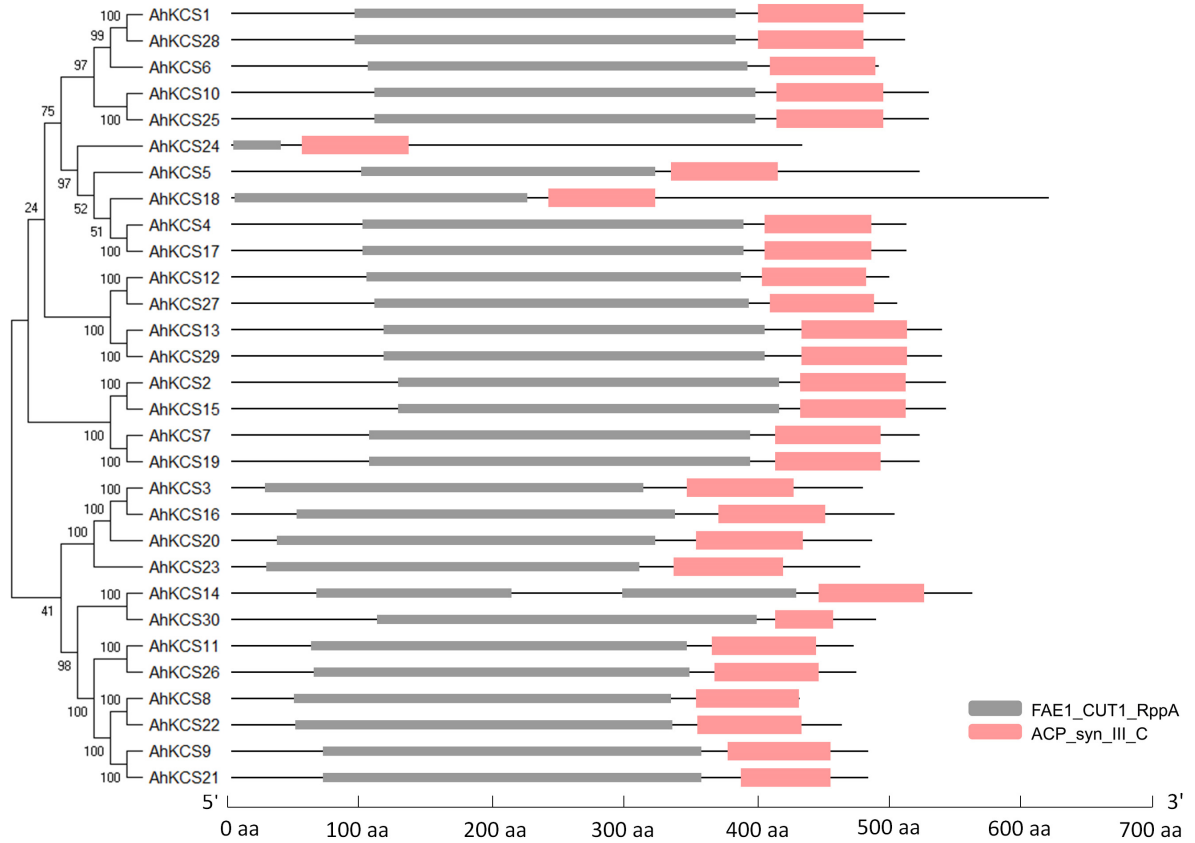

FIGURE 1 | The conserved domains of AhKCSs from peanut. FAE1_CUT1_RppA: FAE1/Type III polyketide synthase-like protein domain (PF08392); ACP_syn_III_C: 3-Oxoacyl-[acyl-carrier-protein (ACP)] synthase III C terminal domain (PF08541).

It has been proved that the seed specific expressed AtKCS18/FAE1 controls the VLCFA content in seed of *Arabidopsis* (James et al., 1995), so the peanut ortholog which was grouped with AtKCS18/FAE1 was of interest. However, there was no AhKCS classified into Group ε with AtKCS18/FAE1 (**Figure 3**). This might imply that there was no seed-specific AhKCS that regulated VLCFA content only in the seed.

Expression Patterns of *AhKCS* Genes in Peanut Plants

The expression levels of *AhKCS* genes in 22 tissues of the peanut were investigated using transcriptome data to identify those with the highest expression in the developing seed (Clevenger et al., 2016). The FPKM values of *AhKCS* genes were calculated by mapping reads to the peanut genome. A heat-map of *AhKCS* genes was created to demonstrate their expression profile (**Figure 4**).

In total, the expression of 22 *AhKCS* genes was detected in at least one tissue of the peanut (**Figure 4**). Six *AhKCS* genes (*AhKCS5*, *AhKCS6*, *AhKCS8*, *AhKCS11*, *AhKCS22*, and *AhKCS26*) were not expressed in any of the tested tissues from which the transcriptome data were derived (**Figure 4**). Eleven *AhKCS* genes (*AhKCS1*, *AhKCS2*, *AhKCS4*, *AhKCS7*, *AhKCS10*, *AhKCS13*, *AhKCS17*, *AhKCS19*, *AhKCS25*, *AhKCS28*, and *AhKCS29*) were constitutively expressed in the 22 tissues (**Figure 4**). *AhKCS12* and *AhKCS27* were specifically expressed in the leaf and stem, while *AhKCS3*, *AhKCS16*, and *AhKCS20* were specifically expressed in the flower (**Figure 4**). No *AhKCS* gene was specifically expressed in the roots or gynophores (**Figure 4**). None of the *AhKCS* genes showed seed-specific expression, though *AhKCS23* was dominantly expressed in both developing seeds and flowers (**Figure 4**).

Nine *AhKCS* genes, namely, *AhKCS1*, *AhKCS4*, *AhKCS10*, *AhKCS13*, *AhKCS17*, *AhKCS23*, *AhKCS25*, *AhKCS28*, and *AhKCS29*, were expressed in developing seeds (**Figure 4**). Except for *AhKCS23*, the other genes were constitutively expressed (**Figure 4**). From these results, candidate genes that might regulate VLCFA content in the developing peanut seed were selected for further characterization.

Correlation Analyses on Expression Levels of *AhKCS* and Contents of VLCFAs

Analysis of VLCFA content in developing seeds of Zhonghua16 were conducted at 20, 30, 40, 50, and 60 DAP. During the development of the seed, no decrease was observed in the

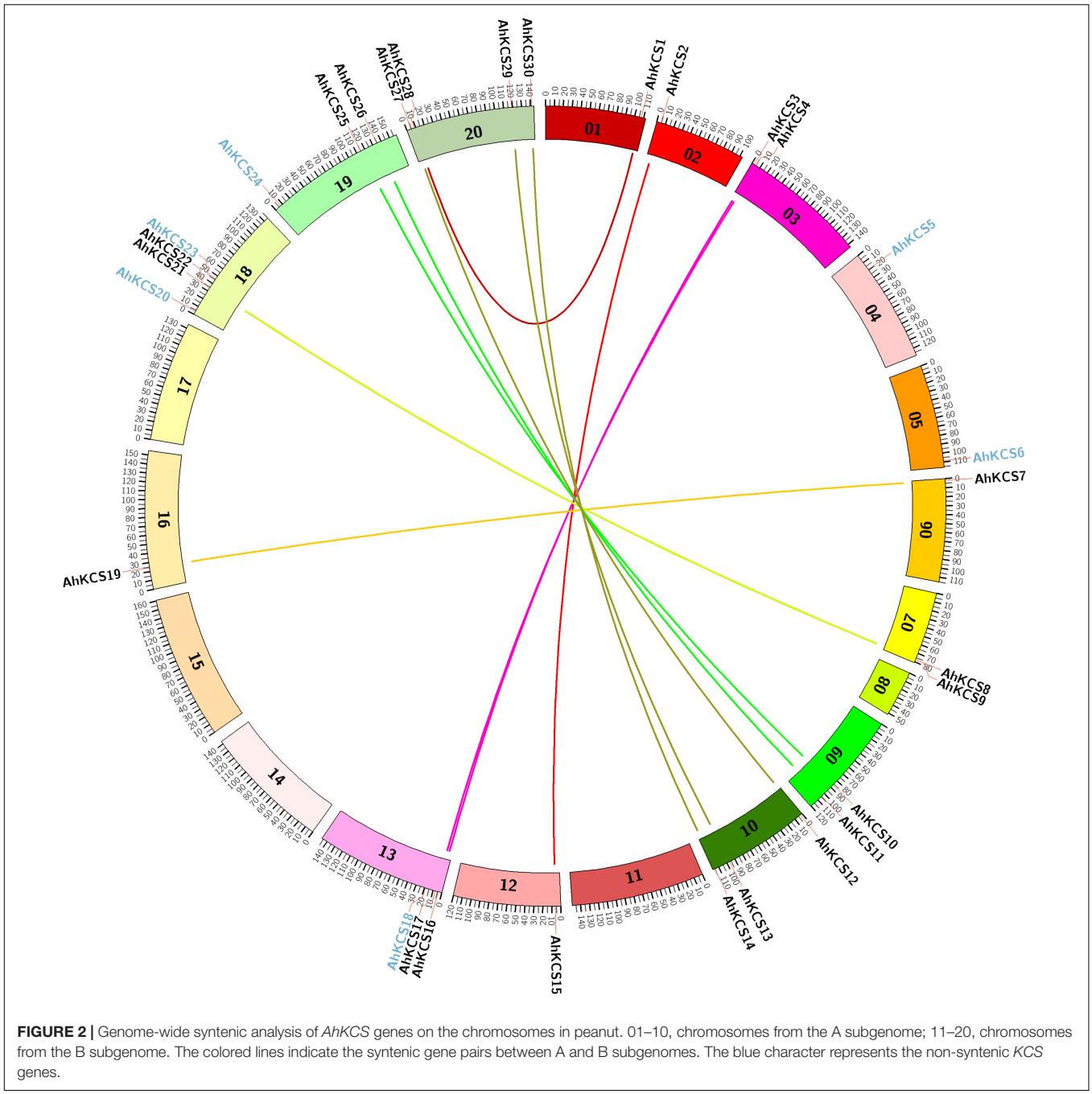

FIGURE 2 | Genome-wide syntenic analysis of *AhKCS* genes on the chromosomes in peanut. 01–10, chromosomes from the A subgenome; 11–20, chromosomes from the B subgenome. The colored lines indicate the syntenic gene pairs between A and B subgenomes. The blue character represents the non-syntenic *KCS* genes.

accumulation of VLCFAs, except for C22:0 (**Figure 5B**). The contents of C20:0 and C24:0 continuously increased during the tested developmental stages (**Figure 5B**). The content of C20:1 soared during 20–40 DAP, plateaued during 40–50 DAP, and then sharply increased during 50–60 DAP (**Figure 5B**). However, the content of C22:0 sharply increased during 20–40 DAP, and then slightly decreased during 40-50 DAP followed by a moderate increase in the last 10 days (**Figure 5B**). The total content of VLCFA increased during 20–40 DAP, plateaued during 40–50 DAP, and then continued to increase (**Figure 5B**).

Nevertheless, the relative contents of VLCFA first increased and then decreased during seed development (**Figure 5C**). The relative content of C20:0 gradually increased to a peak at 50 DAP, while the relative content of other VLCFAs, including total content of VLCFA, dramatically rose to a peak at 30 DAP (**Figure 5C**), suggesting that the relative contents of VLCFAs in the mature seed were lower.

AhKCS gene expression levels in developing peanut seeds were confirmed by qPCR at the same developing stages. Except for *AhKCS4* and *AhKCS17*, the expression levels of other *AhKCS* genes rapidly increased during 20–40 DAP, and then slightly

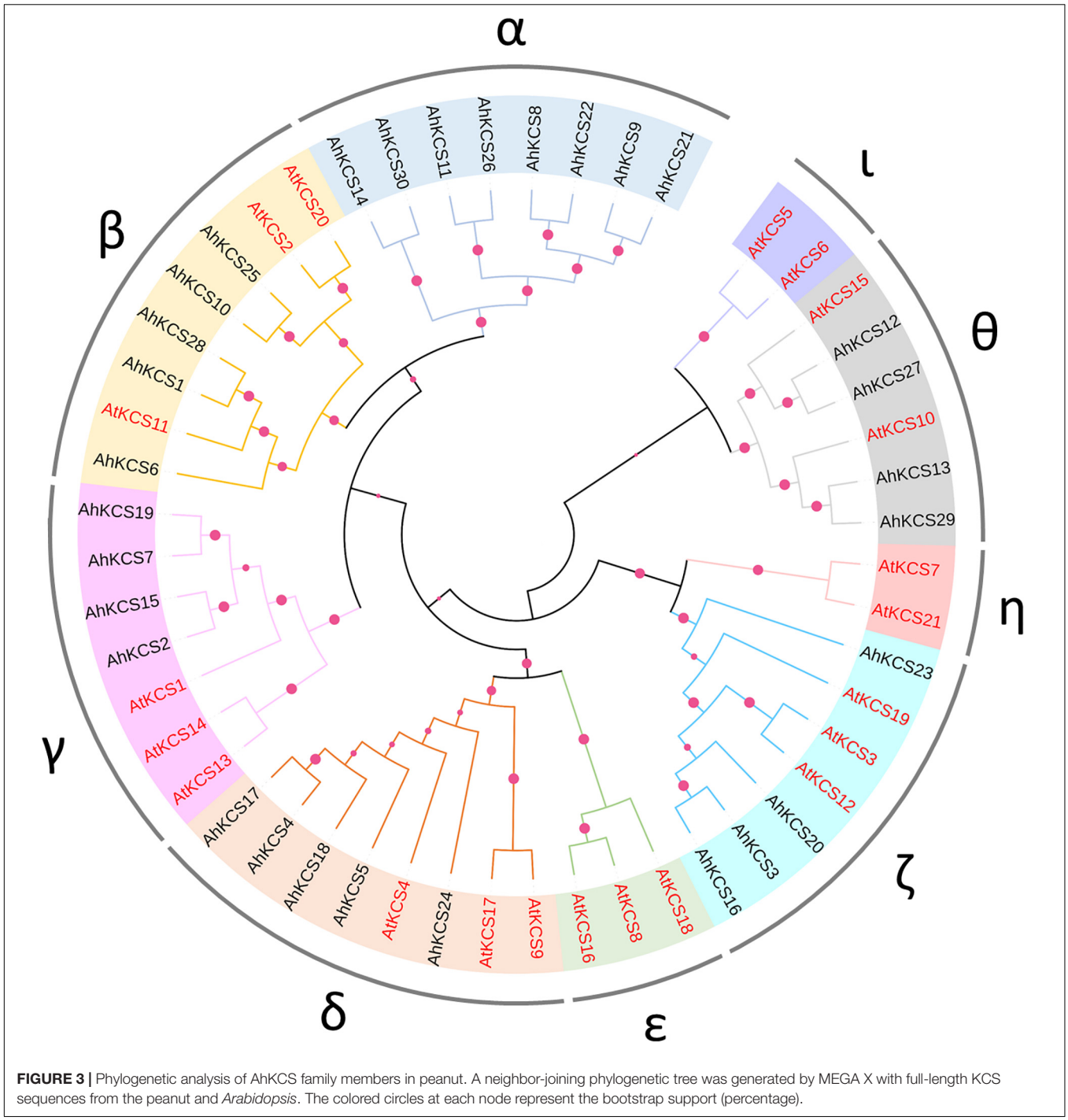

FIGURE 3 | Phylogenetic analysis of AhKCS family members in peanut. A neighbor-joining phylogenetic tree was generated by MEGA X with full-length KCS sequences from the peanut and *Arabidopsis*. The colored circles at each node represent the bootstrap support (percentage).

decreased during 40–60 DAP (**Figure 5A**). In contrast, the expression level of *AhKCS4* and *AhKCS17* first decreased during 20–40 DAP, then increased during 40–60 DAP (**Figure 5A**). The expression level of *AhKCS1* and *AhKCS28* were 5–10-fold higher than that of any other *AhKCS* gene in all developing stages except for stage I (**Figure 5A**). In later stages of development, no significant difference among the expression levels of the remaining *AhKCS* genes was detected, except for *AhKCS1* and *AhKCS28* (**Figure 5A**). These results confirmed that the expression patterns of *AhKCS* genes by qPCR analysis (**Figure 5A**) were consistent with transcriptome data (**Figure 4**).

The correlation analysis on expression levels of *AhKCS* genes and VLCFA contents was conducted. Only the expression levels of *AhKCS1* and *AhKCS28* were significantly and positively correlated with the content of C22:0 (R^2 = 0.90, p < 0.05) (**Supplementary Table S6**). Unfortunately, the expression levels of other *AhKCS* genes were not correlated with any content of VLCFA (**Supplementary Table S6**). These results implied that

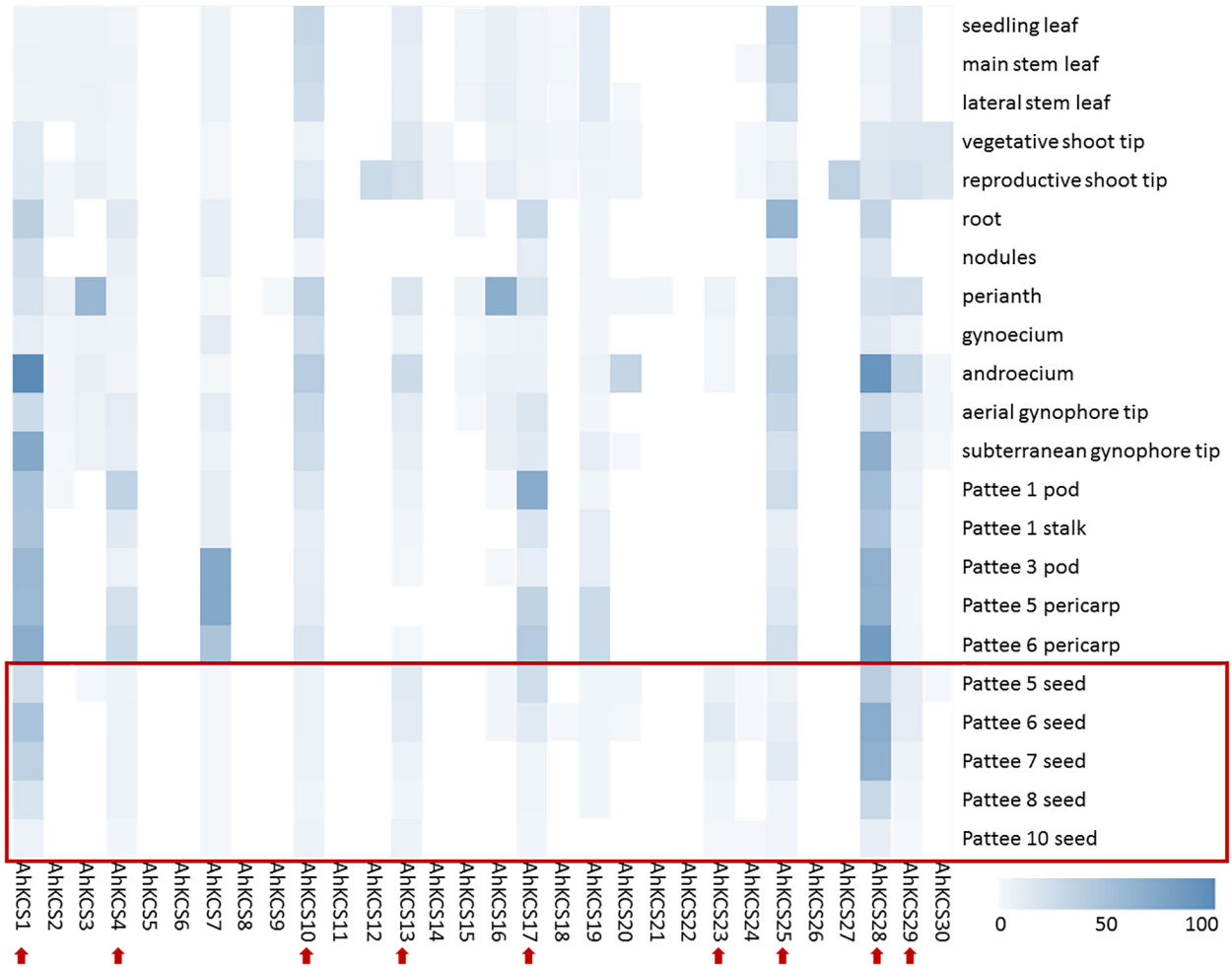

FIGURE 4 | Heat map showing the expression patterns of *AhKCS* genes in 22 tissues of peanut. Seedling leaves and roots were collected 10 days post emergence; nodules were collected 25 days post emergence; main stem leaves, lateral leaves, vegetative shoot tips from main stem, and reproductive shoot tips from first lateral were collected when the first flower appeared; perianth, gynoecia and androecia were collected when flowers were blooming in the morning of anthesis; aerial gynophore tips were collected at elongating pegs prior to soil penetration; subterranean gynophore tips were collected 24 h after soil penetration; Pattee 1 pod, whole pod at pod swelling; Pattee 1 stalk, gynophore stalk at pod swelling; Pattee 3 pod, pericarp very watery, embryo very small and not easily removed; Pattee 5 pericarp, pericarp soft, not as watery, inner pericarp without cracks; Pattee 5 seed, embryo flat, white or just turning pink at one end; Pattee 6 pericarp, inner pericarp tissue beginning to show cracks or cottony; Pattee 6 seed, torpedo shaped, generally pink at embryonic-axis end of kernels; Pattee 7 seed, torpedo to round shaped, embryonic axis end of kernel pink, other end white to light pink; Pattee 8 seed, round, light pink all over; Pattee 10 seed, large, generally dark pink all over, seed coat beginning to dry out. Red arrows indicate *AhKCS* genes with some expression level in developing seed. The data was downloaded from NCBI (Clevenger et al., 2016).

among these nine *AhKCS* genes, *AhKCS1,* and *AhKCS28* are the best candidate contributors to the accumulation of VLCFA in the peanut seed.

Heterologous Expression of *AhKCS* Genes in Yeast

To analyze the functions of the proteins encoded by the *AhKCS* genes, the coding regions of each gene was inserted to the vector pYX242 and transformed into yeast, along with *BnaA.FAE1* and *BnaC.FAE1* genes from rapeseed (*Brassic napus* L.) (Huai et al., 2018) as controls. Fatty acid profiles of the induced yeast cell were obtained as the evidence of substrate preference.

New peaks of saturated and monounsaturated VLCFAs, which are normally present in low abundance in yeast, were detected in yeast cells expressing *AhKCS* genes, and the VLCFA content in these cells was significantly increased (**Figure 6** and **Table 2**). This result indicated that all the tested AhKCSs possessed fatty acid elongase activities. However, the VLCFA compositions in yeast cells with *AhKCS* genes were not the same. Five peaks for C20:0, C22:0, C22:1, C24:0, and C26:0 were detected in yeast cells with *AhKCS1*, *AhKCS10*, *AhKCS23*, *AhKCS25*, and *AhKCS28* genes, while only two peaks for C20:0 and C26:0 were detected in yeast cells with *AhKCS13* and *AhKCS29* (**Table 2**). There were four peaks for C20:0, C22:0, C22:1, and C26:0 identified in yeast cells with *AhKCS4* and *AhKCS17* (**Table 2**). These results

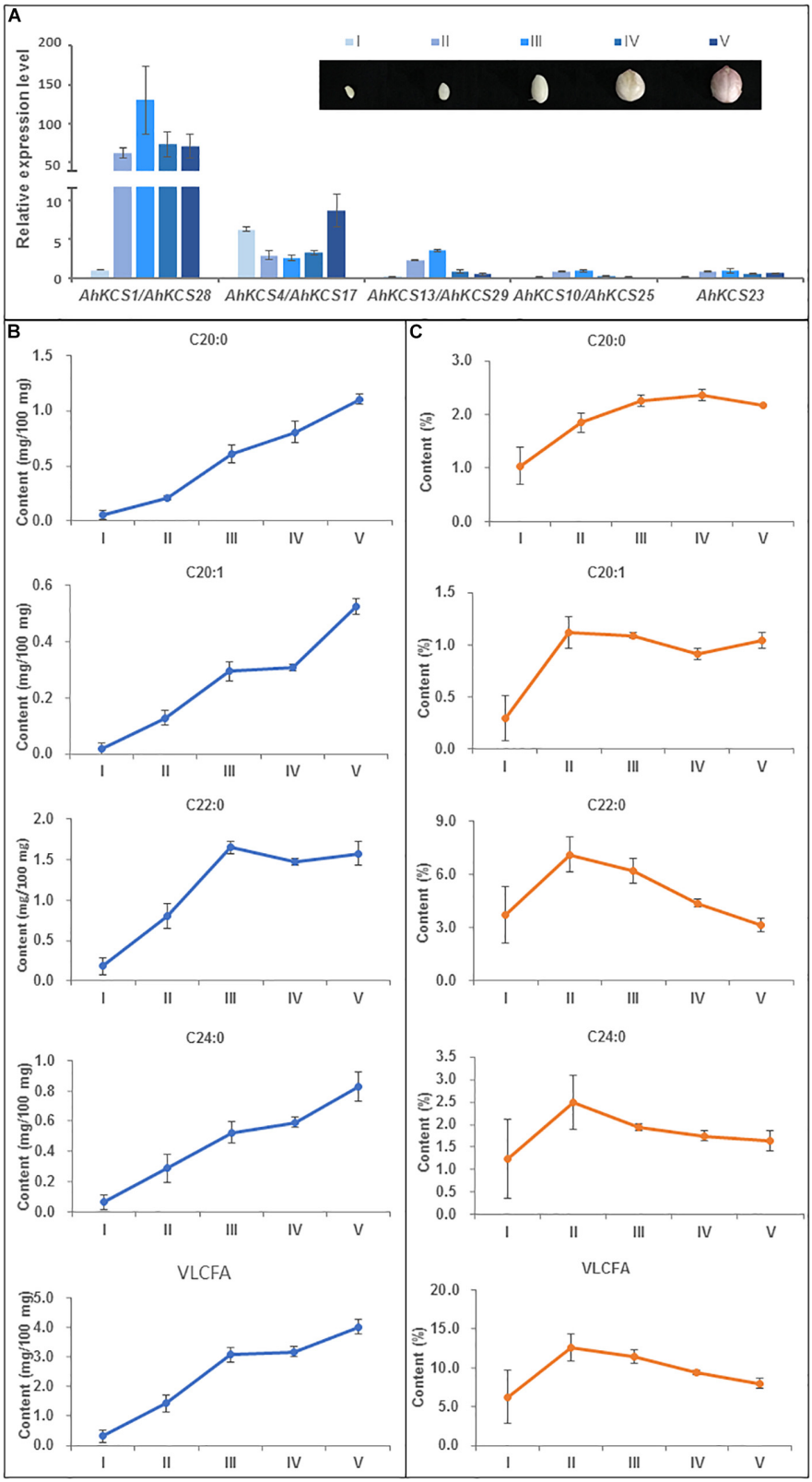

FIGURE 5 | Relationship between *AhKCS* gene expression and the accumulation of VLCFAs during peanut seed development. **(A)** qRT-PCR analysis of *AhKCS* genes in developing peanut seeds. **(B)** Absolute contents of VLCFAs during peanut seed development. **(C)** Relative contents of VLCFAs during peanut seed

(Continued)

FIGURE 5 | Continued
development. Developing peanut seeds were harvested at five specific stages: I – white and flat embryo [approximately 20 days after pollination (DAP)]; II – white and teardrop-shaped embryo (30 DAP); III – white and torpedo to round shaped embryo (40 DAP); IV – light pink and round embryo (50 DAP); V – dark pink, large, and round embryo (60 DAP). *AhACTIN* gene expression level was used as a constitutive control. Data are presented as means with standard error bars SD, which were calculated based on 3–4 independent replicates. Samples from each replicate were measured using 5–10 developing seeds. Statistical significance was evaluated by ANOVA and Fisher's least significant difference (LSD) multiple comparison.

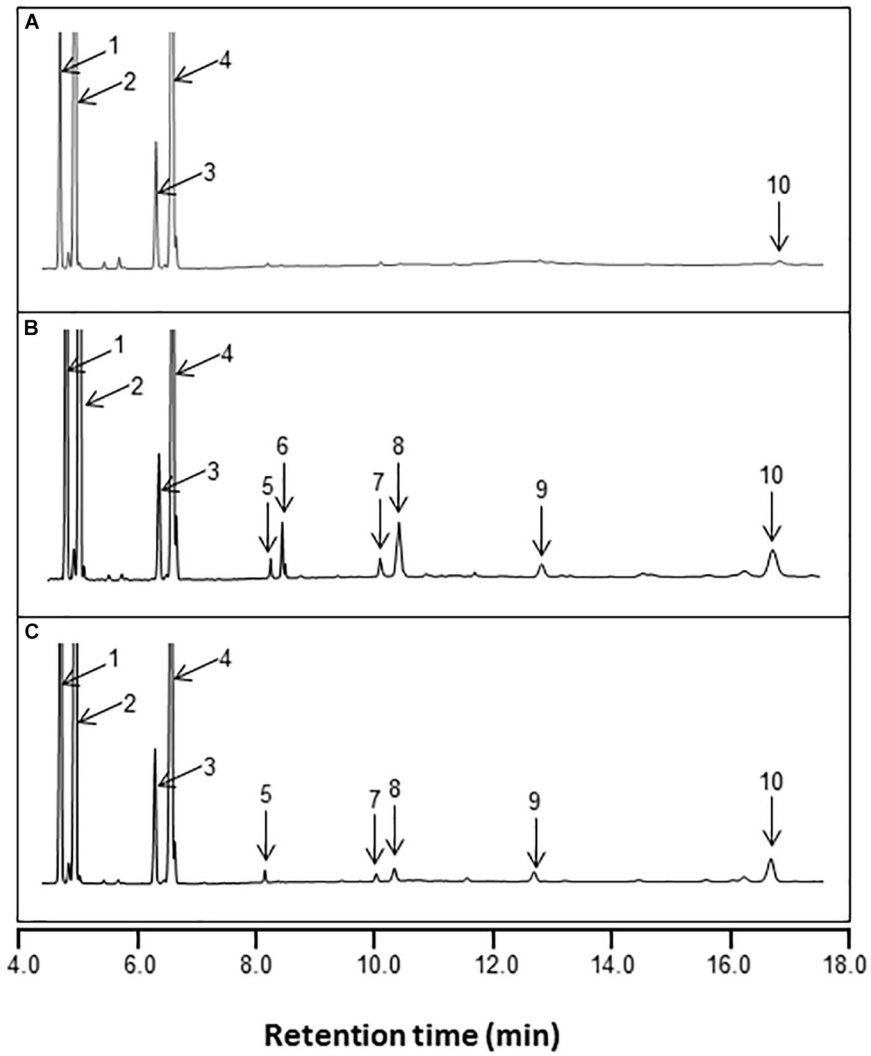

FIGURE 6 | GC analysis of fatty acid methyl esters (FAMEs) from the total lipid fraction of yeast transformed with pYX242 **(A)**, pYX242-BnaA.FAE1 **(B),** and pYX242-AhKCS1 **(C)**. Fatty acid peak identifies are: 1 = C16:0; 2 = C16:1Δ9; 3 = C18:0; 4 = C18:1Δ9 and C18:1Δ11; 5 = C20:0; 6 = C20:1Δ11; 7 = C22:0; 8 = C22:1Δ13; 9 = C24:0; 10 = C26:0. C16:0, palmitic acid; C16:1, palmitoleic acid; C18:0, stearic acid; C18:1, oleic acid; C20:0, arachidic acid; C20:1, eicosenoic acid; C22:0, behenic acid; C22:1, erucic acid; C24:0, lignoceric acid; C26:0, hexacosanoic acid.

suggested that the substrate specificities of AhKCSs differed: AhKCS13 and AhKCS29 tended to accumulate C20:0; AhKCS4 and AhKCS17 preferentially stored C26 fatty acids; AhKCS1, AhKCS10, AhKCS23, AhKCS25, and AhKCS28 actively produced a variety of VLCFAs.

Compared to BnaA.FAE1 and BnaC.FAE1 from rapeseed, AhKCSs exhibited higher preference for C16 and/or C18 SFAs as substrates. In yeast cells expressing *BnaA.FAE1* or *BnaC.FAE1*, C20:1 and C22:1 were detected but only C22:1 was found in *AhKCSs*-expressing cells (**Figure 6** and **Table 2**). The content of very long-chain unsaturated fatty acids (VLCUFAs; C20:1 + C22:1) was significantly higher than that of very long-chain saturated fatty acids (VLCSFAs; C20:0 + C22:0 + C24:0 + C26:0) in yeast cells expressing *BnaC.FAE1* ($P < 0.05$), though no obvious difference was observed in yeast cells expressing *BnaA.FAE1*. Conversely,

TABLE 2 | VLCFA contents (%) in yeast transformed with empty vector and *AhKCS* genes.

Construct	C20:0	C20:1	C22:0	C22:1	C24:0	C26:0	VLCFA	VLCSFA	VLCUFA	VLCSFA/VLCUFA
pYX242	ND	ND	ND	ND	ND	0.4 ± 0.1^{b}	0.4 ± 0.1^{e}	0.4 ± 0.1^{e}	ND	
pYX242-BnaA.FAE1	0.5 ± 0.1^{b}	1.1 ± 0.1^{b}	0.9 ± 0.2^{a}	3.0 ± 1.1^{b}	1.5 ± 0.3^{a}	0.3 ± 0.2^{b}	7.4 ± 1.6^{ab}	3.2 ± 0.2^{bc}	4.1 ± 1.2^{b}	0.9 ± 0.3^{b}
pYX242-BnaC.FAE1	0.4 ± 0.1^{b}	1.4 ± 0.1^{a}	0.7 ± 0.1^{ab}	4.3 ± 0.5^{a}	1.5 ± 0.7^{a}	0.2 ± 0.1^{b}	8.5 ± 1.2^{a}	2.7 ± 0.9^{cd}	5.8 ± 0.5^{a}	0.5 ± 0.1^{b}
pYX242-AhKCS1	0.5 ± 0.1^{b}	ND	0.4 ± 0.1^{bc}	0.6 ± 0.2^{c}	0.6 ± 0.1^{ab}	3.3 ± 0.6^{a}	5.4 ± 0.6^{bc}	4.8 ± 0.8^{ab}	0.6 ± 0.2^{c}	9.8 ± 4.1^{a}
pYX242-AhKCS4	0.2 ± 0.1^{b}	ND	0.1 ± 0.0^{c}	0.5 ± 0.2^{c}	ND	2.8 ± 0.7^{a}	3.6 ± 1.0^{cd}	3.1 ± 0.8^{bcd}	0.5 ± 0.2^{c}	7.4 ± 2.3^{a}
pYX242-AhKCS10	0.1 ± 0.0^{b}	ND	0.2 ± 0.1^{c}	0.1 ± 0.1^{c}	0.2 ± 0.1^{b}	1.0 ± 0.2^{b}	1.5 ± 0.3^{d}	1.4 ± 0.2^{d}	0.1 ± 0.1^{c}	12.7 ± 5.7^{a}
pYX242-AhKCS13	2.5 ± 0.9^{a}	ND	ND	ND	ND	0.6 ± 0.2^{b}	3.1 ± 0.8^{d}	3.1 ± 0.8^{bcd}	ND	
pYX242-AhKCS17	0.3 ± 0.1^{b}	ND	0.2 ± 0.0^{c}	0.5 ± 0.1^{c}	ND	3.6 ± 0.4^{a}	4.3 ± 0.6^{c}	3.9 ± 0.5^{abc}	0.5 ± 0.1^{c}	8.5 ± 2.7^{a}
pYX242-AhKCS23	0.5 ± 0.1^{b}	ND	0.5 ± 0.2^{b}	0.7 ± 0.2^{c}	0.9 ± 0.3^{ab}	3.0 ± 0.2^{a}	5.6 ± 0.9^{b}	4.9 ± 0.8^{ab}	0.7 ± 0.2^{c}	7.0 ± 1.0^{a}
pYX242-AhKCS25	0.3 ± 0.1^{b}	ND	0.4 ± 0.0^{c}	0.6 ± 0.1^{c}	0.8 ± 0.2^{ab}	0.9 ± 0.3^{b}	3.0 ± 0.7^{d}	2.4 ± 0.6^{cd}	0.6 ± 0.1^{c}	5.8 ± 2.4^{a}
pYX242-AhKCS28	0.4 ± 0.1^{b}	ND	0.5 ± 0.2^{bc}	0.7 ± 0.3^{c}	0.9 ± 0.3^{ab}	3.7 ± 0.4^{a}	6.1 ± 0.9^{b}	5.4 ± 0.4^{ab}	0.7 ± 0.3^{c}	9.6 ± 3.3^{a}
pYX242-AhKCS29	3.1 ± 1.3^{a}	ND	ND	ND	ND	0.8 ± 0.3^{b}	4.0 ± 1.1^{d}	4.0 ± 1.1^{bcd}	ND	

ND, not detected. C20:0: arachidic acid; C20:1: eicosenoic acid; C22:0: behenic acid; C22:1: erucic acid; C24:0: lignoceric acid; C26:0: hexacosanoic acid. VLCFA = C20:0 + C20:1 + C22:0 + C22:1 + C24:0 + C26:0; VLCSFA = C20:0 + C22:0 + C24:0 + C26:0; VLCUFA = C20:1 + C22:1. Means ± SD were calculated based on 3–5 independent replicates. a, b, c, d, and e in each column represent significant difference at P < 0.05 based on ANOVA and Fisher's least significant difference (LSD) multiple-comparison. Each letter is significantly different from any other letter and any combination of other letters but is not significantly different from itself and any combination of these letters including itself. For example, a is significantly different from b, c, d, e, bc, cd, de, bcd, cde, and bcde, but is not significantly different from a, ab, abc and abcd. ab is significantly different from c, d, e, cd, de, and cde, but is not significantly different from a, b, ab, abc and abcd. abc is significantly different from d, e and de, but is not significantly different from a, b, c, ab, bc, abc and abcd. abcd is significantly different from e, but is not significantly different from a, b, c, d, ab, bc, cd, abc, bcd, and abcd. The same for b, c, d, and e.

the content of VLCUFA was significantly lower than that of VLCSFA in all yeast cells expressing any *AhKCS* gene ($P < 0.05$). Additionally, the ratio of VLCSFA to VLCUFA in yeast cells expressing BnaA.FAE1 or BnaC.FAE1 were 0.9 and 0.5, respectively, while the ratios in all yeast cells expressing any *AhKCS* gene were greater than 5.0 (**Table 2**). These results indicated that AhKCSs were more specific to saturated fatty acid substrates than Bna.FAE1s.

Analyses of AhKCS Genes in Peanut Lines With Different Contents of VLCFA

To confirm the roles of AhKCSs in regulating the VLCFA content of the peanut, these nine *AhKCS* genes were isolated and sequenced from six lines with different VLCFA contents in their seeds. The VLCFA contents in C-34, C-119, and C-140 were 4.6, 4.3, and 4.7%, while the VLCFA contents in C-178, C-296, and C-224 were 9.4, 9.6, and 9.8% (**Figure 7B** and **Supplementary Table S7**). However, no single nucleotide polymorphism (SNP) was detected in the coding sequences of *AhKCS1*, *AhKCS4*, *AhKCS10*, *AhKCS13*, *AhKCS25*, *AhKCS28*, and *AhKCS29* among these six lines. One nucleotide substitution (C:G → A:T) at position 39 was identified in *AhKCS17* of C-119, with no amino acid alternation (**Supplementary Figure S3A**). Another nucleotide substation (T:A → C:G) at position 1330 was identified in *AhKCS23* of C-34 without changing the amino acid (**Supplementary Figure S3B**). None of the SNPs were therefore associated with VLCFA content.

The expression levels of AhKCS genes were further investigated in the developing seeds from these six lines (**Figure 7**). All nine *AhKCS* genes were expressed, but only the expression levels of *AhKCS1* and *AhKCS28* were positively correlated with the VLCFA content ($R^2 = 0.93$, $p < 0.05$) (**Supplementary Table S8**). The expression levels of *AhKCS1* and *AhKCS28* in C-34, C-119, and C-140 were at least twice as low as those in C-178, C-296, and C-224 (**Figure 7A**). There was no significant correlation between the expression levels of other *AhKCS* genes and the seed VLCFA content (**Figure 7** and **Supplementary Table S8**). Based on these results, *AhKCS1* and *AhKCS28* were proposed to regulate the VLCFA content in peanut.

Subcellular Localization of AhKCS1 and AhKCS28

To examine the subcellular localization of AhKCS1 and AhKCS28, they were separately fused with GFP, and then co-expressed with the ER marker in *Arabidopsis* protoplasts by PEG induction. As expected, the green signal of the empty vector spread throughout the whole cell (**Figure 8A**). But the green signal of AhKCS1 (**Figure 8B**) and AhKCS28 (**Figure 8C**) were completely co-localized with the red ER marker, respectively. No green signal was observed in the nucleus (**Figures 8B,C**). These results indicated that AhKCS1 and AhKCS28 were located on the ER, where fatty acid elongase complex functions (Haslam and Kunst, 2013).

Heterologous Expression of *AhKCS1* and *AhKCS28* Genes in *Arabidopsis*

To further confirm the function of AhKCS1 and AhKCS28 in plants, the *AhKCS1* and *AhKCS28* genes were heterologous expressed in the *Arabidopsis fae1/fad2* double mutant. Eight *AhKCS1*-expressing T_1 lines and five *AhKCS28*-expressing T_1 lines were obtained, respectively (**Supplementary Table S9**). The fatty acid composition of the DsRed positive seeds from each line was determined. The VLCFA contents in seeds from the *Arabidopsis fae1/fad2* double mutant with *BnaA.FAE1* or

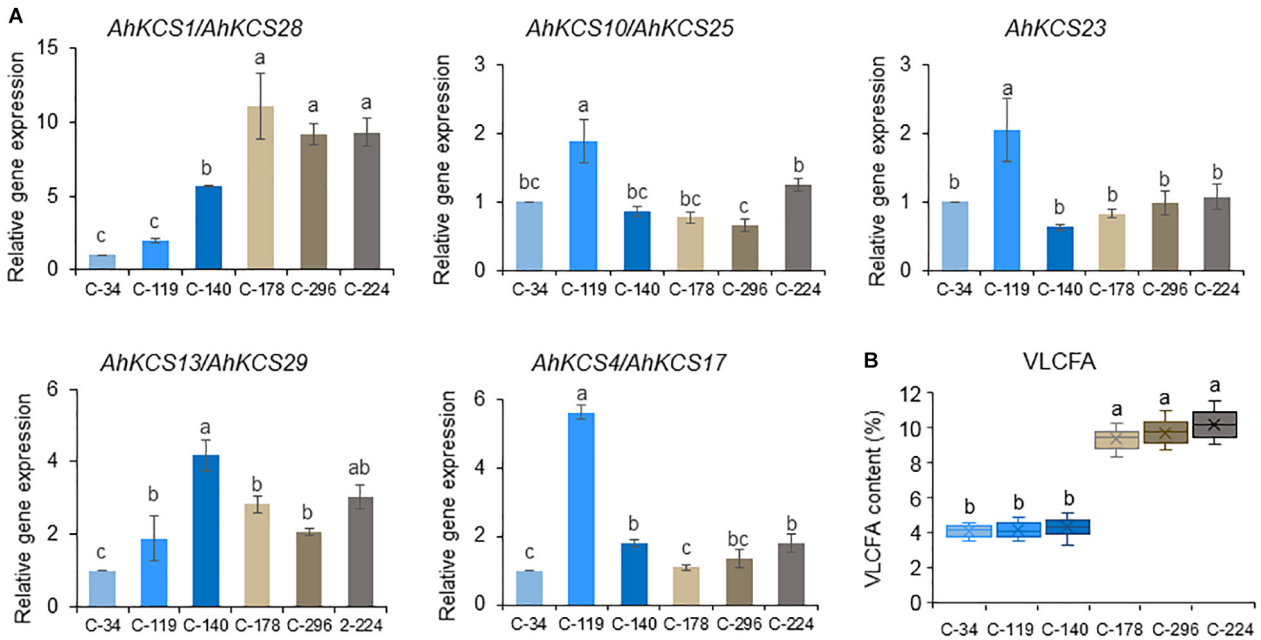

FIGURE 7 | Expression levels of *AhKCS* genes in developing seeds from peanut lines with different VLCFA contents. **(A)** qRT-PCR analysis of *AhKCS* genes in developing seeds from peanut lines with different VLCFA contents. **(B)** VLCFA contents in mature seeds harvested from C-34, C-119, C-140, C-178, C-296, and C-224. The relative expression values of genes were measured on developing seeds harvested at 50 days after pollination. *AhACTIN* gene expression level was used as a constitutive control. Values are the means and SD of three independent biological replicates. a, b, and c represent significant difference at $P < 0.05$ based on ANOVA and Fisher's least significant difference (LSD) multiple-comparison. Each letter is significantly different from any other letter and any combination of other letters but is not significantly different from itself and any combination of these letters including itself. For example, a is significantly different from b, c and bc, but is not significantly different from a and ab. b is significantly different from a and c, but is not significantly different from b, ab, and bc. c is significantly different from a, b, and ab, but is not significantly different from c and bc. ab is significantly different from c, but is not significantly different from a and b. bc is significantly different from a, but is not significantly different from b and c.

BnaC.FAE1 (Huai et al., 2018) were also used as controls to compare the substrate specificity.

In seeds of the *Arabidopsis fae1/fad2* double mutant, there were 3.2% of C20:0 and 2.2% of C20:1, without other VLCFAs (**Figure 9A** and **Supplementary Table S9**). In the seeds from *AhKCS1*- or *AhKCS28*-expressing lines, an extra VLCFA C22:0 was detected, and the contents of C20:0 and C20:1 were significantly increased. Moreover, the total VLCFA content was significantly increased from 5.5 to 25.8% and 28.4% in the *AhKCS1*- or *AhKCS28*-expressing lines, respectively (**Figure 9A** and **Supplementary Table S9**). These results suggested that AhKCS1 and AhKCS28 catalyzed fatty acid elongase activity in plants.

The compositions of VLCFAs in the seeds from *AhKCS1*- or *AhKCS28*-expressing lines were different to those in the seeds from *BnaA.FAE1*- and *BnaC.FAE1*-expressing lines (**Figure 9A** and **Supplementary Table S9**). In the *BnaA.FAE1*- and *BnaC.FAE1*-expressing lines, two extra VLCFAs were presented such as C22:0 and C22:1, compared to the VLCFAs in the *fae1/fad2* double mutant. C22:1 was absent in the seeds from the *AhKCS1*- or *AhKCS28*-expressing lines (**Figure 9A**). The C20:0 content was significantly increased from 3.2 to 6.9% in *AhKCS1*- and 7.2% in *AhKCS28*-expressing lines, while it was significantly decreased to 0.6% in *BnaA.FAE1*- and 0.7% in *BnaC.FAE1*-expressing lines (0.7%) (**Figure 9A**). In addition, there were more VLCSFAs and less VLCUFA accumulated in *AhKCS1*- or *AhKCS28*-expressing lines compared to *BnaA.FAE1*- or *BnaC.FAE1*-expressing lines (**Figure 9B**). Furthermore, the VLCSFA/VLCUFA ratio in *AhKCS1*- and *AhKCS28*-expressing lines were 2.6 and 2.8, but the ratios in *BnaA.FAE1*- and in *BnaC.FAE1*-expressing lines were 0.5 and 0.6 (**Figure 9C**). These results again confirmed that AhKCS1 and AhKCS28 were inclined to use saturated fatty acids as the substrate.

DISCUSSION

The high content of SFAs (15.5–27.5%) is a major negative quality factor in peanut oil. In the peanut, VLCSFA content varies from 2.5 to 8.5%, which accounts for 20–40% of the SFA content. Therefore, decreasing the VLCSFA content is an effective way to reduce SFA total content. It has been proved that the VLCFA content is mainly controlled by KCS in plants (James et al., 1995; Joubes et al., 2008; Huai et al., 2015), so we identified 30 *AhKCS* genes in the peanut genome (**Table 1**). There were approximately 20-30 members of the *KCS* gene family in angiosperms, such as 21 in *Arabidopsis*, 27 in soybean, and 19 in *Medicago truncatula* (Guo et al., 2016) – consistent with the large numbers of AhKCS family members in the peanut. All the identified AhKCSs contained two domains: an ACP_syn_III_C

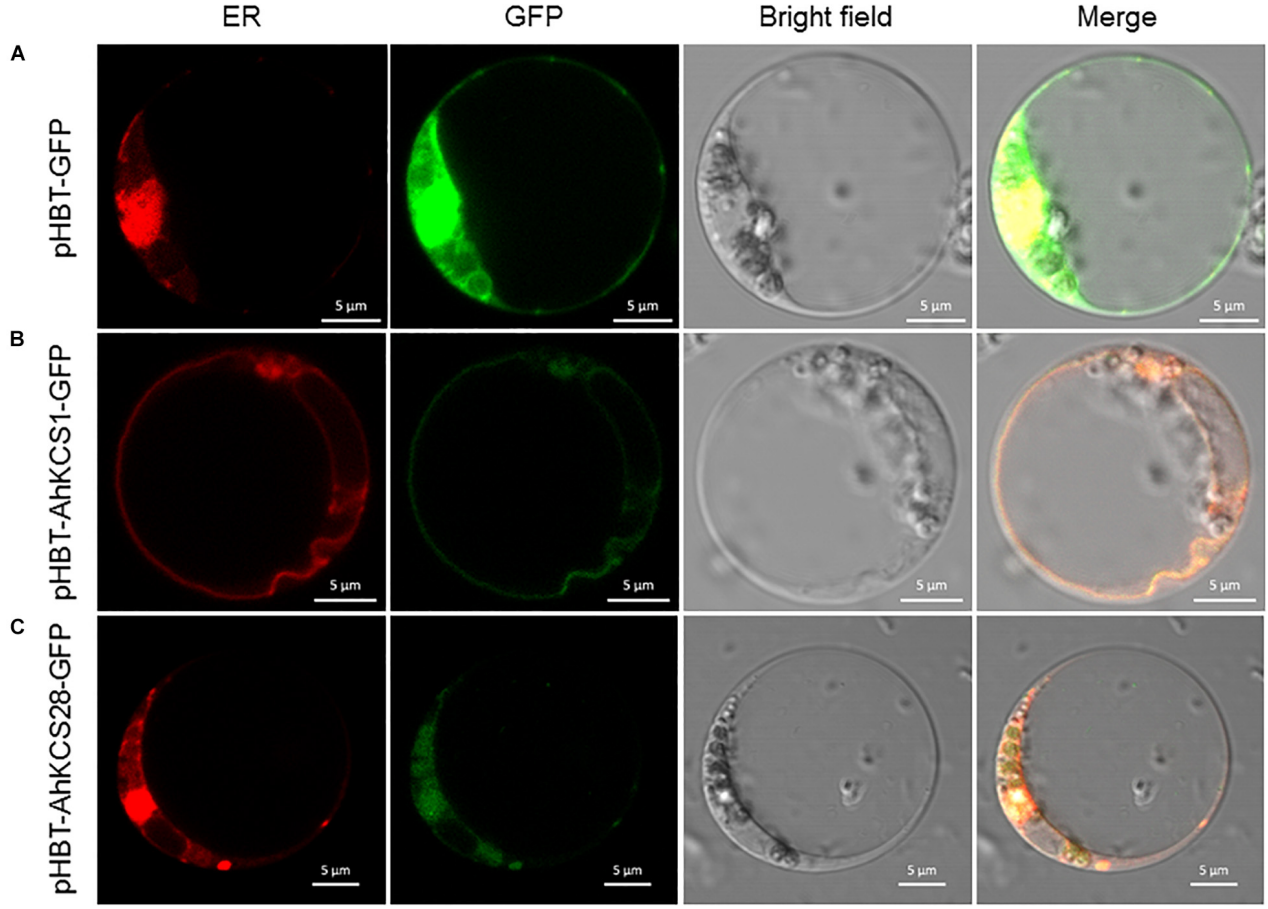

FIGURE 8 | Subcellular location of AhKCS1 and AhKCS28 in the *Arabidopsis* protoplast cell. **(A)** An empty GFP vector served as the control. **(B)** AhKCS1-GFP (green) merged with endoplasmic reticulum (ER) marker (red). **(C)** AhKCS28-GFP (green) merged with ER marker (red).

domain and a FAE1_CUT1_RppA domain, which have been proven to be necessary for KCSs (**Figure 1**; Sagar et al., 2015; Guo et al., 2016; Xiao et al., 2016). The ACP_syn_III_C domain is found in 3-Oxoacyl-[acyl-carrier-protein (ACP)] synthase III (EC:2.3.1.41), and is responsible for initiating the chain of fatty acid synthase reactions in plants and bacteria (Abbadi et al., 2000). KCS members harboring the FAE1_CUT1_RppA domain are described as 3-ketoacyl-CoA synthases, type III polyketide synthases, fatty acid elongases or fatty acid condensing enzymes, and are found in both prokaryotic and eukaryotic (mainly plant) species. This domain contains active site residues, as well as motifs involved in substrate binding (Nobutaka et al., 2002). The characteristics of ACP_syn_III_C and FAE1_CUT1_RppA domains supported that the genes identified in this study belong to *KCS* gene families.

Based on the phylogenetic analysis, all the AtKCS proteins were classified into eight groups (β, γ, δ, ε, ζ, η, θ, and ι) (**Figure 3**), which is consistent with previous studies (Joubes et al., 2008). All the identified AhKCS proteins were grouped into six groups: α, β, γ, δ, ζ, and θ (**Figure 3**). The AhKCSs in Group α were not grouped with any AtKCS (**Figure 3**), suggesting that these AhKCSs might be specific and acquired a different function in the peanut. The AhKCSs in group β were closely related to AtKCS2 and AtKCS20 (**Figure 3**), which were involved in the biosynthesis of suberin (Lee et al., 2009). The AhKCSs in group θ were grouped with AtKCS10 and AtKCS15 (**Figure 3**), which were reported to have participated in the biosynthesis of VLCFA in the epidermal cell (Pruitt et al., 2000). The AhKCSs in these two groups might also be involved in the development of the epidermis. Group ι was composed of AtKCS5/CER60 and AtKCS6/Cer6 only (**Figure 3**), which were responsible for the biosynthesis of cuticular wax (Fiebig et al., 2000). It hinted that the original homolog of AtKCS5/CER60 and AtKCS6/Cer6 might be deleted or functionally diverged in the peanut.

It has been shown that the VLCFA content in the seed is controlled by seed-specific expressed *KCS* genes, such as *AtFAE1* in *Arabidopsis* (James et al., 1995), *BnFAE1* in *B. napus* (Wang et al., 2010), and *CaFAE1* in *Crambe abyssinica* (Mietkiewska et al., 2007). However, no seed-specific expressing *AhKCS* gene was found in the peanut (**Figure 4**). Furthermore, no AhKCS was grouped with AtKCS18/FAE1 (**Figure 3**). Perhaps because the VLCFAs in the peanut are not as abundant as those in *Brassicaceae*, the seed-specific *AhKCS* genes eliminated during evolution.

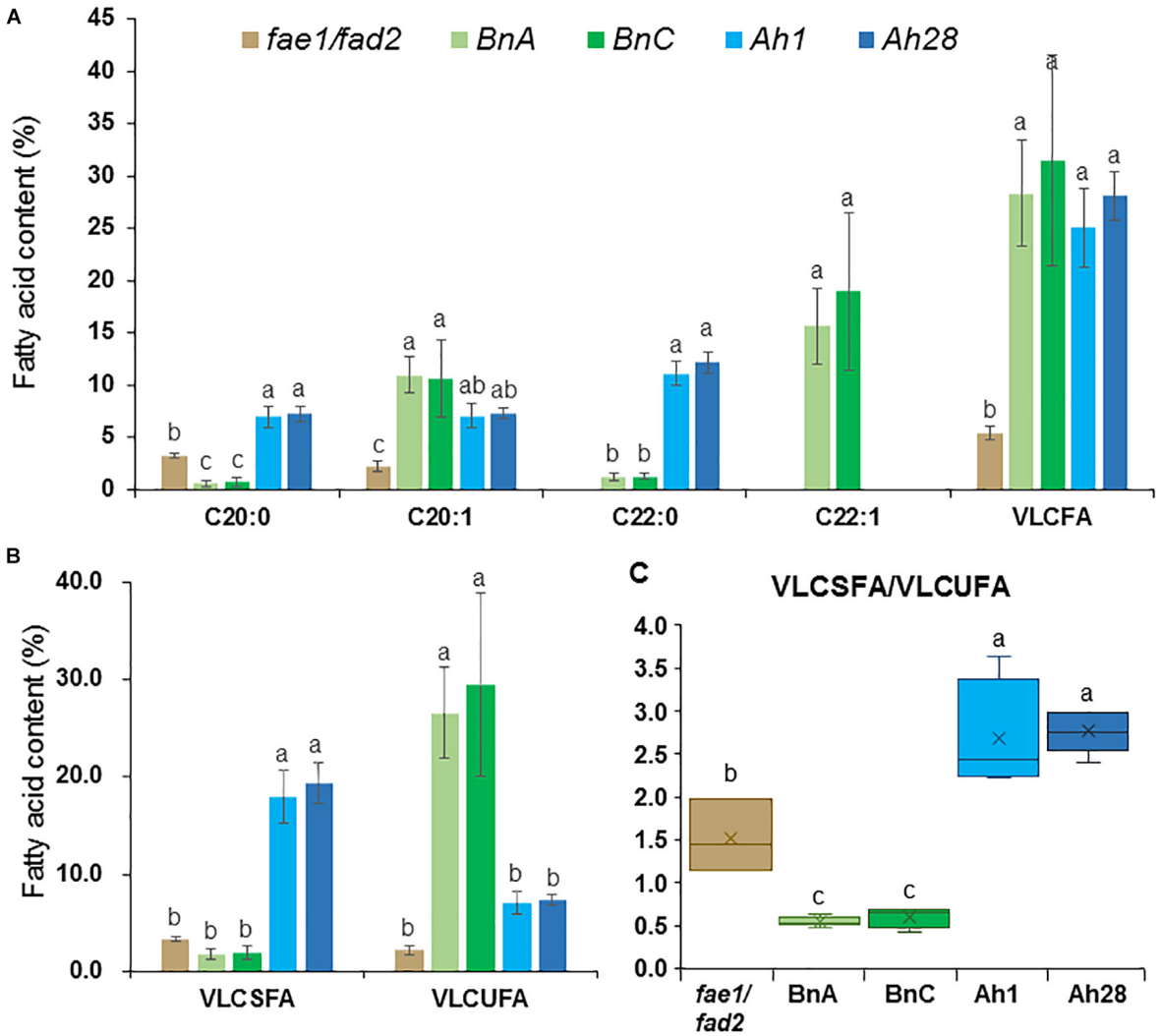

FIGURE 9 | The VLCFA content in mature seeds harvested from *Arabidopsis fae1/fad2* double mutant and T_2 transgenic lines. **(A)** The contents of C20:0, C20:1, C22:0, C22:1 and VLCFA. **(B)** The contents of very long chain saturated fatty acid (VLCSFA) and very long chain unsaturated fatty acid (VLCUFA). **(C)** The ratio of VLCSFA to VLCUFA. VLCFA = C20:0 + C20:1 + C22:0 + C22:1; VLCSFA = C20:0 + C22:0; VLCUFA = C20:1 + C22:1. BnA, T_2 lines transformed with *BnaA.FAE1*; BnC, T_2 lines transformed with *BnaC.FAE1*; Ah1, T_2 lines transformed with *AhKCS1*; Ah28, T_2 lines transformed with *AhKCS28*. At least three replicates were used for each sample. Samples from each replicate were measured using 25 mg mature seeds. Different letters indicated statistically different at $P < 0.05$ based on ANOVA and Fisher's least significant difference (LSD) multiple-comparison. The data was shown in **Supplementary Table S9**.

AhKCS1 and *AhKCS28* were considered to be the genes that regulate the content of VLCFA in the peanut for three reasons. First, the expression level of these two genes was the highest in developing seed (**Figure 5A**), suggesting that these two genes could be one of the main factors to regulate VLCFA biosynthesis in the peanut seed. Second, *AhKCS1* and *AhKCS28* were the only two genes, whose expression level was significantly and positively correlated with the VLCFA content (**Figure 7A** and **Supplementary Table S8**), indicating that the expression level of these two genes might affect the VLCFA content in the peanut seed. Third, AhKCS1 and AhKCS28 exhibited substrate preference for SFA, which were different from BnFAE1s (**Table 2** and **Figure 9**). The substrate specificities are in accordance with the features of VLCFA composition in the peanut and rapeseed, showing that the substrate specificities of these two AhKCSs were involved in determining the VLCFA compositions in the peanut seed. In summary, AhKCS1 and AhKCS28 could be candidate genes for decreasing VLCFA content in the peanut seed.

Due to the high identity of the syntenic AhKCS pairs, the expression level detected in this study is the sum of both genes. For example, the expression level of *AhKCS1/AhKCS28* represented the total amount of expression levels of *AhKCS1* and *AhKCS28*. According to the expression profile of *AhKCS1* and *AhKCS28*, both of them were expressed in the developing seed (**Figure 4**). But the homology between *AhKCS1*and *AhKCS28* was 97.8%, and there were only 14 SNPs between these two genes (**Supplementary Figure S4**). It is difficult to distinguish

the expression levels from each other by qPCR. We designed five pairs of SNP specific primers, but we still failed to separate the expression levels between these two genes (data not shown). Although we could not figure out whose expression level decreased between *AhKCS1* and *AhKCS28*, we still proved that both were involved in the biosynthesis of VLCFAs in the peanut, since both *AhKCS1* and *AhKCS28* were highly expressed in the developing seed and possessed the fatty acid elongase activities.

Many studies have demonstrated that knocking out the *KCS* genes with a high expression level in seeds could significantly reduce the VLCFAs. For example, the VLCFA contents were dramatically decreased from >20% to <1% in the *Arabidopsis fae1* mutant (James et al., 1995), and from >40% to <2% in canola, which is the fae1 mutant of *B. napus* (Wang et al., 2010). The *fae1* mutants of *Camelina sativa* were created by the CRISPR/Cas9 technology, and the VLCFA content was reduced from 22 to <2% (Ozseyhan et al., 2018). Suppressing the expression level of *KCS* genes in seeds could also decrease the VLCFA content. When the expression of *FAE1* was silenced by RNAi in seeds of *B.napus*, the erucic acid was undetectable (Peng et al., 2010; Tian et al., 2011; Shi et al., 2017). Down-regulation of *FAE1* genes in *Crambe abyssinica* significantly reduced the erucic acid content (Li et al., 2016). Therefore, knockout or silencing of the *AhKCS1* and *AhKCS28* genes in the peanut might be an effective way to decrease the VLCFA content and improve the health-promoting and nutritional qualities of the peanut.

DATA AVAILABILITY STATEMENT

All datasets generated for this study are included in the article/**Supplementary Material**.

AUTHOR CONTRIBUTIONS

DH, YLei, and BL conceived and designed the experiments. HJ supplied the peanut lines. XX, JL, LY, YC, XW, NL, YK, and ZW performed the experiments. DH, YLi, PW, and YH analyzed the data. DH wrote the manuscript. DH, HJ, YLei, and BL revised the manuscript. All authors read and approved the final version of the manuscript.

FUNDING

This work was supported by the Natural Science Foundation of Hubei Province (2017CFB161), the National Natural Science Foundation of China (31671734 and 31871662), the National Key R&D Program of China (2018YFD1000901) and the Fundamental Research Funds for Central Non-profit Scientific Institution (Y2018PT52). The funders had no role in experiment design, data analysis, decision to publish, or preparation of the manuscript.

ACKNOWLEDGMENTS

We thank Dr. Edgar B. Cahoon (Center for Plant Science Innovation and Department of Biochemistry, University of Nebraska-Lincoln) for supplying the vectors and editing the manuscript.

SUPPLEMENTARY MATERIAL

The Supplementary Material for this article can be found online at: https://www.frontiersin.org/articles/10.3389/fpls.2020.00406/full#supplementary-material

REFERENCES

Abbadi, A., Brummel, M., Schütt, B. S., Slabaugh, M. B., Schuch, R., and Spener, F. (2000). Reaction mechanism of recombinant 3-oxoacyl-(acyl-carrier-protein) synthase III from *Cuphea wrightii* embryo, a fatty acid synthase type II condensing enzyme. *Biochem. J.* 345, 153–160.

Bertioli, D. J., Cannon, S. B., Froenicke, L., Huang, G., Farmer, A. D., Cannon, E. K., et al. (2015). The genome sequences of *Arachis duranensis* and *Arachis ipaensis*, the diploid ancestors of cultivated peanut. *Nat. Genet.* 47, 438–446.

Bertioli, D. J., Jenkins, J., Clevenger, J., Dudchenko, O., Gao, D., Seijo, G., et al. (2019). The genome sequence of segmental allotetraploid peanut Arachis hypogaea. *Nat. Genet.* 51, 877–884.

Blacklock, B. J., and Jaworski, J. G. (2002). Studies into factors contributing to substrate specificity of membrane-bound 3-ketoacyl-CoA synthases. *Eur. J. Biochem.* 269, 4789–4798.

Blacklock, B. J., and Jaworski, J. G. (2006). Substrate specificity of *Arabidopsis* 3-ketoacyl-CoA synthases. *Biochem. Biophys. Res. Commun.* 346, 583–590.

Briggs, M., Petersen, K., and Kris-Etherton, P. (2017). Saturated fatty acids and cardiovascular disease: replacements for saturated fat to reduce cardiovascular risk. *Healthcare* 5:29. doi: 10.3390/healthcare5020029

Camacho, C., Coulouris, G., Avagyan, V., Ma, N., Papadopoulos, J., Bealer, K., et al. (2009). BLAST+: architecture and applications. *BMC Bioinform.* 10:421.

Clevenger, J., Chu, Y., Scheffler, B., and Ozias-Akins, P. (2016). A developmental transcriptome map for allotetraploid *Arachis hypogaea*. *Fron. Plant Sci.* 7:1446. doi: 10.3389/fpls.2016.01446

Denic, V., and Weissman, J. S. (2007). A molecular caliper mechanism for determining very long-chain fatty acid length. *Cell* 130, 663–677.

Fiebig, A., Mayfield, J. A., Miley, N. L., Chau, S., Fischer, R. L., and Preuss, D. (2000). Alterations in *CER6*, a gene identical to *CUT1*, differentially affect long-chain lipid content on the surface of pollen and stems. *Plant Cell* 12, 2001–2008.

Franke, R., Höfer, R., Briesen, I., Emsermann, M., Efremova, N., Yephremov, A., et al. (2009). The *DAISY* gene from *Arabidopsis* encodes a fatty acid elongase condensing enzyme involved in the biosynthesis of aliphatic suberin in roots and the chalaza-micropyle region of seeds. *Plant J.* 57, 80–95. doi: 10.1111/j.1365-313X.2008.03674.x

Giakoumis, E. G. (2018). Analysis of 22 vegetable oils' physico-chemical properties and fatty acid composition on a statistical basis, and correlation with the degree of unsaturation. *Renewab. Energy* 126, 403–419.

Gray, J. E., Holroyd, G. H., Van Der Lee, F. M., Bahrami, A. R., Sijmons, P. C., Woodward, F. I., et al. (2000). The HIC signalling pathway links CO_2 perception to stomatal development. *Nature* 408, 713–716.

Guo, H.-S., Zhang, Y.-M., Sun, X.-Q., Li, M.-M., Hang, Y.-Y., and Xue, J.-Y. (2016). Evolution of the *KCS* gene family in plants: the history of gene duplication, sub/neofunctionalization and redundancy. *Mol. Genet. Genomics* 291, 739–752. doi: 10.1007/s00438-015-1142-3

Guo, Y., Mietkiewska, E., Francis, T., Katavic, V., Brost, J. M., Giblin, M., et al. (2009). Increase in nervonic acid content in transformed yeast and transgenic plants by introduction of a *Lunaria annua* L. 3-ketoacyl-CoA synthase (*KCS*) gene. *Plant Mol. Biol.* 69, 565–575. doi: 10.1007/s11103-008-9439-9

Han, B. (2016). Genomics: decoding the ancestors of peanut. *Nat. Plants* 2:16042.

Haslam, T. M., and Kunst, L. (2013). Extending the story of very-long-chain fatty acid elongation. *Plant Sci.* 210, 93–107. doi: 10.1016/j.plantsci.2013.05.008

Hegebarth, D., Buschhaus, C., Joubès, J., Thoraval, D., Bird, D., and Jetter, R. (2017). *Arabidopsis* ketoacyl-CoA synthase 16 (KCS16) forms C36/C38 acyl precursors for leaf trichome and pavement surface wax. *Plant Cell Environ.* 40, 1761–1776. doi: 10.1111/pce.12981

Huai, D., Zhang, Y., Zhang, C., Cahoon, E. B., and Zhou, Y. (2015). Combinatorial effects of fatty acid elongase enzymes on nervonic acid production in *Camelina sativa*. *Plos One* 10:e0131755. doi: 10.1371/journal.pone.0131755

Huai, D., Zhang, Y., Zhang, C., Cahoon, E. B., and Zhou, Y. (2018). Substrate specificities of fatty acid elongae BnaA.FAE1 and BnaC.FAE1 from rapeseed (*Brassica napus* L.). *Chin. J. Oil Crop Sci.* 40, 624–632.

James, D. W. Jr., and Dooner, H. K. (1990). Isolation of EMS-induced mutants in *Arabidopsis* altered in seed fatty acid composition. *Theoret. Appl. Genet.* 80, 241–245. doi: 10.1007/BF00224393

James, D. W., Lim, E., Keller, J., Plooy, I., Ralston, E., and Dooner, H. K. (1995). Directed Tagging of the Arabidopsis FATTY ACID ELONGATION1 (FAE1) Gene with the maize transposon activator. *Plant Cell* 7, 309–319.

Joubes, J. M., Raffaele, S., Bourdenx, B., Garcia, C., Laroche-Traineau, J., Moreau, P., et al. (2008). The VLCFA elongase gene family in *Arabidopsis thaliana*: phylogenetic analysis, 3D modelling and expression profiling. *Plant Mol. Biol.* 67, 547–566. doi: 10.1007/s11103-008-9339-z

Katavic, V., Friesen, W., Barton, D. L., Gossen, K. K., Giblin, E. M., Luciw, T., et al. (2001). Improving erucic acid content in rapeseed through biotechnology: what can the *Arabidopsis FAE1* and the yeast *SLC1-1* genes contribute? *Crop Sci.* 41, 739–747.

Kim, D., Pertea, G., Trapnell, C., Pimentel, H., Kelley, R., and Salzberg, S. L. (2013). TopHat2: accurate alignment of transcriptomes in the presence of insertions, deletions and gene fusions. *Genome Biol.* 14:R36. doi: 10.1186/gb-2013-14-4-r36

Kim, J., Jung, J. H., Lee, S. B., Go, Y. S., Kim, H. J., Cahoon, R., et al. (2013). *Arabidopsis* 3-ketoacyl-coenzyme A synthase9 is involved in the synthesis of tetracosanoic acids as precursors of cuticular waxes, suberins, sphingolipids, and phospholipids. *Plant Physiol.* 162, 567–580. doi: 10.1104/pp.112.210450

Krzywinski, M. I., Schein, J. E., Birol, I., Connors, J., Gascoyne, R., Horsman, D., et al. (2009). Circos: an information aesthetic for comparative genomics. *Genome Res.* 19, 1639–1645.

Kumar, S., Stecher, G., Li, M., Knyaz, C., and Tamura, K. (2018). MEGA X: molecular evolutionary genetics analysis across computing platforms. *Mol. Biol. Evol.* 35, 1547–1549. doi: 10.1093/molbev/msy096

Kunst, L., Taylor, D. C., and Underhill, E. W. (1992). Fatty acid elongation in developing seeds of *Arabidopsis thaliana*. *Plant Physiol. Biochem.* 30, 425–434.

Lamesch, P., Berardini, T. Z., Li, D., Swarbreck, D., Wilks, C., Sasidharan, R., et al. (2011). The *Arabidopsis* information resource (TAIR): improved gene annotation and new tools. *Nucleic Acids Res.* 40, D1202–D1210. doi: 10.1093/nar/gkr1090

Lee, S. B., Jung, S. J., Go, Y. S., Kim, H. U., Kim, J. K., Cho, H. J., et al. (2009). Two Arabidopsis 3-ketoacyl CoA synthase genes, *KCS20* and *KCS2/DAISY*, are functionally redundant in cuticular wax and root suberin biosynthesis, but differentially controlled by osmotic stress. *Plant J.* 60, 462–475.

Lemieux, B., Miquel, M., Somerville, C., and Browse, J. (1990). Mutants of *Arabidopsis* with alterations in seed lipid fatty acid composition. *Theoret. Appl. Genet.* 80, 234–240. doi: 10.1007/BF00224392

Leonard, A. E., Pereira, S. L., Sprecher, H., and Huang, Y.-S. (2004). Elongation of long-chain fatty acids. *Prog. Lipid Res.* 43, 36–54.

Li, X., Mei, D., Liu, Q., Fan, J., Singh, S., Green, A., et al. (2016). Down-regulation of crambe fatty acid desaturase and elongase in *Arabidopsis* and crambe resulted in significantly increased oleic acid content in seed oil. *Plant Biotechnol. J.* 14, 323–331. doi: 10.1111/pbi.12386

Li, X., Van Loo, E. N., Gruber, J., Fan, J., Guan, R., Frentzen, M., et al. (2012). Development of ultra-high erucic acid oil in the industrial oil crop *Crambe abyssinica*. *Plant Biotechnol. J.* 10, 862–870. doi: 10.1111/j.1467-7652.2012.00709.x

List, G. R. (2004). Decreasing trans and saturated fatty acid content in food oils. *Food Technol.* 1, 23–20.

Liu, N., Chen, H., Huai, D., Xia, F., Huang, L., Chen, W., et al. (2019). Four QTL clusters containing major and stable QTLs for saturated fatty acid contents in a dense genetic map of cultivated peanut (*Arachis hypogaea* L.). *Mol. Breed.* 39:23.

Mietkiewska, E., Brost, J. M., Giblin, E. M., Barton, D. L., and Taylor, D. C. (2007). Cloning and functional characterization of the fatty acid elongase 1 (FAE1) gene from high erucic *Crambe abyssinica* cv. Prophet. *Plant Biotechnol. J.* 5, 636–645.

Napier, J. A., and Graham, I. A. (2010). Tailoring plant lipid composition: designer oilseeds come of age. *Curr. Opin. Plant Biol.* 13, 329–336. doi: 10.1016/j.pbi.2010.01.008

Napier, J. A., Haslam, R. P., Beaudoin, F., and Cahoon, E. B. (2014). Understanding and manipulating plant lipid composition: metabolic engineering leads the way. *Curr. Opin. Plant Biol.* 19, 68–75. doi: 10.1016/j.pbi.2014.04.001

Nath, U. K., Wilmer, J. A., Wallington, E. J., Becker, H. C., and Möllers, C. (2009). Increasing erucic acid content through combination of endogenous low polyunsaturated fatty acids alleles with *Ld-LPAAT+ Bn-fae1* transgenes in rapeseed (*Brassica napus* L.). *Theoret. Appl. Genet.* 118, 765–773. doi: 10.1007/s00122-008-0936-7

Nelson, B. K., Cai, X., and Nebenführ, A. (2007). A multicolored set of in vivo organelle markers for co-localization studies in *Arabidopsis* and other plants. *Plant J.* 51, 1126–1136.

Nobutaka, F., Ohnishi, Y., Ebizuka, Y., and Horinouchi, S. (2002). Alteration of reaction and substrate specificity of a bacterial type III polyketide synthase by site-directed mutagenesis. *Biochem. J.* 367, 781–789.

Ozseyhan, M. E., Kang, J., Mu, X., and Lu, C. (2018). Mutagenesis of the *FAE1* genes significantly changes fatty acid composition in seeds of *Camelina sativa*. *Plant Physiol. Biochem.* 123, 1–7. doi: 10.1016/j.plaphy.2017.11.021

Peng, Q., Hu, Y., Wei, R., Zhang, Y., Guan, C., Ruan, Y., et al. (2010). Simultaneous silencing of FAD2 and FAE1 genes affects both oleic acid and erucic acid contents in Brassica napus seeds. *Plant Cell Rep.* 29, 317–325. doi: 10.1007/s00299-010-0823-y

Pruitt, R. E., Vielle-Calzada, J.-P., Ploense, S. E., Grossniklaus, U., and Lolle, S. J. (2000). *FIDDLEHEAD*, a gene required to suppress epidermal cell interactions in *Arabidopsis*, encodes a putative lipid biosynthetic enzyme. *Proc. Natl. Acad. Sci. U.S.A.* 97, 1311–1316.

Quist, T. M., Sokolchik, I., Shi, H., Joly, R. J., Bressan, R. A., Maggio, A., et al. (2009). HOS3, an *ELO*-Like Gene, inhibits effects of ABA and implicates a S-1-P/ceramide control system for abiotic stress responses in *Arabidopsis thaliana*. *Mol. Plant* 2, 138–151. doi: 10.1093/mp/ssn085

Sagar, M., Pandey, N., Qamar, N., Singh, B., and Shukla, A. (2015). Domain analysis of 3 Keto Acyl-CoA synthase for structural variations in *Vitis vinifera* and *Oryza brachyantha* using comparative modelling. *Interdiscip. Sci.*7, 7–20. doi: 10.1007/s12539-013-0017-8

Sassa, T., and Kihara, A. (2014). Metabolism of very long-chain fatty acids: genes and pathophysiology. *Biomol. Ther.* 22, 83–92. doi: 10.4062/biomolther.2014.017

Shi, J., Lang, C., Wang, F., Wu, X., Liu, R., Zheng, T., et al. (2017). Depressed expression of *FAE1* and *FAD2* genes modifies fatty acid profiles and storage compounds accumulation in *Brassica napus* seeds. *Plant Sci.* 263, 177–182. doi: 10.1016/j.plantsci.2017.07.014

Smith, M. A., Moon, H., Chowrira, G., and Kunst, L. (2003). Heterologous expression of a fatty acid hydroxylase gene in developing seeds of *Arabidopsis thaliana*. *Planta* 217, 507–516.

Sun, X., Pang, H., Li, M., Peng, B., Guo, H., Yan, Q., et al. (2013). Evolutionary pattern of the *FAE1* gene in *Brassicaceae* and its correlation with the erucic acid trait. *Plos One* 8:e83535. doi: 10.1371/journal.pone.0083535

Thompson, J. D., Higgins, D. G., and Gibson, T. J. (1994). CLUSTAL W: improving the sensitivity of progressive multiple sequence alignment through sequence weighting, position-specific gap penalties and weight matrix choice. *Nucleic Acids Res.* 22, 4673–4680.

Tian, B., Wei, F., Shu, H., Zhang, Q., Zang, X., and Lian, Y. (2011). Decreasing erucic acid level by RNAi-mediated silencing of fatty acid elongase 1 (BnFAE1.1) in rapeseeds (Brassica napus L.). *Afr. J. Biotechnol.* 10, 13194–13201.

Todd, J., Post-Beittenmiller, D., and Jaworski, J. G. (1999). *KCS1* encodes a fatty acid elongase 3-ketoacyl-CoA synthase affecting wax biosynthesis in *Arabidopsis thaliana*. *Plant J.* 17, 119–130.

USDA (2010). *US Department of Health and Human Services. Dietary Guidelines for Americans*. Washington, DC: US Government Printing Office.

Usher, S., Han, L., Haslam, R. P., Michaelson, L. V., Sturtevant, D., Aziz, M., et al. (2017). Tailoring seed oil composition in the real world: optimising omega-3 long chain polyunsaturated fatty acid accumulation in transgenic *Camelina sativa*. *Sci. Rep.* 7:6570. doi: 10.1038/s41598-017-06838-0

Wang, M. L., Chen, C. Y., Tonnis, B., Barkley, N. A., Pinnow, D. L., Pittman, R. N., et al. (2013). Oil, fatty acid, flavonoid, and resveratrol content variability and FAD2A functional SNP genotypes in the US peanut mini-core collection. *J. Agricul. Food Chem.* 61, 2875–2882.

Wang, N., Shi, L., Tian, F., Ning, H., Wu, X., Long, Y., et al. (2010). Assessment of *FAE1* polymorphisms in three *Brassica* species using EcoTILLING and their association with differences in seed erucic acid contents. *BMC Plant Biol.* 10:137. doi: 10.1186/1471-2229-10-137

Xiao, G. H., Wang, K., Huang, G., and Zhu, Y. X. (2016). Genome-scale analysis of the cotton *KCS* gene family revealed a binary mode of action for gibberellin A regulated fiber growth. *J. Integrat. Plant Biol.* 58, 577–589. doi: 10.1111/jipb.12429

Zhang, Y., Huai, D., Yang, Q., Cheng, Y., Ma, M., Kliebenstein, D. J., et al. (2015). Overexpression of three glucosinolate biosynthesis genes in *Brassica napus* identifies enhanced resistance to *Sclerotinia sclerotiorum* and *Botrytis cinerea*. *Plos One* 10:e0140491. doi: 10.1371/journal.pone.0140491

Conflict of Interest: The authors declare that the research was conducted in the absence of any commercial or financial relationships that could be construed as a potential conflict of interest.

frontiers in Plant Science

REVIEW
published: 20 May 2020
doi: 10.3389/fpls.2020.00580

Mechanism and Regulation of Silique Dehiscence, Which Affects Oil Seed Production

*Yan-Kun Yu, Yu-Long Li, Li-Na Ding, Rehman Sarwar, Feng-Yun Zhao and Xiao-Li Tan**

Institute of Life Sciences, Jiangsu University, Zhenjiang, China

Silique dehiscence is an important physiological process during natural growth that enables mature seeds to be released from plants, which then undergo reproduction and ensure the survival of future generations. In agricultural production, the time and degree of silique dehiscence affect the harvest time and processing of crops. Premature silique dehiscence leads to seeds being shed before harvest, resulting in substantial reductions to yields. Conversely, late silique dehiscence is not conducive to harvesting, and grain weight and oil content will be reduced due to the respiratory needs of seeds. In this paper, the mechanisms and regulation of silique dehiscence, and its application in agricultural production is reviewed.

Keywords: silique dehiscence, agronomic traits, phytohormone, signal transduction, agriculture production

OPEN ACCESS

Edited by:
Xue-Rong Zhou, Commonwealth Scientific and Industrial Research Organisation (CSIRO), Australia

Reviewed by:
Anders S. Carlsson, Swedish University of Agricultural Sciences, Sweden
Surinder Pal Singh, Commonwealth Scientific and Industrial Research Organisation (CSIRO), Australia

***Correspondence:**
Xiao-Li Tan
xltan@ujs.edu.cn

Specialty section:
This article was submitted to Plant Biotechnology, a section of the journal Frontiers in Plant Science

Received: *31 December 2019*
Accepted: *17 April 2020*
Published: *20 May 2020*

Citation:
Yu Y-K, Li Y-L, Ding L-N, Sarwar R, Zhao F-Y and Tan X-L (2020) Mechanism and Regulation of Silique Dehiscence, Which Affects Oil Seed Production. Front. Plant Sci. 11:580. doi: 10.3389/fpls.2020.00580

INTRODUCTION

Silique dehiscence is of great significance, as it is the process by which seeds are released from mature siliques. Silique dehiscence is required to expand the growth range of offspring plants, and to provide favorable conditions for prospering species and enriching plant adaptability. Silique dehiscence also plays an important role in plant reproduction and maintains biodiversity among species. However, the specific mechanisms by which plants perform the dehiscence process are not clear.

MORPHOLOGY AND DEHISCENCE OF *Arabidopsis Thaliana* SILIQUES

Arabidopsis thaliana, a model plant, which has seed-shattering characteristics and was used to study silique dehiscence (Spence et al., 1996). Studies have shown that the development of early flowers and siliques in *A. thaliana* can be divided into 20 stages (Smyth et al., 1990). Early flower development occurs from stage 1 to 12, and silique development occurs from stage 13 to 20. The corresponding characteristics of each stage have also been described (Jeffrey and Hill, 1989; Smyth et al., 1990; Robinson-Beers et al., 1992; Spence, 1992; Bowman, 1994; Sessions, 1997; Ferrandiz et al., 1999).

The *Arabidopsis* silique develops from a gynoecium composed of two fused carpels, which consists of a stigma, style, ovary and gynophore (internode and nectaries) (**Figure 1**; Ferrandiz et al., 1999). The dried silique is called the silique (Bowman, 1994; Schmid and Rollins, 1994; Sessions, 1999). The silique contains an ovary with two chambers consisting of two linear valves, a replum, and a putative septum between the two valves and valve margins (Bowman et al., 1999). The valve

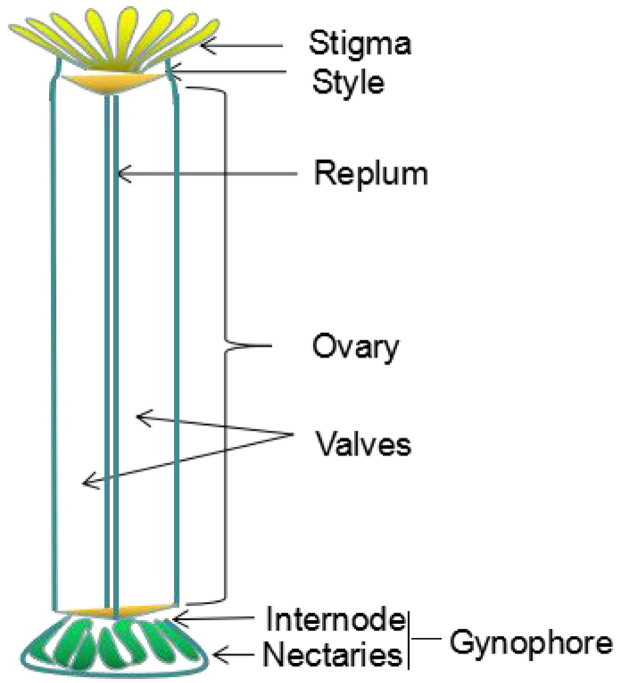

FIGURE 1 | Schematic diagram of gynoecium organization in *Arabidopsis thaliana*, the different parts are indicated. Revised from Ferrandiz et al. (1999).

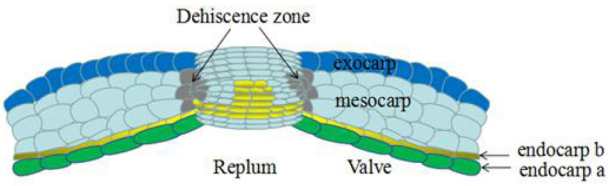

FIGURE 2 | Transversal section of mature silique in *Arabidopsis thaliana*, the different parts are indicated. The silique dehiscence from dehiscence zone, which consists of a lignified layer and a separation layer (Not shown in the figure). Revised from Rajani and Sundaresan (2002).

develops from the ovary wall and encloses the seed. It then elongates as seed develops, and separates from the separation layer when the silique is mature; thus resulting in the seeds being released from the dehiscent silique (Smyth et al., 1990).

Previous studies have shown that the dehiscence of the *A. thaliana* siliques is mainly related to the lignification of the endocarp layer and valve margin (Liljegren et al., 2000). The *A. thaliana* silique is composed of two layers of valves, a replum, a septum, and the dehiscence zone (DZ) between the valves and the septum. The silique valve usually contains six cell layers. The outermost layer, called the exocarp, is a single rectangular layer of cells interspersed with immature, unopened stomata, which are required for respiration and transpiration. The following three layers, called the mesocarp, are composed of thin-walled cells containing chloroplasts, and can perform photosynthesis and provide nutrition during seed development. The endocarp consists of two differentiated cell layers: an inner epidermis with large, isodiametric, thin-walled cells (endocarp a), and a subepidermal layer of small and tightly packed cells (endocarp b), which can be elongated longitudinally and lignified (Rajani and Sundaresan, 2002; **Figure 2**).

Seed spreading is accomplished by silique dehiscence, a process that involves a programmed series of events, during which the valves separate from the replum to release the seed. This process requires the prior development of the DZ at the valve margin, followed by the cells separating in the separation layer. The valve margin consists of a narrow band of four cell layers in entire silique at the valve-replum boundary. During the process of silique extension, the cells of the valve margin extend more slowly than the valve, thus, causing constriction at the valve margin. The DZ is located at the boundary between the valve and replum. The DZ develops from the cells of the valve margin, including both lignified and unlignified cells (Ferrandiz et al., 1999). During the process of silique ripening, thin-walled cells secrete hydrolase to dissolve the middle-lamella and separate the cells from each other (Meakin, 1990; Meakin and Roberts, 1990). Differential shrinkage between the lignified endocarp b cells and the thin-walled non-lignified cells of the valve create mechanical tensions within the silique, which act in a spring-like manner. As the silique matures, a discrete group of cells in the DZ rupture, and the tension in the silique enables the valve to separate from the replum. Whether it is the shedding of fleshy fruit or the dehiscence of dry fruit, the formation of separation zone is needed (Estornell et al., 2013).

In leguminous plants, the varieties of silique indehiscence are the result of interactive selection under long-term domestication and drought conditions, and the silique dehiscence resistance-associated genes selected in different environments may be different (Parker et al., 2020). Some studies have made an anatomical observation on the ventral suture pods of dehiscence-susceptible and dehiscence-resistant varieties of leguminous plants, the results showed that the structures are quite different. It is also found that RFCV (route from the top of fiber cap cells to the connecting point of the two valves), FCC length (fiber cap cell length), VBA (vascular bundle area), VBT (vascular bundle thickness), and LA (bundle cap slope) are related to silique dehiscence (Tu et al., 2019). A recent study identified 163 SNPs (single nucleotide polymorphisms) associated with silique dehiscence, and identified the candidate gene Glyma09g06290, related to silique dehiscence by soybean genomic association analysis (GWAS) and developed molecular markers for silique dehiscence. These findings enrich our understanding of molecular breeding for silique dehiscence (Hu et al., 2019). And in recent study on rice, it has been found that the apetala2-like transcription factor supernumerary bract (SNB) controls rice seed size and shattering, and they found that a SNB allele gene SSH1 is related to seed shttering. In the SSH1 mutant seed shttering decreases and the grain becomes larger, These data indicating that searching for SNB alleles has the potential to increase rice yield (Jiang et al., 2019). The results of this study not only provide a reference for the genetic regulation mechanism of rice shattering, but also provide important target genes for the molecular design

and breeding of rice shedding and yield. This method also provides a reference for the study of silique dehiscence in other species. Some researchers also carried out GWAS and linkage analysis on dehiscence-susceptible and dehiscence-resistant in Chinese rapeseed germplasm. It was found that silique dehiscence was controlled by multiple gene loci, and SNP markers significantly related to silique dehiscence were identified, which provide an effective method for improving resistance of silique dehiscence in rapeseed (Liu et al., 2016). Recently, the evolution of silique dehiscence in different species, including *A. thaliana*, legumes, cereals and rice, has been reported. It is found that phenotypic evolution under domestication may be caused by mutations at homologous sites and different types of fruits show phenotypic assimilation at the tissue level (Di Vittori et al., 2019).

In leguminous plants, silique shattering occurs by two modes: one is active silique shattering, which is independent of external forces, but is dependent on the tension between its own cells. The other mechanism is passive silique shattering or enzyme regulated dehiscence; that is, cell wall modification enzymes in the DZ decompose the cells in the separation zone, leading to silique shattering (Luo et al., 2015). Active silique shattering occurs in *A. thaliana*, oilseed rape and other cruciferous siliques. Upon silique maturation in *A. thaliana*, the inner cells of the valve layer become lignified, while the outer thin-walled cells constrict to produce tension, which cause the siliques to dehisce along the separated layer (Rajani and Sundaresan, 2002). In contrast, the oilseed rape silique is composed of two silique valves, which are linked by a group of narrow, non-lignified cells. Those valves are then pulled in different directions under tension when the siliques are mature (Child et al., 2003). Some studies have found that the arrangement of fibers in the valve and degree of lignification also affect the degree of dehiscence of the silique (Řepková and Hofbauer, 2009; Yang et al., 1990). Cruciferae and leguminous plants have multiple similarities in the mechanisms of silique shattering, which necessitate further study.

Oilseed rape siliques are similar to those of *A. thaliana*, and are composed of two layers of valves, a replum, a septum, and the DZ between the valves and septum. Valves usually contain six cell layers (the exocarp, mesocarp, endocarp a, and endocarp b). The septum, silique stalk, and beak are integral, and the seeds are inserted on the septum. There may also be great similarities to *A. thaliana* in the mode and mechanism of dehiscence based on structure similarities. It has been reported that the dehiscence of oilseed rape siliques not only requires the differentiation and separation of specific cells, but also requires a specific water content in the silique. When the water content of the silique becomes less than 80%, the silique begins to dehisce (Zheng et al., 1999).

THE GENETICS OF SILIQUE DEHISCENCE

In *A. thaliana* and oilseed rape, silique dehiscence is the result of natural evolution, which facilitates the spread of seeds. Many genes have been identified as being involved in DZ differentiation and related biochemical and physiological changes prior to cell separation during silique dehiscence. Two main methods were used to detect and identify such genes. One method was to identify mutants by classical gene mutagenesis and reverse genetics (Rajani and Sundaresan, 2002), while the other method used reporter genes to identify genes that were specifically expressed in the DZ. Genes expressed specifically in the DZ were identified mainly by isolating mRNA expressed in the valve margins (Coupe et al., 1994; Petersen et al., 1996; Whitelaw et al., 1999). The collection of enhancer or gene trap lines based on the random insertion of reporter genes in the *Arabidopsis* genome provides materials for this study. When inserted near the enhancer or within the gene, neighboring regulatory sequences would regulate the expression of reporter genes (Sundaresan et al., 1995). Silique dehiscence resistance is a recessive trait, study showed that trait has little variation of dehiscence resistance in *Brassica napus*, but a great variation in *Brassica* crops such as *Brassica campestris*, *Brassica juncea*, *Brassica carinata,* and *Brassica nigra* (Morgan et al., 1998). The dehiscence resistance genes were introduced into *B. napus* by interspecific hybridization and synthetic *B. napus*, so as to select the lines with dehiscence resistance. Researchers hybridized the dehiscence resistance line with the dehiscence sensitive lines, and the subsequent genetic analyses revealed that the additional effect of the gene in the dehiscence resistance traits reached a higher level, and the traits related to dehiscence resistance were stably inherited (Morgan et al., 2000).

GENES ASSOCIATED WITH CELL DIFFERENTIATION IN THE *Arabidopsis Thaliana* SILIQUE DEHISCENCE ZONE

Shatterproof1 (SHP1) and Shatterproof2 (SHP2)

Shatterproof1 and *Shatterproof2* are transcriptional regulators belonging to the MCMl AGAMOUS DEFICIENS SRF box (MADS-box) gene family, which are involved in various aspects of plant development (Rounsley et al., 1995). They regulate the differentiation of the DZ and promote the lignification of cells adjacent to the valve, as well as promote the formation of the valve margin. Phylogenetic and functional studies revealed extensive functional redundancy among members of the MADS-box gene family (Bowman et al., 1991; Kempin et al., 1995; Purugganan, 1997; Riechmann and Meyerowitz, 1997). *SHP1* and *SHP2* are two such genes with high functional redundancy, and share 87% homology at the amino acid sequence level (Ma et al., 1991; Savidge et al., 1995; Flanagan et al., 2010). There is no significant difference between single mutants of *shp1*, *shp2,* and wild-type *A. thaliana*; however, the *shp1shp2* double mutant exhibited an indehiscent phenotype (Liljegren et al., 2000).

Because lignification within the silique may lead to silique dehiscence (Spence et al., 1996), phloroglucinol was used to detect the lignification pattern in *shp1shp2* and wild-type siliques. Such studies found that, in wild-type plants, the valve margin

cells adjacent to the DZ were lignified throughout the silique, while lignification was reduced in *shp1shp2* double-mutant plants (Liljegren et al., 2000). Scanning electron microscopy and transverse sections showed that, compared with wild-type siliques, *shp1shp2* siliques exhibited less constriction of the valve margins, fewer lignification cells at the valve margin, and the absence of DZs (Liljegren et al., 2000). These results confirmed that *SHP1* or *SHP2* was necessary for dehiscence in *A. thaliana* siliques. *SHP2* expression is repressed by *FUL* in the valves (Ferrándiz et al., 2000b) and is repressed by *APETALA 1* (*AP1*) in the outer whorls of the flower (Kaufmann et al., 2010). A recent study has led to a further understanding of the transcription factor SHP2. Studies have shown that there are redundant cArG box *cis* elements upstream of *SHP2*, which regulate the expression of *SHP2* in the pistil, valve margin and cleavage zone (Sehra and Franks, 2017).

Fruitfull (FUL)

Fruitfull is a member of the extended MADS-box gene family, which is specifically expressed at different stages of plant development. It is involved in the regulation of flower and silique development in *A. thaliana*. During flower development, *FUL* is first expressed in the carpel primordia, and then accumulates in the flower meristem, which can promote flower initiation and development (Alvarez and Smyth, 1997). During the development of siliques, *FUL* promotes the normal development and differentiation of valve cells, and also controls the extension of the silique (Gu et al., 1998; Ferrándiz et al., 2000a). Studies showed that the most obvious difference between the *ful-1* mutant and wild-type plants was that the length of siliques become shorter in the *ful-1* mutant, with crowded seeds inside (Gu et al., 1998). The phenotype of *ful-1* siliqus was due to the lack of lateral valve expansion, differentiation defects of the outer epidermis of the vale, ectopic lignification of the valve mesophyll layers, and a significantly increased number of inner epidermal cells in valves, resulting in seeds becoming crowded within the smaller silique. Additionally, the carpels ceased development soon after pistil fertilization in the *ful-1* mutant. Compared to the wild-type plants, the number of seeds and the dry weight of siliques both decreased the *ful-1* mutant, while the length of siliques was also significantly reduced (Gu et al., 1998).

The epidermis cells of *ful-1* mutant silique valves were irregularly arranged, small with no stomatal precursor cells, and the boundary between the valves and the replum was not distinct. Additionally, after developmental stage 15, cell differentiation and expansion in the replum and valves did not proceed normally (Bowman et al., 1989). The epidermal cells outside the replum failed to form a parallel arrangement, which otherwise occurs in the wild-type plant, but were arranged in a zigzag shape, perpendicular to the main axis of the silique (Gu et al., 1998).

Studies showed that *FUL* is an upstream regulator of *SHP1* and *SHP2*, which affects the formation of the separation layer and lignification of the valve margin (Liljegren et al., 2000). The *shp1shp2* loss-of-function mutants, and *35S:FUL* gain-of-function line showed similar phenotypes (Benfey and Chua, 1990), and both produced indehiscent fruit. Thus, those data suggest that *SHP* and *FUL* genes may interact antagonistically during valve margin development (Ferrándiz et al., 2000b). And some studies have shown that FUL play its role through cArG boxes, and there are cArG box motifs upstream of SHP2, which further illustrates the inhibitory of SHP2 by FUL (Bemer et al., 2017). The regulatory networks of silique dehiscence is continuously updating, from the basic transcription factors necessary for silique dehiscence zone differentiation to the genes related to the development of leaves, flowers and flanking organs, to plant hormones, which play an important role in the differentiation of silique dehiscence zone. And the core regulatory module SHP-FUL which controls the development of dehiscence zone is highly conservative from the model plant *A. thaliana* to closely related crops in the regulation of silique dehiscence (Dong and Wang, 2015). A recent study proved the conservation of SHPS-FUL module in the dehiscence zone differentiation. They selected two local rape varieties namely "*Pakola*" (dehiscence-resistant) and "*PunjabSarsoon3*" (dehiscence-susceptible) to analyze silique morphology, Greater difference was found in silique morphology, which indicated that there was a certain relationship between silique dehiscence and silique morphology. The homologous gene of SHP-FUL was isolated from *Pakola*. Through sequence alignment and expression pattern analysis, it was found that the sequence was highly conserved and there was no significant difference in expression among different varieties (Khan et al., 2019). These studies show that SHP-FUL is highly conservative in regulating the differentiation of dehiscence zone, and also provides a genetic basis for gene editing and breeding varieties suitable for mechanized harvest in the future.

In addition, silique anatomy and microarray analyses were employed to examine the gene expression patterns and related functional analyses during silique dehiscence in *Arabidopsis*. By the end stage of silique dehiscence, a large number of glycosyl hydrolases were enriched in the DZ. Transcription factor enrichment analyses showed that the MADS domain family transcription factors, SEPALLATA3 and AGL15, may be key regulators of silique dehiscence, targeting glycosyl hydrolases related to cell wall degradation (Jiang et al., 2016).

Alcatraz (ALC)

The *ALC* gene encodes a protein related to the myc/bHLH transcription factors expressed in the valves of siliques, which is the site of cell separation during silique dehiscence. *ALC* is involved in the recognition and development of the separation layer of silique valve margins (Liljegren et al., 2000; Rajani and Sundaresan, 2002). Similar to the *shp1shp2* double mutant, the *alc* mutant plant also showed indehiscent siliques, which could be opened manually by applying external pressure at the valve margins. By stage 19 in wild-type plants, the siliques turned yellow and the valves gradually separated from the replum to release the seeds (Ferrandiz et al., 1999). However, in the *alc* mutant, valve separation from the replum fails to occur (Rajani and Sundaresan, 2002). The patterns of DZ formation at the valve margin, as well as lignification of the internal valve layer in *alc* mutants was examined by scanning electron microscopy, and exhibited no significant difference compared to wild-type plants.

Thus, those results indicated that mutation of the *ALC* gene did not disrupt the formation of the DZ, or lignification of the valve layer (Liljegren et al., 2000).

Because there was no visible difference in the exterior of the *alc* mutants, the internal cells of the DZ were examined. A narrow layer of non-lignified cells (NLC) between the lignification cells and the replum cells that exist in wild-type plants were absent in the *alc* mutant. Evaluations of transverse sections of the non-lignified cell layers in mutant siliques revealed that the ectopically lignified cells of the inner valve margin create a lignified bridge between the lignified inner valve cell layers and the lignified replum vasculature, which prevents silique dehiscence. Similarly, loss of the *ALC* gene leads to the non-lignified replum-like cells to occupy the separation site at the outer valve margin, with the ectopic lignified cells toward the inner margin (Gu et al., 1998).

Alcatraz is widely expressed throughout the gynoecium before fertilization and is limited to the valve margin after fertilization. In addition to its functional redundancy with other genes during silique dehiscence, *ALC* is also functionally redundant with genes in other regulatory processes (Gu et al., 1998; Rajani and Sundaresan, 2002). Recently, there is a new discovery on *ALC* that the point mutation of *ALC* homologous gene induced by EMS improves the dehiscence resistance of *B. napus*. This work is carried out in oilseed "*EXPRESS*" with silique dehiscence-susceptible (Braatz et al., 2018a). The point mutation of this gene is expected to be widely used in *B. napus*, thus the yield loss of *B. napus* would be greatly reduced.

Indehiscence (IND)

Indehiscence encodes a unique and atypical basic helix-loop-helix (bHLH) protein. It is known that transcription factors with bHLH domain bind to DNA through residues in the basic region. The helix-loop-helix domain promotes the dimerization of proteins with other bHLH factors to form hetero- or homodimers (Murre et al., 1989). Most *Arabidopsis* bHLH proteins contain a key glutamic acid residue (E) in their basic region, which is responsible for DNA binding. Conversely, IND has an alanine residue (A) in the corresponding site (Fisher and Goding, 1992; Buck and Atchley, 2003; Toledo-Ortiz et al., 2003). ALC, another bHLH protein mentioned above, though, the identity of bHLH domain to IND is lower, they both play an important role in silique dehiscence (Liljegren et al., 2004).

Indehiscence is necessary for silique dehiscence and is involved in the differentiation of three necessary cell types required for seed dispersal (i.e., the valve, replum and valve margin) (Liljegren et al., 2004; Wu et al., 2006; Van Gelderen et al., 2016). *IND* is essential for the lignification of valve and the development of valve margin cells (Liljegren et al., 2004). The *ind* mutant exhibited indehiscent siliques, similar to the *shp1shp2* mutant, but also exhibited serious defects, such as indistinctive margins at the silique apex (Liljegren et al., 2000, 2004). Evaluation of the silique section showed that the small cells, characteristic of the separation zone and lignified cell layers at the wild-type margin, were not obvious in the siliques of *ind* mutants, predicting markedly decreased constriction of the margin than that of wild-type plant (Liljegren et al., 2004). The lignification of vascular bundles in the replum and valve layer were unaffected in *ind* siliques; however, the lignified cells were not observed throughout the margins of *ind-2* mutant siliques. As margin lignification is only partially affected in *shp* silique and unaffected in *alc* siliques, those data indicated that IND played an important role in regulating the lignification of margin cells (Liljegren et al., 2000, 2004; Rajani and Sundaresan, 2002).

During the development of siliques in wild-type plants, *IND* is expressed at the inner valve layer and throughout a strip at the margin. Those tissues then become lignified later in silique development. The expression of *IND* in the *ful* mutant line extends throughout the complete valve, which indicates that *FUL* is required to restrict *IND* expression to the valve margins. The length of siliques in *ful* mutants is 25% that of wild-type siliques, while the length of silique in *ind/ful* double mutants is restored. Additionally studies showed that *IND* activity was the cause of the loss of e epidermal cell expansion valves (Liljegren et al., 2004). In wild-type siliques, lignification of a single inner valve layer is considered to be conducive to silique dehiscence, but there are four valve layers in *ful* siliques, resulting in ectopic lignification. However, lignification of the inner valve layer was observed in *ind/ful* siliques, which is normal, and further indicates that the activity of IND is also responsible for ectopic valve lignification (Ferrándiz et al., 2000b).

Bayer CropScience has also been committed to the study of silique dehiscence. A published patent applied by Bayer CropScience shows that *IND* allele gene *IND-A1* or *IND-C1* have been obtained in Brassica. The mutations of *IND* allele gene can effectively reduce silique dehisecnce or delay silique dehiscence until after harvest, and can be used for increasing yield. The patent also provides methods to identify molecular markers associated with reduced or delayed silique dehiscence in a population of dehiscence seed plants (Laga et al., 2012). The patent finally was assigned to BASF(Badische Anilin-und-Soda-Fabrik). Later, they claimed to have acquired *Bnind* and *Bnalc* double mutants with increased dehiscence resistance of rapeseed (Laga et al., 2016). However, the research results of silique dehiscence resistance of other well-known breeding companies remain secret. As a result, smaller breeding companies must make greater efforts to integrate dehiscence resistance into their varieties. Silique dehiscence resistance is an important factor to improve and stabilize the yield of rapeseed. Obtaining rape varieties that are easy to be harvested mechanically will undoubtedly promote large-scale production of rape and bring greater economic value. Recent studies have found that several *Bnind* single mutants obtained in *B. napus* by TILLING technology did not show dehiscence resistance, but the double mutants obtained by hybridization showed strong silique dehiscence resistance, these results indicated that the mutation of *Bnind* is recessive. Based on the analysis of *IND* double mutants, it was found that there was a positive correlation between silique length and dehiscence resistance, and the joint area of replum-valve increased, and the cells in the dehiscence zone became smaller and denser, which required more force to dehisce. This study made an important contribution to acquire *B. napus* with strong dehiscence resistance and provided a new direction for rapeseed breeding (Braatz et al., 2018b). Studies showed that *IND* which plays an important role in regulating valve margin

differentiation in *A. thaliana* and its homologous gene *HECATE3*, *SHATTERPROOF1/2*, play a role in regulating reproductive tissue development, and they also involved in network regulated by Gibberellin (GA) and auxin. Studies showed that *IND* promotes the development of pollen and anther by regulating GA and auxin, and these hormones also play a role in the development of valve margin, such as IND regulates the development of separation layer by regulating the level of GA through GA degrading enzyme (GA3OX1) (Kay et al., 2013; Dong and Wang, 2015). Some studies have found that the excessive Lignification of fiber cap cells in the ventral suture is the cellular basis and molecular mechanism of indehiscent pods in leguminous plants. In cultivated soybean, it was found that *SHATTERING1-5* (SHAT1-5) and *PDH1* were located in pod dehiscent QTL. In *Phaseolus vulgaris*, *PVIND1*, homologous to *AtIND*, was located near the quantitative trait locus ST of silique dehiscence. But *PVIND1* may not be directly involved in the regulation of silique dehiscence, because study showed it is not linked to the genotype at the ST locus (Gioia et al., 2013; Dong and Wang, 2015; Parker et al., 2020). How it participates in the regulation of silique dehiscence and whether other homologous genes with *AtIND* are involved still need further research to confirm.

Replumless (RPL)

Replumless encodes a transcription factor belonging to the BEL1-Like (BEL1L) family, which is mainly involved in the development of the replum. Previous studies have shown that BEL1L transcription factors regulate ovule development through the negative regulator *AGAMOUS*, a MADS-box gene that is closely related to the *SHP* gene (Modrusan et al., 1994; Western and Haughn, 1999). Similarly, *RPL* may negatively regulates the *SHP* gene to control the development of the replum (Roeder et al., 2003).

In *rpl* mutants, the overall morphology of silique was similar to that of the wild-type, except that the length was half as long as that of the wild-type. The replum cells of *rpl* mutants are also replaced by a narrow file of cells that resemble the cells located in the valve margin. In order to detect whether the narrow file of cells adopted a valve margin identity, examinations of the known expression patterns of the valve margin molecular markers, GT140 (Sundaresan et al., 1995; Ferrándiz et al., 2000b; Liljegren et al., 2000) and SHP2:GUS (Savidge et al., 1995) revealed that those genes were ectopically expressed in the replum region of the *rpl* mutant (Roeder et al., 2003). Those data proved that replum cells developed into valve margin cells. Since the *SHP* genes are ectopically expressed in the replum of the *rpl* mutant, and also control the development of the valve margin, a *rplshp1shp2* triple mutant was constructed to remove the activity of *SHP,* and to detect whether the ectopic expression of *SHP* caused the replum cells to develop into valve margin cells. The results showed that the replum was restored in the triple mutant; thus, indicating that the ectopic expression of *SHP* genes caused the loss of the replum in *rpl* mutants. Another study also suggested that *RPL* is not a direct factor controlling the formation of the replum, but rather, it is necessary to prevent the ectopic expression of *SHPs* in the replum (Roeder et al., 2003).

It is known that there are three main tissues in *A. thaliana* siliques: the valve, the valve margins, and the replum. Previous studies have shown that the formation and development of valve margins is regulated by *SHP1/2, IND,* and *ALC* (Liljegren et al., 2000). Valve development is controlled by the transcription factor, *FUL* (Gu et al., 1998), which negatively regulates *SHP* to prevent valve cells from adopting the identity of valve margin cells (Ferrándiz et al., 2000b). The development of the replum is negatively regulated by *RPL* to prevent the formation of valve margin cells (Roeder et al., 2003). In conclusion, the expression of *SHP1/2, IND,* and *ALC* genes in the valve margin is negatively regulated by *RPL* and *FUL* to control the development of the valve and replum. *SHP1*/2 positively regulate the *IND* and *ALC* genes. *IND* is involved in the identification and development of the lignification layer and the separation layer at the valve margin, while *ALC* is involved in the identification and development of the separation layer at the valve margin (Dinneny et al., 2005; Tang et al., 2007). Besides, some new factors were identified to involve in silique dehiscence. Recently, it has been revealed that *APETALA2* (*AP2*) regulates *SHP* and *IND*, *RPL* to ensure their proper expression level during silique dehiscence (Ripoll et al., 2011). Some studies have shown that *FILAMENTOUS FLOWER* (*FIL*) and *YABBY3* (*YAB3*) and *ASYMMETRIC LEAVES1/2* (*AS1/AS2*) (Sawa et al., 1999; Eshed et al., 2004; Alonso-Cantabrana et al., 2007) related to lateral organ development, and *JAGGED* (*JAG*) (Dinneny et al., 2004; Ohno et al., 2004) promoting the growth of lateral organs jointly promote the expression of *FUL* and *SHP* (Dinneny et al., 2005). Genes generally associated to meristem-related functions act in the replum and control replum width, such as *BREVIPEDICELLUS* (*BP*), *NO TRANSMITTING TRACT* (*NTT*) or *WUSCHEL-RELATED HOMEOBOX 13* (*WOX13*) (Alonso-Cantabrana et al., 2007; Romera et al., 2012; Marsch-Martinez et al., 2014). Study show that boundary genes, like *CUP-SHAPED COTYLEDON* (*CUC*) and *KNOTTED1-LIKE FROM A. THALIANA 2/6* (*KNAT2/6*), are also expressed in the valve margins (Hepworth and Pautot, 2015).

DOWNSTREAM EFFECTORS ASSOCIATED WITH SILIQUE DEHISCENCE

Cellulose, hemicellulose, and pectin are the main components of plant cell walls (Keegstra, 2010). During plant cell differentiation, organ shedding and dehiscence, Cellulase, hemicellulase, and pectinase are responsible for the modification and degradation of these components of cell walls, respectively. Although the biochemical reactions of these enzymes are known, little is known about their biological functions during developmental processes.

The downstream of silique dehiscence is ultimately related to cell wall rupture, cell senescence, and apoptosis, especially the degradation of the middle lamella, which is an important process during dehiscence and is also a feature that is shared with other processes, such as abscission or senescence (Roberts et al., 2000; Patterson, 2001). Cell wall rupture proceeds through the action of

enzymes such as cellulases, hemicellulases and pectinases. Several such enzymatic activities have been identified in *A. thaliana*.

The first gene identified as being associated with silique dehiscence encodes a polygalacturonase (PG), a pectinase exist in the DZ of *B. napus* silique, which is called *B. napus* endo-polygalacturonase *(RDPG1, SAC66)* (Jenkins et al., 1996; Petersen et al., 1996). Its homologous genes in *A. thaliana* are *Arabidopsis* endo-polygalacturonases (*ADPG1, SAC70*), which were isolated based on sequence similarity (Sander et al., 2001; Jenkins et al., 2010). The expression patterns of the *RDPG1* promoter in *A. thaliana* transgenic plants (Sander et al., 2001) and the *ADPG1* promoter in *Brassica* plants (Jenkins et al., 2010) were detected and analyzed in heterologous systems. In *Brassica* plants, the reporter gene driven by the *ADPG1* promoter was expressed in regions where cell separation occured such as at the anther dehiscence site and the DZ. Similar results were observed in *A. thaliana* (Roberts et al., 2002). A tomato pectinase, *positional sterility-2* (*PS-2)*, is a homologous gene of *ADPG1*, which is required for anther dehiscence (Gorguet et al., 2006, 2009). Thus, those results show that the function of pectinase in abscission and dehiscence is highly conserved. Studies showed that the expression of *ADPG1* in the silique DZ and the seed abscission zone is regulated by the INDEHISCENT and HECATE3 transcription factors, respectively (Ogawa et al., 2009). In apple and tomato, the expression of the gene encoding pectinase in the pedicel abscission zone is controlled by the MADS-box transcription factors, JOINTLESS (J), MACROCALYX (C), and SIMBP21 (Nakano et al., 2015). PG expression is controlled at the transcriptional and post-translational levels. *PGs* expressed in the silique dehiscence and abscission zones contain a cleavable N-terminal domain, which seems to prevent PG from being targeted to the cell wall. When the plant is triggered by development signals, the cleavable N-terminal domain of PG is removed, and the mature proteins are transported extracellularly to play their roles (Degan et al., 2001). A study show that pectin methylesterases may be associated to the degradation of the middle lamella at valve separation, although there is no direct evidence (Jaradat et al., 2014), A recent study showed that *A. thaliana* ADPG1 is involved in the defense system, which changes the content or composition of lignin through ectopic expression. Thus, ADPG1 could trigger the expression of defense response genes and release of elicitors, and activates cell wall remodeling to maintain cell integrity and prevent external invasion (Gallego-Giraldo et al., 2020).

It is well-known that cellulase and hemicellulase are involved in abscission and dehiscence, as well as other cell separation processes in plants. In plants, cellulases have tissue-specific expression patterns for many development processes, such as tissue expansion, silique ripening or organ abscission (Brummell and Harpster, 2001). Cellulase activity increased during *B. napus* silique dehiscence, although the corresponding genes for such activity have not been determined (Meakin and Roberts, 1990). Similar to pectinase genes, the expression of cellulase genes in the pedicel abscission zone of tomato are also regulated by the MADS-box transcription factors, J, MC, and SIMBP21. The expression of the tomato cellulase gene, *CELLULASE4*, is involved in rapid cell expansion in some organs, such as hypocotyls and leaves (Brummell et al., 1997). Similarly, the cellulase gene, *KORRIGAN,* in *A. thaliana* is also associated with rapid cell elongation (Nicol et al., 1998; Lane et al., 2001). Hemicellulose is another main component of plant cell walls (Heredia et al., 1995). Hemicellulase may have similar effects on plant development as cellulase and pectinase. In the *A. thaliana* genome, there are 25 cellulase genes (Urbanowicz et al., 2007) and eight mannanase genes (Yuan et al., 2007). Recent studies have confirmed that these genes play a role in *A. thaliana* silique dehiscence. The cellulase gene, *CELLULASE6* (*CEL6*) and the hemicellulase gene, *MANNANASE7* (*MAN7*), were isolated from *A. thaliana*, and their functions in the development and dehiscence of *A. thaliana* siliques was elucidated. Those genes were expressed in both vegetative and reproductive organs, and their expressions in the silique was partially regulated by the INDEHISCENT and ALCATRAZ transcription factors. They indirectly affect the time of cell differentiation in valves and promote the degradation of the separation layer cells to facilitate silique dehiscence (He et al., 2018). Xyloglucan endotransglycosylase (XET) is another enzyme involved in cell wall loosening (Fry et al., 1992). Studies showed that during the final stage of silique development in *B. napus*, an XET-encoding gene was up-regulated in the DZ, while an enhancer trap line (YJ8) found in *A. thaliana* appeared to be positively regulated by *SHP1/2* (Roberts et al., 2000; Ferrandiz, 2002). In order to complete silique dehiscence, many enzymatic activities are required, as well as others whose association with dehiscence still need to be detailed. Previous studies have showed that several genes involved in lignification and remodeling of the cell wall also have function in silique dehiscence. For example, NAC SECONDARY WALL THICKENING PROMOTING FACTOR 1 (*NST1*) and related *NST3* regulate a suite of genes involved in lignin and cellulose synthesis (Mitsuda and Ohme-Takagi, 2008). In addition, lignin is a characteristic of differentiation in many cell types, including xylem, and the endocarp b layer of valves, in which the spatial pattern of lignin deposition is closely related to the function of the cells (Roppolo and Geldner, 2012; Hofhuis et al., 2016). Previous studies have shown that lignin forms a honeycomb-shaped structure, which provides a mechanical constraint to limit the diffusion of cell wall-degrading enzymes at the site of cell-cell detachment. Lignin molecular brace playing an important role in organ separation (Yuree et al., 2018). The continuous improvement of gene editing techniques such as CRISPR-CAS9 system and the development of molecular markers will accelerate the research process of silique dehiscence, and finally achieve large-scale mechanized harvest of oilseed rape. At the same time, the research results on silique dehiscence of leguminous plants will also provide reference for oilseed rape silique dehiscence (Ogutcen et al., 2018).

SIGNAL OF SILIQUE DEHISCENCE

Signal transduction during silique dehiscence is essential for the completion of each event in the process of silique dehiscence.

So far, the signaling molecules and mechanisms by which intercellular communication occurs during silique dehiscence have not been clarified. However, some candidate factors can be proposed based on sequence similarity and expressions pattern. Two putative membrane-binding proteins have been identified as participants in silique dehiscence, including *YJ80* and *YJ115*. *YJ80* is inserted near a gene encoding a mammalian anchor protein-like protein and is expressed at the valve margins and abscission zones of seeds (Ferrandiz, 2002). *YJ115* is inserted into the upstream of a gene unknown function that contains a putative transmembrane domain and is expressed in the abaxial replum and the valve margins (Ferrandiz, 2002). It has been reported that *DEFENSE*, *NO DEATH1* (DND1), which is expressed in the DZ of *Arabidopsis* siliques, encodes cyclic nucleotide-gated ion channel (CNGC) (Köhler et al., 2001). The CNGC is a membrane protein capable of transducing $K^+$and Ca^{2+} ions, and has the same function as other animal CNGCs involved in signal transduction (Leng et al., 1999). One study has also shown that the MADS domain family transcription factors, *SEPALLATA3* and *AG15,* may be involved in *A. thaliana* silique dehiscence by regulating glycosyl hydrolases (Jiang et al., 2016).

Dehiscence and abscission are closely related physiological processes, They all involve the dissolution of intercellular junctions and the degradation of cell walls leading to cell separation (Lewis et al., 2006). And polygalacturonase is needed to loosen the abscission or dehiscence zone cells before cell separation (Ogawa et al., 2009). However, dehiscence and abscission are controlled by different genes in *A. thaliana.* Studies have shown that mutants with flower shedding defects have normal silique dehiscence, on the contrary, there are also mutants with silique indehiscence, whose floral organs shedding normally (Liljegren et al., 2000; Butenko et al., 2003; Patharkar and Walker, 2018). It is reported that a leucine-rich repeat receptor-like protein kinase (LRR-RLK), HAESA, is involved in the regulation of floral organ abscission in *A. thaliana* (Jinn et al., 2000). Some members of LRR-RKs are involved in different developmental processes, but it is not clear whether LRR-RLK is involved in the regulation of silique dehiscence. One study showed that SAC29 is an mRNA specifically up-regulated in the DZ during late silique development in *B. napus*. The protein encoded by *SAC29* is homologous to the receiver domain of response regulator proteins, and may be involved in responding to different stimuli, such as ethylene and cytokinin signals (D'agostino and Kieber, 1999; Whitelaw et al., 1999).

The antagonistic effects of the plant hormones, ethylene and auxin, are known to be involved in abscission (González-Carranza et al., 1998). Ethylene promotes abscission, while auxin delays it. If the delay of silique dehiscence is due to reductions in ethylene, the application of exogenous ethylene can restore the normal timing of cell separation (Child et al., 1998). Increases in cellulase activity in the DZ are due to decreases in auxin concentrations. The application of exogenous auxin analogs delayed DZ cell separation by inhibiting cellulase activity and preventing RDPG1 pectinase secretion into the cell wall (Chauvaux et al., 1997; Degan et al., 2001). Some studies have shown that maintaining auxin minimum in valve margin is necessary for the formation of the separation layer, and this needs to be coordinated by *IND*. *IND* can target several genes related to auxin transport in the valve margin, like *PINOID (PID)* and *WAG2,* which control the distribution of the auxin efflux carrier *PIN-FORMED3 (PIN3)* (Sorefan et al., 2009; Dong and Wang, 2015; Ballester and Ferrandiz, 2017). Studies have shown that cytokinins not only play an early proliferation-inducing role at the medial tissues of the developing gynoecia, but also play a late role in fruit patterning and morphogenesis at the valve margin of developing fruits. The application of exogenous synthetic cytokinins in *shp1*, *shp2,* and *ind* mutants can restore the formation of valve margin, which further show the cytokinins involved in the regulation of silique dehiscence (Marsch-Martinez et al., 2012; Zuniga-Mayo et al., 2014). GA can regulate the differentiation of *Arabidopsis* fruit morphology and silique dehiscence zone, which is also regulated by *IND*. *IND* promotes GA accumulation by regulating gibberellin biosynthesis enzyme GA3OX1, while GA can promote the degradation of DELLA protein bound to ALC, thus releasing ALC to play its role in regulate differentiation of separation layer (Arnaud et al., 2010; Ballester and Ferrandiz, 2017). Abscisic acid may act as a coordination signal (Young and Gallie, 2000). Transcriptome data of *Arabidopsis* siliques development analysis showed that abscisic acid was enriched during silique dehiscence in *A. thaliana*, which confirmed that abscisic acid may play a role in silique dehiscence (Wagstaff et al., 2009). Jasmonic acid (JA) is involved in anther dehiscence. Mutants of JA showed altered timings of anther opening (Sanders et al., 2000; Ishiguro et al., 2001), but there have been no reports on the function of JA in silique dehiscence. However, its positive regulation on flower organ abscission has been proved (Kim et al., 2013). Some studies have shown that salicylic acid (SA) is involved in the process of floral organ abscission, whether it is involved in the silique dehiscence still needs further exploration (Cai and Lashbrook, 2008; Patharkar and Walker, 2015). Recently, studies have shown that auxin controlled by IND specifies the separation layer in *Arabidopsis* siliques (Van Gelderen et al., 2016). In addition, interactions between IND and SPATULA (SPT) promote the development of the separation layer by regulating auxin formation (Girin et al., 2011).

In recent years, the application of plant biostimulants to affect development has achieved preliminary results, but its specific mechanism is not clear (Du Jardin, 2015). Recently, it has been reported that Sealicate, a biological stimulant from the seaweed Ascophyllum nodosum, has effects on the fruit development and seed dispersal of *A. thaliana* and rapeseed. Sealicit was developed utilizing a targeted plant signal induction (PSI) approach to formulation development. Sealicit affects the expression of *IND*, the main regulator of silique dehiscence, and destroys the auxin minimum. These two factors would affect the formation of dehisecnce zone. This provide new direction for the breeding varieties with dehiscence-resistant (Łangowski et al., 2019).

Transcriptome data of *A. thaliana* and tomato fruit development have been analyzed and compared in order to

find more similar regulator (Gomez et al., 2014). Preliminary results have been achieved in the application of synthetic plant hormone analogs and related chemical reagents in fruits, such as synthetic auxins and ethylene blockers, which partially block abscission, are sprayed on Citrus and apple trees about a month before harvest (Anthony, 1999; Yuan and Carbaugh, 2007). Plant hormone analogs and related chemical reagents were sprayed before harvest in *B. napus*, the effects of silique dehiscence were observed. If strains which were beneficial to mechanized harvest without affecting their quality were screened, it would show that these chemical sprays have a certain potential in silique dehiscence. With the development of biotechnology and the ability of high-throughput data analysis, the study on silique dehiscence may bring great commercial value.

In conclusion, hormones play a role in both DZ differentiation and the coordination of physiological events that lead to cell separation. Few studies have directly addressed these questions so far; however, they can be studied by collecting different *A. thaliana* mutants that have altered hormone synthetic pathways and hormone responses. Based on the findings of previous studies, the mechanism and regulation of silique dehiscence involves many factors that interact in a complex network (Ferrandiz, 2002; Dinneny et al., 2005; Ballester and Ferrandiz, 2017; Di Vittori et al., 2019) (**Figure 3**).

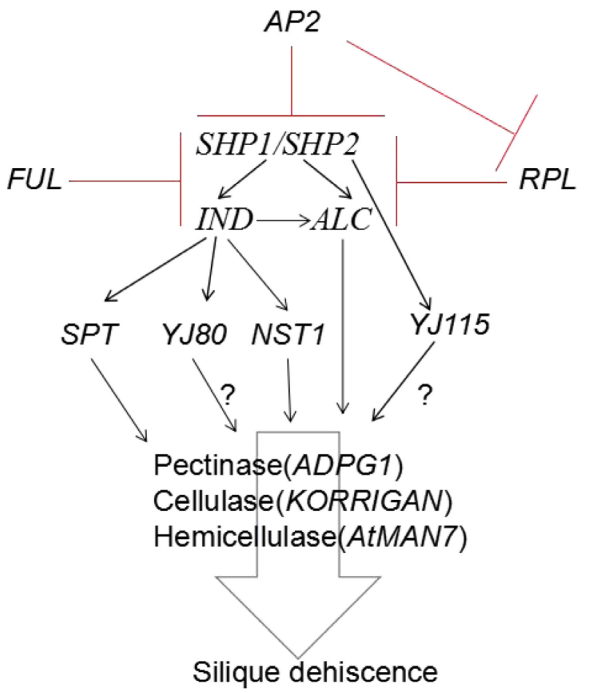

FIGURE 3 | Model for regulation of silique dehiscence in *Arabidopsis thaliana*, The major transcription factors and their regulatory interactions, as well as degradation enzyme of cell wall are included. Hormone coordinate signal transduction in silique dehiscence which not shown in figure. Negative regulation represented by red lines, Positive regulation represented by black arrow. Question marker means hypothetical relationships not well supported by experimental data.

ADVANCES FROM STUDIES OF SILIQUE DEHISCENCE IN *Brassica Napus* AGRICULTURE PRODUCTION

Brassica napus is one of the five major crops, that belongs to Brassicaceae, and can be divided into three categories, including *B. campestris L.*, *B. Juncea,* and *B. napus L.*, among which *B. napus* has the highest grain yield. In China, *B. napus L.* is mainly planted in the middle and lower reaches of the Yangtze River, and is one of the most widely planted oilseed rape in China, accounting for about 20% of the world's yield. With the development of the social economy, the demand for, and quality requirements of, oilseed rape are becoming increasingly higher. According to the United States Department of Agriculture (USDA), global edible oil production was 204 million tonnes and consumption was 200 million tonnes in 2018. China produced 26.86 million tonnes of edible oil, consumed 37.67 million tonnes, and imported 8.087 million tonnes in 2018; an increase of 8.9% from 2017. As a major vegetable oil consuming country, a large amount of oil consumption depends on imports, and its production and development are directly related to whether it can meet the edible oil needs of individuals. Taking various measures to continuously increase yield and improve production efficiency is an important goal for oilseed rape research. Mechanized production is an inevitable direction for the development of agricultural production technology. In order to improve the production efficiency of oilseed rape cultivation, improvements in the level of mechanized production are necessary. However, compared with other crops, oilseed rape silique is easy to dehiscence, so it is difficult to realize mechanized harvest.

Researchers have performed long-term explorations of the resistance of oilseed rape silique dehiscence, and developed different methods to detect the character of silique dehiscence. The earliest of such methods was the European Scholars' Field Investigation Method. The investigation items included the number of seeds lost in the container, the ratio of direct harvest to advance harvest, the number of seedlings germinated by scattered seeds in the field after harvest, the number of seeds scattered in the field, and the number of broken siliques (Kadkol et al., 1984). Although this method is simple to perform, it is time consuming. Moreover, such manual methods are greatly influenced by the investigator's subjectivity, and are also affected by the environment. Thus, the error in the method is large and the reliability is low. Anatomical methods were used to observe the vascular bundles of oilseed rape (Morgan et al., 1998; Child et al., 2003). It was found that there were large differences in the distribution range, size, quantity and position of vascular bundles in different rape lines. This method overcomes the low reliability of the field investigation method, and identifies the physiologica differences of silique dehiscence traits among different species, but it can only identify obvious differences, and those species with few differences cannot be accurately judged. Additionally, this method is only qualitative, and quantitative. In recent years,

a mechanical instrument identification method for simulating the natural dehiscence of siliques in the field has been developed rapidly (Wen et al., 2009).

Researchers proposed a random impact test to detect the resistance of silique dehiscence, the shaking time required to open 50% of dried siliques is tested, but the resistant ability of single silique cannot be detected (Morgan et al., 1998). On this basis, researchers using a shaking table replace the original random collider, adopting multiple collisions, and using the silique dehiscence resistant index instead of the original percentage of broken siliques as an index (Wen et al., 2008). The stability and repeatability of the results were good. In addition, studies reported a new random impact test, in which siliques were baked at 80°C for 30 min to remove the moisture from siliques, which overcame the problem of low resistance to dehiscence in some oilseed rape species (Peng et al., 2012).

Some researchers propose that the dehiscence resistance could be directly evaluated by measuring the tensile force needed for mechanically break siliques (Kadkol et al., 1984; Tys, 1985; Tan et al., 2006). The maximum tensile force at the moment of silique dehiscence represents the dehiscence resistance of the siliques. Other investigators suggested the suspended fracturing method, in which siliques were put on a cantilever beam supporting frame, on which a load force was exerted, and peak force on behalf the resistance of silique dehiscence. The method is simple and rapid, but the reliability and influencing factors must be further explored (Li et al., 2012). Another method of detecting the resistance of oilseed rape to silique dehiscence was designed using a variable speed anti-cracking tester suitable for a single silique on the basis of a single plant thresher. The input current frequency of the silique dehiscence moment was used as an index to measure the resistance of silique dehiscence. When an input current frequency above 60 Hz was applied, the varieties remaining unruptured were regarded as dehiscence-resistant varieties. However, the relationship between this method and dehiscence resistance remains uncertain, and must be verified by further experimentation (Squires et al., 2003). The above-described methods for the identification of oilseed rape silique dehiscence resistance have their own advantages and disadvantages, and further research is necessary to put forward a stable, reliable, time-saving and labor-saving determination method.

The resistance of silique dehiscence is different among different oilseed rape varieties. Some studies reported that the dehiscence of oilseed rape siliques was dependent on the thickness of the pericarp and the degree of development of mechanical tissues in the pericarp (Liu, 1987). The resistance to dehiscence of *B. napus* siliques was the worst, while that of *B. juncea* was second, and *B. campestris* was the highest. Some studies showed that the resistance of siliques was dependent on the length of the siliques, and the content of water and cellulose (Zheng et al., 1999). Studies showed that the dehiscence resistance index of oilseed rape was positively correlated with silique length, pericarp weight, thousand grain weight and seed diameter, and negatively correlated with silique density and the seed number per silique (Cui et al., 2013). A recent study is related to the relationship between replum and silique dehiscence, they study silique morphological structure of rapeseed lines (including dehiscence-susceptible and dehiscence-resistant), it is found that a thick replum structure could produce high silique dehiscence resistance. The replum-valve joint area offers a good method to screen high resistance materials beneficial for breeding (Hu et al., 2015).

The dehiscence resistance of oilseed rape siliques is affected by multiple factors. The most economical and effective way to reduce grain abscission in oilseed rape is to select oilseed rape varieties exhibiting both dehiscence resistance and high yield. Such selection can not only achieve the overall mechanization of oilseed rape harvesting, but also improve the yield of such plants.

SUMMARY AND PROSPECT OF SILIQUE DEHISCENCE

Silique dehiscence is the result of the joint action of a variety of cell activities, during which a set of physiological and biochemical regulators are involved. First, the early regulators of cell differentiation must play a role in regulating cell specification. Second, after different cell types are determined, disparate enzyme activities must proceed to complete the respective processes, such as changes in cell wall composition, lignification, and the disintegration of the middle-lamella in the separation layer. The differentiation processes and downstream enzymatic activity must be strictly controlled. The signaling mechanism plays a key role in ensuring the coordinated operation of dehiscence-related events.

Controlling silique dehiscence is of great significance in agriculture. For oilseed rape and soybean, it is particularly important to control silique dehiscence and optimize yield. The identification of genes involved in silique dehiscence and the signal regulation mechanism remains a vital problem, for which substantial research still needs to be done. With the completion of the *Brassica* genome sequence, and the ongoing comprehensive analyses of expression patterns and metabolic pathways being performed, useful information may soon be available to provide a better understanding of dehiscence. At present, we are studying the genes related to silique dehiscence in *B. napus L.* with the aim of detailing the molecular mechanisms involved in silique dehiscence.

AUTHOR CONTRIBUTIONS

Y-KY was involved in the review writing. X-LT supervised the review. Y-LL, RS, L-ND, and F-YZ was involved in the manuscript refinement. All authors read and approved the manuscript.

FUNDING

This work was supported by the National Key R&D Program of China (2016YFD0101900 and 2016YFD0100305).

REFERENCES

Alonso-Cantabrana, H., Ripoll, J. J., Ochando, I., Vera, A., Ferrándiz, C., and Martínez-Laborda, A. (2007). Common regulatory networks in leaf and fruit patterning revealed by mutations in the Arabidopsis ASYMMETRIC LEAVES1 gene. *Development (Camb. Engl.)* 134, 2663–2671. doi: 10.1242/dev.02864

Alvarez, J., and Smyth, D. R. (1997). Carpel development genes in "*Arabidopsis*". *Flow. Newslett.* 41, 12–17.

Anthony, M. C. Jr. (1999). The efficacy of five forms of 2,4-D in controlling preharvest fruit drop in citrus. *Sci. Horticult.* 81, 267–277.

Arnaud, N., Girin, T., Sorefan, K., Fuentes, S., Wood, T. A., Lawrenson, T., et al. (2010). Gibberellins control fruit patterning in *Arabidopsis thaliana*. *Genes Dev.* 24, 2127–2132. doi: 10.1101/gad.593410

Ballester, P., and Ferrandiz, C. (2017). Shattering fruits: variations on a dehiscent theme. *Curr. Opin. Plant Biol.* 35, 68–75. doi: 10.1016/j.pbi.2016.11.008

Bemer, M., Van Mourik, H., Muino, J. M., Ferrandiz, C., Kaufmann, K., and Angenent, G. C. (2017). FRUITFULL controls SAUR10 expression and regulates *Arabidopsis* growth and architecture. *J. Exp. Bot.* 68, 3391–3403. doi: 10.1093/jxb/erx184

Benfey, P. N., and Chua, N. H. (1990). The cauliflower mosaic virus 35S promoter: combinatorial regulation of transcription in plants. *Science* 250, 959–966. doi: 10.1126/science.250.4983.959

Bowman, J. (ed.). (1994). *Arabidopsis: An Atlas of Morphology and Development*. New York, NY: Springer.

Bowman, J. L., Alvarez, J., Weigel, D., Meyerowitz, E. M., and Smyth, D. R. (1991). Control of flower development in *Arabidopsis thaliana* by APETALA1 and interacting genes. *Development* 119, 721–743.

Bowman, J. L., Baum, S. F., Eshed, Y., Putterill, J., and Alvarez, J. (1999). Molecular genetics of gynoecium development in *Arabidopsis*. *Curr. Top. Dev. Biol.* 45, 155–205. doi: 10.1016/s0070-2153(08)60316-6

Bowman, J. L., Smyth, D. R., and Meyerowitz, E. M. (1989). Genes directing flower development in *Arabidopsis*. *Plant Cell* 1, 37–52.

Braatz, J., Harloff, H.-J., and Jung, C. (2018a). EMS-induced point mutations in ALCATRAZ homoeologs increase silique shatter resistance of oilseed rape (Brassica napus). *Euphytica* 214:29.

Braatz, J., Harloff, H. J., Emrani, N., Elisha, C., Heepe, L., Gorb, S. N., et al. (2018b). The effect of INDEHISCENT point mutations on silique shatter resistance in oilseed rape (Brassica napus). *Theor. Appl. Genet.* 131, 959–971. doi: 10.1007/s00122-018-3051-4

Brummell, D. A., Bird, C. R., Schuch, W., and Bennett, A. B. (1997). An endo-1,4-β-glucanase expressed at high levels in rapidly expanding tissues. *Plant Mol. Biol.* 33, 87–95. doi: 10.1023/a:1005733213856

Brummell, D. A., and Harpster, M. H. (2001). Cell wall metabolism in fruit softening and quality and its manipulation in transgenic plants. *Plant Mol. Biol.* 47, 311–340.

Buck, M. J., and Atchley, W. R. (2003). Phylogenetic analysis of plant basic helix-loop-helix proteins. *J. Mol. Evol.* 56, 742–750. doi: 10.1007/s00239-002-2449-3

Butenko, M. A., Patterson, S. E., Grini, P. E., Stenvik, G. E., Amundsen, S. S., Mandal, A., et al. (2003). Inflorescence deficient in abscission controls floral organ abscission in Arabidopsis and identifies a novel family of putative ligands in plants. *Plant Cell* 15, 2296–2307. doi: 10.1105/tpc.014365

Cai, S., and Lashbrook, C. C. (2008). Stamen abscission zone transcriptome profiling reveals new candidates for abscission control: enhanced retention of floral organs in transgenic plants overexpressing Arabidopsis ZINC FINGER PROTEIN2. *Plant Physiol.* 146, 1305–1321. doi: 10.1104/pp.107.110908

Chauvaux, N., Child, R., John, K., Ulvskov, P., Borkhardt, B., Prinsen, E., et al. (1997). The role of auxin in cell separation in the dehiscence zone of oilseed rape pods. *J. Exp. Bot.* 48, 1423–1429.

Child, R. D., Summers, J. J., Farrent, J. W., and Bruce, D. M. (2003). Increased resistance to pod shatter is associated with changes in the vascular structure in pods of a resynthesized *Brassica napus* line. *J. Exp. Bot.* 54:1919. doi: 10.1093/jxb/erg209

Child, R. N., John, K., Ulvskov, P., Van, O. H., and Van Onckelen, H. A. (1998). Ethylene biosynthesis in oilseed rape pods in relation to pod shatter. *J. Exp. Bot.* 49, 829–838.

Coupe, S. A., Taylor, J. E., Isaac, P. G., and Roberts, J. A. (1994). Characterisation of a mRNA that accumulates during development of rape pods. *Plant Mol. Biol.* 24, 223–227. doi: 10.1007/bf00040589

Cui, J. C., Liu, J., Mei, D. S., Yun-Chang, L. I., Li, F. U., Peng, P. F., et al. (2013). Genetic and correlation analysis on pod shattering traits in *Brassica napus* L. *Acta Agronom. Sin.* 39:1791.

D'agostino, I. B., and Kieber, J. J. (1999). Phosphorelay signal transduction: the emerging family of plant response regulators. *Trends Biochem. Sci.* 24, 452–456. doi: 10.1016/s0968-0004(99)01465-6

Degan, F. D., Child, R., Svendsen, I., and Ulvskov, P. (2001). The cleavable N-terminal domain of plant endopolygalacturonases from clade B may be involved in a regulated secretion mechanism. *J. Biol. Chem.* 276, 35297–35304. doi: 10.1074/jbc.M102136200

Di Vittori, V., Gioia, T., Rodriguez, M., Bellucci, E., Bitocchi, E., Nanni, L., et al. (2019). Convergent evolution of the seed shattering trait. *Genes (Basel)* 10:68. doi: 10.3390/genes10010068

Dinneny, J. R., Weigel, D., and Yanofsky, M. F. (2005). A genetic framework for fruit patterning in *Arabidopsis thaliana*. *Development* 132, 4687–4696. doi: 10.1242/dev.02062

Dinneny, J. R., Yadegari, R., Fischer, R. L., Yanofsky, M. F., and Weigel, D. (2004). The role of JAGGED in shaping lateral organs. *Development* 131, 1101–1110. doi: 10.1242/dev.00949

Dong, Y., and Wang, Y. Z. (2015). Seed shattering: from models to crops. *Front. Plant Sci.* 6:476. doi: 10.3389/fpls.2015.00476

Du Jardin, P. (2015). Plant biostimulants: definition, concept, main categories and regulation. *Sci. Horticult.* 196, 3–14.

Eshed, Y., Izhaki, A., Baum, S. F., Floyd, S. K., and Bowman, J. L. (2004). Asymmetric leaf development and blade expansion in Arabidopsis are mediated by KANADI and YABBY activities. *Development* 131, 2997–3006. doi: 10.1242/dev.01186

Estornell, L. H., Agusti, J., Merelo, P., Talon, M., and Tadeo, F. R. (2013). Elucidating mechanisms underlying organ abscission. *Plant Sci.* 199–200, 48–60. doi: 10.1016/j.plantsci.2012.10.008

Ferrandiz, C. (2002). Regulation of fruit dehiscence in *Arabidopsis*. *J. Exp. Bot.* 53, 2031–2038.

Ferrándiz, C., Gu, Q., Martienssen, R., and Yanofsky, M. F. (2000a). Redundant regulation of meristem identity and plant architecture by FRUITFULL, APETALA1 and CAULIFLOWER. *Development* 127, 725–734.

Ferrándiz, C., Liljegren, S. J., and Yanofsky, M. F. (2000b). Negative regulation of the SHATTERPROOF genes by FRUITFULL during *Arabidopsis* fruit development. *Science* 289, 436–438. doi: 10.1126/science.289.5478.436

Ferrandiz, C., Pelaz, S., and Yanofsky, M. F. (1999). Control of carpel and fruit development in *Arabidopsis*. *Annu. Rev. Biochem.* 68, 321–354.

Fisher, F., and Goding, C. R. (1992). Single amino acid substitutions alter helix-loop-helix protein specificity for bases flanking the core CANNTG motif. *EMBO J.* 11, 4103–4109.

Flanagan, C. A., Hu, Y., and Ma, H. (2010). Specific expression of the AGL1 MADS-box gene suggests regulatory functions in Arabidopsis gynoecium and ovule development. *Plant J.* 10, 343–353. doi: 10.1046/j.1365-313x.1996.10020343.x

Fry, S. C., Smith, R. C., Renwick, K. F., Martin, D. J., Hodge, S. K., and Matthews, K. J. (1992). Xyloglucan endotransglycosylase, a new wall-loosening enzyme activity from plants. *Biochem J.* 282(Pt 3), 821–828. doi: 10.1042/bj2820821

Gallego-Giraldo, L., Liu, C., Pose-Albacete, S., Pattathil, S., Peralta, A. G., Young, J., et al. (2020). ARABIDOPSIS DEHISCENCE ZONE POLYGALACTURONASE 1 (ADPG1) releases latent defense signals in stems with reduced lignin content. *Proc. Natl. Acad. Sci. USA.* 117, 3281–3290. doi: 10.1073/pnas.1914422117

Gioia, T., Logozzo, G., Kami, J., Spagnoletti Zeuli, P., and Gepts, P. (2013). Identification and characterization of a homologue to the *Arabidopsis* INDEHISCENT gene in common Bean. *J. Hered* 104, 273–286. doi: 10.1093/jhered/ess102

Girin, T., Paicu, T., Stephenson, P., Fuentes, S., Körner, E., O'Brien, M., et al. (2011). INDEHISCENT and SPATULA interact to specify carpel and valve margin tissue and thus promote seed dispersal in *Arabidopsis*. *Plant Cell* 23, 3641–3653. doi: 10.1105/tpc.111.090944

Gomez, M. D., Vera-Sirera, F., and Perez-Amador, M. A. (2014). Molecular programme of senescence in dry and fleshy fruits. *J. Exp. Bot.* 65, 4515–4526. doi: 10.1093/jxb/eru093

González-Carranza, Z. H., Lozoya-Gloria, E., and Roberts, J. A. (1998). Recent developments in abscission: shedding light on the shedding process. *Trends Plant Sci.* 3, 10–14.

Gorguet, B., Schipper, D., Heusden, A. W. V., and Lindhout, P. (2006). High-resolution fine mapping of ps-2, a mutated gene conferring functional male sterility in tomato due to non-dehiscent anthers. *Theor. Appl. Genet.* 113, 1437–1448. doi: 10.1007/s00122-006-0389-9

Gorguet, B., Schipper, D., Van Lammeren, A., Visser, R. G. F., and Van Heusden, A. W. (2009). ps-2, the gene responsible for functional sterility in tomato, due to non-dehiscent anthers, is the result of a mutation in a novel polygalacturonase gene. *Theor. Appl. Genet.* 118, 1199–1209. doi: 10.1007/s00122-009-0974-9

Gu, Q., Ferrándiz, C., Yanofsky, M. F., and Martienssen, R. (1998). The FRUITFULL MADS-box gene mediates cell differentiation during Arabidopsis fruit development. *Development* 125, 1509–1517.

He, H., Bai, M., Tong, P., Hu, Y., Yang, M., and Wu, H. (2018). CELLULASE6 and MANNANASE7 affect cell differentiation and silique dehiscence. *Plant Physiol.* 176, 2186–2201. doi: 10.1104/pp.17.01494

Hepworth, S. R., and Pautot, V. A. (2015). Beyond the divide: boundaries for patterning and stem cell regulation in plants. *Front. Plant Sci.* 6:1052. doi: 10.3389/fpls.2015.01052

Heredia, A., Jimenez, A., and Guillen, R. (1995). Composition of plant cell walls. *Z. Lebensm. Unters Forsch.* 200, 24–31. doi: 10.1093/jxb/erv107

Hofhuis, H., Moulton, D., Lessinnes, T., Routier-Kierzkowska, A. L., Bomphrey, R. J., Mosca, G., et al. (2016). Morphomechanical innovation drives explosive seed dispersal. *Cell* 166, 222–233. doi: 10.1016/j.cell.2016.05.002

Hu, D., Kan, G., Hu, W., Li, Y., Hao, D., Li, X., et al. (2019). Identification of loci and candidate genes responsible for pod dehiscence in soybean via genome-wide association analysis across multiple environments. *Front. Plant Sci.* 10:811. doi: 10.3389/fpls.2019.00811

Hu, Z., Yang, H., Zhang, L., Wang, X., Liu, G., Wang, H., et al. (2015). A large replum-valve joint area is associated with increased resistance to pod shattering in rapeseed. *J. Plant Res.* 128, 813–819. doi: 10.1007/s10265-015-0732-9

Ishiguro, S., Kawai-Oda, A., Ueda, J., Nishida, I., and Okada, K. (2001). The DEFECTIVE IN ANTHER DEHISCIENCE gene encodes a novel phospholipase A1 catalyzing the initial step of jasmonic acid biosynthesis, which synchronizes pollen maturation, anther dehiscence, and flower opening in *Arabidopsis*. *Plant Cell* 13, 2191–2209. doi: 10.1105/tpc.010192

Jaradat, M. R., Ruegger, M., Bowling, A., Butler, H., and Cutler, A. J. (2014). A comprehensive transcriptome analysis of silique development and dehiscence in *Arabidopsis* and *Brassica* integrating genotypic, interspecies and developmental comparisons. *GM Crops Food* 5, 302–320. doi: 10.4161/21645698.2014.947827

Jeffrey, P., and Hill, E. M. L. (1989). Floral development in *Arabidopsis thaliana* : a comparison of the wild type and the homeotic pistillata mutant. *Can. J. Bot.* 67, 2922–2936.

Jenkins, E. S., Paul, W., Coupe, S. A., Bell, S. J., Davies, E. C., and Roberts, J. A. (1996). Characterization of an mRNA encoding a polygalacturonase expressed during pod development in oilseed rape (*Brassica napus* L.). *J. Exp. Bot.* 47, 111–115.

Jenkins, E. S., Paul, W., Craze, M., Whitelaw, C. A., Weigand, A., and Roberts, J. A. (2010). Dehiscence-related expression of an *Arabidopsis thaliana* gene encoding a polygalacturonase in transgenic plants of *Brassica napus*. *Plant Cell Environ.* 22, 159–167.

Jiang, L., Ma, X., Zhao, S., Tang, Y., Liu, F., Gu, P., et al. (2019). The APETALA2-like transcription factor SUPERNUMERARY BRACT controls rice seed shattering and seed size. *Plant Cell* 31, 17–36. doi: 10.1105/tpc.18.00304

Jiang, X., He, H., Wang, T., Wang, X., and Hong, W. (2016). Gene expression profile analysis indicate SEPALLATA3 and AGL15 potentially involved in arabidopsis silique dehiscence by regulating glycosyl hydrolase. *J. Plant Biol.* 59, 133–142.

Jinn, T. L., Stone, J. M., and Walker, J. C. (2000). HAESA, an Arabidopsis leucine-rich repeat receptor kinase, controls floral organ abscission. *Genes Dev.* 14, 108–117.

Kadkol, G. P., Macmillan, R. H., Burrow, R. P., and Halloran, G. M. (1984). Evaluation of Brassica genotypes for resistance to shatter. *Dev. Lab. Test. Euphy.* 33, 63–73.

Kaufmann, K., Wellmer, F., Muino, J. M., Ferrier, T., Wuest, S. E., Kumar, V., et al. (2010). Orchestration of floral initiation by APETALA1. *Science* 328, 85–89. doi: 10.1126/science.1185244

Kay, P., Groszmann, M., Ross, J. J., Parish, R. W., and Swain, S. M. (2013). Modifications of a conserved regulatory network involving INDEHISCENT controls multiple aspects of reproductive tissue development in Arabidopsis. *New Phytol.* 197, 73–87. doi: 10.1111/j.1469-8137.2012.04373.x

Keegstra, K. (2010). Plant cell walls. *Plant Physiol.* 154, 483–486.

Kempin, S. A., Savidge, B., and Yanofsky, M. F. (1995). Molecular basis of the cauliflower phenotype in *Arabidopsis*. *Science* 267, 522–525.

Khan, M. R., Rehman, O., and Riaz, M. (2019). Expression Pattern analysis of core regulatory module SHPs-FUL transcripts in rapeseed pod shattering. *Sarhad J. Agricult.* 35:696.

Kim, J., Dotson, B., Rey, C., Lindsey, J., Bleecker, A., Binder, B., et al. (2013). New clothes for the jasmonic acid receptor COI1: delayed abscission, meristem arrest and apical dominance. *PLoS One* 8:e60505. doi: 10.1371/journal.pone.0119063

Köhler, C., Merkle, T., Roby, D., and Neuhaus, G. (2001). Developmentally regulated expression of a cyclic nucleotide-gated ion channel from *Arabidopsis* indicates its involvement in programmed cell death. *Planta* 213, 327–332. doi: 10.1007/s004250000510

Laga, B., Den, B. B., and Lambert, B. (2012). *Brassica Plant Comprising a Mutant Indehiscent Allele. U.S. Patent No 9475849*. Washington, DC: U.S. Patent and Trademark Office

Laga, B., Den, B. B., and Lambert, B. (2016). *Brassica Plant Comprising A Mutant Indehiscent Allele. U.S. Patent No 8809635*. Washington, DC: U.S. Patent and Trademark Office.

Lane, D. R., Wiedemeier Apeng, L. C., Hofte, H., Vernhettes, S., and Desprez, T. (2001). Temperature-sensitive alleles of RSW2 link the KORRIGANendo-1,4-beta-glucanase to cellulose synthesis and cytokinesis inarabidopsis. *Plant Physiol.* 126, 278–288. doi: 10.1104/pp.126.1.278

Łangowski, Ł, Goñi, O., Quille, P., Stephenson, P., Carmody, N., Feeney, E., et al. (2019). A plant biostimulant from the seaweed Ascophyllum nodosum (Sealicit) reduces podshatter and yield loss in oilseed rape through modulation of IND expression. *Sci. Rep.* 9:16644. doi: 10.1038/s41598-019-52958-0

Leng, Q., Mercier, R. W., Yao, W. Z., and Berkowitz, G. A. (1999). Cloning and first functional characterization of a plant cyclic nucleotide-gated cation channel. *Plant Physiol.* 121, 753–761. doi: 10.1104/pp.121.3.753

Lewis, M. W., Leslie, M. E., and Liljegren, S. J. (2006). Plant separation: 50 ways to leave your mother. *Curr. Opin. Plant Biol.* 9, 59–65. doi: 10.1016/j.pbi.2005.11.009

Li, Y., Zhu, J., Xu, L., and Zhao, Z. (2012). Experiment on strength of rapeseed pod dehiscence based on impending fracturing method. *Nongye Gong. Xuebao Transact. Chinese Soc. Agricult. Eng.* 28, 111–115.

Liljegren, S. J., Ditta, G. S., Eshed, Y., Savidge, B., and Yanofsky, M. F. (2000). SHATTERPROOF MADS-box genes control seed dispersal in *Arabidopsis*. *Nature* 404, 766–770. doi: 10.1038/35008089

Liljegren, S. J., Roeder, A. H. K., Kempin, S. A., Gremski, K., Ostergaard, L., Guimil, S., et al. (2004). Control of fruit patterning in *Arabidopsis* by INDEHISCENT. *Cell* 116, 843–853. doi: 10.1016/s0092-8674(04)00217-x

Liu, H. (1987). *Practical Rape Cultivation*. Shanghai: Shanghai Scientific & Technical Publishers.

Liu, J., Wang, J., Wang, H., Wang, W., Zhou, R., Mei, D., et al. (2016). Multigenic control of pod shattering resistance in chinese rapeseed germplasm revealed by genome-wide association and linkage analyses. *Front. Plant Sci.* 7:1058. doi: 10.3389/fpls.2016.01058

Luo, D., Wang, Y. R., and Liu, Z. P. (2015). Research progress in the biological basis of legume pod dehiscence. *Acta Agrestia Sinica* 23, 927–935.

Ma, H., Yanofsky, M. F., and Meyerowitz, E. M. (1991). AGL1-AGL6, an Arabidopsis gene family with similarity to floral homeotic and transcription factor genes. *Genes Dev.* 5, 484–495. doi: 10.1101/gad.5.3.484

Marsch-Martinez, N., Ramos-Cruz, D., Irepan Reyes-Olalde, J., Lozano-Sotomayor, P., Zuniga-Mayo, V. M., and De Folter, S. (2012). The role of cytokinin during *Arabidopsis gynoecia* and fruit morphogenesis and patterning. *Plant J.* 72, 222–234. doi: 10.1111/j.1365-313X.2012.05062.x

Marsch-Martinez, N., Zuniga-Mayo, V. M., Herrera-Ubaldo, H., Ouwerkerk, P. B., Pablo-Villa, J., Lozano-Sotomayor, P., et al. (2014). The NTT transcription

factor promotes replum development in *Arabidopsis fruits*. *Plant J.* 80, 69–81. doi: 10.1111/tpj.12617

Meakin, P. J. (1990). Dehiscence of fruit in oilseed rape (*Brassica napus* L.). I. Anatomy of pod dehiscence. *J. Exp. Bot.* 41, 995–1002.

Meakin, P. J., and Roberts, J. A. (1990). Dehiscence of fruit in oilseed rape (Brassica nap us L.): II. The role of cell wall degrading enzymes and ethylene. *J. Exp. Bot.* 41, 1003–1011.

Mitsuda, N., and Ohme-Takagi, M. (2008). NAC transcription factors NST1 and NST3 regulate pod shattering in a partially redundant manner by promoting secondary wall formation after the establishment of tissue identity. *Plant J. Cell Mol. Biol.* 56, 768–778. doi: 10.1111/j.1365-313X.2008.03633.x

Modrusan, Z., Reiser, L., Feldmann, K. A., Fischer, R. L., and Haughn, G. W. (1994). Homeotic transformation of ovules into carpel-like structures in *Arabidopsis*. *Plant Cell* 6:333. doi: 10.1105/tpc.6.3.333

Morgan, C. L., Bruce, D. M., Child, R., Ladbrooke, Z. L., and Arthur, A. E. (1998). Genetic variation for pod shatter resistance among lines of oilseed rape developed from synthetic B. napus. *Field Crops Res.* 58, 160–165.

Morgan, C. L., Ladbrooke, Z. L., Bruce, D. M., Child, R., and Arthur, A. E. (2000). Breeding oilseed rape for pod shattering resistance. *J. Agricult. Sci.* 135, 347–359.

Murre, C., Mccaw, P. S., and Baltimore, D. (1989). A new DNA binding and dimerization motif in immunoglobulin enhancer binding, daughterless. MyoD, and myc proteins. *Cell* 56, 777–783. doi: 10.1016/0092-8674(89)90682-x

Nakano, T., Kato, H., Shima, Y., and Ito, Y. (2015). Apple SVP Family MADS-box proteins and the tomato pedicel abscission zone regulator JOINTLESS have similar molecular activities. *Plant Cell Physiol.* 56, 1097–1106. doi: 10.1093/pcp/pcv034

Nicol, F., His, I., Jauneau, A., Vernhettes, S., Canut, H., and Hofte, H. (1998). A plasma membrane-bound putative endo-1,4-beta-D-glucanase is required for normal wall assembly and cell elongation in *Arabidopsis*. *EMBO J.* 17, 5563–5576. doi: 10.1093/emboj/17.19.5563

Ogawa, M., Kay, P., Wilson, S., and Swain, S. M. (2009). ARABIDOPSIS DEHISCENCE ZONE POLYGALACTURONASE1 (ADPG1), ADPG2, and QUARTET2 are Polygalacturonases required for cell separation during reproductive development in *Arabidopsis*. *Plant Cell* 21, 216–233. doi: 10.1105/tpc.108.063768

Ogutcen, E., Biotech, A., Khan, M., Marques, E., Penmetsa, R., Kahraman, A., et al. (2018). Pod shattering: a homologous series of variation underlying domestication and an avenue for crop improvement. *Agronomy* 8:137.

Ohno, C. K., Reddy, G. V., Heisler, M. G. B., and Meyerowitz, E. M. (2004). The *Arabidopsis* JAGGED gene encodes a zinc finger protein that promotes leaf tissue development. *Development* 131, 1111–1122. doi: 10.1242/dev.00991

Parker, T. A., Berny Mier, Y., Teran, J. C., Palkovic, A., Jernstedt, J., and Gepts, P. (2020). Pod indehiscence is a domestication and aridity resilience trait in common bean. *New Phytol.* 225, 558–570. doi: 10.1111/nph.16164

Patharkar, O., and Walker, J. (2015). Floral organ abscission is regulated by a positive feedback loop. *Proc. Natl. Acad. Sci. U.S.A.* 112, 2906–2911. doi: 10.1073/pnas.1423595112

Patharkar, O. R., and Walker, J. C. (2018). Advances in abscission signaling. *J. Exp. Bot.* 69, 733–740.

Patterson, S. E. (2001). Cutting loose. Abscission and dehiscence in *Arabidopsis*. *Plant Physiol.* 126, 494–500. doi: 10.1104/pp.126.2.494

Peng, P., Li, Y., Mei, D., Liu, D., Fu, L., Wang, H., et al. (2012). Optimization and experiment of assessment method for pod shatter resistance in *Brassica napus* L. *Transact. Chinese Soc. Agricult. Eng.* 29, 19–25.

Petersen, M., Sander, L., Child, R., Van Onckelen, H., Ulvskov, P., and Borkhardt, B. (1996). Isolation and characterisation of a pod dehiscence zone-specific polygalacturonase from *Brassica napus*. *Plant Mol. Biol.* 31, 517–527. doi: 10.1007/bf00042225

Purugganan, M. D. (1997). The MADS-box floral homeotic gene lineages predate the origin of seed plants: phylogenetic and molecular clock estimates. *J. Mol. Evol.* 45:392. doi: 10.1007/pl00006244

Rajani, S., and Sundaresan, V. (2002). The *Arabidopsis* myc/bHLH gene ALCATRAZ enables cell separation in fruit dehiscence. *Curr. Biol.* 11, 1914–1922. doi: 10.1016/s0960-9822(01)00593-0

Riechmann, J. L., and Meyerowitz, E. M. (1997). MADS domain proteins in plant development. *Biol. Chem.* 378, 1079–1101.

Ripoll, J. J., Roeder, A. H., Ditta, G. S., and Yanofsky, M. F. (2011). A novel role for the floral homeotic gene APETALA2 during *Arabidopsis* fruit development. *Development* 138, 5167–5176. doi: 10.1242/dev.073031

Roberts, J. A., Elliott, K. A., and Gonzalez-Carranza, Z. H. (2002). Abscission, dehiscence, and other cell separation processes. *Annu. Rev. Plant Biol.* 53, 131–158. doi: 10.1146/annurev.arplant.53.092701.180236

Roberts, J. A., Whitelaw, C. A., Gonzalez-Carranza, Z. H., and Mcmanus, M. T. (2000). Cell separation processes in plants-Models, mechanisms and manipulation. *Ann. Bot.* 86, 223–235.

Robinson-Beers, K., Pruitt, R. E., and Gasser, C. S. (1992). Ovule development in wild-type arabidopsis and two female-sterile mutants. *Plant Cell* 4, 1237–1249. doi: 10.1105/tpc.4.10.1237

Roeder, A. H. K., Ferrándiz, C., and Yanofsky, M. F. (2003). The role of the REPLUMLESS homeodomain protein in patterning the arabidopsis fruit. *Curr. Biol.* 13, 1630–1635. doi: 10.1016/j.cub.2003.08.027

Romera, B. M., Ripoll, J.-J., Yanofsky, M., and Pelaz, S. (2012). The WOX13 homeobox gene promotes replum formation in the *Arabidopsis thaliana* fruit. *Plant J. Cell Mol. Biol.* 73, 37–49. doi: 10.1111/tpj.12010

Roppolo, D., and Geldner, N. (2012). Membrane and walls: who is master, who is servant? *Curr. Opin. Plant Biol.* 15, 608–617. doi: 10.1016/j.pbi.2012.09.009

Rounsley, S. D., Ditta, G. S., and Yanofsky, M. F. (1995). Diverse roles for MADS box genes in *Arabidopsis* development. *Plant Cell* 7, 1259–1269. doi: 10.1105/tpc.7.8.1259

Řepková, J., and Hofbauer, J. (2009). Seed pod shattering in the genus Lotus and its overcoming. *Czech J. Genet. Plant Breed. UZEI (Czech Repub.)* 45, 39–44.

Sander, L., Child, R. P., Albrechtsen, M., and Borkhardt, B. (2001). Analysis of a dehiscence zone endo-polygalacturonase in oilseed rape (*Brassica napus*) and *Arabidopsis thaliana*: evidence for roles in cell separation in dehiscence and abscission zones, and in stylar tissues during pollen tube growth. *Plant Mol. Biol.* 46, 469–479. doi: 10.1023/a:1010619002833

Sanders, P. M., Lee, P. Y., Biesgen, C., Boone, J. D., Beals, T. P., Weiler, E. W., et al. (2000). The *Arabidopsis* DELAYED DEHISCENCE1 gene encodes an enzyme in the jasmonic acid synthesis pathway. *Plant Cell* 12, 1041–1061. doi: 10.1105/tpc.12.7.1041

Savidge, B., Rounsley, S. D., and Yanofsky, M. F. (1995). Temporal relationship between the transcription of two *Arabidopsis* MADS box genes and the floral organ identity genes. *Plant Cell* 7, 721–733. doi: 10.1105/tpc.7.6.721

Sawa, S., Watanabe, K., Goto, K., Liu, Y. G., Shibata, D., Kanaya, E., et al. (1999). FILAMENTOUS FLOWER, a meristem and organ identity gene of *Arabidopsis*, encodes a protein with a zinc finger and HMG-related domains. *Genes Dev.* 13, 1079–1088. doi: 10.1101/gad.13.9.1079

Schmid, R., and Rollins, R. C. (1994). The cruciferae of continental north america: systematics of the mustard family from the arctic to panama. *Taxon* 43:153.

Sehra, B., and Franks, R. G. (2017). Redundant CArG box cis-motif activity mediates SHATTERPROOF2 transcriptional regulation during *Arabidopsis thaliana* gynoecium development. *Front. Plant Sci.* 8:1712. doi: 10.3389/fpls.2017.01712

Sessions, A. (1999). Piecing together the *Arabidopsis gynoecium*. *Trends Plant Sci.* 4, 296–297.

Sessions, R. (1997). *Arabidopsis* (Brassicaceae) flower development and gynoecium patterning in wild type and Ettin mutants. *Am. J. Bot.* 84, 1179–1191.

Smyth, D. R., Bowman, J. L., and Meyerowitz, E. M. (1990). Early flower development in *Arabidopsis*. *Plant Cell* 2, 755–767.

Sorefan, K., Girin, T., Liljegren, S., Ljung, K., Robles, P., Galván-Ampudia, C., et al. (2009). A regulated auxin minimum is required for seed dispersal in *Arabidopsis*. *Nature* 459, 583–586. doi: 10.1038/nature07875

Spence, J. (1992). *Development of the Silique of Arabidopsis thaliana*. Ph.D. thesis, Durham University, Durham.

Spence, J., Vercher, Y., Gates, P., and Harris, N. (1996). 'Pod shatter' in *Arabidopsis thaliana*, *Brassica napus* and B. juncea. *J. Microscopy* 181, 195–203.

Squires, T. M., Gruwel, M. L. H., Zhou, R., Sokhansanj, S., Abrams, S. R., and Cutler, A. J. (2003). Dehydration and dehiscence in siliques of *Brassica napus* and *Brassica rapa*. *Canad. J. Bot. Revue Canad. Bot.* 81, 248–254.

Sundaresan, V., Springer, P., Volpe, T., Haward, S., Jones, J. D., Dean, C., et al. (1995). Patterns of gene action in plant development revealed by enhancer trap and gene trap transposable elements. *Genes Dev.* 9, 1797–1810. doi: 10.1101/gad.9.14.1797

Tan, X. L., Zhang, J. F., Li, Y., Zhang, Z. Y., Jia, Z., Song, J., et al. (2006). Quantitive determination of the strength of rapeseed pod dehiscence. *Transact. Chinese Soc. Agricult. Eng.* 22, 40–43.

Tang, G. X., Qin, Y. B., Song, W. J., and Zhou, W. J. (2007). Mechanism to control fruit development and disperse in *Arabidopsis* and the application for rapeseed(*Brassica napus*) breeding. *Chinese J. Cell Biol.* 29, 864–868.

Toledo-Ortiz, G., Huq, E., and Quail, P. H. (2003). The *Arabidopsis* basic/helix-loop-helix transcription factor family. *Plant Cell* 15, 1749–1770.

Tu, B., Liu, C., Wang, X., Li, Y., Zhang, Q., Liu, X., et al. (2019). Greater anatomical differences of pod ventral suture in shatter-susceptible and shatter-resistant soybean cultivars. *Crop Sci.* 59, 2784–2793.

Tys, J. (1985). Evaluation of the mechanical properties of winter rape siliques in respect to their susceptibility to cracking. *J. Public Admin. Policy Res.* 115, e512–e517.

Urbanowicz, B. R., Bennett, A. B., Elena, D. C., Carmen, C., Takahisa, H., Bernard, H., et al. (2007). Structural organization and a standardized nomenclature for plant endo-1,4-beta-glucanases (cellulases) of glycosyl hydrolase family 9. *Plant Physiol.* 144:1693. doi: 10.1104/pp.107.102574

Van Gelderen, K., Van Rongen, M., Liu, A., Otten, A., and Offringa, R. (2016). An INDEHISCENT-controlled auxin response specifies the separation layer in early *Arabidopsis* fruit. *Mol. Plant* 9, 857–869. doi: 10.1016/j.molp.2016.03.005

Wagstaff, C., Yang, T. J. W., Stead, A. D., Buchanan-Wollaston, V., and Roberts, J. A. (2009). A molecular and structural characterization of senescing *Arabidopsis siliques* and comparison of transcriptional profiles with senescing petals and leaves. *Plant J.* 57, 690–705. doi: 10.1111/j.1365-313X.2008.03722.x

Wen, Y. C., Fu, T. D., and Tu, J. X. (2008). Screening and analysis of resistance to silique shattering in rape (*Brassica napus* L.). *Acta Agronom. Sin.* 34, 163–166.

Wen, Y. C., Ting-Dong, F. U., Jin-Xing, T. U., Chao-Zhi, M. A., Shen, J. X., and Zhang, S. F. (2009). Advances in studies of pod shattering resistance in rapeseed. *J. Plant Genet. Resour.* 1, 140–145.

Western, T. L., and Haughn, G. W. (1999). BELL1 and AGAMOUS genes promote ovule identity in Arabidopsis thaliana. *Plant J.* 18, 329–336. doi: 10.1046/j.1365-313x.1999.00448.x

Whitelaw, C. A., Paul, W., Jenkins, E. S., Taylor, V. M., and Roberts, J. A. (1999). An mRNA encoding a response regulator protein from *Brassica napus* is up-regulated during pod development. *J. Exp. Bot.* 50, 335–341.

Wu, H., Mori, A., Jiang, X., Wang, Y., and Yang, M. (2006). The INDEHISCENT protein regulates unequal cell divisions in *Arabidopsis* fruit. *Planta* 224, 971–979. doi: 10.1007/s00425-006-0351-8

Yang, J. B., Somers, D. A., Wright, R. L., and Mcgraw, R. L. (1990). Seed pod dehiscence in birdsfoot trefoil, Lotus conimbricensis, and their interspecific somatic hybrid. *Can. J.Plant Sci.* 70, 279–284.

Young, T. E., and Gallie, D. R. (2000). Programmed cell death during endosperm development. *Plant Mol. Biol.* 44, 283–301.

Yuan, J. S., Yang, X., Lai, J., Lin, H., Cheng, Z. M., Nonogaki, H., et al. (2007). The endo-beta-mannanase gene families in *Arabidopsis*, rice, and poplar. *Funct. Integr. Genomics* 7, 1–16. doi: 10.1007/s10142-006-0034-3

Yuan, R., and Carbaugh, D. (2007). Effects of NAA, AVG, and 1-MCP on ethylene biosynthesis, preharvest fruit drop, fruit maturity, and quality of 'Golden Supreme' and 'Golden Delicious' apples. *Hortscience* 42, 101–105.

Yuree, L., Yoon, T. H., Lee, J., Jeon, S. Y., Lee, J. H., Lee, M. K., et al. (2018). A lignin molecular brace controls precision processing of cell walls critical for surface integrity in *Arabidopsis*. *Cell* 173, 1468–1480. doi: 10.1016/j.cell.2018.03.060

Zheng, S. Q., Mo, X. R., Zhu, C., and Zeng, G. W. (1999). Study on the formation of silique dehiscence susceptabil ity in oilseed rape. *J. Zheji. Univ. (Agricult. Life Sci.)* 25, 462–466.

Zuniga-Mayo, V. M., Reyes-Olalde, J. I., Marsch-Martinez, N., and De Folter, S. (2014). Cytokinin treatments affect the apical-basal patterning of the *Arabidopsis gynoecium* and resemble the effects of polar auxin transport inhibition. *Front. Plant Sci.* 5:191. doi: 10.3389/fpls.2014.00191

Conflict of Interest: The authors declare that the research was conducted in the absence of any commercial or financial relationships that could be construed as a potential conflict of interest.

frontiers in Plant Science

ORIGINAL RESEARCH
published: 12 June 2020
doi: 10.3389/fpls.2020.00727

Development of a *Brassica napus* (Canola) Crop Containing Fish Oil-Like Levels of DHA in the Seed Oil

*James R. Petrie[1†], Xue-Rong Zhou[1], Antonio Leonforte[2], Jason McAllister[3], Pushkar Shrestha[1], Yoko Kennedy[1], Srinivas Belide[1], Greg Buzza[2], Nelson Gororo[2], Wenxiang Gao[4], Geraldine Lester[1], Maged P. Mansour[5], Roger J. Mulder[6], Qing Liu[1], Lijun Tian[1], Claudio Silva[7], Noel O. I. Cogan[8], Peter D. Nichols[9], Allan G. Green[1], Robert de Feyter[1], Malcolm D. Devine[10] and Surinder P. Singh[1]**

[1] CSIRO Agriculture and Food, Canberra, ACT, Australia, [2] Nuseed Pty Ltd., Horsham, VIC, Australia, [3] Nuseed Pty Ltd., Laverton North, VIC, Australia, [4] Nuseed Americas Inc., Woodland, CA, United States, [5] CSIRO Agriculture and Food, Werribee, VIC, Australia, [6] CSIRO Manufacturing, Clayton, VIC, Australia, [7] Nufarm Ltd., Laverton North, VIC, Australia, [8] Department of Primary Industries, Melbourne, VIC, Australia, [9] CSIRO Ocean & Atmosphere, Hobart, TAS, Australia, [10] Nuseed Global, Calgary, AB, Canada

OPEN ACCESS

Edited by:
Ian Douglas Godwin, The University of Queensland, Australia

Reviewed by:
Jay Shockey, United States Department of Agriculture, United States
Enrique Martinez Force, Instituto de la Grasa (IG), Spain

***Correspondence:**
Surinder P. Singh
Surinder.Singh@csiro.au

†Present address:
James R. Petrie, Nourish Ingredients Pty Ltd., Brighton, QLD, Australia

Specialty section:
This article was submitted to Plant Biotechnology, a section of the journal Frontiers in Plant Science

Received: *25 February 2020*
Accepted: *06 May 2020*
Published: *12 June 2020*

Citation:
Petrie JR, Zhou X-R, Leonforte A, McAllister J, Shrestha P, Kennedy Y, Belide S, Buzza G, Gororo N, Gao W, Lester G, Mansour MP, Mulder RJ, Liu Q, Tian L, Silva C, Cogan NOI, Nichols PD, Green AG, de Feyter R, Devine MD and Singh SP (2020) Development of a Brassica napus (Canola) Crop Containing Fish Oil-Like Levels of DHA in the Seed Oil. Front. Plant Sci. 11:727. doi: 10.3389/fpls.2020.00727

Plant seeds have long been promoted as a production platform for novel fatty acids such as the ω3 long-chain (≥ C_{20}) polyunsaturated fatty acids eicosapentaenoic acid (EPA) and docosahexaenoic acid (DHA) commonly found in fish oil. In this article we describe the creation of a canola (*Brassica napus*) variety producing fish oil-like levels of DHA in the seed. This was achieved by the introduction of a microalgal/yeast transgenic pathway of seven consecutive enzymatic steps which converted the native substrate oleic acid to α-linolenic acid and, subsequently, to EPA, docosapentaenoic acid (DPA) and DHA. This paper describes construct design and evaluation, plant transformation, event selection, field testing in a wide range of environments, and oil profile stability of the transgenic seed. The stable, high-performing event NS-B50027-4 produced fish oil-like levels of DHA (9–11%) in open field trials of T_3 to T_7 generation plants in several locations in Australia and Canada. This study also describes the highest seed DHA levels reported thus far and is one of the first examples of a deregulated genetically modified crop with clear health benefits to the consumer.

Keywords: ω3 long-chain polyunsaturated fatty acid, DHA, canola, elite event, field trial

INTRODUCTION

The long-chain (≥ C20) polyunsaturated fatty acids (LC-PUFA) such as eicosapentaenoic acid (EPA; 20:5ω3) and docosahexaenoic acid (DHA; 22:6ω3) are essential components of animal cell membranes and important contributors to human health. Certain tissues and organs, including eyes, brain and heart, are particularly rich in EPA and DHA and there is an abundance of evidence supporting the beneficial role of EPA and/or DHA in promoting eye health, heart health and cognitive function (Simopoulos, 1999; Martin, 2011; Hashimoto et al., 2017). Although primary production of these fatty acids occurs predominantly in ocean-based microalgae and some bacteria, the major sources of EPA and DHA for human consumption are oil extracted from various fish species, either wild or farmed (for example, salmon, trout, anchoveta, menhaden, etc.) that accumulate these LC-PUFA through the marine food web or through their supplied diet

(Abedi and Sahari, 2014). Various assessments indicate that most humans consume lower than optimal amounts of EPA and DHA required, and the total ocean supply of LC-PUFA is insufficient to meet the recommended daily intake for the global population (Stark et al., 2016). Rising human populations and increased awareness of the health benefits of LC-PUFAs on one hand, and restrictions on the allowable catch of the marine sources of LC-PUFAs on the other, are expected to create a shortage of these key nutrients in the near future (Adarme-Vega et al., 2014; Sprague et al., 2017).

There is a compelling sustainability argument in favor of supplementing the marine supply of LC-PUFA with a land-based source (Napier et al., 2015). High oil yield and relatively low production costs of oil crops would provide economic and sustainable production platform of oil containing EPA and DHA. We identified canola (*Brassica napus* L.) as a potential oil crop for EPA and DHA production. Canola seed production is up to 4 T.ha^{-1}, with 40–45% seed oil content. It has broad agronomic and geographic adaptation, great genetic resources and substantially developed germplasms. If canola can be used producing DHA at levels of 10–15% in its oil, 2.5 million ha of such canola (about 2% of global cultivation of major oilseed crops) would provide the equivalent amount of DHA currently harvested from all fish oils (Zhou et al., 2019).

In the past 15 years, two approaches have been taken to produce EPA and DHA in oil crops: first, the expression of the microalgal polyketide synthase system (Metz et al., 2001) which synthesizes DHA from malonyl-CoA (Walsh et al., 2016) and, second, the stepwise extension of the endogenous higher plant lipid biosynthetic system through addition of the alternate fatty acid desaturases and elongases from the more conventional aerobic pathway to produce EPA and DHA (Robert et al., 2005; Wu et al., 2005; Petrie et al., 2012; Ruiz-Lopez et al., 2014). Substantially higher total levels of EPA and DHA have been reported in plant seeds by engineering the aerobic desaturase and elongase pathway, particularly the Δ6-desaturase mediated version of this pathway (**Figure 1**). The successful accumulation of EPA and DHA into the seed oil of plant hosts by this method has been reported in the model species *Arabidopsis thaliana* (Robert et al., 2005; Petrie et al., 2012). This technology was subsequently transferred to *Camelina sativa* as a minor oilseed crop by assembling five to seven genes from marine microalgae and fungi to engineer an EPA-alone or an EPA+DHA oil (Ruiz-Lopez et al., 2014). Independent work by our group, harnessing expression of a different set of seven transgenes from yeast and microalgae, demonstrated DHA production of up to 12.4% of total fatty acids in oil from transgenic *C. sativa*, similar to the level found in DHA-rich fish oil, and an EPA content of 0.8–3.3% (Petrie et al., 2014). More recently, Usher et al. (2017) reported 16–17% EPA, and 4–5% EPA plus 4% DHA in field tests of an EPA and DHA constructs, respectively, in field-grown *C. sativa*.

In this paper we report the successful translation of our high DHA technology, initially demonstrated in *Arabidopsis* and *C. sativa*, into canola (*B. napus*), the world's second most important annual oilseed crop, to provide a highly scalable platform for commercially sustainable DHA production. We describe construct design and evaluation, plant transformation, event selection, field testing in a wide range of environments, and stability testing of the transgenic seed and oil. The completion of molecular, biochemical, genetic stability and agronomic characterisation of this canola event has resulted in regulatory approval for cultivation of the crop in Australia for human and animal consumption of the oil (FSANZ, 2017; OGTR, 2018) and cultivation approval in the USA. Similar approvals are pending in Canada.

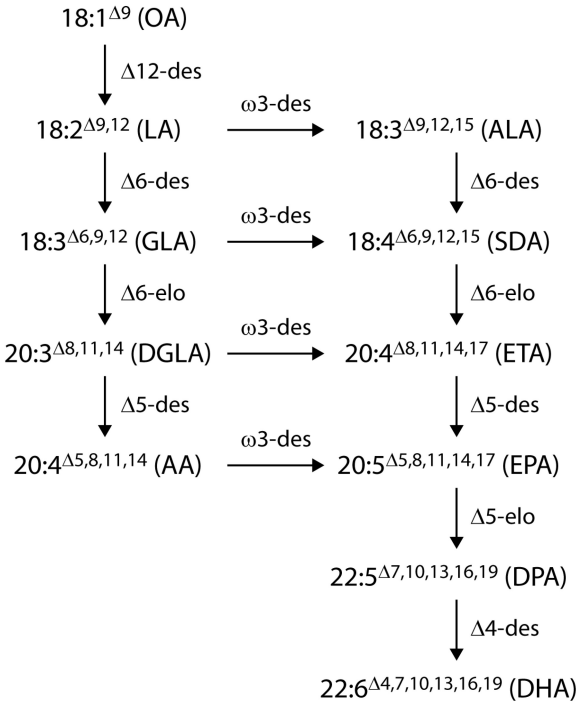

FIGURE 1 | The Δ6-desaturase aerobic long-chain (≥ C20) polyunsaturated fatty acid synthesis pathways. Desaturases are denoted by 'des' and elongases by 'elo'. The ω6 pathway runs in parallel with the ω3 pathway with fatty acids converted across by the action of an ω3-desaturase. Abbreviations are OA, oleic acid; LA, linoleic acid; ALA, α-linolenic acid; GLA, γ-linolenic acid; SDA, stearidonic acid; DGLA, dihomo-γ-linolenic acid; ETA, eicosatetraenoic acid; AA, arachidonic acid; EPA, eicosapentaenoic acid; DPA, docosapentaenoic acid; DHA, docosahexaenoic acid.

MATERIALS AND METHODS

Oligonucleotides

The oligonucleotides used in this work were chemically synthesized by Sigma-Aldrich (Castle Hill, NSW, Australia). The oligonucleotide sequences are listed in **Supplementary Table 1**.

Plasmid Construction

A set of binary vector GA7 (Petrie et al., 2012) variants GA7_mod-B, GA7_mod-D, GA7_mod-E, GA7_mod-F and GA7_mod-G were constructed. The seven fatty acid biosynthesis genes were chemically synthesized at GeneArt (Regensburg, Germany) as a single 19,750 bp fragment flanked with *Not*I sites, which was then cloned into vector pJP3416 to generate

GA7 (Petrie et al., 2012). The vector GA7_mod-B was built by re-arranging the two elongase genes and replacing the promoter for Micpu-Δ6D in the existing vector GA7 (**Figure 2A**). A fragment with Pro-FAE1::Pyrco-Δ6E::Ter-Lectin was first cloned into the two *Sbf*I sites of GA7 to replace Pro-FAE1::Pyrco-Δ5E::Ter-Lectin near the left border with Pyrco-Δ6E, generating intermediate GA7_mod-A. The original Micpu-Δ6D expression cassette and the adjacent Pyrco-Δ6E in GA7_mod-A was replaced with a *Pme*I-*Asc*I fragment containing Pro-Cnl2::Micpu-Δ6D::Ter-Cnl2 and Pro-FAE1::Pyrco-Δ5E to

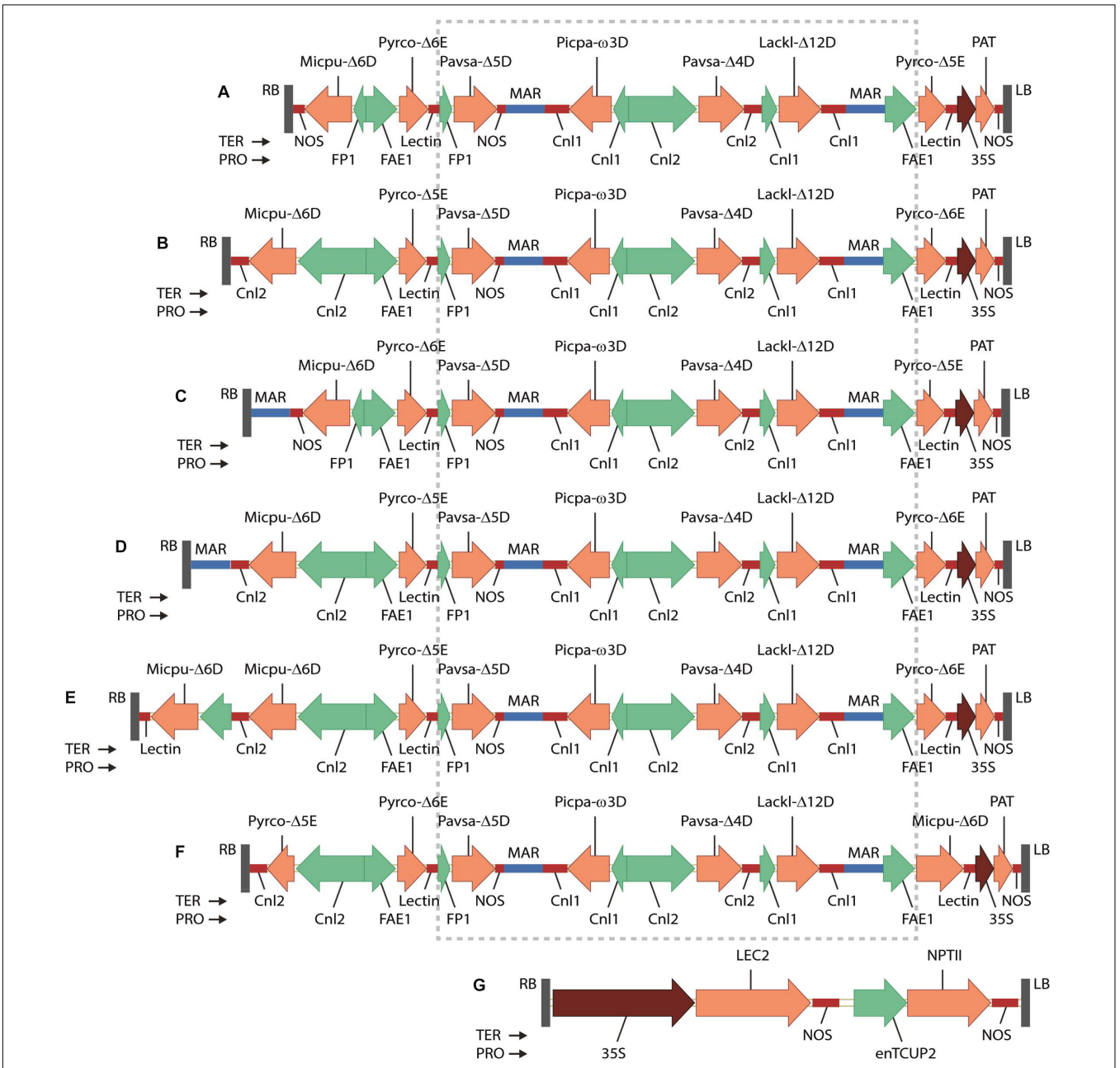

FIGURE 2 | T-DNA regions of binary vectors tested in this study shown in the right border (RB) to left border (LB) orientation: **(A)** GA7; **(B)** GA7_mod-B; **(C)** GA7_mod-D; **(D)** GA7_mod-E; **(E)** GA7_mod-F; **(F)** GA7_mod-G; **(G)** pJP3129. The boxed region of the GA7 series is common to all constructs. Genes are: Micpu-Δ6D, *Micromonas pusilla* Δ6-desaturase; Pyrco-Δ6E, *Pyramimonas cordata* Δ6-elongase; Pavsa-Δ5D, *Pavlova salina* Δ5-desaturase; Picpa-ω3D, *Pichia pastoris* ω3-desaturase; Pavsa-Δ4D, *P. salina* Δ4-desaturase; Lackl-Δ12D, *Lachancea kluyveri* Δ12-desaturase; Pyrco-Δ5E, *P. cordata* Δ5-elongase; PAT, phosphinothricin N-acetyltransferase from *Streptomyces viridochromogenes*. Promoters are: FP1, truncated napin promoter from *Brassica napus*; FAE1, *Arabidopsis thaliana* FATTY ACID ELONGATION1 promoter; Cnl1, *Linum usitatissimum* CONLININ1 promoter; Cnl2, *L. usitatissimum* CONLIIN2 promoter; 35S, Cauliflower mosaic virus 35S promoter with duplicated enhancer region. Terminators are: NOS, *Agrobacterium tumefaciens* NOS; Lectin, *Glycine max* Lectin; Cnl1, *L. usitatissimum* conlinin1; Cnl2, *L. usitatissimum* conlinin2. MAR denotes the Rb7 matrix attachment region from *Nicotiana tabacum*.

yield the final vector, GA7_mod-B (**Figure 2B**). A fragment containing *Nicotiana tabacum* Rb7 matrix attachment region (MAR) was inserted at *Pme*I site between right border and Micpu-Δ6D expression cassette in GA7, generating GA7_mod-D (**Figure 2C**). The same MAR fragment was also inserted into same *Pme*I site between right border and NOS terminator in GA7_mod-B, generating GA7_mod-E (**Figure 2D**). The variants GA7_mod-F and GA7_mod-G were previously reported (Petrie et al., 2014; **Figures 2E,F**). All these binary vectors were transferred to *Agrobacterium tumefaciens* strain AGL1 (Lazo et al., 1991).

Expression of Seed Specific Constructs in LEC2-Induced Canola Somatic Embryos

B. napus somatic embryos were generated by co-transformation of a 35S::LEC2 vector with a seed-specific GA7 construct variant as previously described (Belide et al., 2013). The DHA levels as a percentage of the somatic embryo total fatty acids were analyzed by gas chromatography (see below). The conversion efficiencies of each enzymatic step involved in DHA biosynthesis pathway are calculated as the sum of the products divided by the sum of the substrate and the products.

Canola Stable Transformation

Several canola varieties were used as transformation recipients, including the 'Oscar' cultivar and elite commercial varieties such as AV-Jade, AV-Spectrum, AV-Zircon, and the high-oleic 'Monola' variety. *B. napus* cotyledonary petioles were transformed with the binary vector GA7_mod-B essentially as described by Belide et al. (2013) with slight modification. Briefly, infected cotyledonary petioles were cultured on MS media as described (Belide et al., 2013) except using 5 mg L^{-1} PPT for selection with a biweekly subculture. Shoots from the resistant callus were transferred to shooting media (MS media with 0.1 mg L^{-1} gibberelic acid + 3 mg L^{-1} $AgNO_3$ + 250 mg L^{-1} cefotaxime + 5 mg L^{-1} PPT) to extend the shoots for another two weeks. Selected healthy shoots with one or two leaves were transferred to rooting media (1/2 MS with 1 mg L^{-1} NAA + 20 mg L^{-1} ADS + 3 mg/mg L^{-1} $AgNO_3$ + 250 mg L^{-1} cefotaxime). DNA was isolated from leaf with plant DNA isolation kit (Bioline, Alexandria, NSW, Australia) to confirm the T-DNA insertion by PCR. The confirmed lines were transferred to pots and grown in glasshouse.

Characterization of T-DNA Copy Number by Digital PCR

Genomic DNA was isolated from leaf tissues as described by Mieog et al. (2013) using TissueLyser II (Qiagen, Hilden, Germany). Primers and probes were designed with Primer 3 plus[1] (Rozen and Skaletsky, 1999) and tested in AutoDimer[2] to study the potential interaction between the reference and target oligonucleotide trio (**Supplementary Table 1**). High-mobility-group (HMG) protein, a single copy in the genome of *Brassica* species (Weng et al., 2004), was used as a reference. The primer set for HMG protein (HMG-F/HMG-R) combined with the HMG-P probe was designed to detect a 73 bp of HMG. As for the target genes, we used PPT selectable marker and delta-6 desaturase (Δ6D) fragment, positioned at the left and right borders, respectively, in GA7_mod-B. The PPT-F/PPT-R primer pair combined with PPT-P, and the Δ6D-F/Δ6D-R primer pair combined with Δ6D-P, were used to amplify fragments of 82 and 89 bp, respectively. The reference gene probe was labeled with 5′HEX (hexachloro-fluorescein) and the transgene probes were labeled with 5′FAM (6-fluorescein). Probes were doubled-quenched with ZEN™ and Iowa Black Hole Quencher 1. We obtained primers and probe from SIGMA and Integrated DNA Technologies Inc., respectively.

A range of 50 to 100 ng genomic DNA was digested with 4 units each of *Bam*HI and *Eco*RI (New England Biolabs, Ipswich, MA, United States) in a final volume of 20 μL, at 37°C, 4 h to overnight. Digested DNA was added to the Bio-Rad 2XddPCR™ Supermix for Probes (no dUTP) (Bio-Rad, Gladesville, Australia) at concentrations ranging from 20 to 120 ng DNA per 20 μL dd-PCR reaction. TaqMan assay primers and probes were used at the final concentrations of 900 and 250 nM, respectively. For triplex assay, Δ6D-P was reduced to 50 nM. Samples were placed onto Droplet Generator QX200™ (Bio-Rad) or QX200AutoDG and heat sealed with a pierceable foil heat seal with PX1 PCR plate sealer (Bio-Rad). Plates were placed in C1000 Thermal Cycler (Bio-Rad) and reactions were run with the following cycles: 95°C for 10 min followed by 40 cycles at 94°C for 30 s; 61°C for 1 min, then 98°C for 10 min and maintained at 12°C finally. The ramping rate of 2.5°C/s in all temperature change steps were used. After amplification, the plates were loaded onto the QX200 Droplet Reader (Bio-Rad). Data analysis was performed using Quanta soft™ software (Bio-Rad).

Sequencing of T-DNA Integration Site in Elite Events

Genomic DNA of eight T_3 and T_4 lines were randomly sheared using the Covaris Technology (Covaris, Woburn, MA, United States) and fragments with size of 700–900 bp were collected. Both ends of the sheared DNA fragments were ligated with a single Illumina adaptor (universal primer PE2, **Supplementary Table 1**). A total of 78 vector-specific primers (data not shown) were designed to span the whole GA7_mod-B vector (31,564 bp). These primers were ligated to another Illumina adaptor (universal primer PE1, **Supplementary Table 1**). T-DNA containing fragments were enriched by nested PCRs with the Illumina universal primer PE2 and vector-specific primers, followed by further enrichment through PCR amplification with Illumina universal primer PE2 and the T-DNA linked Illumina universal primer PE1. Sequencing of fragments from both ends (paired end) was performed on an Illumina MiSeq (Illumina, San Diego, CA, United States) with Illumina universal primers PE2 and PE1, generating 2 × 250 bp sequencing reads. More than 250,000 raw reads were generated. The raw reads were trimmed and cleaned filtered with the following criteria by a custom computational script written in Perl. The reads were trimmed if > 3 "N" nucleotides were

[1]http://www.bioinformatics.nl/cgi-bin/primer3plus/primer3plus.cgi
[2]http://www.cstl.nist.gov/strbase/AutoDimerHomepage/AutoDimerProgramHomepage.htm

called, > 3 nucleotides had PHRED quality score ≤ 20, or the median PHRED score ≤ 20. The reads were discarded when sequence read length was < 75 nucleotides, or mate pair was discarded, or if Illumina adaptor was missing. The reads passed the criteria and kept by Perl were then passed through the Cutadapt v1.4.1 (Martin, 2011) program to trim any remaining adaptor sequences. After the two-step quality filtering successfully removed all of these adaptors, about 10% of the raw sequence reads were removed. The clean sequences of the enriched fragments were then aligned to 31,564 bp reference sequences of vector, using BWA software package[3] and the MEM Algorithm was used to generate T-DNA sequence in FASTA format. The alignments were then converted into an indexed BAM file using the SAMtools software package[4] and can be visualized in software packages such as Tablet[5].

The sequence reads aligned to the vector reference at only a single read of the paired-end reads were used for further analysis. Specific sub-sets of reads generated in the right and left border regions were specifically targeted for junction sequence from canola genome by aligning to the reference genome sequences of *B. napus* ($2n = 4x =$ AACC[6]), *B. rapa* ($2n = 2x =$ AA[7]) and *B. oleracea* ($2n = 2x =$ CC[8]). The identified sequence reads were assembled using the CAP3 software[9], and BLASTed to the reference genomes of *Brassica*. The contigs that had significant matches to the reference sequence of both *Brassica* and the binary vector were used to define the copy number and integration sites of T-DNA inserts in DHA canola.

Genetic Stability of the T-DNA Inserts in DHA Canola

A total of 100 seeds from T_3 to T_7 generation (20 seeds / generation) of DHA canola were used for DNA extraction based on LGC Oktopure DNA Extraction System (LGC, Boston, MA, United States). DNA concentration was measured with NanoDrop 8000 UV-Vis Spectrophotometers (Thermo Fisher Scientific, Wilmington, DE, United States). One non-GMO control (AV-Jade) and one event positive control (transgenic GA7_mod-B *Brassica napus* event) were included. This positive control was previously used to characterize DHA canola through PCR amplicon sequencing.

Four assays (EAD02DJ517, EA05DJ380, EA02UJ284 and EA05UJ200) were designed with Primer3Plus[10] for primer melting temperature (Tm) of 59–60°C. Each assay was targeting one of the four junction regions of the two T-DNA copies in DHA canola. To facilitate the electrophoresis with four assays simultaneously, the assays were designed with distributed amplicon size (517, 380, 284 and 200 bp). All four assays spanned the junctions of *B. napus* genomic sequence and the T-DNA inserts.

PCR amplification was performed in 25 μL reaction according to the recipe of OneTaq PCR Amplification Kit (New England Biolabs, Ipswich, MA, United States). Touchdown PCR was used for amplification with the following parameters: 1 cycle of 94°C for 30 s, followed by 6 cycles of 94°C for 30 s, 64–58°C (dropping 1.0°C per cycle) for 20 s and 68°C for 30 s, and followed by 33 cycles of 94°C for 30 s, 58°C for 20 s and 68°C for 30 s with an final extension at 68°C for 5 min.

Each DNA sample was PCR amplified individually with each assay. After PCR amplification, 2.25 μL of PCR amplicons from each of the four assays were mixed together with 1.0 μL of 10 × Ambion gel loading buffer (Thermo Fisher Scientific, Wilmington, DE, United States) for electrophoresis on 1.5% agarose gel.

Field Evaluation

Event NS-B50027-4 was grown in the field at several Australian sites in 2015 and 2016 and in Canada in 2016 to determine both agronomic performance and whether growing conditions affected DHA synthesis and accumulation. AV Jade and other non-transgenic varieties, and the A02 and A05 segregants were also included in the 2016 trials. Canola was grown in open field plots or in pure seed production tests under the relevant isolation and monitoring regulations, and agronomic parameters, including grain and oil yield and the fatty acid profiles of harvested seed were evaluated. The experimental sites were at different locations with varying environments for soil type, growing season rainfall and agronomic management practices. When available, irrigation was supplied on a limited basis at some sites as required to supplement rainfall. In all cases plot size was 10 m^2 and seeding rate adjusted on the basis of seed size and germination percentage to approximately 35 plants per m^2 in Australia and 70 plants per m^2 in Canada. Each trial experiment was designed with a randomized block consisting of 5 replicates with 12–14 entries (combination of transgenic lines and 6–8 check cultivars). The Australian cultivar entries represented a range of agronomic diversity including plant habit, phenology and yield potential in the Australian cropping zones. These cultivars are open pollinated and have been described in the Australian National Variety Testing Program and Regional annual crop reports[11]. AV-Jade is the non-transformed isoline of NS-B0050-24. The two Canadian commercial cultivars (DK7444 and LL130) were high-yielding, herbicide-tolerant hybrids. The transgenic lines included T_3, T_5 and T_7 generations of NS-B0050-24. In 2016, segregant lines containing the A05 or A02 loci were included in the trials.

Agronomic data were collected for each plot in all trials including plant emergence (number of emerged plants per m^{-2} approximately 14 to 24 days post-sowing; plant vigor (estimate of ground cover at about the 6-leaf stage, using a 1 to 9 score, where 1, 5 and 9 represent ≤ 10%, 40–50% and >90% ground cover, respectively); flowering time (number of days from sowing to when 50% of plants had at least one open flower); flowering

[3]http://bio-bwa.sourceforge.net/

[4]http://samtools.sourceforge.net/

[5]https://ics.hutton.ac.uk/tablet/

[6]http://www.genoscope.cns.fr/blat-server/cgi-bin/colza/webBlat

[7]http://brassicadb.org/brad/blastPage.php

[8]http://plants.ensembl.org/Brassica_oleracea/Tools/Blast?db=core

[9]http://doua.prabi.fr/software/cap3

[10]http://primer3plus.com/cgi-bin/dev/primer3plus.cgi

[11]http://www.nvtonline.com.au

end time (days from sowing to when 90–95% of plants had no open flowers); flowering duration (difference in days between flowering time and end flowering time); plant height (cm) at maturity; seed shattering (seed collected over a 2-week period in two trays (total 0.12 m^{-2}) placed between rows); lodging resistance (1 to 9 score based on plant angle from the base of the plant, where 1 = erect plants, 5 = moderate lodging and 9 = complete lodging); plant stand at harvest (plants in two 1-m^{-2} quadrants within each plot); and plant survival (plant count as a % of site mean for plant emergence).

Severity symptoms of Blackleg leaf from representative pathogens *Leptosphaeria maculans* and *L. biglobosa* were recorded as scores of 1 to 9, where 1 = 0–5%, 5 = 20–25% and 9 $\geq$ 40% leaf infection, respectively across five sites. Symptoms associated with cankering and stem breakage were not observed. Opportunistic disease or insect stress that could be recorded were also observed in all field trials.

Grain was harvested when seed was physiologically mature and dry (∼7% moisture content) using a plot harvester and yield recorded (metric tons per ha). Grain moisture at harvest was determined on a bulk sample using a hand-held moisture meter (Wile 65 Moisture Meter, Farmcomp Agroelectronics; Australia) or with a Harvest Master Classic Grain Gauge with an Allegro CX (Juniper Systems; Logan, UT, United States).

Restricted estimated likelihood analysis was undertaken on factors measured using ASReml procedures in GenStat (Version 17). A statistical method with linear mixed model was used to account for field spatial variation. This method has been extensively described and used for plant breeding in field and genetics research (Smith et al., 2001).

Generation of A02 and A05 Segregants

A backcrossing program was undertaken in glasshouses at Nuseed (Horsham, VIC, Australia) to transfer the GMO inserts from NS-B50027-4 to non-GMO canola genotypes. Segregating progeny from the BC1F3 generation varying for the presence or absence of locus inserts (A02, A05) and zygosity were identified using linked molecular markers. The segregant populations were used to investigate the individual and additive contributions of the two loci to the phenotypic expression of higher DHA in mature seed.

Seed Oil Content Analysis

Oil content was determined using an Spinlock SLK-200 Benchtop NMR Spectrometer (Cordoba, Argentina). Approximately 5–8 g of seed was accurately weighed into an NMR tube for analysis, and seed oil content generated by a software calibration created using 20 reference canola samples with known % oil content. The % oil contents of these 20 samples were determined by gravimetric oil extraction (extraction method based on AOF method AOF 4-1.25).

Seed Moisture Content

For moisture correction of % oil results (field trial seed), moisture content was determined using an oven drying method based on AOF method 4-1.5. Five grams of pre-weighed seeds were dried in an open tin at 130°C for 1 hr. Samples were cooled in a desiccator for 40 min then weighed and % moisture determined as % loss of mass.

Fatty Acid Profile Analysis

Fatty acid profile analysis of LEC2-induced somatic embryo and canola seeds harvested from CSIRO glasshouses was performed. For pooled seed, 100 mg of seed was crushed in a mixture of 0.9 mL chloroform/methanol (2/1, v/v) in the argon-filled Safe-lock tubes (2.0 mL; Eppendorf) using a metal ball (0.5 cm diameter) and Reicht Tissue lyser (Qiagen) at a frequency of 22 Hz. The homogenate was transferred to a 2 mL glass vial and the solvents were evaporated under the nitrogen flow on a 40°C hot plate. Fatty acid methyl esters (FAME) of the seed homogenate was carried out by incubating the sample in 0.7 mL of 1 N methanolic-HCl (Supelco) at 80°C for 2 h. After cooling the sample to room temperature, 0.3 mL 0.9% NaCl and 0.6 mL hexane were added and vortexed for 5 min. The FAME layer was separated by centrifuging the mixture at 1700 × *g* for 5 min and transferred to a GC vial. FAME were analyzed by GC as described in Zhou et al. (2011). For single seed analysis, the seed was transferred to the argon-filled 2 mL GC vial and the seed was pressed by a metal rod to crack the seed coat. FAME preparation and analysis were carried out essentially as mentioned above, except the seed was incubated in 0.5 mL 1 N methanolic-HCl and FAME were extracted in 0.3 mL hexane. FAME were transferred to a glass insert inside a GC vial. The somatic embryo was freeze dried. The FAME GC analysis was performed as above.

Fatty acid profile analysis of the field trial harvested seed was performed at Nuseed's facility in Laverton, VIC, Australia. Pooled seed samples from individual plants (typically 20 seeds) were hand-crushed in a culture tube using a metal crushing tool. Seed samples were ground in a Cole-Parmer 4301-02 water-cooled analytical mill, fitted with a reduction lid for small samples, and a chilled water-circulator attached. Approx. 5–7 g of seed was ground, and a subsample transferred to a culture tube. The seed oil was extracted with petroleum ether and the solvent was then evaporated under a stream of nitrogen. An aliquot of the seed oil was derivatised using thermally assisted hydrolysis and methylation (THM). The derivatising reagent was a 1 in 4 dilution of Meth Prep II (Grace™ Alltech™) with the resulting reagent being 1.25% 3-(trifluoromethyl)phenyltrimethylammonium hydroxide in methanol. In brief, 10 μL of seed oil was transferred to a test tube and 1990 μL of 50:50 chloroform:methanol (with 0.01% BHT) was added and vortexed. 100 μL of the solution was transferred to a 9 mm-mouth GC vial with 400 μL flat-bottomed glass insert. A further 50 μL of 50:50 chloroform:methanol was added followed by 50 μL of 1.25% Meth Prep II solution. The vial was capped, vortexed and placed in a heating block at 40°C for 30 min. The FAME were analyzed using a Shimadzu GC-2010plus fitted with an SGE BPX-70 capillary column (0.32 mm i.d. and 0.25 μm film thickness), a FID, a split/splitless injector and an AOC-20S auto sampler and AOC-20I injector. Hydrogen was the carrier gas and was set to constant linear velocity mode of either 40 or 65 cm/sec. Injection volume was either 0.5 or 1 μL with a split ratio of 25:1. The injector was held at 250°C and the detector was held at 300°C. For standard screening, a

30 m column was used. After injection of 0.5 μL sample, the oven temperature was held at 140°C for 1.2 min, raised to 172°C at a rate of 6°C/min, then raised to 200°C at a rate of 10°C/min, held for 1.8 min and finally raised to 250°C at a rate of 50°C/min and held for 0.5 min. The carrier gas linear velocity was 65 cm/sec. The standard screen provided data for all fatty acids in the long-chain omega 3 synthesis pathway leading from oleic acid to DHA. For detailed profiles, a 60 or 90 m BPX-70 column was used. The 90 m column consisted of a 30 m and a 60 m BPX-70 column joined together with a GlasSeal^{TM} capillary column connector. After injection of a 1 μL sample, the oven temperature was held at 50°C for 4 min, raised to 140°C at 50°C/min, raised to 232°C at 3°C/min and finally raised to 250°C at 50°C/min and held for 1 min. The carrier gas linear velocity was 40 cm/sec. The detailed profile provided fatty acid results for all the major and many of the minor fatty acids. Fatty acid profiles were quantified using area normalization with Shimadzu LabSolutions software.

Seed Oil Profile Stability

Wild type (cultivar AV-Jade) and transgenic seeds, either freshly harvested or stored at 4°C, 24°C or 32°C for 6 months, were used in the determination of oil quantity and fatty acid profile. Total lipids were extracted from the seeds and the amount and the compostion of fatty acids were quantified by GC analysis.

Fatty Acid Positional Analysis in Seed Oil and Triacylglycerols

Positional analysis of DHA in purified TAG from T_4 homozygous seeds was performed by ^{13}C NMR analysis as described in Petrie et al. (2014).

RESULTS

Metabolic Engineering of *B. napus* to Produce DHA

We designed several candidate constructs (**Figure 2**) to optimize promoter choice for individual genes as well as the order and orientation of genes in the expression vector. Earlier work had demonstrated the functionality of our selected gene set (*Lachancea kluyveri* Δ12-desaturase, *Pichia pastoris* ω3-desaturase, *Micromonas pusilla* Δ6-desaturase, *Pyramimonas cordata* Δ6-elongase, *Pavlova salina* Δ5-desaturase, *P. cordata* Δ5-elongase, and *P. salina* Δ4-desaturase) in plant seeds (Petrie et al., 2013, 2014). The additional constructs were designed in attempts to optimize both the conversion of native plant fatty acid substrates to DHA and reduce accumulation of intermediate fatty acids. GA7_mod-B (**Figure 2B**) was produced from the parental construct GA7 (Petrie et al., 2013) using a combination of DNA syntheses to produce new DNA fragments and restriction enzyme cloning to swap the position of the Δ5- and Δ6-elongases. The Δ6-desaturase promoter was also changed from the truncated *B. napus* napin (FP1) promoter to the *Linum usitatissimum* conlinin2 promoter (Truksa et al., 2003). These changes sought to increase the Δ6-desaturation of ALA to SDA and the Δ6-elongation of SDA to ETA; the Δ5-elongase efficiency in the original GA7 construct was exceptionally high, but the relatively low Δ6-elongase activity had resulted in the accumulation of SDA in both *A. thaliana* and *C. sativa*. Additional constructs, GA7_mod-D and GA7_mod-E, were generated from GA7 and GA7_mod-B, respectively, and contained a third matrix attachment region (MAR; Halweg et al., 2005) spacer between the T-DNA right border and the Δ6-desaturase expression cassette. This MAR insertion was designed to 'insulate' the Δ6-desaturase from the *B. napus* genomic DNA because the close proximity of transgenes to genomic DNA regulatory elements might impair transgene expression. GA7_mod-G switched the positions of the Δ6-desaturase and Δ6-elongase coding regions in the GA7_mod-B format. Finally, GA7_mod-F was based on GA7_mod-B, but contained an additional Δ6-desaturase expression cassette (*A. thaliana FAE1* promoter::*M. pusilla* Δ6-desaturase::*Glycine max* lectin terminator). This variation was designed to both increase the Δ6-desaturase transcript abundance and broaden the expression window by overlapping the FAE1 promoter (Rossak et al., 2001) with the Cnl2 seed storage protein promoter. Finally, a different codon usage was used for the additional Δ6-desturase coding region to avoid any potential secondary structure and silencing issues. The same plant selectable marker, *Streptomyces viridochromogenes* phosphinothricin-N-acetyltransferase (PAT), was used in all vectors.

Brassica napus seedling explants were co-transformed with a 35S::LEC2 binary vector (pJP3129, **Figure 2G**) and one of the binary vectors GA7_mod-B, GA7_mod-D, GA7_mod-E, GA7_mod-F, or GA7_mod-G. Multiple somatic embryos were generated and their fatty acid profiles analyzed. Representative conversion efficiencies for each construct variant in this somatic embryo assay are shown in **Supplementary Table 2**. GA7_mod-B embryos were generally found to have a high conversion efficiency from SDA through to DHA, although Δ6-desaturation was consistently low, with only a quarter of the ALA being converted. Δ6-elongation was high in this variant (91.6%) without a concomitant reduction in Δ5-elongation. In contrast, the Δ6-elongase efficiency in GA7_mod-D, which differed from the original GA7 parent construct only in the addition of a MAR spacer at the right border, was lower at 69.8%. Δ6-desaturation was not greatly increased in this variant, although it is difficult to conclude that border spacing is not effective in the somatic embryo assay. The addition of a second Δ6-desaturase in GA7_mod-F did increase activity at this step, indicating that expression level was contributing to conversion levels. Finally, the Δ6-desaturation in GA7_mod-G was reduced as a result of switching the positions of the Δ6-elongase and Δ6-desaturase coding regions. The binary vector GA7_mod-B was selected for large-scale *B. napus* transformation.

Canola Transformation and Event Selection

Copy number varied greatly across the 1,550 T_0 *B. napus* lines generated from all varieties, ranging from 0 (presumably selection escapes) to 23, with DHA levels in T_1 seeds (seeds from the primary transformants) ranging from 0 to 8.7% based on 5 single seeds per line. **Supplementary Figures 1A,B** show the T-DNA insertion copy number and the DHA levels in

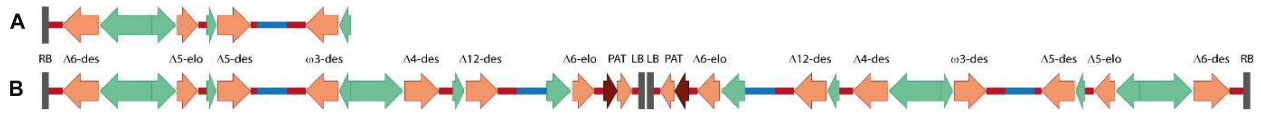

FIGURE 3 | Structure of transgenic loci in *Brassica napus* line NS-B50027-4 following transformation with binary vector GA7_mod-B (**Figure 2B**): **(A)** Partial T-DNA insertion in chromosome A02; **(B)** Two complete T-DNA inserts in chromosome A05 arranged as an inverted repeat at the left border (linking DNA is shown for illustrative purposes).

T_1 seeds of 750 representative transgenic T_0 lines in AG-Spectrum, AV-Jade and Oscar varieties. We selected low-copy (1-2) events useful for backcrossing and breeding. DHA levels in individual transgenic T_1 seed ranged from 0 to 5.6% of total fatty acids in low-copy events, with both range and average values differing between different canola varieties (**Supplementary Figure 1C**). High-DHA, low insert copy number T_1 plants were grown and selfed, and T_2 seed subjected to a further round of selection on the same criteria. This was repeated for T_2 plants, using more stringent selection criteria. Genomic DNA from the progeny of several candidate events was isolated and sequenced by Illumina sequencing to determine the structures of the transgenic loci. Ultimately, a single transgenic event, designated by the OECD Identifier NS-B50027-4, was selected for advancement. Transgenic DNA from binary vector GA7_mod-B was inserted in chromosomes A02 and A05 of the canola genome in this event. The transgenic locus at A02 consisted of a partial insertion which included the T-DNA right-border, along with intact Δ6-desaturase, Δ5-elongase, Δ5-desaturase and ω3-desaturase expression cassettes (**Figure 3A**), while the transgenic locus at A05 was comprised of two complete T-DNA right-border to left-border insertions oriented in a head-head manner (**Figure 3B**). No vector backbone (vector DNA from beyond the T-DNA border regions) was detected in the genomic DNA of event NS-B50027-4 either by Southern blot (data not shown) or Illumina sequencing of the genome using primers which spanned the complete GA7_mod-B vector. The sequences of the transgene insert and *B. napus* flanking regions at A02 and A05 were deposited in GenBank under accession numbers MP172039 and MP172040.

Fatty Acid Composition of Transgenic Lines

Initial transgenic events contained a wide range in the levels of DHA measured in the seed oil, with levels of 20–25% not uncommon and one event with 34% DHA. However, these tended to be multi-copy events. Multiple lines accumulated DHA in the 10–15% range when homozygous, including progeny from event NS-B50027-4; in comparison, bulk Peruvian anchovy oil, the major marine source, typically contains 11–12% DHA. Omega-3 fatty acid profiles, transgenic enzyme conversion efficiencies, and ω3: ω6 ratios from a range of homozygous mature seed varying in T-DNA copy number are shown in **Figure 4**, and detailed fatty acid profiles of field-grown NS-B50027-4, the A02 and A05 segregants and the parent, AV-Jade, are shown in **Table 1**. In general, fatty acid profiles were very consistent across glasshouse and multi-location field trials. As expected,

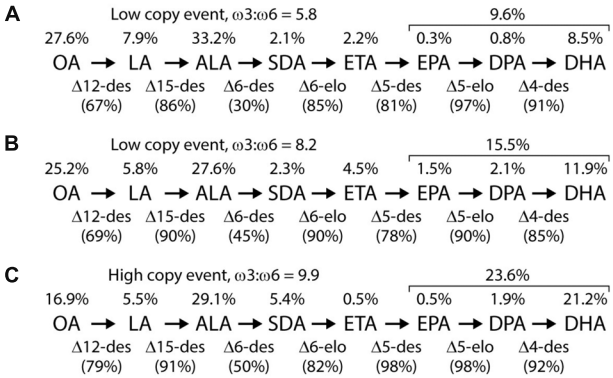

FIGURE 4 | Representative fatty acid profiles of transgenic GA7_mod-B *Brassica napus* events ranging from moderate to high levels of DHA. The bottleneck step is typically Δ6-desaturation, with other enzymatic steps tending to occur at high or very high efficiency. Bracketed values above the pathway describe the total EPA, DPA and DHA levels. Enzyme conversion efficiencies are shown in parentheses and the ω3 to ω6 ratio (all chain lengths) for each event is reported. **(A,B)** Representative events with low copy (1–3 copies), and **(C)** representative event with high copy (> 3 copies) of the T-DNA inserts.

DHA was highest in NS-B50027-4 and found at intermediate levels in plants that contained only the A05 insert. Plants that contained only the A02 partial insert had only trace levels of DHA. No DHA was detected in AV-Jade. Additionally, oleic acid (18:1ω9) content was significantly lower and ALA significantly higher in the transgenic lines. Production of novel ω6 fatty acids was typically very low in the transgenic lines. Total ω3 fatty acids increased in NS-B50027-4 and total ω6 declined, resulting in a considerably higher ω3:ω6 ratio than in the parental line (4-5 cf. < 1). Saturated fatty acid levels remained similar in all lines, at approximately 7–8% of total fatty acids. Of note, no erucic acid (22:1ω9) was produced in NS-B50027-4.

Interestingly, the lipid class distribution in seed of line NS-B50027-4 was almost identical to that in the parental cultivar Jade: triacylglycerol (TAG) made up 38.9% of total seed mass in NS-B0027-4 (39.6% in Jade), diacylglycerol (DAG) contributed 0.4% (0.3% in Jade), free fatty acids (FFA) contributed 0.3% (0.1% in Jade), and phosphatidylcholine (PC) contributed 1.1% (1.2% in Jade). Retention of DHA and intermediate fatty acids in polar lipids tended to be low relative to retention in the neutral lipids TAG and DAG. DHA was very strongly enriched (97%) in the *sn*-1/3 (α) positions of the TAG molecule (**Supplementary Figure 2**).

TABLE 1 | Mean fatty acid profile of field-derived seed oil from transgenic line NS-B50027-4, segregant progeny containing each of the transgenic loci on chromosome A05 or A02, and the parental line AV-Jade.

Fatty acid	Common name	Percent of total seed fatty acids			
		NS-B50027-4	A02 Insert	A05 Insert	AV-Jade
14:0	Myristic	0.1 ± 0.0	–	0.1 ± 0.0	–
16:0	Palmitic	4.2 ± 0.0	4.1 ± 0.0	3.9 ± 0.1	4.0 ± 0.0
16:1ω7	Palmitoleic	0.2 ± 0.0	0.2 ± 0.0	0.2 ± 0.0	0.2 ± 0.0
18:0	Stearic	2.7 ± 0.1	2.3 ± 0.1	2.4 ± 0.0	2.2 ± 0.0
18:1ω9	Oleic	42.0 ± 1.0	59.1 ± 0.3	54.6 ± 1.1	59.1 ± 0.4
18:1ω7	Cis-vaccenic	3.2 ± 0.1	3.0 ± 0.0	2.9 ± 0.1	2.8 ± 0.1
18:2ω6	Linoleic	7.0 ± 0.2	7.2 ± 0.3	11.9 ± 0.4	19.3 ± 0.2
18:3ω6	γ-Linolenic	0.4 ± 0.0	0.1 ± 0.0	0.1 ± 0.0	–
18:3ω3	α-Linolenic	20.0 ± 0.5	17.0 ± 0.2	15.9 ± 0.3	9.5 ± 0.1
20:0	Arachidic	0.8 ± 0.0	0.7 ± 0.0	0.7 ± 0.0	0.5 ± 0.0
18:4ω3	Stearidonic	2.2 ± 0.1	2.2 ± 0.0	0.5 ± 0.0	–
20:1ω9	Gondoic	1.2 ± 0.0	1.6 ± 0.0	1.3 ± 0.0	1.0 ± 0.0
22:0	Behenic	0.3 ± 0.0	0.3 ± 0.0	0.3 ± 0.0	0.2 ± 0.0
20:3ω3	Eicosatrienoic	0.6 ± 0.0	0.1 ± 0.0	0.6 ± 0.0	–
20:4ω3	Eicosatetraenoic	1.3 ± 0.1	0.1 ± 0.0	0.6 ± 0.0	–
22:1ω9	Erucic	–	–	–	–
20:5ω3 (EPA)	Eicosapentaenoic	0.5 ± 0.0	–	0.1 ± 0.0	–
24:0	Lignoceric	0.1 ± 0.0	0.2 ± 0.0	0.1 ± 0.0	0.1 ± 0.0
24:1ω9	Nervonic	0.1 ± 0.0	0.1 ± 0.0	0.1 ± 0.0	0.1 ± 0.0
22:5ω3 (DPA)	Docosapentaenoic	1.0 ± 0.0	0.3 ± 0.0	0.2 ± 0.0	–
22:6ω3 (DHA)	Docosahexaenoic	9.7 ± 0.3	0.1 ± 0.0	2.1 ± 0.1	–
Other		2.5 ± 0.1	1.3 ± 0.0	1.3 ± 0.0	0.7 ± 0.0
Σ EPA, DPA, DHA		11.1 ± 0.4	0.3 ± 0.0	2.4 ± 0.1	–
Total ω3		35.3 ± 1.0	19.8 ± 0.2	20.0 ± 0.5	9.6 ± 0.1
Total ω6		7.4 ± 0.2	7.3 ± 0.3	12.0 ± 0.4	19.4 ± 0.2
ω3:ω6		4.8 ± 0.2	2.7 ± 0.1	1.7 ± 0.0	0.5 ± 0.0
Total saturates		8.2 ± 0.1	7.6 ± 0.1	7.5 ± 0.1	7.1 ± 0.0
			Conversion efficiencies		
Δ12-des		50%	31%	36%	32%
Δ15-des		83%	73%	63%	33%
ω3 Δ6-des		42%	14%	18%	–
ω3 Δ6-elo		85%	19%	86%	–
ω3 Δ5-des		90%	80%	80%	–
ω3 Δ5-elo		96%	100%	96%	–
ω3 Δ4-des		91%	25%	91%	–

Data from Ararat, VIC, Australia, 2017; n = 5. Conversion efficiencies are calculated as sum(products)/sum(substrate + products). Fatty acids are given as a percentage of seed total fatty acids.

Field Evaluation

Genotype and environmental conditions (rainfall/available moisture in particular) were the most important determinants of crop yield, resulting in considerable variation in canola yields across sites and years among different varieties tested (**Supplementary Table 3**). Grain yield of AV Jade was higher than that of NS-B50027-4 in some instances, but not all, indicating that the presence of the transgenic construct did not significantly reduce overall crop yield. There was no significant variation in other agronomic parameters (crop emergence, time to flowering and maturity, pod shattering, disease incidence, pest predation) between NS-B50027-4 and other genotypes included in the field tests. In addition, the junction specific PCR test for the two T-DNA copies in DHA canola from the T_3 to T_7 generations indicated that the T-DNA inserts in this event were stably inherited (**Supplementary Figure 3**).

Production of EPA, DPA and DHA in NS-B50027-4 was remarkably consistent across all experimental sites, averaging 0.5, 1.0 and 10% of total seed fatty acid content, respectively. EPA, DPA, DHA, and total LC-PUFA levels from the T_3-T_7 generations of NS-B50027-4 are shown in **Table 2**. T_7 NS-B50027-4 progeny accumulated 12.5% DHA in open field conditions at Nurrabiel (Victoria, Australia) in 2016. Seed oil content (**Supplementary Table 3**) was negatively correlated with

TABLE 2 | EPA, DPA, and DHA composition (as percentage of seed total fatty acids) in line NS-B50027-4 over multiple generations.

Gen.	Sample	Environment	Year in Field	Location	EPA	DPA	DHA	Sum of EPA, DPA, DHA
T_3	Single plant	GH	N/A	Horsham	0.5	0.8	12.6	14.0
T_3	Bulk	Field (tent)	2014	Nurrabiel	0.4	0.8	8.9	10.1
T_3	Bulk	Open field	2015	St Helens Plains	0.4	1.1	9	10.5
T_4	Single plant	GH	N/A	Horsham	0.5	0.8	11.9	13.2
T_5	Single plant	GH	N/A	Horsham	0.6	0.6	13.4	14.6
T_5	Bulk	Field (tent)	2015	Nurrabiel	0.6	1.1	12.1	13.7
T_5	Bulk	Open field	2016	St Helens Plains	0.5	0.9	9.7	11.1
T_6	Single plant	GH	N/A	Horsham	0.6	0.8	12.9	14.3
T_6	Bulk	Field (tent)	2016	Green Lake	0.5	1.0	10.6	12.1
T_7	Single plant	GH	N/A	Horsham	0.6	0.7	13.8	15.1
T_7	Bulk	Field (tent)	2016	Nurrabiel	0.6	1.0	12.5	14.1

'Gen.' denotes the seed generation, 'GH' denotes glasshouse-produced seed; 'Field (tent)' denotes pure seed produced in an isolation tent in the field. All sites are in VIC, Australia and were grown in the Australian winter/spring season (May-November/December). Each row shows one measurement from pooled seeds of bulk or single plant at multiple sites with multiple generations.

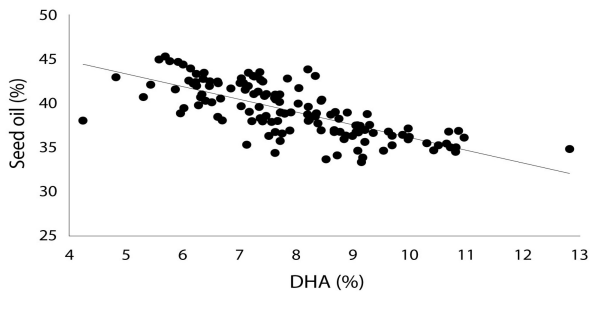

FIGURE 5 | DHA composition (as percentage of total fatty acids in oil) vs. seed oil content (percentage of seed weight) in field-grown GA7_mod-B transgenic *Brassica napus* showing a negative correlation between seed oil yield and DHA composition.

DHA accumulation (**Figure 5**) over the range of oil content observed across locations and was reduced by approximately 4% (46% to 42%) in NS-B50027-4. This effect was confirmed by comparing the oil content of NS-B50027-4 with lines that contained only the A02 or A05 locus; NS-B50027-4 (highest DHA) tended to have the lowest oil content, followed by A05 events (intermediate DHA level) and then events only carrying the partial insert in chromosome A02 (no DHA) (**Supplementary Table 3**).

Finally, the long-term stability of the seed oil was tested by storing seed from line NS-B50027-4 and Jade at 4°C, 24°C, and 32°C for 6 months and subsequently examining the fatty acid profile of the seed oil. Fatty acid profiles and DHA levels in the seed oil were not significantly affected by storage under these conditions, analyzed by One Way Analysis of Variance (ANOVA), confirming the long-term stability of LC-PUFAs in the canola seed (**Figure 6**).

DISCUSSION

We were primarily focused on achieving a high level of DHA accumulation with low levels of ω6 LC-PUFA and intermediate fatty acids beyond ALA. Earlier studies indicated that co-production of EPA and DHA in seed tended to result in reduced accumulation of at least one of these fatty acids. We decided to focus on the production of the maximal level of DHA rather than co-producing EPA and DHA for a number of reasons. Commodity fish oil (e.g., anchovy) contains a higher level of EPA compared to DHA (16–18% vs 12%) so from a purely source-oriented perspective DHA is the rarer molecule. DHA also appears to be more difficult for aquaculture species to synthesize *de novo* and must be exogenously supplied during feeding, whereas EPA can be synthesized from ALA at a higher rate (Emery et al., 2016; Bou et al., 2017). Finally, the linear nature of DHA biosynthesis in seed means that a successful DHA production pathway can easily be converted to an EPA or DPA production pathway by omitting the Δ5-elongase or Δ4-desaturase, respectively. In fact, we have initiated development of an EPA-only pathway in canola which will be the subject of a separate study.

Key considerations in achieving a high level of DHA accumulation included (1) avoiding excessive 'pool shuffling' between acyl-CoA and acyl-PC pools, (2) use of a Δ6-desaturase with ω3 preference, (3) promoter timing designed to reduce accumulation of intermediate fatty acids, and (4) duplicating parts of the pathway to increase gene expression and efficiency. Rapid testing of alternative construct designs in the somatic embryo assay facilitated these goals.

We elected to use the Δ6-desaturase pathway (**Figure 1**) with supplementation of the native FAD2 (Δ12-desaturase) and FAD3 (Δ15-desaturase) activities to increase the production of the substrate ALA. Accumulation of intermediate fatty acids and higher flux (> 78%) through the post SDA part of the pathway was achieved by reducing the amount of fatty acid 'pool shuffling' between acyl-CoA (where elongation occurs) and acyl-PC (where desaturation typically occurs in plant metabolism) (Abbadi et al., 2004; Robert et al., 2005). In choosing the front-end desaturases we deliberately selected desaturases that act on fatty acid substrates in the acyl-CoA pool. For example, the acyl-CoA desaturation ability of the *M. pusilla* Δ6-desaturase was described in Petrie et al. (2010). In addition, Yilmaz et al. (2017) demonstrated that the *P. lutheri* Δ4-desaturase, a gene

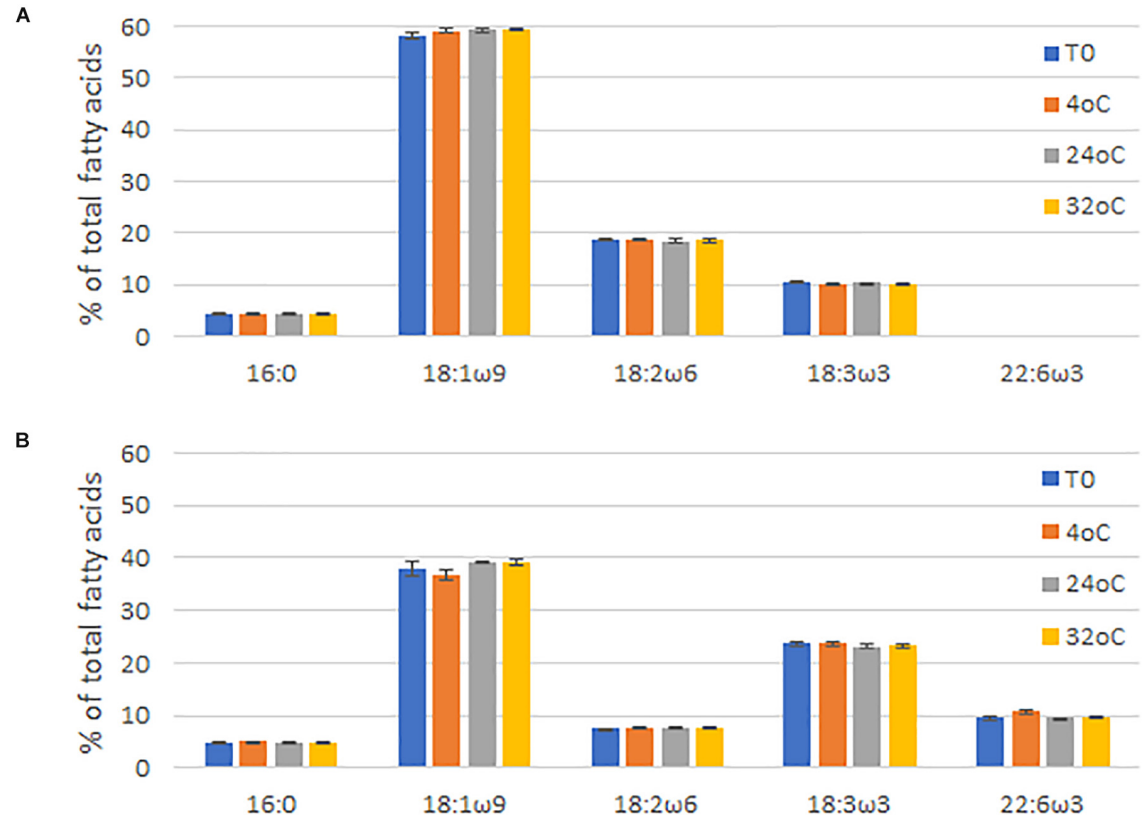

FIGURE 6 | Fatty acid profiles of **(A)** *Brassica napus* AV-Jade cultivar (parental), and **(B)** GA7_mod-B transgenic *B. napus* seeds after being stored for six months at 4°C, 24°C, or 32°C. T0 = time zero (no storage). Data were analyzed by One Way Analysis of Variance (ANOVA) using Sigmaplot (v13) by the Holm-Sidak method. Differences were considered significant at the 5% level. Data are shown as the mean of three repeats ± standard deviation (SD).

that is very closely related to the *P. salina* Δ4–desaturase used in this study, was able to desaturate acyl-CoA substrates to reduce pool shuffling. This resulted not only in the desaturated fatty acids but also the subsequent elongated fatty acids being produced with high efficiency, thus avoiding intermediate fatty acid accumulation. Based on a phylogenetic analysis of amino acid sequences (data not shown), the *P. salina* Δ5-desaturase clusters with other demonstrated acyl-CoA desaturases and is therefore predicted to use ETA-CoA as its primary substrate. In this study, the retention of fatty acid intermediates in the acyl-CoA pool provided for very efficient Δ6- and Δ5-elongase steps. Furthermore, we achieved an extremely high long-chain ω3 to ω6 ratio by limiting the amount of ω6 pathway flux with a Δ6-desaturase that had a strong preference for the ω3 substrate, ALA (Petrie et al., 2010). We also used an ω3-desaturase that converted LA to ALA (Zhang et al., 2008).

A common feature of the fatty acid profiles described in **Figure 4** and **Table 1** is that Δ6-desaturation is the rate-limiting step for this engineered pathway with only about half the ALA converted to SDA. There are several possible reasons for this. First, it could simply be a matter of low transcript abundance leading to low protein levels. This is unlikely, because although there is a clear gene dosage effect, high copy number events, possibly resulting in higher transcript levels, somewhat improved but did not overcome rate limitation at this step. It is also noteworthy that the majority of evidence suggests that fatty acid desaturation activity is regulated primarily at the post-translational level and hence higher transcript levels might not necessarily result in higher desaturase activity or protein levels (O'Quin et al., 2010). Interestingly, in a separate but related study, the *M. pusilla* Δ6-desaturase protein was the least abundant of the three algal front-end desaturases used in our DHA pathway. For example, *P. salina*-Δ4D protein levels ranged from up to 1,500 ng/mg total seed protein in mature seed and up to 5,600 ng/mg seed protein in developing transgenic canola seed. In contrast, *M. pusilla* Δ6-desaturase protein levels ranged from 220 ng/mg total seed protein in mature seed and up to 870 ng/mg total seed protein in developing transgenic canola seed (Colgrave et al., 2019b). Another possibility is that the *M. pusilla* Δ6-desaturase has low activity from a functional perspective. In fact, a study published recently indicates that there is a constraint imposed by increased preference for ALA over LA by *M. pusilla* Δ6-desaturase which results in the enzyme inherently displaying lower activity (Li et al., 2020). Finally, it is possible that the *M. pusilla* Δ6-desaturase enzyme has a very strong preference for acyl-CoA substrates, such that the bulk of the naturally produced acyl-PC ALA is unavailable for conversion until it enters the acyl-CoA pool. It is also conceivable that much

of the acyl-PC ALA simply ends up in triacylglycerol via the action of PDAT without ever entering the acyl-CoA pool (Pan et al., 2013). Further work is required to develop strategies to increase activity at this rate-limiting step.

This study further highlighted the importance of construct design and promoter selection when introducing new metabolic pathways to plant hosts (Cheng et al., 2010). For example, synthesis of intermediate fatty acids in the absence of an enzyme that can perform further conversion might result in the removal of the intermediate fatty acid from the metabolically active lipid pool into storage lipids where they are no longer accessible as a substrate. We used relatively late promoters (seed storage protein promoters Cnl2 and napin) to express the first committed step of synthesis, Δ6-desaturation. An example of this principle can be seen in the relatively poor Δ6-elongation observed in GA7_mod-F embryos (**Supplementary Table 2**): although the Δ6-desaturation was higher following the addition of a FAE1::Δ6-desaturase expression cassette, the subsequent conversion of SDA to ETA was lower, indicating that the additional SDA was not entirely available for conversion.

To speed up the process of selecting a construct for large-scale transformation, we used a rapid somatic embryo assay instead of testing each construct variant in canola seed. Constitutive expression of the LEC2 transcription factor during the early stages of tissue culture can result in the production of somatic embryos with seed-like fatty acid profiles (Stone et al., 2008). This system provides the activation of seed-specific promoters, allowing rapid assessment of seed-specific construct function after co-transformation (Petrie et al., 2013). The fatty acid profiles achieved in the somatic embryos described in this study shared some characteristics despite the varying DHA levels: a very high ω3 to ω6 LC-PUFA ratio, high total ω3 PUFA levels, high conversion efficiency from SDA through to DHA, and low accumulation of intermediate fatty acids. These profiles indicate that the conversion efficiency from SDA through to DHA is remarkably high, with little loss of substrate along the pathway. This is likely due to the selection of LC-PUFA desaturases which are capable of acting in the acyl-CoA pool, resulting in both elongation and desaturation in the same metabolite pool as described above.

Interestingly, expression of the GA7_mod-B construct was found to be highly stable when integrated into the canola genome, even with the twin T-DNA insertions in an inverted repeat arrangement on the A05 chromosome. DHA levels have been remarkably stable in both glasshouse and field trials over several years and up to the T_7 generation, under a wide range of growing conditions (**Table 2**). The effect of the A02 partial construct locus is also interesting: this fragment is effectively acting as a 'booster' for the full pathway insertion in chromosome A05 which increased gene dosage without increasing the number of genes in the construct. Notably, DHA levels increased from 2.1% in the absence of the A02 partial construct to 9.7% when present with the A05 locus (**Table 1**). The use of partial pathway insertions to provide multiple copies of some genes should not be overlooked when engineering complex pathways, especially for the specific use of increasing flux through bottlenecks. In addition, proteomics combined with a targeted LC-MS/MS approaches were applied to simultaneously measure the relative low abundance of seven transgenic enzymes involved in the docosahexaenoic acid (DHA) biosynthetic in DHA canola from multiple filed trials, which are all membrane-bound (Colgrave et al., 2019b). The results demonstrated that the seed-specifically expressed enzymes that drive the production of DHA were only detected in mature and developing seed of DHA canola. *In vitro* protein digestibility analysis using a strategy with two-stage digestion including simulated gastric fluid trypsin showed that these proteins were rapidly degraded by > 95% within 5 min (Colgrave et al., 2019a).

The field trial results confirm that NS-B50027-4 retains the seed yield of the parental line, with only a slight reduction in total seed oil content. However, the value proposition for this crop is very different from conventional canola, and the value of the oil is expected to compensate for the oil content reduction. Previous research has shown either no significant effect of LC-PUFA expression (14% total LC-PUFA) on seed oil content (Napier et al., 2015), or an oil content reduction of 3.0–8.3% in plants expressing 16–17% EPA (Usher et al., 2017). Further research to incorporate the trait in other germplasm, high-yielding open-pollinated and hybrid lines, may be undertaken. Although NS-B50027-4 is primarily adapted to Australian conditions, the field results indicated that it performed adequately in Canada and the United States, with reasonable grain yield and, more importantly, consistent LC-PUFA yields.

The oil from NS-B50027-4 has several unique features: it is relatively high in DHA, a highly beneficial LC-PUFA for dietary supplementation (Napier et al., 2019), but also contains a small amount of EPA and a significant amount of DPA, a fatty acid in which there appears to be increasing interest from the medical community (Kaur et al., 2016). In addition, the oil contains a high level of ALA (ca. 20%, compared to 10% in typical canola oil). This provides a substantially increased ω3:ω6 ratio, with concomitant health benefits. In addition, the predominance of DHA at *sn*-1 and *sn*-3 on TAG suggests it will be highly available upon ingestion. The long-term stability of the LC-PUFA in NS-B50037-4 suggests there will be little loss of the key fatty acids during storage and transportation of grain from this crop, removing some of the logistical concerns with protecting LC-PUFA from premature oxidation.

Omega-3 canola oil is expected to have multiple applications in human and animal nutrition. The high DHA and total ω3 levels achieved suggest that this oil is particularly suitable as an ingredient in aquaculture feed. Vegetable and poultry oils with a low ω3 to ω6 ratio have become a major energy source in commercial aquaculture feeds, resulting in a significant reduction in the ω3 to ω6 ratio in farmed Atlantic salmon compared to wild-caught fish (Strobel et al., 2012) or fish raised on high fish-oil diets (Nichols et al., 2014). Dietary supplementation with this ω3 canola oil results in a high ω3 and DHA content in fillets of Atlantic salmon (Ruyter et al., 2019), with consequent benefits to consumers of such fillets. This and a more recent study (Betancor et al., 2018) indicated no negative effects on fish health, growth and survival, confirming that such oils are safe and effective replacements for fish oils in aquaculture diets.

The optimal levels of EPA and DHA for fish growth and health are not yet clearly established, although the low level of EPA in the omega-3 canola oil does not appear to be a detriment to fish nutrition. Indeed, there is evidence that EPA may not be required by Atlantic salmon under certain conditions (Bou et al., 2017; Usher et al., 2017). Evidence for forward conversion of ALA to EPA and DHA has been demonstrated in Atlantic salmon (Stubhaug et al., 2005; Sanden et al., 2011; Bou et al., 2017) and rainbow trout (Turchini et al., 2011; Hixson et al., 2014), particularly when the LC-PUFA are incorporated in the feed at low levels, as occurs with the presence and use of any fish meal in the feed. The high ALA content of the omega-3 canola oil may therefore alleviate its relatively low EPA content, making it a suitable replacement for fish oil in aquaculture diets. Conversion of EPA to DHA is very inefficient in humans (Kitessa et al., 2014), with use of a DHA-containing oil being seen therefore as considerably more beneficial from both an animal (farmed fish) and then the resulting human nutrition perspective.

Oil from line NS-B50027-4 may also provide a direct increase in LC-PUFA availability for human nutrition and health. Based on a Recommended Daily Intake (RDI) of 500 mg (Nichols et al., 2010), as proposed by various national health bodies, a global population reaching 8 billion by 2025, and assuming that fish contain on average 0.3 g (range 0.2–3.5 g) of EPA and DHA per 100 g of edible flesh, it is estimated that the current global fish harvest (93 million tons per annum) will fall well short of meeting this requirement (Naylor et al., 2009). In addition to the nutritional benefits occurring for both the farmed fish and the human consumers, the use of omega-3 canola oil in aquaculture feeds (Ruyter et al., 2019) will also provide substantial environmental benefits through the reduced pressure on the wild harvest fisheries which presently no longer meet the market demand.

Cultivation of the DHA canola crop and human and animal consumption of the oil in Australia and cultivation in USA has been approved by the relevant regulators (FSANZ, 2017; OGTR, 2018; USDA, 2018). Also, the successful engineering of high levels of DHA in canola opens the door to large-scale production of other important LC-PUFA such as EPA and DPA. These fatty acids are intermediates in the metabolic pathway we have used to produce DHA in this study. For example, the use of different versions of the GA7 construct may yield fish oil-like levels of EPA and even higher levels of the relatively rare fatty acid DPA, or possibly further increase the amount of DHA that can be produced in canola seed (Shrestha et al., 2018).

DATA AVAILABILITY STATEMENT

The sequences of the transgene insert and *B. napus* flanking regions at A02 and A05 were deposited in GenBank under accession numbers MP172039 and MP172040.

AUTHOR CONTRIBUTIONS

JP, X-RZ, PN, RF, MD, and SS made substantial contributions to the conception and design of the work, analysis and interpretation of data, and extensive drafting or editing of the manuscript. JM, PS, YK, WG, GL, MM, RM, QL, LT, CS, and NC analyzed and interpreted data. AL, SB, GB, and NG made substantial contributions to the design of the work and analyzed and interpreted data. AG made substantial contributions to the conception of the work.

FUNDING

This work was supported by CSIRO, Nuseed Pty Ltd. and Australian Grains Research and Development Corporation (GRDC).

ACKNOWLEDGMENTS

We thank Dawar Hussain, Lina Ma, Anne Mackenzie, Nathalie Niesner, Carolyn Klowss, and Lisa Kennedy for their excellent technical assistance, the Australian Grains Research and Development Corporation (GRDC) for their guidance and financial support, and Dr. Matthew Morell and Dr. Bruce Lee for their support.

SUPPLEMENTARY MATERIAL

The Supplementary Material for this article can be found online at: https://www.frontiersin.org/articles/10.3389/fpls.2020.00727/full#supplementary-material

REFERENCES

Abbadi, A., Domergue, F., Bauer, J., Napier, J. A., Welti, R., Zahringer, U., et al. (2004). Biosynthesis of very-long-chain polyunsaturated fatty acids in transgenic oilseeds: constraints on their accumulation. *Plant Cell* 16, 2734–2748. doi: 10.1105/tpc.104.026070

Abedi, E., and Sahari, M. A. (2014). Long-chain polyunsaturated fatty acid sources and evaluation of their nutritional and functional properties. *Food Sci. Nutr.* 2, 443–463. doi: 10.1002/fsn3.121

Adarme-Vega, T. C., Thomas-Hall, S. R., and Schenk, P. M. (2014). Towards sustainable sources for omega-3 fatty acids production. *Curr. Opin. Biotechnol.* 26, 14–18. doi: 10.1016/j.copbio.2013.08.003

Belide, S., Zhou, X.-R., Kennedy, Y., Lester, G., Shrestha, P., Petrie, J. R., et al. (2013). Rapid expression and validation of seed-specific constructs in transgenic LEC2 induced somatic embryos of *Brassica napus*. *Plant Cell Tiss. Organ. Cult.* 113, 543–553. doi: 10.1007/s11240-013-0295-1

Betancor, M. B., Li, K., Bucerzan, V. S., Sprague, M., Sayanova, O., Usher, S., et al. (2018). Oil from transgenic *Camelina sativa* containing over 25 % *n*-3 long-chain PUFA as the major lipid source in feed for Atlantic salmon (*Salmo salar*). *Br. J. Nutr.* 119, 1378–1392. doi: 10.1017/S0007114518001125

Bou, M., Berge, G. M., Baeverfjord, G., Sigholt, T., Østbye, T.-K., Romarheim, O. H., et al. (2017). Requirements of *n*-3 very long-chain PUFA in Atlantic salmon (*Salmo salar* L): effects of different dietary levels of EPA and DHA on

fish performance and tissue composition and integrity. *Br. J. Nutr.* 117, 30–47. doi: 10.1017/S0007114516004396

Cheng, B. F., Wu, G. H., Vrinten, P., Falk, K., Bauer, J., and Qiu, X. (2010). Towards the production of high levels of eicosapentaenoic acid in transgenic plants: the effects of different host species, genes and promoters. *Transgenic Res.* 19, 221–229. doi: 10.1007/s11248-009-9302-z

Colgrave, M. L., Byrne, K., Caine, J., Kowalczyk, L., Vibhakaran Pillai, S., Dong, B., et al. (2019a). Proteomics reveals the in vitro protein digestibility of seven transmembrane enzymes from the docosahexaenoic acid biosynthesis pathway. *Food Chem. Toxicol.* 130, 89–98. doi: 10.1016/j.fct.2019.05.015

Colgrave, M. L., Byrne, K., Pillai, S. V., Dong, B., Leonforte, A., Caine, J., et al. (2019b). Quantitation of seven transmembrane proteins from the DHA biosynthesis pathway in genetically engineered canola by targeted mass spectrometry. *Food Chem. Toxicol.* 126, 313–321. doi: 10.1016/j.fct.2019.02.035

Emery, J. A., Norambuena, F., Trushenski, J., and Turchini, G. M. (2016). Uncoupling EPA and DHA in fish nutrition: dietary demand is limited in Atlantic salmon and effectively met by DHA alone. *Lipids* 51, 399–412. doi: 10.1007/s11745-016-4136-y

FSANZ, (2017). http://www.foodstandards.gov.au/code/applications/Pages/A1143-DHA-Canola-Line-NS%E2%80%93B500274.aspx (accessed December 20, 2017).

Halweg, C., Thompson, W. F., and Spiker, S. (2005). The Rb7 matrix attachment region increases the likelihood and magnitude of transgene expression in tobacco cells: a flow cytometric study. *Plant Cell* 17, 418–429. doi: 10.1105/tpc.104.028100

Hashimoto, M., Hossain, S., Al Mamun, A., Matsuzaki, K., and Arai, H. (2017). Docosahexaenoic acid: one molecule diverse functions. *Crit. Rev. Biotechnol.* 37, 579–597. doi: 10.1080/07388551.2016.1207153

Hixson, S. M., Parrish, C. C., and Anderson, D. M. (2014). Changes in tissue lipid and fatty acid composition of farmed rainbow trout in response to dietary camelina oil and a replacement of fish oil. *Lipids* 49, 97–111. doi: 10.1007/s11745-013-3862-7

Kaur, G., Guo, X.-F., and Sinclair, A. J. (2016). Short update on docosapentaenoic acid: a bioactive long-chain n-3 fatty acid. *Curr. Opin. Clin. Nutr. Metab. Care* 19, 88–91. doi: 10.1097/mco.0000000000000252

Kitessa, S. M., Abeywardena, M., Wijesundera, C., and Nichols, P. D. (2014). DHA-containing oilseed: a timely solution for the sustainability issues surrounding fish oil sources of the health-benefitting long-chain omega-3 oils. *Nutrients* 6, 2035–2058. doi: 10.3390/nu6052035

Lazo, G. R., Stein, P. A., and Ludwig, R. A. (1991). A DNA transformation competent *Arabidopsis* genomic library in *Agrobacterium*. *Biotechnology* 9, 963–967. doi: 10.1038/nbt1091-963

Li, D., Damry, A. M., Petrie, J. R., Vanhercke, T., Singh, S. P., and Jackson, C. J. (2020). Consensus mutagenesis and ancestral reconstruction provide insight into the substrate specificity and evolution of the front-end Δ6-desaturase family. *Biochemistry* 59, 1398–1409. doi: 10.1021/acs.biochem.0c00110

Martin, M. (2011). Cutadapt removes adapter sequences from high-throughput sequencing reads. *EMBnet. J.* 17, 10–12. doi: 10.14806/ej.17.1.200

Metz, J. G., Roessler, P., Facciotti, D., Levering, C., Dittrich, F., Lassner, M., et al. (2001). Production of polyunsaturated fatty acids by polyketide synthases in both prokaryotes and eukaryotes. *Science* 293, 290–293. doi: 10.1126/science.1059593

Mieog, J. C., Howitt, C. A., and Ral, J.-P. (2013). Fast-tracking development of homozygous transgenic cereal lines using a simple and highly flexible real-time PCR assay. *BMC Plant Biol.* 13:71. doi: 10.1186/1471-2229-13-71

Napier, J. A., Olsen, R.-E., and Tocher, D. R. (2019). Update on GM canola crops as novel sources of omega-3 fish oils. *Plant Biotechnol. J.* 17, 703–705. doi: 10.1111/pbi.13045

Napier, J. A., Usher, S., and Haslam, R. P. (2015). Transgenic plants as a sustainable, terrestrial source of fish oils. *Eur. J. Lipid Sci. Technol.* 117, 1317–1324. doi: 10.1002/ejlt.201400452

Naylor, R. L., Hardy, R. W., Bureau, D. P., Chiu, A., Elliott, M., Farrell, A. P., et al. (2009). Feeding aquaculture in an era of finite resources. *Proc. Natl. Acad. Sci. U.S.A.* 106, 15103–15110. doi: 10.1073/pnas.0905235106

Nichols, P. D., Glencross, B., Petrie, J. R., and Singh, S. P. (2014). Readily available sources of long-chain omega-3 oils: is farmed Australian seafood a better source of the good oil than wild-caught seafood? *Nutrients* 6, 1063–1079. doi: 10.3390/nu6031063

Nichols, P. D., Petrie, J., and Singh, S. (2010). Long-chain omega-3 oils – An update on sustainable sources. *Nutrients* 2, 572–585.

OGTR, (2018). http://www.ogtr.gov.au/internet/ogtr/publishing.nsf/Content/DIR155 (accessed February 13, 2018).

O'Quin, J. B., Bourassa, L., Zhang, D. Y., Shockey, J. M., Gidda, S. K., Fosnot, S., et al. (2010). Temperature-sensitive post-translational regulation of plant omega-3 fatty-acid desaturases is mediated by the endoplasmic reticulum-associated degradation pathway. *J. Biol. Chem.* 285, 21781–21796. doi: 10.1074/jbc.M110.135236

Pan, X., Siloto, R. M., Wickramarathna, A. D., Mietkiewska, E., and Weselake, R. J. (2013). Identification of a pair of phospholipid:diacylglycerol acyltransferases from developing flax (*Linum usitatissimum* L.) seed catalyzing the selective production of trilinolenin. *J. Biol. Chem.* 288, 24173–24188. doi: 10.1074/jbc.M113.475699

Petrie, J. R., Nichols, P. D., Devine, M. D., and Singh, S. P. (2013). Engineered oil crops with fish oil DHA levels. *Inform* 24, 648–651.

Petrie, J. R., Shrestha, P., Belide, S., Kennedy, Y., Lester, G., Liu, Q., et al. (2014). Metabolic engineering *Camelina sativa* with fish oil-like levels of DHA. *PLoS One* 9:e85061. doi: 10.1371/journal.pone.0085061

Petrie, J. R., Shrestha, P., Liu, Q., Mansour, M. P., Wood, C. C., Zhou, X.-R., et al. (2010). Rapid expression of transgenes driven by seed-specific constructs in leaf tissue: DHA production. *Plant Meth.* 6:6. doi: 10.1186/1746-4811-6-8

Petrie, J. R., Shrestha, P., Zhou, X.-R., Mansour, M. P., Liu, Q., Belide, S., et al. (2012). Metabolic engineering plant seeds with fish oil-like levels of DHA. *PLoS One* 7:e49165. doi: 10.1371/journal.pone.0049165

Robert, S. S., Singh, S. P., Zhou, X.-R., Petrie, J. R., Blackburn, S. I., Mansour, P. M., et al. (2005). Metabolic engineering of *Arabidopsis* to produce nutritionally important DHA in seed oil. *Func. Plant Biol.* 32, 473–479. doi: 10.1371/journal.pone.0049165

Rossak, M., Smith, M., and Kunst, L. (2001). Expression of the FAE1 gene and FAE1 promoter activity in developing seeds of *Arabidopsis thaliana*. *Plant Mol. Biol.* 46, 717–725. doi: 10.1023/a:1011603923889

Rozen, S., and Skaletsky, H. (1999). *Bioinformatics Methods and Protocols*. Totowa, NJ: Humana Press.

Ruiz-Lopez, N., Haslam, R. P., Napier, J. A., and Sayanova, O. (2014). Successful high-level accumulation of fish oil omega-3 long-chain polyunsaturated fatty acids in a transgenic oilseed crop. *Plant J.* 77, 198–208. doi: 10.1111/tpj.12378

Ruyter, B., Sissener, N. H., Østbye, T.-K., Simon, C. J., Krasnov, A., Bou, M., et al. (2019). *n*-3 Canola oil effectively replaces fish oil as a new safe dietary source of DHA in feed for juvenile Atlantic salmon. *Br. J. Nutr.* 122, 1329–1345. doi: 10.1017/S0007114519002356

Sanden, M., Stubhaug, I., Berntssen, M. H. G., Lie, Ø, and Torstensen, B. E. (2011). Atlantic salmon (*Salmo salar* L.) as a net producer of long-chain marine ω-3 fatty acids. *J. Agric. Food Chem.* 59, 12697–12706. doi: 10.1021/jf203289s

Shrestha, P., Hussain, D., Mulder, R. J., Taylor, M. C., Singh, S. P., Petrie, J. R., et al. (2018). Increased DHA production in seed oil using a selective lysophosphatidic acid acyltransferase. *Front. Plant Sci.* 9:1234. doi: 10.3389/fpls.2018.01234

Simopoulos, A. P. (1999). Essential fatty acids in health and chronic disease. *Amer. J. Clin. Nutr.* 70, 560S–569S. doi: 10.1093/ajcn/70.3.560s

Smith, A., Cullis, B., and Thompson, R. (2001). Analysing variety by environment data using multiplicative missed modes and adjustments for spatial field trend. *Biometrics* 57, 1138–1147. doi: 10.1111/j.0006-341X.2001.01138.x

Sprague, M., Betancor, M. B., and Tocher, D. R. (2017). Microbial and genetically engineered oils as replacements for fish oil in aquaculture feeds. *Biotechnol. Letts.* 39, 1599–1609. doi: 10.1007/s10529-017-2402-6

Stark, K. D., Van Elswyk, M. E., Higgins, M. R., Weatherford, C. A., and Salem, N. Jr. (2016). Global survey of the omega-3 fatty acids, docosahexaenoic acid and eicosapentaenoic acid in the blood stream of healthy adults. *Prog. Lipid Res.* 63, 132–152. doi: 10.1016/j.plipres.2016.05.001

Stone, S. L., Braybrook, S. A., Paula, S. L., Kwong, L. W., Meuser, J., Pelletier, J., et al. (2008). Arabidopsis LEAFY COTYLEDON2 induces maturation traits and auxin activity: implications for somatic embryogenesis. *Proc. Natl. Acad. Sci. U.S.A.* 105, 3151–3156. doi: 10.1073/pnas.0712364105

Strobel, C., Jahreis, G., and Kuhnt, K. (2012). Survey of *n*-3 and *n*-6 polyunsaturated fatty acids in fish and fish products. *Lipids Health Dis.* 11, 144–144. doi: 10.1186/1476-511X-11-144

Stubhaug, I., Tocher, D. R., Bell, J. G., Dick, J. R., and Torstensen, B. E. (2005). Fatty acid metabolism in Atlantic salmon (*Salmo salar* L.) hepatocytes and

influence of dietary vegetable oil. *Biochim. Biophys. Acta* 1734, 277–288. doi: 10.1016/j.bbalip.2005.04.003

Truksa, M., MacKenzie, S. L., and Qiu, X. (2003). Molecular analysis of flax 2S storage protein conlinin and seed specific activity of its promoter. *Plant Physiol. Biochem.* 41, 141–147. doi: 10.1016/S0981-9428(02)00022-0

Turchini, G. M., Francis, D. S., Keast, R. S. J., and Sinclair, A. J. (2011). Transforming salmonid aquaculture from a consumer to a producer of long chain omega-3 fatty acids. *Food Chem.* 124, 609–614. doi: 10.1016/j.foodchem.2010.06.083

USDA, (2018). https://www.aphis.usda.gov/brs/aphisdocs/17_23601p_det.pdf (accessed August 30, 2018).

Usher, S., Han, L., Haslam, R. P., Michaelson, L. V., Sturtevant, D., Aziz, M., et al. (2017). Tailoring seed oil composition in the real world: optimising omega-3 long chain polyunsaturated fatty acid accumulation in transgenic *Camelina sativa*. *Sci. Rep.* 7:6570. doi: 10.1038/s41598-017-06838-0

Walsh, T. A., Bevan, S. A., Gachotte, D. J., Larsen, C. M., Moskal, W. A., Merlo, P. A. O., et al. (2016). Canola engineered with a microalgal polyketide synthase-like system produces oil enriched in docosahexaenoic acid. *Nat. Biotechnol.* 34, 881–887. doi: 10.1038/nbt.3585

Weng, H., Pan, A., Yang, L., Zhang, C., Liu, Z., and Zhang, D. (2004). Estimating number of transgene copies in transgenic rapeseed by real-time PCR assay with HMG I/Y as an endogenous reference gene. *Plant Mol. Biol. Rep.* 22, 289–300. doi: 10.1007/bf02773139

Wu, G. H., Truksa, M., Datla, N., Vrinten, P., Bauer, J., Zank, T., et al. (2005). Stepwise engineering to produce high yields of very long-chain polyunsaturated fatty acids in plants. *Nat. Biotechnol.* 23, 1013–1017. doi: 10.1038/nbt1107

Yilmaz, J. L., Lim, Z. L., Beganovic, M., Breazeale, S., Andre, C., Stymne, S., et al. (2017). Determination of substrate preferences for desaturases and elongases for production of docosahexaenoic acid from oleic acid in engineered canola. *Lipids* 52, 207–222. doi: 10.1007/s11745-017-4235-4

Zhang, X., Li, M., Wei, D., and Xing, L. (2008). Identification and characterization of a novel yeast ω3-fatty acid desaturase acting on long-chain n-6 fatty acid substrates from *Pichia pastoris*. *Yeast* 25, 21–27. doi: 10.1002/yea.1546

Zhou, X.-R., Green, A. G., and Singh, S. P. (2011). *Caenorhabditis elegans* Δ12-desaturase FAT-2 is a bifunctional desaturase able to desaturate a diverse range of fatty acid substrates at the Δ12 and Δ15 positions. *J. Biol. Chem.* 286, 43644–43650. doi: 10.1074/jbc.M111.266114

Zhou, X.-R., Li, J., Wan, X., Hua, W., and Singh, S. (2019). Harnessing biotechnology for the development of new seed lipid traits in *Brassica*. *Plant Cell Physiol.* 60, 1197–1204. doi: 10.1093/pcp/pcz070

Conflict of Interest: The authors declare that this study received funding partially from CSIRO, Nuseed and GRDC. CSIRO is not an affiliate of any of the Nuseed entities. The Nuseed entities had the following involvement with the study: Authors AL, GB and NG participated in event selection and were responsible for all breeding, line advancement and genetic analysis; JM and CS were responsible for oil and fatty acid analysis; WG was responsible for molecular analysis and marker development; MD was responsible for overall project planning and writing parts of the manuscript.

The remaining authors declare that the research was conducted in the absence of any commercial or financial relationships that could be construed as a potential conflict of interest.

frontiers in Plant Science

ORIGINAL RESEARCH
published: 03 July 2020
doi: 10.3389/fpls.2020.00895

AP2/DREB Transcription Factor RAP2.4 Activates Cuticular Wax Biosynthesis in *Arabidopsis* Leaves Under Drought

Sun Ui Yang[1†], Hyojin Kim[2†], Ryeo Jin Kim[2], Jungmook Kim[1] and Mi Chung Suh[2]*

[1] Department of Bioenergy Science and Technology, Chonnam National University, Gwangju, South Korea, [2] Department of Life Science, Sogang University, Seoul, South Korea

Drought is a critical environmental stress that limits growth and development of plants and reduces crop productivity. The aerial part of land plants is covered with cuticular waxes to minimize water loss. To understand the regulatory mechanisms underlying cuticular wax biosynthesis in *Arabidopsis* under drought stress conditions, we characterized the role of an AP2/DREB type transcription factor, RAP2.4. *RAP2.4* expression was detected in one-week-old seedlings and rosette leaves, stems, stem epidermis, cauline leaves, buds, flowers, and siliques of 6-week-old *Arabidopsis*. The levels of *RAP2.4* transcripts increased with treatments of abscisic acid (ABA), mannitol, NaCl, and drought stress. Under drought, total wax loads decreased by approximately 11% and 10%, and in particular, the levels of alkanes, which are a major wax component, decreased by approximately 11% and 12% in *rap2.4-1* and *rap2.4-2* leaves, respectively, compared with wild type (WT) leaves. Moreover, the transcript levels of cuticular wax biosynthetic genes, *KCS2* and *CER1,* decreased by approximately 15–23% and 32–40% in *rap2.4-1* and *rap2.4-2* leaves, respectively, relative to WT 4 h after drought treatment, but increased by 2- to 12-fold and 3- to 70-fold, respectively, in three independent *RAP2.4* OX leaves relative to WT. Epicuticular wax crystals were observed on the leaves of *RAP2.4* OX plants, but not on the leaves of WT. Total wax loads increased by 1.5- to 3.3-fold in leaves of *RAP2.4* OX plants relative to WT. Cuticular transpiration and chlorophyll leaching occurred slowly in the leaves of *RAP2.4* OX plants relative to WT. Transcriptional activation assay in tobacco protoplasts showed that RAP2.4 activates the expression of *KCS2* and *CER1* through the involvement of the consensus CCGAC or GCC motifs present in the *KCS2* and *CER1* promoter regions. Overall, our results revealed that RAP2.4 is a transcription factor that activates cuticular wax biosynthesis in *Arabidopsis* leaves under drought stress conditions.

Keywords: AP2/DREB-type, *Arabidopsis*, cuticular wax, drought, RAP2.4, transcription factor

OPEN ACCESS

Edited by:
Guodong Wang,
Institute of Genetics and Developmental Biology, Chinese Academy of Sciences, China

Reviewed by:
Rongfeng Huang,
Institute of Biotechnology (CAAS), China
Qiao Zhao,
Shenzhen Institutes of Advanced Technology, Chinese Academy of Sciences, China

****Correspondence:***
Mi Chung Suh
mcsuh@sogang.ac.kr

† These authors have contributed equally to this work

Specialty section:
This article was submitted to Plant Metabolism and Chemodiversity, a section of the journal Frontiers in Plant Science

Received: *02 October 2019*
Accepted: *02 June 2020*
Published: *03 July 2020*

Citation:
Yang SU, Kim H, Kim RJ, Kim J and Suh MC (2020) AP2/DREB Transcription Factor RAP2.4 Activates Cuticular Wax Biosynthesis in Arabidopsis Leaves Under Drought. Front. Plant Sci. 11:895. doi: 10.3389/fpls.2020.00895

INTRODUCTION

Drought is a severe environmental stress implicated in the reduction of plant growth and crop productivity. As plants are sessile, they must cope with drought stress for their optimal growth and development. During the transition of land plants from aquatic to terrestrial environments, they developed a key surface structure, the outermost cuticle layer covering their aerial tissues, to

protect them from terrestrial stresses such as drought, excess light, and UV light (Shepherd and Griffiths, 2006; Bernard and Joubès, 2013; Yeats and Rose, 2013). Therefore, the primary function of the cuticle layer is to reduce water-loss through the epidermis, except through the stomata (Yeats and Rose, 2013; Lee and Suh, 2015a). The cuticle, which is the first physical barrier between plants and the environment, plays a role in the protection of plants from excess UV light, pathogenic spores, and insect attack (Eigenbrode and Espelie, 1995; Sieber et al., 2000; Holmes and Keiller, 2002; Yeats and Rose, 2013) and also in the prevention of organ fusion during plant development (Ingram and Nawrath, 2017). The hydrophobic cuticle layer mainly comprises the cutin polyester matrix, intracuticular waxes embedded in the cutin matrix, and epicuticular waxes. Cutin polyester is mainly formed by interlinking through ester bonds of ω-hydroxy C16 or C18 fatty acids and their derivatives (Beisson et al., 2012; Bakan and Marion, 2017). Major components of cuticular waxes are very long chain fatty acids (VLCFA, longer than C20) and their derivatives including alkanes, aldehydes, primary and secondary alcohols, and wax esters (Lee and Suh, 2013; Hegebarth and Jetter, 2017).

Cuticular wax biosynthesis mainly occurs in the epidermal cells of plants (Suh et al., 2005). The C16 and C18 fatty acids synthesized in the plastids are further elongated to VLCFAs by the fatty acid elongase (FAE) complex in the endoplasmic reticulum (ER) (Millar et al., 1999; Zheng et al., 2005; Bach et al., 2008; Beaudoin et al., 2009; Kunst and Samuels, 2009; Haslam and Kunst, 2013; Kim et al., 2013; Morineau et al., 2016). The VLCFAs are modified to VLC aliphatic compounds, which are aldehydes, alkenes, secondary alcohols, and ketones via the alkane-forming pathway and primary alcohols and wax-esters via the alcohol-forming pathway (Rowland et al., 2006; Greer et al., 2007; Li et al., 2008; Bourdenx et al., 2011; Li-Beisson et al., 2013; Bernard and Joubès, 2013; Lee and Suh, 2015a). The wax molecules synthesized in the ER are secreted through the ATP-binding cassette transporter in the plasma membrane and with the help of glycosylphosphatidyl-anchored lipid transfer proteins to extracellular space, and then deposited on the surface of epidermal cells (DeBono et al., 2009; Lee et al., 2009; Kim et al., 2012). The total wax load and composition varied greatly among plant species, in an organ-specific manner, or by environmental factors (Holmes and Keiller, 2002; Shepherd and Griffiths, 2006; Kosma et al., 2009; Seo et al., 2011; Go et al., 2014; Lee et al., 2016; Kim et al., 2018). In particular, the total wax load increased by approximately 2-fold in *Arabidopsis* and tree tobacco (*Nicotiana glauca*) leaves under drought stress conditions (Kosma et al., 2009; Seo et al., 2011; Lee et al., 2016). Increased total wax loads in leaves reduced cuticular transpiration rate and conferred resistance to drought (Seo et al., 2011; Lee et al., 2016). Noticeably, the increased levels of VLC-alkane components in *Arabidopsis* are prominent under drought stress conditions, indicating that the molecular regulatory mechanism underlying the alkane-forming pathway may be important to understand one of the plant strategies to cope with drought (Kosma et al., 2009; Xue et al., 2017).

It has long been questioned how land plants precisely regulate total wax loads in response to drought stress. Several transcription factors have been reported to be implicated in the upregulation of wax biosynthesis in plants under drought (Seo et al., 2011; Lee et al., 2016). WIN1/SHN1, which belongs to the AP2/ERF transcription factor family, is a transcriptional activator that induces the expression of *KCS1*, *ECERIFERUM1* (*CER1)*, and *CER2* genes and its overexpression in *Arabidopsis* and *N. tabacum* caused increased resistance to drought (Aharoni et al., 2004; Broun et al., 2004; Kannangara et al., 2007; Djemal and Khoudi, 2019). Similarly, ectopic expression of *Medicago truncatula WXP1* and *WXP2* transcription factors containing the AP2 domain led to increased wax load and enhanced drought tolerance (Zhang et al., 2005; Zhang et al., 2007). In addition, the *Arabidopsis* R2R3-type transcription factor MYB96, which is induced by drought and ABA treatment, directly activates the expression of *KCS1, KCS2, KCS6, KCR1*, and *CER3* genes involved in wax biosynthesis (Seo et al., 2011). Its functional homolog, MYB94, is a transcription activator that increases the levels of *WSD1, KCS2, CER2, FAR3*, and *ECR* transcripts in *Arabidopsis* (Lee and Suh, 2015b). MYB94 and MYB96 additively activate cuticular wax biosynthesis by binding to the same MYB consensus motifs in wax biosynthetic gene promoters (Lee et al., 2016). Interestingly, total wax loads of double knockout *myb94 myb96* leaves decreased by approximately 44% and 52% relative to the wild type under well-watered and drought stress conditions, respectively, indicating that about 50% of total wax biosynthesis in *Arabidopsis* leaves is dependent on both MYB94 and MYB96 (Lee et al., 2016). However, it is still unclear how the biosynthesis of the remaining wax in *myb94 myb96* is regulated in *Arabidopsis* under both conditions.

Arabidopsis transcriptome analysis showed that the expression of an AP2/DREB transcription factor, RELATED TO APETALA 2.4 (RAP2.4, At1g78080) was induced by drought and salt stress treatments (Feng et al., 2005). *M. truncatula* WXP1, which shares the highest sequence homology with *Arabidopsis* RAP2.4, displayed increased total wax loads and enhanced drought tolerance in transgenic alfalfa (*Medicago sativa*) (Zhang et al., 2005). Lin et al. (2008) observed enhanced drought tolerance in *Arabidopsis* overexpressing *RAP2.4* (*RAP2.4* OX), but no significant differences were detected in water loss between wild type and *RAP2.4* OX lines. These results suggest that regulation of cuticular wax biosynthesis may be involved in the drought stress response mediated by *Arabidopsis* RAP2.4.

In this study, we investigated the role of an AP2/DREB-type transcription factor, RAP2.4 in cuticular wax biosynthesis in *Arabidopsis* leaves under drought stress condition. Quantitative Real-Time-PCR (qRT-PCR) analysis showed that *RAP2.4* expression is induced by treatment with ABA, and drought, salt, and osmotic stress. Under drought stress condition, total wax loads significantly decreased in *Arabidopsis rap2.4-1* and *rap2.4-2* leaves relative to the wild type under drought stress conditions, but no remarkable differences between the wild type and *rap2.4* mutants were observed under well-watered conditions. In addition, we observed that ectopic expression of *RAP2.4* increased total wax loads in *Arabidopsis* leaves and delayed water-loss through the cuticular layer of leaves.

Transactivation assay of RAP2.4 in *N. benthamiana* protoplasts revealed that the expression of *KCS2* and *CER1* involved in VLCFA and alkane biosynthesis, respectively, is induced by *RAP2.4* expression and in particular, the CCGAC or GCC consensus motifs present in the *KCS2* and *CER1* promoter regions are required for RAP2.4-mediated elevation of *KCS2* and *CER1* expression. These results demonstrate that an AP2/DREB-type transcription factor, RAP2.4 activates cuticular wax biosynthesis by increasing the expression of *KCS2* and *CER1* in *Arabidopsis* leaves under drought. This study suggests that RAP2.4, in addition to MYB96 and MYB94, is also an important component of the transcriptional gene regulatory network involved in drought-induced wax biosynthesis in *Arabidopsis*.

MATERIALS AND METHODS

Plant Materials and Growth Conditions

The *Arabidopsis* T-DNA insertion mutants *rap2.4-1* (SALK_020767) and *rap2.4-2* (SALK_093377) were obtained from the Arabidopsis Biological Resource Center (ABRC[1]). To isolate *rap2.4* mutants, the genomic DNA was isolated from rosette leaves of 2-week-old *Arabidopsis* using DNA extraction buffer [200 mM Tris-Cl (pH 8.0), 250 mM NaCl, 25 mM EDTA (pH 8.0), 0.5% SDS]. Genomic DNA and gene-specific primers (**Supplementary Table 1**) were used for DNA-based PCR. The seeds of *Arabidopsis* wild type (Col-0), transgenic *Arabidopsis* lines overexpressing *RAP2.4*, and *rap2.4 Arabidopsis* mutants were surface-sterilized with 75% EtOH solution containing 0.05% Triton X-100 and 100% EtOH. The *Arabidopsis* seeds were germinated in 1/2 MS medium (0.22% Murashige and Skoog media, 1% sucrose, 0.7% phytoagar, pH 5.7). Transgenic *Arabidopsis* seeds were germinated in 1/2 MS medium containing kanamycin (25 μg/ml). Seven-day-old *Arabidopsis* seedlings were transferred to sterile soil (soil:vermiculite:perlite, 3:2:1). All growth conditions were maintained at 24 ± 2°C under long-day conditions (16 h/8 h).

For treatment of drought stress, 7-day-old seedlings of wild type (Col-0) and *rap2.4* mutants were transferred to plastic pots [350 (W) × 270 (D) × 130 (H)] filled with 500 g of soil. The transferred seedlings were covered with plastic wrap to maintain humidity for 5 days, The plastic wrap was punched with a razor blade to maintain ambient humidity; the plastic wrap was removed after 2 days. The soil was first soaked with water and then the plants were exposed to drought stress for 2 weeks. Next, the soil was re-soaked with water and then, the plants were subjected to a second drought treatment for 2 weeks.

Construction of Binary Vectors and *Arabidopsis* Transformation

To generate transgenic *Arabidopsis* overexpressing *RAP2.4*, *RAP2.4* cDNA was amplified using At1g78080 F1/At1g78080 R1 primers (**Supplementary Table 1**) and *Arabidopsis* seedling cDNA. The amplified products were translationally fused with the gene encoding enhanced yellow fluorescent protein (eYFP) between the CaMV35S promoter and the terminator of ribulose 1,5-biphosphate carboxylase/oxygenase small subunit (rbc-T) from *Pisum sativum* in the modified pPZP212 binary vector[2] (Hajdukiewicz et al., 1994). The recombinant vector was introduced into *Arabidopsis* (ecotype, Col-0) using *Agrobacterium*-mediated transformation (Clough and Bent, 1998). Transgenic *Arabidopsis* seedlings (*RAP2.4* OX) were selected in 1/2 MS medium containing carbenicillin (100 μg/ml) and kanamycin (25 μg/ml). The selected transgenic plants (T_2 or T_3 plants) were used for further experiments.

Isolation of Total RNA and Gene Expression Analysis

To analyze the expression of *RAP2.4* in various organs or tissues of *Arabidopsis*, we collected 1-week-old seedlings and rosette leaves, stems, flowers, buds, and siliques of 6-week-old *Arabidopsis*. To investigate the expression patterns after treatment of osmotic stress, salt stress, or exogenous ABA, 10-day-old seedlings were floated and incubated in 1/2 MS liquid medium containing 200 mM mannitol, 200 mM NaCl, or 100 μM ABA for 1, 2, and 6 h at 25]°C with shaking at 40 rpm. For exposure to drought stress, 10-day-old seedlings were transferred to cellulose paper (Whatman) and air-dried for 1 and 2 h. To investigate the expression patterns of cuticular wax biosynthetic genes in 4-week-old *Arabidopsis* wild type and *rap2.4* mutants after the drying event, the aerial parts of wild type and *rap2.4* mutants were cut and placed on the cellulose paper and air-dried for 1, 2, and 4 h. To analyze the expression patterns of cuticular wax biosynthetic genes in the wild type and transgenic *Arabidopsis* overexpressing *RAP2.4*, the rosette leaves were collected from 4-week-old *Arabidopsis*. Total RNA was isolated using the Nucleospin RNA Plant Extraction Kit (MACHEREY-NAGEL) following the manufacturer's protocols. Total RNA was used for cDNA synthesis using Gostrip™ Reverse Transcriptase (Promega) following the manufacturer's protocols. The cDNA and gene-specific primers (**Supplementary Table 1**) were used for both the semi-RT-PCR and the quantitative RT-PCR (CFX96 thermal cycler, Bio-Rad). The KAPA SYBR FAST qRT-PCR kit (KAPA Biosystems) was used for quantitative RT-PCR. Quantification of the *PP2AA3* (At1g13320) transcripts was used for normalization of the *RAP2.4* transcripts and cuticular wax biosynthetic genes.

Scanning Electron Microscope (SEM) Analysis

To observe the cuticular wax crystal on the surface of leaves, rosette leaves from 4-week-old wild type and transgenic *Arabidopsis* overexpressing *RAP2.4* were used according to methods described in a previous study (Lee and Suh, 2015b).

Cuticular Wax Analysis Using Gas Chromatography (GC)

The cuticular wax were extracted from rosette leaves of 5- to 6-week-old wild type, *rap2.4* mutants, and three independent

[1]https://www.arabidopsis.org/

[2]https://www.novoprolabs.com/vector/V10826, pRAP2.4.

transgenic *Arabidopsis* overexpressing *RAP2.4* (OX20, OX26, and OX31) by shaking in chloroform for 30 s. Extracts were evaporated under nitrogen gas after adding the internal standard (1-tricosanol, docosanoic acid, and *n*-octacosane). Then, concentrated wax was dissolved in a solution of pyridine and bis-*N,O*-trimethylsilyl trifluoroacetamide (BSTFA, Sigma) (1:1, v/v) and incubated at 90°C for 30 min. The silylated waxes were concentrated under nitrogen gas and they were re-dissolved with premixed heptane-toluene solution (1:1, v/v). The conditions of the GC analysis were described in a previous study (Lee and Suh, 2015b).

Transpiration and Chlorophyll Leaching Assays

For the cuticular transpiration assay, well-watered 3-week-old *Arabidopsis* plants were incubated in the dark for 12 h, and the shoot was carefully separated from the root. Subsequently the shoot was fully watered for 1 h by floating on water. After removal of water from the shoot surface, the weights of the shoots were measured for 2.5 h with 15 min. intervals while maintaining the dark condition.

For the chlorophyll leaching assay, the shoots without roots of well-watered 3-week-old *Arabidopsis* were exposed to the dark for 12 h, and then immediately immersed in 80% ethanol with shaking at 40 rpm. The extracted chlorophyll content was measured for 3 h with 15 min. intervals on a spectrophotometer (Ultrasec 3100 pro; Amersham Biosciences) at wavelengths of 647 and 664 nm. The chlorophyll content was calculated as μmol Chlorophyll/fresh weight (FW, g) = [7.93 (A664) + 19.53 × (A647)]/FW (g).

Transcriptional Activation Assay in *N. benthamiana* Protoplasts

The transcriptional activation assays were performed as described in Lee and Suh (2015b). For making reporter constructs, the minimal *CaMV 35S* promoter and *LUC* gene of *Gal4(3X):LUC* plasmid (Tiwari et al., 2003) were amplified with Min35S pro_*Pst*I-F/Min35S pro_*Xba*I-R primer set and Luc *Xma*I F/Luc *Sac*I R primer set, respectively, and then the *CaMV 35S* promoter and *GUS* gene of pBI221 were replaced with the amplified DNA fragments, minimal *CaMV 35S* promoter and *LUC* gene, respectively (**Supplementary Table 1**). The generated vector named as pBI:LUC. Next, the oligonucleotides (KCS2 BS1, KCS2 BS2, CER1 BS1, and CER1 BS2) containing the consensus CCGAC or GCC motifs, which are present in the promoter regions of *KCS2* and *CER1* and their mutated oligonucleotides (KCS2 mBS1, KCS2 mBS2, CER1 mBS1, and CER1 mBS2), where the consensus CCGAC and GCC sequences were changed to TTTTT and TTT sequences, were designed. The *Hin*dIII and *Sal*I restriction enzyme sites were included in the designed oligonucleotides at 5'- and 3'-end, respectively. The synthesized oligonucleotides were annealed, and then the DNA fragments were cloned in *Hin*dIII and *Sal*I sites of the *pBI:LUC* vector. The *pPZP212* and *pRAP2.4* binary vectors were used as the effector. The *pPZP212* or *pRAP2.4.* binary vector was co-transfected with each reporter vector into *N. benthamiana* leaf protoplast using polyethylene glycol (PEG)-mediated transfection (Yoo et al., 2007). The *pBI221* expression vector was used as the normalization factor. Twenty hours after transfection, total protein extracted from the protoplasts was subjected to enzymatic assays to quantifyluciferase (LUC) activity using a dual-luciferase assay system (Promega). Quantification of the GUS level was used for normalization of quantification of LUC activity. The fluorescence of LUC and GUS were detected under GLOMAX (Promega).

RESULTS

Expression of *RAP2.4* in *Arabidopsis*

To investigate the expression levels of *RAP2.4* gene in various *Arabidopsis* organs, we isolated total RNAs from 7-day-old seedlings and rosette leaves, stem, cauline leaves, floral buds, flowers, and siliques of 6-week-old plants, and then subjected them to qRT-PCR. When the transcript level of *RAP2.4* was compared with that of *PP2AA3*, which is used as a reference gene to assess the quantity and quality of RNA samples (Czechowski et al., 2005), the level of *RAP2.4* transcripts was approximately 1.6- to 3.4-fold higher in the various *Arabidopsis* organs tested (**Figure 1A**). The highest expression of *RAP2.4* was observed in cauline leaves. To measure the increased levels of *RAP2.4* transcripts in *Arabidopsis* after drought, osmotic, and salt stress treatments or ABA applications, 10-day-old seedlings were air-dried or incubated on 1/2 MS media supplemented with 200 mM mannitol, 200 mM NaCl, or 100 μM ABA for 0, 1, 2, or 6 h. The transcript levels of *RAP2.4* increased by approximately 2.9- to 3.1-fold with drought treatment, 2.0- to 3.2-fold with 200 mM mannitol treatment, 1.8- to 2.9-fold with salt stress, and 2.1- to 3.1-fold with ABA applications (**Figure 1B**).

Isolation of *rap2.4* Knock-Out Mutants and Generation of Transgenic Arabidopsis Plants Overexpressing *rap2.4*

To investigate the role of the *RAP2.4* gene in cuticular wax biosynthesis, T-DNA-inserted *rap2.4* mutant seeds (SALK_020767C and SALK_093377) were obtained from the Arabidopsis Biological Resource Center (www.arabidopsis.org). The T-DNA insertions were designated between 710 and 711 bp from initiation of transcription in *rap2.4-1* (SALK_020767C) and 1504 and 1505 bp from initiation of transcription in *rap2.4-2* (SALK_093377) in the TAIR site (see footnote 1) (**Figure 2A**). To check the T-DNA insertions from *rap2.4-1* and *rap2.4-2* mutants, genomic DNA was extracted from leaves of *rap2.4-1* and *rap2.4-2*, and then genomic DNA PCR was performed. PCR bands, which were amplified using At1g78080-NF1 and At1g78080-CR1 primers, were detected in wild type (Col-0) but not in *rap2.4-1* and *rap2.4-2* mutants. However, PCR bands, which were amplified using LBa1 and At1g78080-CR1 or At1g78080-NF1 and LBa1 primers, were detected in *rap2.4-1* and *rap2.4-2* mutants but not in the wild type (Col-0) (**Figure 2B**). In

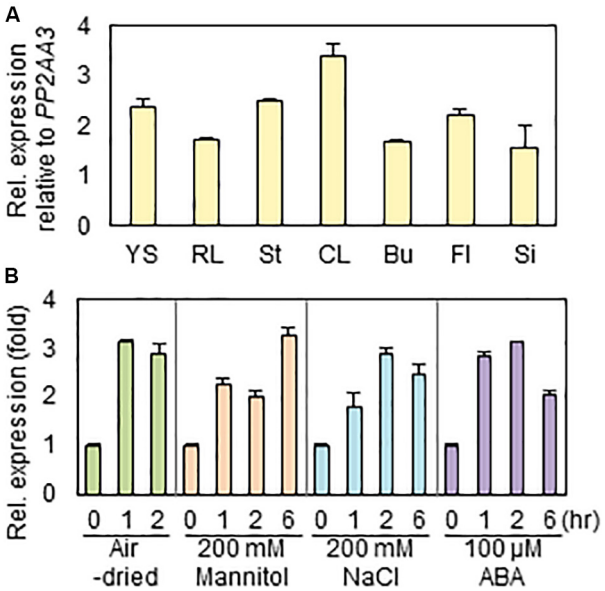

FIGURE 1 | Expression of *RAP2.4* in *Arabidopsis*. **(A)** The transcript level of *RAP2.4* in various organs of *Arabidopsis*. Total RNA was isolated from 1-week-old seedlings (YS), rosette leaves (RL), stems (St), cauline leaves (CL), buds (Bu), flowers (Fl), and silique (Si) of 6-week-old *Arabidopsis*. Transcript levels were determined by quantitative Real Time-Polymerase Chain Reaction (qRT-PCR) and relative expression was determined using the ΔΔCt method. *PP2AA3* (At1g13320) was used to determine the quantity and quality of the cDNAs. Each value is the mean ± SD of three independent measurements. **(B)** Expression of *RAP2.4* transcripts after application of exogenous ABA and treatment of salt and osmotic stress, and drought. One-week-old seedlings were transferred to the 1/2 MS liquid medium supplemented with 200 mM mannitol, 200 mM NaCl, or 100 μM ABA for the indicated times. For drought stress, the transferred seedlings were air-dried for the indicated times. Transcript levels were determined by qRT-PCR and relative expression was determined using the ΔΔCt method. *PP2AA3* (At1g13320) was used to determine the quantity and quality of the cDNAs. Each value is the mean ± SD of three independent measurements.

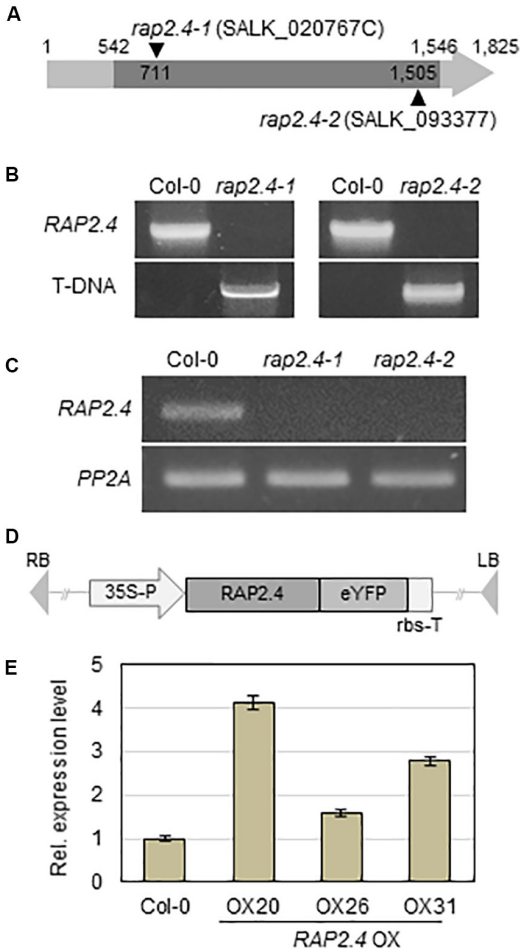

FIGURE 2 | Isolation of *Arabidopsis RAP2.4* knock-out mutant and generation of transgenic *Arabidopsis* overexpressing *RAP2.4*. **(A)** Schematic diagram of T-DNA-inserted *Arabidopsis rap2.4* mutants. The *rap2.4-1* and *rap2.4-2* are *RAP2.4* knock-out mutant alleles. Genomic DNA-PCR **(B)** and reverse transcription (RT)-PCR **(C)** analyses of *RAP2.4* in *Arabidopsis* wild type (Col-0) and *rap2.4* mutants. Total RNA was extracted from 4-week-old rosette leaves and subjected to RT-PCR. *PP2AA3* (At1g13320) was used to determine the quantity and quality of the cDNAs. **(D)** Schematic diagram of *RAP2.4* overexpression construct under the control of the CaMV 35S promoter (35S-P). rbs-T, terminator of ribulose 1,5-biphosphate carboxylase/oxygenase small subunit from *Pisum sativum*. eYFP, enhanced yellow fluorescent protein. RB, right border. LB, left border. **(E)** Quantitative real-time (RT)-PCR analysis of three independent transgenic *Arabidopsis* plants overexpressing *RAP2.4* (OX20, OX26, and OX31). Total RNA was extracted from 4-week-old rosette leaves. *PP2AA3* (At1g13320) was used to determine the quantity and quality of the cDNAs. Transcript levels were determined by qRT-PCR and relative expression was determined using the ΔΔCt method. Each value is the mean of three independent measurements. Bars indicate standard deviation.

RT-PCR analysis of 4-week-old wild type *rap2.4-1*, and *rap2.4-2* leaves, *RAP2.4* transcripts were detected in the wild type but not in *rap2.4-1* and *rap2.4-2*, indicating that *rap2.4-1* and *rap2.4-2* are knockout mutants (**Figure 2C**).

To generate transgenic *Arabidopsis* plants overexpressing *RAP2.4*, *RAP2.4* was inserted between the *CaMV 35S* promoter and the terminator of ribulose 1,5-biphosphate carboxylase/oxygenase small subunit (rbs-T) (**Figure 2D**). The generated binary vector was transformed into *Arabidopsis* plants via the *Agrobacterium*-mediated transformation method. qRT-PCR showed that the levels of *RAP2.4* transcripts in *RAP2.4* overexpression lines, OX20, OX26, and OX31 increased by 4.7-fold, 1.6-fold, and 2.8-fold, respectively, compared to the wild type (**Figure 2E**). During growth and development, we observed that growth of *RAP2.4* OX lines was smaller than that of the wild type and the growth-retarded phenotype was prominent in *RAP2.4* OX20. However, no noticeable differences in growth and development were observed between wild type and *rap2.4* mutants (**Supplementary Figure 1**).

Cuticular Wax Content and Composition in Arabidopsis Wild Type and *rap2.4* Mutants Under Well-Watered and Drought Stress Conditions

To investigate the effect of loss-of-function of *RAP2.4* on cuticular wax composition and amount, cuticular waxes were

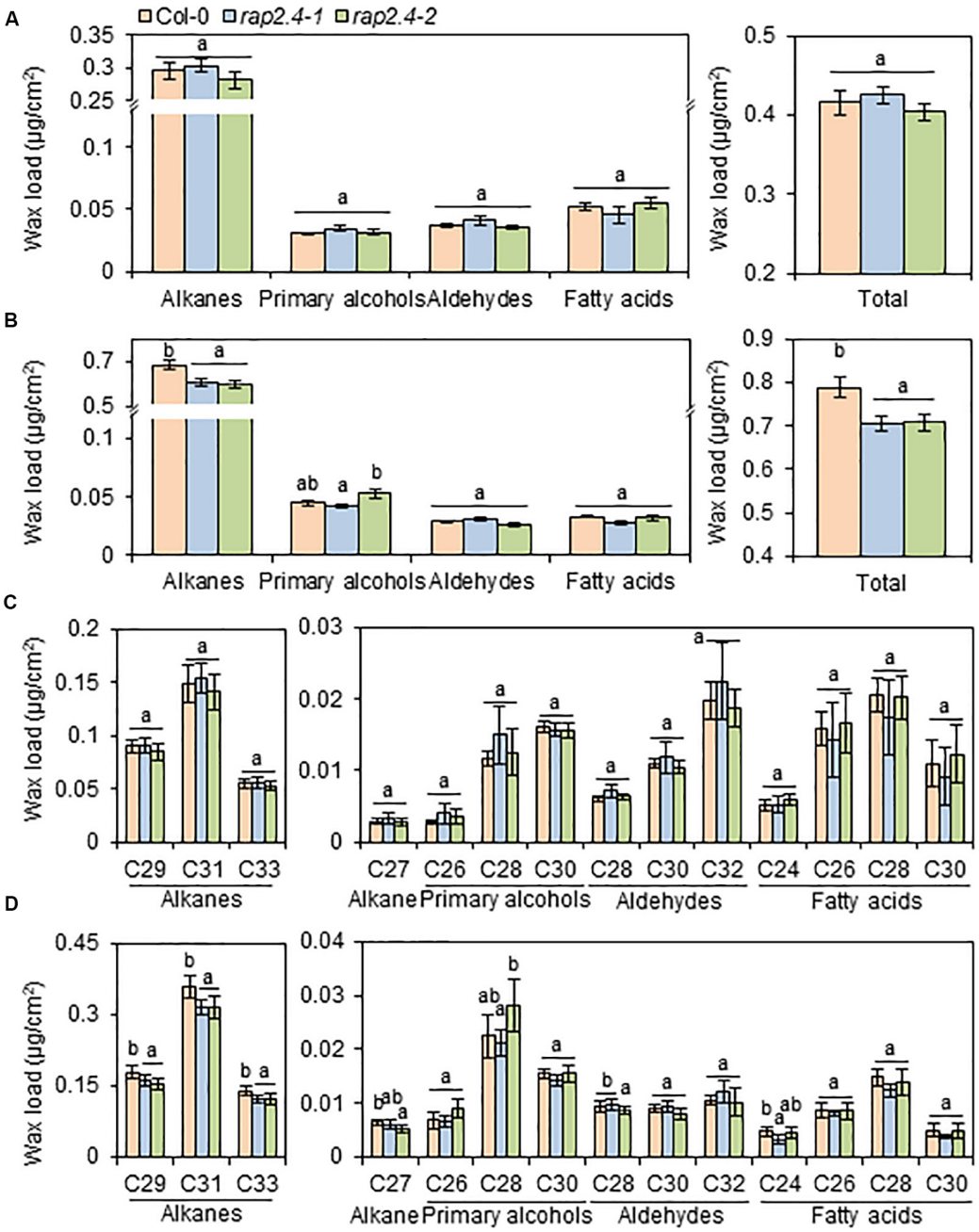

FIGURE 3 | Cuticular wax amount and composition in the leaves of *Arabidopsis* wild type (Col-0) and *rap2.4* mutants under normal and drought conditions. **(A)** Cuticular wax amount in leaves of plants grown under the normal growth conditions (temperature, 24 ± 2°C; humidity, approximately 50%; light condition, 100–120 μmol $m^{-2}s^{-1}$). **(B)** Cuticular wax amount in leaves of plants grown under the drought stress conditions. **(C)** Cuticular wax composition in leaves of plants grown under normal growth conditions. **(D)** Cuticular wax composition in leaves of plants grown under drought stress conditions. Cuticular waxes were extracted from leaves of 5- to 6-week-old *Arabidopsis* grown under normal growth and drought stress conditions. Each value is the mean of three independent measurements. Bars indicate standard deviation. Different letters denote statistically significant differences at $P < 0.05$ (Tukey's test), following a one-way ANOVA test with treatment as the variable factor.

extracted from leaves and stems of wild type, *rap2.4-1,* and *rap2.4-2* mutants which were grown under well-watered or drought stress conditions, and measured by gas chromatography (GC) with a flame ionization detector (FID). Wild type and *rap2.4* mutants showed no significant differences in leaf wax content and composition under sufficiently watered conditions (**Figures 3A,C**). Under the drought stress condition, however, total wax loads decreased by approximately 10% in both *rap2.4-1* and *rap2.4-2* leaves relative to the wild type (**Figures 3B,D**). Approximately 13–19%, 11–14%, 11–12%, and 12% reduction

in the levels of each VLC-alkane, C27, C29, C31, and C33, respectively, were observed in *rap2.4* mutants relative to the wild type under drought (**Figures 3B,D**). However, there were no significant differences in the levels of other wax components even though plants were grown under drought (**Figures 3B,D**).

Epicuticular Wax Crystals and Cuticular Wax Content and Composition in *Arabidopsis* Wild Type and *RAP2.4* Overexpression Lines

Because the wax-deficient phenotype of *rap2.4* mutants was observed under drought, we next examined the formation of epicuticular wax crystals in leaves of wild type and *RAP2.4* overexpression lines using SEM. SEM analysis showed that epicuticular wax crystals were clearly observed in leaves of *RAP2.4* OX20, OX26, and OX31 lines, but not in leaves of the wild type (**Figure 4A**).

Subsequently, the content and composition of cuticular waxes were measured from leaves and stems of wild type and *RAP2.4* overexpression lines using GC-FID (**Supplementary Figure 2**). Total wax content increased by approximately 3.3-, 1.5-, and 1.8-fold in *RAP2.4* OX20, OX26, and OX31, respectively, compared with to that in the wild type (**Figure 4B**). The largest increase (1.7- to 4.2-fold) in leaves of all three *RAP2.4* OX lines relative to that in the wild type was observed in the levels of VLC-alkanes (C27, C29, C31, and C33), which are major wax components (more than 70% of total wax loads) in *Arabidopsis* leaves (**Figure 4C**). In particular, approximately 3.2-, 5.3-, 4.0-, and 3.1-fold increase in the levels of C27, C29, C31, and C33, respectively, was observed in leaves of *RAP2.4* OX20 compared with that of the wild type (**Figure 4C**). The significant increase in the levels of C29, C31, and C33 VLC-alkanes was also observed in leaves of *RAP2.4* OX26, and OX31 relative to wild type (**Figure 4C**). An increase in the levels of other components, VLC-primary alcohols (C26, and C28), VLC-aldehydes (C28, C30, and C32), and VLC-fatty acids (C24 and C30) was also detected in leaves of *RAP2.4* OX20 and OX31 relative to the levels in the wild type, except for C30 VLC-PA and C28 VLCFAs (**Figure 4C**). The levels of C28 and C30 VLC-PA were increased in leaves of *RAP2.4* OX26 relative to wild type (**Figure 4C**).

Cuticular Transpiration and Chlorophyll Leaching Assays in *Arabidopsis* Wild Type and *RAP2.4* Overexpression Lines

An increase in total wax loads in leaves of *RAP2.4* OX lines prompted us to measure cuticular transpiration and chlorophyll leaching assays in the *Arabidopsis* wild type and *RAP2.4* overexpression lines. For the cuticular transpiration assay, 3-week-old wild type and *RAP2.4* OX lines were dark-treated for 12 h to completely close stomata in leaves, whole aerial parts of plants were floated on water under dark for 1 h, and then, cuticular transpiration rate was measured. As shown in **Figure 5A**, the water loss through the cuticle was slower in all three *RAP2.4* OX lines than in the wild type.

For the chlorophyll leaching assay, 3-week-old wild type and *RAP2.4* OX lines were incubated for 12 h under dark, whole aerial parts of the plants were immersed in 80% ethanol, and then, the chlorophyll content leached from the leaves was measured. As shown in **Figure 5B**, the rate of chlorophyll leaching was slower in the *RAP2.4* OX lines than in the wild type.

Expression of Genes Involved in Cuticular Wax Biosynthesis and Its Regulation in Arabidopsis Wild Type, *rap2.4* Mutants, and *RAP2.4* OX Leaves Under Well-Watered and/or Drought

Next, we examined whether the significant decrease in total wax loads and levels of alkanes observed in *rap2.4-1* and *rap2.4-2* leaves relative to that in the wild type under drought stress conditions correlates with the reduced expression of genes involved in cuticular wax biosynthesis and its regulation. Total RNA was isolated from wild type and *rap2.4* mutant leaves, which were air-dried for 0, 1, 2, and 4 h and then subjected to qRT-PCR analysis. The *RAP2.4* gene displayed the highest expression in wild type leaves 1 to 2 h after drought treatment. The expression of *RD29A* (*At5g52310*), which is known as a drought-inducible gene (Shinozaki and Yamaguchi-Shinozaki, 2007), was upregulated in both wild type and *rap2.4* mutant leaves 1 h after drought treatment and continuously increased in the wild type up to 4 h after drought treatment. However, no further increase in the levels of *RD29A* was detected in *rap2.4* mutant leaves 2 and 4 h after drought treatment. Increased levels of *KCS2* (*At1g04220*) and *CER1* (*At1g02205*) transcripts were approximately 20% and 40% lower, respectively, in *rap2.4* leaves than in wild type leaves 4 h after drought treatment (**Figure 6A**). However, no significant differences were observed in the levels of *KCR1* (*At1g67730*), *PAS2* (*At5g10480*), *KCS6* (*At1g68530*), *CER3* (*At5g57800*), *MYB94* (*At3g47600*), and *MYB96* (*At5g62470*) expression between wild type and *rap2.4* leaves after drought treatment (**Supplementary Figure 3**).

In addition, the expression of *KCS2* and *CER1* was markedly upregulated in all three *RAP2.4* OX lines relative to that in the wild type (**Figure 6B**). The levels of *KCS1* (*At1g01120*), *KCS6*, *CER3*, and *CER4*/*FAR3* (*At4g33790*) were increased by 1.2- to 2.0-fold in 2 or 3 *RAP2.4* OX lines compared with that in the wild type, but no significant change in the levels of *PAS2* and *ECR* (*At3g55360*) expression was observed between the wild type and *RAP2.4* OX lines (**Figure 6B**). These results indicate that *KCS2* and *CER1* are directly or indirectly regulated by the *RAP2.4* transcription factor under drought.

Transcriptional Activation Assay of RAP2.4 in *N. benthamiana* Protoplasts

Based on the observation that the expression of *KCS2* and *CER1* was altered in *rap2.4* mutants and *RAP2.4* OX lines compared with that in the wild type, we further examined whether RAP2.4 directly regulate the expression of *KCS2* and *CER1*. According to the previous report that RAP2.4 specifically recognizes the CCGAC core sequences of the drought response element (DRE) and GCC box (Rae et al., 2011), the consensus CCGAC and GCC motifs were searched in the promoter regions of *KCS2* and *CER1*. For reporter constructs, the selected

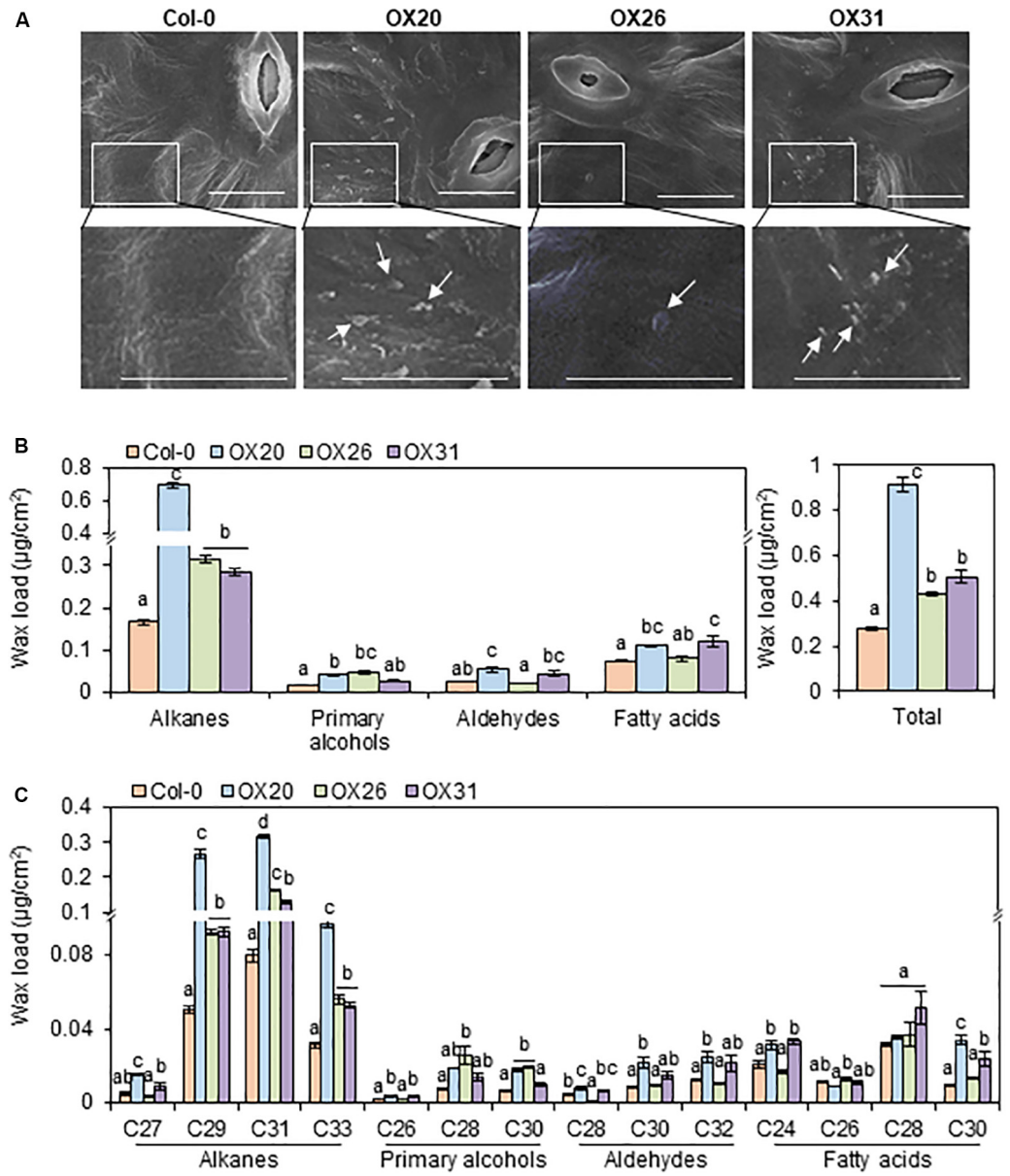

FIGURE 4 | Epicuticular wax crystals **(A)** and cuticular wax amount and composition **(B)** in the leaves of *Arabidopsis* wild type (Col-0) and *RAP2.4* OX lines. **(A)** Scanning electron microscopy analysis of epicuticular wax crystals on leaves of 3- to 4-week-old *Arabidopsis* wild type (Col-0) and *RAP2.4* OX lines. The images (inset) in the upper panel were magnified and shown in the lower panel. Bars = 10 μm. White arrows indicate wax crystals. **(B)** Cuticular wax amount in leaves of 5-week-old *Arabidopsis* wild type (Col-0) and *RAP2.4* OX lines. **(C)** Cuticular wax composition in leaves of 5-week-old *Arabidopsis* wild type (Col-0) and *RAP2.4* OX lines. Each value is the mean of three independent measurements. Bars indicate standard error. Different letters denote statistically significant differences at $P < 0.05$ (Tukey's test), following a one-way ANOVA test with treatment as the variable factor.

DNA fragments (KCS2 BS1, KCS2 BS2, CER1 BS1, and CER1 BS2] containing the consensus CCGAC or GCC motifs and their mutated DNA fragments (KCS2 mBS1, KCS2 mBS2, CER1 mBS1, and CER1 mBS2), where the consensus CCGAC and GCC sequences were converted to TTTTT and TTT sequences, respectively, were transcriptionally ligated to the minimal *CaMV 35S* promoter in the pBI:LUC harboring the luciferase reporter gene (**Figures 7A,B**). For effector constructs, the coding region of *RAP2.4* was inserted between the *CaMV 35S* promoter and nopaline synthase (Nos) terminator in the *pPZP212* vector and named *pRAP2.4* (**Figure 7B**). The reporter and effector vectors were co-transfected into *N. benthamiana* protoplasts with a vector harboring *GUS* for internal control to monitor transformation efficiencies and luciferase and GUS activities were measured. The ratio of LUC activity to GUS activity in protoplasts expressing *LUC* driven by the *KCS2-P1, KCS2-P2*, and *CER1-P1* promoters was approximately 14.5-, 3.5-, and 2.8-fold elevated, respectively, but no significant increase

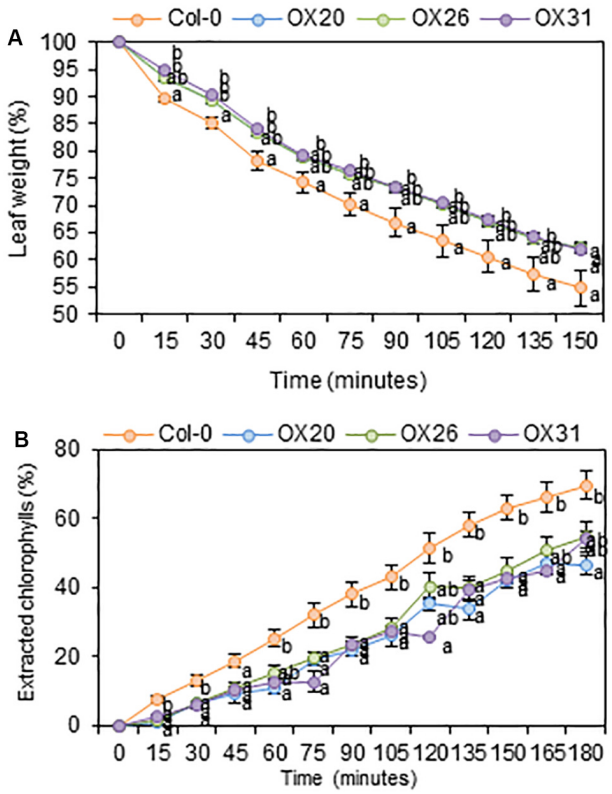

FIGURE 5 | Cuticular transpiration **(A)** and chlorophyll leaching **(B)** assays of *Arabidopsis* wild type (Col-0) and *RAP2.4* OX lines. **(A)** Cuticular transpiration assay in leaves of 3-week-old *Arabidopsis* wild type (Col-0) and *RAP2.4* OX lines. **(B)** Chlorophyll leaching in leaves of 3-week-old *Arabidopsis* wild type (Col-0) and *RAP2.4* OX lines. Each value represents the mean of three independent measurements. Bars indicate the standard error of the mean. Different letters denote statistically significant differences at $P < 0.05$ (Tukey's test), following a one-way ANOVA test with treatment as the variable factor.

in *LUC* gene expression driven by the *CER1-P2* promoter was observed, upon co-expression with *RAP2.4* compared with the *pPZP212* control. By contrast, the co-transformation of *pRAP2.4* with *KCS2-mP1, KCS2-mP2, CER1-mP1, or CER1-mP2* did not elevate the *LUC* gene expression (**Figure 7C**), indicating that the CCGAC or GCC consensus motifs present in the *KCS2* (BS1 and BS2) and *CER1* (BS1) promoter regions are essential for the expression of *KCS2* and *CER1* by RAP2.4 and RAP2.4 may be directly involved in the transcriptional activation of *KCS2* and *CER1* genes.

DISCUSSION

When land plants face water deficit stress, they close the stomata (Brodribb and McAdam, 2017) and the aerial organs of land plants increase total loads of cuticular waxes, which are present in the outermost layer of the cuticle, to reduce non-stomatal water loss (Riederer and Schreiber, 2001; Domínguez et al., 2017). In particular, an increase in the levels of alkanes among the diverse wax components is prominent in *Arabidopsis* under drought (Kosma et al., 2009; Lee and Suh, 2015a). Although involvement of MYB96 and MYB94 transcription factors has been reported in the upregulation of cuticular wax biosynthesis in *Arabidopsis* (Seo et al., 2011; Lee and Suh, 2015b; Lee et al., 2016), increased total wax loads were still observed in *myb96 myb94* mutants relative to the wild type under drought. This observation prompted us to find another transcription factor, which upregulates cuticular wax biosynthesis in *Arabidopsis* under drought. In this study, we show that ABA-, drought-, osmotic-, and salt-stress inducible *RAP2.4* activates cuticular wax biosynthesis in *Arabidopsis* leaves under drought stress conditions. qRT-PCR and transcriptional activation assays revealed that RAP2.4 upregulates the expression of *KCS2* and *CER1*, which are required for the production of alkanes, and contributes to an increase in total wax loads which is critical for drought resistance in *Arabidopsis* leaves.

The aerial parts of land plants increase or decrease total wax loads by the up- or down-regulation of genes involved in cuticular wax biosynthesis under different environmental conditions such as drought, dark, or pathogen infection or in an organ-specific manner (Raffaele et al., 2008; Buschhaus and Jetter, 2011; Seo et al., 2011; Go et al., 2014; Park et al., 2016). Therefore, it has been speculated that cuticular wax biosynthesis is mainly regulated by transcriptional regulatory mechanism, which is supported by the identification of several transcription factors, WIN1/SHN1, MYB30, MYB96, MYB94, DEWAX, DEWAX2, and WRI4 involved in the regulation of wax biosynthesis (Aharoni et al., 2004; Raffaele et al., 2008; Seo et al., 2011; Go et al., 2014; Lee and Suh, 2015b; Park et al., 2016; Kim et al., 2018). Among the several transcription factors, ABA- and drought-inducible MYB96 and MYB94 transcription factors were reported to additively function in the upregulation of cuticular wax biosynthesis under both well-watered and water-deficit conditions (Lee et al., 2016). However, the wax-deficient phenotype was observed in the leaves of *rap2.4-1* and *rap2.4-2* mutants under only drought stress conditions (**Figure 3**), suggesting that *RAP2.4* plays a role in the upregulation of cuticular wax biosynthesis under drought. The hypothesis is consistent with the enhanced expression of *RAP2.4* by ABA, salt, drought, and osmotic stress treatments (**Figure 1B**). In addition, in microarray analyses of 2-week-old Arabidopsis WT versus *myb96-D* (*MYB96* OX) leaves and 3- to 4-week-old Arabidopsis WT versus *MYB94* OX leaves, the levels of *RAP2.4* expression was only approximately 1.4- and 1.2-fold elevated in *myb96-D* (*MYB96* OX) and *MYB94* OX leaves relative to WT, respectively (Seo et al., 2011; Lee et al., 2016). No significant differences were observed in the levels of *MYB94* and *MYB96* expression between Arabidopsis WT and *rap2.4* leaves 1 h and 2 h after drought treatment (**Supplementary Figure 2**). Therefore, these results suggest that a DERB-type RAP2.4 transcription factor and MYB96/MYB94 transcription factors might independently regulate cuticular wax biosynthesis under drought stress conditions.

In wax chemical analysis in the leaves of *rap2.4-1* and *rap2.4-2* relative to that of the wild type under drought, a significant reduction was observed in the levels of alkanes, C29, C31, and C33, which comprise approximately 85% of total wax loads (**Figure 3**). Whereas a remarkable increase in the alkanes loads was observed in the leaves of *RAP2.4* OX lines, although an elevation in the content of other components was detected

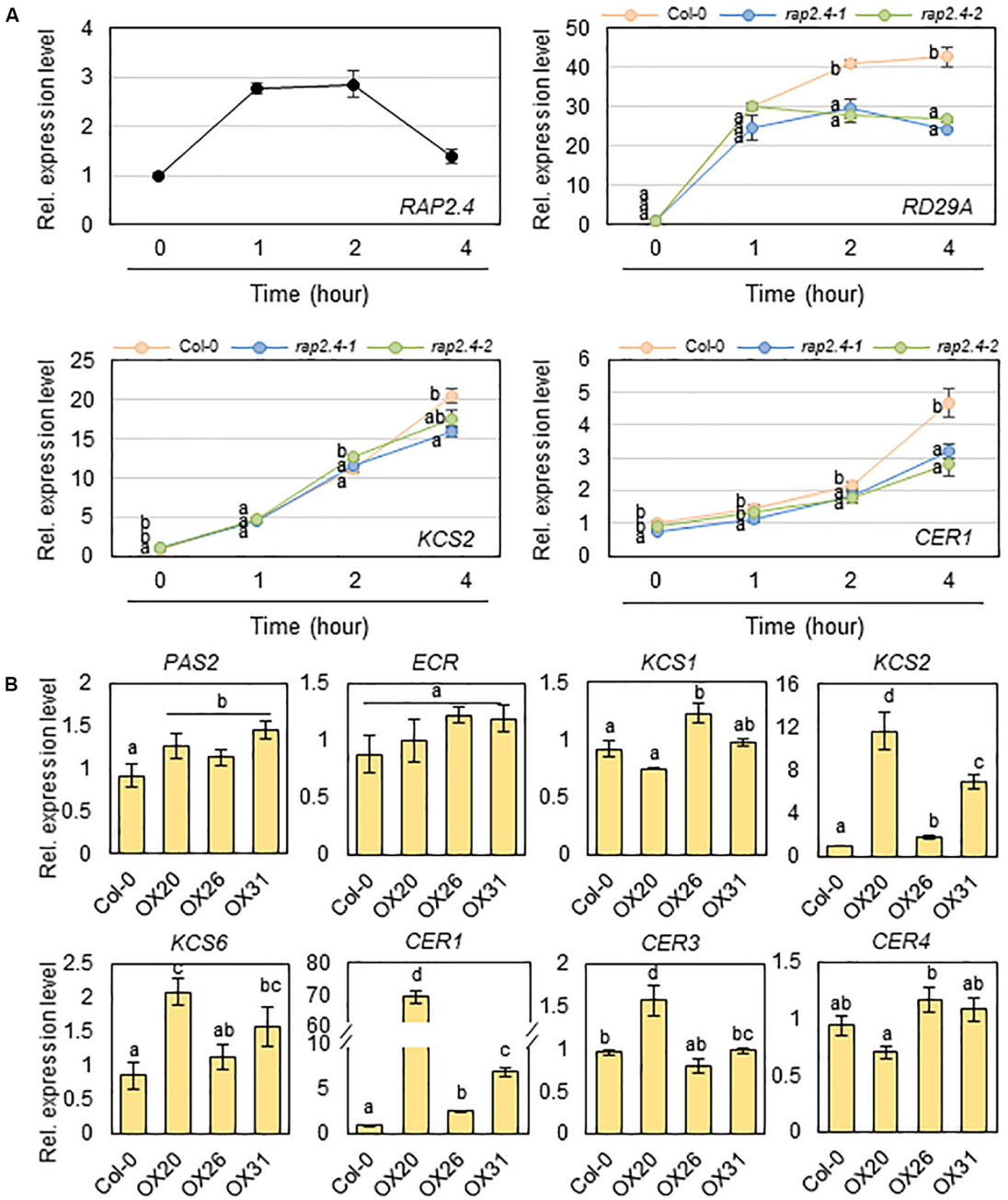

FIGURE 6 | Quantitative RT-PCR analysis of wax biosynthetic genes in 4-week-old wild type (Col-0), *rap2.4* mutants, and *RAP2.4* OX lines. **(A)** The transcript level of *RAP2.4* in 4-week-old *Arabidopsis* wild type (Col-0) and the transcript level of *RD29A*, *KCS2*, and *CER1* in 4-week-old *Arabidopsis* wild type (Col-0) and *rap2.4* mutants. Rosette leaves from 4-week-old *Arabidopsis* grown in soil were air-dried for 0, 1, 2, and 4 h. Each value represents the mean of three independent measurements. Bars indicate the standard deviation of the mean. Different letters denote statistically significant differences at $P < 0.05$ (Tukey's test), following a one-way ANOVA test with treatment as the variable factor. **(B)** Quantitative RT-PCR analysis of wax biosynthetic genes in 4-week-old *Arabidopsis* wild type (Col-0) and *RAP2.4* OX lines. The RNAs were extracted from rosette leaves of *Arabidopsis* grown in soil for three weeks. Each value represents the mean of three independent measurements. Bars indicate the standard deviation of the mean. Different letters denote statistically significant differences at $P < 0.05$ (Tukey's test), following a one-way ANOVA test with treatment as the variable factor.

(**Figure 4**). These results are consistent with the upregulation of *KCS2* and *CER1*, which function in VLCFA and alkane synthesis, respectively (**Figure 6**). Transcriptional activation assay (**Figure 7**) showed that the expression *KCS2* and *CER1* is increased by the expression of *RAP2.4* in tobacco protoplasts, indicating that *KCS2* and *CER1* are the target genes of RAP2.4. Among wax biosynthetic genes, the expression of *KCS2* and *CER1* genes are the most highly induced (approximately 10-

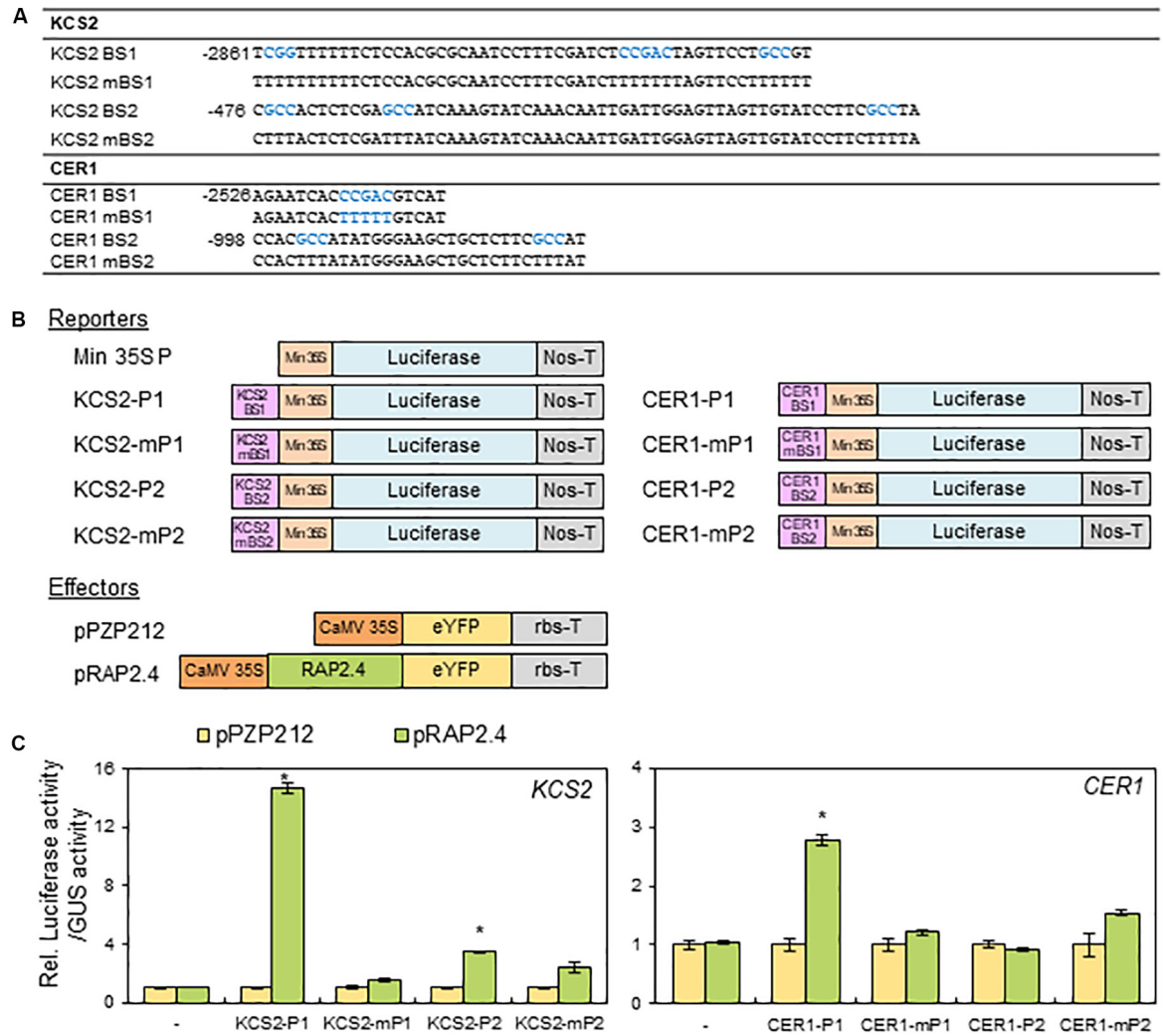

FIGURE 7 | Transactivation assay of *RAP2.4* in *N. benthamiana*. **(A)** The oligonucleotide sequences (BS) including RAP2.4 binding consensus sequences, which are present in the promoter regions of *KCS2* and *CER1* genes. Core binding sequences shown in blue were mutated, resulting in mBSs, to verify specific binding. **(B)** Schematic diagrams of reporter and effector constructs for transcriptional activation assay. For the reporter constructs, the synthesized oligonucleotides were annealed, and then the DNA fragments were ligated between the CaMV 35S minimal promoter (Min 35S) and the luciferase gene. For the effector construct, *RAP2.4* was translationally fused with the gene encoding eYFP between the CaMV 35S promoter (CaMV35SP) and the terminator of ribulose 1,5-biphosphate carboxylase/oxygenase small subunit from *Pisum sativum* (rbs-T). Nos-T, The terminator of the nopaline synthase gene. **(C)** Transcriptional activation assay in *N. benthamiana* leaf protoplasts. *N. benthamiana* leaf protoplasts were co-transformed with reporter and effector constructs, and luciferase and GUS activities were determined fluorometrically. Luciferase activity was normalized by dividing this value by GUS activity. Each value is the mean of four independent measurements (*t* test, $^*P < 0.01$). Bars indicate the standard error of the mean.

and 5-fold, respectively) in *Arabidopsis* in response to drought (Seo et al., 2011). In *myb96 myb94* seedlings, approximately 2- or 10-fold increase in the levels of *KCS2* and *CER1* transcripts were still detected under drought-treated conditions compared with that in the well-watered conditions (Lee et al., 2016). In addition to MYB96 and MYB94, therefore, RAP2.4 functions in the upregulation of *KCS2* and *CER1* under drought. In particular, electrophoretic mobility shift assay (EMSA) and/or chromatin immunoprecipitation (ChIP) assay showed that MYB96 and MYB94 transcription factors directly interact with the same cis-element (TAACTACTAACTA) in the promoter region of *KCS2* gene, suggesting that it is possible that ABA- and drought-induced expression of *KCS2* is synergistically regulated by MYB96 and MYB94 transcription factors (Seo et al., 2011; Lee et al., 2016). However, neither MYB96 nor MYB94 transcription factors were able to specifically bind to the putative consensus sequences in the *CER1* promoter region (Seo et al., 2011; Lee et al., 2016). In this study, transcriptional activation assay of RAP2.4 in *N. benthamiana* protoplasts revealed that the CCGAC or GCC consensus motifs in the promoter regions of *KCS2* and *CER1* are required for the expression of *KCS2* and *CER1* driven by RAP2.4 (**Figure 7**), indicating that ABA- and drought-inducible RAP2.4 may be directly involved in the transcriptional activation of *KCS2* and *CER1* genes under drought.

The stability of the MYB96 and MYB30 proteins was reported to be controlled by MYB30-INTERACTING E3 LIGASE 1 (MIEL1) E3 ubiquitin ligase, which controls protein turnover (Lee et al., 2017). In particular, Lee et al. (2017) reported that wax accumulation is balanced in *Arabidopsis* stems by preventing the adverse effects of excess MYB96 protein through degradation of MYB96. Based on the evidence that the transcript levels of *MIEL1* decreased significantly in 18-day-old *Arabidopsis* under osmotic (300 mM mannitol), salt (150 mM NaCl), and drought stress conditions[3], MYB96 could be stabilized to play a role in the activation of wax biosynthesis under drought (Seo et al., 2011). It was reported that BTB/POZ and MATH domain (BPM) proteins, which are substrate adaptors for Cullin 3-based E3 ubiquitin ligase, are negative regulators to control the stability of AP2/ERF transcription factors, DREB2A and WRI1, which are critical in the modulation of heat stress response and fatty acid metabolism, respectively (Chen et al., 2013; Morimoto et al., 2017). As Weber and Hellmann (2009) reported that RAP2.4 interacts with BPM proteins, it will be interesting to investigate whether the BPM and RAP2.4 interaction is involved in the molecular mechanisms underlying the regulation of drought-induced wax biosynthesis. The recent evidence that the Kelch-domain containing F-box protein, Small and Glossy Leaves 1(SAGL1) regulates cuticular wax biosynthesis by modulating the stability of CER3 in response to changes in humidity (Kim et al., 2019) supports that post-translational regulatory mechanism as well as transcriptional and post-transcriptional control mechanisms play important roles in the regulation of cuticular wax biosynthesis (Aharoni et al., 2004; Hooker et al., 2007; Raffaele et al., 2008; Seo et al., 2011; Lam et al., 2012, 2015; Go et al., 2014; Lee and Suh, 2015b; Park et al., 2016; Kim et al., 2018, 2019).

RAP2.4/WOUND INDUCED DEDIFFERENTIATION 1 (WIND1) has been reported to be implicated in plant development regulated by light and ethylene (Lin et al., 2008) and promotion of somatic cell dedifferentiation in response to wounding (Iwase et al., 2011). In particular, Lin et al. (2008) reported that *RAP2.4* OX seedlings or plants displayed shorter hypocotyls, reduced apical hook curvature in darkness, increased and longer root hairs, reduced size of cotyledons, and early flowering. In addition to the developmental defects in *RAP2.4* OX plants, overexpression of *RAP2.4* confers an enhanced tolerance to drought stress (Lin et al., 2008), but little was known about the molecular mechanism underlying drought tolerance in *RAP2.4* OX plants. In this study, we observed a wax-deficient phenotype in drought-treated *rap2.4-1* and *rap2.4-2* mutants, even though no noticeable phenotype was observed in the *rap2.4* mutants (Lin et al., 2008). In conclusion, an AP2/DREB-type transcription factor, RAP2.4, is a transcriptional activator which upregulates *KCS2* and *CER1* genes and thereby, the total wax loads increased in *Arabidopsis* leaves under drought. This study also suggests that RAP2.4 might be useful in the production of alkanes and the development of crops with enhanced drought tolerance.

[3] http://bar.utoronto.ca/efp/cgi-bin/efpWeb.cgi

DATA AVAILABILITY STATEMENT

All datasets for this study are included in the article/**Supplementary Material**.

AUTHOR CONTRIBUTIONS

SY, HK, and MS conceived and designed the research and wrote the manuscript. SY, HK, and RK conducted the experiments. SY, HK, RK, JK, and MS analyzed the data. JK edited the manuscript. All authors read and approved the manuscript.

FUNDING

This work was supported by grants from the National Research Foundation (NRF-2019R1A2B5B02070204) of South Korea and the Next-Generation BioGreen 21 Program (No. PJ013422) of the Rural Development Administration, South Korea.

ACKNOWLEDGMENTS

We thank Young Sam Go and Juyoung Kim for technical assistance.

SUPPLEMENTARY MATERIAL

The Supplementary Material for this article can be found online at: https://www.frontiersin.org/articles/10.3389/fpls.2020.00895/full#supplementary-material

REFERENCES

Aharoni, A., Dixit, S., Jetter, R., Thoenes, E., van Arkel, G., and Pereira, A. (2004). The SHINE clade of AP2 domain transcription factors activates wax biosynthesis, alters cuticle properties, and confers drought tolerance when overexpressed in *Arabidopsis*. *Plant Cell* 16, 2463–2480. doi: 10.1105/tpc.104.022897

Bach, L., Michaelson, L. V., Haslam, R., Bellec, Y., Gissot, L., and Marion, J. (2008). The very-long-chain hydroxy fatty acyl-CoA dehydratase PASTICCINO2 is essential and limiting for plant development. *Proc. Natl. Acad. Sci. U.S.A.* 105, 14727–14731. doi: 10.1073/pnas.0805089105

Bakan, B., and Marion, D. (2017). Assembly of the cutin polyester: from cells to extracellular cell walls. *Plants* 6:E57. doi: 10.3390/plants6040057

Beaudoin, F., Wu, X., Li, F., Haslam, R. P., Markham, J. E., Zheng, H., et al. (2009). Functional characterization of the *Arabidopsis* β-ketoacyl-coenzyme A reductase candidates of the fatty acid elongase. *Plant Physiol.* 150, 1174–1191. doi: 10.1104/pp.109.137497

Beisson, F., Li-Beisson, Y., and Pollard, M. (2012). Solving the puzzles of cutin and suberin polymer biosynthesis. *Curr. Opin. Plant Biol.* 15, 329–337. doi: 10.1016/j.pbi.2012.03.003

Bernard, A., and Joubès, J. (2013). *Arabidopsis* cuticular waxes: advances in synthesis, export and regulation. *Prog. Lipid Res.* 52, 110–129. doi: 10.1016/j.plipres.2012.10.002Get

Bourdenx, B., Bernard, A., Domergue, F., Pascal, S., Léger, A., Roby, D., et al. (2011). Overexpression of *Arabidopsis ECERIFEFUM1* promotes wax VLC-alkane biosynthesis and influences plant response to biotic and abiotic stresses. *Plant Physiol.* 156, 29–45. doi: 10.1104/pp.111.172320

Brodribb, T. J., and McAdam, S. A. M. (2017). Evolution of the stomatal regulation of plant water content. *Plant Physiol.* 174, 639–649. doi: 10.1104/pp.17.00078

Broun, P., Poindexter, P., Osborne, E., Jiang, C. Z., and Riechmann, J. L. (2004). WIN1, a transcriptional activator of epidermal wax accumulation in *Arabidopsis*. *Proc. Natl. Acad. Sci. U.S.A.* 101, 4706–4711. doi: 10.1073/pnas.0305574101

Buschhaus, C., and Jetter, R. (2011). Composition differences between epicuticular and intracuticular wax substructures: how do plants seal their epidermal surfaces? *J. Exp. Bot.* 62, 841–853. doi: 10.1093/jxb/erq366

Chen, L., Lee, J. H., Weber, H., Tohge, T., Witt, S., Roje, S., et al. (2013). *Arabidopsis* BPM proteins function as substrate adaptors to a cullin3-based E3 ligase to affect fatty acid metabolism in plants. *Plant Cell* 25, 2253–2264. doi: 10.1105/tpc.112.107292

Clough, S. J., and Bent, A. F. (1998). Floral dip: a simplified method for Agrobacterium-mediated transformation of *Arabidopsis thaliana*. *Plant J.* 16, 735–743. doi: 10.1046/j.1365-313x.1998.00343.x

Czechowski, T., Stitt, M., Altmann, T., Udvardi, M. K., and Scheible, W. R. (2005). Genome-wide identification and testing of superior reference genes for transcript normalization in *Arabidopsis*. *Plant Physiol.* 139, 5–17. doi: 10.1104/pp.105.063743

DeBono, A., Yeats, T. H., Rose, J. K., Bird, D., Jetter, R., Kunst, L., et al. (2009). *Arabidopsis* LTPG is a glycosylphosphatidylinositol-anchored lipid transfer protein required for export of lipids to the plant surface. *Plant Cell* 21, 1230–1238. doi: 10.1105/tpc.108.064451

Djemal, R., and Khoudi, H. (2019). Combination of the endogenous promoter-intron significantly improves salt and drought tolerance conferred by TdSHN1 transcription factor in transgenic tobacco. *Plant Physiol. Biochem.* 139, 435–445. doi: 10.1016/j.plaphy.2019.04.009

Domínguez, E., Heredia-Guerrero, J. A., and Heredia, A. (2017). The plant cuticle: old challenges, new perspectives. *J. Exp. Bot.* 68, 5251–5255. doi: 10.1093/jxb/erx389

Eigenbrode, S. D., and Espelie, K. E. (1995). Effects of plant epicuticular lipids on insect herbivores. *Annu. Rev. Entomol.* 40, 171–194. doi: 10.1146/annurev.en.40.010195.001131

Feng, J. X., Liu, D., Pan, Y., Gong, W., Ma, L. G., Luo, J. C., et al. (2005). An annotation update via cDNA sequence analysis and comprehensive profiling of developmental, hormonal or environmental responsiveness of the *Arabidopsis* AP2/EREBP transcription factor gene family. *Plant Mol. Biol.* 59, 853–868. doi: 10.1007/s11103-005-1511-0

Go, Y. S., Kim, H., Kim, H. J., and Suh, M. C. (2014). *Arabidopsis* cuticular wax biosynthesis is negatively regulated by the DEWAX gene encoding an AP2/ERF-type transcription factor. *Plant Cell* 26, 1666–1680. doi: 10.1105/tpc.114.123307

Greer, S., Wen, M., Bird, D., Wu, X., Samuels, L., Kunst, L., et al. (2007). The cytochrome P450 enzyme CYP96A15 is the midchain alkane hydroxylase responsible for formation of secondary alcohols and ketones in stem cuticular wax of *Arabidopsis*. *Plant Physiol.* 145, 653–667. doi: 10.1104/pp.107.107300

Hajdukiewicz, P., Svab, Z., and Maliga, P. (1994). The small, versatile pPZP family of Agrobacterium binary vectors for plant transformation. *Plant Mol. Biol.* 25, 989–994. doi: 10.1007/bf00014672

Haslam, T. M., and Kunst, L. (2013). Extending the story of very-long-chain fatty acid elongation. *Plant Sci.* 210, 93–107. doi: 10.1016/j.plantsci.2013.05.008

Hegebarth, D., and Jetter, R. (2017). Cuticular waxes of *Arabidopsis thaliana* shoots: cell-type-specific composition and biosynthesis. *Plants* 6:27. doi: 10.3390/plants6030027

Holmes, M. G., and Keiller, D. R. (2002). Effects of pubescence and waxes on the reflectance of leaves in the ultraviolet and photosynthetic wavebands: a comparison of a range of species. *Plant Cell Environ.* 25, 85–93. doi: 10.1046/j.1365-3040.2002.00779.x

Hooker, T. S., Lam, P., Zheng, H., and Kunst, L. (2007). A core subunit of the RNA processing/degrading exosome specifically influences cuticular wax biosynthesis in *Arabidopsis*. *Plant Cell* 19, 904–913. doi: 10.1105/tpc.106.049304

Ingram, G., and Nawrath, C. (2017). The roles of the cuticle in plant development: organ adhesions and beyond. *J. Exp. Bot.* 68, 5307–5321. doi: 10.1093/jxb/erx313

Iwase, A., Mitsuda, N., Koyama, T., Hiratsu, K., Kojima, M., Arai, T., et al. (2011). The AP2/ERF transcription factor WIND1 controls cell dedifferentiation in *Arabidopsis*. *Cur. Biol.* 21, 508–514. doi: 10.1016/j.cub.2011.02.020

Kannangara, R., Branigan, C., Liu, Y., Penfield, T., Rao, V., Mouille, G., et al. (2007). The transcription factor WIN1/SHN1 regulates cutin biosynthesis in *Arabidopsis thaliana*. *Plant Cell* 19, 1278–1294. doi: 10.1105/tpc.106.047076

Kim, H., Go, Y. S., and Suh, M. C. (2018). DEWAX2 transcription factor negatively regulates cuticular wax biosynthesis in *Arabidopsis* leaves. *Plant Cell Physiol.* 59, 966–977. doi: 10.1093/pcp/pcy033

Kim, H., Lee, S. B., Kim, H. J., Min, M. K., Hwang, I., and Suh, M. C. (2012). Characterization of glycosylphosphatidylinositol-anchored lipid transfer protein 2 (LTPG2) and overlapping function between LTPG/LTPG1 and LTPG2 in cuticular wax export or accumulation in *Arabidopsis thaliana*. *Plant Cell Physiol.* 53, 1391–1403. doi: 10.1093/pcp/pcs083

Kim, H., Yu, S.-I., Jung, S. H., Lee, B.-H., and Suh, M. C. (2019). The F-box protein SAGL1 and ECERIFERUM3 regulate cuticular wax biosynthesis in response to changes in humidity in *Arabidopsis*. *Science* 31, 2223–2240. doi: 10.1105/tpc.19.00152

Kim, J., Jung, J. H., Lee, S. B., Go, Y. S., Kim, H. J., Cahoon, R., et al. (2013). *Arabidopsis* 3-ketoacyl-coenzyme a synthase9 is involved in the synthesis of tetracosanoic acids as precursors of cuticular waxes, suberins, sphingolipids, and phospholipids. *Plant Physiol.* 162, 567–580. doi: 10.1104/pp.112.210450

Kosma, D. K., Bourdenx, B., Bernard, A., Parsons, E. P., Lü, S., Joubès, J., et al. (2009). The impact of water deficiency on leaf cuticle lipids of *Arabidopsis*. *Plant Physiol.* 151, 1918–1929. doi: 10.1104/pp.109.141911

Kunst, L., and Samuels, L. (2009). Plant cuticles shine: advances in wax biosynthesis and export. *Curr. Opin. Plant Biol.* 12, 721–727. doi: 10.1016/j.pbi.2009.09.009

Lam, P., Zhao, L., Eveleigh, N., Yu, Y., Chen, X., and Kunst, L. (2015). The exosome and trans-acting small interfering RNAs regulate cuticular wax biosynthesis during *Arabidopsis* inflorescence stem development. *Plant Physiol.* 167, 323–336. doi: 10.1104/pp.114.252825

Lam, P., Zhao, L., McFarlane, H. E., Aiga, M., Lam, V., Hooker, T. S., et al. (2012). RDR1 and SGS3, components of RNA-mediated gene silencing, are required for the regulation of cuticular wax biosynthesis in developing inflorescence stems of *Arabidopsis*. *Plant Physiol.* 159, 1385–1395. doi: 10.1104/pp.112.199646

Lee, H. G., Kim, J., Suh, M. C., and Seo, P. J. (2017). The MIEL1 E3 ubiquitin ligase negatively regulates cuticular wax biosynthesis in *Arabidopsis* stems. *Plant Cell Physiol.* 58, 1249–1259. doi: 10.1093/pcp/pcx065

Lee, S. B., Go, Y. S., Bae, H. J., Park, J. H., Cho, S. H., Cho, H. J., et al. (2009). Disruption of glycosylphosphatidylinositol-anchored lipid transfer protein gene altered cuticular lipid composition, increased plastoglobules, and enhanced susceptibility to infection by the fungal pathogen *Alternaria brassicicola*. *Plant Physiol.* 150, 42–54. doi: 10.1104/pp.109.137745

Lee, S. B., Kim, H. U., and Suh, M. C. (2016). MYB94 and MYB96 additively activate cuticular wax biosynthesis in *Arabidopsis*. *Plant Cell Physiol.* 57, 2300–2311. doi: 10.1093/pcp/pcw147

Lee, S. B., and Suh, M. C. (2013). Recent advances in cuticular wax biosynthesis and its regulation in *Arabidopsis*. *Mol. Plant* 6, 246–249. doi: 10.1093/mp/sss159

Lee, S. B., and Suh, M. C. (2015a). Advances in the understanding of cuticular waxes in *Arabidopsis thaliana* and crop species. *Plant Cell Rep.* 34, 557–572. doi: 10.1007/s00299-015-1772-2

Lee, S. B., and Suh, M. C. (2015b). Cuticular wax biosynthesis is up-regulated by the MYB94 transcription factor in *Arabidopsis*. *Plant Cell Physiol.* 56, 48–60. doi: 10.1093/pcp/pcu142

Li, F., Wu, X., Lam, P., Bird, D., Zheng, H., Samuels, L., et al. (2008). Identification of the wax ester synthase/acyl-coenzyme A: diacylglycerol acyltransferase WSD1 required for stem wax ester biosynthesis in *Arabidopsis*. *Plant Physio.* 148, 97–107. doi: 10.1104/pp.108.123471

Li-Beisson, Y., Shorrosh, B., Beisson, F., Andersson, M. X., Arondel, V., Bates, P. D., et al. (2013). Acyl-lipid metabolism. *Arabidopsis Book* 11:e0161. doi: 10.1199/tab.0161

Lin, R. C., Park, H. J., and Wang, H. Y. (2008). Role of *Arabidopsis* RAP2.4 in regulating light- and ethylene-mediated developmental processes and drought stress tolerance. *Mol. Plant* 1, 42–57. doi: 10.1093/mp/ssm004

Millar, A. A., Clemens, S., Zachgo, S., Giblin, E. M., Taylor, D. C., and Kunst, L. (1999). CUT1, an *Arabidopsis* gene required for cuticular wax biosynthesis and pollen fertility, encodes a very-long-chain fatty acid condensing enzyme. *Plant Cell* 11, 825–838. doi: 10.1105/tpc.11.5.825

Morimoto, K., Ohama, N., Kidokoro, S., Mizoi, J., Takahashi, F., Todaka, D., et al. (2017). BPM-CUL3 E3 ligase modulates thermotolerance by facilitating negative regulatory domain-mediated degradation of DREB2A in *Arabidopsis*. *Proc. Natl. Acad. Sci. U.S.A.* 114, E8528–E8536. doi: 10.1073/pnas.1704189114

Morineau, C., Gissot, L., Bellec, Y., Hematy, K., Tellier, F., Renne, C., et al. (2016). Dual fatty acid elongase complex interactions in *Arabidopsis*. *PLoS One* 11:e0160631. doi: 10.1371/journal.pone.0160631

Park, C. S., Go, Y. S., and Suh, M. C. (2016). Cuticular wax biosynthesis is positively regulated by WRINKLED4, an AP2/ERF-type transcription factor, in *Arabidopsis* stems. *Plant J.* 88, 257–270. doi: 10.1111/tpj.13248

Rae, L., Lao, N. T., and Kavanagh, T. A. (2011). Regulation of multiple aquaporin genes in *Arabidopsis* by a pair of recently duplicated DREB transcription factors. *Planta* 234, 429–444. doi: 10.1007/s00425-011-1414-z

Raffaele, S., Vailleau, F., Léger, A., Joubès, J., Miersch, O., Huard, C., et al. (2008). A MYB transcription factor regulates very-long-chain fatty acid biosynthesis for activation of the hypersensitive cell death response in *Arabidopsis*. *Plant Cell* 20, 752–767. doi: 10.1105/tpc.107.054858

Riederer, M., and Schreiber, L. (2001). Protecting against water loss: analysis of the barrier properties of plant cuticles. *J. Exp. Bot.* 52, 2023–2032. doi: 10.1093/jexbot/52.363.2023

Rowland, O., Zheng, H., Hepworth, S. R., Lam, P., Jetter, R., and Kunst, L. (2006). CER4 encodes an alcohol-forming fatty acyl-coenzyme A reductase involved in cuticular wax production in *Arabidopsis*. *Plant Physiol.* 142, 866–877. doi: 10.1104/pp.106.086785

Seo, P. J., Lee, S. B., Suh, M. C., Park, M. J., Go, Y. S., and Park, C. M. (2011). The MYB96 transcription factor regulates cuticular wax biosynthesis under drought conditions in *Arabidopsis*. *Plant Cell* 23, 1138–1152. doi: 10.1105/tpc.111.083485

Shepherd, T., and Griffiths, W. D. (2006). The effects of stress on plant cuticular waxes. *New Phytol.* 171, 469–499. doi: 10.1111/j.1469-8137.2006.01826.x

Shinozaki, K., and Yamaguchi-Shinozaki, K. (2007). Gene networks involved in drought stress response and tolerance. *J. Exp. Bot.* 58, 221–227. doi: 10.1093/jxb/erl164

Sieber, P., Schorderet, M., Ryser, U., Buchala, A., Kolattukudy, P., Métraux, J. P., et al. (2000). Transgenic *Arabidopsis* plants expressing a fungal cutinase show alterations in the structure and properties of the cuticle and postgenital organ fusions. *Plant Cell* 12, 721–738. doi: 10.1105/tpc.12.5.721

Suh, M. C., Samuels, A. L., Jetter, R., Kunst, L., Pollard, M., Ohlrogge, J., et al. (2005). Cuticular lipid composition, surface structure, and gene expression in *Arabidopsis* stem epidermis. *Plant Physiol.* 139, 1649–1665. doi: 10.1104/pp.105.070805

Tiwari, S. B., Hagen, G., and Guilfoyle, T. (2003). The roles of auxin response factor domains in auxin-responsive transcription. *Plant Cell* 15, 533–543. doi: 10.1105/tpc.008417

Weber, H., and Hellmann, H. (2009). *Arabidopsis thaliana* BTB/ POZ-MATH proteins interact with members of the ERF/AP2 transcription factor family. *FEBS J.* 276, 6624–6635. doi: 10.1111/j.1742-4658.2009.07373.x

Xue, D., Zhang, X., Lu, X., Chen, G., and Chen, Z. H. (2017). Molecular and evolutionary mechanisms of cuticular wax for plant drought tolerance. *Front. Plant Sci.* 8:621. doi: 10.3389/fpls.2017.00621

Yeats, T. H., and Rose, J. K. (2013). The formation and function of plant cuticles. *Plant Physiol.* 163, 5–20. doi: 10.1104/pp.113.222737

Yoo, S., Cho, Y., and Sheen, J. (2007). *Arabidopsis* mesophyll protoplasts: a versatile cell system for transient gene expression analysis. *Nat. Protoc.* 2, 1565–1572. doi: 10.1038/nprot.2007.199

Zhang, J. Y., Broeckling, C. D., Blancaflor, E. B., Sledge, M. K., Sumner, L. W., and Wang, Z. Y. (2005). Overexpression of WXP1, a putative *Medicago truncatula* AP2 domain-containing transcription factor gene, increases cuticular wax accumulation and enhances drought tolerance in transgenic alfalfa (*Medicago sativa*). *Plant J.* 42, 689–707. doi: 10.1111/j.1365-313X.2005.02405.x

Zhang, J. Y., Broeckling, C. D., Sumner, L. W., and Wang, Z. Y. (2007). Heterologous expression of two *Medicago truncatula* putative ERF transcription factor genes, WXP1 and WXP2, in *Arabidopsis* led to increased leaf wax accumulation and improved drought tolerance, but differential response in freezing tolerance. *Plant Mol. Biol.* 64, 265–278. doi: 10.1007/s11103-007-9150-2

Zheng, H., Rowland, O., and Kunst, L. (2005). Disruptions of the *Arabidopsis* enoyl-CoA reductase gene reveal an essential role for very-long chain fatty acid synthesis in cell expansion during plant morphogenesis. *Plant Cell* 17, 1467–1481. doi: 10.1105/tpc.104.030155

Conflict of Interest: The authors declare that the research was conducted in the absence of any commercial or financial relationships that could be construed as a potential conflict of interest.

frontiers in Plant Science

ORIGINAL RESEARCH
published: 08 July 2020
doi: 10.3389/fpls.2020.00804

hetN and *patS* Mutations Enhance Accumulation of Fatty Alcohols in the *hglT* Mutants of *Anabaena* sp. PCC 7120

Heli Siti Halimatul Munawaroh[1,2], *Egi Tritya Apdila*[2] *and Koichiro Awai*[2,3,4]*

[1] Laboratory of Chemistry Study Program, Department of Chemistry Education, Universitas Pendidikan Indonesia, Bandung, Indonesia, [2] Graduate School of Science and Technology, Shizuoka University, Shizuoka, Japan, [3] Research Institute of Electronics, Shizuoka University, Hamamatsu, Japan, [4] Department of Biological Science, Faculty of Science, Shizuoka University, Shizuoka, Japan

The heterocysts present in filamentous cyanobacteria such as *Anabaena* sp. PCC 7120 are known to be regulated by HetN and PatS, the repressors of heterocyst differentiation; therefore, the inactivation of these proteins will result in the formation of multiple heterocysts. To enhance the accumulation of fatty alcohols synthesized in the heterocyst, we introduced mutations of these repressors to increase heterocyst frequency. First, we isolated double mutants of *hetN* and *patS* and confirmed that the null mutation of these genes promoted higher frequencies of heterocyst formation and higher accumulation of heterocyst-specific glycolipids (Hgls) compared with its wild type. Next, we combined *hetN* and *patS* mutations with an *hglT* (encoding glycosyltransferase, an enzyme involved in Hgl synthesis) mutation to increase the accumulation of fatty alcohols since knockout mutation of *hglT* results in accumulation of very long chain fatty alcohol, the precursor of Hgl. We also observed retarded growth, lower chlorophyll content and up to a five-fold decrease in photosynthetic activity of the *hetN*/*patS*/*hglT* triple mutants. In contrast, the triple mutants showed three times higher heterocyst formation frequencies than the *hglT* single mutant and wild type. The production rate of fatty alcohol in the triple mutants attained a value 1.41 nmol/mL OD_{730}, whereas accumulation of Hgls in the wild type was 0.90 nmol/mL OD_{730}. Aeration of culture improved the accumulation of fatty alcohols in *hetN*/*patS*/*hglT* mutant cells up to 2.97 nmol/mL OD_{730} compared with cells cultured by rotation. Our study outlines an alternative strategy for fatty alcohol production supported by photosynthesis and nitrogen fixation.

Keywords: ***Anabaena*** **sp. PCC 7120, heterocyst, heterocyst-specific glycolipids, fatty alcohol, aeration**

OPEN ACCESS

Edited by:
Mi Chung Suh,
Sogang University, South Korea

Reviewed by:
Vicente Mariscal,
Institute of Plant Biochemistry and Photosynthesis (IBVF), Spain
Iris Maldener,
University of Tübingen, Germany

***Correspondence:**
Koichiro Awai
awai.koichiro@shizuoka.ac.jp

Specialty section:
This article was submitted to Plant Biotechnology, a section of the journal Frontiers in Plant Science

Received: *27 January 2020*
Accepted: *19 May 2020*
Published: *08 July 2020*

Citation:
Munawaroh HSH, Apdila ET and Awai K (2020) hetN and patS Mutations Enhance Accumulation of Fatty Alcohols in the hglT Mutants of Anabaena sp. PCC 7120. Front. Plant Sci. 11:804. doi: 10.3389/fpls.2020.00804

INTRODUCTION

Anabaena sp. PCC 7120 (hereinafter Anabaena) is a multicellular cyanobacterium that possesses a long filament comprising 100 or more vegetative cells usually in the presence of combined nitrogen sources in the medium. When the combined nitrogen concentration in the environment reduces, Anabaena develops heterocyst cells to separate oxygen-labile nitrogen fixation from oxygen produced due to photosynthesis in the vegetative cells. Heterocyst cells are typically distinguishable

from vegetative cells by their morphology, such as a large and round shape, reduction of pigments, thick cellular envelopes, and cyanophycin granules at poles adjacent to the vegetative cells. These cells are surrounded by a glycolipid layer to provide a micro-oxic environment that protects the enzyme nitrogenase from oxygen diffusion from outside the cells (Ernst et al., 1992; Fay, 1992; Wolk, 1996; Maldener et al., 2003; Huang et al., 2004; Awai et al., 2009).

Numerous proteins have been found to be involved in heterocyst development, including repressors. In Anabaena, HetR is a well-known protein that is involved in the early stage of heterocyst formation. PatS and HetN are known to play a prominent role in heterocyst development and its formation pattern maintenance (Buikema and Haselkorn, 1991; Golden and Yoon, 2003). Both *patS* and *hetN* have been reported to encode a diffusible inhibitor of differentiation, the RGSGR pentapeptide, which affects heterocyst formation pattern. The product of *patS* is proposed to control heterocyst formation through *hetR* regulation. The *patS* gene product is thought to function through the means of cell-to-cell signaling to prevent the formation of multiple contiguous heterocysts. The pattern of heterocyst formation possibly requires the interaction between HetR and PatS (Huang et al., 2004). PatS diffuses laterally to inhibit the differentiation of neighboring cells by hampering the DNA binding activity of HetR (Golden and Yoon, 2003; Zhang et al., 2006). Another gene, *hetN*, is required for the maintenance of the heterocyst pattern (Callahan and Buikema, 2001). Unlike *patS* mutants, the deletion of *hetN* in Anabaena shows no alteration in the heterocyst formation pattern and the vegetative cell interval. However, this null mutant also forms multiple heterocysts after the normal pattern of heterocyst formation (Fan et al., 2005), indicating that HetN is not required for the formation of the initial heterocyst pattern in response to nitrogen-starved conditions. Yet, this gene plays an important role in the maintenance of the heterocyst pattern (Callahan and Buikema, 2001).

Borthakur et al. (2005) analyzed the effects of *patS* and *hetN* mutations on heterocyst development. They found that the double mutant of *patS* and *hetN* had significantly higher heterocyst frequency than the single mutant of *patS* or *hetN*, suggesting that *patS* and *hetN* suppress heterocyst differentiation by different pathways. Surprisingly, the inactivation of both genes leads to the differentiation of almost all vegetative cells into heterocyst cells under nitrogen-starved conditions (Borthakur et al., 2005). This double mutant was not a null mutant; the inducible repression system for *hetN* was used for this procedure because it was thought that the double mutant is lethal under nitrogen-starved conditions. Afterward, Corrales-Guerrero et al. (2014) reported the double null mutant of *patS* and *hetN* in Anabaena. However, a recent study found that substrains of Anabaena maintained separately in different laboratories have higher number of genomic variations, such as SNPs, and these polymorphisms change the heterocyst differentiation patterns (Wang et al., 2018).

As described above, to prevent oxygen diffusion into the heterocyst, their cellular envelope develops a structural barrier called the heterocyst-specific glycolipid layer (HGL). HGL is composed of heterocyst-specific glycolipids (Hgls) that comprise glucose attached to a very long chain fatty alcohol by an ether bond. The final step of Hgl synthesis is catalyzed by the enzyme glucosyltransferase HglT (Awai and Wolk, 2007). The null mutant of *hglT* differentiates into heterocysts but fails to form the HGL and instead accumulates fatty alcohol (Halimatul et al., 2014). The accumulation of fatty alcohols in the *hglT* mutants could be of biotechnological interest that may help in finding an alternative route for fatty alcohol production. Long chain hydrocarbons including long chain fatty alcohols are nowadays drawing more attention due to their high energy density, low moisture absorption, low vitality, and compatibility with existing engines and transport facilities. However, fatty alcohol is mostly prepared from natural oil through the processes of transesterification and hydrogenation. These processes require harsh production environments or introduce harmful materials into the environment (Zheng et al., 2012). For these reasons, researchers are on the lookout for organisms that efficiently produce fatty alcohols. Recently, the production of fatty acid ethyl esters and fatty alcohols have been reported in genetically modified *Escherichia coli* (Steen et al., 2010). However, this system requires the addition of a stable carbon source which in turn increases production costs.

To enhance the accumulation of fatty alcohols, we combined the genes of mutants' *hetN* and *patS* with that of *hglT* gene. The knockout mutants of *hetN* and *patS* formed approximately three times more heterocysts than the wild type under nitrogen-starved conditions. In the triple mutants of *hetN*, *patS*, and *hglT* genes, more fatty alcohols were accumulated compared with the single *hglT* mutant. In this study, we demonstrated that increased ratio of heterocyst per filament in the *hglT* mutants of Anabaena enhances the accumulation of fatty alcohols.

MATERIALS AND METHODS

Growth Conditions of the Wild Type and Mutants of Anabaena

Anabaena and *hglT* mutant strains were grown in the liquid medium of BG11 (containing nitrate as a nitrogen source) (Stanier et al., 1971) at a temperature of 30°C in the presence of light (50–80 μmol m^{-2} s^{-1}) on a rotary shaker (120 rpm) as described previously (Awai et al., 2007). For the nitrogen-starved condition experiments, cells were first grown in the BG11 medium to an optical density of 0.8–1.2 at 730 nm (OD_{730}), washed thrice with nitrogen-free medium ($BG11_0$: BG11 without nitrate), and resuspended in $BG11_0$. For cultures exposed to air bubbling, 50 ml of $BG11_0$ was used in a 93 ml test tube.

Isolation of Mutants of Anabaena

The knockout vector of the *hetN* gene was constructed: DNA fragments upstream and downstream of *hetN* gene were amplified by the polymerase chain reaction (PCR) technique using the primer pairs #1 and #2 and #3 and #4, respectively (see **Supplementary Table S1**). The upstream fragment was cloned into the *Sma*I site of pMobΩ1 (Saito and Awai, 2020) using In-Fusion HD Cloning Kit with a Cloning Enhancer (Takara Bio,

Shiga, Japan), and the downstream fragment was cloned into the *Apa*I site to construct the knockout vector, pMO1hetNKO.

The knockout vector of *patS* was also constructed by amplifying the DNA fragments upstream and downstream of *PatS*. The upstream fragment was amplified by PCR using primers #5 and #6, and the downstream fragment of *patS* was amplified using primers #7 and #8. The upstream fragment was cloned into the *Apa*I site of pMobEm1 (Awai et al., 2014) using the In-Fusion HD Cloning Kit with Cloning Enhancer, and the downstream fragment was cloned into the *Sma*I site to construct the knockout vector, pME1patSKO.

The knockout vector of the *hglT* gene was constructed as described previously (Halimatul et al., 2014). The constructed plasmid vectors were introduced consecutively into the wild type and the mutant strains of Anabaena by the triparental mating method of Elhai and Wolk (1988). The constructed vectors above contain the *sacB* gene, and we used 6% sucrose for positive selections of mutants with double recombination.

The genomic DNA from the wild type and transformed cells were used as templates for PCR genotyping with the primers described below using HybriPol DNA polymerase (Bioline). Genomic DNA was extracted from the cells macerated with glass beads in TE buffer, followed by phenol/chloroform extraction and ethanol precipitation, as seen elsewhere. PCR-based confirmation of gene disruption was performed using external and internal primers to amplify the full length of *hglT, hetN, or patS* to confirm the insertion of the antibiotic resistance gene into the target gene and for the detection of deletion of the central part of *hglT, hetN,* or *patS*. Genotyping for *hglT* gene disruption was performed using primers #9 and #10 for the amplification of full-length *hglT*, #10 and #11 for insertion of the kanamycin resistance gene into *hglT*, and #9 and #12 for detection of deletion of the central part of *hglT*.

Polymerase chain reaction-based confirmation of *hetN* deletion was conducted using primers #1 and #4 for the amplification of full-length *hetN*, #4 and #13 for insertion of the spectinomycin/streptomycin resistance gene into *hetN*, and #4 and #14 for detection of deletion of the central part of *hetN*.

Genotyping for *patS* gene deletion was performed using primers #5 and #8 for the amplification of full-length *patS*, #8 and #15 for insertion of the erythromycin resistance gene into *patS*, and #5 and #16 and #5 and#17 for detection of deletions of the central part of *patS* in the Δ*hetN/patS* double and Δ*hetN/patS/hglT* triple mutants, respectively.

Chlorophyll Content, Cell Spectrum, Lipid Content, and Oxygen Evolution Analysis

Cells of each strain were precipitated from 1 mL culture (OD_{730} = 0.8–1.2), resuspended in 90% methanol and measured using the method reported by Meeks and Castenholz (1971). The absorption spectra of the cells were determined by harvesting 1 mL of the cells and resuspending in fresh BG11 medium prior to measurement. The cells were subsequently scanned from 350 to 800 nm using a spectrophotometer UV-2450 (Shimadzu, Kyoto, Japan) with an integrating sphere. The lipid content was measured as described previously (Halimatul et al., 2014).

Bulk photosynthetic activities were determined by measuring the oxygen evolution rate at a temperature of 25°C with a Clark-type oxygen electrode (Hansatech instruments, Norfolk, United Kindom) using 1 mL cell suspension of the samples (approximately 5–7 μg Chl *a*/mL). The Anabaena cells were illuminated with a halogen lamp at light intensity intervals of 0 (dark conditions), 33, 58, 113, 222, and 416 μmol photons/mg Chl/h.

RNA Extraction, Reverse Transcription, and qRT-PCR

Total RNA was isolated from whole filaments according to the manufacturer's protocol (RNeasy, Qiagen, Hilden, Germany) and treated with DNase I (Takara Bio, Shiga, Japan). cDNA synthesis was performed using 400 ng of purified RNA with random

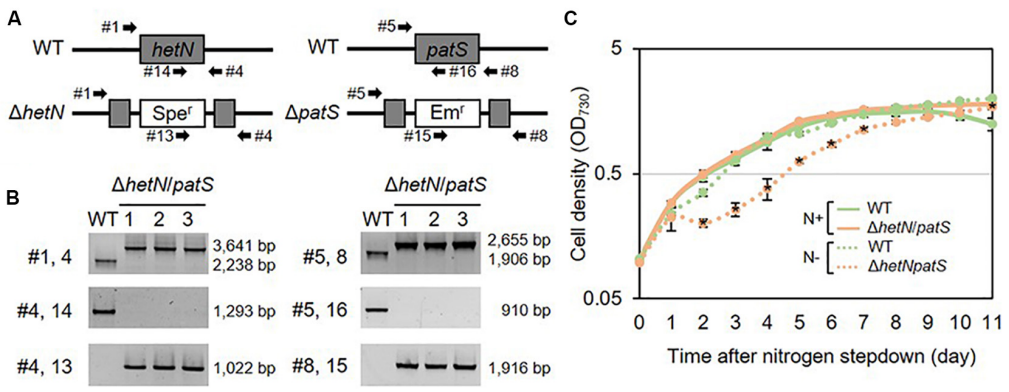

FIGURE 1 | Genotype and growth curve of *hetN/patS* double mutants. **(A)** Schematic representation of *hetN* and *patS* regions of the wild type and mutant genomes. Spe^r: spectinomycin, Em^r: erythromycin resistance cassettes. **(B)** Genotype analysis of the double mutants using the primers highlighted in **(A)** by arrows. **(C)** Growth curve of the double mutants. Solid line: N+, hashed line: N–. Error bars indicate the SD based on three independent experiments. Asterisks in the markers indicate significant differences from the wild type grown under same conditions ($P < 0.01$, Welch's *t* test).

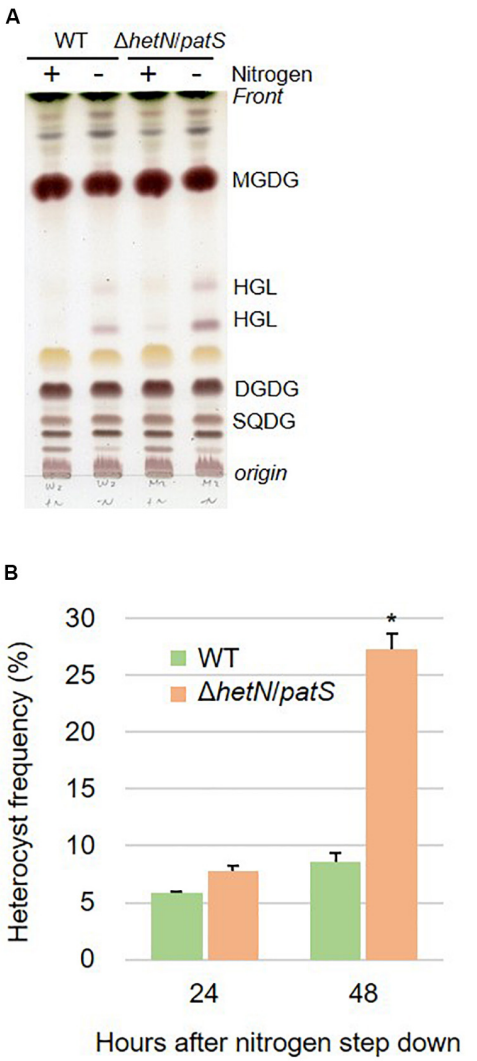

FIGURE 2 | Lipid composition and heterocyst frequency of the wild type (WT) and double mutant. **(A)** Lipids separated by TLC of the wild type (WT) and the double mutant. Lipids were extracted from the cells grown in BG11 and $BG11_0$ (48 h of nitrogen step-down). **(B)** Heterocyst frequency. Error bars indicate the SD based on three independent experiments. Approximately 500 cells were counted per experiment. An asterisk indicates a significant difference from the wild type grown under same conditions ($P < 0.01$, Welch's *t* test).

hexamer and PrimeScript II Reverse Transcriptase (Takara Bio) according to the manufacturer's protocol. The generated cDNA was used as a template for qRT-PCR analysis. qRT-PCR was performed with Thermal Cycler Dice Real Time System (Takara Bio) in a 20-μl reaction mixture containing 10 μl of SYBR Premix Ex Taq (Takara Bio) and 0.4 μM each of *nifH* gene-specific forward and reverse primers (#18 and #19). Relative volume ratios were normalized with the values for *rnpB*, which encodes a subunit of RNaseP, amplified with the primer set #20 and #21. The relative quantities are represented as means of duplicate experiments.

RESULTS

Deletions of *hetN* and *patS* Enhanced Heterocyst Frequency and Hgl Accumulation

To increase the heterocyst frequency of Anabaena, we first knocked out the two genes encoding suppressors of heterocyst differentiation, HetN and PatS. Both proteins are known to inhibit heterocyst differentiation in an independent manner; PatS contributes at the initial stage of heterocyst development and HetN maintains the ratio between heterocyst and vegetative cells under nitrogen-starved conditions. As shown in **Figures 1A,B**, the double null mutants of *hetN* and *patS* (Δ*hetN*/*patS*) were isolated. A PCR analysis using primers external to *hetN* (**Figure 1A**, #1 and #4) resulted in two PCR fragments of different sizes. The wild type strain produced a 2,238 bp fragment, and the mutant produced a larger 3,641 bp fragment because of the presence of the spectinomycin resistance cassette. PCR with a primer that annealed to the middle region of *hetN*, #14, produced an amplicon only from the wild type genome as the necessary region was not present in the mutant genome. PCR with primer #13, which anneals to the spectinomycin resistance cassette, produced amplicons only from the mutant genome. These results indicated that no wild type copies of *hetN* were present in the mutant cells. Similar analysis was conducted for *patS*, and null mutation was also confirmed. There were no obvious differences of growth between the double mutant and wild type under nitrogen-replete conditions. Under nitrogen-starved conditions, however, the double mutants exhibited retarded growth, especially from the second day after nitrogen step-down (**Figure 1C**). This is probably because the double mutant required extra energy to develop more heterocyst cells compare to the wild type. Lipid analysis showed that the double mutants accumulate more Hgl compared with the wild type (**Figure 2A**). A thick band of Hgl was seen in the double mutant after 48 h of nitrogen step-down, whereas a faint band in the wild type appeared under same conditions. We also analyzed heterocyst frequency of the double mutants. Compared with the wild type, similar differentiation rate was observed in the double mutants after 24 h, but they showed approximately 3.5-fold more heterocyst cells after 48 h of nitrogen step-down (27.2%, **Figure 2B**). These results imply that knockout mutations of *hetN* and *patS* can enhance the accumulation of Hgls and/or their precursor, fatty alcohols. It is of note that our Δ*hetN*/*patS* double mutant could grow diazotrophically, which is not same as the previously reported Δ*hetN*/*patS* mutants (Corrales-Guerrero et al., 2014).

Triple Mutant of *hetN, patS*, and *hglT* Showed Lower Growth Rate, Chlorophyll Content, and Photosynthetic Activity Under Nitrogen-Starved Conditions

Next, we tried to knockout *hglT* in Δ*hetN*/*patS*. **Figure 3** shows the results of genotyping of the isolated triple mutant of *hetN*,

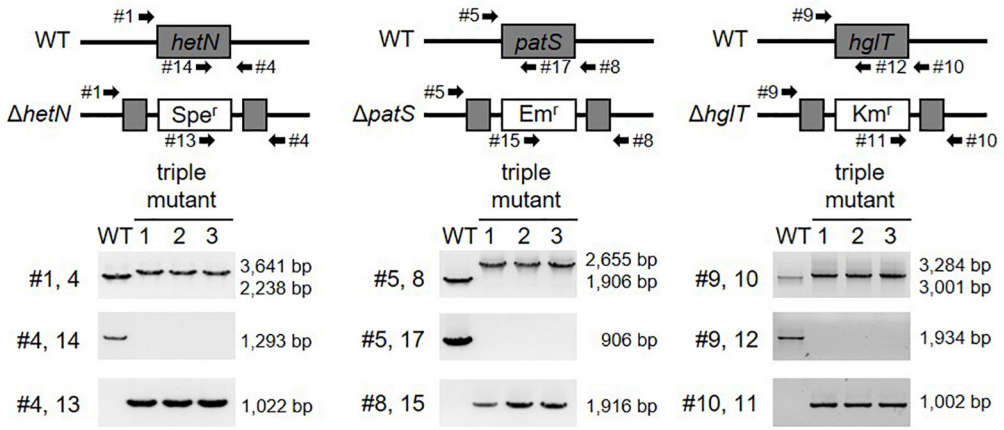

FIGURE 3 | Genotype of *hetN/patS/hglT* triple mutants. Upper layer shows schematic representations of *hetN*, *patS*, and *hglT* regions of the wild type and mutant genomes. Bottom layer shows genotype analysis of the triple mutants using the primers highlighted by arrows in the upper layer. Spe^r: spectinomycin resistance cassette, Em^r: erythromycin resistance cassette, Km^r: kanamycin resistance cassette.

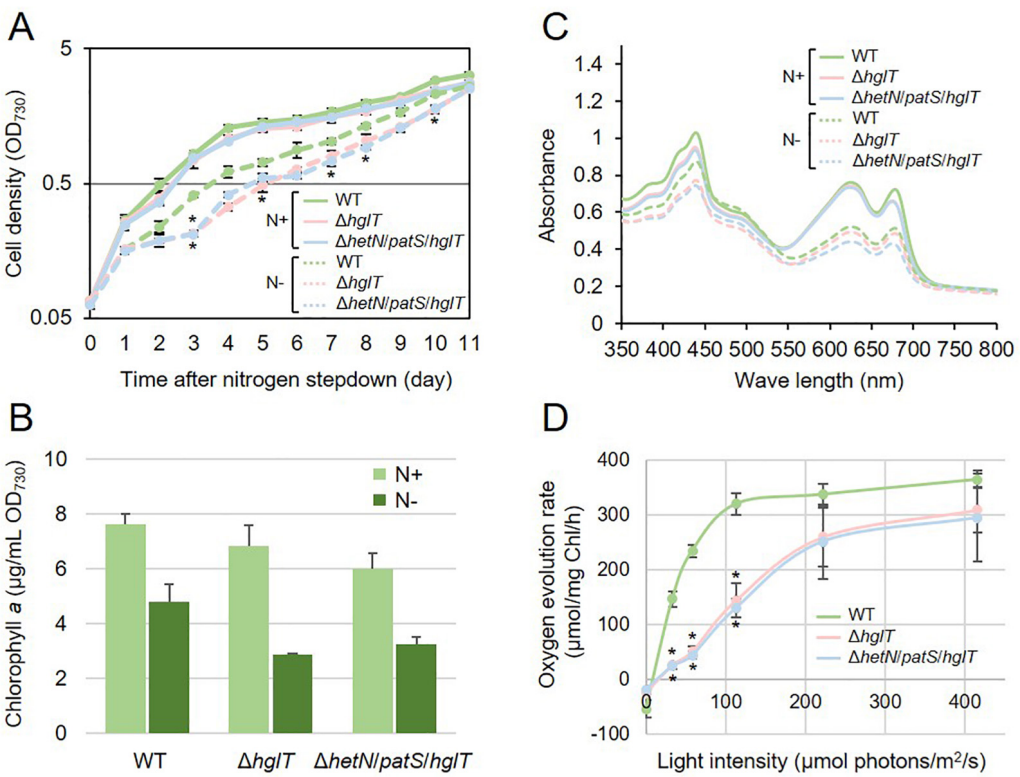

FIGURE 4 | Growth curve, chlorophyll contents, and cell spectra of *hglT* mutants. The wild type and mutant cells were grown in BG11 (N+) or BG11$_0$ [N–, 48 h of nitrogen step-down in **B,C**]. **(A)** Growth curve of the *hglT* mutants. Solid line: N+, hashed line: N–. Error bars indicate the SD based on three independent experiments. Asterisks indicate significant differences from the wild type grown under same conditions ($P < 0.01$, Welch's *t* test). **(B)** Chlorophyll *a* contents of the wild type (WT), *hglT* single mutant (Δ*hglT*), and *hetN/patS/hglT* triple mutant (Δ*hetN/patS/hglT*). Error bars indicate the SD based on three independent experiments. **(C)** Cell spectra. Solid line: N+, hashed line: N–. Representative data are shown. **(D)** Oxygen evolution rate. Error bars indicate the SD based on three independent experiments. Asterisks indicate significant differences from the wild type at the same light intensities ($P < 0.01$, Welch's *t* test).

patS, and *hglT* (Δ*hetN*/*patS*/*hglT*). Similar genotyping analyses as described above were conducted for *hetN*, *patS*, and *hglT*, and null mutation of each gene was confirmed. Using these triple mutants, first the growth rates were compared with the wild type and single *hglT* mutants. There were no obvious differences among these three strains under nitrogen-replete conditions.

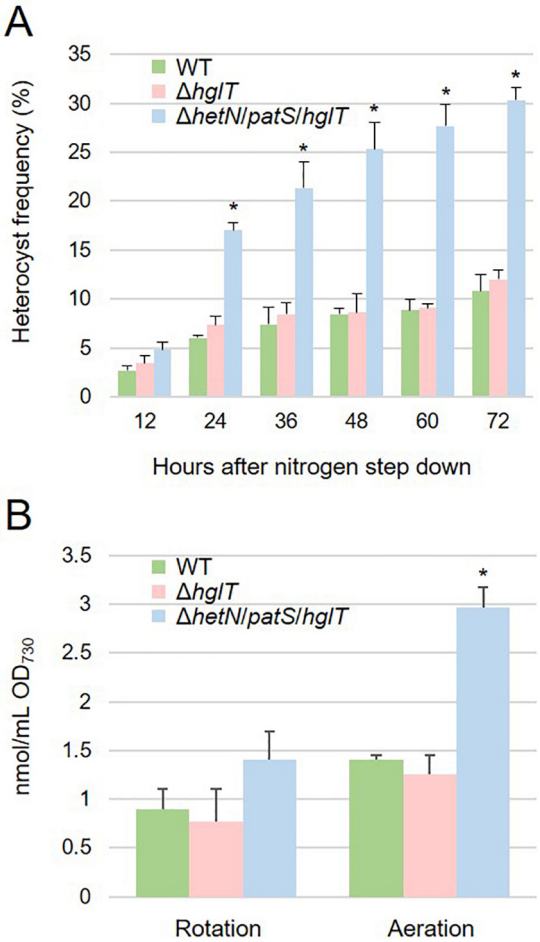

FIGURE 5 | (A) Heterocyst frequency of the wild type (WT), *hglT* single mutant (Δ*hglT*) and *hetN*/*patS*/*hglT* triple mutant (Δ*hetN*/*patS*/*hglT*). Error bars indicate the SD based on three independent experiments. Approximately 500 cells were counted per experiment. Asterisks indicate significant differences from the wild type at the same timepoints ($P < 0.01$, Welch's *t* test). **(B)** Accumulation of the heterocystous lipids. Wild type accumulated HGLs while the mutants accumulated aglycones (fatty alcohols). Error bars indicate the SD based on three independent experiments. Rotation: cells cultured on rotary shaker in Erlenmeyer flasks, Aeration: cells cultured in test tubes with bubbling. An asterisk indicates a significant difference from the wild type grown under same conditions ($P < 0.01$, Welch's *t* test).

Under nitrogen-starved conditions, however, both the single and triple mutants exhibited retarded growth, especially from the second day after nitrogen step-down (**Figure 4A**). There are probably two parallel reasons to explain this growth retardation in the triple mutant. First is that, as was seen in the Δ*hetN*/*patS* double mutants, more energy and carbon sources were used for development of heterocyst cells, rather than cell divisions. Second is that the accumulated aglycones (fatty alcohols) of Hgls by the *hglT* mutation are not sufficient to complement functions of Hgls and lower the efficiency of nitrogen fixation in the heterocyst cells (Halimatul et al., 2014). Δ*hetN*/*patS*/*hglT* had less chlorophyll *a* compared with the wild type under both nitrogen-replete and -starved conditions (**Figure 4B**), which can be also seen in the cell spectra (**Figure 4C**: 678 nm peak). The cell spectra of both Δ*hglT* and Δ*hetN*/*patS*/*hglT* mutant cells showed no significant alteration in the phycocyanin peak (625 nm) under nitrogen-replete conditions compared with the wild type. Under nitrogen-starved conditions, 625 nm peaks were reduced in both single and triple mutants, which fit to the observation of delayed growth in these mutants (**Figure 4A**). Because the chlorophyll content was low in the mutants, photosynthetic activity was measured (**Figure 4D**). Both the Δ*hglT* and Δ*hetN*/*patS*/*hglT* cells showed retarded photosynthetic activity, especially under low light conditions, such as ∼100 μmol photons/mg Chl/h. The values are around five times lower in the mutants at low light conditions (30–60 μmol photons/mg Chl/h) but around 1.2 times lower at middle to high light conditions (200–400 μmol photons/mg Chl/h). Oxygen evolution rates of the single and triple mutant cells were very similar, indicating that their retarded photosynthetic activity is due to the inactivation of *hgl*T, not *patS* and/or *hetN*.

hetN/patS/hglT Triple Mutants Exhibited More Heterocysts but Little Accumulation of Fatty Alcohols

Heterocyst frequency of the Δ*hetN*/*patS*/*hglT* triple mutant was analyzed. **Figure 5A** shows that the triple mutant exhibited a higher heterocyst differentiation rate (approximately three times) compared with the wild type and Δ*hglT* single mutant, especially after 24 h of nitrogen step-down. The heterocyst frequency kept increasing; after 72 h, the rate stabilized at 30.3%, which was much more than the wild type (10.8%) and Δ*hglT* single mutant (12.0%). Since the triple mutant had a high heterocyst frequency, we analyzed the expression level of *nifH*, the gene encoding a subunit of nitrogenase that is specifically expressed in heterocyst cells. As shown in **Supplementary Figure S1**, mRNA level of *nifH* was similar among the wild type, Δ*hglT* mutant, and Δ*hetN*/*patS*/*hglT*. This result indicates that the triple mutant cells have less nitrogenase per heterocyst cell, at least the expression of *nifH*, because they have three times higher rate of heterocyst formation compared with the wild type and Δ*hglT* single mutant; the expression rate of *nifH* remained the same. We then finally analyzed lipid composition of the mutants. As seen in **Figure 5B**, the triple mutant harbored 1.41 nmol/mL OD_{730} of fatty alcohols. This was about 157% of the accumulation of Hgls in the wild type (0.90 nmol/mL OD_{730}). Since the heterocyst frequency was approximately three times higher than the wild type, it was about half less the amount we expected.

Aeration of Culture Enhanced Accumulation of Fatty Alcohol in the *hetN/patS/hglT* Triple Mutant

To enhance the accumulation of fatty alcohols in Δ*hetN*/*patS*/*hglT*, we optimized the cultural conditions. Since the experiments described above were conducted using a rotary shaker, we speculated whether the efficiency of Hgl and its aglycones, fatty alcohols, can be boosted by aeration, since aeration in general has been shown to promote better cyanobacterial growth than rotation. As expected, the cells

cultured with aeration showed higher accumulation of Hgls and aglycones than those cultured by rotation (**Figure 5B**). Accumulation of Hgl in the wild type increased to 1.5-fold compared with the cells cultured by rotation (1.41 nmol/mL OD_{730}). This increase was also seen in the *hglT* single mutant (0.77–1.25 nmol/mL OD_{730}). In the triple mutant, the amount of fatty alcohols increased to 2.97 nmol/mL OD_{730}, which is more than twice that of the cells cultured by rotation.

DISCUSSION

Aeration Might Boost the CO_2 Uptake and/or Oxygen Diffusion Into the Cells

In this study, we initially used rotary shakers to grow cells of cyanobacteria. However, we found that the effectiveness of lipid production is dependent on the degree of aeration. The mutants cultured with continuous aeration accumulated fatty alcohol with a maximum production rate, over twice that obtained by rotary shaking (**Figure 5B**). This might be because influx of CO_2 from aeration increased the intracellular C/N ratio and induced the accumulation of carbon products in the cells. Another possibility is that aeration led to oxygen saturation in the culture, which led the thickening of the heterocyst envelope, especially the glycolipid layer. It has been reported that when the heterocyst containing cyanobacteria (*Anabaena flos-aquae*) are cultured in high partial pressure of oxygen under nitrogen-starved conditions, their heterocyst cells develop an envelope with a very thick HGL (Kangatharalingam et al., 1992). Therefore, it is possible that the Δ*hetN*/*patS*/*hglT* cells are able to sense oxygen concentration in the culture and develop a thicker envelope under aeration. We have not tried the additional CO_2 and/or O_2 in the air for bubbling yet, but it would be interesting topic for future investigation.

Possible Modifications to Enhance Fatty Alcohol Production

Culturing the *hetN*/*patS*/*hglT* triple mutant cells with bubbling led to an accumulation of 2.97 nmol/mL OD_{730} fatty alcohols. This amount is equivalent to 1.23 mg/L OD_{730} and lower than those previously reported for the production of fatty acids in other cyanobacteria. For example, genetically modified *Synechocystis* PCC 6803 has been reported to synthesize >200 mg/L of fatty acids (Eungrasamee et al., 2019). Kato et al. (2017) reported that the removal of the product from the medium enhances bioproduction in cyanobacteria. They overlaid isopropyl myristate to remove the toxic product, palmitic acid, from the medium of the unicellular cyanobacterium *Synechococcus elongatus* PCC 7942 and found that this two-phase cultural system also accelerated the production of the fatty acid. To adopt this two-phase system, it was very important to let our cells secrete the product into the growth medium. It has been proposed that Hgl aglycones localize to the space between the outer membrane and the heterocyst envelop polysaccharide (HEP) layer and as do the Hgls in the wild type (Halimatul et al., 2014). The disruption of HEP layer in our mutants may allow the cells to secrete the fatty alcohol into the medium under nitrogen-starved conditions and enable its extraction into the overlaid solvent, such as isopropyl myristate.

Anabaena Is a Useful Platform for Bioproduction

Anabaena can fix gaseous nitrogen, an ability that makes them a great candidate for use as a platform for bioproduction. For example, ethanol production using heterocyst cells has been reported by Ehira et al. (2018). They reported more than a hundred times yield (∼170 mg/L) compared with anthropogenic production, indicating that Anabaena has a huge potential for bioproduction. Fatty alcohol in this report was synthesized through reactions of polyketide synthases (PKS). Presently, PKS and non-ribosomal peptide synthase (NRPS) are in the spotlight. In cyanobacteria, PKS has been known to synthesize toxic compounds such as microcystin (Shishido et al., 2019) and swinholide (Humisto et al., 2018). In some marine bacteria, PKS synthesize very long chain fatty acids, such as docosahexaenoic acids (Okuyama et al., 2007). Recently, NRPSs have successfully been expressed in Anabaena for bioproduction (Videau et al., 2016, 2019). The replacement of genes involved in the synthesis of Hgl with desired PKS/NRPS will be of great interest.

DATA AVAILABILITY STATEMENT

All datasets generated for this study are included in the article/**Supplementary Material**.

AUTHOR CONTRIBUTIONS

HM and KA conceived the research and wrote the manuscript. HM and EA conducted the experiments. HM, EA, and KA performed the data analysis. All authors contributed to the article and approved the submitted version.

FUNDING

This research was supported by the Directorate General of Science and Technology and Higher Education Resources, Republic of Indonesia, through World Class Professor Program-Scheme A 2019 (T/44/D.2.3/KK.04.05/2019) and PRESTO, Japan Science and Technology Agency, Japan.

SUPPLEMENTARY MATERIAL

The Supplementary Material for this article can be found online at: https://www.frontiersin.org/articles/10.3389/fpls.2020.00804/full#supplementary-material

FIGURE S1 | Transcript level of *nifH* under nitrogen starvation. The relative quantities of *nifH* were determined by qRT-PCR in the wild type (WT), *hglT* single mutant (Δ*hglT*), and the triple mutant for the indicated time. Values are expressed as the means of duplicated experiments.

REFERENCES

Awai, K., Lechno-Yossef, S., and Wolk, C. P. (2009). "Heterocyst envelope glycolipids," in *Lipid in Photosynthesis Essential and Regulatory Functions*, eds H. Wada and N. Murata (Netherlands: Springer), 179–202. doi: 10.1007/978-90-481-2863-1_9

Awai, K., Ohta, H., and Sato, N. (2014). Oxygenic photosynthesis without galactolipids. *Proc. Natl. Acad. Sci. U.S.A.* 111, 13571–13575. doi: 10.1073/pnas.1403708111

Awai, K., Watanabe, H., Benning, C., and Nishida, I. (2007). Digalactosyldiacylglycerol is required for better photosynthetic growth of *Synechocystis* sp. PCC6803 under phosphate limitation. *Plant Cell Physiol.* 48, 1517–1523. doi: 10.1093/pcp/pcm134

Awai, K., and Wolk, C. P. (2007) Identification of the glycosyl transferase required for synthesis of the principal glycolipid characteristic of heterocysts of *Anabaena* sp. strain PCC 7120. *FEMS Microbiol. Lett.* 266, 98–102. doi: 10.1111/j.1574-6968.2006.00512.x

Borthakur, P. B., Orozco, C. C., Young-Robbins, S. S., Haselkorn, R., and Callahan, S. M. (2005). Inactivation of patS and hetN causes lethal levels of heterocyst differentiation in the filamentous cyanobacterium *Anabaena* sp. PCC 7120. *Mol. Microbiol.* 57, 111–123. doi: 10.1111/j.1365-2958.2005.04678.x

Buikema, W. J., and Haselkorn, R. (1991). Characterization of a gene controlling heterocyst differentiation in the cyanobacterium Anabaena 7120. *Genes Dev.* 5, 321–330. doi: 10.1101/gad.5.2.321

Callahan, S. M., and Buikema, W. J. (2001). The role of HetN in maintenance of the heterocyst pattern in *Anabaena* sp. PCC 7120. Mol Microbiol 40, 941–950. doi: 10.1046/j.1365-2958.2001.02437.x

Corrales-Guerrero, L., Flores, E., and Herrero, A. (2014). Relationships between the ABC-exporter HetC and peptides that regulate the spatiotemporal pattern of heterocyst distribution in *Anabaena*. *PLoS One* 9:e104571. doi: 10.1371/journal.pone.0104571

Ehira, S., Takeuchi, T., and Higo, A. (2018). Spatial separation of photosynthesis and ethanol production by cell type-specific metabolic engineering of filamentous cyanobacteria. *Appl. Microbiol. Biotechnol.* 102, 1523–1531. doi: 10.1007/s00253-017-8620-y

Elhai, J., and Wolk, C. P. (1988). Conjugal transfer of DNA to cyanobacteria. *Methods Enzymol.* 167, 747–754. doi: 10.1016/0076-6879(88)67086-8

Ernst, A., Black, T., Cai, Y., Panoff, J. M., Tiwari, D. N., and Wolk, C. P. (1992). Synthesis of nitrogenase in mutants of the cyanobacterium *Anabaena* sp. strain PCC 7120 affected in heterocyst development or metabolism. *J. Bacteriol.* 174, 6025–6032. doi: 10.1128/jb.174.19.6025-6032.1992

Eungrasamee, K., Miao, R., Incharoensakdi, A., Lindblad, P., and Jantaro, S. (2019). Improved lipid production via fatty acid biosynthesis and free fatty acid recycling in engineered *Synechocystis* sp. PCC 6803. *Biotechnol. Biofuels* 12:8. doi: 10.1186/s13068-018-1349-8

Fan, Q., Huang, G., Lechno-Yossef, S., Wolk, C. P., Kaneko, T., and Tabata, S. (2005). Clustered genes required for synthesis and deposition of envelope glycolipids in *Anabaena* sp. strain PCC 7120. *Mol. Microbiol.* 58, 227–243. doi: 10.1111/j.1365-2958.2005.04818.x

Fay, P. (1992). Oxygen relations of nitrogen fixation in cyanobacteria. *Microbiol. Rev.* 56, 340–373. doi: 10.1128/mmbr.56.2.340-373.1992

Golden, J. W., and Yoon, H. S. (2003). Heterocyst development in *Anabaena*. *Curr. Opin. Microbiol.* 6, 557–563. doi: 10.1016/j.mib.2003.10.004

Halimatul, H. S., Ehira, S., and Awai, K. (2014). Fatty alcohols can complement functions of heterocyst specific glycolipids in *Anabaena* sp. PCC 7120. *Biochem. Biophys. Res. Commun.* 450, 178–183. doi: 10.1016/j.bbrc.2014.05.093

Huang, X., Dong, Y., and Zhao, J. (2004). HetR homodimer is a DNA-binding protein required for heterocyst differentiation, and the DNA-binding activity is inhibited by PatS. *Proc. Natl. Acad. Sci. U.S.A.* 101, 4848–4853. doi: 10.1073/pnas.0400429101

Humisto, A., Jokela, J., Liu, L., Wahlsten, M., Wang, H., Permi, P., et al. (2018). The swinholide biosynthesis gene cluster from a terrestrial *Cyanobacterium*, Nostoc sp. Strain UHCC 0450. *Appl. Environ. Microbiol.* 84:e02321-17. doi: 10.1128/AEM.02321-17

Kangatharalingam, N., Priscu, J. C., and Paerl, H. W. (1992). Heterocyst envelope thickness, heterocyst frequency and nitrogenase activity in Anabaena flos-aquae: influence of exogenous oxygen tension. *Microbiology* 138, 2673–2678. doi: 10.1099/00221287-138-12-2673

Kato, A., Takatani, N., Ikeda, K., Maeda, S. I., and Omata, T. (2017). Removal of the product from the culture medium strongly enhances free fatty acid production by genetically engineered *Synechococcus elongatus*. *Biotechnol. Biofuels* 10, 141. doi: 10.1186/s13068-017-0831-z

Maldener, I., Hannus, S., and Kammerer, M. (2003). Description of five mutants of the cyanobacterium *Anabaena* sp strain PCC 7120 affected in heterocyst differentiation and identification of the transposon-tagged genes. *FEMS Microbiol. Lett.* 224, 205–213. doi: 10.1016/S0378-1097(03)00444-0

Meeks, J. C., and Castenholz, R. W. (1971). Growth and photosynthesis in an extreme thermophile, *Synechococcus lividus* (Cyanophyta). *Arch. Mikrobiol.* 78, 25–41. doi: 10.1007/bf00409086

Okuyama, H., Orikasa, Y., Nishida, T., Watanabe, K., and Morita, N. (2007). Bacterial genes responsible for the biosynthesis of eicosapentaenoic and docosahexaenoic acids and their heterologous expression. *Appl. Environ. Microbiol.* 73, 665–670. doi: 10.1128/AEM.02270-06

Saito, T., and Awai, K. (2020). A polyketide synthase HglEA, but not HglE2, synthesizes heterocyst specific glycolipids in *Anabaena* sp. PCC 7120. *J. Gen. Appl. Microbiol.* 66, 99–105. doi: 10.2323/jgam.2019.11.004

Shishido, T. K., Jokela, J., Humisto, A., Suurnakki, S., Wahlsten, M., Alvarenga, D. O., et al. (2019). The biosynthesis of rare homo-amino acid containing variants of microcystin by a benthic cyanobacterium. *Mar. Drugs* 17:271. doi: 10.3390/md17050271

Stanier, R. Y., Kunisawa, R., Mandel, M., and Cohen-Bazire, G. (1971). Purification and properties of unicellular blue-green algae (order Chroococcales). *Bacteriol. Rev.* 35, 171–205. doi: 10.1128/mmbr.35.2.171-205.1971

Steen, E. J., Kang, Y., Bokinsky, G., Hu, Z., Schirmer, A., McClure, A., et al. (2010). Microbial production of fatty-acid-derived fuels and chemicals from plant biomass. *Nature* 463, 559–562. doi: 10.1038/nature08721

Videau, P., Wells, K. N., Singh, A. J., Eiting, J., Proteau, P., and Philmus, B. (2019). Expanding the natural products heterologous expression repertoire in the model Cyanobacterium *Anabaena* sp. strain PCC 7120: production of pendolmycin and teleocidin B-4. *ACS Synth. Biol.* 9, 63–75. doi: 10.26434/chemrxiv.11316098.v1

Videau, P., Wells, K. N., Singh, A. J., Gerwick, W. H., and Philmus, B. (2016). Assessment of *Anabaena* sp. Strain PCC 7120 as a heterologous expression host for cyanobacterial natural products: production of Lyngbyatoxin A. *ACS Synth. Biol.* 5, 978–988. doi: 10.1021/acssynbio.6b00038

Wang, Y., Gao, Y., Li, C., Gao, H., Zhang, C. C., and Xu, X. (2018). Three Substrains of the Cyanobacterium *Anabaena* sp. Strain PCC 7120 Display Divergence in Genomic Sequences and hetC Function. *J. Bacteriol.* 200:e00076-18. doi: 10.1128/JB.00076-18

Wolk, C. P. (1996). Heterocyst formation. *Annu. Rev. Genet.* 30, 59–78. doi: 10.1146/annurev.genet.30.1.59

Zhang, C. C., Laurent, S., Sakr, S., Peng, L., and Bedu, S. (2006). Heterocyst differentiation and pattern formation in cyanobacteria: a chorus of signals. *Mol. Microbiol.* 59, 367–375. doi: 10.1111/j.1365-2958.2005.04979.x

Zheng, Y. N., Li, L. L., Liu, Q., Yang, J. M., Wang, X. W., Liu, W., et al. (2012). Optimization of fatty alcohol biosynthesis pathway for selectively enhanced production of C12/14 and C16/18 fatty alcohols in engineered *Escherichia coli*. *Microb. Cell Fact.* 11:65. doi: 10.1186/1475-2859-11-65

Conflict of Interest: The authors declare that the research was conducted in the absence of any commercial or financial relationships that could be construed as a potential conflict of interest.

Advantages of publishing in Frontiers

OPEN ACCESS
Articles are free to read for greatest visibility and readership

FAST PUBLICATION
Around 90 days from submission to decision

HIGH QUALITY PEER-REVIEW
Rigorous, collaborative, and constructive peer-review

TRANSPARENT PEER-REVIEW
Editors and reviewers acknowledged by name on published articles

Frontiers
Avenue du Tribunal-Fédéral 34
1005 Lausanne | Switzerland

Visit us: www.frontiersin.org
Contact us: frontiersin.org/about/contact

REPRODUCIBILITY OF RESEARCH
Support open data and methods to enhance research reproducibility

DIGITAL PUBLISHING
Articles designed for optimal readership across devices

FOLLOW US
@frontiersin

IMPACT METRICS
Advanced article metrics track visibility across digital media

EXTENSIVE PROMOTION
Marketing and promotion of impactful research

LOOP RESEARCH NETWORK
Our network increases your article's readership